2D AND 3D PHENOTYPING MURINE MODELS OF *Amelogenesis imperfecta*

Thesis submitted in accordance with the requirements of the University of Liverpool for the degree of Doctor in Philosophy

by

Thomas Liam Coxon

July 2010

ABSTRACT

Introduction

Odontogenesis is a paradigm for biomineralisation. *Amelogenesis imperfecta* (AI) is an inherited tooth enamel defect displaying genetic and phenotypic heterogeneity. The enamel extra-cellular matrix proteins amelogenin and enamelin are coded for by human genes (*AMELX,* OMIM300391 and *ENAM,* OMIM606585) and mice genes (*Amelx* and *Enam*) that are implicated in the aetiology of AI. Mouse models containing specific gene mutations are comparable to those found in humans because they disrupt protein function during the different stages of enamel formation that are reflected in the overlapping range of AI phenotypes; $Amelx^{Y64H}$ and $Enam^{Rgsc395}$ mutant mice display similar phenotypes to humans with X-linked AI and autosomal dominant local hypoplastic AI respectively.

The mouse model is accessible and amenable to experimental investigation. The mandible represents a series of developmental units and the incisor tooth continuously grows giving a permanent record of all stages of enamel formation. Accurately measuring mandible morphology, incisor morphology and enamel colour and whiteness can quantify morphological development and enamel mineralisation.

Aims

To develop, test the reliability of and validate four novel measurement methods; a 2D image analysis system (IAS) to measure murine (i) mandible morphology, (ii) incisor tooth morphology, (iii) incisor enamel colour and whiteness, and (v) a 3D IAS to measure incisor morphology and enamel surface structure. To use the new methods to characterise the phenotypes of an experimental population of *Amelx* and *Enam* mutant mice that model human AI. To use the wild-type genotype groups as controls and as baselines for comparison with the respective mutant littermate genotype groups. To investigate the phenotype variation between the genotype groups and use the significantly different variables to differentiate between the affected and unaffected groups. To demonstrate the effect of the specific gene mutations on the function of the amelogenin and enamelin proteins. To explore mandible and incisor morphological development and enamel mineralisation.

Methods

An established 2D IAS was modified with a macro-lens for the small mouse application. A standardised algorithm was developed in-house for the enamel colour and whiteness assessment. A bespoke 3D IAS was developed by adapting a high resolution measurement device with a rotary stage to obtain 3D images in 360°. 2D and 3D analytical measurement tools and 3D modelling software were also customised.

A homogenous reliability population ($n = 20$) containing left and right mandibles and incisors was measured from the buccal, lingual and labial aspects using the new 2D IAS, 3D IAS and colour and whiteness methods. A heterogeneous experimental population ($n = 35$) containing the *Amelx*^{WT} and *Enam*^{WT} (wild-type) control genotype groups and the *Amelx*$^{X/Y64H}$ (heterozygous), *Amelx*$^{Y/Y64H}$ (hemizygous) and *Amelx*$^{Y64H/Y64H}$ (homozygous) and the *Enam*^{Rgsc} *heterozygous* and *Enam*^{Rgsc} *homozygous* mutant genotype groups were similarly measured.

Measurement reliability was determined by multiple operator correlation, method agreement and descriptive statistics. Bonferonni corrected significant differences ($p = 0.002$) were identified by Analysis of Variance, Multiple Comparisons and Tuckey Honestly Significant Differences tests.

Results

The intra-operator and inter-operator measurement reliability of the 2D IAS mandible morphology (ICC $\geq$ 0.77), incisor morphology (ICC $\geq$ 0.75) and colour and whiteness assessment (ICC $\geq$ 0.13) methods were predominantly classified as excellent. The 2D and 3D methods demonstrated significant ($p < 0.01$) agreement (PCC $\geq$ 0.71) with no significant differences ($p < 0.01$) between measurements, except in one variable. The confidence intervals, limits of agreement and bias assessments were all highly satisfactory. A principal component analysis highlighted strong size and shape defining relationships between the morphological variables.

Significant differences ($p \leq 0.002$) in morphology and colour and whiteness were evident between the unaffected *Amelx*^{WT} group and the three affected mutant groups *Amelx*$^{X/Y64H}$, *Amelx*$^{Y/Y64H}$ and *Amelx*$^{Y64H/Y64H}$. Mandibles and incisors were largest in the *Amelx*^{WT} group and smallest in the *Amelx*$^{Y64H/Y6H}$ group. The *Amelx*$^{X/Y64H}$ incisors were of intermediate size, shape and colour. The *Amelx*^{WT} incisors constituted high *yellow* and low *whiteness* and low *lightness* colour components in complete contrast to the discoloured *Amelx*$^{Y/Y64H}$ and *Amelx*$^{Y64H/Y64H}$ incisors; the significant differences were identified in the *incisal* and *whole* enamel surface regions that corresponded to the *mature* and *all* stages of enamel development respectively.

Significant differences ($p \leq 0.002$) in morphology and colour and whiteness were evident between the unaffected *Enam*^{WT} and the two affected mutant groups *Enam*^{Rgsc} *heterozygous* and *homozygous*. Mandibles and incisors were largest in the *Enam*^{WT} group and smallest in the *Enam*^{Rgsc} *heterozygous* group. The *Enam*^{WT} incisors constituted high *yellow* and low *whiteness* and low *lightness* colour components in complete contrast to the similarly discoloured *Enam*^{Rgsc} *heterozygous* and *homozygous* incisors; the significant differences were identified the in the *middle*, *incisal* and *whole* enamel surface regions that corresponded to the *secretory*, *mature* and *all* stages of enamel development respectively.

Conclusions

The novel 2D IAS, colour and whiteness and 3D IAS have provided a series of macro-metric morphological and micro-metric surface parameters that were highly reliable and selective. The methods were successfully validated as practical, objective and quantitative approaches to accurate phenotyping of mice mandibles, incisors and enamel.

The experimental comparison detected significant differences between the unaffected wild-type controls and affected experimental mutants in mandible morphology, incisor morphology, and in enamel colour and whiteness. This was directly attributed to the specific gene mutations that were proposed to have caused protein truncation and loss of function, which disrupted enamel formation and led to severe enamel defects. The *Amelx* and *Enam* mouse models phenocopied AIH1 and AIH2 respectively; the $Amelx^{Y/Y64H}$ and $Amelx^{Y64H/Y64H}$ incisor displayed thin hypoplastic enamel characteristic of AIH1; the $Amelx^{X/Y64H}$ incisors displayed hypomineralised enamel characteristic of AIH1; the $Enam^{Rgsc}$ *heterozygous* and *homozygous* incisors showed localised hypoplastic enamel characteristic of AIH2.

The sites of the significant enamel discolouration were different in the *Amelx* groups (*incisal*, *whole*) and the *Enam* groups (*middle*, *incisal*, *whole*), supporting the different affects of the two proteins and the respective mutations; amelogenin disrupted the *mature* stage of enamel formation and enamelin disrupted both the *secretory* and *mature* stages. Overlapping enamel phenotypes were differentiated by separate and specific surface regions that corresponded to the different developmental stages of enamel formation.

This study supported the multifunctional role of amelogenin in alveolar bone formation during mandible development. The $Amelx^{X/Y64H}$ intermediate enamel phenotype was concordant with lionisation and X-chromosomal inactivation. This study supported the critical involvement of the amelogenin and enamelin proteins in controlling enamel structural organisation and generating the full thickness of enamel during mineralisation. This study supported the intracellular protein-protein trafficking/ chaperoning secretory pathway recently proposed as an explanatory mechanism for dysplastic enamel mineralisation. The phenotype was correlated to the genotype in two pertinent mouse models of human AI.

CONTENTS

ACKNOWLEDGEMENTS

I acknowledge The Wellcome Trust for funding my position as a full-time Research Technician & part-time PhD student in The School of Dental Sciences at The University of Liverpool, UK.

I gratefully acknowledge the consummate professionalism & personal supervision of Dr. Richard N. Smith and Professor Alan H. Brook (International Collaborating Centre in Oro-Facial Genetics & Development, School of Dental Sciences, University of Liverpool, UK) who afforded me this generous opportunity & to whom I am sincerely deeply indebted.

My thanks extend to Dr. Paul Anderson (Biophysics Centre for Oral Growth & Development, Queen Mary & Westfield College, University of London, UK), Professor Lassi J. Alvesalo (Institute of Dentistry, University of Oulu, Finland) and Professor Grant C. Townsend (School of Dentistry, University of Adelaide, Australia) for their valuable collaborative input.

This project would not have been possible without the support of my good friends & colleagues in The Research Wing of The School of Dental Sciences at The University of Liverpool, UK.

DEDICATION

To My Family... Past, Present & Future.

DECLARATION

This thesis is the result of my own work. The material contained herein has not been presented, nor is currently being presented, either wholly or in any part for any other degree or qualification.

Ethics approval was granted by the Wellcome Trust programme (reference 06/Q0104/38).

The research was carried out in the School of Dental Sciences at The University of Liverpool.

ABBREVIATIONS

2D	Two-dimensional
3D	Three-dimensional
AI	*Amelogenesis imperfecta*
AIH1	X-linked *Amelogenesis imperfecta*
AIH2	Autosomal Dominant Local Hypoplastic Amelogenesis imperfecta
AMELX	Amelogenin human X chromosome gene
Amelx	Amelogenin mouse X chromosome gene
$Amelx^{WT}$	Amelogenin wild-type
$Amelx^{X/Y64H}$	Heterozygous Y64H mutation
$Amelx^{Y/Y64H}$	Hemizygous Y64H mutation
$Amelx^{Y64H/Y64H}$	Homozygous Y64H mutation
ECM	Extra-cellular Matrix
ENAM	Enamelin human gene
Enam	Enamelin mouse gene
$Enam^{WT}$	Enamelin wild-type
$Enam^{Rgsc395}$	heterozygous S55I mutation
$Enam^{Rgsc395}$	homozygous S55I mutation
IAS	Image Analysis System
ICC	Intra-class Correlation Coefficient
MD	Mean Difference
NCSP	Non-contact Surface Profilometer
OMIM	Online Mendelian Inheritance in Man
PCA	Principal Component Analysis
PCC	Pearson's Correlation Coefficient
SD	Standard Deviation
SD Diff.	Standard Deviation of the Difference

LIST OF FIGURES

LIST OF TABLES

1. INTRODUCTION

1.1. INTRODUCTION

This project aims to further the information on normal and abnormal dental enamel mineralisation using novel 2D and 3D imaging and analytical measurement tools. This project used murine models to enhance the phenotypic differentiation and further the aetiological understanding of an inherited group of dental enamel defects known as the *Amelogenesis imperfectas*.

The project was the result of work carried out at The University of Liverpool, School of Dental Sciences. It was undertaken as part of the five year Wellcome programme grant (ref. 075945/c/04/z) that involved separate but allied parallel clinical and laboratory molecular and biochemical investigations at three other institutions; The University of Leeds, The University of Manchester and The University of Sheffield, and their respective University Hospital and National Health Service Primary Care Trusts.

Ethical approval was granted according to the Wellcome Trust programme grant.

1.2. EXPERIMENTAL DESIGN AND METHODS

1.2.1. Animal Models of *Amelogenesis imperfecta*

Odontogenesis is a paradigm for biomineralisation. The murine tooth model affords substantial opportunities for investigating the role of the extra-cellular matrix (ECM) proteins in enamel mineralisation. *Amelogenesis imperfecta* (AI) is an inherited enamel defect displaying genetic and phenotypic heterogeneity. The predominant ECM proteins amelogenin and enamelin are encoded by human (*AMELX,* OMIM300391 and *ENAM,* OMIM606585) and mouse (*Amelx* and *Enam*) gene homologues that are implicated in the aetiology of AI. Mouse models containing specific gene mutations are comparable to those found in humans because they disrupt protein function during different stages of enamel formation that are reflected in the overlapping range of AI phenotypes; $Amelx^{Y64H}$ and $Enam^{Rgsc395}$ mutant mice display similar phenotypes to humans with X-linked AI (A1H1, OMIM301200) and autosomal dominant local hypoplastic AI (A1H2, OMIM104500) respectively.

Mouse heads were obtained from Professor Michael Dixon's laboratory at The University of Manchester, UK, where the breeding colony was established from RIKEN (Riken, Wako, Japan) parent stock generated by N-Ethyl-N-nitrosourea (ENU) mutagenesis and identified during large scale phenotype driven screening (www.gsc.riken.go.jp/Mouse/). ENU mutagenesis generates point mutations to appropriately model human genetic diseases.

The mouse models are accessible and amenable to experimental investigation. Mouse mandibles and mandibular incisors are well suited to the quantitative study of tooth morphological development and enamel mineralisation respectively. The mouse mandible is a homologous developmental unit and the continuously growing mouse incisor represents all stages of enamel formation. Incisor enamel surface structure exhibits the *pre-secretory*, *secretory* and *mature* developmental stages of enamel formation. The tooth provides a permanent record of tooth development and enamel formation (amelogenesis). This permits direct correlation between the observable phenotype and the underlying genetic lesion.

Mandible and incisor morphological measurement (morphometry) and colour and whiteness assessment are excellent methods by which to quantify the developmental plasticity and the effect of the specific gene mutations on the critical function of amelogenin and enamelin in

the phenotype variation of AI. Relating the macro-metric and micro-metric phenotype to the genotype helps to understand the aetiology of AI. The quantifiable effect on enamel mineralisation will lead to new information relating to the biological function of amelogenin and enamelin proteins *in vivo* in mice and in humans.

1.2.2. Detailed Phenotyping

New murine dental phenotyping approaches permit essential method reliability and validity to be determined for four new measurement methods; a modified 2D image analysis system (2D IAS) for (i) mandible morphology, (ii) incisor morphology (iii) enamel colour and whiteness assessment, and (v) a new 3D IAS incisor morphology and surface analysis method. A homogeneous wild-type population of extracted mouse mandibles and incisors will be used in a statistically comprehensive study of method reliability. The in-house developments - e.g. the novel colour and whiteness software algorithm, the customised hardware modifications and the novel specialised analytical software - will present major research outcomes that specifically meet the requirements of the small mammalian tooth application.

The new measurement methods will quantitatively characterise the phenotypes of mandibles, incisors and enamel mineralisation of an experimental population of two mouse models of AI. The unaffected *Amelx*^{WT} and *Enam*^{WT} (wild-type) control mice will serve as a baseline for comparative analysis with their respective affected *Amelx*$^{X/Y64H}$ (heterozygous), *Amelx*$^{Y/Y64H}$ (hemizygous) and *Amelx*$^{Y64H/Y64H}$ (homozygous) and the *Enam*^{Rgsc} *heterozygous* and *Enam*^{Rgsc} *homozygous* phenocopy mutant mice groups. A multiple comparison analysis of variance will provide robust statistical support.

1.3. RELATING PHENOTYPE TO GENOTYPE

Standardised and comprehensive characterisation of the two animal models will permit valid phenotype to genotype correlation providing fundamental information in respect of the role of the specific ECM proteins in enamel mineralisation, while increasing the relevance of the research to end users/ patients by translation to the human condition. The 2Ds and 3D investigations will provide significant additional quantitative data to describe previously inaccessible information on animal tooth morphology, lesion pattern and enamel distribution in respect of the macro-metric and micro-metric effect on the AI phenotype.

The new 3D IAS will facilitate new 3D surface analysis to provide a unique and accurate topographical examination of animal model lesion size and surface deficiencies and, furthermore, the nature and extent of structural defects present. Analysing the phenotype in relation to the genotype will address questions such as the causes of the variation in phenotype between individuals with the same single gene mutation and the variation in degree to which different teeth are affected in the same individual.

This will not only provide new information on defective dental mineralisation in respect of the effects of specific mutations in the ECM protein components but will also facilitate extrapolation from the animal to the human situation.

1.4. SUMMARY

In addition to providing a robust platform against which to interpret the roles of specific ECM components during odontogenic mineralisation, this study provides micro-metric and macro-metric observations for the systematic characterisation of dental defects and enamel phenotypes of animal teeth. This will permit correlations between the phenotype and the underlying genetic pathogenesis. This will provide quantitative phenotype level evidence to support the biochemical and histological data that has recently proposed the intracellular protein-protein interactions and trafficking/ chaperoning secretory pathways to be a key mechanistic factor underpinning the aberrant enamel mineralisation observed in AI.

2. LITERATURE REVIEW

2.1 INTRODUCTION

2.1.1. 2D and 3D Morphometric and Colour and Whiteness Assessment

Image analysis has long been applied in dental morphology research because morphometric methods are well suited to experimental studies of anatomical form, structural development and morphogenesis. Image analysis increases understanding because it is objective and can simplify phenotypes into shapes and sizes that may be explored quantitatively.

Tooth colour is significantly influenced by the combined physico-optical properties of the dental hard tissues and enamel surface topography. Therefore, the normal and abnormal mineralisation of enamel and dentine affects tooth colour, and conversely, measurement of colour and whiteness measurement can be used as an indicator of levels of mineralisation.

Innovation in methodology can have important applications in addressing research questions. The numerous 2D and 3D imaging methods provide versatile techniques for morphological investigation that can be quickly and conveniently stored on a personal computer. The rise of digital imaging, the fall of photographic film use and the increased accessibility of digital technologies has expanded the applications of image analysis.

The literature review will detail a wide variety of 2D and 3D approaches to recording and measuring human and mouse dental morphology, and colour and whiteness. In assessing techniques for image acquisition, quantitative analysis and comparison, the available and developing technologies will be discussed in the context of those that can be translated from the human and optimised for the mouse application. Economy, speed, practicality, measurement accuracy, reliability, and breadth of parameters will be used as criteria for evaluating the limitations and efficacy of each method, and for assessing its relative advantages and disadvantages in terms of potential use for the small mouse application. The review will focus on image analysis systems that accurately quantify developmental morphologies to investigate the structure-function relationships of disease aetiologies. The combination of 2D and 3D techniques will provide a complementary multilevel approach to studying the complex multifactorial aetiologies of various abnormal dental phenotypes.

2.1.2. Tooth Development and The Mammalian Model

The accessibility of teeth makes them a convenient model for studying organogenesis. The similar developmental processes of human and mouse odontogenesis makes inbred strains of laboratory mice the mammalian model of choice for human dental disease, for a number of reasons. For example, mice and humans share a similar genome size, share many gene sequence homologies and orthologous proteins, and share many molecular regulatory mechanisms/ pathways during odontogenesis and skeletogenesis. The mouse incisor displays all of the distinct stages of initiation, morphogenesis, differentiation and mineralisation, including the complex processes that determine tooth number, size, shape, morphology and enamel surface structure. The genetic homogeneity of specially bred mice ensures a baseline level for experimentally introduced anomalies. Targeted gene mutation causes a single protein change that can be detected at the macroscopic phenotype level. This affect may then be attributed to the mutation under investigation, to provide insight into the processes of morphological development and enamel mineralisation. The mouse is the only mammalian model with which it is possible to employ both the phenotype to genotype (phenotype-driven) and genotype to phenotype (gene-driven) approaches.

Odontogenesis is a paradigm for biomineralisation. The important roles of the enamel ECM proteins in structural development, surface morphogenesis and mineralisation make the tooth a unique location to explore the phenotype-genotype relationship.

2.1.3. Mineralisation and the Predominant Extra-Cellular Matrix (ECM) Proteins

The precise ECM mediated orchestration of mammalian biomineralisation remains obscure but a number of important genes and proteins involved in dental mineralised tissue formation are recognised to provide instructional templates for crystal deposition, growth and morphology. The predominant enamel ECM proteins are amelogenin and enamelin. They are encoded by the *Amelx* and *Enam* genes respectively, which are evolutionarily conserved orthologues in humans and mice. Amelogenin constitutes 90% of developing enamel and enamelin is the largest but least abundant ECM protein (1-5%). Amelogenin and enamelin provided some of the earliest evidence of the ECM involvement in enamel mineralisation and have been extensively characterised. They are both secreted by ameloblasts in the various

stages of enamel formation or amelogenesis. Their respective structures relate to their specific segregated functions in amelogenesis.

2.1.4. Phenotyping Murine Models of *Amelogenesis Imperfecta*

Mutations in *Amelx* and *Enam* genes are implicated in the aetiology of *Amelogenesis imperfecta* (AI), a clinically and genetically heterogeneous group of inherited dental defects. Three main deficiencies in the quality or quantity of enamel are broadly classified into three main AI phenotypes; hypoplastic, hypomineralised and hypomature. The diverse spectrum of phenotypes is dependent on the type and location of the specific gene mutations. Thus far, 15 *AMELX* and 8 *ENAM* gene mutations have been identified in humans.

The *Amlex* and *Enam* mouse models contain similar mutations to those found in humans. The targeted mutations are engineered to alter protein structure and disrupt function and have generated similar enamel phenotypes. These phenocopy mouse models substantiate the dynamic involvement of the ECM proteins in enamel formation. By detecting the affect of the specific protein changes on the macroscopic tooth morphology and microscopic enamel surface phenotype, in the distinct stages of amelogenesis, it may be possible to understand more about the specific roles of these proteins during enamel mineralisation and furthermore in the causality of AI.

2.2. 2D DENTAL MEASUREMENT METHODS

2.2.1. Direct Methods

2.2.2.1. Callipers and Dividers:

The early dental surveying instruments designed for reproducing tooth shape and dental arch form were reported to be tedious, relatively imprecise and practically unsuitable for measurements on teeth (Biggerstaff, 1969). Dividers, sliding callipers, vernier callipers and dial callipers were among the first manual techniques used to obtain linear measurements from dental study models (Moorees *et al.,* 1957; Bolton, 1962). The use of engineering dividers advanced with a millimetre rule (Bolton, 1958) and the desire for increased accuracy brought about the popular use of sliding callipers (Hixon and Oldfather, 1958; Hunter and Priest, 1960; Barrett *et al.,* 1963; Moorrees and Reed, 1964). Conventional engineering callipers were also a readily available instrument for measuring tooth dimensions.

Comparing manual measurements using engineering dividers and sliding callipers found measurements on study models to be systematically 0.1mm larger than the equivalent intra-oral measurements (Hunter and Priest, 1960). This was likely to have been caused by errors introduced by the impression and/ or casting procedures. Sliding callipers and Boley gauge callipers demonstrated higher reproducibility and were reportedly easier to use, more accurate and consistent than the needle point dividers (Moorees *et al.,* 1957; Shellhart *et al.,* 1995). The introduction of digital callipers linked to a personal computer brought about a more rapid measurement and data acquisition (Mik and Cooke, 1998) and reduced measurement transfer and calculation errors (Ho and Freer, 1999). However, the measurement error associated with manual landmark positioning on the cast and other factors involving operator subjectivity, such as landmark determination and repositioning (Hunter and Priest, 1960), meant that digital callipers did not provide a sufficient degree of accuracy (Mik and Cooke, 1998) or appropriate scale for morphometric measurement of murine teeth (Hillson *et al.,* 2005). The use of callipers would therefore be inappropriate in the current application.

2.2.2. Indirect methods

2.2.2.1. Early Photographic Method:

An early 2D technique that digitised photographic negatives of study models with manually marked anatomical landmarks showed good method reliability (Biggerstaff, 1969). The system used a number of linear and surface area measurements to assess cusp variation with good intra-operator (MD ±0.014mm) and inter-operator (MD ±0.083mm) precision (Biggerstaff, 1969). Although the overall method was less expensive and more versatile compared with the early direct techniques (Stanton *et al.,* 1931). The method for defining anatomical landmarks was ambiguous and callipers were still recommended for traditional dental measurements.

This semi-automatic system represented an early move towards reduced subjectivity and associated error and the predominance of the indirect methods for dental measurement. However, restricted measurement capacity and questionable practicality made this particular photographic method unsuitable for the current murine application.

2.2.2.2. Savara's Data Acquisition Method:

An indirect method that used photocopied reproductions of manually marked dental casts and reported no significant measurements differences ($p < 0.001$) was said to be reproducible, simple, economical and timesaving compared to the direct manual methods (Singh and Savara, 1964). However, a similar method showed substantial differences between the actual cast measurements taken with callipers and photocopies of dental casts (Champagne, 1992). Although this technique was said to avoid the limitations of elaborate equipment, factors of enlargement, object to image distance and lighting methods, it presented numerous problems such as magnification and the inability to precisely duplicate a 3D object into a 2D planar image.

A photogrammetric method by the same author quantified human tooth form by way of a modified comparator and a decimal converter (Savara, 1965). This essentially photographic technique used semi-automated computer based data reduction and data analysis to avoid common errors associated with callipers, i.e. reading scales and transcribing the figures, but introduced new sources of error (Savara and Sanin, 1969). The method showed fair cast reorientation and mesio-distal measurement (SD Diff. ±0.09mm) but only a limited number of

repeat measurements were carried out. The claimed benefits of this method were arguable and the expensive equipment and the need for skilled operators did not lead to its widespread use.

2.2.2.3. Transverse Micro-Radiography (TMR):

Transverse micro-radiography (TMR) is a 2D technique that allows the mineral content of the hard tissues to be quantified using X-ray absorption, which is proportional to the optical density of the photographic film or plate (Arends and ten Bosch, 1992). TMR is a practical and reliable technique but is also destructive, involving sample sectioning and polishing (Arends and ten Bosch, 1992). This is disadvantageous in terms of preparation time and also limits experimental design but TMR directly measures the mineral content of the dental hard tissues and quantifies mineral changes and distribution in enamel, dentine, and cementum (Higham *et al.,* 2009). TMR allows very detailed examination of mineralisation, e.g in rodent incisors (Sato *et al.,* 1996), but cannot investigate the macro-structure of the whole tooth.

2.2.2.4. 2D Image Analysis System:

The 2D Image Analysis System (IAS) was introduced to objectively measure tooth dimensions on dental casts (Brook *et al.,* 1983). The early apparatus consisted of a black and white television camera, an adjustable calibrated stage and a macro-stand illuminated by four adjustable lamps. Operators were able to control image acquisition, storage and on-screen display by a mini-computer and host software. Calibrated images were derived from multiple views and the configuration files containing the camera settings and stage orientation data could be saved electronically in order to reposition models exactly during repeat measurements (Brook *et al.,* 1983).

Large numbers of recognised dental measurements (Moores *et al.,* 1957) were taken using computer software with reasonable speed and intra-operator repeatability measurements (±0.1mm) compared to previous manual processes (Brook *et al.,* 1983). Comparing the IAS to a classical dial calliper on 50 individuals with a mean reliability for occlusal (81%) and buccal (66%) view measurements validated this system with lower reliability than the classic manual measurements (96%) (Brook *et al.,* 1986). This was because the dial callipers focused on individual teeth separately whereas the new technique enabled tooth measurements from the complete dentition and from multiple views. Calibration and alignment errors on the monitor were reported to be the cause of the measurement variation. However, the IAS introduced a

versatile orientation stage and an increasingly automated computer analysis approach that reduced experimental error and expedited data comparison of different samples.

The new 2D IAS demonstrated numerous advantages over the direct methods and previous indirect methods, e.g almost double the range of measurements of previous studies (Keiser, 1990) and a greater accuracy (±0.01mm) than digital callipers (Mitutoyo Ltd., Japan) (Brook *et al.,* 1999). Novel software programmes called macros aided morphological analysis and provided a greater variety of measurements (Khalaf *et al.,* 2001). The method measured all tooth types from various views with excellent intra-operator repeatability (ICC $\geq$ 0.97) (Brook *et al.,* 1999). Several considerable improvements contributed to the good to excellent multiple independent operator reliability (ICC 0.60 - 0.96), e.g. calibrated illumination and standardised model positioning, and have produced a comprehensive total imaging system (Brook *et al.,* 2005a), valid under both *in-vitro* and *in-vivo* conditions (Smith *et al.,* 2008a).

The application of the 2D IAS has been expanded for multiple purposes that include tooth size comparisons (Khalaf *et al.,* 2001, 2005a, 2009), analysis of curvature (Smith *et al.,* 2007), tooth symmetry (Khalaf *et al.,* 2005b; Di Biase *et al.,* 2006), tooth colour (Brook *et al.,* 2007; Lath *et al.,* 2007a), stain (Lath *et al.,* 2006; Lath *et al.,* 2007b), plaque (Smith *et al.,* 2001, 2004, 2006) and gingival inflammation assessment (Smith *et al.,* 2008b). A series of studies on hypodontia (McKeown *et al.,* 2002), supernumerary teeth (Khalaf *et al.,* 2001, 2005a, 2009), enamel defects (Brook *et al.,* 2001; Elcock *et al.,* 2006; Smith *et al.,* 2009a) and examination of Romano-Briton populations (Brook *et al.,* 1995, 2006) has highlighted the diverse functionality of the 2D IAS in investigating the multifactorial influences of genetic, epigenetic and the environment on tooth morphology and development (Brook *et al.,* 20002, 2005b), and disease aetiologies (Brook *et al.,* 2009). Indeed, the system upholds the gold standard for measuring dental morphology in 2D, and in validation studies on novel 3D measurement methods (Smith *et al.,* 2009b; Horrocks *et al.,* 2009).

2.3. MORPHOMETRICS

2.3.1. Mandible Morphometrics

A variety of non-morphometric methods have furthered the understanding of the molecular and cellular processes that effect morphogenesis, e.g. fluorescent protein assays in cleft lip and palate (Parsons *et al.,* 2008) and 3D serial histology of developing teeth (Lesot *et al.,* 1996, 1998) and mandibles (Ramaesh and Bard, 2003). However, although quantifying biochemical activity and microscopic ultra-structural growth has proven invaluable, particularly in studies of development and embryogenesis, these approaches would not be applicable for measuring tooth morphology or enamel surface structure analysis. Typically they have given little attention to subtle differences among the developmental mechanisms of conspecific organisms, despite the fact that experimental manipulations frequently produced a range of overlapping phenotypic manifestations (Bailey, 1985, 1986; Cooper and Albertson, 2008). Therefore, non-morphometric investigations can overlook the important overlapping variation in a range of phenotypes that have ramifications for differentiation in diagnosis.

Considering multiple biometric characters or morphometric variables allows quantitative estimation of morphological variation and divergence among populations as a result of genetic relationship in a complimentary approach to non-morphometric microscopic and histological methods (Ansorge, 2001). Furthermore, quantitative analysis of morphological variation provides a baseline framework for determining if fine scale phenotypic changes between control and mutant populations are the result of an experimentally induced alteration or developmental noise. Classical targeted disruptions of specific genetic pathways have lead to a significantly deeper understanding of the molecular regulation of morphogenesis and development. However, this extensive multidisciplinary research does not quantify how anatomical traits are affected at the phenotype level to give a more holistic view of the genotype-phenotype interactions. The bioinformatic methods that mathematically model developmental systems (Jernvall *et al.,* 2000) and/ or data-mine phenotypes (Plyusnin *et al.,* 2008) are out of the scope of this review.

On the other hand morphometric techniques quantify shape descriptions and calculate morphological variation when powerfully combined with statistical methods (Bookstein, 1984), e.g. Principal Component Analysis (Harris *et al.,* 1988; Khalaf *et al.,* 2001) or Planar

Procrustes Analysis (Robinson *et al.,* 2001, 2002). A great wealth of information about the genetic basis and development of anatomical form was generated from the use of comparative morphology in evolutionary genetics (Wentworth-Thompson, 1942; Bookstein, 1998; Klingenberg, 2002). Most biological forms contain specific landmarks that are structurally consistent loci (or points) and have evolutionary, ontogenetic, and/or functional significance (Lele and Richtsmeier, 1991). Homologous landmarks correspond between two or more characteristics of organisms cause continuity of information between groups/ populations in experimental studies (van Valen, 1982). Such landmarks may be useful in morphometric analysis when they are consistently and reliably located with a measurable degree of accuracy on all forms considered (Roth, 1988; Bookstein, 1997).

Skeletal features have long provided an amenable system for quantifying anatomical form; in particular the mouse mandible has been an excellent model for the complex morphological development of oro-facial structures (Gaunt, 1964; Atchley *et al.,* 1985; Atchley and Hall, 1991; Bookstein, 1998). Such features can be analysed using (i) direct measurements (Gaunt, 1964; Bailey, 1985, 1986), which characterise relative sizes of parts by linear distance measurements, (ii) the Cartesian coordinate locations of anatomical landmarks (geometric morphometrics) (Moore, 1973; Klingenberg *et al.,* 2001; 2004), or (iii) by the outline shapes of structures of interest (Lavelle, 1983; Moss, 1988; Cheveraud *et al.,* 1990; 1996). Investigations into the variability of size and shape in inbred mouse mandibles have used multivariate statistical analysis (Zelditch *et al.,* 1989) or finite element scaling analysis (Moore, 1973; Moss, 1988; Cheverud *et al.,* 1983, 1990) to quantify morphological divergence between well defined genotype groups.

Geometric methods combined with the multivariate generalisation of linkage analysis that reflect the entire diversity of spatial patterns of gene effects have been successfully used to analyse mandible size and shape by quantitative trait loci (Cheverud *et al.,* 1996) and Procrustes landmark superimposition (Klingenberg *et al.,* 2001). Principal Component Analysis (PCA) has been shown to spread the measure of variation evenly across factors so that size variation does not dominate and that new parameters avoid landmark overlap in the same regions with sparse sampling and missing variation in regions spanned by long measurements (Zelditch *et al.,* 1989). Other statistical methods have been also effective in analysing population differences and showed phenotypic variation was an effective exploratory strategy (Klingenberg, 2002).

Homologous landmark features between individuals illustrate morphogenetic traits and make it possible to detect the magnitude of developmental and phenotypic variation between inbred, genetically identical strains of model organisms. For example, skeletal modules or units may be used for linear measurements of both aspects of the mandible (Gaunt, 1964) and measurements between anatomical landmark points correspond to biometric regions of biomechanical significance (Moore, 1973). In fact, using characteristic mandibular landmarks the systematic morphometric analysis of 15 previously indistinguishable strains of inbred mice were differentiated using morphometric measurements with 98% accuracy (Festing, 1972). Also inaccuracies associated with poorly defined non-homologous biological landmarks were eliminated by datum point coordinate measurement methods that described the profile of the mandible in outline form, using a strip chart digitiser (Lavelle, 1973) and triangulation truss (Strauss *et al.,* 1982; Zelditch *et al.,* 1989). A number of more recent examples that successfully quantify form to describe the mutational effects on anatomical growth and formation may be found in Cooper and Albertson (2008).

2.3.2. Landmark/ Measurement Determination

By using a combination of direct linear methods (Moore, 1973; Bailey, 1985, 1986) and outline analysis (Lavelle, 1972, 1983; Moss, 1988) it will be possible to achieve new meaningful morphometric variables that will be more than the sum of the traditional anatomical landmark measurements (Figure 1.).

Figure 1. Mandible Morphometrics

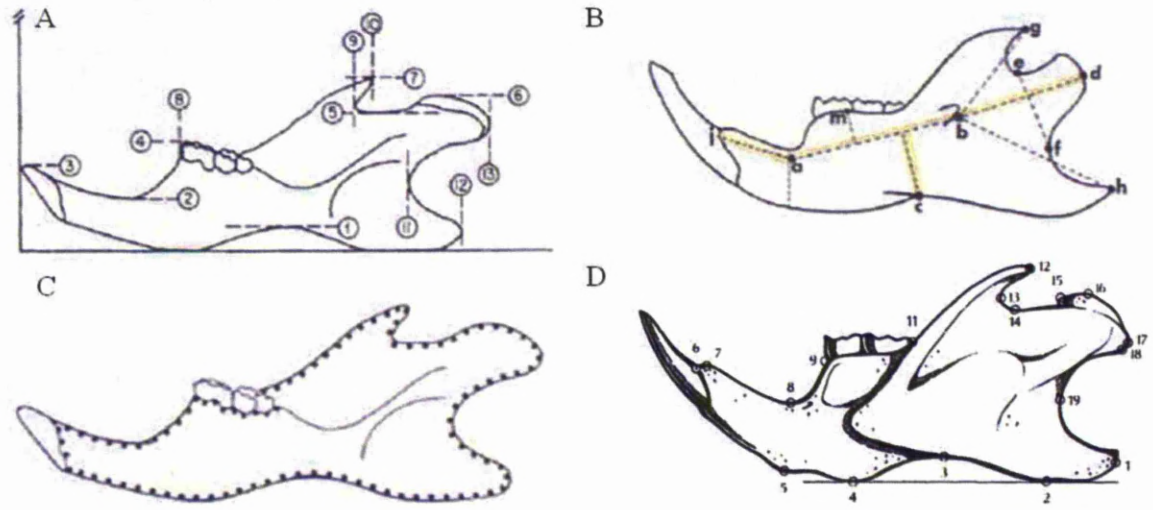

(A) landmark points used to determine features for investigation (Festing 1972); (B) linear measurements between landmarks (Moore, 1973); (C) outline description of form by equidistant data points (Lavelle, 1973); (D) morphogenetic features that represent functional and developmental traits (Atchely *et al.,* 1985). Right and left hemi-mandibles shown.

The mandible morphology will be characterised by integrating established morphological landmarks with those from new measurement techniques to provide further parameters for anatomical and morphogenetic linear measurements within and between developmental units. Equally spaced data points have previously described the outline form or profile of both aspects of mandibles (Lavelle, 1973) and prominent morphogenetic features representing functional and developmental traits (Atchley *et al.,* 1985) will be combined to define new measurements, e.g. *perimeter* and *surface-area*. The benefits of the 2D IAS include increased automation and minimal operator subjectivity (Brook *et al*, 2005a) that will help define additional measurement parameters and extended the versatility of the existing system to provide an exciting possibility for exploring phenotype variation in dental morphology and development.

2.4. 3D DENTAL MEASUREMENT METHODS

2.4.1. Direct Methods

The direct methods employed specifically constructed instruments to measure tooth dimensions by direct mechanical contact, e.g. the Symmetrograph (Korkhaus, 1930) and the Optocom (van Der Linden, 1972). The Symmetrograph was a simple manual appliance that transformed the 3D contours of dental casts into a 2D profile on graph paper (Moyers, 1988; Ciambotti *et al.*, 2001). The Optocom consisted of a light microscope mounted onto a moveable table that positioned dental casts for imaging (van Der Linden, 1972). Their method reliability was reasonable but only after experienced operation (Bhatia and Harrison, 1986; Moyers, 1988).

The direct methods relied on mechanical or physical contact principles meaning that linear measurement errors were proportional to - and dependent on - the vertical Z coordinate data. Some direct 3D methods required more mechanical contact than others and the transformation of the 3D coordinates into a 2D medium was often approximated. This showed that the direct methods were full of many uncertainties, which was a considerable disadvantage that limited measurement accuracy and compromised morphological detail. The direct methods had a narrower measurement capacity and smaller range of measurements than both the manual calliper methods and the 2D IAS. By recording the 3D data in a 2D medium it was a challenge to make a complete comparison with the more contemporary 3D techniques. These effectively 2D methods can not be considered for the current study.

2.4.2. Indirect Methods

The indirect 3D approaches invariably used optical principals in a variety of methods.

2.4.2.1 Photogrammetry:

The early photogrammetry methods captured stereo-pairs of images that were combined to reconstruct the third dimension (Tham, 1956; Savara, 1965). Dental casts were positioned on a movable stage, in front of a horizontally mounted analogue camera. Occlusal surface photographs were developed and contour maps were drawn. The early 'stereo-photometric' methods recorded tooth dimensions on grid paper in terms of 3D coordinate point positions

(Berkowitz and Pruzansky, 1968; Taverne *et al.,* 1979), which effectively performed a 2D analysis in much the same way as the early direct methods (Korkhaus, 1930; van Der Linden, 1972). The limitations of the photogrammetry methods were reflected in their low measurement accuracy ±0.1mm (Savara, 1969) and high measurement variation ±0.3mm (Berkowitz and Pruzansky, 1968).

The alignment of stereo image pairs was problematic primarily because the movable carrier used for sequential images made the non-standard orientation of the models in 3D difficult and subsequently restricted accuracy. Therefore, photogrammetry could not be applied to a small mammalian application and was more suited to the large engineering and surveying applications from where the techniques were originally adopted.

Later investigations attempted to overcome the alignment problems by projecting a reference grid on to the dental cast surface with a light (Pirttiniemi *et al.* 1999). This illuminating method was more effective than using grid paper (Berkowitz and Pruzansky, 1968) and represented a precursor to Moiré Contourography (Kanazawa *et al.,* 1984; Mayhall and Alvesalo, 1992). The light projection apparatus was an early example of the use of the developing optical technologies and it indicated the start of a transition from the direct mechanical methods to the predominant use of the indirect optical methods.

2.4.2.2. Reflex Metrograph:

The Reflex Metrograph was based on the reflex plot system of Scott (1981) that generated 3D Cartesian coordinates with the aid of a microprocessor. The use of marked points on human dental study models improved coordinate point accuracy (X ±0.06; Y ±0.08; Z ±0.10) (Takada *et al.,* 1983) and showed satisfactory intra-operator and inter-operator measurement reliability (Bhatia and Harrison, 1987; Richmond, 1987). For example, there were no significant differences (MD ± 0.50-0.20) between the linear measurements when comparing the following three methods, (i) Vernier Caliper, (ii) a Reflex Metrograph (Butcher and Stephens, 1981) and (iii) Reflex Holograms (Benatar *et al.,* 1989). Although the Reflex Metrograph was reported to be quicker, simpler and more accurate than the previously discussed methods (Takada *et al.,* 1983) it did not provide sufficient precision, reliability or flexibility (Rossouw *et al.,* 1993) and was superseded by other indirect methods with a closer capacity to work at the small murine scale.

2.4.2.3. Travelling Microscope:

The travelling microscope, a binocular microscope fitted onto a movable carriage, was first used to investigate murine dental characteristics by Bader (1965). It was later used to measure 3D linear measurements on dental study models with a high Z-coordinate resolution of 1.0μm and a good measurement repeatability (±2.0-3.0μm) (Bhatia and Harrison, 1986). Low measurement errors of marked (±0.067mm) and unmarked (±0.22mm) anatomical landmarks were smaller than those of the Reflex Metrograph (Takada *et al.,* 1983) and were almost 10 magnitudes smaller on marked casts (Bhatia and Harrison, 1986). The high Z-coordinate resolution of the microscope improved accuracy over the previous direct and indirect optical methods discussed. The mechanised horizontal and vertical movement also enabled good practicality and utility, offering a more automated process with considerable development potential.

2.4.2.4. Measuring Microscope:

The Measuring Microscope was first used to measure bucco-lingual diameters of murine molars with a resolution of 10.0μm (Grünberg, 1951). It defined morphological landmarks on dental casts with a high precision (1.0μm) and low positioning error (SE X ±0.02mm; Y ±0.02mm; Z ±0.03- 0.02mm) (Theilke *et al.,* 1998). The Measuring Microscope was used for investigating the cusps, grooves and pits of dental cast occlusal morphology but not for full 360° analysis. It showed potential for mechanised automation similar to that of the Travelling Microscope.

2.4.2.5. Moiré Contourography:

Moiré Contourography (Rowe and Welford, 1967) was first used in dentistry to obtain 3D occlusal surface data and measure individual tooth cusp morphology (Kanazawa *et al.,* 1984; Mayhall and Alvesalo, 1992). A light was projected through a master and a reference grating and the resulting contour lines on the tooth surface were captured originally in an analogue photograph (Kanazawa *et al.,* 1984) and latterly by a digital camera (Mayhall and Alvesalo, 1992).

The equipment resolution was determined by the width (or interval) of the light contours (0.2mm) (Kanazawa *et al.,* 1984). The later technique used a computer program to magnify the digital photographs for more precise (±0.02mm) on-screen measurement (Mayhall and Alvesalo, 1992). The measurement reliability was fair for the mesio-distal measurement (SD

±0.40mm) and bucco-lingual (SD ±0.68mm) measurement but the resolution was poor and the image analysis was limited to molar occlusal surfaces. The data collection time of 30 minutes for each tooth by experienced operators was prohibitively long (Mayhall and Kageyama 1997). A higher power light source and narrower width reference gratings would have reduced contour widths and increased the equipment resolution. The restricted range of measurements on the occlusal surface made this procedure of limited appeal when compared to modern indirect 3D optical methods.

2.4.2.6. Lasers in Dentistry:

The use of the indirect optical methods expanded in the dental literature as the prevalence of laser techniques escalated in the 1980s because of an increasingly competitive digitisation market that improved the commercial availability, affordability and awareness of laser devices (Rekow 2006). A variety of laser devices have found many specific applications in clinical (Keller and Hibst, 1993) and cosmetic dentistry (Mindermann *et al.,* 1993). They are most frequently employed in computer aided design (CAD) and computer aided manufacturing (CAM) applications in technical laboratories, wherein they automate the fabrication of prostheses and restorative implants through coordinate measuring machines (CMM) and 3D printer attachments (Duret *et al.,* 1988).

In the current context, the principal advantage of the CAD and CAM systems is that they are high throughput tools with high levels of automation. However, this has compromised resolution and versatility by design to speed up product development and standardise manufacturing quality respectively. Therefore, the specific design orientated operation does not give a high enough resolution or enough customisation potential for these systems to be suitable for the current purpose. Never the less, these methods have contributed to the momentum and technological foundation of the advancing 3D market and there are numerous other laser applications in dentistry that do require further consideration.

2.4.2.7. Laser Scanners:

The abundance of laser technologies on the commercial market has led to many dental research publications describing the use of 3D dental study models and on-screen computer measurements (Apuzzo, 2006). Invariably the laser scanner based optical devices use the geometric principal of triangulation to collect 3D point cloud data that is used for surface digitisation or 3D model reconstruction (Figure 2.).

Figure 2. 3D Model Reconstruction

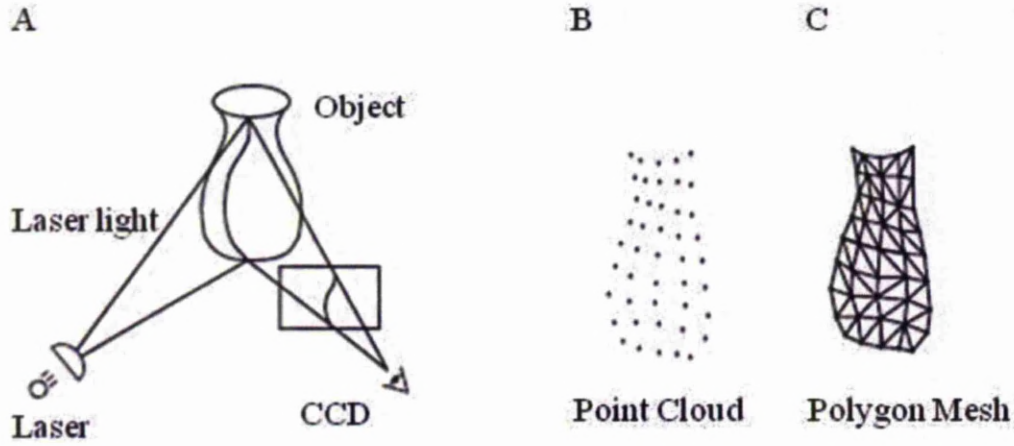

(A) image acquisition by laser light projection and Charged Coupled Device (CCD) sensor (B) rudimentary point cloud data; (C) post-imaging computational processing to generate reconstructed triangular polygon mesh.

3D computer software renders virtual models of objects to provide a more comprehensive morphological quantification than was previously achievable by any of the 2D tools. Comparing the new 3D techniques with the previously described 2D methods typically reported a more detailed surface representation than was previously described because of the high density of point cloud information, e.g. on dental casts (Halazonetis 2001; Hajeer *et al.,* 2004). However, the resulting 3D models were dependent on the resolution of the individual scanners and the image processing parameters of the associated computer software (Curless and Levoy, 1996; Reich, 1998).

The term laser scanning has been applied across multiple disciplines, and was often used synonymously to describe both identical and different techniques. The following account of laser scanners, used for dental applications, adopts the native terms used by the authors. Although tautologies may exist, a complete review of the literature would otherwise not have been possible. The laser devices were separated into Slit Ray Laser Scanner, Laser Line Scanner, Stripe Laser Scanner and Laser Range Scanner. The following account may not be exhaustive but it is presented here in chronological order to represent the continuity of the laser technologies in dental applications.

2.4.2.8. Slit Ray Laser Scanner:

The slit-ray laser device was composed of a laser projector, a revolving mirror, two video cameras and a computer post-processing work-station (Kuroda *et al.,* 1996). The primary

advantage of this system was that it used a rotary table to move the dental cast in 360° while a stationary laser fan collected the point cloud data. The method reconstructed complete virtual 3D models in 40 minutes with low measurement error (< 0.05mm) (Kuroda *et al.,* 1996). There were no conventional dental measurements or statistical analysis presented but the introduction of a full 360° image acquisition system represented a noteworthy step towards a complete morphological assessment of human dental casts.

A similar technique using a stereo pair of video cameras reconstructed casts with a so called 'textured' illumination source (Ayoub *et al.,* 1997) that superimposed a conventional 2D digital image on to the 3D model surface. This approach was said to aid measurement landmark positioning and showed only small differences between the repeated manual measurements on dental study models (MD = 0.17 mm, SD = 0.08mm) and those obtained from the 3D virtual models (MD 0.06mm, SD 0.03mm) (Bell *et al.,* 2003).

Intra-operator measurement variation on the 3D casts (0.02–0.14mm) was suggested to be related to the positioning of landmark measurement points but was less than that observed when directly measuring the models with callipers (0.14–0.48mm) (Bell *et al.,* 2003). Therefore, the slit ray laser was of moderate accuracy and reproducibility but had errors associated with landmark positioning. There was no indication of economy or of the complete time taken for full cast image acquisition, analysis and measurement so some questions remained unanswered. Moreover, there were various problems associated with incomplete data sets or holes in the virtual 3D models.

One approach to improving 3D data collection was to use multiple images from multiple views (multi-view images) that were combined using advances in post-processing computer imaging software (Motohashi and Kuroda, 1999). Projected measurements between landmarks, that were equivalent to the mesio-distal calliper measurement and 2D methods, could now be attained in 3D and were comparable on the virtual and actual study models (MD ±0.02mm) (Motohashi and Kuroda, 1999).

Good resolution (0.01mm) and good precision (±0.05mm) was demonstrated (Hayashi *et al.,* 2003) but did not indicate any major advances in the time period between publications. This suggested an upper limit to the Slit Ray Laser technique. A more rigorous reliability study for a morphometric investigation would be expected to have examined more variables, included

a greater sample of models, and would have been strengthened by reproducibility of multiple independent operators. Nevertheless, important capabilities such as range of measurements, measurement precision and reliability had improved.

Importantly, two significant method improvements were represented here; (i) the combination of multi-view images by a rotary table system (Kuroda *et al.,* 1996) and (ii) the advances in image combination software (Motohashi and Kuroda, 1999).

2.4.2.9. Laser Line Scanner:

A laser line scanner (VIVID 700, Minolta, Osaka, Japan) improved on the speed of earlier multi-view methods by collecting four separate images quickly (25 minutes) using a goniometer to reposition the dental casts (Sohmura *et al.,* 2000). Digital callipers measurements taken on 10 actual casts and virtual on-screen measurements taken on 10 3D models showed good coordinate point accuracy (SD ±0.015mm) and a high measurement correlation (R^2 0.9854) (Sohmura *et al.,* 2000). The Cubesper laser line scanner (Topcon Inc., Tokyo, Japan) was less precise (MD >0.3mm) (Hirogaki *et al.,* 2001). The low resolution of the VIVID 700 (0.4mm) provided gross morphological images that were not good enough to reproduce detailed occlusal surface structure, e.g. hypoplastic lesions or fissures.

The goniometer contributed to a good overall operating speed and was a simple and effective method of collecting multi-view data. However, its fixed tilt angle (±30°) and 90 ° interval positioning was restrictive and the 3D reconstructed models contained surfaces with incomplete data sets or holes, particularly around areas of undercut. The previously described rotary table (Kuroda *et al.,* 1996) was considered to be the superior positioning tool (Sohmura *et al.,* 2000). The computer algorithm used to combine the multi-view images was a substantial software improvement but there was no indication of how the image combination errors (X ±0.08mm; Y ±0.35mm) were derived.

2.4.2.10. Stripe Laser Scanner:

A stripe laser scanner (VIVID 900, Minolta, Osaka, Japan) with a moderate resolution (0.18mm) (Sohmura *et al.,* 2004a) was higher than the two similar models that were previously described as laser line scanners VIVID 700 (Sohmura *et al.,* 2000) and Cubesper (0.25mm) (Hirogaki *et al.,* 2001). The stripe laser scanner linear measurements error (MD ±0.3mm) was reasonable compared to the other model VIVID 700 (MD ±0.2mm) (Sohmura

et al., 2000) but the multi-view image combination errors of both instruments were too large for dental casts (Sohmura *et al.,* 2004a) and would entirely prohibit any accurate investigation of a small mouse tooth subject.

2.4.2.11. Laser Range Scanner:

A laser range scanner with a moderate resolution (0.1mm) combined multi-view images using a fiducial marker with a small average error (±0.08mm) and standard deviation (±0.04mm) (Goshtasby *et al.,* 1997). This procedure involved subjective operator input during the placement of markers and the mathematical calibration was reported to be difficult and time consuming (Goshtasby *et al.,* 1997). The resolution of this method did not improve the morphological analysis beyond other comparable methods that were simply used for digitising models for archiving and display purposes (Apuzzo *et al.,* 2006).

A laser range scanner method with a moderate resolution (X 0.15-1.00mm; Y 0.30mm; Z 0.05-0.20mm) independently analysed teeth sectioned from 3D models and was able to export these images in various file formats (Kondo *et al.,* 2004). However, there were no considerable advantages to this technique over other 3D laser techniques (Chuah *et al.,* 2001) and the inadequate resolution and absence of other method assessment criteria, e.g. measurement details and reliability, made the technique unsuitable for the murine application.

The various laser methods described and presented so far represent a single technology. The methods projected a variety of laser light patterns (line, stripe, slit ray and range) onto the surface of dental casts and may be collectively referred to as the structured light methods (Figure 3.).

Figure 3. 3D Structured Light Methods

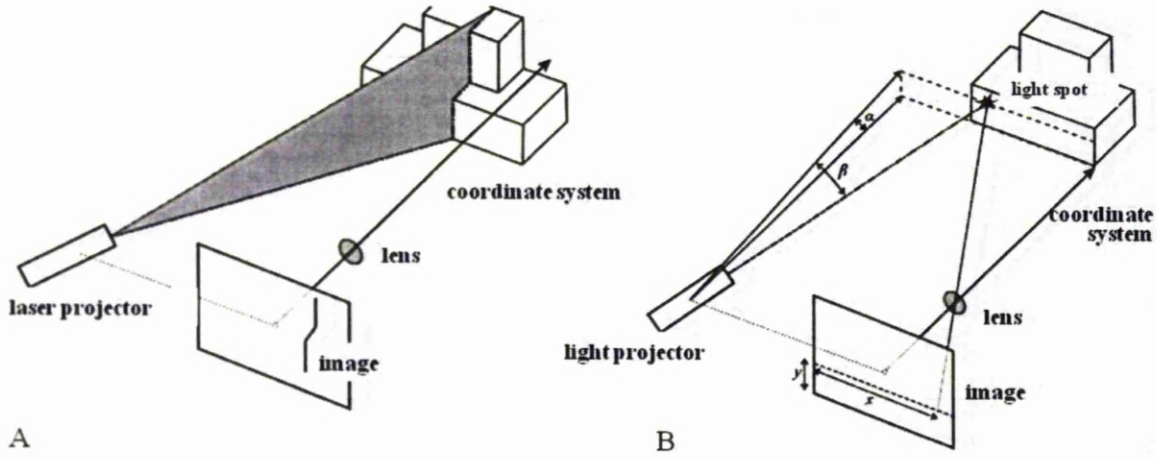

(A) a continuous light stripe (or fan) swept the object; (C) a light spot laser projection or single point laser. The object was either stationary, while the projected light scanned the object, or the object was moved as the light remained stationary. Both obtained 3D data using the optical principal of triangulation. Image modified from Halazonetis (2001).

2.4.2.12. Commercial Digitisation:

Commercial digitisation methods became increasingly versatile and included both *in-vitro* systems (OrthoCAD, Cadent, New Jersey, USA) and *in-vivo* systems (e-Models, GeoDigm Corp, Minnesota, USA) with sophisticated measurement tools well targeted to clinical dental practices (Hajeer *et al.* 2004; Joffe, 2004). Classical Vernier callipers were compared with three computerised methods; (i) QuickCeph 3D digital models with on-screen measurements (Quick Ceph SystemsInc., California, USA), (ii) OrthoCAD 3D digital models with on-screen measurements, and (iii) the Hamilton Arch Tooth System (HATS) digital callipers (Tomassetti *et al.,* 2001). The QuickCeph (MD ±1.84 mm; PCC 0.432), HATS (mean difference = 0.99mm, PCC 0.885) and OrthoCAD (MD ±1.20 mm; PCC 0.715) methods compared well with the Vernier callipers that were the most repeatable (MD ±0.77mm; PCC 0.934). The QuickCeph method was the fastest but had the lowest measurement correlation, followed in order of decreasing speed by the HATS, OrthoCAD and the Vernier callipers methods (Othman and Harradine, 2006). The compromise between measurement speed and precision was consistent with their respective levels of automation. The anatomical landmarks were difficult to distinguish with the two commercial digitisation systems (OrthoCAD and QuickCeph) (Tomassetti *et al.,* 2001). This reinforces the proposition that the greatest source of random error is caused by difficulties identifying and defining

anatomical landmarks (Houston, 1986). Therefore, the classical 2D hand measurements here proved to be more accurate, reliable and faster to operate when considering the overall setup time and dependence on computing facilities.

The OrthoCAD system was later evaluated against the Boley gauge by two examiners with good inter-operator measurement reproducibility (PCC <0.001) (Santoro *et al.,* 2003). On the other hand, the measurements were smaller on the 3D model than the actual model suggesting systematic error that was believed to have been caused by a combination of alginate shrinkage during transportation to the OrthoCAD location, differences in operator training and abilities, and the effect of operator preferences for measuring on a computer screen (Santoro *et al.,* 2003; Quimby *et al.,* 2004). The validity, reproducibility, efficacy and effectiveness of the OrthoCAD method was also tested against digital callipers by one examiner measuring 10 standard models, two examiners measuring 50 models and 10 operators measuring 10 models (Quimby *et al.,* 2004). The two measurements methods were equally accurate, reliable and clinically acceptable with excellent reproducibility (ICC >0.90), according to Donner and Eliasziw (1987). The 3D measurement method was superior to the Boley Gauge method (Santoro *et al.,* 2003) despite the ambiguous sources of error and variance ascribed to alginate shrinkage and operator subjectivity (Quimby *et al.,* 2004).

A Peer Assessment Rating (PAR) index score of intra-operator measurements on plaster models with digital callipers (ICC 0.98) and on 3D OrthoCAD models with onscreen measurement (ICC = 0.96) showed excellent reliability (Zilberman *et al.,* 2003; Mayers *et al.,* 2005) with no clinically significant differences between the two methods (Stevens *et al.,* 2006). Therefore, the accuracy of these commercial 3D methods was clinically acceptable but was not as suitable for scientific work as digital callipers (Lin *et al.,* 1998; Tomassetti *et al.,* 2001; Santoro *et al.,* 2003; Quimby *et al.,* 2004; Mayers *et al.,* 2005; Othman and Harradine, 2006).

2.4.2.13. Non-Contact Surface Profilometry:

The non-contact surface profilometer (NCSP) has been used to describe a number of single point methods that employed laser triangulation (Lee and Chang, 2005; Apuzzo, 2006) and chromatic confocal sensors (Chen *et al.,* 2000; Higham *et al.,* 2009). In dentistry, the technology has been employed to investigate dental biomaterials (Zhang *et al.,* 2000; Chrzanowski *et al.,* 2008), and enamel erosion and abrasion (Barbour *et al.,* 2006; Ablal *et*

al., 2009; Elton *et al.,* 2009). In both cases images were acquired from a single laser point or laser spot projected onto and reflected from a tooth surface using different optical principals and technologies (Chen *et al.,* 2000; Apuzzo, 2006; Higham *et al.,* 2009). The term laser was only correctly applied to the laser triangulation technique because the chromatic confocal sensor technique used polychromatic (white) light.

Single point laser methods overcame some of the shortcomings of the laser scanning techniques for a small mammalian teeth application because they had a shorter working distance (180mm) and measuring range (45mm) (Lee and Chan, 2005). Typical close range single point lasers, e.g. *Scantech st600* (Scantech, Ringsted, Denmark) and *Callidus CT900* (Callidus, Halle, Germany), had a similar resolution (50μm) and accuracy (±0.1mm) but both these criteria decreased proportionally as the working distance from the tooth surface increased (100-400mm and 0-900mm respectively). On the other hand, the NCSP equipment was available in a modular setup so operators could design their own system to suit their application specifications (e.g. different chromatic confocal sensors). This was a major advantage that would benefit the current requirements for both macro-scopic morphological analysis and micro-scopic surface analysis.

The micro-metric performance of the NCSP resolved a huge variety of surfaces to create 3D micro-topological surface maps because the chromatic confocal sensor tolerated optical heterogeneity, surface colour and transparency differences and irregularities. The sensor was not influenced by variable reflectivity or ambient illumination and was appropriate for all types of dental materials - transparent/ opaque, specular/ diffuse and polished/ rough - including the transparent or semitransparent surface layers of the enamel and dentine. Also, it eliminated the light scattering/ specular reflection associated with incomplete data or holes from laser sources (Kuroda *et al.,* 1996; Motohashi and Kuroda, 1999; Sohmura *et al.,* 2000), it avoided beam spot reflection and stray light effects to provide more accuracy than the more widely used position sensitive detectors of single point lasers (Chen *et al.,* 2000; Lee and Chang, 2005).

The NCSP technique employs axial chromatism within the chromatic confocal optical sensor. When white light passes through a lens with a high degree of chromatic aberration this causes the different wavelengths to be focused at different positions in the Z coordinate measurement range, so that within a continuum of monochromatic diffraction limited planes,

only one part of the object is focused at any one position, thus introducing a new level of sub-micron accuracy (Tiziani and Uhde, 1994). As the reflected light passes through a beam splitter projected onto an optical pin hole it has a double or confocal filtering effect that excludes all out of focus wavelengths in much the same way as classical monochromatic confocal microscopes that eliminate light that is thicker than the focal plane (Carlsson and Alund, 1987). A spectrometer then deflects the different wavelengths by different amounts and the sensor detects, processes and converts these different signals into a precise depth discriminating distance measurement with a high (>1.0μm) Z-coordinate resolution. The Z-coordinate data then combines with the X and Y coordinate location of the precise (25 nm) CMM mechanically moveable stage to achieve a highly competitive overall systematic resolution of 1.0μm.

Also, the NCSP could be customised. Hardware modification can combine the X and Y coordinate automation of the travelling microscope (Bader, 1965; Bhatia and Harrison, 1987) and the high resolution of the measuring microscope (Gruenberg, 1951; Thielke *et al.,* 1998) with a rotary table for multi-view image acquisition (Kuroda *et al.,* 1996). An appropriately chosen chromatic optical sensor would provide a sufficiently high resolution and the versatile system would be sufficiently automated to suit the current application of investigating both the 360° macro-morphology and the enamel surface micro-structure of small murine teeth. Fabricating a rotary table to adapt the CMM stage to hold and move a mouse incisor (e.g. at defined intervals such as 360°/60° = 6 images) within a suitable measuring range would establish a central axis of rotation about which mathematical offsets or spatial adjustments could be made to register the multiple multi-view image files together. The growing 3D imaging software market may provide a suitable solution.

Therefore, a rotary stage modification would be multi-purpose, serving to; (i) facilitate tooth positioning within the measuring range, (ii) be the absolute reference in the local coordinate system, and (iii) be the central axis of rotation for combining multiple multi-view images into a single 3D model. The NCSP (including chromatic confocal sensor) represents a highly suitable method for the current study because of its high resolution, versatility, relatively economical adaptation cost (£25,000) and proven ability to interrogate enamel surface mineralisation. However, other competing methodologies needed consideration.

2.4.2.14. Computer Tomography (CT):

Computer Tomography (CT) is a digital imaging technique that involves the geometric reconstruction of a large series of high resolution 2D sections, taken about a single axis of rotation. The multiple cross-sections, or slices, are reconstructed by various computer software algorithms to generate a complete 3D image. The many applications of CT have had a globally important impact, e.g. Magnetic Resonance Imaging (MRI), Confocal Microscopy, Micro-Computed Tomography (μCT), Nano-Computed Tomography (nano-CT).

As CT resolves structures like bone it has become an attractive method for recording and measuring 3D morphological data, particularly as dental cast die stone study models have a high radio-density (Pirttiniemi *et al.,* 1999). Attempts to combine skeletal hard-tissue information from CT scans with other laser scanning dental information reported significant errors and difficulties (Nishii *et al.,* 1998; Terai *et al.,* 1999; Nakasima *et al.,* 2005). Conventional diagnostic multi-detector CT and multi-slice helical CT scanners combine multi-slice images less than 1.0mm in thickness (Fuchs *et al.,* 2000; Khambay *et al.,* 2002), and a medical X-ray CT technique can complete scans of dental casts in a few seconds and reconstruct 3D models within 10 minutes (Sohumura *et al.,* 2004b). This represents a useful reduction in scan time, e.g. when compared to the laser line scanner (25 minutes) (Sohumura *et al.,* 2000), the stripe laser scanner (40 minutes) (Hirogaki *et al.,* 2001) and the other laser devices (Kuroda *et al.,* 1996; Goshtasby *et al.,* 1997; Motohashi and Kuroda, 1999; Bell *et al.,* 2003; Kondo *et al.,* 2004).

The introduction of industrial specification CT scanners with a serial reconstruction slice thickness of 10μm have demonstrated the power of this method to visualise and analyse biological specimens that were once considered too small to image with medical diagnostic machines (Rowe *et al.,* 2001). The anatomical investigation of small mammals using high resolution X-ray CT has dramatically improved the quality and quantity of 3D information available (http://digimorph.org/index.phtml) (Rowe *et al.,* 2001) and has been used to visualise the 3D morphology of teeth, measure enamel and dentine distribution, thickness and volume (Gant *et al.,* 2001).

2.4.2.15. X-ray Micro-Tomography (XMT) and Micro-Computed Tomography (μCT):

X-ray micro-tomography (XMT) is a miniaturised version of CT or computed axial tomography (CAT) scanning (Elliot *et al.,* 1994). It amasses large amounts of information that can be represented as 2D or 3D images with a resolution of between 5-30μm (Anderson *et al.,* 1996). μCT resolves cross-sectional image pixel sizes in the micron range and has a potential threshold of detectability of small details 1–2μm in dimension (Higham *et al.,* 2009). In XMT, unlike μCT, the specimen is rotated not the X-ray source and detector, so that a series of X-ray projections recorded at a number of angles around the specimen give a 360° radioscopic image (Davis and Wong, 1996). The 2D data projections are obtained in a single plane using an X-ray intensifier and the resulting images are used to reconstruct a 3D model.

The early XMT attenuation images were limited to 40 μm and did not discriminate sufficiently between the mineralised dental tissues (Tachibana and Matsumoto, 1990) but the method has since been useful in the study of mineral concentrations (Anderson *et al.,* 1996; Davis and Wong, 1996) and in remineralisation and demineralisation studies (Anderson *et al.,* 1998; Anderson *et al.,* 2004; Dowker *et al.,* 2003; Fearne *et al.,* 2004). XMT has also been used to illustrate enamel and dentine distribution, thickness and mineral concentrations in mouse incisors (Wong *et al.,* 1995; Wong *et al.,* 2000) and molars (Lazzari *et al.,* 2009). Recent advances in μCT have used high intensity synchrotron sources to improve image resolution (1–30 μm), e.g. SkyScan-1072 (SkyScan, Antwerpen, Belgium) (Wazen *et al.,* 2009) and a μCT system (IMTEK Inc, Knoxville, TN) (Tsutsui *et al.,* 2008).

Kim *et al.,* (2007) evaluated the accuracy of measurements taken on (i) twelve extracted teeth using digital callipers (Mitutoyo Corp., Japan; accuracy ± 0.02mm) that were used as a reference and compared to (ii) calibrated 2D digital photographs with Image-J 1.27z software (National Institutes of Health, USA), (iii) noncontact 3D optical scanner Topometric 3D-Sensor optoTOP (resolution 2μm, accuracy 6-15μm) (Breukmann GmbH, Germany), with RapidForm 2002 software (INUS Technology Inc., Korea), and (v) a desktop μCT scanner SkyScan-1072 (detail detectability of 3μm and a resolution of 8μm) (Skyscan, Antwerpen, Belgium) measured using V-works software (CyberMed, Inc., Korea). All the distance measurements from the four methods were highly correlated (PCC, $p < 0.01$). The 3D optical scanner was in very close agreement with the calliper measurements but the measurement on

the 2D digital photographs were significantly ($p < 0.01$) overestimated when compared to other methods (Kim *et al.,* 2007). Volume measurements from the μCT were significantly ($p < 0.01$) underestimated compared to the 3D optical scanner (Mean Standard Deviation of the difference -50.40 ± 22.78, (Kim *et al.,* 2007). The overestimation and underestimation was attributed to a number of non-standardised systematic errors described by the authors, e.g. differences in magnification and calibration, which highlighted the central importance of reliability testing and method validation of new imaging techniques. The ability to measure the volume of each portion of a tooth with a density by the XMT and μCT methods was an advantage but appropriate thresholds must be defined to distinguish between the various tissues and structures from the surrounding materials/ tissues (Kim *et al.,* 2007). The XMT and μCT methods were undoubtedly powerful but meaningful morphological measurement using this new tool still requires considerable refinement.

2.4.2.16. Nano- Computed Tomography (Nano-CT):

Nano-CT, like μCT, uses X-rays to non-destructively image slices or cross-sections of a 3D object for reconstruction into a 3D virtual model. The term nano indicates that the pixel sizes of the cross-sections are in the nanometer range. A high-resolution (200–300nm) SkyScan-2011 nano-CT (Skyscan, Antwerpen, Belgium) was used to examine the internal morphology of dentin and resolve its porous sub-structure (Parkinson and Sasov, 2008). Nano-CT has also been used for accurate enamel mineral density and thickness determination (Myers *et al.,* 2009). In this case, a TMR sectioned (100μm) murine incisor was used as a reference or 'standard' for the enamel mineral density measurement and was then re-assembled using cyanoacrylate and scanned using nano-CT. Ten nano-CT slices (10 μm) were reconstructed into 100μm sections for analysis using SkyScan software (Myers *et al.,* 2009). The nano-CT and TMR data exactly matched demonstrating that nano-CT can provide a quantitative, rapid and non-destructive method for the determination of enamel mineral density on a continuous 3D basis. A few commercially available systems exist at present but the technology is prohibitively expensive and shows only marginal benefits over μCT. Nonetheless, as accessibility of this powerful new technique improves it will gradually be compared more and more with existing techniques and is likely to be highly competitive.

2.4.2.17. Magnetic Resonance Imaging (MRI):

Magnetic Resonance Imaging (MRI) is a non-invasive method that renders tomographic images to demonstrate the biochemical, physiological and/ or pathological conditions of

organs and other internal structures. It is most frequently used for medical diagnosis and has diversified into numerous specialised forms, e.g. *diffusion* MRI, *functional* MRI, *interventional* MRI and *experimental* MRI. MRI uses non-ionising radio frequency signals and does not expose patients to harmful radiation. It is best suited to non-calcified tissues because of their low radio density, but a contrast-enhanced dental MRI technique that used intra-oral disclosing medium was able 3D visualise the mandible and teeth in the oral cavity (Olt and Jakob, 2004). It was a feasible alternative to other X-ray based imaging, such as conventional radiography and CT, because of its high resolution (0.6mm x 0.6mm x 0.8mm) and very fast scan times (2 minutes for a full cast) (Olt and Jakob, 2004).

However, CT scanners make better tools for examining bone and calcified tissues such as enamel and dentine. Both CT and MRI generate multiple 2D cross-sectional images of tissues to build 3D reconstructions but because MRI is capable of superior image contrast, by varying a number of scanning parameters, it can enhance and alter tissue contrast to detect different features and readily discriminate soft tissues. Therefore, MRI is intended for *in-vivo* imaging and would not be a practical reality for the current small murine dental application. CT is more widely available, more economical, and more convenient than MRI but both methods are very expensive (> £1,000,000) compared to the previously described techniques.

2.4.2.18. Scanning and Transmission Electron Microscopy:

Scanning Electron Microscopy (SEM) is capable of imaging fine morphological detail at tens of thousands of times higher resolution (1-5nmn) than light microscopes. SEM magnification can be controlled between 10 and 500,000 times and is capable of relating the microanatomy and surface morphology of a wide variety of samples. SEM typically yields images with a characteristic 3D appearance that would be useful for examining the tooth morphology and surface structure of teeth but 3D measurements cannot be made directly (although some dimensions may be determined by stereo-photogrammetry). Transmission Electron Microscopy (TEM) is a related technique that forms another chief image analysis method which is applied in a range of scientific, biological and medical fields. TEM and SEM are microscopic techniques rather than macroscopic techniques and as such are more often than not used for histological investigations of internal tissues *in-vitro*. SEM and TEM samples require chemical preparation before imaging, which makes them both relatively time consuming and expensive processes with a low throughput. The SEM and TEM techniques

are very powerful, particularly as TEM can be combined with 3D representation using CT methods, but the cost of the equipment is expensive (> £100,000).

2.4.2.19. Confocal Microscopy:

The use of the confocal microscope has been instrumental in progressing both the micro- and macro-relief (Jernvall and Selaenne, 1999) inspection of small mammalian tooth morphology, e.g. a laser scanning confocal microscope (LeicaTCS NT, Leica Ltd, Sydney, Australia) was used to image fluorescently stained urethane casts of bat teeth (Evans *et al.,* 2001). The topographical and shaded relief maps reconstruct the tooth surface topology from optical sections either by reflection or by fluorescence imaging. The laser point source mapped the surface topography of the cast at high resolution (X = ±35μm, Y = ±10μm, Z = number of pixels 128 x 128 or 256 x 256, or sampling interval between stacks) with rapid scan times but the large amount of data made substantial demands on computer processing power and increased image processing time. Moreover, the method imaged a cast rather than the actual dentition and because of optical heterogeneity (caused by loss of signal intensity and signal degradation) accurate models were not possible (Evans *et al.,* 2001). The chromatic optics of the NCSP method does not have this problem.

The laser scanning confocal microscope was effective because of the combined single point laser source and confocal optics. However, the optical sectioning technique would more be more appropriately used to represent the internal micro-structure of tissues, cells and organelles (similar to SEM and TEM) and would not be suitable for the current investigation.

2.4.2.20. Combined Methods:

Much of the direct and indirect methods, except CT and MRI, have been limited to the erupted tooth crown. Using a combination of methods (e.g. laser scanned occlusal surface images and radiographic root structure images) it was possible to explore the whole tooth and obtain previously inaccessible information (Nishii *et al.,* 1998). Other combined approaches have reconstructed images from different methods by using a generic example of a tooth and best fit landmark registration (Enciso *et al.,* 2003) or the individual occlusal surface morphology and different algorithms (Buchaillard *et al.,* 2007). The benefit of these combined approaches was that they exploited all clinical information available for a given tooth, which may be advantageous for patient specific dentistry, but there were no overall

timings given for image acquisition or of individual procedures, only the computer processing was reported to be fast.

If μCT and 3D laser scanning data is to be accumulated and properly correlated in the future it might be possible to predict the internal structures of teeth from the 3D surface (Kim *et al.*, 2007). However, further hardware and software developments would be necessary for this to become a reality. Nevertheless, once the various CT methods become more widely available and financially accessible their part in a combined approach would be very attractive, especially in an increasingly collaborative multi-disciplinary clinical research field.

2.5. COLOUR AND WHITENESS ASSESSMENT

2.5.1. Tooth Colour and Whiteness Variation

There is a wide range of tooth colour variation in the population. Enamel and dentine defects dramatically affect observable tooth colour and whiteness, e.g. *Amelogenesis imperfecta* exhibits discolouration varying from cream and yellow opacities to brown and black colours (Brook *et al.,* 2007). Natural variation occurs within and between regions of the same tooth, from tooth to tooth, and is influenced by extrinsic colourations or environmental factors (Brook *et al.,* 2007). These extrinsic factors can be minimised or excluded in congenic animal populations by the uniform conditions of animal husbandry.

In humans, colour changes caused by developmental defects of enamel are included in the subjectively assessed indices (i) the Federation Dentaire Internationale (FDI) Developmental Defects of Dental Enamel Index and/ or (ii) Epidemiological Index of Developmental Defects of Dental Enamel (FDI, 1992; Brook *et al.,* 2001; Elcock *et al.,* 2006; Smith *et al.,* 2009a). Currently no measurement methods of murine tooth colour and whiteness exist. The human clinical indices may not be directly translated for the assessment of murine dental anomalies but their qualitative terminology can be used to initially identify defects (opacities, hypoplasias and discoloured enamel) and record them on the Mouse Dental Anomalies Database Record Form.

2.5.2. Colour Distribution

In humans, incisor colour distribution is typically assessed in three anatomical thirds - cervical (or gingival), middle and incisal - of which the middle third is the most representative portion in terms of colour and whiteness (Brook *et al.,* 2007). In mice, incisor enamel is distributed asymmetrically along the labial surface, reaching further in the buccal direction than the lingual direction (Hay, 1961; Moinchen *et al.,* 1996). The normal colour distribution of a wild-type mouse incisor is opaque white with yellow/ orange/ brown pigmentation at the distal-tip being consistent with the presence of dentin and iron pigments as the major colour constituents (Halse, 1972). The translucent whiteness fades in a proximal direction through horizontal bands into more opaque white. The un-erupted part of the incisor

(within the hemi-mandible) becomes progressively red/ brown towards the apical end where there is no enamel.

Enamel mineralisation in the rodent mandibular incisor has been divided into three histological stages of enamel formation or amelogenesis; (i) *pre-secretory*, (ii) *secretory* and (iii) *maturation* (Smith and Warshawsky, 1975, 1976). Five developmental stages were identified in the appearance of enamel as: (i) soft translucent, (ii) soft cracked, (iii) white opaque, (iv) hard translucent and (v) yellow/ brown pigmented (Robinson *et al.,* 1983). These colour changes related to the chemistry and histology of the enamel organ (Robinson *et al.,* 1981a, 1981b) where, from the proximal-end to the distal-tip, Ca and P increased (Hiller *et al.,* 1975), as did enamel and dentine mineral concentrations (Wong *et al.,* 1995). The rat mandibular incisor was sampled in three stages of amelogenesis (*pre-secretory*, secretory and *maturation*) using external reference points on the molars as landmarks for strip dissection (Smith and Nanci, 1989). Also, enamel mineralisation was separated into primary and secondary stages corresponding to pre-secretory/ secretory and maturation stages of development respectively (Allan *et al.,* 1967 *loc cit* Wong *et al.,* 2000). Most recently, using a backscatter SEM method, the developing mouse mandibular incisor was imaged along the labial surface in three enamel surface regions; (i) apical (secretory), (ii) middle (nearly mature) and (iii) incisal (erupted) (Smith *et al.,* 2009c).

These techniques were applied to extracted murine teeth and could not be used to image the human condition *in vivo*. As colour distribution is typically assessed in three anatomical thirds (or regions) in human incisors, and because these regions have a relationship to the apparent *pre-secretory*, *secretory* and *mature* histological stages of enamel formation in the hypsledont (continuously growing) murine incisor, they may be representatively applied to assess the enamel surface colour and whiteness assessment in three developmental stages of enamel formation.

2.5.3. Colour Space

A number of standardised colour scales have been developed to objectively model colour (Wright, 1928; Guild, 1931), e.g. the Commission Internationale de l' E'clairage (CIE) have mathematically defined colour space (L = *Lightness*, A = *green/ red*, B = *yellow/ blue*) and whiteness (WI = *whiteness*) in terms that represented the human perception of colour (CIE,

1986). Human teeth show a significant contribution of the B *yellow* component (Joiner *et al.,* 2008). The CIE LAB and WI model expressed variation in colour and whiteness in clinically significant units (Jarad *et al.,* 2005) and served as a device independent reference capable of making accurate colour balance corrections (Smith *et al.,* 2008a). To date, murine teeth have not been described using any such measure.

2.5.4. Methods of Assessing Tooth Colour and Whiteness

The predominant methods used to assess human tooth colour and whiteness range from shade guides to instrumental methods such as spectrophotometers, colourimeters and digital image analysis systems.

2.5.4.1. Shade Guides:

Shade guides depend largely on operator judgment. They are inherently subjective (Okubo *et al.,* 1998; Lath *et al.,* 2007a), lack consistency and reliability (Khurana *et al.,* 2007). They are most frequently used for prosthetic/ prosthodontic shade matching. Increasingly available digital spectrophotometery based shade guide devices are more consistent (Paul *et al.,* 2002; Hammad *et al.,* 2003) and accurate (Jarad *et al,* 2005; Lath *et al.,* 2007b) but have similar disadvantages, e.g. unnatural colour shades, systematic errors and an incompatibility with the CIE colour space model (Joiner, 2004; Wee *et al.,* 2006).

2.5.4.2. Spectrophotometers:

Spectrophotometers measure tooth colour reflectance or transmittance (Paul *et al.,* 2002). They have been used in clinical and research settings for many years (Macantee and Lakowski, 1981; Goodkind and Schwabacher, 1987). Three commercially available instruments were evaluated by Khurana *et al.,* (2007); (i) the Spectroshade Micro showed good agreement between repeats and the highest proportion (87%) of complete agreement when compared to (ii) Vita Easyshade (59.7%), a spot measurement spectrophotometer, and (iii) an X-Rite ShadeVision (50%) colorimeter. The spectrophotometers showed reliable results (kappa value = 0.8) and compatibility with the CIE colour space model (Khurana *et al.,* 2007) but their widespread clinical and research use has been slow because of complexity, impracticality and expense (Joiner, 2004; Guan *et al.,* 2005; Lath *et al.,* 2007a, 2007b). However, a non-contact digital matching method has shown less operator variation

(61.1% correct) and reasonable CIE LAB correlations compared to the Vita Lumin shade matching tabs (43% correct) (Jarad *et al.,* 2005).

The methods required contact or were designed for use on the flat surfaces of human incisors. This would make measurements on small murine incisors difficult and impractical.

2.5.4.3. Colourimeters:

Colourimeters filter colour to approximate a standard observer's eye and generally measure colour in tristimulus terms or CIE LAB values (Joiner, 2004). Comparing colourimeters and spectrophotometers, colourimeters were deemed to give acceptable colour measurement differences (van der Burgt *et al.,* 1990; ten Bosch and Coops; 1995) but there was little correlation with human observations (Douglas, 1997; Watts and Addy, 2001). Also, a number of systematic errors were reported to limit reliability and precision (van der Burgt *et al.,* 1990; ten Bosch and Coops; 1995; Douglas, 1997; Wee *et al.,* 2006).

2.4.5.4. 2D Digital Image Analysis:

In recent years computer based digital image analysis has been the most successful approach to measuring human tooth colour and whiteness (Brook *et al.,* 2007). The system has evaluated tooth surface colour and whiteness objectively both *in-vivo* and *in-vitro* with a high degree of multiple operator reliability (Smith *et al.,* 2008a) under standardised conditions of illumination, orientation and magnification (Brook *et al.,* 2005a). Similar systems have also shown highly reliable results when modified for monitoring the effects of bleaching (Garcia-Goody *et al.,* 2004), assessing gingival inflammation (Smith *et al.,* 2008b) and quantifying dental plaque (Smith *et al.,* 2001, 2004; Smith *et al.,* 2006). During validation, the digital image analysis systems have shown high method correlation and compared favourably with colourimeters (Joiner, 2004), spectrophotometers (Guan *et al.,* 2005; Lath *et al.,* 2007a) and shade guides (Lath *et al.,* 2007b).

The advantages of digital image analysis include minimised subjectivity, high accuracy and reliability. Also, the system provided a permanent database of images and was quick and simple to use without being restricted to experienced operators (Wee *et al.,* 2006). Compared to the alternatives digital image analysis was more economical, practical and more widely available in dentistry (Jarad *et al.,* 2005). Importantly, the system could be made to be suitable for assessing small curved murine teeth as it has been successfully standardised for

CIE (Jarad *et al.,* 2005) and it has demonstrated versatility and flexibility with potential for customised modification (Brook *et al.,* 2005a; Guan *et al.,* 2005; Smith *et al.,* 2008a).

2.6. DENTAL DEVELOPMENT

2.6.1. The Murine Model System

Mus musculus is the most widely used experimental animal for human disease (Qui, 2006). The mouse is the mammalian model of choice because it is amenable and easy to keep, has non-specific inexpensive nutritional requirements, breeds all year round (with a short life span and generation time) and has large stocks of progenies (Guénet and Bonhomme, 2004). Mice and humans have almost the same genome size and share a number of gene sequence homologies and evolutionary conserved orthologue genes (Waterstone *et al.,* 2002). The majority of global gene banks are derived from studies on mice and they are available on public databases (www.ncbi.nlm.nih.gov/genome/guide/mouse/) making mice the most valuable experimental model organism. Mice overcome a number limitations of human subjects, and several other model organisms (Loew and Cohen, 2002), for example; (i) numerous inbred strains are available with different phenotypes, (ii) heterozygous genetic backgrounds are available, (iii) mice can be maintained under strictly controlled environments to minimise environmental influences, (iv) mice can be crossed to generate congenic animals to isolate the genes relevant to the phenotype under study, and (v) the ability to test gene function by gene targeted mutagenesis approaches.

ENU mutagenesis induces 1000-fold more random point mutations than naturally occur. ENU is the most effective mutagen as most human genetic diseases are caused by partial loss of the gene function due to point mutations (Seedorf *et al.,* 2004). Rodentia is therefore the only mammalian order within which it is possible to employ both the phenotype to genotype (phenotype-driven) and the genotype to phenotype (gene-driven) approaches that are essential to understanding the heterogeneity and complexity of the phenotypes of many human diseases (Masuyama *et al.,* 2005).

The similar processes of human and mouse odontogenesis make the mouse the most suitable experimental model for human dental disease (Fleischmannova *et al.,* 2008) and the amenable non-essential nature of teeth is convenient for studying organogenesis (Pipsa and Thesleff, 2003; Tucker and Sharpe, 2004). All teeth are composed of diverse tissue types involved in both tooth morphogenesis (Fukumoto and Yamada, 2005) and mineralisation (Veis, 2005). In particular, the mouse incisor exhibits all stages of development at any one

time making it ideal for studying the several distinct stages of enamel formation along the tooth axis (Smith and Warshawsky, 1976; Leblond and Warshawsky, 1979; Smith and Nanci, 1989; Sato *et al.,* 1996). Also, functional data from gene targeting shows tooth morphogenesis and skeletal morphogenesis share many key genes (Smith and Coates, 2000; McCollum and Sharpe, 2001a).

2.6.1.1. Dental Patterns:

The mineralised hard parts of teeth are well preserved in the vertebrate fossil record so dental records have long been used to infer the phylogeny of species (Luckett and Hartenberger, 1985). This data is increasingly supported by molecular methods (Frye and Hedges 1995; Boursot, 1996; Salazar-Ciudad *et al.,* 2002) but the evolutionary origin of teeth debate remains current (Reif, 1982; Weiss *et al.,* 1998; Smith and Coates, 2000; Holland and Chen, 2001). A dual origin of heterodont teeth, from both external denticles and internal pharyngeal teeth is now thought to account for the necessary flexibility required for the evolution of complex heterodont dentitions (Smith 2003; Smith and Johansen, 2003). The heterodont tooth types located anteriorly to posteriorly are incisiform, caniniform and molariform. Comparing human and mice dental formulas, humans have 20 primary (deciduous) and 32 secondary (permanent) teeth - incisors 2/2, canine 1/1, premolars 2/2, molars 3/3 - while mice have 16 teeth - incisor 1/1, canine 0/0, pre-molar 0/0, molars 3/3 - representing a less complex reduced dental pattern (Shellis and Berkovitz, 1981). The characteristic toothless diastema region between the incisors and molars and the absence of canine or premolar teeth make the mouse a simplified version for study (Addison and Appleton, 1915).

Although there are limitations, e.g. mice posses only one set of molars (monophylodont) that are not replaced, whereas humans have two generations of all tooth types (diphyodont) (Shellis and Berkovitz, 1981), both the mouse mandible and mouse incisor are proven to be excellent models for studying complex morphological development (Gaunt, 1964; Atchley *et al.,* 1985; Atchley and Hall, 1991; Bookstein, 1998). The mouse incisor is continuously growing and is especially useful for studying the dynamic process of odontogenesis (Tucker and Sharpe, 1999; Salazar-Ciudad *et al.,* 2003; Fleischmannova *et al.,* 2008).

2.6.1.2. Mouse Mandibles:

The mouse hemi-mandible was chosen because it was well studied both developmentally (Frommer, 1964; Hall, 1991; Ramesh and Bard, 2003), evolutionarily (Crompton, 1963;

Klingenberg, 2002) and functionally (Moore, 1973; Mao and Nah, 2004). Human and mice skeletal and dental morphogenesis share many key genes (McCollum and Sharpe, 2001b) and the genetic variability of mandible form has been well documented in man and mouse (Beamer, 1993; Bailey, 1985, 1986). The left and right hemi-maxilla and hemi-mandible incisor pairs each contain a single incisor and are joined at the mandibular symphysis. As representative units of development they can be separated into developmental modules by homologous landmarks useful for structural analysis (Atchley and Hall, 1991).

2.6.1.3. Mouse Incisors:

Human and mice incisors exhibit the same basic architecture with little fundamental difference between their basic structure and mode of formation (Tomes, 1850; Shellis and Berkovitz, 1981; Warshawsky *et al.,* 1981). In particular the mouse mandibular incisor gives a relatively high yield of enamel that is thicker than the maxillary incisors (Moinichen *et al.,* 1996) and is an important established experimental model of enamel morphology, biochemistry and molecular biology (Robinson *et al.,* 1981a, 1983). Its continuous growth and eruption has been attributed to stem cell populations in the cervical loop (Harada *et al.,* 1999; Wang *et al.,* 2007) and its constant length is proposed to be maintained by a balance of cell proliferation at the proximal-end and abrasion/ attrition at the distal-tip (Ohshima *et al.,* 2005; Krinke, 2004). Mandibular incisors are curved from the proximal-end to the distal-tip and run the entire length of the mandible (Hay, 1961; Shellis and Berkovitz, 1981). A slight narrowing at the distal-tip is the result of ameloblast cells depositing enamel asymmetrically and bilaterally on the labial surface (Amar *et al.,* 1986; Wang *et al.,* 2004). Enamel reaches further onto the labial surface in the buccal direction than in the lingual direction (Moinchen *et al.,* 1996). The lingual surface is covered with dentin and cementum, and is more flat than the curved buccal surface because of the adjacent position of each incisor within the hemi-mandible pair.

As a odontogenic model the mouse incisor can be longitudinally divided into labial crown and lingual root analogues (Amar *et al.,* 1986) and is comparable to other tooth types (and human teeth) in terms of its directional development (Ohshima *et al.,* 2005).

2.6.2. Developmental Models

In the 19th century, embryology tested evolutionary theories against observations of early tooth development, e.g. experiments on amphibia discovered the neural crest to be the source of mesenchymmal cells (Platt, 1893). In the 20th century, experimental embryology extended to the mouse model began to describe development in more causal terms (Mitisiadis and Smith, 2006); numerous early texts contributed to the understanding of dental patterning of the teeth and jaws in mice and men (Butler, 1939, 1956; 1995a; Wentworth-Thompson, 1942; Dahlberg, 1945; Gaunt, 1955, 1964; Crompton, 1963; Grünberg, 1951, 1963, 1965; Wolpert, 1969; Sofaer, 1975; Osborn, 1978; Atchely, 1985; Bailey, 1985).

2.6.2.1. Morphogenetic Fields:

The regional field theory proposed a gradient of external morphogens were responsible for the different sizes and shapes of mammalian teeth (Butler, 1939, 1956). It was suggested that the different tooth classes displayed local similarities because of the influence of graded positional differences within distinct morphogenetic fields. This was supported by grouping teeth into families according to their distinct morphology and location, and was applied to the human dentition (Dahlberg, 1945).

2.6.2.2. Clone Theory:

As developmental biology became increasingly based on genetics rather than physiology and anatomy a clone theory emerged (Osborn, 1971, 1978). The theory suggested that teeth developed from a single clone of pre-programmed mesenchymal cells, each capable of giving rise to the different tooth types. However, the intrinsic autonomous control mechanisms of the clone model did not explain how regional tooth shape differences were achieved or how the dentition developed as a whole (Townsend *et al.,* 2009).

Studies that investigated the inductive relationships between epithelium and mesenchyme cells began to generate a greater understanding of the important role of embryonic germ layers and molecular signaling during odontogenesis (Lumsden, 1988). Attempts were made to reconcile the prevailing theories by proposing a dynamic self organising theory based on the modular organisation and expression patterns of regulatory molecules within specific embryonic domains (Maas and Bei *et al.,* 1997; Weiss *et al.,* 1998). Successive theories combined those of their predecessors to purport that initiation of dental development may

occur according to the morphogenetic field model and that tooth germ formation may occur according to the clone model (Smith and Coates, 2000). The concept of a molecular morphogenetic field should not be limited to the expression of a single gene or its protein product but must consider how the various genetic and epigenetic influences modulate their affect on dental development (Line, 2001, 2003).

2.6.2.3. Molecular Model:

Much recent progress has come from identifying potential mechanisms at the genetic level to invoke the roles of homeobox genes, transcription factors and the expression patterns of various other vital signalling molecules (Pipsa and Thesleff, 2003; Tucker and Sharpe, 2004; Mitsiadis and Smith, 2006).

Important observations of the distinct spatial expression of homeobox genes, coding for regulatory transcription factors, proposed the odontogenic homeobox code thought to control dental patterning (Sharpe, 1995). This theory was developed using targeted gene disruption experiments in incisor and molar teeth and explained how the overlapping homeobox gene expression domains combine to determine the intermediate morphologies of human canines and premolars (Tucker *et al.,* 1998; Thomas and Sharpe, 1999). Further experimental support came from altering the specific signalling molecules that modulated the homeobox domains to modify tooth number, size and shape (Tucker and Sharpe, 1998; Sharpe, 2000). Within the epithelium and mesenchyme positive auto-regulatory loops and mutual repression patterns have been shown to spatially restrict gene expression and establish presumptive incisor and molar fields (Tucker and Sharpe, 2004). Bone morphogenetic protein (BMP) and fibroblast growth factor (FGF) families of genes and proteins reciprocally induce and inhibit the expression of the various homeobox genes (Tucker, 2006). These complex patterns of gene expression also establish the proximal–distal and oral–aboral/ rostral–caudal developmental axes of the body plan (Mitsiadis and Smith, 2006).

2.6.2.4. Unifying of Theories:

The field, clone and odontogenic homoebox theories are complementary not contradictory and propose a unifying view that can be applied to developmental anomalies (Townsend *et al.,* 2009). This is reflected in the multifactorial model of tooth development (Brook, 1984) and extends to the multilevel, multidimensional orchestration of dental development (Brook, 2009).

2.6.3. Tooth Development

To date, more than 300 genes are associated with important signals, receptors and transcription factors that control normal and abnormal tooth development (http://bite-it.helsinki.fi). The majority are part of the evolutionarily conserved signalling pathways that mediate cell communication, tissue growth and differentiation, and thereby regulate tooth initiation and morphogenesis (Jernvall and Thesleff, 2000a; Salazar-Ciudad *et al.,* 2002, 2003). The reciprocal epithelial-mesechymal interactions occur reiteratively throughout tooth development (Jernvall and Thesleff, 2000a) and many mutations that cause dental defects in humans have also been partially recapitulated in mouse models (Thesleff, 2006; Fleischmannova *et al.,* 2008; Brook, 2009) (Figure 4.).

Figure 4. The Genetic Regulation of Odontogenesis

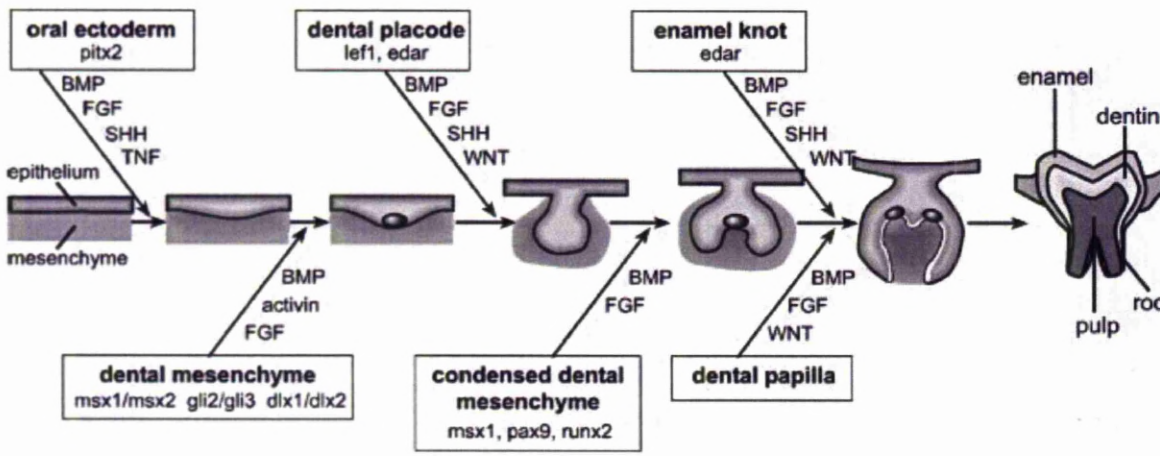

The multigene families of conserved signal pathways mediate sequential and reciprocal interactions between the ectoderm and mesenchyme and regulate key transcription factors associated with dental defects in humans; Fibroblast growth Factor (FGF), Bone Morphogenetic Proteins (BMP), Sonic Hedgehog (SHH), WNT, Tumor Necrosis Factor (TNF). Image modified from (Thesleff, 2006).

Five histologically distinct developmental stages are recognised during odontogenesis; (i) Initiation, (ii) Bud, (iii) Cap, (iv), Bell and (vi) Eruption. The initiation of tooth formation is morphologically distinguishable as a thickening of the dental epithelium, or dental placode, at embryonic day (ED10-11) in mice and during embryonic weeks (7-11) in humans (Miletich and Sharpe, 2003). The epithelium sends signals to the dental mesenchyme inducing its odontogenic potential and initiating the dental lamina at prospective tooth sites. The dental lamina proliferates (ED12-13) and begins to invaginate into the underlying mesenchyme that

condenses around the forming epithelial tooth bud (ED11-13). At the tip of the epithelial tooth bud a restricted subset of cells form a transient signalling center called the primary enamel knot (Jernvall *et al.,* 1994). The enamel knot organises differential cell growth through the transition from the bud to cap stage that marks the onset of tooth crown development (Vaahtokari *et al.,* 1996; Jernvall and Thesleff, 2000b). The epithelium convolutes around the condensed mesenchyme, or dental papilla, during cap morphogenesis (ED13-15) as the progressive folding and growth eventually develops into a bell shape tooth germ (ED15-17). Apoptosis in the enamel knot has an important role in regulating tooth size and shape (Kim *et al.,* 2006a).

Spatio-temporal induction of a secondary enamel knot directs the subsequent folding and invagination of the inner enamel epithelium at the sites of future cusps (Jernvall and Thesleff, 2000b; Kim *et al.,* 2006a). At this stage repeated activation and inhibition of signalling related to differential growth and folding within the tooth germ determines tooth dimensions and cusp morphology (Jernvall and Thesleff, 2000a).

During the late bell stage, differentiation of two tooth-specific cell types occurs along the epithelio-mesenchymal interface of tooth germs (Miletich and Sharpe, 2003); (i) mesenchymal cells in contact with the inner enamel epithelium facing the basement membrane differentiate into odontoblasts (Linde and Goldberg, 1993); odontoblasts lining the pulp chamber secrete a layer of pre-dentin that serves as a scaffold for the deposition of the organic dentin matrix (Butler, 1995b); (ii) immediately after the initial deposition of the predentin layer, adjacent epithelial cells terminally differentiate into pre-ameloblasts and then ameloblasts (Ruch and Lesot, 2000; Lesot and Brook, 2009). Ameloblast cells secret the organic enamel extra-cellular matrix (ECM) that mediates the process of enamel formation (Deutsch, 1989).

Murine incisors are an excellent location to simultaneously observe the series of cell differentiation and migration events during the dynamic process of amelogenesis. Mineralised tissue formation begins at the cusp tips and proceeds in a cervical direction, from the crown to the root (Nanci, 2003). Hertwig's epithelial sheath determines the form of the roots and the fully differentiated tooth is ready to erupt.

In longitudinal section, the stages of ameloblast differentiation can be seen as a gradient with less differentiated cells located posteriorly and the more mature cells located anteriorly on the labial surface (Figure 5.).

Figure 5. Mouse Incisor Morphogenesis and Development

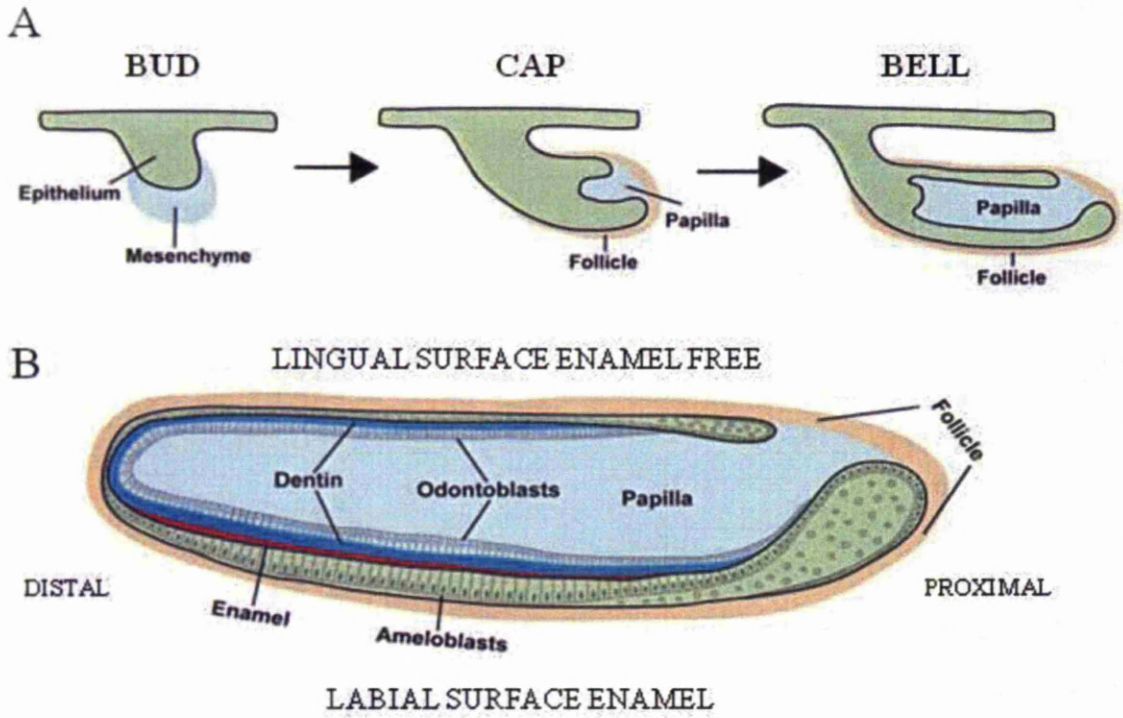

(A) after initiation, the mouse mandibular incisor bud rotates antero-posteriorly, parallel to the long axis of the incisor; (B) during the late bell stage, cell differentiation and ECM secretion occurs. The mesenchymal (light blue) cells that contact the epithelium (green) give rise to the single layer of odontoblasts that secrete dentin (dark blue) and to the labially orientated ameloblasts that secrete enamel (red). Image modified from Wang *et al.*, (2004).

A proximally located stem cell compartment provides progenitor populations for epithelial ameloblasts and mesenchymal odontoblasts (Wang *et al.*, 2004). The mesenchyme diverges into two lineages, (i) the dental papilla and (ii) the dental follicle; the papilla gives rise to the tooth pulp and odontoblasts, while the follicle gives rise to the cementoblasts, cementum and periodontal tissues (Nanci, 2003). Classical tissue recombination experiments in mice show odontoblasts and dentin are distributed similarly on the labial and lingual surface (Amar *et al.*, 1986). On the lingual surface odontoblasts differentiate and produce dentin but the epithelial cells do not differentiate into ameloblasts (Gaunt, 1956). On the labial surface the epithelial cells, adjacent to odontoblasts and dentin, differentiate into tall, polarised ameloblasts that secrete the enamel ECM (Wang *et al,* 2004). This accounts for the labial-

lingual asymmetry in enamel secretion and formation (Wang *et al.,* 2007) and for the enamel-free areas that are a mixture of enamel and cementum related proteins (Sakakura *et al.,* 1989).

2.7. MINERALISATION

2.7.1 Dentine

In the multilayered process, dentine is the first hard tissue to commence mineralisation (Brook, 2009). Dentine secreting odontoblast cell terminal differentiation is controlled by the molecular signals from the secondary enamel knot (Ruch and Lesot, 2000; Lesot and Brook, 2009). Dentine is highly permeable because it is primarily composed of inter-tubular dentine, a fibrous network of collagen with deposited mineral crystals, and peritubular dentine, a highly mineralised sheath around the dentinal tubules that radiate from the pulp (Linde and Goldberg 1993).

During early tooth development pre-odontoblasts differentiate first into functional odontoblasts and start to secrete a collagen-rich pre-dentin matrix (Ruch and Lesot, 2000). The pre-dentin matrix consists of type I collagen (86%) and some non-collagenous proteins, including proteoglycans and glycoproteins (MacDougall *et al.,* 1998; Butler *et al.,* 2002). Mantle dentine formed during primary dentinogenesis at the dentino-enamel junction is rich in proteoglycans, more irregular and less mineralised than the following layers (Linde and Goldberg 1993). During secretion of the pre-dentin matrix odontoblasts become columnar and form long cell processes that become embedded in the dentin matrix secreted directly beneath the basal lamina – at which point components such as laminin play an important role (Salmivirta *et al.,* 1997).

Dentin mineralisation does not occur until the basement membrane material is degraded and removed, which allows direct interactions between pre-dentin and pre-ameloblast (Linde and Goldberg, 1993; Butler, 1995b). The presence of functional odontoblasts and/ or predentin-dentin matrix is required for reciprocal epithelial-mesenchymal interactions to regulate pre-ameloblast differentiation into ameloblasts (Ruch and Lesot, 2000). The subsequent secretion of enamel ECM is only initiated after the dentin matrix starts to mineralise (Ruch and Lesot, 2000). Dentin starts to mineralise as the basal lamina disappears and the apical surfaces of ameloblasts associate with the superficial collagen fibrils of the mantle dentin. Differentiating

ameloblasts now start to express small amounts of enamel proteins as they begin to send cytoplasmic projections through the gaps in the fragmenting basal lamina (Butler *et al.,* 2002).

Dentinogenesis involves controlled reactions that dynamically convert unmineralised pre-dentin into dentin at the pre-dentin-dentin boarder as apatite crystals form (Butler *et al.,* 2002). The constant thickness of pre-dentin suggests the transition is highly controlled and involves a gradient of events that regulate the proteolysis of ECM macromolecules (Butler *et al.,* 2002). Some confusion exists over the timing of the start of secondary dentinogenesis in humans, and the exact details of the complex proteolytic cleavage processes are not completely known, but in rodent molars dentine formation occurs with no apparent transition from the former to the latter (Butler, 1995b). Tertiary dentinogenesis is stimulated as a reparative response to perturbations during tooth ontogeny.

The dentine ECM is associated with dentinal defects such as *Dentinal Dysplasia* (DD) (OMIM125400, Wiktop, 1957, 1975) and *Dentinogenesis imperfecta* (DI) (OMIM125490, Xiao *et al.,* 2001; Zhang *et al.,* 2001), and with gene mutations in the various collagen structural proteins (Butler, 1995b). DI results in exposed sensitive and softened dentine that lacks resilience and undergoes rapid attrition (Wiktop, 1975) manifests as severe discolouration of the teeth (Witkop, 1989). The non-collagenous proteins, such as dentine sialoprotein (DSP) and dentin phosphoprotein (DPP), mapped to a shared chromosomal location (4q21-q23), are derived from a single parent gene that codes for dentin sialophosphoprotein (DSPP) (*DSPP*, OMIM125485, MacDougall *et al.,* 2002; MacDougall *et al.,* 2003). The cleavage products of DSPP play a significant role in controlling crystal size and/ or morphology and mineralisation (Butler, 1995b). Dpp may act as a nucleator of hydroxapatite crystals during dentine morphogenesis, histodifferentiation and patterning (MacDougall *et al.,* 1998). The proteolytic processing of DSPP is hypothesised to be catalyzed by BMP-1 (Zhu *et al.,* 2010).

2.7.2. Enamel

Enamel covers the anatomical crown of teeth and is the most highly mineralised tissue in the human body (Tomes, 1850). It is acellular, insensitive and inert (Robinson *et al.,* 1981a; Deutsch, 1989) and when mature contains less than 1% organic material (Brookes *et al.,* 1995; Simmer and Fincham, 1995). Inorganic enamel mineral is composed of calcium

hydroxyapatite crystals (25nm thick and 65nm wide), that extend as much as 2.0 mm from the enamel-dentino junction to the tooth surface (Meckel *et al.,* 1965; Dacusi and Kerebel, 1978). The hydroxyapatite crystallites grow parallel to one another in bundles or rods (Boyde, 1967), with about 10,000 crystallites per rod (Warshawsky *et al.,* 1987). Hydroxyapatite is responsible for more than 95% mineral by weight of mature enamel (Robinson *et al.,* 1989; Simmer and Fincham, 1995; Fincham *et al.,* 1999).

Enamel mineral crystals are unusually large when compared with crystals of bone, dentin, cementum and other mammalian hydroxyapatite (Veis, 2003a). The structure of enamel in murine rodents (Boyde, 1969), such as rats (Risnes 1979a; Rinses, 1979b) and mice (Moinichen *et al.,* 1996; Lyngstadaas, 1998), is unique in that its shows extreme enamel prism decussation (Boyde, 1969), where prisms in adjacent rows are inclined in opposite directions across each other (Risnes, 1987; Risnes, 1999). Rodent incisor enamel has characteristic and distinct inner and outer enamel layers; the thickness of the outer enamel in the central labial region is about 22 μm in the mandibular incisor (Rinses *et al.,* 1979b; Moinichen *et al.,* 1996).

The structure of murine incisor enamel is established at the interface between secretory ameloblasts and forming enamel (Leblond 1979), the topography of which has a complex three-dimensional configuration (Warshawsky *et al.,* 1987; Rinses *et al.,* 2002). The crystal surface of murine enamel has been characterised by Atomic Force Microscopy (Kirkham *et al.,* 1998) and its size and form is a reflection of the restrictions imposed during tissue morphogenesis (Robinson *et al.,* 1998; Kirkham *et al.,* 2002).

2.7.3. Amelogenin Proteins

The amelogenins are a family of evolutionarily conserved proteins (Fincham *et al.,* 1983). Amelogenins provided the earliest evidence of the ECM involvement in enamel mineralisation (Termine *et al.,* 1980; Fincham *et al.,* 1983; Deutsch, 1989) and they constitute up to 90% of the developing enamel (Robinson *et al.,* 1989; Fincham *et al.,* 1994; Robinson *et al.,* 1995). The predominant enamel ECM protein, amelogenin, is secreted from and expressed in ameloblasts throughout the various stages of enamel formation or amelogenesis (Hu *et al.,* 2001). The ECM is transiently formed in the extra-cellular space during enamel crystal deposition, progressive protein degradation and secondary crystal

growth (Deutsch, 1995; Robinson *et al.,* 1998). It is the ECM that finalises the enamel surface morphology (Jernvall and Thesleff, 2000a; Margolis *et al.,* 2006).

2.7.3.1. Amelogenin:

Amelogenin is a 180-amino acid hydrophobic prolein rich (25-30%) protein with a bipolar nature due to its hydrophilic 12-carboxy-terminal residues (Simmer *et al.,* 1994; Simmer, 1995; Fincham *et al.,* 1999). It is secreted primarily (80%) as a protein isoform of 175 amino acids with a signal peptide (16 amino acids) that includes three distinct domains: an N-terminal positively charged (N-region), a central hydrophobic part (H-region), and a more polar C-terminal domain (C-region) (Deutsch *et al.,* 1995). Amelogenin is the most abundant ECM protein, greater than 95% mineral by weight in mature enamel and it is almost completely removed during mineralisation (Smith, 1998).

The amelogenin monomer subunits self-assemble into spherical structures called nanospheres (15-20nm) that are found between the growing ribbon-like crystals (Fearnhead, 1960; Robinson *et al.,* 1981b; Fincham *et al.,* 1995). Nanospheres spatially organise the initial crystallites, control crystal habit and create anionic channels that facilitate ion transport within the mineralising ECM (Fincham *et al.,* 1995). Therefore, nanospheres are thought to provide the scaffold that guides crystal growth as the amelogenin proteins are deposited and hydrolysed in an orchestrated manner (Fincham *et al.,* 1999; Paine *et al.,* 2000). The highly conserved amelogenin N-terminal tri-tyrosyl domain may be involved in the formation of nanospheres (Ravindranath *et al,* 1999) and/or binding to other enamel or dentin proteins (Ravindranath *et al.,* 2003). The N-terminal region may have a role in amelogenin self-assembly related to enamel defects (Paine *et al.,* 2002). The C-terminal region may contribute to nanosphere stability and size homogeneity (Moradian-Oldak *et al.,* 2000). Nanospheres either provide the environment for the initiation of mineral crystals in normal enamel or have an essential interactive relationship between nanosphere self-assembly and mineral growth (Robinson *et al.,* 2003; Margolis *et al.,* 2006). Enamel surface topology suggests that ECM processing may generate nuclei leading to fusion and transformation into long apatite crystals (Kirkham *et al.,* 2000; Robinson *et al.,* 2003). The C-terminus has an affinity for forming enamel crystallites and likely plays a critical role in amelogenin scaffold assembly during enamel development (Wright, 2006).

In the mouse, the amelogenin gene (*Amelx*) is mapped to the X chromosome (Lau *et al.*, 1989; Fincham *et al.*, 1983), whereas in humans the amelogenin gene (*AMEL*) is sexually dimorphic and maps to both the Xp22.1-p22.3 and Yp11.2 chromosomes (Lau *et al.*, 1989; Salido *et al.*, 1992). In human males, 90% of the amelogenin gene transcripts are expressed from the X chromosomal copy of the gene (*AMELX*), while only 10% is expressed from the Y chromosomal copy (*AMELY*) (Snead *et al.*, 1989). Despite being expressed in the same cells, the X and Y chromosomal copies are processed differently (Nakahori *et al.*, 1991; Salido *et al.*, 1992).

Amelogenin was originally thought to be an enamel specific protein of exclusively epithelial origin with an isoated function in controlling the size, shape and the direction of hydroxyapatite crystal formation during enamel structural organisation and mineralisation (Robinson *et al.*, 1981a, 1983, 1989). However, alternatively spliced RNA transcripts that translate into multiple isoforms and result in the heterogeneous mixture of amelogenin proteins that are found in developing mouse tooth extracts suggests otherwise (Simmer *et al.*, 1994; Simmer, 1995; Hu *et al.*, 1997). There are thought to be up to nine exon coding regions of amelogenin (*AMELX/ Amelx*) in many species (Li *et al.*, 1998; Baba *et al.*, 2002; Papagerakis *et al.*, 2005). So it has been difficult to assign specific functions to individual amelogenins because of the large number of isoforms with potentially different functions (Deutsch *et al.*, 1989; Stephanopoulos *et al.*, 2005; Gibson *et al.*, 2005). Nonetheless, this mechanism produces species-specific variations in enamel structure and has resulted in the finely tuned process of amelogenesis.

Also, amelogenin is now known to be expressed in the dentin matrix (Nebgen *et al.*, 1999), odontoblasts (Papagerakis *et al.*, 2003), in Hertwig's root sheath and periodontal ligament cells (Fong *et al.*, 1998; Fong and Hammarstrom, 2000), in long bone cells, such as osteocytes, osteoblasts and osteoclasts, in periosteum, in chondrocytes of the articular cartilage and the epiphyseal growth plate (Haze *et al.*, 2007), in glial cells, in salivary glands and in some hematopoietic cells (Li *et al.*, 2006; Deutsch *et al.*, 2006). The expression of amelogenin in alveolar bone regions suggests it may be active in bone formation and remodelling (Haze *et al.*, 2007).

Several amelogenin isoforms display different signalling effects on ameloblast and odontoblast differentiation (Nebgen *et al.*, 1999; Veis, 2003b). Amelogenin's signalling roles

during early craniofacial development was supported by its early expression in mouse embryogenesis (ED10.5), long before initiation of tooth formation, and its detection in the dental lamina (ED13.5-ED16.5) before extra-cellular enamel or dentin formation (Li *et al.,* 2006; Gruenbaum-Cohen *et al.,* 2008). Amelogenin also encourages progenitor cell recruitment during periodontal regeneration (Hammarstrom *et al.,* 1997) and promotes regeneration of other supporting tissues (e.g. periodontal ligament and cementum) (Hu *et al.,* 2006; Zhu *et al.,* 2006).

The expression of amelogenin occurs in a variety of tissues of the craniofacial complex, including non-mineralising cells of the neural crest that give rise to non-neuronal ecto-mesenchymal tissues in bone, cartilage and mesenchymal regions of the teeth (and in the eye-lens, which is not thought to be neural crest derived) (Gruenbaum-Cohen *et al.,* 2008). This means that during these developmental stages amelogenin must have additional functions to those described in the early ECM studies. The expression patterns in the eye-lens, brain and nerve fibers (Deutsch *et al.,* 2006) suggested a possible role for amelogenin in elongating structures that may be of possible relevance to the model of nanosphere elongation (Paine *et al.,* 2002; Du *et al.,* 2005; Margolis *et al.,* 2006). Therefore, amelogenin is proposed to be a multifunctional protein (Li *et al.,* 2006; Gruenbaum-Cohen *et al.,* 2008).

2.7.4. Non-Amelogenin proteins

Non-amelogenin ECM proteins are also important in enamel mineralisation. They too may have yet to be discovered roles in the craniofacial complex.

2.7.4.1. Ameloblastin:

Ameloblastin (formerly amelin or sheathlin) is the most abundant non-amelogenin ECM protein (5% of total protein). It is expressed at high levels in ameloblasts, at low levels in odontoblasts and pre-odontoblasts (Toyosawa *et al.,* 2000). Human ameloblastin (*AMBN*) is located on chromosome 4q21 (Karrman *et al.,* 1997; MacDougall *et al.,* 1997), near other genes associated with the mineralised tissues (MacDougall *et al.,* 2003), and it shares high sequence homology with mice (chromosome 5) (Toyosawa *et al.,* 2000). Ameloblastin is alternatively spliced in humans and mice and the fate of its cleavage products are thought to be similar to that of other ECM proteins (Brookes *et al.,* 2001; Iwata *et al.,* 2007).

2.7.4.2. Amelotin:

Amelotin is a structural enamel protein component of the basal lamina, with only few post translational modifications (Iwasaki *et al.,* 2005). The human amelotin gene (*AMTN)* shows significant sequence homology with its mouse orthologue, displaying a similar exon-intron structure and expression loci on chromosomes 4 and 5 respectively (Iwasaki *et al.,* 2005). Thus far, amelotin is only known to be expressed in ameloblasts during the maturation-stage of amelogenesis and may therefore be engaged in proteolytic processing/ degradation of the ECM (Iwasaki *et al.,* 2005).

2.7.4.3. Enamelin:

Enamelin is the largest (1103 amino-acids with a 39 amino-acid signal peptide) and least abundant (1 to 5% of total amount) enamel ECM protein (Hu *et al.,* 2001a). The human enamelin gene (*ENAM*) is located at chromosome 4q21 (Hu *et al.,* 2000; Dong *et al.,* 2000) and the mouse enamelin gene (*Enam*) is located at chromosome 5 (Hu *et al.,* 1998, 2001a). *ENAM* and *Enam* are evolutionarily conserved, sharing 73% gene sequence homology (Dong *et al.,* 2000). Enamelin is a tooth-specific protein that is secreted solely and specifically by ameloblasts (Hu *et al.,* 2008). Unlike ameloblastin and amelogenin, no alternatively spliced enamelin RNA has been reported (Hu *et al.,* 1997) but nucleotide polymorphisms do affect the produced amino acid (Stephanopoulos *et al.,* 2005).

Extensive proteolytic processing of enamelin gives rise to multiple cleavage products that accumulate in different parts of the enamel ECM (Deutsch *et al.,* 1995). Enamelin is present at the dentino-enamel junction, throughout the entire thickness of enamel during the secretory stage, and disappears early in the maturation stage (Hu *et al.,* 1997, 2000, 2001a). These cleavage products are uniquely different to their precursors and demonstrate vital regulatory functions at the different stages of enamel growth and formation (Hu *et al.,* 2007).

Therefore, enamelin is thought to control multiple steps (nucleation, growth and organisation) in the crystallisation of hydroxyapatite during enamel formation (Hu *et al.,* 2007; Hu and Simmer, 2007).

2.7.4.4. Enamelysin and Kallikrein-4 Proteases:

Enamelysin (or matrix-metalloproteinase-20) is a calcium-dependent proteinase coded for a tooth specific human (*MMP-20*) and mice (*mmp-20*) genes (Bartlett *et al.,* 1996). It is heavily

expressed by ameloblasts adjacent to the Tomes' process throughout the secretory stage and into the early maturation stage where it is thought to be necessary for the process of crystal elongation (Bartlett *et al.,* 2004, 2006). Kallikrein-4, a calcium-independent serine proteinase, is coded for by the human (*KLK-4*) and mice (*klk-4*) genes (Simmer *et al.,* 1998). Kallikrein-4 is expressed later than enamelysin, starting in the transition stage and early maturation stage ameloblasts and continuing through to tooth eruption (Hu *et al.,* 2002; Simmer *et al.,* 2009).

MMP-20 steadily cleaves enamel proteins that have accumulated in the space between crystal ribbons for support during the secretory stage, their concentration decreasing with depth as enamel crystals thicken away from the enamel surface (Lu *et al.,* 2008). *KLK-4* more aggressively degrades the retained ECM as enamel protein secretion terminates. Despite these important differences in the timing of their expression and proposed functions, *MMP-20* and *KLK-4* mutations cause a similar autosomal recessive pigmented hypomaturation AI phenotype in humans (Wright *et al.,* 2006; Hu and Simmer, 2007). Therefore, the principle functions of *MMP*-20 and *KLK-4* are thought to be in facilitating the orderly replacement of ECM with mineral, generating an enamel layer that is harder, less porous, and does not retain excess enamel proteins (Lu *et al.,* 2008).

In mice, *Mmp-20* and *Klk-4* studies have suggested that *Mmp-20* alone processes amelogenin during the secretory stage of amelogenesis (Simmer *et al.,* 1998; Hu *et al.,* 2002; Nagano *et al.,* 2009). *Mmp-20* also has a major role alongside *Klk4* in removing enamel proteins (Bartlett *et al.,* 2004, 2006), which is crucial for the proper maturation of enamel crystals (Fleischmannova et al., 2008; Simmer *et al.,* 2009).

2.8. AMELOGENESIS

2.8.1. Amelogenesis

Ameloblasts control the critical ionic, pH and fluid concentration of the intra- / extra-cellular micro-environment whilst undergoing morphological changes and accommodating diverse physiological functions (Deutsch *et al.,* 1995). Amelogenesis can be observed in three distinct stages; (i) *pre-secretory*, (ii) *secretory* and (iii) *maturation* (and post-maturation) identifiable in both the ameloblast and in the extra-cellular enamel that they produce (Rinses, 1987; Robinson *et al.,* 1998; Smith and Nanci, 1989) (Figure 6.).

Figure 6. Stages of Enamel Formation.

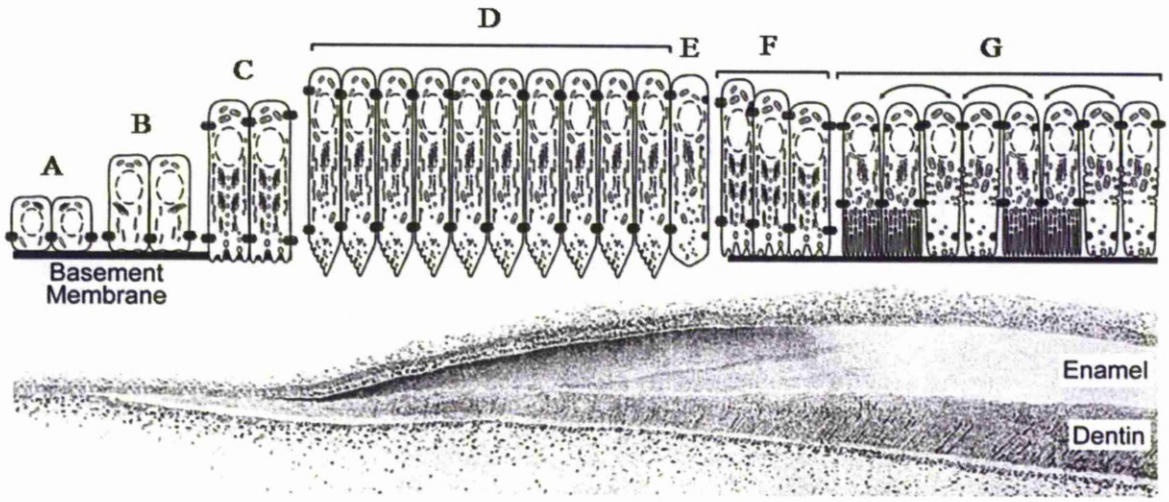

Ameloblast changes during enamel formation: (A) epithelial cells rest on the basement membrane; (B) they increase in length as they differentiate into ameloblasts above the pre-dentin matrix; (C) **pre-secretory** ameloblasts send processes through the degenerating basement membrane as they initiate enamel protein secretion onto the surface of the mineralising dentin; (D) the start of the **secretory-stage** sees the dentino-enamel junction established as a thin layer of aprismatic enamel begins to mineralise. Ameloblasts develop a specialisation, or Tomes' process, in place of the absent basement membrane, and enamel proteins are secreted at a mineralisation front where the enamel crystals grow in length. Each enamel rod follows a retreating Tomes' process from a single ameloblast; (E) at the end of the secretory stage, ameloblasts lose their Tomes' process and produce a thin layer of aprismatic enamel; (F) at this point the enamel has achieved its final thickness. During a transition stage, ameloblasts restructure, reduce their secretory activity and change the types of proteins secreted; (G) e.g. *KLK-4* begins to degrade the accumulated protein matrix. During the **maturation stage** ameloblasts modulate between ruffled and smooth-ended phases. Ameloblast activity promotes the deposition of mineral on the sides of enamel crystals as the enamel layer hardens. Image modified from Hu *et al*, (2007).

2.8.1.1. Pre-secretory Stage:

During the *pre-secretory* stage of amelogenesis the basement membrane (epithelial sheet) forms apically and differentiates, longitudinally towards the incisal tip, into tall ameloblasts that secrete the enamel ECM and transport calcium ions that begin mineralisation (Deutsch *et al.,* 1989, 1995). Amelogenins first appear on the surface of recently deposited dentin where they are secreted on top of and around existing crystallites (dentin crystals initially and enamel crystals thereafter), and into the spaces that were previously occupied by the basal lamina (Robinson *et al.,* 1989; Ruch and Lesot, 2000). This forming dentino-enamel junction is particularly susceptible to failure as the enamel layer tends to shear from the underlying dentin (Sato *et al.,* 1996; Deutsch *et al.,* 1995).

Secretory ameloblasts recede as patches of enamel grow larger and merge as a continuous and uniform layer of initial aprismatic enamel is deposited (i.e. not separated into rod and inter-rod) (Boyde, 1967). At the secretory ends of ameloblasts, a specialised cell extension called a Tomes process forms with secretory and non-secretory regions (Tomes, 1850). Adjacent to the matrix depositing ameloblasts, the mineralisation front (a concentration of the secreted enamel proteins) retreats with the Tomes process as the enamel crystals grow in length (Risnes, 1998). The radial movement of the ameloblasts away from the mineralisation front provides the architectural basis for organising enamel crystals into prisms (Meckel *et al.,* 1965; Rinses *et al.,* 2002). After secretion amelogenin quickly passes through the mineralisation front (Smith and Nanci, 1989) and assembles into nano-spheres (Fincham and Simmer, 1995) that are thought to regulate crystal spacing (Robinson *et al.,* 1989; Deutsch *et al.,* 1998). The developing ECM is predominantly formed of amelogenin (90%) which continues to be essential for crystal growth and structural maintenance into the mid-secretory stage (Paine *et al.,* 2005).

2.8.1.2. Secretory Stage:

During the secretory stage of amelogenesis uncleaved enamelin is only observed in the surface enamel at the mineralisation front, near the Tomes' process of the ameloblast, where it is thought to be critical in maintaining crystallite elongation (Hu *et al.,* 1997). Many enamelin cleavage products are found throughout the entire thickness of developing enamel (Deutsch *et al.,* 1989), concentrated in the rod and inter-rod enamel, where they may bind to the sides of developing enamel crystals and regulate their shape (Hu *et al.,* 2000). Enamelin is

rapidly cleaved shortly after secretion and disappears early in the maturation stage suggesting it plays an early role during enamel formation (Hu *et al.*, 2001b, 2007).

Ameloblastin maintains the differentiation state of secreting ameloblasts (Fukumoto *et al.*, 2004) which continue to secrete enamel proteins as the crystals elongate and grow (primarily in length) as the enamel layer thickens (Robinson *et al.*, 1989). The final length of the enamel crystals (and the thickness of the enamel layer as a whole) is determined by the length of time ameloblasts continue to deposit enamel proteins, or how long they remain in the secretory stage (Hu *et al.*, 2007). Ameloblastin expression is diminished by the maturation stage.

During the secretory stage ameloblasts progressively decrease in height, increase in width and reduce their secretion of enamel proteins (Deutsch *et al.*, 1995). As enamel crystals achieve their final length the ECM (separating individual crystallites) begins to be degraded and reabsorbed (Robinson *et al.*, 1995) into the early maturational stage (Lu *et al.*, 2008). Ameloblasts initiate the secretion of enamelysin that cleaves amelogenin in the secretory stage (Bartlett *et al.*, 1996; Bartlett *et al.*, 2004). Kallikrein-4 later degrades amelogenin as the process of ECM proteolysis continues into the maturation phase (Simmer *et al.*, 1998; Hu *et al.*, 2002). Amelotin is also secreted at this point as part of a newly forming basement membrane (Iwasaki *et al.*, 2005).

2.8.1.3. Maturation Stage:

Further towards the incisal tip the epithelium enters a maturation stage wherein ameloblasts shorten and begin to cycle through smooth-ended and ruffle-ended phases as they lose their secretory characteristics (Smith and Warshawsky, 1975, 1976; Nanci, 2003). At this stage the rapid removal of the ECM terminates the longitudinal growth of enamel crystals, accelerates their latitudinal growth and thickness, and exposes the sides of the thin crystals to ion deposition (Hu *et al.*, 2007). The predominant site of mineral deposition now shifts from the enamel surface, and as mineralisation speeds up the enamel layer hardens (or matures) as mineral ions are increasingly deposited either side of the crystals until adjacent crystallites contact (Robinson *et al.*, 1998). By the end of this stage, normal enamel thickness is thought to be achieved by the suppressed expression of a variety of protein genes, e.g. *Amelx* and *Enam* (Lezot *et al.*, 2000, 2002, 2008).

In the human permanent dentition, crystallites continue to grow in width and thickness over about 3–6 years during which time the enamel layer becomes hard, fully mineralised and fully mature (Termine *et al.,* 1980; Robinson *et al.,* 1998). The ECM has been completely removed and secondary enamel crystal growth occludes the spaces previously occupied by water, amelogenins and other ECM proteins that were replaced by calcium and phosphorus mineral ions (Deutsch *et al.,* 1995). The fully mineralised enamel layer is neither replaceable nor repairable because during maturation ameloblasts become cuboidal, progress towards the gingival margin and are lost as the tooth erupts (Nanci, 2003).

2.9. AMELOGENESIS IMPERFECTA

2.9.1. Amelogenesis imperfecta

The *Amelogenesis imperfectas* (AI) are a clinically and genetically heterogeneous group of inherited dental defects that are exhibited in the absence of non-dental symptoms (Witkop, 1957, 1975; Witkop and Sauk, 1976). The prevalence of AI appears to vary geographically, e.g. 1:8000 in Israel (Chosack *et al.,* 1979), 1:700 in Sweden (Backman and Holm, 1986) and 1:14000 in the USA (Witkop and Sauk, 1989). A broadly classified spectrum of human AI phenotypes exists with three main types; (i) autosomal dominant (85%), (ii) autosomal recessive (10%) and (iii) X-linked (5%). These phenotypes are subdivided into a combination of at least 14 different subtypes that result in three main deficiencies in the quality or quantity of enamel; (i) hypoplastic, (ii) hypomineralised/calcified and (ii) hypomature (Winter and Brook, 1975; Witkop, 1989; Aldred *et al.,* 2003; Wright *et al.,* 2006; Crawford *et al.,* 2007).

The range of enamel dysplasias observed in patients with AI is classified according to the thickness, hardness and smoothness of the affected enamel (Crawford *et al.,* 2007). These differences are believed to reflect the different stage of amelogenesis when the disruption occurs (Hu *et al.,* 2007): e.g. a *pre-secretory* stage failure in mineralisation, in its most extreme hypomineralised/ hypocalcified form, leaves enamel of normal thickness but rough and soft, lacking resilience and susceptible to rapid attrition (Wiktop, 1957; Hart *et al.,* 2003a; Kim *et al.,* 2008); in the *secretory* stage insufficient enamel protein deposition/ secretion and associated crystal elongation leaves the enamel layer pathologically thin or hypoplastic (Chosack *et al.,* 1979; Lench and Winter, 1995; Lagerstrom-Fermer *et al.,* 1995; Rajpar *et al.,* 2001); in the *maturation* stage a failure to fully remove the ECM and promote the hardening of the enamel layer leads to crowns of normal size but pathologically soft or hypomature (Sauk *et al.,* 1972; Lagerstrom-Fermer *et al.,* 1991; Hart *et al.,* 2000).

A number of specific mutations have been identified in the amelogenin gene (*AMELX,* OMIM300391, Hart *et al.,* 2002a, 2002b; Kim *et al.,* 2004) and in the enamelin gene (*ENAM,* OMIM606585 Rajpar *et al.,* 2001; Mardh *et al.,* 2002; Hart *et al.,* 2003b), which are human and mouse orthologues involved in enamel formation. The other significant genes implicated in the aetiologies of enamel defects encode the ameloblastin protein (*AMBN,* OMIM601259, AI1B, OMIM104500; MacDougall *et al.,* 1997, Toyosawa *et al.,* 2000), the *FAM83H* protein

(*FAM83H*, OMIM611927, AI3, OMIM130900, Kim *et al.*, 2008) and two proteases kallikrein-4 (*KLK-4*, OMINM603767, Hart *et al.*, 2004) and enamelysin (*MMP-20*, OMIM604629, Kim *et al.*, 2005a, Papagerakis *et al.*, 2008). Amelogenin, enamelin and ameloblastin are critical for proper enamel mineralisation and they all belong to a secretory calcium-binding phosphoprotein gene family (Kawasaki and Weiss, 2003).

AMELX and *ENAM* mutations cause structural changes that alter the functional domains and specificity of the proteins and result in the spectrum of different enamel appearances (Fincham *et al.*, 1999). To date, the 15 known *AMELX* mutations correlate directly to different deletion, mis-sense, frame-shift and non-sense types of mutations (Aldred *et al.*, 2003; Stephanopoulos *et al.*, 2005; Wright *et al.*, 2006; Crawford *et al.*, 2007) (Table 1.).

Table 1. Gene Mutations Causing *Amelogenesis imperfecta*

A

X-linked *Amelogenesis imperfecta*

MALE PHENOTYPE	MUTATION	REFERENCE
hypoplastic (normal mineralisation)	M1T	Kim *et al.*, 2004
hypoplastic (normal mineralisation)	W4S	Kim *et al.*, 2004
hypoplastic (normal mineralisation)	W4X	Sekiguki *et al.*, 2001
smooth hypoplastic (normal mineralisation)	I5_A8delinsT	Lagerström-Fermer and Landegren, 1995
hypomaturation (some hypomineralisation)	18del	Lagerström-Fermer, 1991
hypomaturation (some hypomineralisation) brown colour	T51I	Lench and Winter, 1995
hypoplastic (some hypomineralisation, variable) white opaque	P52fsX53	Aldred *et al.*, 1992a; Lench *et al.*, 1994
hypomaturation (some hypoplasia) white cervical brown coronal	P70T	Collier *et al.*, 1997; Ravassipor *et al.*, 2000; Hart *et al.*, 2002b
hypomaturation (yellow, brown)	H77L	Hart *et al.*, 2002b
smooth hypoplastic	H129fsX187	Sekiguki *et al.*, 2001
smooth hypoplastic	Y141fsX187	Greene *et al.*, 2002
hypocalcified	P158fsX187	Lench and Winter, 1995
smooth hypoplastic (some hypomineralisation/ calcification)	L181fsX187	Kindelan *et al.*, 2000; Hart *et al.*, 2001
smooth hypoplastic	E191X	Lench and Winter, 1995
smooth hypoplastic (yellow)	P52R	Kida *et al.*, 2007
Animal model	Amelx-null Amelx-null; Y64H	Gibson *et al.*, 2001; Gibson *et al.*,2005; Gibson *et al.*, 2007; Wright *et al.*, 2009; Barron *et al.*, 2010

B

autosomal recessive and dominant *Amelogenesis imperfecta*

PHENOTYPE	MUTATION	REFERENCE
dominant localised hypoplastic (AIH2, OMIM104500)	K53X	Mardh *et al.*, 2002; Kim *et al.*, 2006b
dominant severe horizontal grooves	M71_Q157del	Kim *et al.*, 2005b
dominant generalised thin hypoplastic (AIH2, OMIM104500)	A158_Q178del	Rajpar *et al.*, 2001; Urza *et al.*, 2005
dominant generalised thin hypoplastic (AIH3, OMIM204650)	N197fsX277	Kida *et al.*, 2002; Hart *et al.*, 2003b; Kim *et al.*, 2005b
dominant hypoplastic	R170M	Gutierrez *et al.*, 2007
dominant hypoplastic	S246X	Ozdemir *et al.*, 2005
recessive local pitted	V340_M341insSQ	Ozdemir *et al.*, 2005
recessive generalised thin hypoplastic	P422fsX448	Hart *et al.*, 2003b
Animal model	p.S55I; PQ176X PE57G; Enam-null	Matsuya *et al.*, 2005; Seedorf *et al.*, 2007; Hu *et al.*, 2008; Wright *et al.*, 2009

(A) *AMELX* X-linked AI mutations; (B) *ENAM* autosomal dominant and recessive AI mutations. Adapted and updated from Hart *et al.*, (2002), Stephanopoulos *et al.*, (2005) Wright *et al.*, (2006) and Hu *et al.*, (2007).

All of the X-linked forms of AI (AIH1, OMIM301200) are associated with specific mutations in the X-chromosomal amelogenin gene (*AMELX*, OMIM300391, Lagerstrom-Fermer *et al.*, 1991, 1995; Lench and Winter, 1995), located at chromosome Xp22.3-p22.1 (Lau *et al.*, 1989; Salido *et al.*, 1992; Aldred *et al.*, 1992a). One family has been reported as having linkage to another X linked interval (Xq22-28) (Aldred *et al.*, 1992b, OMIM301201) and there are other X-linked conditions that have significant enamel involvement, making it likely that there are other important genes on the X chromosome (Wright, 2006).

AIH1 affects males and females differently and their phenotypes vary markedly in severity and appearance (Witkop, 1967). In males, 90% of the amelogenin transcripts are expressed from *AMELX* and only 10% are expressed from the active human amelogenin gene on the Y chromosome *AMELY* (*AMELY,* OMIM410000) (Salido *et al.*, 1992). Although *AMELY* is thought to contribute proteins no mutations are reported (Fincham *et al.*, 1983; Snead *et al.*, 1989; Nakahori *et al.*, 1991). Affected hemizygous males express only the mutant allele and so display the trait severely, whereas, heterozygous females show a mosaic pattern of expression due to lyonisation (Lyon, 1961) or X-chromosome inactivation (Huynh and Lee, 2005; Heard and Disteche, 2006). This is proposed to be due to alternating clusters of ameloblasts (expressing either the normal or the mutant allele) secreting either the normal or the defective amelogenin protein (Witkop and Sauk, 1976). Affected teeth typically display vertical ridges and grooves as a result of enamel hypoplasia, or they have vertical striated bands of alternating normal and discoloured enamel (Witkop, 1967). Pleiotropic variation is often exhibited (Liao *et al.*, 2008) between affected individuals in the same family, between dentitions in the same individual and even between different teeth in the same dentition (Brook, 2009), e.g. in some families hypoplasia occurs together with other abnormal mineralisation phenotypes (Backman, 1988).

AMELX mutations are categorised as; (i) major deletions or signal peptide coding region mutations that result in the total loss of amelogenin (Lagerstrom-Fermer *et al.*, 1991 and 1995; Kim *et al.*, 2004), this is a human knockout (KO) equivalent that primarily leads to the smooth hypoplastic phenotype of reduced enamel thickness (also described as hard and well-mineralised); (ii) frame-shift mutations in the N-terminal coding region (Aldred *et al.*, 1992b; Lench *et al.*, 1994) that result in hypomaturation hypomineralised enamel that is soft with too much organic material and hypolplastic phenotypes with varying degrees of severity (even between same gender individuals within the same family) (Wright *et al.*, 2003). Mis-sense

T51I mutations in this region result in an enamel phenotype described as hypomineralisation/ hypomaturation (Lench and Winter, 1995), and the P70T and H77L mutations that produce the hypomaturation phenotype both display enamel discoloration (Collier *et al.,* 1997; Ravassipour *et al.,* 2000; Hart *et al.,* 2002b); (iii) premature stop codons in the C-terminus coding region that cause protein truncation and result in a generalised thinning of enamel and a smooth hypoplastic phenotype (Lench and Winter, 1995; Hart *et al.,* 2002b; Aldred *et al.,* 2003).

This overlapping range of enamel phenotypes is not surprising given that amelogenin (and its associated proteins) are all involved in the critical pathways that are related to the secretion, organisation, processing, and/ or mineralisation of developing enamel (Wright *et al.,* 2003; Wright, 2006). For example, in hypoplastic AIH1 a deficiency in the amount of enamel, which is of a normal hardness but does not develop to normal thickness, makes teeth appear small - the surface enamel varies considerably displaying smooth, rough, pitted, or local forms (Witkop, 1989). The hypomature (snowcapped) type of AIH1 arises from defects in the maturation stage of amelogenesis, where, in males the primary teeth are opaque ground-glass white and the secondary teeth are mottled yellow-brown and white (Witkop, 1989) and enamel is moderately soft and of normal thickness, so chips and abrades more easily than normal (Crawford *et al.,* 2007). In hypomature AIH1 teeth may either have only a thin layer of enamel of normal colour and translucency, or the enamel may be of normal thickness but poorly mineralised with loss of translucency and/ or a yellow-brown discolouration (Wright *et al.,* 2003; Wright, 2006; Crawford *et al.,* 2007). In hypocalcified AIH1 the loss of enamel is rapid because the developmental disruption results from early defective initial crystallite mineralisation and growth (Wright, 2006). Understanding the relationship between the enamel phenotype and underlying genetic lesion is made more complex by the extensive alternative splicing of *Amelx* such that a point mutation could potentially affect several different amelogenin proteins but have no effect on others (Gibson *et al.,* 2005, 2009).

In addition to amelogenin, the other important ECM constituent that is implicated in the aetiology of AI is *ENAM* (OMIM606585, Dong *et al.,* 2000; Hu *et al.,* 2000). Multiple *ENAM* allelic mutations are associated with autosomal dominant AI (AIH2) (Rajpar *et al.,* 2001; Kida *et al.,* 2002; Hart *et al.,* 2003a; Hu and Yamakoshi, 2003) mapped to human chromosome 4q11-q21 and encompassing the *AMBN* gene (Karrman *et al.,* 1997). Two clinically distinct forms of AIH2 exist, smooth hypoplastic AI and local hypoplastic AI

(OMIM104500, Rajpar *et al.,* 2001; Mardh *et al.,* 2002). The local hypoplastic phenotype resulting from *ENAM* mutations that essentially stops protein production from one allele is characterised by horizontal bands of hypoplastic pits that encompass the tooth. Mutations that result in a secreted but altered protein are associated with the more severe generalised thin hypoplastic type that display fine horizontal bands and pitting on the enamel surface, hypothesised to result from a dominant negative effect (Mardh *et al.,* 2002; Wright, 2006). Therefore *ENAM* mutations show a haploinsufficiency dose effect so that a single mutant allele causes a mild form of AI and defects in both alleles prevent the whole enamel layer from forming in more severe forms of AI (Hart *et al.,* 2003b; Ozdemir *et al.,* 2005; Hu and Yamakoshi, 2003; Hu *et al.,* 2008).

The subsets of AI conditions offer an unparalleled opportunity to investigate the specific roles of proteins in normal and abnormal enamel formation and to delineate between the various phenotypes (Hart *et al.,* 2002b; Miletich and Sharpe, 2003; Stephanopoulos *et al.,* 2005; Paine and Snead, 2005). Mutations leading to defective processing are thought to impair mineral initiation, fusion, and crystal growth leading to short mineral segments in hypoplastic AI or abnormally large crystals in hypomature AI (Robinson *et al.,* 2003). Further genetic linkage studies are expected to show additional loci for both X-linked and autosomal forms of AI (Aldred *et al.,* 1992b; Karrman *et al.,* 1996; Kim *et al.,* 2006b; Wright, 2006; Hu *et al.,* 2007).

2.9.2. Mouse Models of *Amelogenesis imperfecta*

Numerous murine model studies have targeted particular ECM genes in order to evaluate the effect of the individual protein changes during enamel development. This has gained much of the insight into the structural and functional causes behind the phenotype heterogeneity in AI.

2.9.2.1. Amelogenin (Amelx):

Amelogenin deficient knock-out (KO) mutant mice, with a deletion in the signal peptide sequence that results in the total loss of amelogenin, combine various human phenotypes into one model of AI (Gibson *et al.,* 2001, 2005). The distinctly abnormal phenotypes (chalky-white discoloured teeth) of the amelogenin-null (*Amelx*-null) mice are remarkably similar to severe hypomaturation AI in humans (Sauk *et al.,* 1972; Collier *et al.,* 1997). Micro-radiography and SEM revealed broken incisal tips and disorganised thin hypoplastic enamel

respectively, which suggested incorrect amelogenin assembly, delayed mineral deposition and thin disrupted enamel prism patterning (Gibson *et al.,* 2001). Amelogenin was not required for mineral crystal initiation but was essential for correct structural organisation, crystal pattern formation and elongation during the *secretory* stage of amelogenesis (Gibson *et al.,* 2001). This proposed the critical importance of amelogenin in generating the correct thickness of enamel.

Mice over expressing the most abundant amelogenin isoform (M180) and mice containing a proline - threonine (P70T) mutation in the amelogenin tri-tyrosyl domain (Gibson *et al.,* 2007), have revealed a similar phenotype to the hypomaturation form of AI in humans with a similar mutation (Collier *et al.,* 1997). The P70T mutation is adjacent to a proteolytic cleavage site thought to be required for amelogenin degradation during normal crystal growth (Li *et al.,* 2001). Under light microscopy and SEM the morphology of the molars from the wild-type and the M180 mice showed similar prismatic enamel, while the P70T mice showed markedly aprismatic chalky-white discoloured enamel (Gibson *et al.,* 2007). The resulting delay in the proteolysis was suggested to lead to the retention of excess protein as seen in the hypomature enamel of AI (Li *et al.,* 2001; Gibson *et al.,* 2005). Mating the *Amelx*-null mice (Gibson *et al.,* 2001) and the M180 mice generated M180KO offspring with partially rescued enamel thickness, mineral density and volume (Gibson *et al.,* 2007), but mating the *Amelx*-null and the P70T mutants generated P70TKO offspring that displayed a heterogeneous enamel structure with no evidence of rescue (Li *et al.,* 2008). This supported the dominant-negative effect of the P70T mutation (Gibson *et al.,* 2007).

Also amelogenin cell binding activity may be disrupted by *Amelx* tri-tyrosyl domain mutations that lead to defective enamel, particularly as it was shown to be involved in nanosphere assembly (Ravindranath *et al,* 1999). The tri-tyrosyl domain has received a lot attention because of lectin-like binding activity to glycosylated enamelin proteins at the dentino-enamel junction, such as N-acetyl glucosamine (Ravindranath *et al,* 1999; Wright, 2006) and the N-acetyl glucosamine mimicking domain of cytokeratin 14 and N-acetyl glucosamine residues on cytokeratin 5 (Ravindranath *et al.,* 2003, 2004). Therefore, the actual mechanism that leads to AI may be related to amelogenin cell binding activity and cell signalling function (Gibson *et al.,* 2007). The cooperative function of amelogenin variants, e.g. in nanospheres assembly, may explain the biological importance of the alternative splicing of *Amelx* RNA (Gibson *et al.,* 2009).

Humans from 54 families segregating for AI (18 autosomal dominant, 26 autosomal recessive and 10 X-linked traits) were recently recruited for candidate gene (*AMELX, ENAM, AMTN, AMBN, MMP-20* and *KLK-4*) sequencing (Wright *et al.,* 2009). Mutations were found in the *AMELX, ENAM* and *KLK-4* genes but none were identified in the *MMP-20*, *AMTN* or *AMBN* genes. Comparing wild-type and mutant mice models of AI, *Amelx*-null and *Enam*-null mice displayed a complete loss of enamel prisms similar to that of marked hypoplasia in humans (Wright *et al.,* 2009). The mandibular incisors in the *Amelx*-null and *Enam*-null mice lost the yellow-brown coloration typical of wild-type mice and displayed a rough aberrantly mineralised enamel surface. The AI associated enamel phenotypes in humans and mice appeared to differ depending on whether the mutation/ knockout involved the genes encoding ECM proteins (*Amelx* or *Enam*) or proteases (*Mmp-20* and *Klk-4*) (Wright *et al.,* 2009).

A recently reported novel ENU-induced *Amelx* N-terminal region mis-sense Y64H mutation (in the tri-tyrosl motif of amelogenin) led to enamel that was hypomineralised in the $Amelx^{Y/Y64H}$ male or severely hypoplastic in the $Amelx^{X/Y64H}$ and $Amelx^{Y64H/Y64H}$ female mutant mice (Barron *et al.,* 2010). The engorged endoplasmic reticulum/ golgi apparatus suggested intracellular retention of Y64H amelogenin (Barron *et al.,* 2010). The scarcity of the full-length Y64H amelogenin in the Y64H mutant ECM extracts suggested the failed secretion of amelogenin into the enamel ECM (Barron *et al.,* 2010). In contrast to previous reports (Lei *et al.,* 2001) there appeared to be no difference in Y64H amelogenin degradation rates, which eliminated the possibility of this amelogenin Y64H having an increased susceptibility to normal post secretory processing or enhanced sensitivity to extra-cellular proteolysis (Barron *et al.,* 2010).

Intracellular protein-protein interactions, mediated via the amelogenin tri-tyrosyl motif, were thought to be a key factor underpinning the molecular pathogenesis of AI (Barron *et al.,* 2010). However, amelogenin and ameloblastin were both shown to be accumulated in the ameloblasts of affected mice, which suggested a combination of the Y64H mutant amelogenin and ameloblastin proteins was a pathological factor. This may be related to amelogenin-ameloblastin interactions that result in protein complexes with conformational anomalies that can no longer be trafficked appropriately prior to secretion (Barron *et al.,* 2010).

Mice expressing a truncated ameloblastin share similar histopathological features to the Y64H amelogenin mutant mice (Fukumoto *et al.,* 2004; Wazen *et al.,* 2009), which suggested the *Amelx* mutant phenotype may be due in part to disturbances involving ameloblastin secretion and function (Barron *et al.,* 2010). Considering their relative abundances of amelogenin (95%) and ameloblastin (5%) in the ECM it is conceivable that their synthesis differs commensurately. Abnormal amelogenin-ameloblastin interactions may be only one part of the reason for impaired Y64H amelogenin secretion, and it is likely that other protein-protein interactions may also be affected, such as amelogenin-cytokeratin interactions (Barron *et al.,* 2010). The tri-tyrosyl motif binding to N-acetyl-D-glucosamine residues on cytokeratin 5 (Ravindranath *et al.,* 1999) and the N-acetyl-D-glucosamine mimicking sequence in cytokeratin 14 (Ravindranath *et al.,* 2003) suggests a possible role for cytokeratin 14 in chaperoning amelogenin during amelogenesis (Barron *et al.,* 2010). Therefore, it was also proposed that ameloblast cell binding, amelogenin chaperoning/ trafficking and secretion may have a causative role in the mechanism of dysplastic enamel formation in AI. Importantly the *Amelx* Y464H mutant mice provides an excellent model that phenocopy human X-linked AI.

2.9.2.2. Ameloblastin (Ambn):

Ameloblastin deficiency results in severe enamel hypoplasia in AIH1 in humans (Paine *et al.,* 2002) and transgenic mice that over express ameloblastin exhibit a similar defect (Paine *et al.,* 2003). Recently generated *Ambn* mutants that secreted a truncated ameloblastin protein failed to produce an enamel layer, which demonstrated that ameloblastin was essential during enamel formation (Smith *et al,* 2009c). These findings were consistent with the idea that part of the pathology involves cell adhesion and/ or loss of contact to the ECM (Fukyumoto *et al.,* 2004). Other loss of function models (e.g. ECM glycoproteins laminin and connexion) have shown aborted *secretory* and *maturation* stage enamel formation suggesting that the disruption of many cellular processes was more likely to be the cause of the enamel defects, rather than the absence of a single specific protein (Smith *et al.,* 2009c; Wazen *et al.,* 2009). Ameloblastin was originally thought to be an important determinant of tissue architecture (Brookes *et al.,* 2001) and has more recently been shown to maintain the differentiation state of secreting ameloblasts, control their secretion and have a significant role in cell adhesion (Fukumoto *et al.,* 2004). It has also been shown to interact with amelogenin (Ravindranath *et al.,* 2004) and share a common secretory pathway (Zalzal *et al.,* 2008). This has lead to the suggestion that amelobastin and amelogenin may be functionally dependent (Wazen *et al.,*

2009) and may have synergistic roles during enamel formation (Hatakeyama *et al.,* 2009; Smith *et al.,* 2009c).

2.9.2.3 Enamelin (Enam):

Mutations that disrupted the *maturation* stage removal of the ECM interfered with enamel hardening and resulted in soft/ hypomature forms of AI (Hu *et al.,* 1997, 2000). Several point mutations introduced into the *Enam* gene by ENU mutagenesis have shown enamelin to be crucial for the initiation of enamel crystal formation at the *pre-secretory* and *secretory* stages of amelogenesis (Masuya *et al.,* 2005; Seedorf *et al.,* 2007). Disrupted secretion interfered with crystal elongation (and enamel thickness) resulting in a rough and pitted enamel surface in the $Enam^{+/-}$ heterozygous mice and complete enamel agenesis in the *Enam*-null condition (Hu *et al.,* 2008). The enamel of the $Enam^{+/-}$ heterozyous mice was nearly normal in the maxillary incisors but the mandibular incisors were discoloured and wore rapidly at the incisal contact points. *Enam*-null mice do not make enamel because of a complete failure at the secretory surface mineralisation front of the ameloblast (Hu *et al.,* 2008). Enamelin gene mutations are the single most significant contributing factor to the aetiology of AI (Hu *et al.,* 2007).

The M100888 mis-sense mutation in *Enam* mice (Matsuya *et al.,* 2005) has recently been sequenced and shown to affect the 55th amino acid of the full-length enamelin peptide, changing a serine residue to an isoleucine (Dr. Martin Barron, unpublished personal communication). Therefore, there is a discrepancy depicted in figure 3. of Matsuya *et al.,* (2005) that shows the M100521 mutation as a serine to isoleucine change rather than the M1000395 mutation. The M100521 mutation actually affects the splice junction between exons 4 and 5, and the M1000395 depicted is actually the M100514 mutation (Dr. Martin Barron, unpublished personal communication).

2.10. SUMMARY

Looking forward to the present study, the purpose of this summary is to focus on the aforementioned methods that are most pertinent to the explicit investigation of odontogenesis, tooth morphogenesis and enamel mineralisation.

2.10.1. 2D Measurement Methods

The early manual contact methods, e.g. mechanical callipers, gave a lower reliability compared to the recent digital imaging methods. The later digital calliper methods were reported to be the gold standard for tooth measurement but were also cumbersome to operate. They did not benefit from the highly accurate landmark determination and repositioning of the 2D IAS that will be used in this study. The 2D IAS was simple to operate, required less instruction and could be used by untrained operators. The 2D IAS benefitted from automated technology that maximised reliability and precision. As a quantitative tool the 2D IAS succeeded as the gold standard and was proven to be an optimum technique for measuring human tooth dimensions. However, the 2D IAS was limited to 2D planar data analysis that reduced important 3D tooth morphology. This restricted measurement capacity and was a major limiting factor of all the 2D approaches. Nonetheless, the 2D IAS was the most reliable and precise 2D method. It was adaptable and offered the most modification potential for the small murine application.

2.10.2. 3D Measurement Methods

A wide variety of contemporary 3D methods recorded and measured dental morphology. The direct 3D methods were incomparable to modern 3D methods because they only described 2D planar analysis of 3D objects. The early 3D methods, e.g. the Symmetrograph and the Optocom, depended on mechanical contact that made them subjective and confounded by uncertainty. The direct methods showed high operator and systematic error compared to the indirect approaches. Human dental study model applications dominated the literature.

Technological advances resulted in a succession from the direct contact methods to the indirect non-contact 3D methods, e.g. the Reflex-Metrograph and the Travelling Microscope. The introduction of light projection, e.g. Moiré Contourography, represented the early use of

optical technology and the start of a transition towards the structured light methods. A range of 3D tools became increasingly available because of advances in computer technology, digital imaging devices, electro-optical components, laser and other light sources. These systems digitised the surface of dental casts into 3D models for measurement on a computer screen. The increasing economic availability of the structured light technologies made these techniques more accessible. Many indirect 3D methods were readily commercialised in dentistry and regarded as clinically acceptable alternatives to the conventional plaster model.

The optical principal of triangulation determined the 3D coordinates of the object surface as point cloud data that was transformed from a local to a global coordinate system when rendered into a 3D model by computer software. Three approaches to obtaining 360° 3D models predominated; (i) object rotation, (ii) sensor movement, and (iii) fixed imaging systems. Each had relative advantages and disadvantages, e.g. calibration and multi-view image combination errors. Also, the geometric data transformation was approached by several computer algorithms, again with advantages and disadvantages. The computer integration of the separate image capture, processing and storage steps was demonstrated by many examples, and the most progress towards a fully automated and fast multi-view image combination method was exemplified by the rotary table instrument. Software and hardware developments improved the speed and measurement capacities of many of the most recent 3D methods to provide previously inaccessible data, e.g. Computer Tomography. The majority of the commercially available dental systems were only suitable for assessing the human dentition using dental study models. The laser methods did not provide sufficiently high accuracy or high resolution necessary for a small murine tooth application.

A compromise between resolution and versatility, and the balance between cost and speed was evidently a limitation to the 3D optical technology, e.g. increased accuracy and resolution required long processing durations. However, an expanding market provided increased consumer choice and newly available software became increasingly accurate and reliable.

The structured light techniques were limited by the use of specific calibration surfaces that meant that differences between the calibration and the tooth surface were proportional to the measurement accuracy. In many cases this was too large to accurately assess the small mouse incisor. Light scatter at the surface of reflective materials, e.g. mineralised tissues like

enamel, was also a big disadvantage because it caused areas of missing data, incomplete images or 3D models with holes. This problem occurred because of optical heterogeneity, variations in albedo or weak laser light reflection. Although this was minimised when studying uniform materials like dental plaster or die stone, the optical properties of tooth enamel and dentine allowed light to penetrate the surface layer, scatter back to the sensor and produce an irregular source of systematic error that was difficult to quantify. Algorithms for closing holes in complex morphology exist but may introduce artifice. This was prohibitive and compromised the accurate representation of tooth morphology, even at high resolution. Therefore, the laser methods could not provide the precision required for imaging dental tissues at the small murine scale and were unsuitable for studying the macro-structure and micro-surface morphology of mice teeth and the mineralised tissues.

Of the structured light techniques only the NCSP chromatic sensor was suitable for imaging all types of materials and surfaces (transparent or opaque, specular or diffuse, glossy or mat). The NCSP obtained enamel surface structural information, regardless of ambient illumination or heterogeneous reflectivity in enamel demineralisation, remineralisation, abrasion and attrition studies. The chromatic confocal sensor delivered spatio-chromatic filter high sub-micron resolution Z-coordinate data through modular optics that will be tailored to suit the specifications of the application. The X and Y coordinate data collection was automated by a precise CMM movable platform that had potential for hardware modification.

Thus, an economical and practical approach to the small murine application would be to modify the NCSP CMM platform with a rotary stage, in a similar manner to those previously described for the rotary table. This would adapt the instrument to acquire multiple multi-view 3D images within an established coordinate system and to reconstruct complete 360° 3D models. Although there were limitations to the multi-view image combination methods, the increasingly powerful array of commercial 3D modelling software available could be used to combine the multi-view images and create a new indexing method that would contribute to the future of 3D imaging technology. This modification would introduce a new method of 360° surface metrology able to resolve enamel surface structure at a competitive resolution of 1.0μm. A novel NCSP technique would fall between the discriminating power of the laser scanning, confocal microscopy, CT, XMT, μCT and nano-CT techniques to give excellent relative economy. Unlike the other methods, the NCSP could enable a practical solution to facilitate both the macro-metric and micro-metric investigation of the small murine incisor.

2.10.3. Colour and Whiteness Assessment

With the exception of the digital techniques, the colour and whiteness methods reviewed were not compatible with the CIE colour space model. They were subjective with limited repeatability, showed operator and systematic errors, and had other inconsistencies that were difficult to manage and quantify. In particular, the sectrophotometers and colourimeters were designed for contact on flat surfaces and had many disadvantages that compounded errors making them unsuitable for investigating the curved morphology of the mouse incisor. On the other hand, the 2D IAS method was successfully standardised for CIE colour space (in humans) and could be appropriately modified for the murine application. It quantified enamel phenotypes in measures that were translated to humans.

The distinct anatomical thirds used to assess human incisors were identified in the *gingival*, *middle* and *incisal* regions of the hypsledont murine incisor that correspond to the *pre-secretory*, *secretory* and *mature* histological/ development stages of enamel formation. Therefore, it is hoped that by quantifying enamel surface mineralisation in terms of colour and whiteness at the phenotype level (both overall and separately in these specific regions) it will be possible to attribute the contributions of the important ECM proteins to the specific stages of amelogenesis.

2.10.4. 2D and 3D Morphometric Measurement Systems

The 2D and 3D systems were of variable efficiency and practicality. They offered a highly informative means of documenting mouse mandible and incisor phenotypes for systematic morphometric research. The impact of computerised methods has had economical and storage benefits; recording, archiving and database management made access, communication and data analysis more convenient.

A great variety of 2D and 3D methods have been discussed to examine human and mouse dental morphology. The techniques have significantly improved over the decades and the ever increasing capabilities of 2D digital photography and 3D modelling have facilitated expedient image analysis methods in dental research. Further modifications for the murine application will realise the potential for a sophisticated and objective phenotype to genotype investigative tool that can be readily applied to the mouse model.

The extensive use of the mouse model in morphometric studies has led to a better understanding of the genetic basis of dental development. Investigating developmental anomalies will continue to be important to understand normal and abnormal enamel mineralisation. The application of a 2D IAS will provide a robust and reliable means to assess the involvement of the ECM proteins in the skeletogenesis of hemi-mandibles and in odontogenesis of mandibular incisors. Accurately quantifying the morphometric variation of the observable phenotypes by the modified methods (detailed in the following sections) will enhance our knowledge of the processes by which underlying gene mutations have their affect.

The customised 2D IAS and novel 3D IAS will define previously inaccessible measurement parameters making more information available for phenotype comparisons. This new range of measurements will extend the versatility of the systems and provide further possibilities for exploring phenotype variation. A more complete quantification of dental morphology could be demonstrated by other new variables, e.g. *surface-area* and *volume*, and will give a new handle on comparative analysis of biological variation and development, e.g. the conventional projected straight line measurements between two landmarks (as in the 2D IAS) could be extended to include actual on-surface dimensional measurements. The actual measurement will follow the 3D curvature of the tooth structure to take account of the enamel surface contours for a more meaningful quantitative evaluation of tooth morphology. The 3D method will assess the macro-metric gross structure and micro-metric surface topography of enamel to provide a more sophisticated 3D tool that will interrogate tooth morphogenesis and enamel mineralisation.

2.10.5. Tooth Development and The Mammalian Model

In contrast to human teeth murine incisors are an excellent location to observe the dynamic process of enamel formation and tooth morphogenesis because they form and erupt continuously throughout life and offer access to all stages of enamel development in a single tooth. Thus far, they have been instrumental in understanding the roles of specific genes and proteins during amelogenesis. Early dental development models were useful in describing the patterns of variation observed within the dentition. However, more recent molecular studies have identified the underlying molecular mechanisms (in terms of differential gene expression) and have delineated the strict regulatory pathways that orchestrate the diverse

cellular and extra-cellular processes of oro-facial development conserved in humans and in mice. The three developmental models (Field, Clone and Molecular) may be incorporated into a unified explanatory model for craniofacial development that is complementary.

As the process of odontogenesis progresses the tooth changes into a complete organ consisting of different mineralised and un-mineralised tissues that each contribute to the form and function of the tooth. The reciprocal reiterative and conserved nature of signalling pathways suggests the affect of a single gene mutation can influence the complex interaction of various tissues and cannot be considered in isolation. The need for detailed phenotyping/ morphometric analysis, not just of the teeth known to be directly affected but also the associated structures, e.g. the mandible, would benefit from being documented and may provide a deeper insight into/ understanding of the pleiotropic affects of specific mutations on abnormal development. The current investigation may substantiate a morphometric link between the known disruptions to ECM proteins responsible for enamel defects and skeletal development in the mandible.

2.10.6. Mineralisation and The Predominant ECM Proteins

The importance of the ECM proteins in the mineralisation of enamel defects, e.g. AI, has been well established and increasingly characterised. Numerous clinically defined phenotypes have been described and have indentified various gene mutations in specific homologous domains of the predominant ECM proteins amelogenin and enamelin. It is thought that only 25% of mutations (and associated defects) have been described and the various mechanisms that cause abnormal enamel formation require further elucidation. The interactions of the diverse families of amelogenin and non-amelogenin proteins that orchestrate the formation of the enamel ECM have shown spatially and temporally restricted expression during amelogenesis. The functional significance of this distribution is not fully understood, e.g. there is evidence for multiple roles of amelogenin isoforms with different functions, both before the initiation of tooth formation and in bone formation. This has superseded the once held view of amelogenin functioning specifically as a protein that regulates size, shape and directional growth of organic mineral crystals. Amelogenin is now thought to be a multifunctional protein.

2.10.7. Phenotyping Murine Models of *Amelogenesis imperfecta*

Depending on the type and loci of the different *Amelx* and *Enam* gene mutations, post-translational modification and alternative splicing, a diverse set of protein degradation products are seen. Their cellular distribution patterns are reflected in the mineralisation process thought to be responsible for the range of AI phenotypes, from smooth hypoplastic to hypomineralised/ hypomaturation forms. This highly overlapping spectrum of enamel phenotypes is not surprising given that amelogenin and enamelin have been shown to be involved in the critical pathways related to the secretion and organisation of developing enamel. Different mutant mice groups have already been used to explore the abnormal function of proteins and the causes of the considerable phenotypic variation within and between individuals with AI. Importantly, this overlapping range of phenotypes provides a permanent record of odontogenesis and is an excellent case in which to employ a phenotype-genotype driven approach. Also, to better understand the aetiological roles of amelogenin and enamelin in determining the macro-metric and micro-metric tooth morphology and enamel mineralisation phenotypes indicative of AI.

Contrasting the human and mouse enamel pathologies has shown similarities and differences for several reasons that can be related to the complete loss of protein function in the mouse model compared to the more subtly altered protein function in humans. Therefore, although the experimental model may not fully recapitulate the functional range of AI associated human gene mutations, because of the more diverse genetic background of the human population (not to mention epigenetic interactions), this method of targeted gene exploration has proven to be the most readily available resource and amenable means of characterising protein function. This ability to manipulate murine models has provided a wealth of information thus far, e.g. the amelogenin mouse effectively combines the various AI phenotypes into a single model, and by continuing to characterise the variability and diversity exhibited by AI, through revealing the observable phenotype-genotype relationship, it will be possible to further the understanding of disease pathologies.

There were no known reports in the literature of any detailed 2D or 3D macro-structural investigations of the mouse model for dental anomalies. Also there were no known occurrences of 2D colour and whiteness assessment in the mouse model and/ or 3D quantitative assessment of the phenotype variation of mouse incisors. Therefore, a vacancy exists for a holistic investigation into murine dental phenotyping that could benefit from the

significant impetus for objective and automated biological measurement. The aim of the current study is to provide a complementary macro-metric and micro-metric means of identifying dysmorphologies and quantitatively characterising homologous mandible and incisor craniofacial features that represent a complex developmental module and a site of continuous enamel formation respectively.

The *Amelx* (OMIM300391) and *Enam* (OMIM606585) mutants represent excellent models for investigating the roles of the specific amelogenin and enamelin ECM proteins respectively. Accurate examination of phenocopy mouse models - via four *Amelx* genotypes (*Amelx*^{WT}, *Amelx*$^{X/Y64H}$, *Amelx*$^{Y/Y64H}$ and *Amelx*$^{Y64H/Y64H}$) and three *Enam* genotypes (*Enam*^{WT}, *Enam*^{Rgsc395} *homozygous* and *Enam*^{Rgsc395} *heterozygous*) - gives the opportunity to differentiate between the phenotypes of the wild-type controls and of their specific mutant littermates. Using newly developed 2D and 3D morphometric methods and colour and whiteness assessment it will be possible to distinguish between the wild-type and pheno-deviant mice and to elucidate any affect of the specific gene mutations. The colour and whiteness assessment will illustrate the lack of demarcation between overlapping phenotypes and provide a quantitative means for delineating the different lesions and aberrations in enamel mineralisation. In fact, dissecting out the specific affects of these genetic mutations using regional colour and whiteness assessment may identify and isolate disruptions in a developmental stage specific manner and offer an unparalleled contribution to phenotype-genotype correlations.

Clearer phenotyping of AI phenocopy mice will explicate a deeper understanding of the multifactorial growth and development of the oro-facial features and of the aetiology of enamel mineralisation defects.

3. AIMS AND NULL HYPOTHESES

3.1. AIMS

i. To develop four novel measurement methods; (i) a 2D image analysis system (IAS) to measure murine mandible morphology, (ii) incisor morphology and (iii) incisor enamel colour and whiteness, and (iv) a 3D IAS to measure incisor morphology and enamel surface structure.

ii. To define a novel repertoire of morphometric variables for each new method.

iii. To determine the reliability and validate the new measurement methods and morphometric variables in a homogenous mouse population.

iv. To use the new measurement methods to characterise the phenotype of mouse mandibles, incisors and enamel mineralisation in a heterogeneous experimental population.

v. To use two separate experimental mutant populations with specific gene mutations in the amelogenin (*Amelx*, OMIM 300391) and enamelin (*Enam*, OMIM606585) proteins as models of X-linked *Amelogenesis imperfecta* (AIH1, OMIM301200) and autosomal dominant local hypoplastic *Amelogenesis imperfecta* (AIH2, OMIM104500) respectively.

vi. To use the wild-type genotype groups as a control and as a baseline for comparison with their respective mutant littermate genotype groups.

vii. To demonstrate phenotype variation between the genotype groups in terms of significantly different morphometric variables.

viii. To investigate the effect of the amelogenin and enamelin proteins on mandibular development, tooth morphology and enamel mineralisation.

ix. To differentiate between overlapping phenotypes.

3.2. NULL HYPOTHESES

i. The 2D IAS will not be reliable.

ii. The colour and whiteness assessment will not be reliable.

iii. The 3D IAS will not be reliable.

iv. The 3D IAS will not be valid.

v. The mandible and incisor morphometry, and colour and whiteness assessment will not quantify phenotype.

vi. The mandible and incisor morphology will not represent enamel quantity, growth and development.

vii. The colour and whiteness assessment and 3D surface analysis will not represent enamel quality and mineralisation.

viii. The control and mutant groups will not show evidence of statistically significant phenotype variation.

ix. There will be no significant differences in the mandible dimensions between wild-type and mutant populations.

x. There will be no significant differences in the incisor dimensions between wild-type and mutant populations.

xi. There will be no significant differences in the enamel phenotype between wild-type and mutant populations.

xii. The *Amelx* mutants will not display hypoplastic/ hypomineralised enamel indicative of X-linked AI (AIH1,OMIM301200).

xiii. The *Enam* mutants will not display local hypoplastic enamel indicative of autosomal dominant AI (AIH2, OMIM104500).

4. MATERIALS AND METHODS

4.1. INTRODUCTION

The study sample mice were supplied by The Medical School at The University of Liverpool and by The Dental School at The University of Manchester as part of the collaborative Wellcome Trust programme. The study used one reliability population (n = 20) and one experimental population (n = 35), which itself contained two separate populations; (i) *Amelx* and (ii) *Enam* containing respective wild-type control groups and multiple mutant genotype groups. The experimental group contained recently sequenced gene mutations (Matsuya *et al.,* 2005; Barron *et al.,* 2010). Each of the seven groups contained five individuals. Both the left and right side hemi-mandibles and mandibular incisors were imaged from buccal, lingual and labial aspects (views).

A number of novel hardware and software developments are included here as part of the method development - this involved significant personal input, internal departmental development and inter-disciplinary collaborations. An established 2D IAS was modified with a macro-lens for imaging the mouse dentition. A bespoke colour and whiteness algorithm was developed internally by customising industry standard imaging software for a new approach to the mouse application. The new techniques utilised existing measurement parameters and determined novel morphometric variables for phenotype assessment.

The 3D IAS was an entirely new concept that drew from the technological advances and innovations documented in the recent literature. A novel rotary stage was designed and developed as a modification to a non-contact surface profilometer (NCSP) measurement device that was made available through institutional collaboration. The rotary stage was a removable adaptation fabricated by industrial partners. The NCSP device was adapted to obtain multiple 3D images from multiple angles in 360°. This new system introduced a novel method of multiple-image combination by image indexing, which employed powerful 3D computer aided design software to construct the 3D models. Further collaborative development of bespoke 3D analytical software innovatively expanded the 3D measurement repertoire of the system.

The 3D IAS represents an original approach to 3D imaging of small mouse teeth that would not have been possible without the multi-disciplinary specialities of an extensive collaborative network.

4.2. STUDY SAMPLE

Ethical approval was granted according to the Wellcome Trust programme ethics reference number 06/Q0104/38. Laboratory mice were euthanized using Home Office approved methods according to Chapter 14 of The Animal (*Scientific Procedures*) Act 1986 (www.archive.official-documents.co.uk/document/hoc/321/321-xa.htm).

4.2.1. Criteria for Inclusion

Mouse oral cavities were examined with a dissection microscope (Bresser, Meade Instruments Corp, California, USA) according to protocols outlined in the 'Phenotyping of mouse oral cavity - primary first line and primary extended' standard operating procedure obtained from the European Mouse Phenotyping Resource of Standardised Screens website (www.empress.har.mrc.ac.uk) (Green *et al.*, 2005). Any mice identified with uncharacteristic anatomical malformations were not included in the study sample. Mice were recorded on a Mouse Dental Anomalies Record Form (www.eumorphia.org) (Brown *et al.*, 2008). Any hemi-mandibles or mandibular incisors (specimens) damaged during extraction were not included in the study sample.

4.2.2. Reliability Population

The reliability population was a genetically homogenous inbred multi-purpose strain of Charles River CD-1™ (Charles River Inc., MA, USA) wild-type mice ($n = 20$) obtained from the Medical School Animal House at The University of Liverpool, UK.

A mixed sex population of 20 mice (10 females and 10 males) was euthanized by CO_2 asphyxiation at 3 months (90 days) of age. The mice were decapitated using a laboratory animal guillotine and frozen by Animal House staff according to local protocols. The mice were thawed in a fridge 24 hours before collection. The mice were sexually and skeletally mature. No gross phenotypic variation or sexual dimorphism was evident.

4.2.3. Experimental Population

Two experimental populations (i) *Amelx* and (ii) *Enam* were obtained from RIKEN GSC (Wako, Tokyo, Japan) by Prof. Mike Dixon's Laboratory, School of Dentistry, The University of Manchester, UK. Breeding colonies were established and maintained on a DBA/2J genetic background by Ms. Charlotte Hunt and Dr. Martin Barron, School of Dentistry, The University of Manchester, UK.

The populations were congenic Dilute Brown Agouti strain mice. The separate M100800 (*Amelx*) and M100395 (*Enam*) populations had mutations in their amelogenin gene and enamelin gene respectively. The mutant mice were generated during large-scale ENU mutagenesis (www.brc.riken.jp/lab/gsc/mouse/). The mutations were human orthologues of the *AMELX* gene (OMIM300391) and *ENAM* gene (OMIM606585).

The M100800 mutation in the *Amelx* mice affected the 64th amino acid of the full-length amelogenin peptide, changing a Tyrosine residue to a Histidine residue and resulting in a mis-sense mutation Y64H (Mouse Genome Informatics Accession ID: 3807977). The only difference found between the wild-type (n = 160) littermates and affected male (n = 72) and female (n = 54) mice analysed was a T to C transition at nucleotide 249 of the *Amelx* coding sequence (Barron *et al.,* 2010). This mutation lies within the conserved tri-tyrosyl motif (PYPSYGYEPMGGW) of amelogenin positioned towards the C-terminus of the tyrosine-rich peptide (TRAP) domain (Barron *et al.,* 2010).

The M100395 mutation in the *Enam* mice affected the 55th amino acid of the full-length enamelin peptide, changing a Serine residue to an Isoleucine residue and resulting in a mis-sense mutation p.S55I (Mouse Genome Informatics Accession ID: 3055582). There was a discrepancy as to which amino acid was affected in Figure 3. of the Masuya *et al.,* (2005) paper. The M100521 mutation actually affected the splice junction between exons 4 and 5 (Dr. Martin Barron, unpublished personal communication). The M1000395 depicted was actually the M100514 mutation (Dr. Martin Barron, unpublished personal communication).

The two separate experimental populations (i) *Amelx* and (ii) *Enam* each contained one wild-type control group and multiple mutant genotype groups. The different genotype groups were defined by the inheritance patterns of the individuals within the group.

Each group contained five individual mice.

The *Amelx* population consisted of four genotype groups;

(i) *wild-type* $Amelx^{WT}$ males ($n = 4$) and female ($n = 1$)

(ii) *heterozygous* $Amelx^{X/Y64H}$ females ($n = 5$)

(iii) *hemizygous* $Amelx^{Y/Y64H}$ males ($n = 5$)

(iv) *homozygous* $Amelx^{Y64H/Y64H}$ females ($n = 5$)

The *Enam* population consisted of three genotype groups;

(i) *wild-type* $Enam^{WT}$ males ($n = 2$) and females ($n = 3$)

(ii) *heterozygous* $Enam^{Rgsc395}$ males ($n = 2$) and $Enam^{Rgsc395}$ females ($n = 3$)

(iii) *homozygous* $Enam^{Rgsc395}$ males ($n = 2$) and females ($n = 3$)

There were therefore 20 *Amelx* mice and 15 *Enam* mice. The wild-type mice were unaffected littermate controls. The wild-types were used as a baseline for data comparison.

4.2.4. Animal Husbandry (Prof. Dixon's Laboratory)

All experimental animals were maintained under strict uniform conditions (12 hour light/dark cycle, 22 ± 1 °C ambient room temperature at 60% relative humidity). Mice were fed on a pellet diet (ID#801722 CRM P, Special Diets Service, Essex, UK) that was crushed to a powder. Food and water was available *ad libitum*.

New-born mice were left with their mothers for 21 days and weaned thereafter. Adult female and male mice were separated and housed in same sex cages containing a maximum of 5 mice per cage. Mice were inspected daily and their bedding changed as necessary. All mice were euthanized by cervical dislocation at 3 months (90 days) when the mice were sexually and skeletally mature. Mice were age and weight matched, within and between the genotype groups. No gross phenotypic variation or sexual dimorphism was evident.

4.2.5. Storage and Preparation

All mice were studied as part of an experimental continuum taking place at different institutions (and locations). Due consideration for the various investigations dictated that the

mice were not treated with or exposed to any interferential methods or chemicals, e.g. boiling (Bader, 1965), ethanol fixation (Moinichen *et al.,* 1996), enzymatic digestion (Luther, 1949; Gruneburg, 1951) or skeletonisation by insects (Atchley *et al.,* 1985) were all prohibited.

The most suitable and effective method of preservation during transport was determined by piloting the effects on six specimens, two under each of the following conditions: (i) freeze drying with CO_2 dry-ice; (ii) air drying at room temperature; (iii) preservation in 10% neutral buffered formalin.

The freeze dried specimens were very dehydrated. The surrounding tissues were brittle and flaky/ powdered, and fixed hard to the hemi-mandible. The air dried specimens were also dehydrated but less than when freeze dried. The surrounding tissues were also fixed to the hemi-mandible but less so than when freeze dried. For both the freeze dried and air dried specimens the surrounding tissues were difficult to remove while preparing for imaging.

The 10% neutral buffered Formalin was most suitable transport method because the surrounding tissues were hydrated and removed without difficulty. There were no discernible adverse affects on the gross morphology, colour or phenotype of any specimens.

All specimens used for imaging were stored in $1.5ml^3$ eppendorfs (Eppendorf AG, Hamburg, Germany) in a freezer at -80.0°C after micro-dissection and imaging.

4.2.6. Micro-dissection/ Extraction

Mouse heads arrived in 10% neutral buffered formalin in $50ml^3$ centrifuge tubes. Specimens were repeatedly washed with Phosphate Buffer Solution and distilled water to remove the Formalin. This was carried out under a Fume Cupboard (Holliday Fielding Hocking Ltd, Leeds, UK) according to local protocols because of the carcinogenicity of Formalin.

The hemi-mandible and incisor specimens were extracted in sequence using a pair of tweezers (Swann-Morton, Sheffield UK) and a size 11 surgical blade scalpel (Swann-Morton, Sheffield, UK), in a petri-dish (Barloworld Scientific, Stone, UK) under a dissection microscope (Bresser, Meade Instruments Corp, California, USA) at X1.5 magnification.

Gross dissection of hemi-mandibles removed the skin, attached muscle, ligament and surrounding tissues. Hemi-mandibles were divided at the mandibular symphysis by scalpel incision. Each hemi-mandible was excised separately. Fine dissection prevented damage to the fragile coronoid and other anatomical features that were relatively weak amongst the strong surrounding tissues.

Mandibular incisors were extracted after the hemi-mandibles had been imaged. The supporting bone was progressively removed from around the incisor, from the distal-tip towards the proximal-end. The structural integrity of the incisor was strong at the hard mineralised distal-tip and weak at the soft and vascularised proximal-end. Care was taken to avoid damage or removal of any surface enamel.

All unwanted animal tissues were autoclaved and incinerated according to local protocols. The mouse heads were returned to and stored in the original $50ml^2$ centrifuge bottles in 10% neutral buffered formalin. Specimens used for imaging were stored at -80.0°C.

4.3. 2D IMAGE ANALYSIS SYSTEM

The 2D Image Analysis System (IAS) used for digital imaging and measurement (Brook *et al.*, 2005a, 2005b) was modified with a macro-lens for murine specimen imaging (Figure 7.).

Figure 7. The 2D Image Analysis System

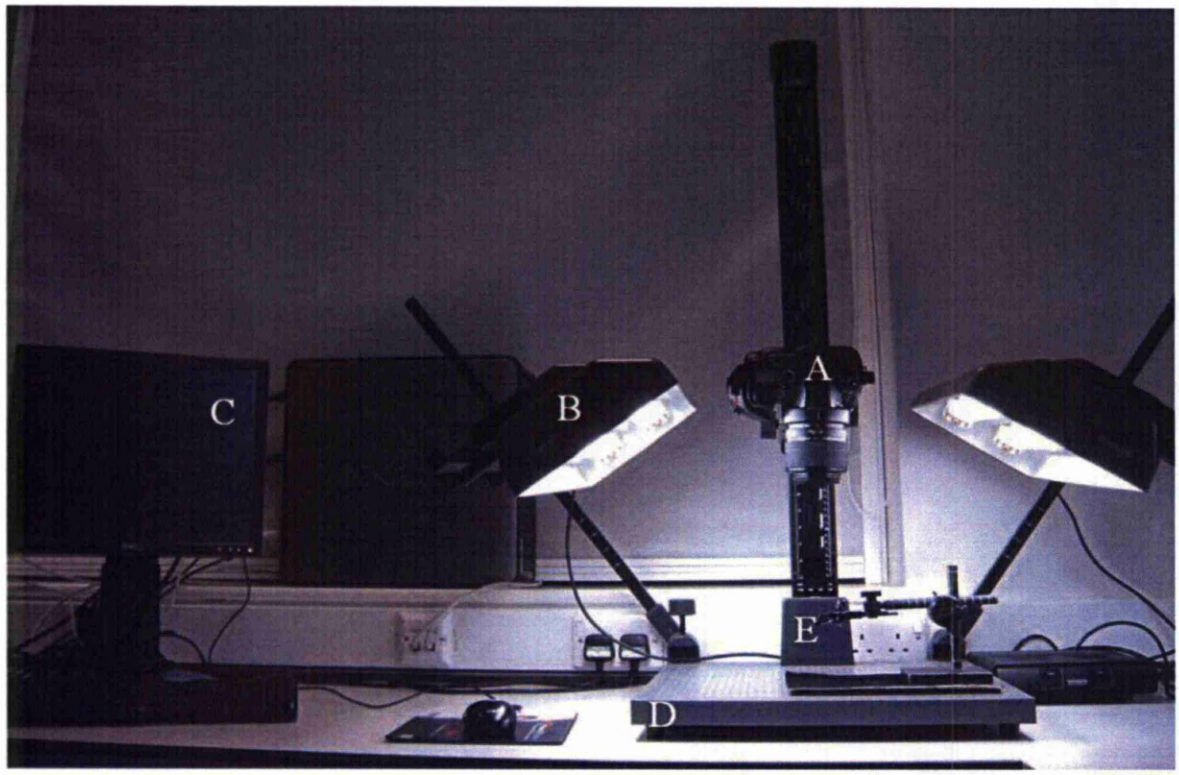

(A) camera and macro-lens; (B) lights; (C) desktop PC; (D) photographic stand; (E) customised tooth holder.

The system was composed of a desktop PC, digital camera, photographic stand and lights. It was operated under standardised conditions of magnification, orientation and illumination.

4.3.1. Personal Computer

The desktop Personal Computer (PC) was a Dell Optiplex620 (Dell Inc, Texas, USA) - Intel® Pentium® 4, 3.40GHz Computer Processing Unit - with 2MB (mega bytes) of RAM (random access memory) and a 250.0GB (giga byte) hard-drive running on the Microsoft Windows XP Professional 2002 SP2 platform (Microsoft Corp, New Mexico, USA). The 19 inch monitor was 32-Bit true-colour with a 1280 X 1024 pixel resolution.

To maximise the efficiency of large file transfer the camera and PC were connected by high speed IEEE 1394 Fire Wire (Belkin International Inc., California, USA). Image files were saved directly to the PC.

4.3.2. Digital Camera

The digital camera was a 13.5 mega pixel Kodak DCS Pro Single Lens Reflex/c (Eastman Kodak Company, Geneva, Switzerland). The camera utilised single lens reflex technology with a system of semi-automatic and moving mirrors so that exactly what was seen through the viewfinder, in the field of view (FOV), was captured in the 2D image. The viewfinder incorporated an eyepiece dioptre that was adjusted to suit each operator's individual eyesight.

The camera contained a photosensitive charge-coupled device (CCD) sensor that converted analogue images into electric signals to produce high resolution (13.5 mega pixel) digital photographs. A 2D image file size was 39.0MB; 13MB per Red, Green and Blue colour channels (RGB). Images were 32-Bit high quality true colour images displayed in an array of 4500 X 3000 pixels.

The camera operating system was the Kodak Professional DCS Firmware version 5.4.1 software. The camera contained a SanDisk (SanDisk Corp, California, USA) Ultra® II Compact Flash 2.0GB memory card.

The camera was operated in manual focus and exposure modes. This was the most versatile means of imaging.

4.3.3. Macro-Lens

The camera was fitted with a Macro Photo Lens MP-E65mm F2.8 1-5X (Sigma Corp, Kanagawa, Japan). The macro-lens facilitated small object imaging by maximising the proximity of the specimen in the FOV. The macro-lens was fitted with an ultra violet (UV) polarising filter during colour and whiteness imaging.

The macro-lens magnification was fixed at X2 and X3 during the morphometric and colour and whiteness imaging respectively. This allowed the FOV to be fully utilised.

4.3.4. Photographic Stand

The camera was mounted vertically onto a photographic copy stand (Kaiser, Odenwald, Germany), aligned perpendicular to the plane of the specimen. This stand was robust and provided stability for long exposures. It had a scale for precise specimen alignment and realignment for consistency, standardisation and reliability.

4.3.4.1. Vertical Height:

The vertical height was determined by the vertical graduated scale between 0.0-50.0cm. It was manually adjusted by a hand cranked rotary arm. This method varied the distance between the camera and the specimens. It was used to focus the camera at a fixed magnification.

4.3.5. Camera Settings

4.3.5.1. Aperture size:

The macro-lens aperture was minimum *f*2.8 and maximum *f16*. An aperture of *f16* was used for morphometric imaging and colour and whiteness assessment to maximise the photographic depth of field (DOF). This gave a greatest distance from the plane of focus in which the image remained sharp, both in front and behind the specimen.

4.3.5.2. Shutter Speed:

The shutter speed was between maximum 1 and minimum 1/1000 seconds. The aperture size and shutter speed were balanced to give an optimum overall exposure that provided the greatest amount of light and DOF. A fast shutter speed (¼ second) was used for morphometric imaging. A slow shutter speed (3.2 seconds) was used for colour and whiteness assessment as less light and a larger DOF were determining factors. The settings minimised the possible effect of camera shake.

4.3.5.3. International Organisation for Standardisation (ISO) Sensitivity:

The ISO sensitivity of a digital camera relates to the original photographic film-speed rating - a measure of light sensitivity of photographic film. The digital equivalent equates to the CCD sensor sensitivity and accounts for sensor noise and lighting conditions. On the ISO scale, between minimum 0 and maximum 1200, daylight = 100 ISO. An ISO of 160 was used throughout as the stability of the photographic stand allowed an optimum balance of image quality.

4.3.5.4. Magnification:

Magnification was fixed at X2 and X3 during the morphometric and colour and whiteness imaging respectively.

4.3.6. Imaging Background

Specimens were positioned on a black mat velvet background that lay flat on the photographic stand base during imaging sessions. Therefore, specimens were readily distinguished from the background. This benefitted objective morphometric measurement, particularly *perimeter* and *surface-area* variables. It also reduced light reflection and was kept free of dust by using a compressed air canister (Dust Off, Falcon Safety products, New Jersey, USA). During colour and whiteness assessment, the incisor perimeter was easily objectively selected against the black background.

4.3.7. Illumination

Illumination was provided by two horizontal fluorescent lights containing D60 daylight bulbs (Osram, Munich, Germany). They were colour 12 with a reproduction index of 90-100. The conditions were designed to replicate average middle of the day ambient sunlight (Guan *et al.*, 2005; Smith *et al.*, 2008a). The light intensity was set to level 4, between minimum 0 and maximum 8.

The photographic stand provided further means to control the lighting. The diagonal height position of each light was determined by their distance from the specimen, on a scale of 1-17 inches (minimum = 1, maximum = 17). The lights were set to 6 inches. This was important because UV radiation emits heat. Illumination was monitored for heat effects.

Also, each light could be adjusted in multiple directions providing additional ways of controlling light intensity and direction. The diagonal angle of each light was set to ±45° to the vertical.

The lights were fitted with removable polarising sheets to give non-polarised and polarised illumination during the colour and whiteness imaging. All other settings were the same for morphometric and colour and whiteness imaging.

4.3.8. Calibration

A 10.0mm scale (Minitool Inc, California, USA), with 0.1mm divisions, was included in all morphometric images for calibration. Each separate image was individually calibrated using a linear scale.

Each colour and whiteness image was individually calibrated against a British Ceramic Research Association white tile that was captured at the start of each imaging session.

4.3.9. Image Capture

All 2D images were acquired using host software Kodak Professional DCS Camera Manager Version 4.2 (Eastman Kodak Company, Geneva, Switzerland). This permitted the operators to control the camera settings and various imaging parameters through the PC. The images were captured by clicking 'Take Image' in the host software, rather than directly through the photographic equipment. This minimised physical interference with the assembly, i.e. from camera shake, and also minimised error and maximised exposure possibilities, i.e. slow shutter speed. The camera settings were adjusted in the 'Camera Properties' tab. The camera time and date settings were 'synchronised to the computer'.

All images were previewed and examined using Kodak Photo Desk Version 4.3 software (Eastman Kodak Company, Geneva, Switzerland). The images were checked and could be discarded and repeated if necessary, e.g. if the exposure and/ or focus were unacceptable.

During imaging the hemi-mandible and incisor specimens were removed from storage in $1.5ml^2$ eppendorfs where they were kept on dry ice in an insulated polystyrene box. Once a

specimen was in position on the background, only the camera vertical height was adjusted for focusing. Image capture took 30 seconds per incisor. Maintaining uniform conditions of temperature and hydration minimised any possibility of fluctuations that could affect size and or colour. Effort was made throughout to minimise experimental error.

4.3.10. File Format and Saving

The 2D image files were automatically saved to the PC in 'raw' .DCR file format. These files contained unprocessed/ uncompressed data from the CCD sensor. The .DCR files were converted into the more common versatile Tagged Image File Format (TIFF) using the Photo Desk software. The DCR and TIFF file formats were typically 12.0MB and 39.0MB in size respectively. Filenames were determined and root directories selected in the 'Capture Session' tab.

No image compression or colour adjustment was required during the imaging process. This prevented data loss and did not compromise quality or quantity of information/ detail.

4.4. 2D MORPHOMETRIC MEASUREMENT

The 2D morphometric measurements were obtained using Image Pro Plus (IPP) software version 5.1 (Media Cyberenetics Inc, Maryland, USA). In the 2D IAS the linear measurements represented projected flat surface distances between two points, rather than the actual 3D measurements that followed the 3D contour of the tooth surface in the 3D IAS.

To open a 2D image (.TIFF file) the 'File' dropdown menu and 'Open' commands were used to select a file from the Microsoft Windows Explorer (Microsoft Corp, New Mexico, USA) directory. Open files were viewed by selecting the '3000 X 4500 resolution' option in the 'File Load Option' dialogue box.

4.4.1. 2D Measurement Procedure

Hemi-mandibles and incisors were carefully orientated during 2D imaging by positioning the measurement markers on the different anatomical landmark features. A 'local zoom' function (200%) enhanced the precise positioning of the measurement markers, the function of the measurement tools and the calibration procedure. The local zoom function contributed to minimising operator measurement errors, and increased operator reliability and consistency.

Using the IPP dropdown menu, the 'Measure', 'Calibration' and 'Spatial Calibration Wizard' options were selected to calibrate each image separately. In the 'create spatial calibration' dialogue box 'active' images were calibrated in mm units using the 'spatial reference' (Figure 8.).

Figure 8. 2D Morphometric Image Calibration

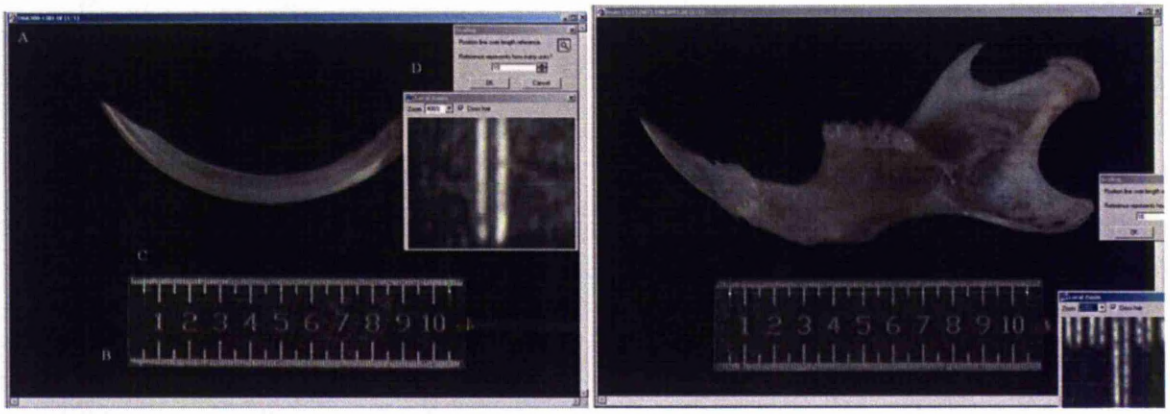

(A) 2D image .TIFF file; (B) 10.0mm linear scale; (C) scaling reference line (green line); (D) local zoom (200%). A calibration report for each image indicated an average calibration was 0.004105 μm/pixel.

The individual calibration of each image allowed for any magnification or focus variation between the images. The precision of the calibration procedure was improved and the potential error minimised when aligning the scaling reference line and linear scale with the 'local zoom' tool.

The following steps were used to obtain the 2D measurements. In the IPP dropdown menu, the 'Measure' and 'Measurements…' options were selected. The measurement markers were placed using the 'click and drag' features, in the 'Measurement' dialogue box. The cursor was used to position the markers on the specific anatomical landmarks. When the cursor moved over an existing marker it changed colour which aided repeatable landmark positioning for the different measurement variables.

4.4.2. 2D Mandible Measurements

The following eight measurements were obtained from 2D images taken from the buccal and lingual view (total = 16 variables), for both the left and right side hemi-mandibles; *overall-length* (mm); *ascending-height* (mm); *basal-length* (mm); *mandible-angle* (°); *coronoid-condyle-length* (mm); *diagonal-length* (mm); *mandible-area* (mm^2); *mandible-perimeter* (mm) (Figure 9.).

Figure 9. Mandible Morphometric Variables

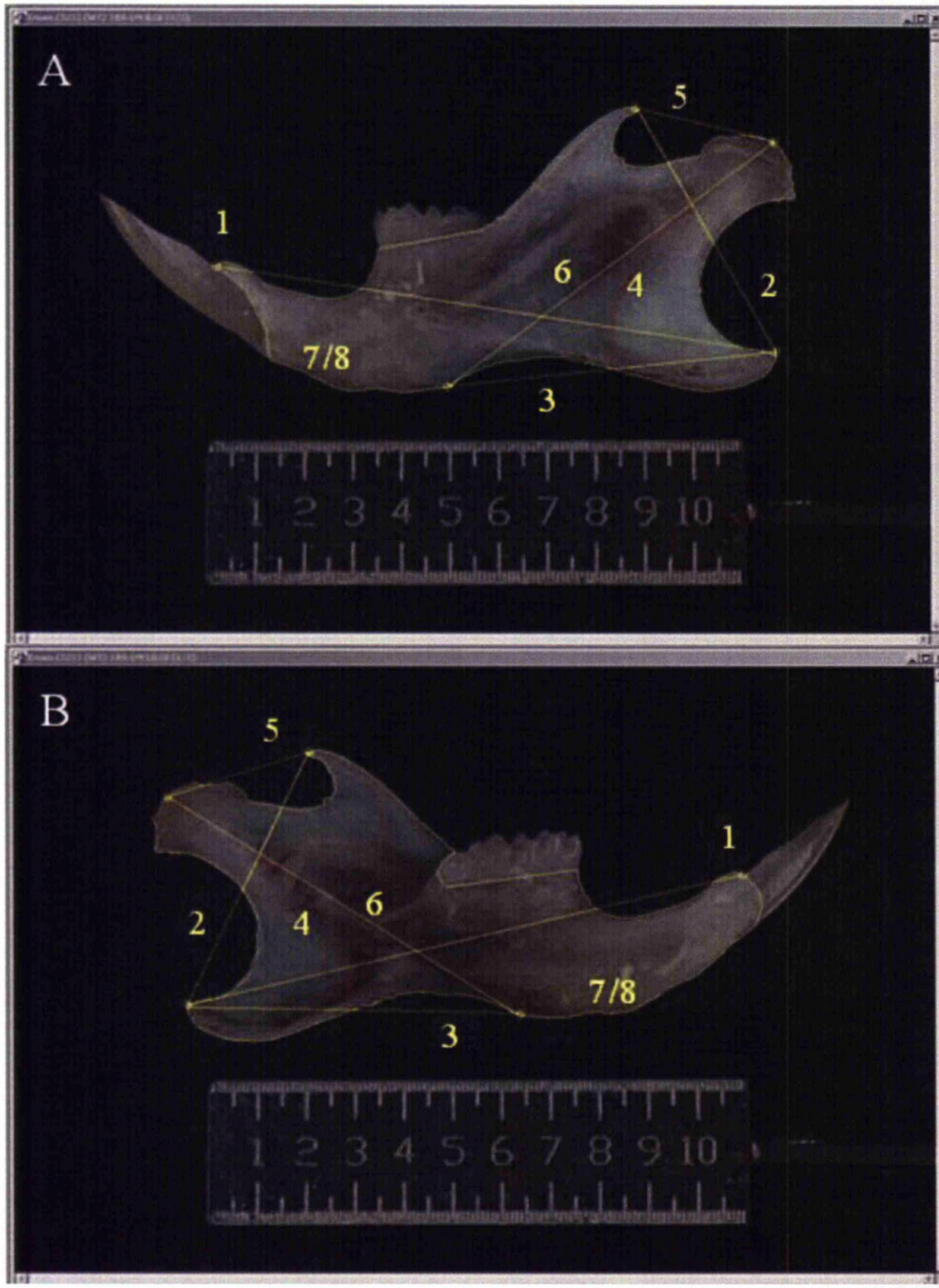

(A) buccal view or lateral aspect; (B) lingual view or medial aspect. Morphometric variables included; (1) o*verall-length* (mm); (2) *ascending-height* (mm); (3) *basal-length* (mm); (4) *mandible-angle* (°); (5) *coronoid-condyle-length* (mm); (6) *diagonal-length* (mm); (7) *mandible-area* (mm^2) and (8) *mandible-perimeter* (mm). Scale = 10.0mm. Left hemi-mandible shown.

To determine the projected *overall-length, ascending-height, basal-length, mandible-angle, coronoid-condyle-length* and *diagonal-length* linear measurement variables, the 'Measure' and 'Measurements…' options were selected from the dropdown menu. In the 'Measurements' dialogue box the 'line', 'angle measurement' and 'trace' click and drag features were used.

To determine the *mandible-perimeter* and projected *surface-area* measurements, the 'Measure' and 'Count Size…' options were selected from the dropdown menu. In the 'Count/ Size' dialogue box, the 'Measure', 'Select Measurements', 'Area' and 'Perimeter' options were selected. In the 'Edit' dropdown box, the 'Draw Merge objects' measurement tool was then used to automatically trace the observable mandible perimeter by double clicking on tooth surface on the black background in the active image. In the 'View' dropdown menu, the 'Measurement Data' Option was selected and the data displayed and recorded.

The 2D mandible morphometric measurements were obtained from both the buccal and lingual surfaces of both the left and right side hemi-mandibles. The morphometric measurement separated the mandibles into different developmental modules (or units) that taken together represented overall growth and morphometry.

4.4.2.1. overall-length: The *overall-length* determined the overall longitudinal length of the mandible from the angular process landmark to the inter-dental spine landmark, from the proximal-end to the distal-tip (Figure 10.).

Figure 10. Mandible *overall-length*

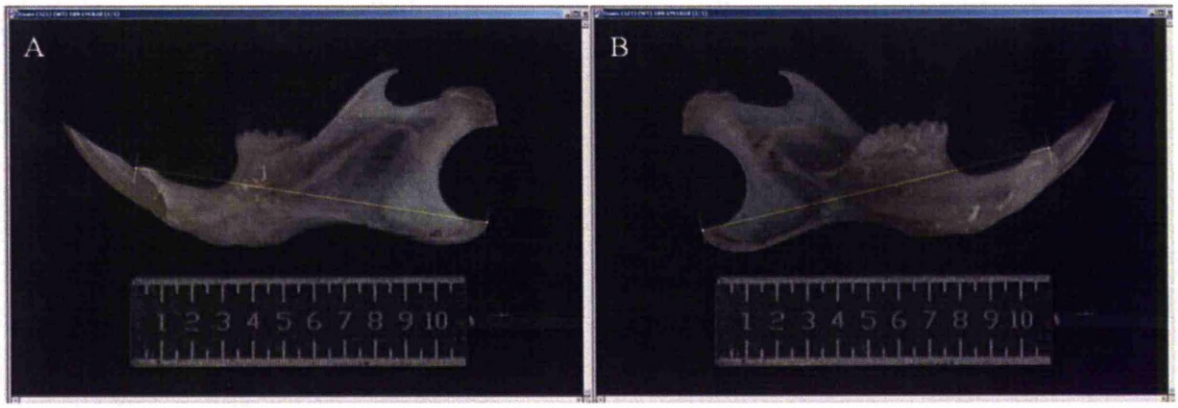

(A) buccal and (B) lingual views. Scale = 10.0mm.

4.4.2.2. ascending-height: The *ascending-height* determined the overall latitudinal length of the mandible from the angular process landmark to the coronoid landmark (Figure 11.).

Figure 11. Mandible *ascending-height*

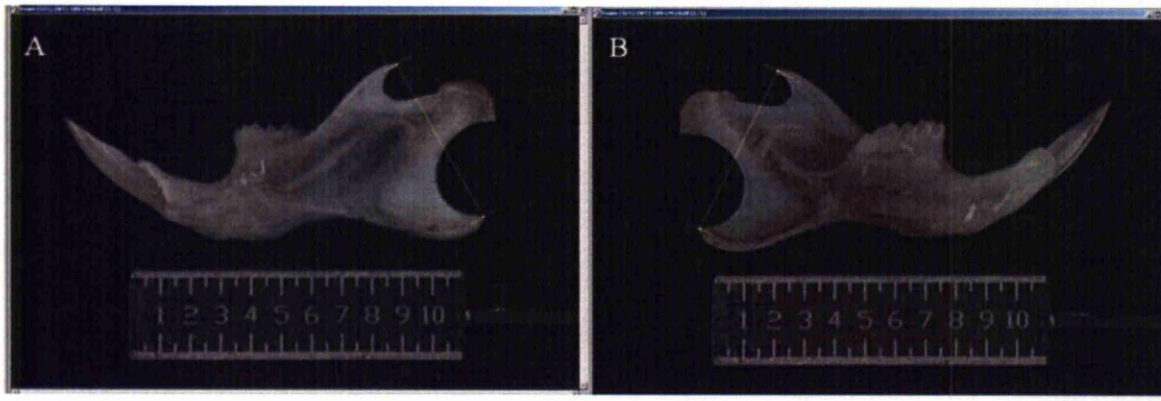

(A) buccal and (B) lingual views. Scale = 10.0mm.

4.4.2.3. basal-length: The *basal-length* determined the length from the mandible angular process landmark to the mandible border landmark (Figure 12.).

Figure 12. Mandible *basal-length*

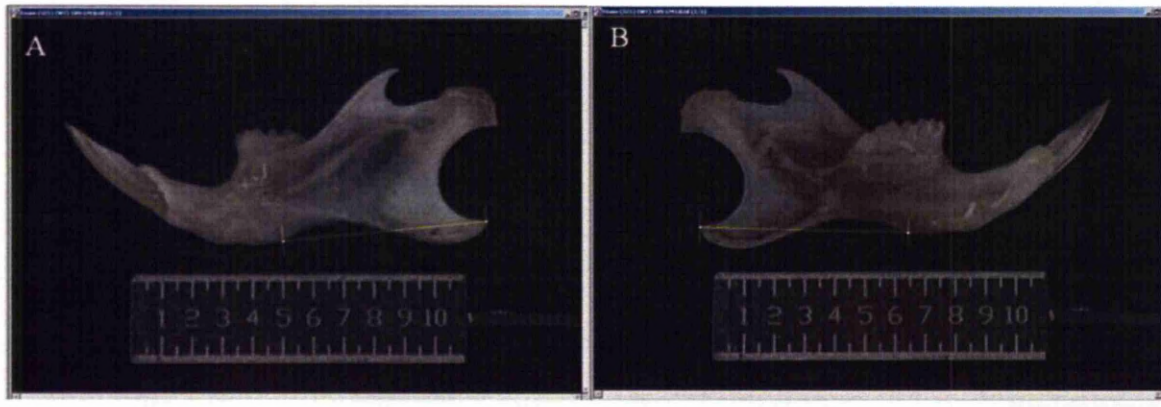

(A) buccal and (B) lingual views. Scale = 10.0mm.

4.2.4.4. mandible-angle: The *mandible-angle* determined the angle between the angular process landmark and the mandible border landmark. This represented the curvature between the *ascending-height* and *basal-length* (Figure 13.).

Figure 13. Mandible *mandible-angle*

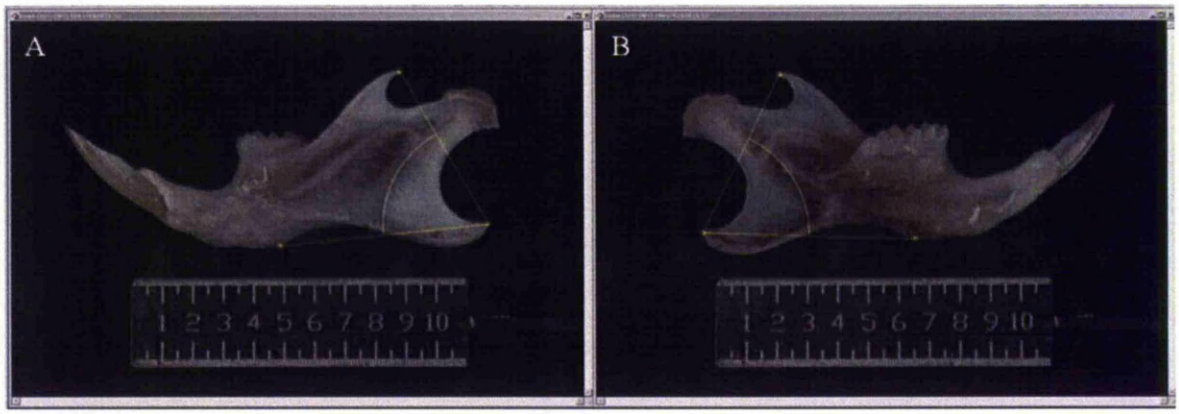

(A) buccal and (B) lingual views. Scale = 10.0mm.

4.4.2.5. coronoid-condyle-length: The *coronoid-condyle-length* determined the length between the coronoid process and condyle process (at the apex of articular surface). It estimated the temporo-mandibular joint growth and morphometry (Figure 14.).

Figure 14. Mandible *coronoid-condyle-length*

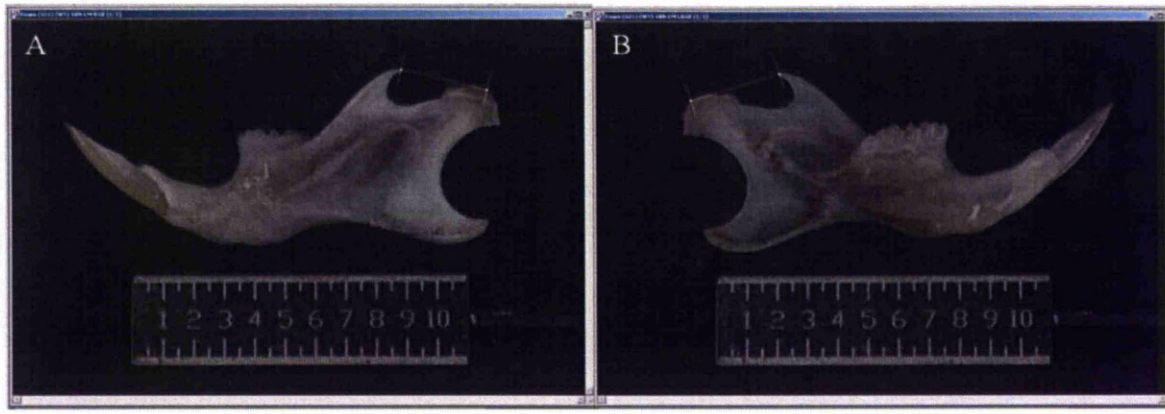

(A) buccal and (B) lingual views. Scale = 10.0mm.

4.4.2.6. diagonal-length: The *diagonal-length* determined the overall diagonal length of the mandible form the condyle process landmark to the mandible boarder landmark (Figure 15.).

Figure 15. Mandible *diagonal-length*

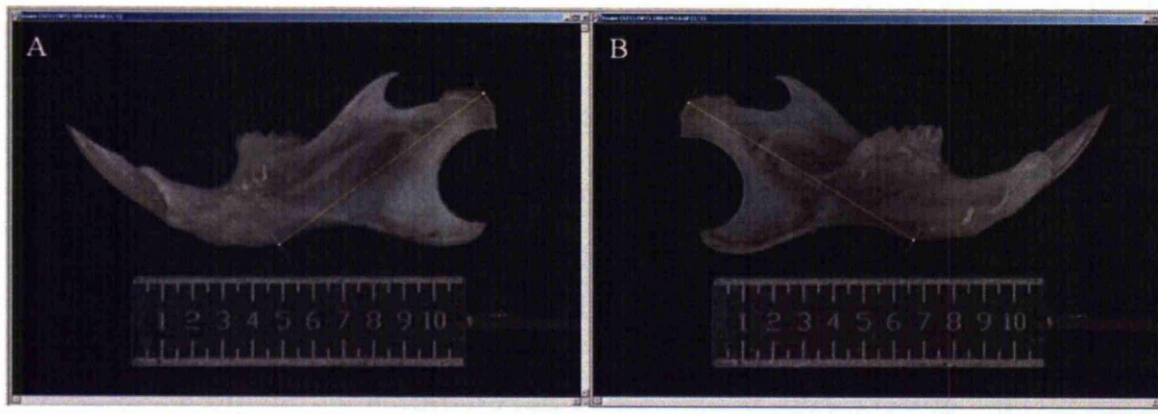

(A) buccal; (B) lingual views. Scale = 10.0mm.

4.4.2.7. mandible-perimeter: The *mandible-perimeter* determined the observable mandible perimeter. It estimated overall growth and morphometry (Figure 16.).

Figure 16. Mandible *mandible-perimeter*

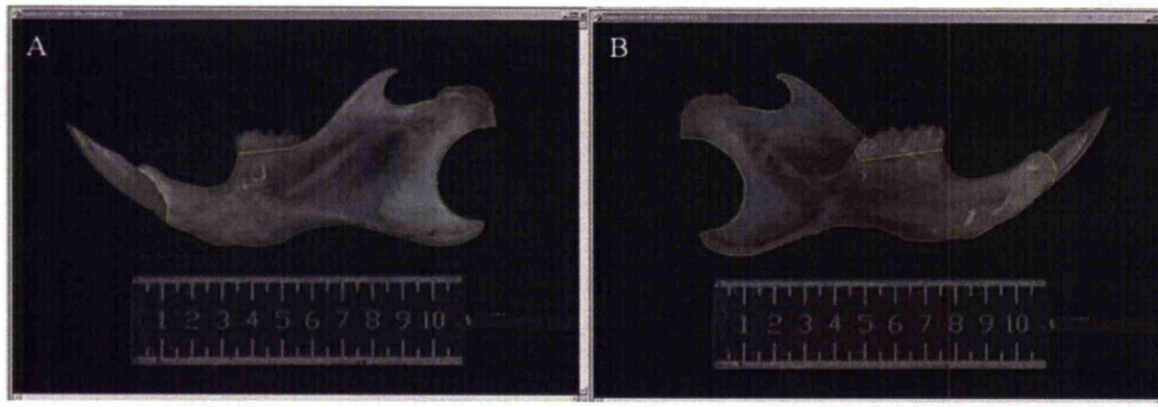

(A) buccal and (B) lingual views. Scale = 10.0mm.

4.4.2.8. mandible-area: The *mandible-area* determined the observable mandible area. It estimated overall growth and morphometry (Figure 17.).

Figure 17. Mandible *mandible-area*

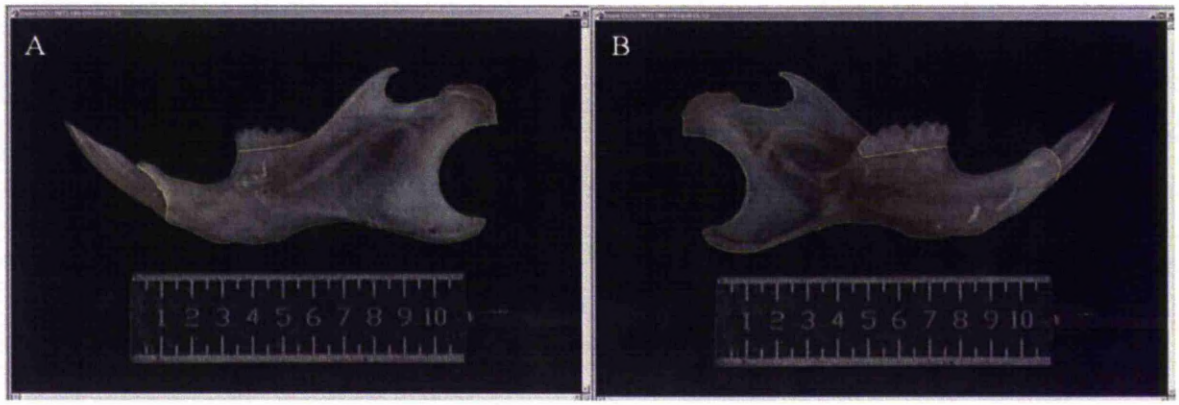

(A) buccal; (B) lingual views. Scale = 10.0mm.

The buccal and lingual surfaces of the hemi-mandibles were anatomically different. These differences in the observable perimeter were traced around the molars and alveolar processes at the dental ridge and reflected in the *mandible-perimeter* and *mandible-area* measurement values.

4.4.3. 2D Incisor Measurements

The following six measurements were obtained from 2D images taken from the buccal and lingual view (total = 11 variables), for both the left and right side incisor; projected *overall-length* (mm); projected *labial-length* (mm); a*ngle-of-curvature* (°); projected *width-at-midpoint* (mm); projected *perimeter* (mm^2); projected *surface-area* (mm^2). The projected *labial-length* was only obtained from the buccal surface view (Figure 18.).

Figure 18. Incisor Morphometric Variables

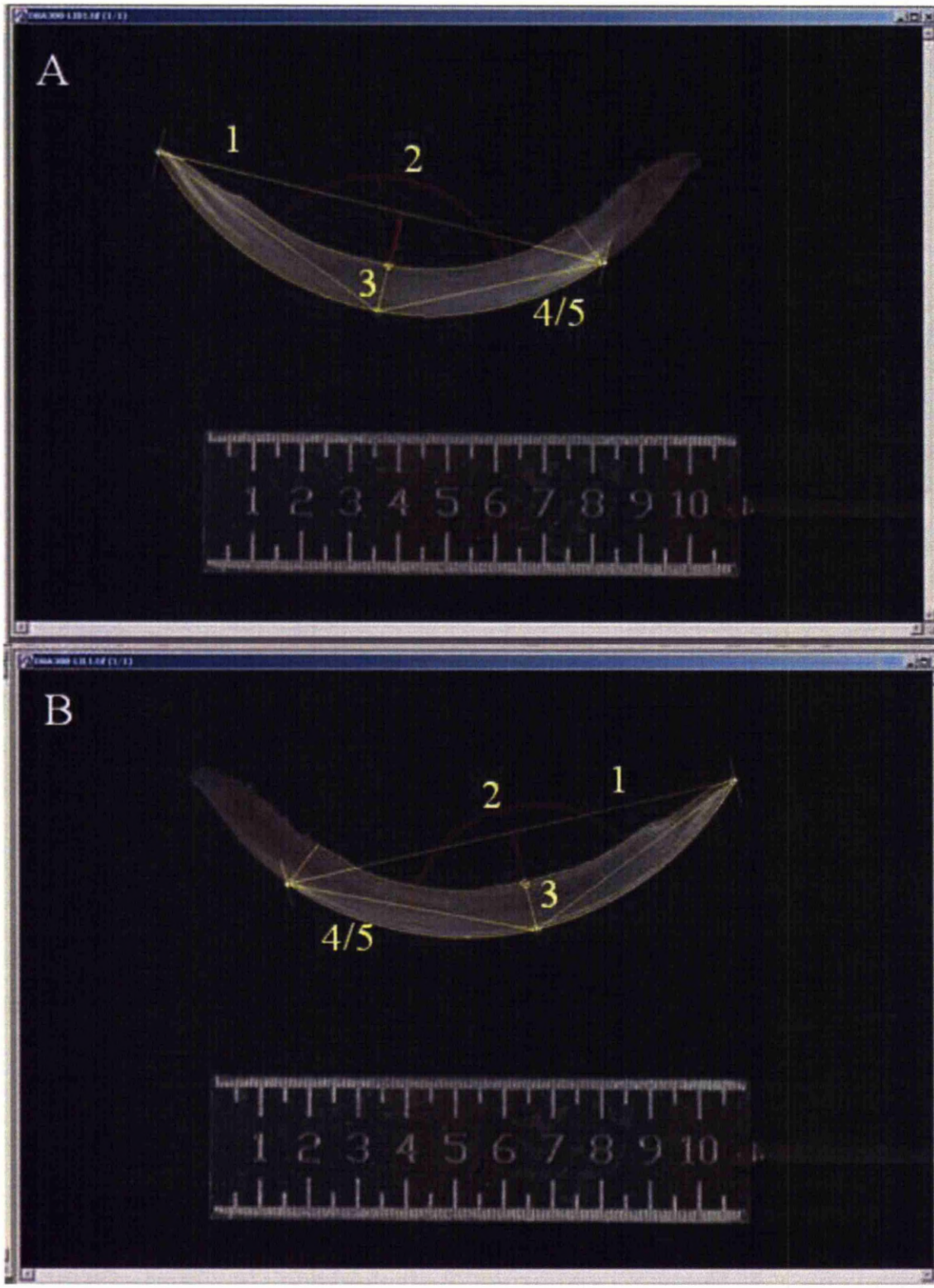

(A) buccal view; (B) lingual view. Morphometric variables included; (1) *overall-length* (mm); (2) *angle-of-curvature* (°); (3) *width-at-midpoint* (mm); (4) *incisor-perimeter* (mm) and (5) *incisor-area* (mm^2). An additional variable (6) *labial-length* (mm) was obtained from the proximal-end to distal-tip landmarks in the buccal image. Scale = 10.0mm. Left incisor shown.

An important landmark was positioned at the beginning of the distinct change in surface texture and colour at the proximal-end. This distinctive feature marked the beginning of the *pre-secretory* stage of enamel formation. It that was readily located in the 2D morphometric images (Figure 18.), in the colour and whiteness images (Figures 27. and 28.) and in the 3D morphometric images (Figure 41.).

To determine the projected *overall-length*, projected *labial-length*, a*ngle-of-curvature*, and projected *width-at-midpoint* linear measurement variables, the 'Measure' and 'Measurements...' options were selected from the IPP dropdown menu. In the 'Measurements' dialogue box the create click and drag features 'add perpendicular distance measurements from a line', 'line', 'angle measurement' and 'trace' tools were used.

To determine the projected *incisor-perimeter* and projected *incisor-area* measurements, the 'Measure' and 'Count Size...' options were selected from the IPP dropdown menu. In the 'Count/ Size' dialogue box, the 'Measure', 'Select Measurements', and 'Area' and 'Perimeter' options were selected. In the 'Edit' dropdown box, the 'Draw Merge objects' measurement tool was used to automatically trace the observable tooth perimeter by double clicking on tooth surface perimeter on the black background in the active image. In the 'View' dropdown menu, the 'Measurement Data' Option was selected and the data displayed and recorded.

The measurement tool automatically traced the *mandible-perimeter* and projected *incisor-perimeter* variables on the black background. The mandible molar teeth (dental ridge), mandibular symphysis (mandible boarder to inter-dental spine), and the incisor proximal-end landmark features required manual operator input but the automated measurement tools minimised operator subjectivity.

4.4.3.1. projected overall-length: The 2D projected *overall-length* was used to determine the overall longitudinal length of an incisor, from the proximal-end to the distal-tip (Figure 19.).

Figure 19. Incisor 2D projected *overall-length*

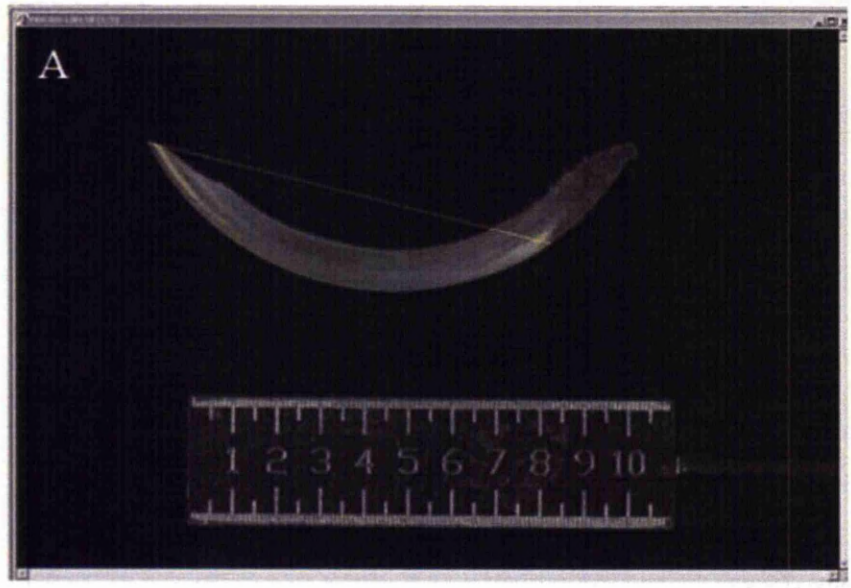

2D projected *overall-length* of a left incisor. Buccal view. Scale = 10.00mm.

4.4.3.2. projected labial-length: The 2D projected *labial-length* determined the overall longitudinal incisor length - along the labial surface - from the proximal-end to the distal-tip landmarks. It accounted for incisor curvature along the labial surface. It estimated the quantity of longitudinal enamel growth/ deposition. The 2D images were taken from the buccal view only, as the values were identical from the labial view (Figure 20.).

Figure 20. Incisor 2D projected *labial-length*

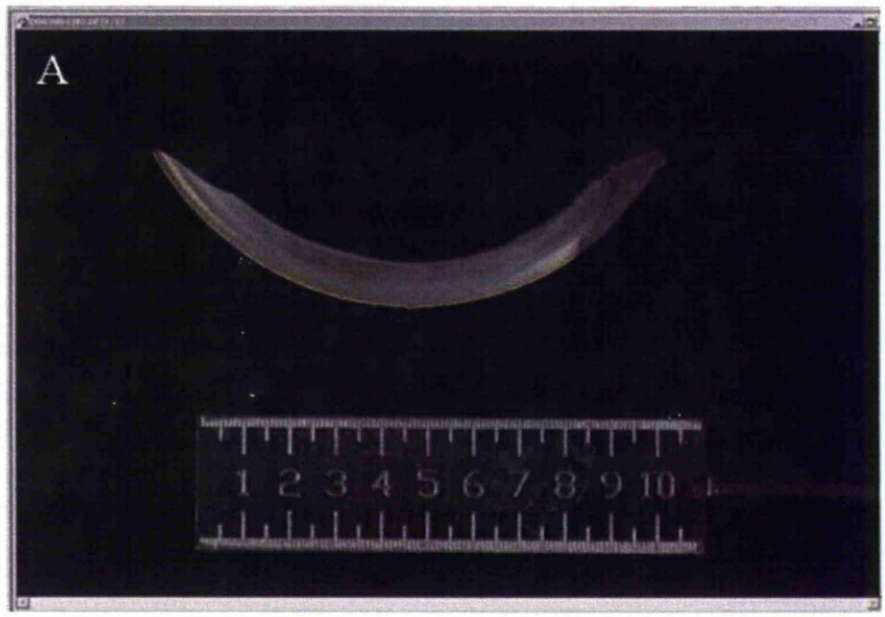

2D projected *labial-length* of a left incisor. Buccal view. Scale = 10.0mm.

4.4.3.3. angle-of-curvature: The *angle-of-curvature* was used to determine the angle between the distal-tip and proximal-end landmarks. It was used to estimate the curved morphology of the incisor. It was taken from the buccal and lingual views (Figure 21.).

Figure 21. Incisor 2D *angle-of-curvature*

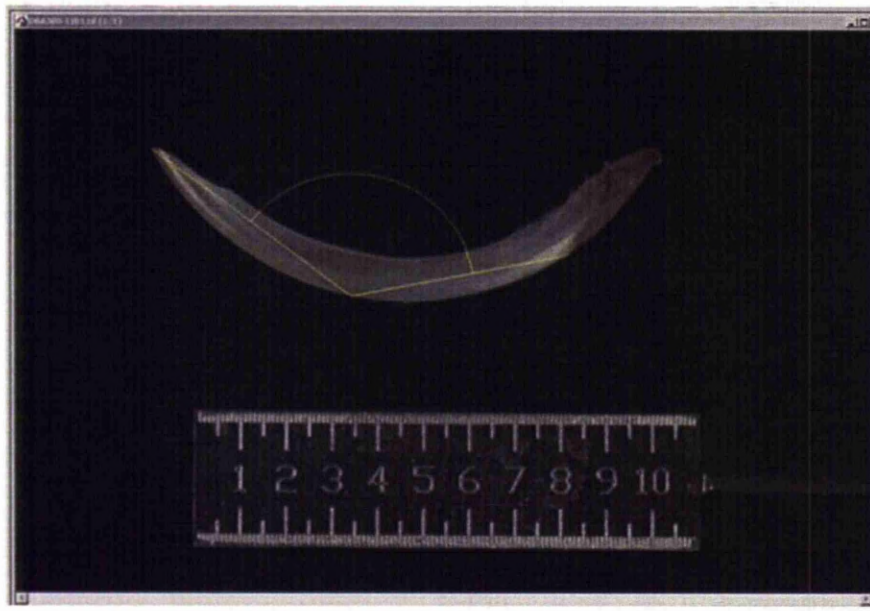

2D *angle-of curvature* of a let incisor. Buccal view. Scale = 10.0mm.

4.4.3.4. projected width-at-midpoint: The 2D projected *width-at-midpoint* was used to determine the incisor antero-posterior diameter. It was used as an estimate of lateral growth and tooth bulk at the tooth curve tangent and was taken from the buccal and lingual views (Figure 22.).

Figure 22. Incisor 2D projected *width-at-midpoint*

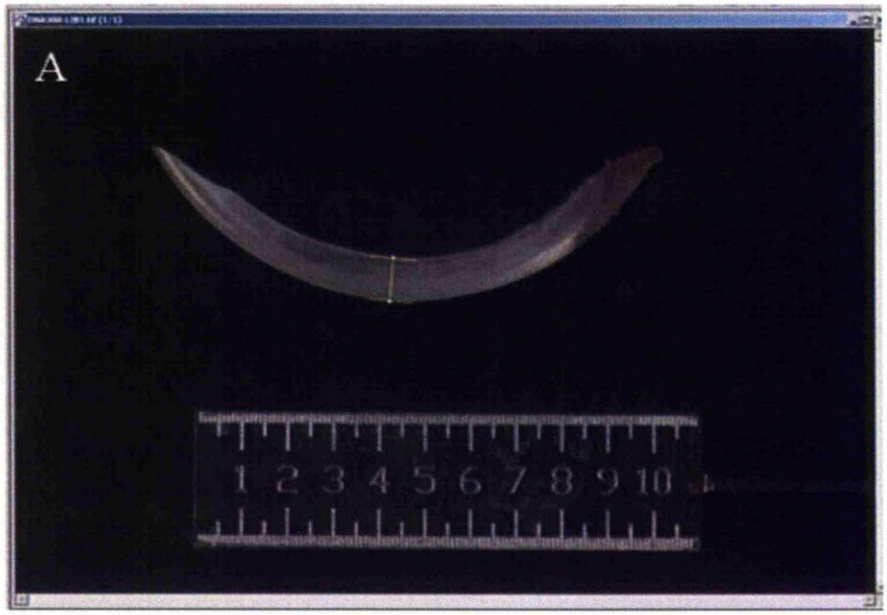

2D projected *width-at-midpoint* of a left incisor. Buccal view. Scale = 10.0mm.

4.4.3.5. incisor perimeter: The 2D projected *perimeter* was used to determine the complete incisor perimeter. It was used as an estimate of the overall quantity of enamel growth/ deposition and was taken from the buccal and lingual views (Figure 23.).

Figure 23. Incisor 2D projected *perimeter*

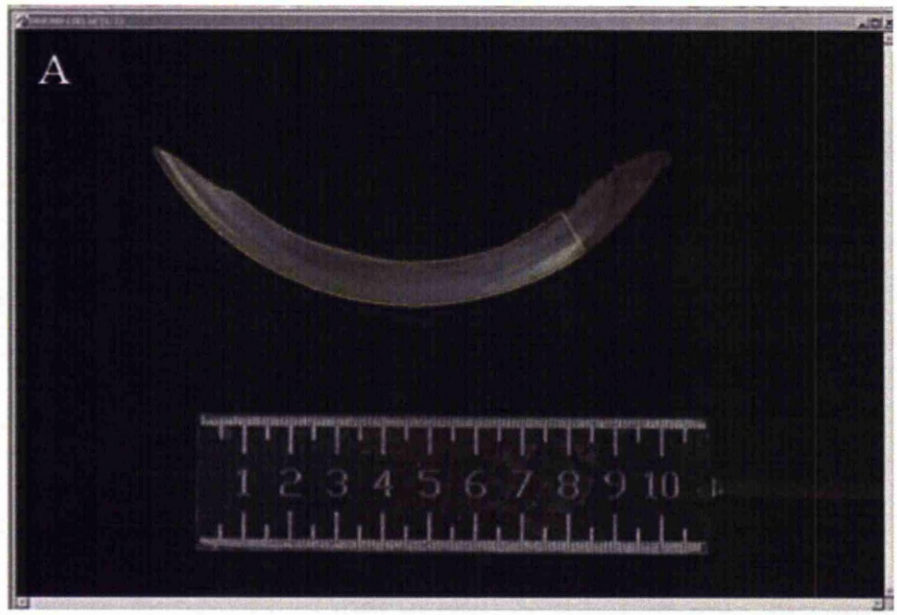

2D projected *perimeter* of a left incisor. Buccal view. Scale = 10.0mm.

4.4.3.6. incisor surface-area: The 2D projected *surface-area* determined the flat surface area of tooth enamel. The measurement estimated of the quantity of enamel growth/ deposition and was taken from the buccal and lingual views (Figure 24.).

Figure 24. Incisor 2D projected *surface-area*

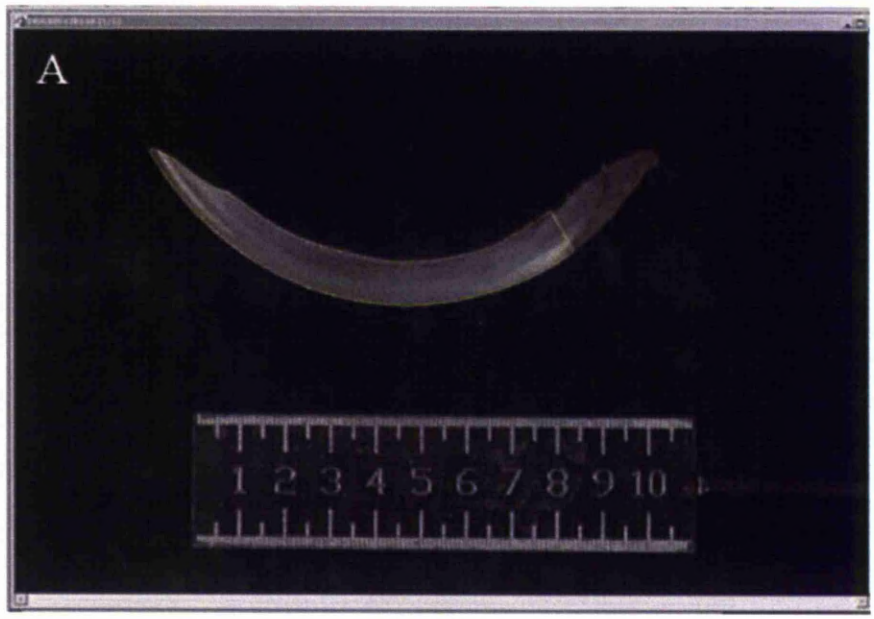

2D projected *surface-area* of a left incisor. Buccal view. Scale = 10.0mm.

4.5. COLOUR AND WHITENESS IMAGING

The colour and whiteness imaging used the same equipment as the 2D IAS with minor camera setting alterations. Incisors were positioned differently using a custom specimen holder (Figure 25.).

Figure 25. Customised Tooth Holder

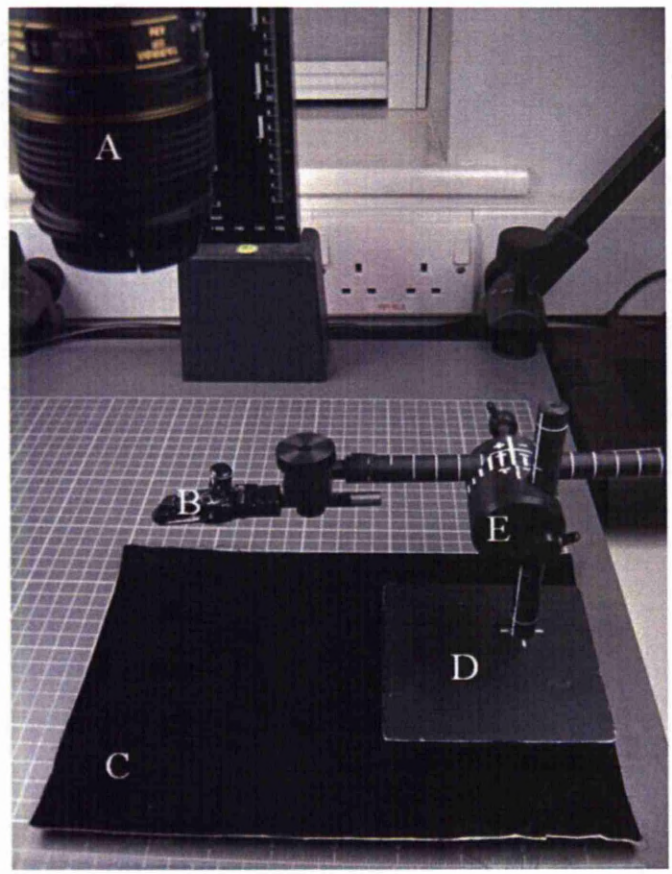

(A) camera lens; (B) incisor clamp and black modelling clay; (C) black matt background; (D) base; (E) adjustable stand.

The versatile holder could be rotated in three planes. Incisors were elevated at 6.0mm from the photographic base. Graduated scales enabled precise positioning and repositioning for consistency, standardisation and reliability. The adjustable clamp secured different incisors with the aid of black modelling clay (Flair PLC, Surrey, UK).

4.5.1. Image Capture

The same 2D IAS macro-lens was fitted with a UV polarising filter. The horizontal lights on the photographic stand were also fitted with removable polarising sheets for the non-polarised and polarised imaging.

4.5.2. Camera Settings

The following settings were the same for non-polarised and polarised illumination;
Aperture = *f*16; Shutter Speed = 3.2 seconds; ISO = 160; Magnification = X3.

4.5.3. Orientation Settings

The enamel colour and whiteness was objectively assessed on the labial surface from the labial view using the 2D IAS because enamel only develops on the labial surface of mouse incisors (Hay, 1961). Incisors were imaged from a slight buccal orientation to maximise the directly observable enamel surface to investigate mineralisation (Figure 26.).

Figure 26. Colour and Whiteness Assessment Image

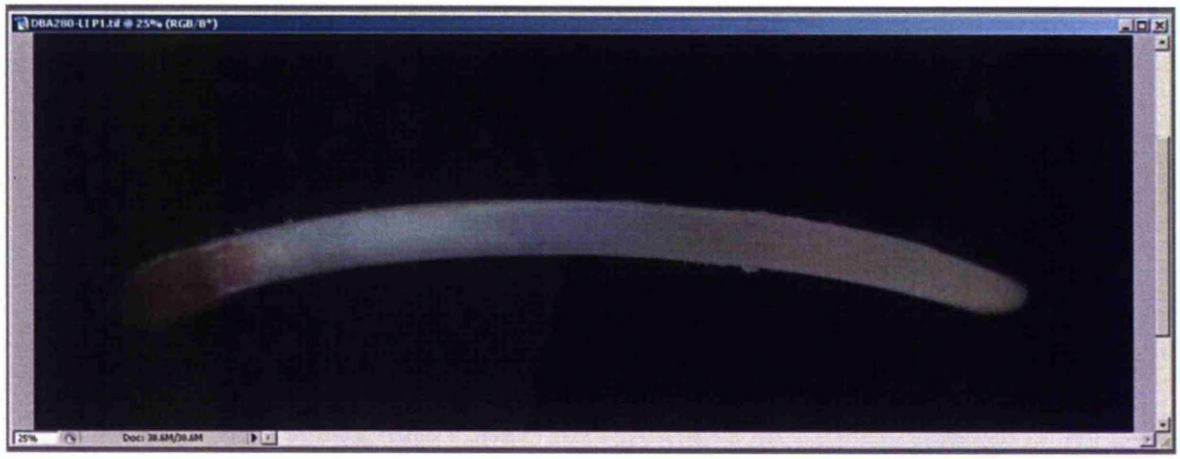

The labial surface enamel from the labial view, in a slight buccal orientation. The black background was discernable. The modelling clay was not seen in polarised images.

Incisors were securely fixed in a horizontal orientation to best utilise the camera FOV. The labial surface was perpendicular to the focal plane in the camera FOV. The mid-point of the incisor was used or focusing. This optimised the focal plane within the DOF.

4.5.4. Non-Polarised and Polarised Images

Non-polarised light describes the normal angle of light wave travel from source relative to a surface. On the other hand, polarised light describes transverse light waves that travel perpendicular to the normal angle. Incisor enamel has a high albedo and has highly reflective properties and optical heterogeneity. Therefore, a Hoya Circular Polarising filter (55mm diameter) (Tokina Co. Ltd., Tokyo, Japan) was used to eliminate polarised light.

The polarising filter was screwed onto the macro-lens. Polarising film sheets were fitted to the copy stand horizontal lights. During imaging a piece of polarisation film (held in front of the macro-lens) was used to ensure polarisation - through the viewfinder the incisors appeared bright when non-polarised or, after turning the filter 90°, appeared dark when polarised. Both non-polarised and polarised images were taken to determine the influence of UV light reflections during colour and whiteness assessment (Figure 27.).

Figure 27. Colour and Whiteness Imaging Illumination

(A) polarised and (B) non-polarised images. No reflection was present in the polarised image.

The colour and whiteness images were sensitive to surface interference from non-polarised light reflection that distorted and introduced artifice. Polarised images contained no light reflection. Although the polarised images lacked the normal translucent appearance, this did not reduce detail and increased contrast, increased colour saturation and did not affect exposure.

4.6. COLOUR AND WHITENESS ASSESSMENT

The 2D colour and whiteness assessment obtained standardised measurements with a bespoke colour calibrated algorithm using in-house customised Adobe Photoshop CS2 Version 9 software (Adobe Systems Inc, California, USA) and Microsoft Excel spreadsheet (Microsoft Corporation, Redmond, Washington, USA).

Adobe Photoshop was customised by installing 'A Set New White Tile.jsx' and' Add Sample.jsx' preset JavaScript files in the PC Program Files root directory of Microsoft Windows Explorer. Two keyboard shortcuts or Hot Keys were created by selecting the 'Edit', 'Keyboard Shortcuts...' options from the dropdown menu. The Application Menu Commands 'File', 'Scripts' 'A Set New White Tile.jsx' and 'File', 'Scripts' 'Add Sample' were mapped to the 'Ctrl +.' and 'Ctrl +,' hot keys respectively.

4.6.1. Calibration

A spectrophotometrically colour standardised British Ceramic Research Association white tile (#0520, Ceram Ltd, Staffordshire, UK) was imaged at the start of each imaging session to ensure colour balanced corrected images, under polarised and non-polarised illumination.

In the Adobe Photoshop dropdown menu, the 'Rectangular Marquee Tool' was used to select a central area of the white tile. Using the Ctrl+. hot key a spreadsheet file was automatically generated that contained the Red Green Blue (RGB) colour data from the selected area. Using the algorithm the RGB values were automatically calculated into calibrated Commission Internationale de l'éclairage (CIE) *lightness* (L); *green/ red* (A); *yellow/ blue* (B) and *whiteness* (WI) colour space outputs. (Negative A values indicated *green* while positive values indicated *red*; negative B values indicated *blue* and positive values indicated *yellow*; L = 0 values yield black and L = 100 values yielded white.) The resulting colour space values were calibrated against the standardised white tile values and accounted for the ambient illumination of a specific imaging session.

To open a colour and whiteness (.TIFF) file the 'File' dropdown menu and 'Open...' options were used to select a file from the Microsoft Windows Explorer directory. The individual incisor images were opened in a batch corresponding to the white tile image taken at the start

of that imaging session. A 'Zoom' tool (25.0%) was used to magnify images to fill the PC monitor screen. The automatic 'Magnetic Lasso Tool' feature was used to objectively trace the enamel surface perimeter. The zoom function minimised operator measurement errors and maximized operator consistency.

4.6.2. Assessment Procedure

Enamel was assessed in four distinct anatomical surface regions; (i) *whole*, and proceeding from the proximal-end to the distal-tip, (ii) *gingival*, (iii) *middle*, and (iv) *incisal*, that corresponded to the *pre-secretory*, *secretory* and *mature* histological stages of enamel formation. The following measurements, CIE L = *lightness; green/ red*; *yellow/ blue* and *whiteness* were obtained in the *whole, gingival, middle* and *incisal* regions (total = 16 variables), for both the left and right hand side incisors, in each of the non-polarised and polarised colour and whiteness images (Figure 28.).

Figure 28. Incisor Colour And Whiteness Assessment

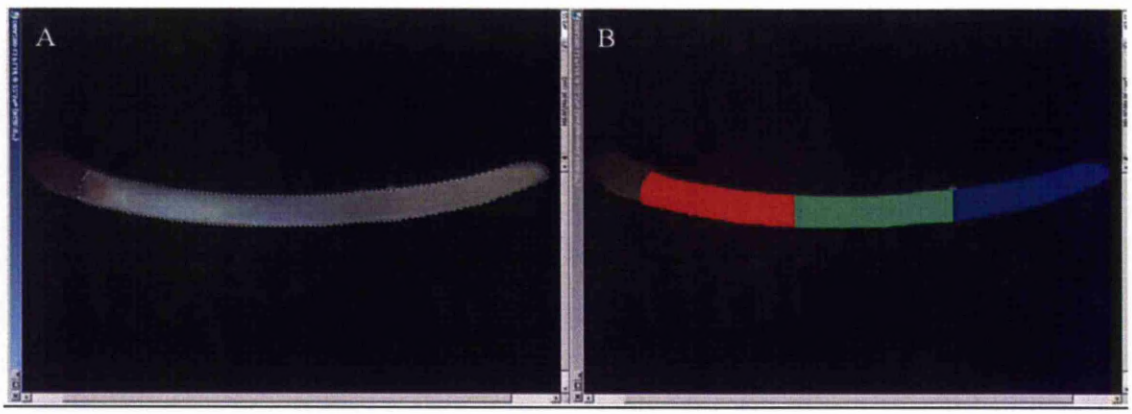

(A) *Whole* enamel surface region selection; (B) *gingival* (red), *middle* (green) and *incisal* (blue) anatomical regions. The automated software separated the anatomical regions equidistantly. The algorithm calculated CIE *lightness; green/ red*; *yellow/ blue and whiteness* colour space values for each of the four regions. Right incisor.

In the Photoshop dropdown menu, the 'Magnetic Lasso Tool' option feature was used to automatically trace the observable incisor perimeter and objectively encompass the labial enamel surface. (The following settings were refined to precisely trace the perimeter variable; feather = 0 pixels, width = 10 pixels, edge contrast = 50% and frequency = 57.) Using the Ctrl+, hot key the *whole* region was either assessed independently or separated into the three colour coordinated regions equidistantly. This minimised human subjective input and error.

Each incisor image was opened in a sequence within the batch and the algorithm used the RGB colour data outputs from each region to automatically calculate CIE LAB and WI colour space values. These calibrated colour space values were automatically exported into a colour coded spreadsheet. All data was collated into a single spreadsheet for analysis. The software and algorithm were objective, practical and minimised human input. They also expedited data collection efficiently with limited data handling.

4.7. 3D IMAGE ANALYSIS SYSTEM

The 3D Image Analysis System (IAS) included image acquisition, file transformation and 3D model reconstruction steps. The 3D morphometric measurement was the last step in the series. The equipment incorporated custom hardware and software modifications of a Non-Contact Surface Profilometer measurement device (NCSP) to deliver a versatile high systematic resolution (1.0μm) 3D IAS (Figure 29.).

Figure 29. 3D IAS Equipment

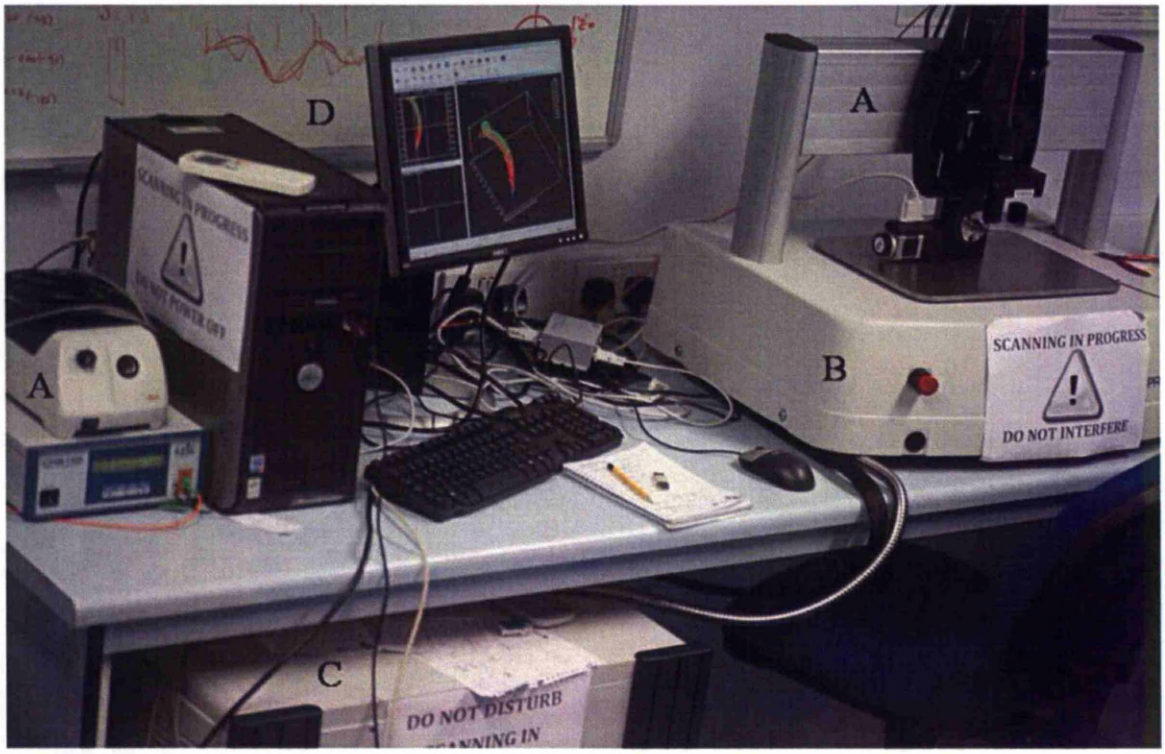

(A) z-distance measurement sensor (including optoelectric control unit on the left); (B) coordinate measuring machine platform and rotary stage; (C) ProScan CPU stack; (D) desktop PC.

The NCSP (Scantron ProScan 2000, ScanTron Industrial Products Ltd., Taunton, UK) collectively referred to a Coordinate Measuring Machine (CMM) mechanical platform, that was movable in the X and Y coordinate directions, and a Z-distance measurement sensor that was movable in the vertical Z coordinate direction. The CMM was connected to a central Computer Processor Unit (CPU) stack in a local area network that was controlled by Scantron ProScan 2000 V2.1.17 software (Scantron Industrial Products Ltd., Taunton, UK). The Microsoft Windows XP Professional 2002 SP2 (Microsoft Corp, New Mexico, USA)

operating system was on a Dell Optiplex620 desktop PC (Dell Inc, Texas, USA) with Intel® Pentium® 4 CPU, 3.40GHz, 5GB RAM and a 250GB hard-drive. The monitor was 19 inch, 32-Bit true-colour 1280 X 1024 pixel resolution, supported by a ATI Radeon Sapphire HD 3650 512MB graphics card (Advanced Micro Devices, Inc., CA, USA).

4.7.1. Non-Contact Surface Profilometer (NCSP)

The Z-distance measurement sensor was precisely movable in the Z coordinate direction for single point dynamic focusing, independent of the CMM. The Z-distance measurement sensor contained a modular optical pen (STIL S.A., Provence, France) which combined a magnifier (range 200mm-210mm focal length) and a chromatic lens (range 100μm-24mm depth of field). The optical pen was connected by a fibre-optic cable (Corning Inc, NY, USA) to a CHR 150-L optoelectric control unit (STIL S.A., Provence, France) containing a high resolution (75.0nm) chromatic confocal sensor.

Also, within the control unit there was a digital signal processing board, a spectrometer and a 50W tungsten halogen lamp that generated polychromatic (white) light. It was essential that the most appropriate sensor was chosen for the murine application because of the heterogeneous albedo of enamel. The S3/16 model optical sensor accepted all kinds of materials. The measurement range (3.5mm) was the interval between the lower and upper measuring limits of the sensor and the maximum deviation on a surface that the sensor could measure. The working distance (16.4mm) was the distance between the sensor and the middle of the measuring range. This allowed enough space to account for the 360° rotation of the incisors.

The small 'Spot Size' (8.0μm) was pertinent to the lateral features being measured, e.g. fissures required a sensor that could adequately resolve fine enamel surface structures. The spectral sensor had a high Z coordinate (axial) resolution of 75.0nm. The linearity or actual error was 0.035μm± (0.1% of range), with a sensor accuracy of 0.4μm (STIL S.A., Provence, France). This was ample to measure the smallest surface feature.

The resolution of the Proscan2000, an axial resolution of 5.0nm measured at a rate of up to 1,000 points per second, equated to the smallest quantity measurable (www.scantron-net.co.uk/proscan2000). The overall systematic resolution took into account the precise

movement of the CMM platform (0.1μm) and the actual 'Step Size' (1.0-25.0μm) parameters. The NCSP systematic resolution was 1.0μm.

4.7.1.1. CMM Movable Platform:

By mechanically moving the specimen in the X and Y coordinate directions, using the CMM platform, and simultaneously measuring the Z coordinate of each point, by the stationary chromatic spectral sensor, it was possible to obtain high resolution micro-topographic images. The CMM travel was predominately in the Y coordinate direction (Figure 30.).

Figure 30. Direction of CMM Platform Travel and Data Collection

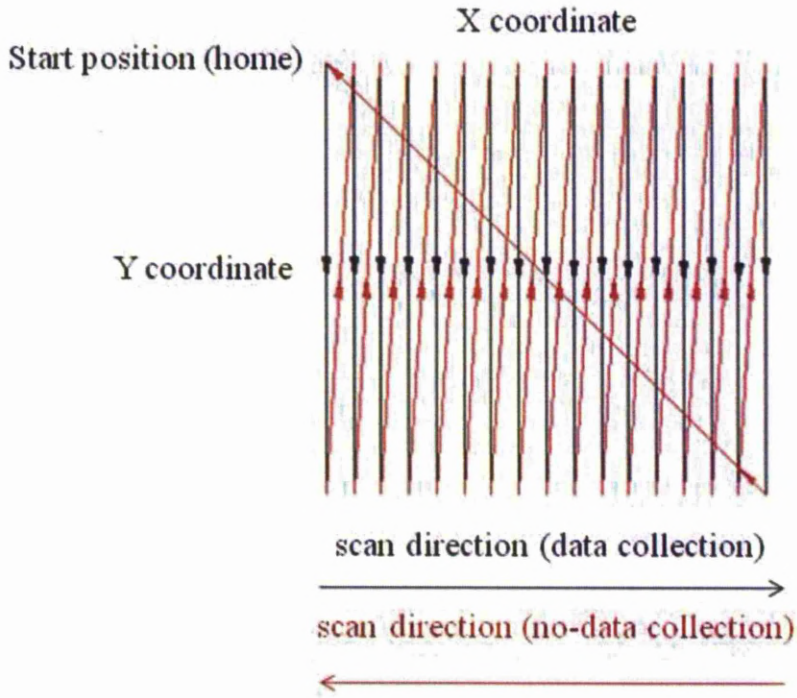

The mechanical movement of the CMM in X and Y coordinate directions from the start position 'home' coordinate point of origin. The lines represent the travel of the CMM beneath the stationary Z-coordinate measurement sensor. Data collection lines scanned in Y (black line) until complete and the CMM platform retraced in X (red line) to the beginning point of the next line. This procedure was repeated one line at a time.

The Y direction travel along the longitudinal axis of the specimens maximised data collection and minimised 'no-data' collection making the most efficient use of scan times (e.g. 15 minutes for the 5.0x10.0mm area). The distance between the black lines equalled the 'Step Size X (mm)'. 'Step Size X' multiplied by 'Number Of Steps X' equalled 'Part Size X'.

Similrly 'Part Size Y' equalled 'Step Size Y' multiplied by 'Number Of Steps Y' (Figure 31.).

Figure 31. The Scanning Setup

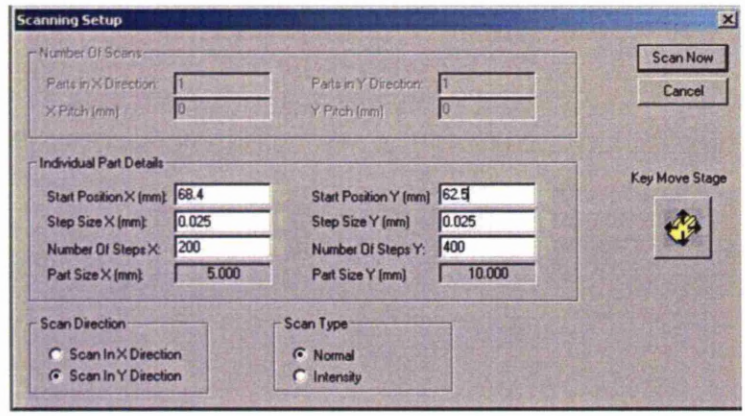

Figure . The 'Scanning Setup' dialogue box in the Proscan2000 software.

The individual scan 'Individual Part Details' coordinate inputs were determined iteratively by preparatory scans. The 'Start Position' coordinates were required later for X and Y offset mathematical calculations. The Z-distance measurement sensor moved in the vertical Z-axis to obtain Z coordinate data by dynamic focusing (Figure 32.).

Figure 32. Z-Distance Measurement

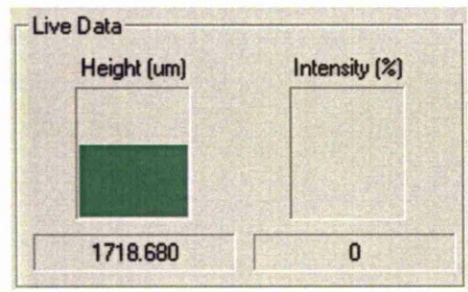

The 'Live Data' screen in Proscan2000 displayed the Z coordinate distance measurement (or height). The middle (1.75mm) of the sensor measuring range (3.5mm) was used to optimise 3D data collection.

Changes in Z-distance ('Height'), displayed in the 'Live Data' screen, between the specimen surface and a known reference point on the rotary stage precisely engineered steel mandrel (c = 6.0mm), were recorded for each specimen. The change in Z-distance (along with the X and

Y coordinates) determined the specimen's position in the local coordinate system. X, Y and Z coordinate data point offset calculations spatially adjusted the 3D image files for each individual specimen in a novel process of image indexing that was used to reconstruct the 3D models.

4.7.1.2. Novel Customised Modifications:

The CMM platform was modified with a novel and customised rotary stage. The rotary stage consisted of a precisely engineered steel mandrel with known dimensions (Figure 33.).

Figure 33. Precisely Engineered Steel Mandrel

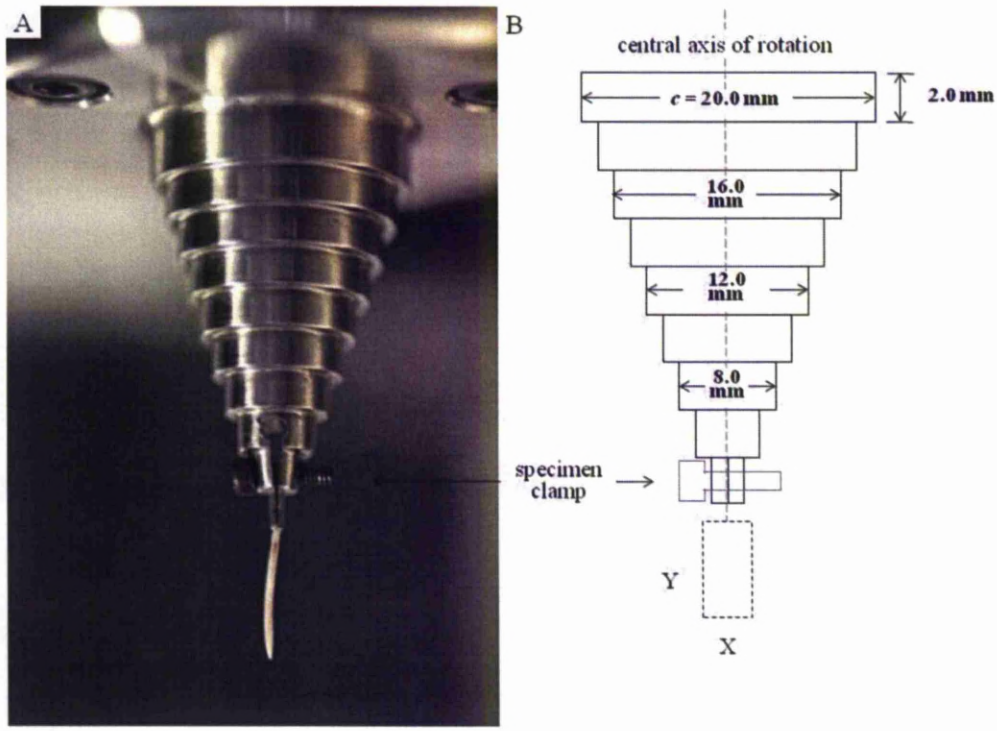

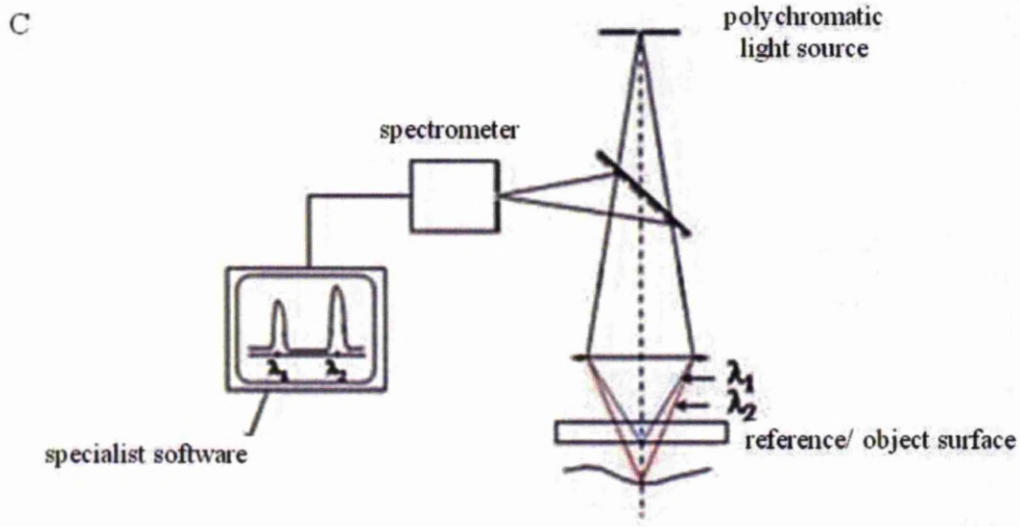

(A) photograph of mandrel (plan view); (B) schematic of mandrel including known dimensions used for calculating the Z coordinate offset; (C) diagram of the mandrel (reference/ object surface) in the NCSP system. The central axis of rotation or datum line (at x = 0) was located within the sensor measuring range. The precisely engineered steel mandrel served as the absolute reference surface within the local coordinate system.

The bespoke rotary stage was mounted on the CMM platform from above using four screws. The adaptation was completely removable (Figure 34.).

Figure 34. The Customised Rotary Stage

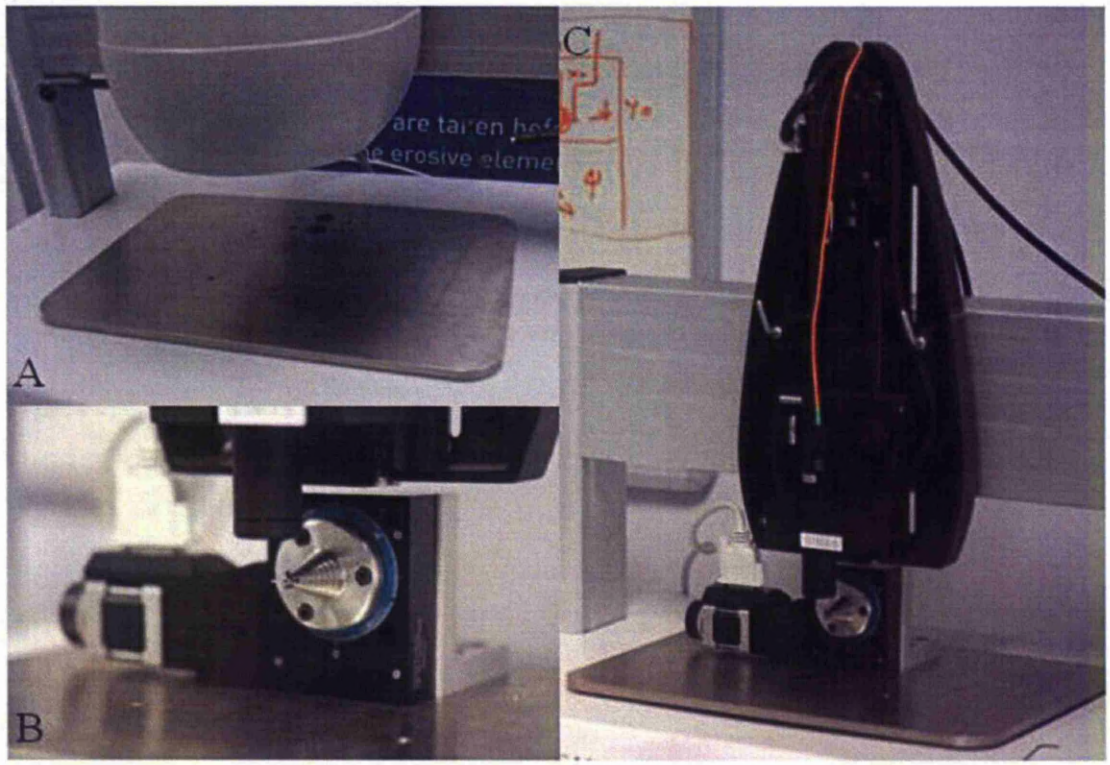

(A) CMM movable platform; (B) customised rotary stage (stepper motor and micro-precision rotation stage); (C) rotary stage in position on the CMM platform. The incisors were secured by a milled clamp at the end of the mandrel, tightened firmly using four 2.0mm diameter screws.

A precision position stepper motor controller (C663 Mercury ™ Step, Physik Instrumente GmbH & Co. KG, Karlsruhe, Germany) and a micro-precision rotation stage (M-006.2S, Physik Instrumente GmbH & Co. KG, Karlsruhe, Germany) were operated from the PC by Rotary software (Physik Instrumente GmbH & Co. KG, Karlsruhe, Germany). The incisors were thereby rotated 360° at predetermined 45° intervals (e.g. 45°, 90°, 135°, 180°, 225°, 270°, 315°, 360°). The 3D data was collected in the intervals between each rotation. The number of intervals related to the number of multi-view micro-topographical surface-maps or 3D images required to reconstruct a complete 360° model (Figure 35.).

Figure 35. Multiple Multi-view Micro-Topographical Surface-maps

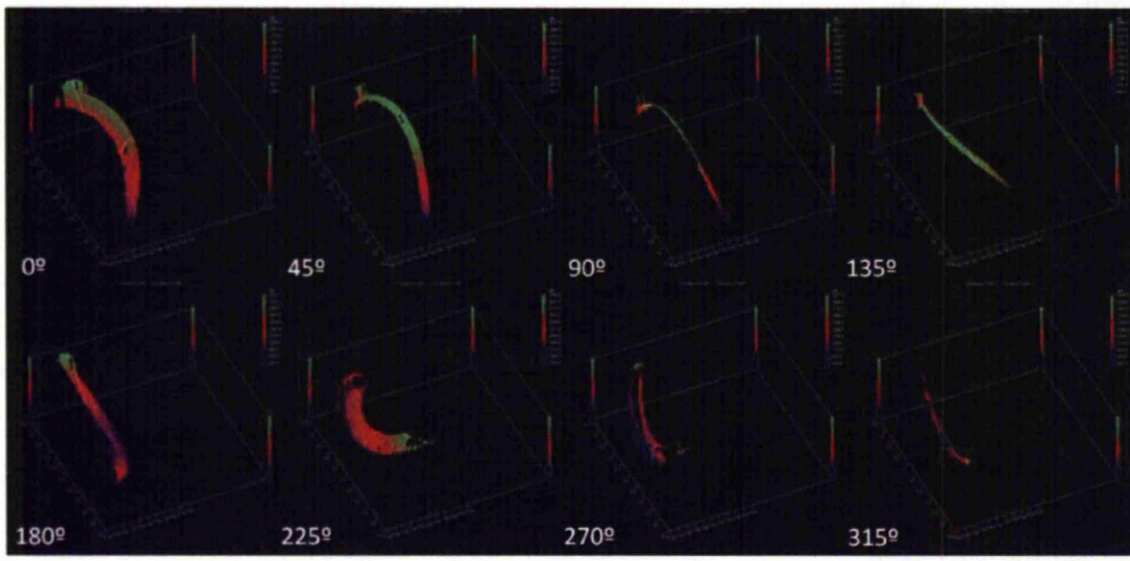

Eight individual micro-topographical surface-maps. At each interval between rotations a micro-topographical surface-map or 3D image file was generated, previewed and saved, e.g. a 360° revolution with 45° intervals produced 8 individual multi-view files (360/45 = 8).

The equipment was largely automated in the X, Y and Z coordinate directions so the inputs, controlling the intervals and degrees of rotation, provided a complementary and versatile means of data collection. (Complete scan time for one incisor model was 15 minutes x 8 files = 2 hours.) The multi-view micro-topographical surface maps or 3D images were previewed and saved in native/ proprietary Proscan (.prn) files. The files went through a series of file type transformations towards a complete 3D surface structural model.

4.7.2. File Format and Saving

In the .prn file type the incisor surface was defined in terms of 3D Cartesian (X,Y and Z) coordinate data points. The 3D spatial location of each point within a local geometric coordinate system was established between the CMM and the Z-distance measurement sensor. In order to correct the relative position of each coordinate data point, the multiple .prn files were imported into Microsoft Excel spreadsheets to be offset by a specific mathematical calculation (Figure 36.).

Figure 36. Calculating Coordinate Data Point Offsets

A (plan view)

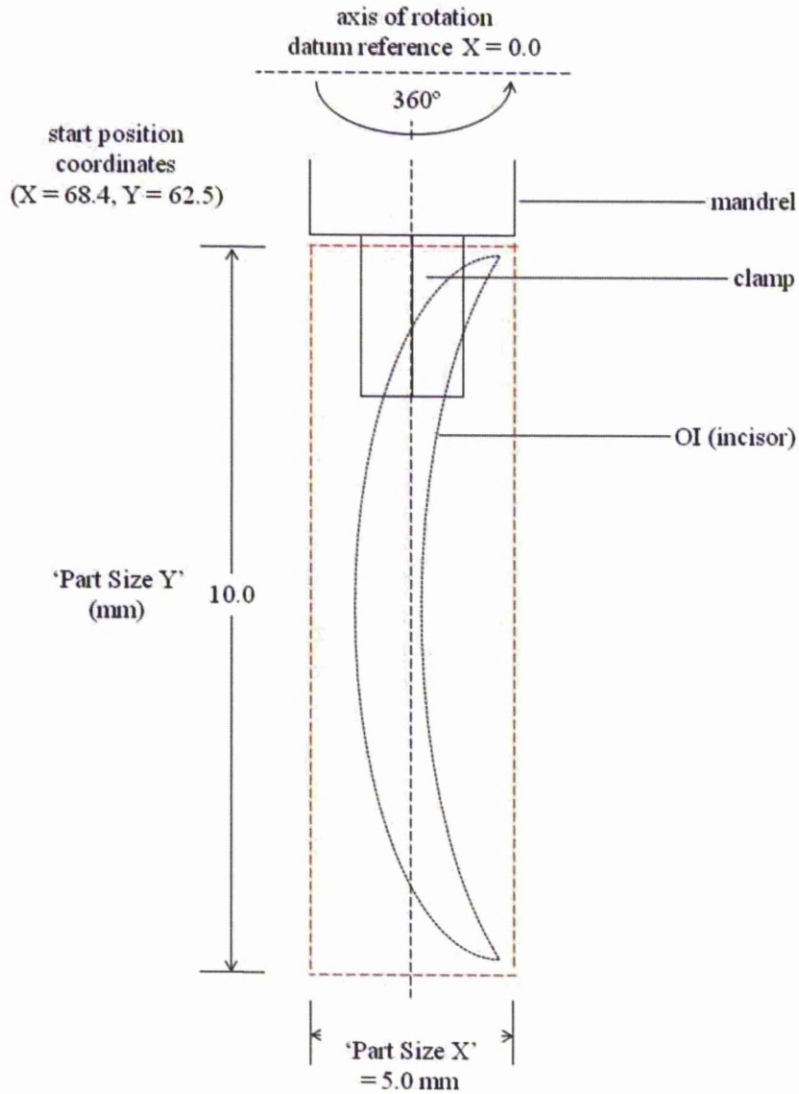

B (front view)

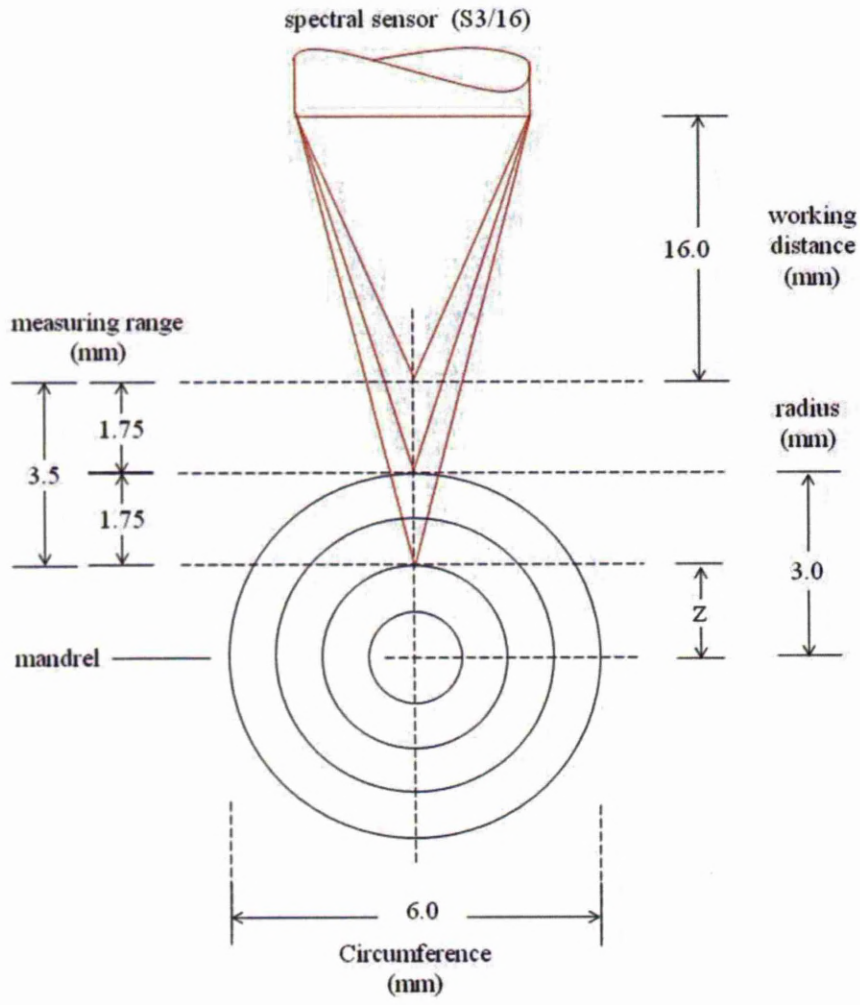

Calculating the geometric mathematical offsets; (A) plan view, the X and Y coordinates were, determined in the 'Scanning Setup'; (B) front view, the Z coordinate was the recorded Z distance (or height) between the specimen clamp to a known point on the 6.0mm circumference step of the mandrel. The offsets were noted for X, Y and Z for all images and were subtracted from the corresponding coordinate data point values in the .prn image files after being imported into a spreadsheet.

The .prn files were imported into a spreadsheet in a 'comma delimited text file format' (.csv file). The offset values were obtained from the 'Start Position' coordinates for the X and Y coordinates, and from the Z-distance between the specimen (at 0° position) and the 6.0mm circumference of the mandrel. The three different values were subtracted from the three different X, Y and Z coordinate data point columns in the spreadsheet. The offset adjusted files were saved in .csv format.

The .csv files were converted to a text file format (.txt file) by changing the file extension in Microsoft Windows Explorer. The .txt file was compatible for import in point cloud data format into SolidWorks Premium2008 software (DassaultSolidWorks, Massachusetts, USA). Each file was spatially corrected according to the novel 3D image registration process of indexing.

Thus, the steel mandrel not only fixed the incisors firmly in position within the measuring range, and established a central axis of rotation (used as a datum line), but it also provided a reference for calculating Z offsets and combining the multiple 3D images.

4.7.3. Final 360° 3D File

To produce a 360° 3D model the multiple multi-view images were assembled together in the local coordinate system using the mandrel as an absolute reference surface. The central axis of rotation of the mandrel served as a datum line (at X = 0) about which each separate image in the series was opened in sequence and spatially adjusted in SolidWorks by the corresponding degrees of rotation (e.g. 45°, 90°, 135°, 180°…) predetermined by the intervals of the rotary stage (Figure 37.).

Figure 37. Combining Multi-view images by Indexing/ Registration

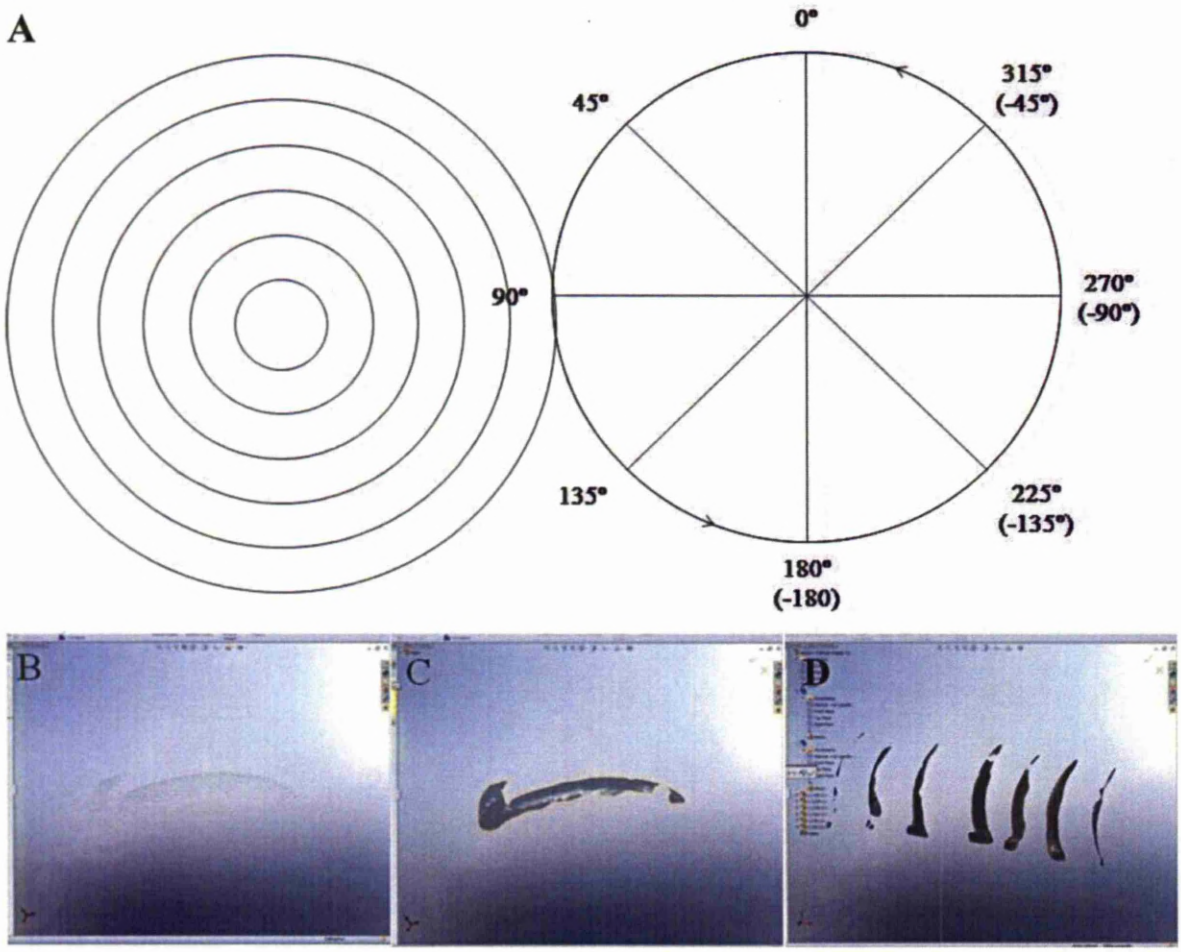

(A) schematic of the mandrel from a front view. The degrees of rotation correspond to the predetermined intervals of the rotary stage. The centre of the circle was the central axis of rotation where the incisor was clamped. Screen-shot image series of file type transformations from; (B) coordinate point cloud data; (C) polygon mesh file conversion; (D) multiple spatially corrected/ adjusted 3D images before 3D modelling.

4.7.4. 3D Modelling (.stl File Production)

After each individual point cloud data .txt file was indexed around the datum line the separate files for each incisor were saved as an .xyz file type. The mathematically offset and spatially corrected .xyz files were then converted back into .txt files by changing the file extension in Microsoft Windows Explorer. The coordinate data from each separate .txt file was copied and pasted into a single .txt file using Microsoft Notepad (Microsoft Corp, New Mexico, USA). This file was opened in the Solidworks software and converted into a single triangulated polygon mesh using the 'Scan to 3D' add-on and 'Mesh Prep Wizard' features (Figure 38.).

Figure 38. 360° 3D Surface Structure Model

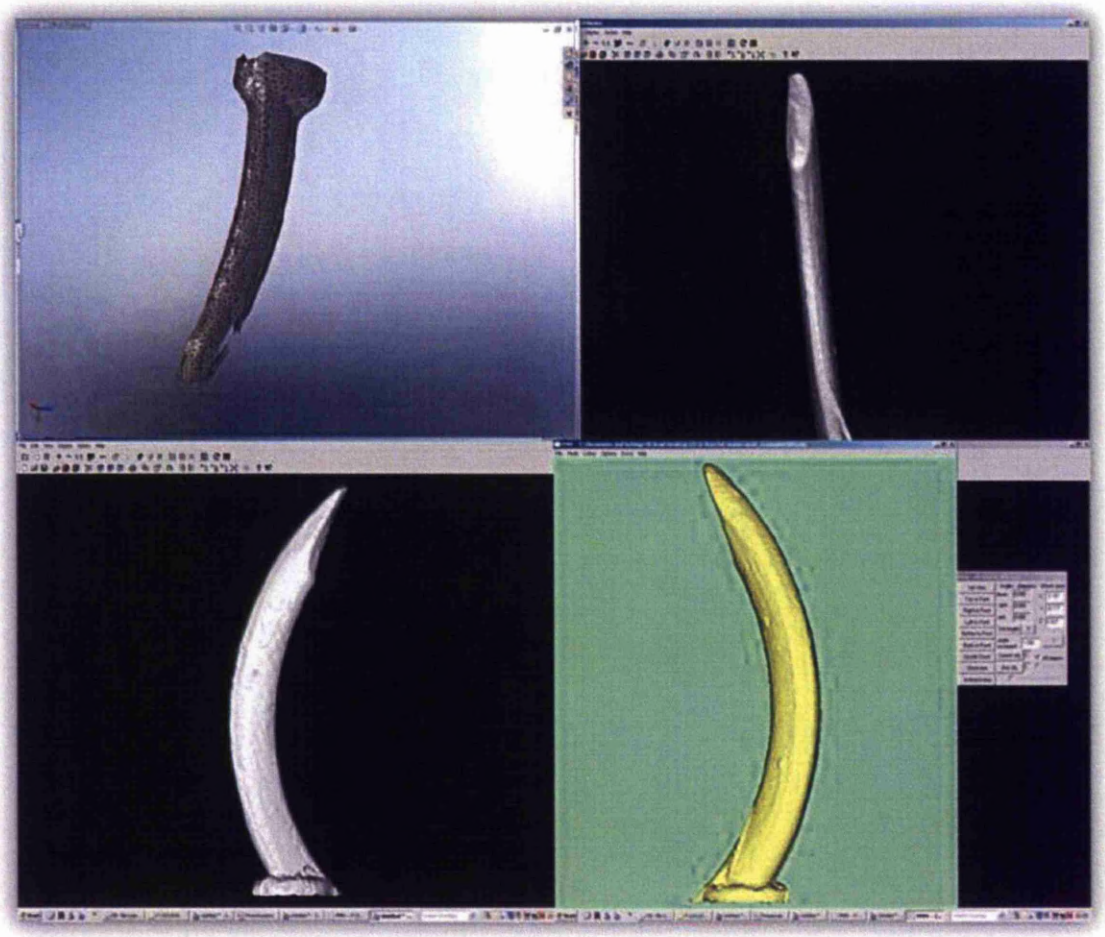

Screen shot images from the 360° 3D surface structure model of a mouse right mandibular incisor. The 3D model files could be exported in various file formats to be compatible with analytic software packages. The 3D model shows the mandrel clamp at the proximal-end.

The 3D models were edited/ trimmed at the proximal-end landmark feature to remove the mandrel clamp and were saved in .stl format. The distinct surface texture change that distinguished the start of the *pre-secretory* stage of enamel formation was used as a landmark feature - it was the same landmark as the 2D IAS morphometric and colour and whiteness assessment images. The feature was located distally from the mandrel clamp. The remaining hole was closed flat using the Solidworks 'Mesh Prep Wizard'.

No image compression occurred during file type transformations. This prevented any data loss and did not compromise quality or quantity of information, or surface detail.

4.8. 3D MORPHOMETRIC MEASUREMENT

All 3D morphometric measurements were obtained using Cloud 3D surface viewer software (Dr. Robin Richards, University College London, UK), except the *surface-roughness* measurement that was obtained using ProScan 2000 software (ScanTron Industrial Products Ltd., Taunton, UK). In the 3D IAS both projected and actual linear measurements were possible. The projected measure represented the flat surface distances between two points, as seen in the 2D IAS, but the additional actual 3D measurement followed the 3D contour of the tooth surface for greater analytical power.

4.8.1. Operating Instructions

To open a 3D model (.STL) the 'File' dropdown menu and 'OpenSTL' commands were used to select a file from the Microsoft Windows Explorer directory. Opened files were viewed by the 'Fit to window' command in the 'Options' dropdown menu.

For each measurement, the precise X, Y and Z coordinate position and orientation of incisors were recorded in the respective 'Offsets (mm)' and 'Angles (degrees)' commands in the 'View – all objects affected' dialogue box. Incisors were consistently repositioned and re-orientated in the exact location for repeat measurements. Therefore, repeat measurement markers were reliably replaced.

Incisors were rotated in all directions by selecting 'Rotate' in the 'Mode' dropdown menu. The incisor 3D models were rotated in fixed X, Y and Z coordinate dimensions/ planes by holding down either the right or both buttons on the mouse and rotating clockwise/ anticlockwise around a fixed central axis.

A 'Zoom' function was operated by holding both the left and right mouse buttons together, moving the mouse forwards to zoom in, and moving the mouse backwards to zoom out. The onscreen zoom was monitored in mm in the 'Size - field of view' dialogue box display. This maintained the different magnifications for the different measurements and ensured consistent measurement marker placement.

There was no additional calibration procedure because the .STL files contained internal calibration data (in mm) established within the 3D IAS.

4.8.2. 3D Measurement Procedure

Incisors were orientated in 3D in a position appropriate to attain each measurement. Measurement markers were placed on the anatomical landmark features of the incisor image surface and did not move.

The following steps were used to obtain the 3D measurements. In the Cloud dropdown menu, the 'Mode', 'PlaceMarkers' options were selected. The cursor displayed ('MARK') and measurement markers were placed on the landmark features of the incisor surface. Measurement lines between markers were displayed by selecting 'Set Ref Point' and 'Set Line Point' in the 'Measurements (mm)' dialogue box. The line was used as a guide for further marker placement. The cross of each marker point was used to ensure all marker points were equidistant. The last marker was superimposed over the final marker (usually marker B) to obtain the projected and actual measurements.

In the 'Meas' dropdown menu of the 'Measurements (mm)' dialogue box, the 'Length of polyline' option was selected and a 'Measure line segments' dialogue box appeared. To obtain the projected measurement, the wanted makers (e.g. A and B) were selected and moved to the 'these markers will be used' box using the 'move to wanted list' button. Alternatively, to obtain the projected measurement the wanted makers (e.g. A, C D...) were selected and moved to the 'these markers will be used' box using the 'move to wanted list' button. The actual and projected measurement data was recorded and saved in a spreadsheet.

The 3D *surface-roughness* measurement was obtained differently using the ProScan2000 software. The rotary stage was not required and the NCSP was used as originally designed. The incisors were placed directly onto the CMM moveable platform and immobilised in modelling clay. The high resolution selected region examples scan parameters were different from those used for the 3D model reconstructions (Figure 39.).

Figure 39. 3D Surface Region Scan Parameters

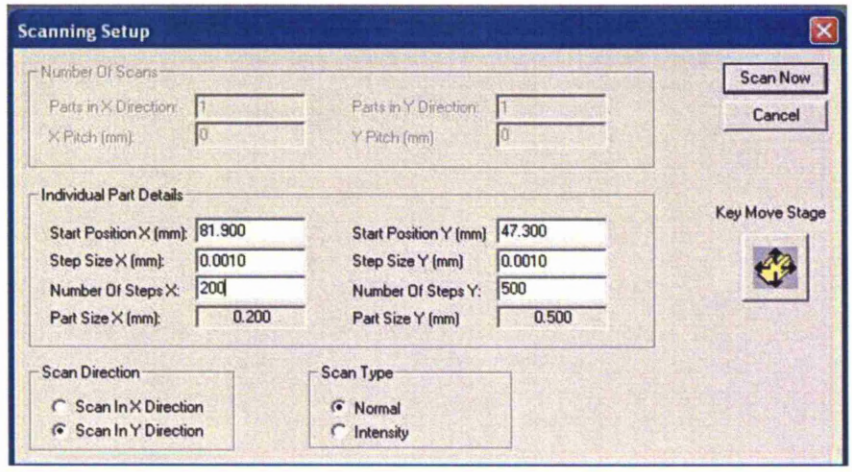

Scan parameters used for the high resolution selected surface regions; Step Size = 1.0μm; Part size = 200x500μm). The *surface-roughness* measurements were automatic data outputs that were saved in a spreadsheet after imaging.

The high resolution scans were obtained using the 'Step Size', 'Number of Steps' and 'Part Size' displayed in the 'Scanning Setup' window. The selected region example images were saved as individual .prn files. They were not multi-view images and did not require combination or reconstruction as in the 3D modelling. Therefore, no offset calculation or indexing was required.

One example scan was obtained for each of the seven genotype groups, in each of three representative regions of enamel surface (i) *gingival*, (ii) *middle* and (iii) *incisal* (Figure 40.).

Figure 40. Selected 3D Surface Region

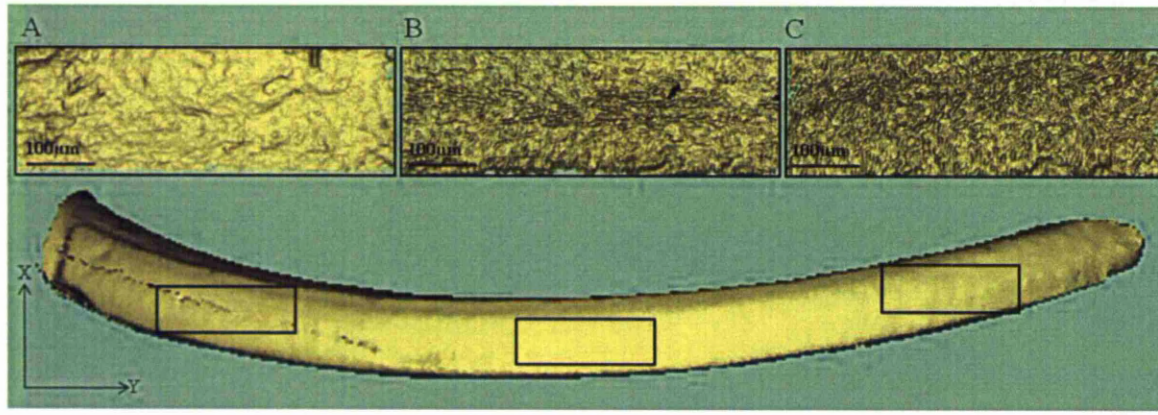

(A) *gingival*; (B) *middle*; (C) *incisal* enamel surface regions corresponded to the anatomical thirds. Left = proximal-end, right = distal-tip. Rectangles represent the high resolution (1.0µm) selected area examples (200x500µm) and contain individual 100µm scales.

The three selected area example scans were obtained along the longitudinal labial axis of the incisors between the proximal-end and the distal-tip. The dimensions (200x500µm) were dictated by the surface under inspection, which according to the recommendations of the International Organisation for Standardisation (ISO 4288-1996) were sufficient to give a true representation of the texture of the enamel surface. The proximal-end was taken to be 0.0mm and the Y coordinate start positions for each image/ region were measured at approximately +3.0mm, +6.0mm and +9.0mm respectively.

The corresponding X coordinate start positions for each image/ region were determined by subtracting 100µm from the X coordinate at the centre of the labial surface. This ensured that the 200x500µm selected region obtained surface data from a central surface for each region. The high resolution examples were obtained from approximately the same regional locations as individual incisor dimensions varied. Each region was equidistant to minimise subjectivity.

4.8.3. 3D Incisor Measurement

The following eleven measurements were obtained from 3D models from the buccal, lingual and labial views (x16 variables), for both the left and right side incisors (x32 variables); projected *overall-length* (mm); projected *labial-length* (mm); actual *labial-length* (mm); projected *width-at-midpoint* (mm); actual *width-at-midpoint* (mm), *circumference* (mm); actual *perimeter* (mm); actual *surface-area* (mm^2); total *surface-area* (mm^2); total *volume* (mm^3) and *surface-roughness* (μm).

All 3D measurements were taken on the buccal and lingual surfaces, except the following; (i) *labial-length*, (ii) *circumference*, (iii) total *surface-area*, (iv) total *volume* and (v) *surface-roughness*. The 3D projected and actual *labial-lengths* were taken in from the labial surface. The 3D *circumference*, total *surface-area* and total *volume* were obtained once for each left and right incisor. *Surface-roughness* was only obtained on the labial surface because of the asymmetrical distribution of enamel.

The distinct surface texture change that distinguished the start of the *gingival* region/ *pre-secretory* stage of enamel was used as a landmark feature - this was the same landmark as the 2D IAS morphometric and colour and whiteness assessment images.

4.8.3.1. projected overall-length: The 3D projected *overall-length* was used to determine the overall longitudinal length of an incisor, from the proximal-end to the distal-tip (Figure 41.).

Figure 41. 3D projected *overall-length*

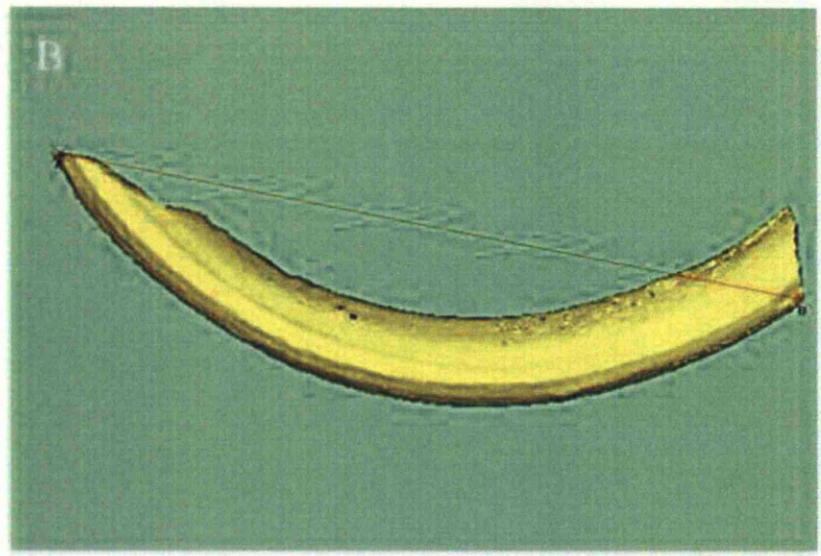

Buccal view of a left incisor. Scale = 10.00mm.

4.8.3.2. labial-length: The 3D *labial-length* determined the overall longitudinal incisor length along the labial surface, from the proximal-end to the distal-tip landmarks. It accounted for incisor curvature along the labial surface. It estimated the quantity of longitudinal enamel growth/ deposition (Figure 42.).

Figure 42. 3D actual *labial-length*

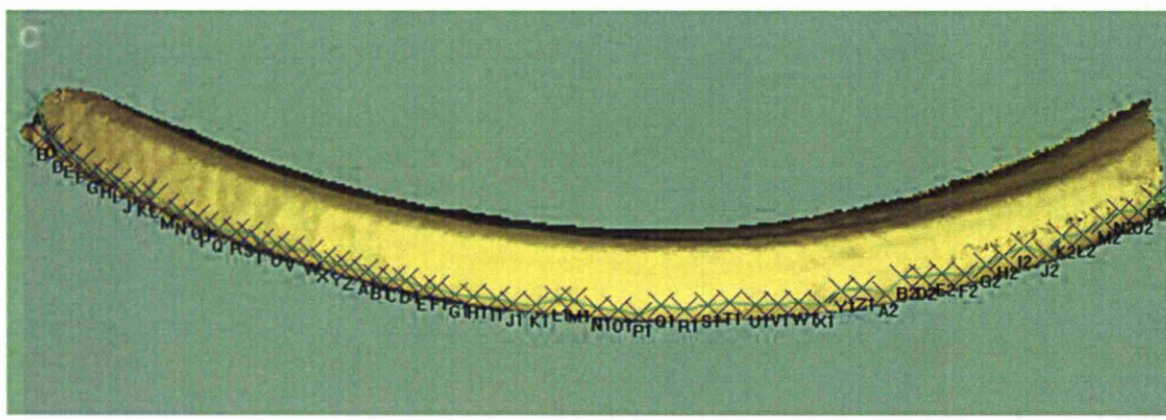

Labial view of a left incisor, slight buccal orientation. Actual surface measurement (green line/ marker crosses). Scale = 10.0mm.

***4.8.3.3. actual labial-length*:** The 3D actual *labial-length* was used to determine the overall longitudinal length of an incisor along the labial surface. The measurement accounted for incisor curvature and topography along the labial surface. It was used to estimate the quantity of longitudinal enamel growth/ deposition. It was taken from the labial view (Figure 43.).

Figure 43. 3D actual *labial-length*

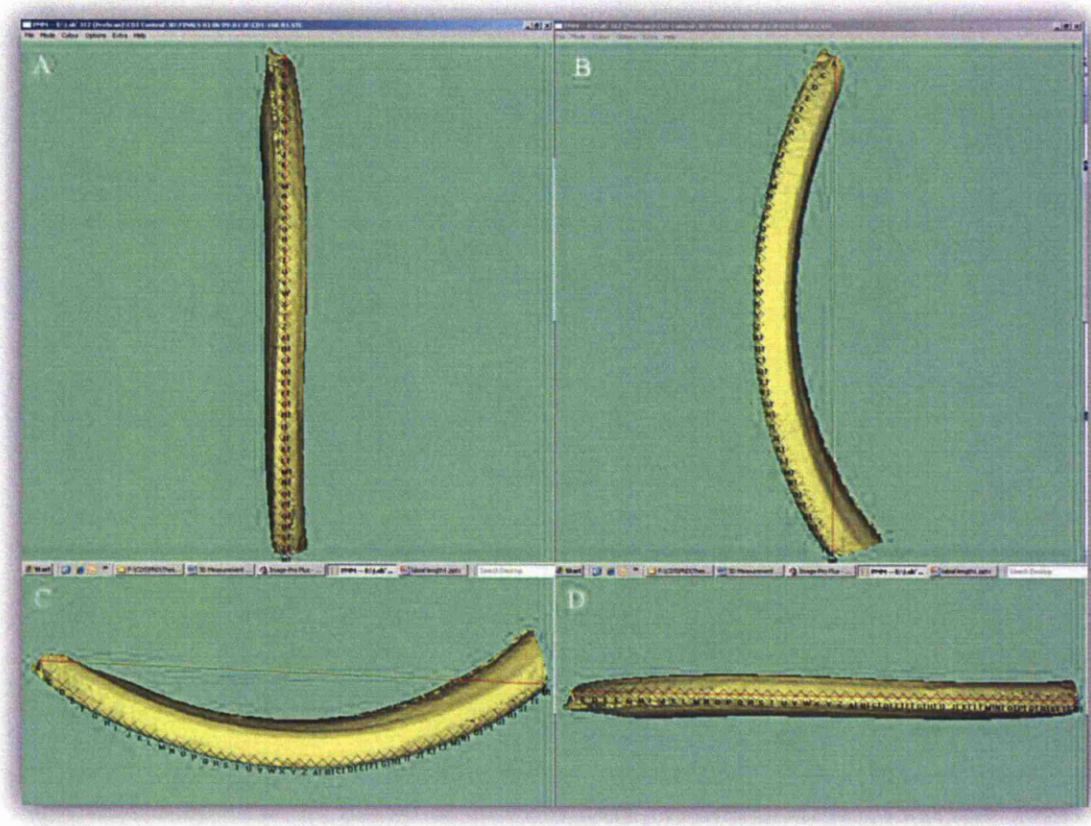

(A) Labial view; (B-D) various labial orientations exhibiting the difference between the actual (red line) and projected (green line/ markers crosses) measurements. Left incisor shown.

4.8.3.4. projected width-at-midpoint: The 2D projected *width-at-midpoint* and 3D projected *width-at-midpoint* were used to determine the incisor antero-posterior diameter. They were used as an estimate of lateral growth and tooth bulk at the tooth curve tangent. Both were taken from the buccal and lingual views (Figure 44.).

Figure 44. 3D projected *width-at-midpoint*

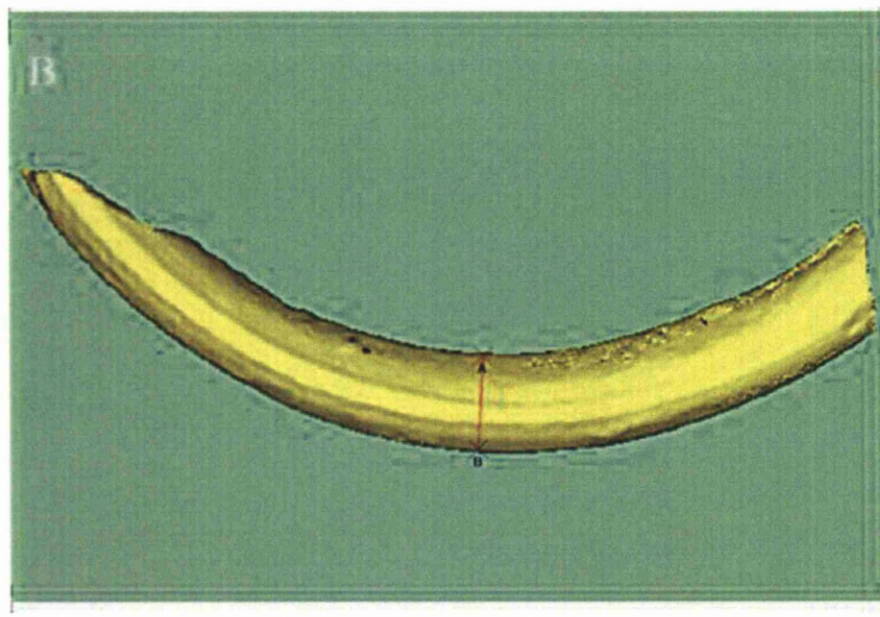

Buccal view of a left incisor. Scale = 10.0mm.

4.8.3.5. actual width-at-midpoint: The 3D actual *width-at-midpoint* was used to determine the incisor antero-posterior diameter. The measurement estimated lateral growth and tooth bulk at the tooth curve tangent and it accounted for incisor curvature and surface topography. It was taken from the buccal and lingual views (Figure 45.).

Figure 45. 3D actual *width-at-midpoint*

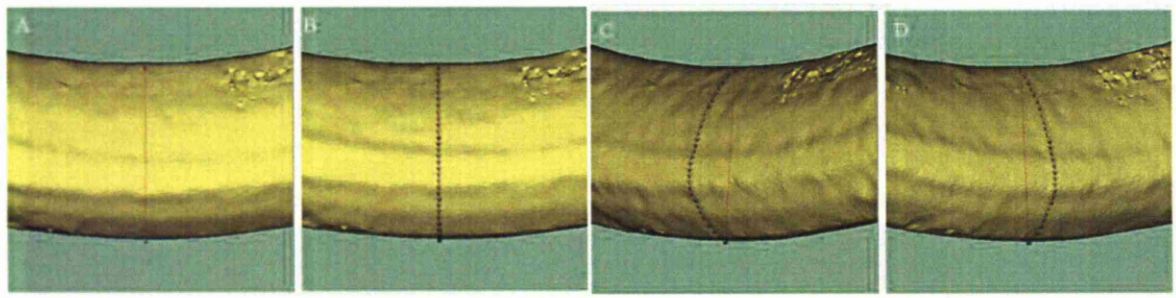

(A) projected measurement; (B) actual surface measurement; (C-D) difference between the projected (red line) and actual measurements (green line/ markers crosses) from two views. Buccal surface of a left incisor.

The *width-at-midpoint* was taken on both buccal and lingual surfaces to investigate the difference between their respective projected and actual measurements, and to identify asymmetry. The *width-at-midpoint* measurement of the buccal and lingual surfaces quantified enamel growth/ deposition as enamel forms on the labial surface only.

4.8.3.6. incisor perimeter: The 3D actual *perimeter* was used to determine the complete incisor perimeter, accounting for incisor surface topography. It was used as an estimate of the overall quantity of enamel growth/ deposition. It was taken from the buccal and lingual views (Figure 46.).

Figure 46. 3D actual *perimeter*

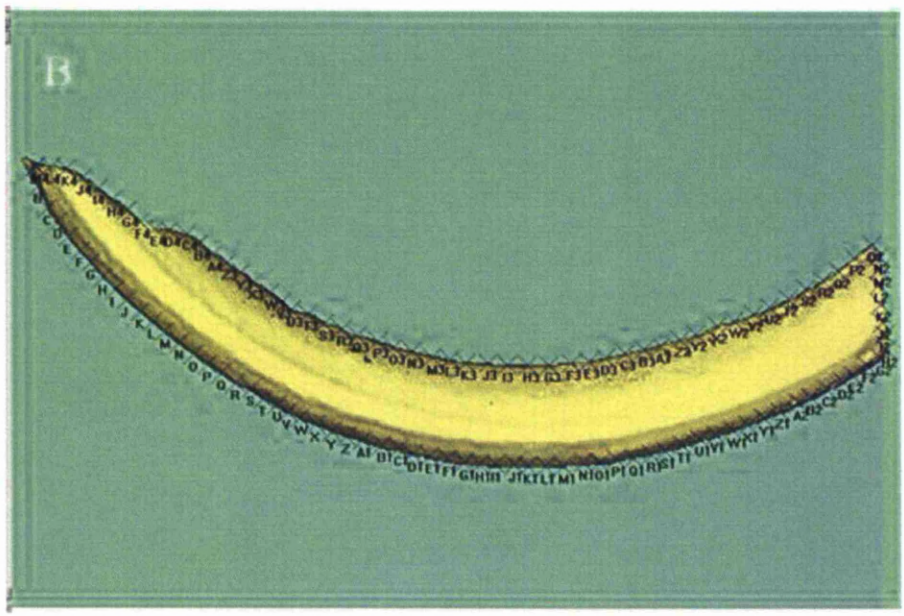

Buccal view of a left incisor. Scale = 10.0mm.

4.8.3.7. total and marked surface-area: The 3D *surface-area* determined both the total and the marked surface area of enamel and accounted for the incisor surface topography. The measurements were used to estimate the quantity of enamel growth/ deposition. The marked *surface-area* measurement was taken from the buccal and lingual view (Figure 47.).

Figure 47. 3D *surface-area*

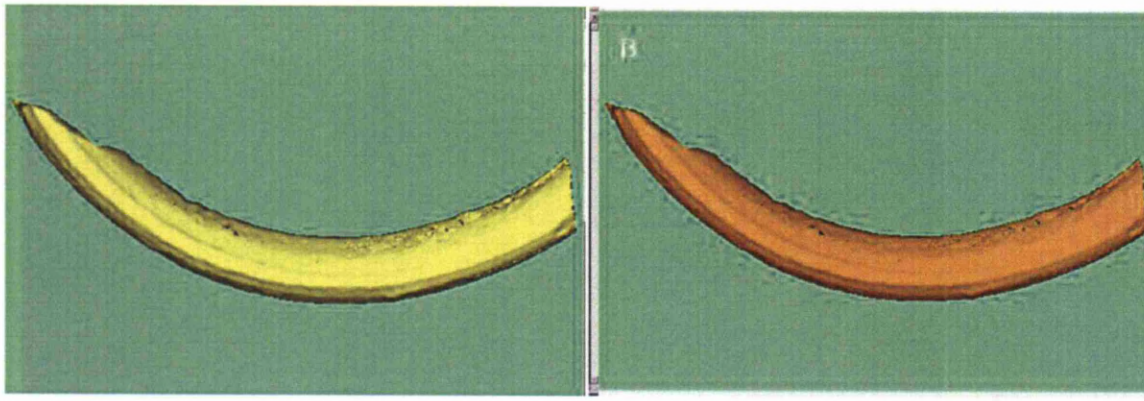

(A) 3D total (yellow) *surface-area*; (B) 3D marked (orange) *surface-area*. Buccal view of a left incisor. Scale = 10.0mm.

4.8.3.8. circumference: The *circumference* was used to determine the antero-posterior circumference. The measurement was used as an estimate of lateral growth and tooth bulk at the tooth curve tangent. It was taken from multiple views in 360° (Figure 48.).

Figure 48. 3D *circumference*

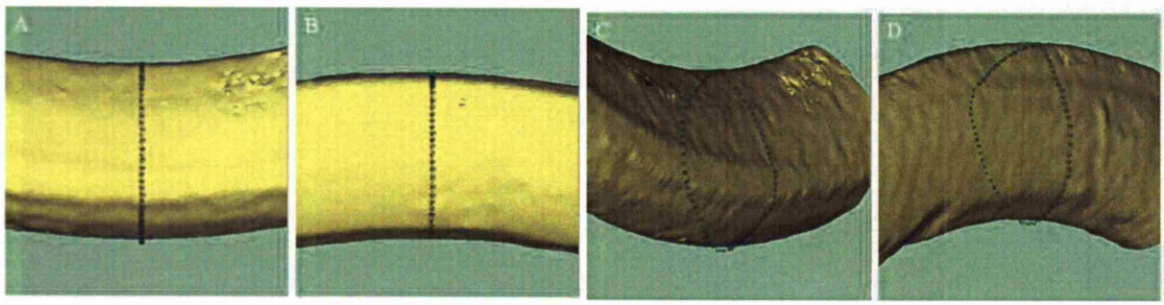

(A) buccal surface; (B) lingual surface; (C-D) buccal and lingual views displaying the actual 'on surface' measurements. Left incisor shown.

4.8.3.9. total volume: The 3D *volume* was used to determine the volume of the incisor. It was used as an estimate of tooth bulk and the quantity of enamel growth/ deposition. It accounted for the incisor's complete surface topography (Figure 49.).

Figure 49. 3D total *volume*

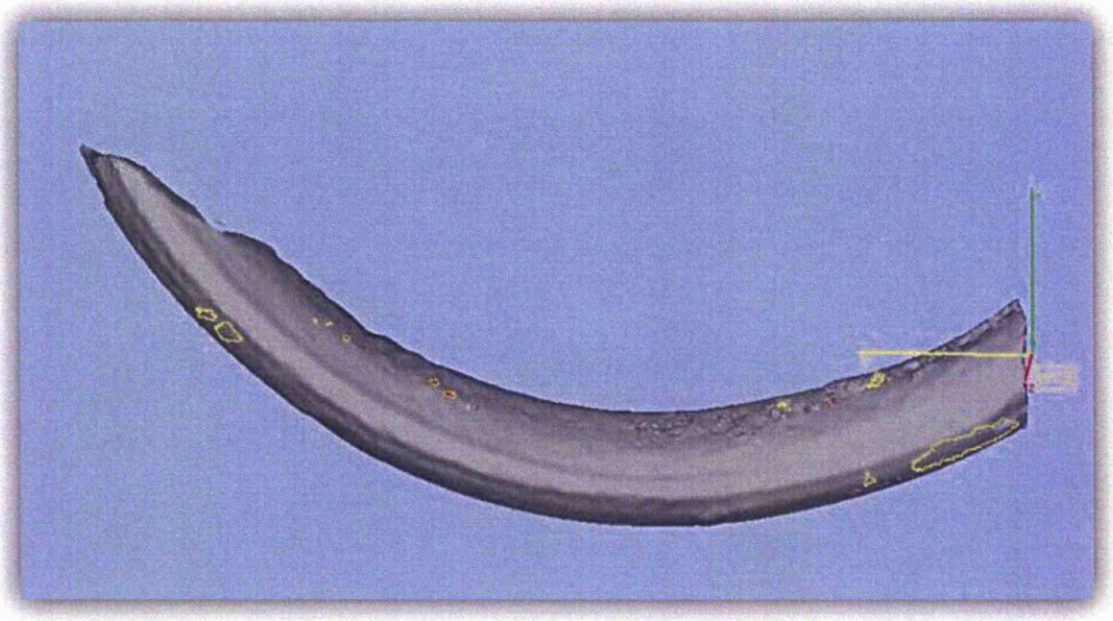

Buccal view of a left incisor.

4.8.3.10. surface-roughness: The *surface-roughness* measurement was used to determine the enamel surface roughness in each of the three representative regions of the labial surface (i) *gingival*, (ii) *middle* and (iii) *incisal* (Figure 50.).

Figure 50. 3D *surface-roughness*

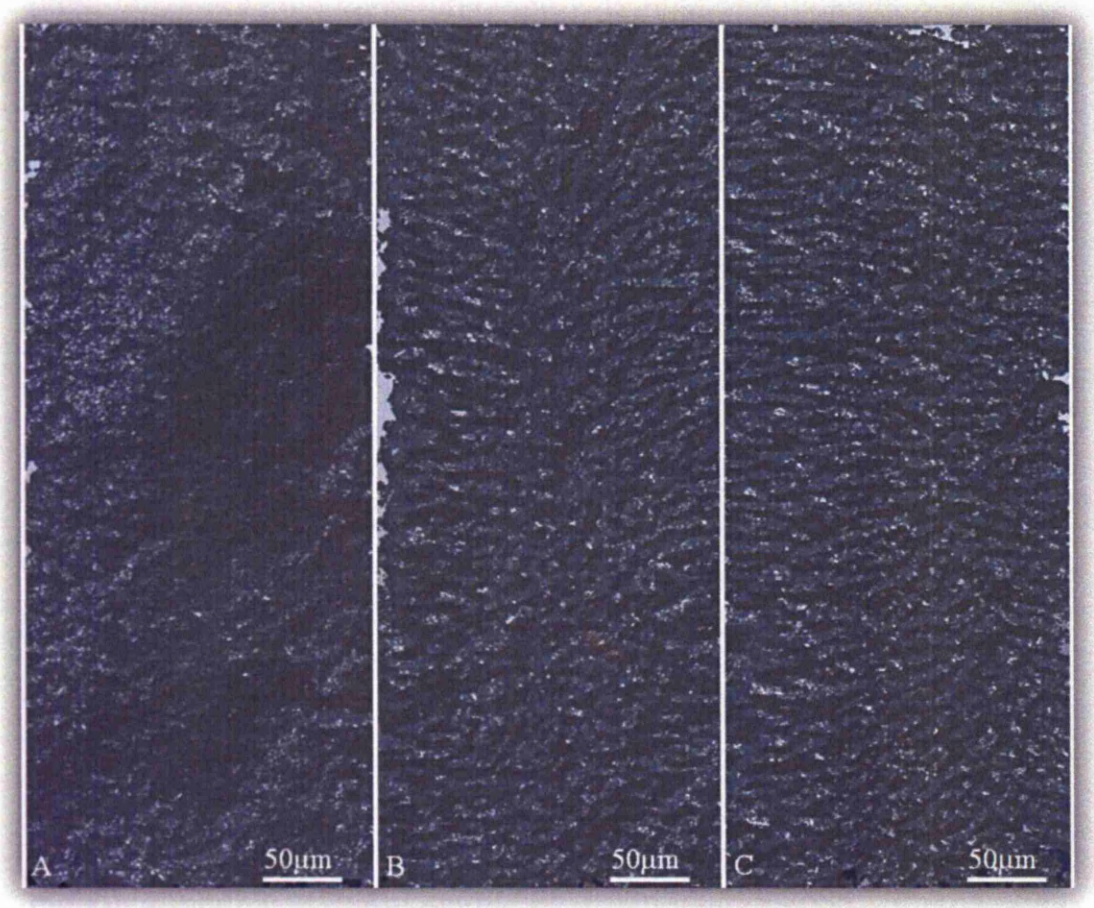

(A) *gingival/ pre-secretory*; (B) *middle/ secretory*; (C) *incisal/ mature* regions. The top of the image represents the proximal-end and the bottom of image represents the distal-tip. The 200X500µm images were obtained at 1.0µm resolution on the labial surface. The recommended ISO cut-off filter was calculated; sampling length (0.25mm), evaluation length (1.25 mm), step-size (1.0µm) and number of steps (1250);[(cut-off 0.25mm / 2) / step-size 0.001mm) = 125].

In the 'General' tab, 'Proscan2000 Configuration' and 'Analysis Functions Required' menu, the Roughness Average (Ra) surface characteristic function was selected. The measurement of form can be separated into roughness and waviness components (Thomas, 1982; Whitehouse, 1994). The 'Surface Filter' function was applied to remove the waviness component and leave the surface roughness information. By clicking 'Profile Analysis' the *surface-roughness* measurement data was exported into a Microsoft Excel spreadsheet (.csv) file containing separate mean X and Y coordinate Ra values.

4.9. 2D AND 3D MORPHOMETRIC MEASUREMENT

4.9.1. 2D and 3D Incisor Measurement

The following four measurements (except the projected and actual *labial-length*) were obtained from 3D models from the buccal and lingual view of the 2D images (total = 6 variables), for both the left and right side incisors: projected *overall-length* (mm); projected *labial-length*; actual *labial-length*; projected *width-at-midpoint* (mm).

All 2D measurements were taken both from the buccal and lingual view of the 2D images except the projected *labial-length* that was only taken from the buccal view as the values were the same. The *angle-of-curvature* was not obtained in 3D as it was limited in the 2D X and Y coordinate dimensions.

4.9.1.1. projected overall-length: The 2D projected and 3D projected *overall-length* were used to determine the overall longitudinal length of an incisor, from the proximal-end to the distal-tip (Figure 51.).

Figure 51. 2D projected *overall-length* and 3D projected *overall-length*

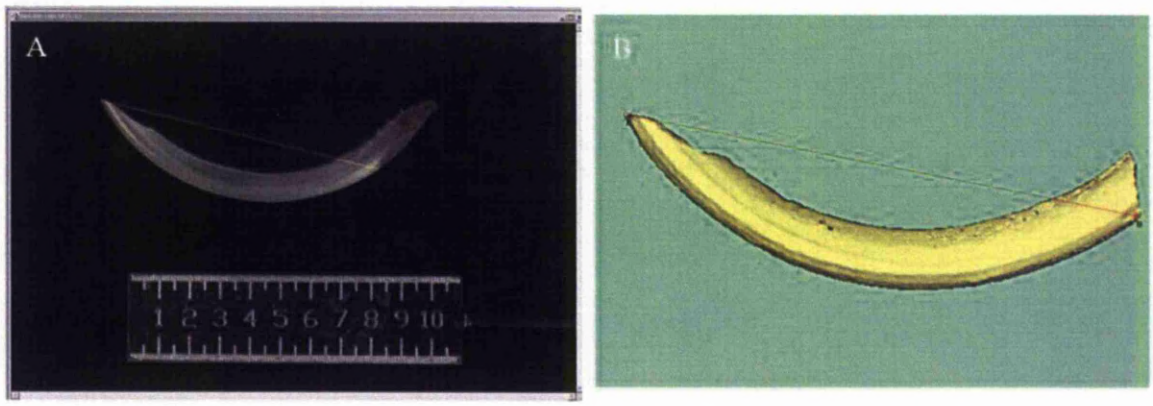

(A) 2D projected; (B) 3D projected. Left incisor, buccal view. Scale = 10.00mm.

The distinct surface texture and colour change that distinguished the start of the *pre-secretory* stage of enamel formation was used as a landmark feature - this was the same landmark as the colour and whiteness assessment images.

4.9.1.2. labial-length: The 2D projected *labial-length* and 3D actual *labial-length* determined the overall longitudinal incisor length along the labial surface, from the proximal-end to the distal-tip landmarks. It accounted for incisor curvature along the labial surface. It estimated the quantity of longitudinal enamel growth/ deposition. The 2D measurement was taken from the buccal view, and the 3D measurement was taken from the labial view (Figure 52.).

Figure 52. 2D projected *labial-length* and 3D actual *labial-length*

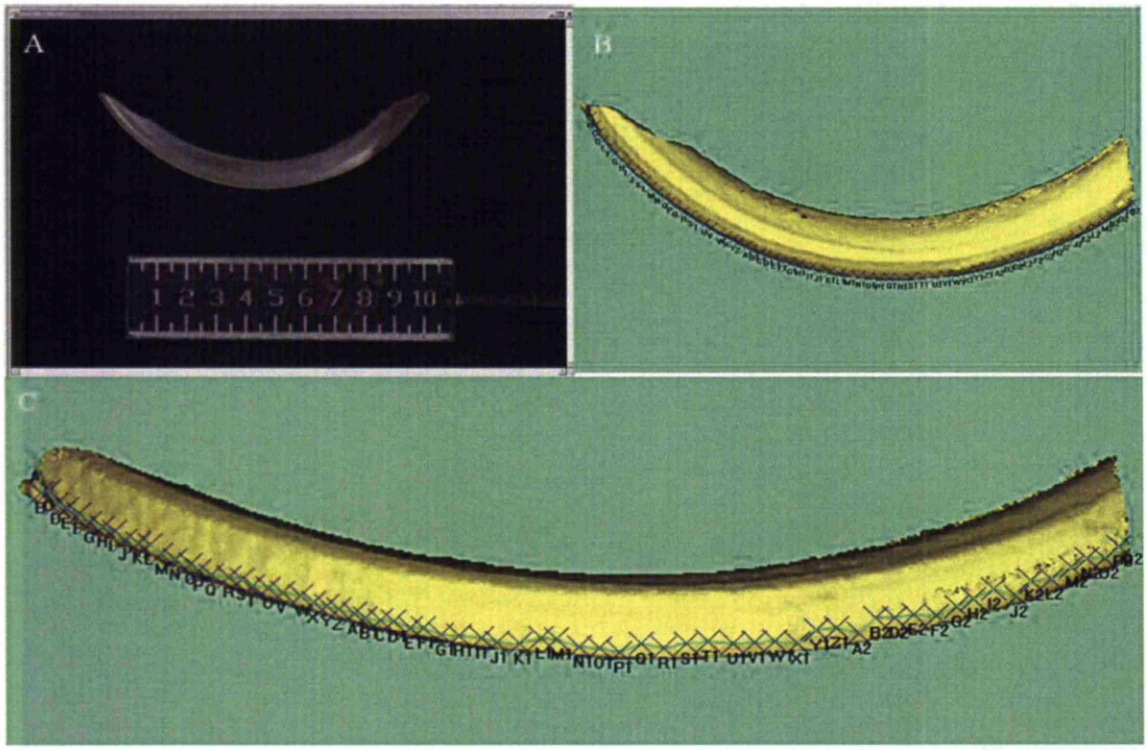

(A) 2D projected (yellow line); (B) 3D actual (buccal view); (C) 3D actual (labial view) Left incisor.
Scale = 10.0mm.

***4.9.1.3. actual labial-length*:** The 3D actual *labial-length* was used to determine the overall longitudinal length of an incisor along the labial surface. The measurement accounted for incisor curvature and topography along the labial surface. It was used to estimate the quantity of longitudinal enamel growth/ deposition. It was taken from the labial view (Figure 52.).

4.9.1.4. projected width-at-midpoint: The 2D projected *width-at-midpoint* and 3D projected *width-at-midpoint* were used to determine the incisor antero-posterior diameter, between the lingual and labial surfaces. They were used as an estimate of lateral growth and tooth bulk at the tooth curve tangent. Both were taken from the buccal and lingual views (Figure 53.).

Figure 53. 2D projected *width-at-midpoint* and 3D projected *width-at-midpoint*

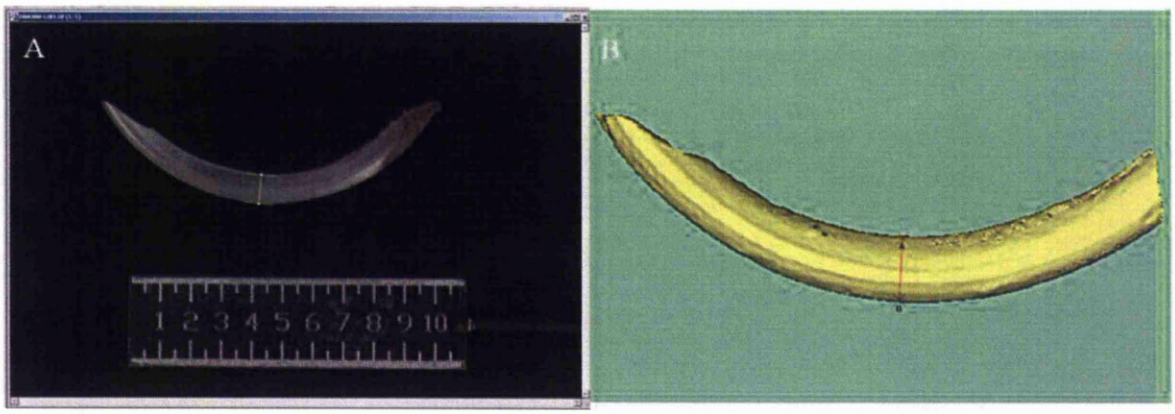

(A) 2D projected (B) 3D projected . Left incisor, buccal view. Scale = 10.0mm.

4.9.1.5. incisor perimeter: The 2D projected *perimeter* was used to determine the complete incisor perimeter. The 3D actual *perimeter* accounted for the incisor surface topography. It was used as an estimate of the overall quantity of enamel growth/ deposition. It was taken from the buccal and lingual views (Figure 54.).

Figure 54. 2D projected *perimeter* and 3D actual *perimeter*

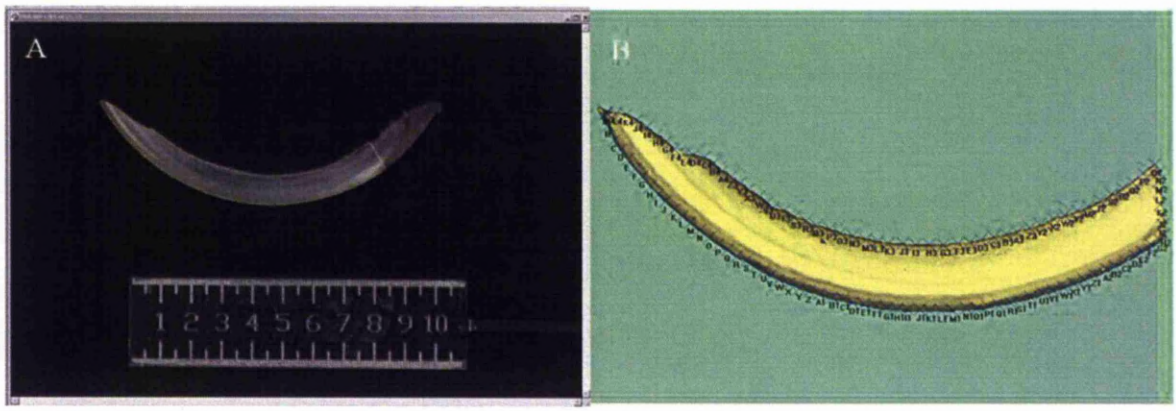

(A) 2D projected ; (B) 3D actual. Left incisor, buccal view. Scale = 10.0mm.

4.9.1.6. incisor surface-area: The 2D projected *surface-area* determined the flat surface area of tooth enamel. The 3D actual *surface-area* determined the marked surface area of enamel and accounted for the incisor surface topography. The measurements estimated of the quantity of enamel growth/ deposition. Both were taken from the buccal and lingual views (Figure 55.).

Figure 55. 2D projected *surface-area* and 3D actual *surface-area*

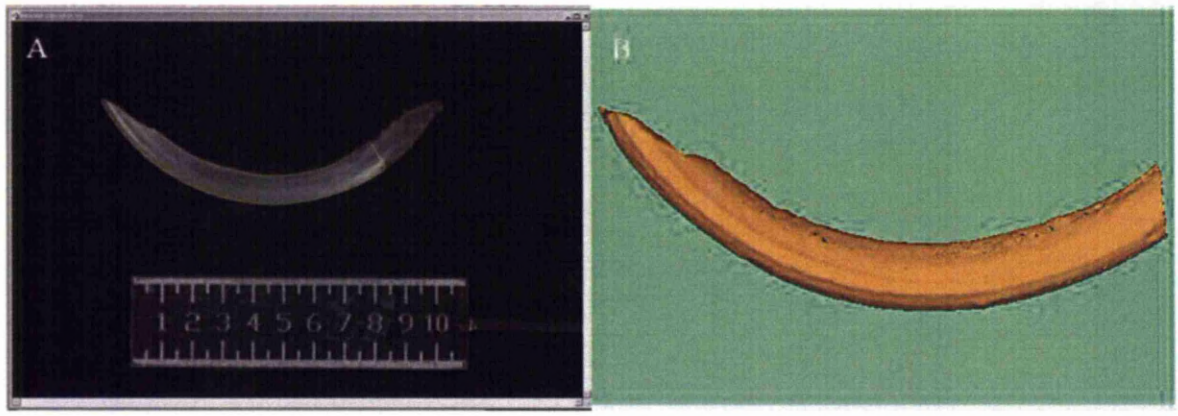

(A) 2D projected; (B) 3D actual marked. Left, incisor, buccal view. Scale = 10.0mm.

4.10. SUMMARY

An established 2D IAS was modified with a macro-lens for the small mouse application. An original standardised algorithm was developed in-house for the enamel colour and whiteness assessment. A bespoke 3D IAS was developed by adapting a high resolution measurement device with a rotary stage to obtain 3D images in 360°. Analytical measurement tools and 3D modelling software were customised for this application.

Two study samples were obtained for (i) multiple-operator method reliability and validation, and (ii) experimental comparative analysis. The reliability sample was a homogenous population of general laboratory mice (n = 20). The experimental sample was heterogenous population of congenic mice consisting of two separate populations each containing a control genotype groups and mutant genotype groups (n = 35) with recently described gene sequence mutations. The left and right side hemi-mandibles and mandibular incisors were imaged.

Hardware and software developments were undertaken and demonstrated novel input through inter-disciplinary collaboration. The new 2D IAS, new colour and whiteness and new 3D IAS were used to image the two study samples. These four approaches extended the measurement capacity for comparative investigation, using established parameters and new variables for objective and quantitative macro-metric and micro-metric murine dental phenotyping.

4.11. METHOD RELIABILTY AND VALIDATION

4.11.1. Introduction

Reliability measured the consistency of the instruments and methods, providing a measure of the total system error. This was determined by the statistical analysis of repeat measurements with the same equipment, on the same object and under the same conditions. Both intra-operator and inter-operator reliability was necessary for complete method assessment and validation (Smith and Harris, 2009). Also, to determine the validity of the new measurement methods it was essential to examine the measurement agreement with those of established methods recognised as benchmarks or as a definitive 'gold standard'. Both operator reliability and method agreement must be demonstrated as a reliable method may still be inaccurate.

The accuracy of each method was tested to identify measurement errors, defined as the difference between a measured and a true value. Measurement inaccuracies may be caused by (i) random (experimental) errors, which may vary from observation to observation, or (ii) systematic errors/ biases. All measurement methods contain experimental error.

Experimental error is inversely related to the degree of the reliability of the measurement method (Hunter and Priest, 1960). The greatest source of experimental error (that affects precision and reliability) may be landmark identification or positioning (Bhatia and Harrison, 1987). On the other hand, systematic errors are predictable, typically constant or proportional to the true value (Houston, 1983). They may be caused by imperfect instrument calibration, imperfect methods of observation or external interference in the measurement process (Keiser, 1990). Experimental errors may be identified by significant bias and eliminated.

There are number of terms associated with error and measurement reliability.

4.11.1.1. Accuracy/ Validity:

Accuracy is the closeness of a measurement to the true value. It was necessary to consider the validity of the measurement methods. The validity was assessed statistically for acceptability.

4.11.1.2. Precision:

The precision (or reliability) of a measurement method is the degree to which repeated measurements give the same value under unchanged conditions. Highly precise instruments have small variability (standard deviation) in the fluctuations of their measurements.

4.11.1.3. Reliability:

Reliability is the consistency of the measurement methods and measurements over a given number of repeat measurements on the same object under identical conditions, ideally by more than one operator. Reliability measures were developed by Bland and Altman (1986, 1999). Methods are deemed reliable (within a range) if they yield consistent results for the same measure, or are unreliable if repeat measurements give different results. Reliability also varies according to the skills of the operator and may improve through training.

4.11.2. Reliability Study

To make consistent observations an investigator must be familiar with a measurement technique. Each measurement method was piloted and standard operating procedures/ measurement protocols were written and revised iteratively. The protocols were used to provide adequate multiple operator training.

Before measuring the study sample the 2D IAS, the colour and whiteness and the 3D IAS measurement methods were all appraised during a reliability study that tested their experimental and systematic errors. The reliability studies established both the closeness of agreement between independent measurements obtained with the same method on an identical object, under the same conditions, by one identical operator (intra-operator repeatability) and by two different operators (inter-operator reproducibility).

Images were obtained with the same equipment, in the same laboratory, on separate occasions with a minimum interval of 1 week. Measurements were carried out after a minimum interval of 24 hours. The three independent operators were (I) Mr. Thomas Liam Coxon (TLC), (II) Mr. James Henry Hibbard (JHH) and (III) Dr. Aliya Stretton (AS). Operator I trained operators II and III in all methods. The first repeat measurements from each intra-operator repeatability study were used for the inter-operator reproducibility.

The exact number of images and measurements used in the comprehensive reliability and validation studies are detailed herein.

4.11.2.1. 2D IAS Mandible Morphometry:

2D images of the left and right hemi-mandibles (x2) were obtained from the buccal and lingual views (x4 images), from each individual in the reliability sample (x80 images). Each image was repeated by operators I and II (total x160 images). Eight variable measurements (x8) were obtained from each image.

4.11.2.2. 2D IAS Incisor Morphometry

2D images of the left and right incisors (x2) were obtained from the buccal and lingual views (x4 images), from each individual in the reliability sample (x80 images). Each image was repeated by operators I and II (total x 160 images). Five measurements were obtained from each image (+1 additional measurement from every buccal image) by operators I and II.

4.11.2.3. 2D IAS and Colour and Whiteness Assessment:

2D images of the left incisors were obtained from the labial view under polarised and non-polarised lighting conditions (x2 images), from each individual in the reliability sample (x40 images). Each image was repeated by operators I and III (total x80 images). Thirty two measurements were obtained from each image by operators I and III.

4.11.2.4. 3D IAS Incisor Morphometry:

3D images/ 3D model files of the left and right incisors (x2) were obtained from each individual in the reliability sample (x40 images). Each model was repeated by operators I and II (total x80 images). Sixteen measurements were obtained from each model by operators I and II.

Repeat images/ 3D model files were obtained by operator I only. Independent (multiple operator) intra-operator repeatability tested for experimental error and systematic error while and inter-operator reproducibility tested experimental error. Inter-operator repeats were not required for the 3D actual *surface-area*, marked *surface-area*, total *volume* and *surface-roughness* measurements because the values were identical computer outputs from the same 3D model files.

4.11.3. Statistics

The following descriptive statistics were used to quantitatively summarise the data.

4.11.3.1. Standard Deviation:

The standard deviation (SD) measured the measurement variability. It may be thought of as the average difference from the mean of the sample.

4.11.3.2. Standard Deviation of the Difference:

The Standard Deviation of the Difference (SD Diff'.) was used to assess measurement variability for the repeat measures.

4.11.3.3. Mean Difference:

The Mean Difference (MD).

4.11.3.4. Standard Error:

The standard error of the sample mean (SE) indicated the variability around the estimate of the mean measurement. It was used to calculate the 95% confidence intervals (1.96xSE) either side of the mean.

4.11.3.5. Intra-class Correlation Coefficient:

The Intra-class Correlation Coefficient (ICC) was used to assess the degree of correlation between quantitative measurement methods and measurements made by independent operators measuring the same quantity for intra-operator repeatability and inter-operator reproducibility (Fleiss and Shrout, 1977; Fleiss, 1986a, 1986b). In paired measurements the ICC was a more natural measure of association than the Pearson's Correlation Coefficient because it accounted for the biological variation of the samples.

Donner and Eliasziw (1986) classified the ICC values as;

Slight (0.000-0.200), Fair (0.210-0.400), Moderate (0.410-0.600), Substantial (0.610-0.800) and excellent (0.810-1.000) correlations.

4.11.3.6. Bland-Altman Plot:

Bland-Altman plots were created to observe operator and method agreement diagrammatically (Bland and Altman, 1986, 1999). They visualise the measurement variation between the two operators and the two methods by plotting the average of two measurements (horizontal X axis) against the difference between each measurement (vertical Y axis). This illustrates the size of the measurement variation and its distribution about zero. Therefore, it is possible to demonstrate not only the overall degree of agreement but also the presence of any biases.

The plots reveal any possible unwanted relationships between the differences and the averages (Figure 56.).

Figure 56. Bland-Altman Plots Measurement Distribution

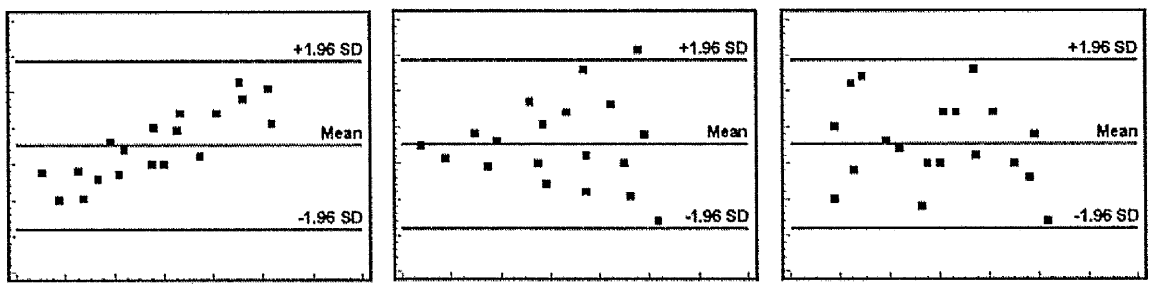

(A) a proportional error; (B) a case where the variation of at least one method depended strongly on the magnitude of the measurements; (C) expected systematic error. The average of the two measurements is displayed on the horizontal X axis against the difference between each measurement on the vertical Y axis.

A horizontal line is drawn at the MD. Dashed lines drawn at the MD ± 1.96 X SD Diff' are equal to the limits of agreement (or the coefficient of repeatability).

4.11.3.7. Coefficient of Repeatability/ Limits of Agreement:

The coefficient of repeatability (CR) was used as a precision measure to determine the agreement strength or repeatability of a measurement. It was calculated as ± SD of Diff' (about MD = zero) X 1.96. The CR was given for the intra-operator repeatability and was equal to the limits of agreement (LOA) given for the inter-operator reproducibility. Both were displayed within the Bland-Altman plots.

4.11.3.8. Confidence Intervals:

Confidence intervals (CI) are typically stated at the 95% confidence level. They specify a range within which 95% of the population would be expected to lie (Bland and Altman, 1986). If the range is too wide it could suggest that either a larger population or a more discriminatory variable is required.

4.11.3.9. Significant Measurement Bias:

A bias estimate was calculated for each variable. A MD less than the SE X 1.96 implied no significant bias.

4.11.4. Validation Study

The new colour and whiteness method was not comparable with any existing murine techniques, as described in the literature review. However, the validity was fully tested (see Appendix 4. List of Original Publications). The novel 3D IAS was validated here against the existing 2D IAS.

The following statistics were used to quantitatively summarise the validation study data.

4.11.4.1. Pearson's Correlation Coefficient:

Pearson's Product-Moment Correlation Coefficient (PCC) was used to measure the strength of agreement between the two methods, at the $p = 0.01$ (1%) significance level (two-tailed). It is the most commonly applied statistic for method agreement studies because it quantifies the differences between measurements made by independent operators on the same variables (Bland and Altman, 1986, 1999). Scatter plots were used to identify outliers.

The interpretation of the PCC depends on the context and purposes of the method comparison and several guidelines are offered (Rodgers and Nicewander, 1988). The PCC ranges in values from -1 (a perfect negative relationship) to +1 (a perfect positive relationship), where a value of 0 indicates no linear relationship. Regarding the size of the measurement correlation, a positive correlation, for example, may be Small (0.1 – 0.3), Medium (0.3 – 0.5) or Large (0.5-1.0).

4.11.4.2. Scatter Plot:

Scatter plots illustrated the degree of correlation between the measurements from the two different methods and showed up any outliers.

4.11.4.3. t-test:

A student's *t*-test (two-tailed) is the most commonly used hypothesis test. In the validation study a Repeated Measures *t*-test was used to reject the null hypothesis; e.g. that there were significant differences ($p \geq 0.01$) between the two measurement methods.

4.11.5. Principal Component Analysis

The PCA was used as an exploratory analysis to discover patterns of relationships between variables. Total Variance Explained tables were given to show how much variance each component (or the combination of multiple variables) accounted for as a percentage of the total variance of shape.

Principal components that accounted for less than one Eigenvalue were extracted. The Scree plot illustrated at what point (Eigenvalue $\geq$ one) additional components no longer had a discernable effect on the amount of variance of shape.

4.11.6. Experimental Study

The following statistics were used to quantitatively summarise the experimental study data.

4.11.6.1. Analysis of Variance (ANOVA):

A one-way Analysis of Variance (ANOVA) measured phenotype variation between the different groups. Multiple pair-wise comparisons simultaneously compared all possible pairs of means to identify which group means were significantly different from one another. A Bonferroni calculation corrected the $p = 0.05$ (5%) significance level for the increased probability of making type-1 errors (false positives) that occur normally when making numerous multiple comparisons. The significance level (α) was divided by the number of variables tested (α/n), e.g. 0.05/ (22 or 32) = 0.002 (2-tailed). The Bonferroni significance level ($p = 0.002$) was a robust adjustment, particularly with respect to the independence of the variables. Therefore, where applicable, any significant differences ($p < 0.05$) observed before the Bonferroni correction were also detailed.

ANOVA was reliable when assuming (i) variables were normally distributed, (ii) samples were independent and (iii) variances were all equal. The F-distribution statistic was presented as a convention.

4.11.6.2. Multiple Comparisons:

Tukey's Honestly Significant Difference (HSD) test was used in conjunction with the ANOVA. It was essentially a multiple *t*-test that also corrected for the increased probability of false positives by requiring a stronger level of evidence for significance to be achieved in each pair-wise test. The $p = 0.05$ (5%) significance level was used (2-tailed).

The one-way ANOVA and Tukey's HSD tests compensated for the large number of inferences being made and were more suitable than doing multiple *t*-tests.

5. RESULTS

5.1. METHOD RELIABILITY AND VALIDATION

5.1.1. Introduction

Fliess Intra-class Correlation Coefficient determined intra-operator repeatability and inter-operator reproducibility. Bland-Altman plots displayed a graphical representation of measurement method agreement, distribution about the mean, bias and limits of agreement. Pearson's Correlation Coefficient, Scatter Plots and Repeated Measures *t*-tests demonstrated the 2D IAS and 3D IAS method agreement towards validation.

Descriptive statistics summarised the reliability, validation and experimental data; Mean Difference, Standard Deviation, Standard Deviation of the difference, Standard Error and Coefficient of Repeatability (or Limits of Agreement).

Principal Component Analysis and Scree Plots revealed a number of underlying variable associations defining the shape of the mandible and incisor.

Bonferroni corrected one-way ANOVA multiple comparisons ($p = 0.002$) and Tukey's HSD tests ($p = 0.05$) identified phenotype variation.

Reliability and validation measurements were carried out by three independent operators.

5.1.2. Reliability - 2D Mandible Measurement

This section details one example variable from each of the intra-operator repeatability and the inter-operator reproducibility datasets for brevity. The full data is recorded in Appendix 1. Tables 1-6).

5.1.2.1. Intra-Operator Repeatability Operator I (TLC):

Table 2. Intra-operator I Statistics - left mandible buccal view *overall-length*

Mean Difference (mm)	0.025
Standard Deviation of Difference (mm)	0.243
Standard Error (mm)	0.054
Bias (Mean Diff. < SE X 1.96)	0.106
Coefficient of Repeatability ±	0.476
Intra-class Correlation Coefficient	0.919

Figure 57. Intra-operator I Bland-Altman Plot - left mandible buccal view *overall-length*

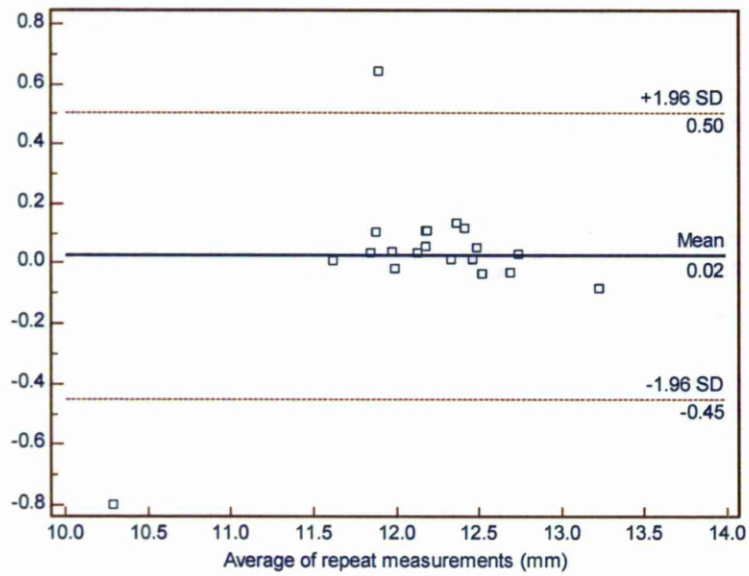

Intra-operator repeatability (ICC 0.791-0.988) was classified as substantial to excellent (Donner and Eliasziw, 1987); right buccal *diagonal-length* (ICC ≥0.791) showed the lowest repeatability and left buccal *overall-length* (ICC ≤ 0.988) showed the highest repeatability (Appendix 1. Tables 1. and 2.).

5.1.2.2. Intra-Operator Repeatability Operator II (JHH):

Table 3. Intra-operator II Statistics - left mandible buccal view *overall-length*

Mean Difference (mm)	0.016
Standard Deviation of Difference (mm)	0.072
Standard Error (mm)	0.016
Bias	0.031
Coefficient of Repeatability ±	0.141
Intra Class Correlation Coefficient	0.993

Figure 58. Intra-operator II Bland-Altman Plot - left mandible buccal view *overall-length*

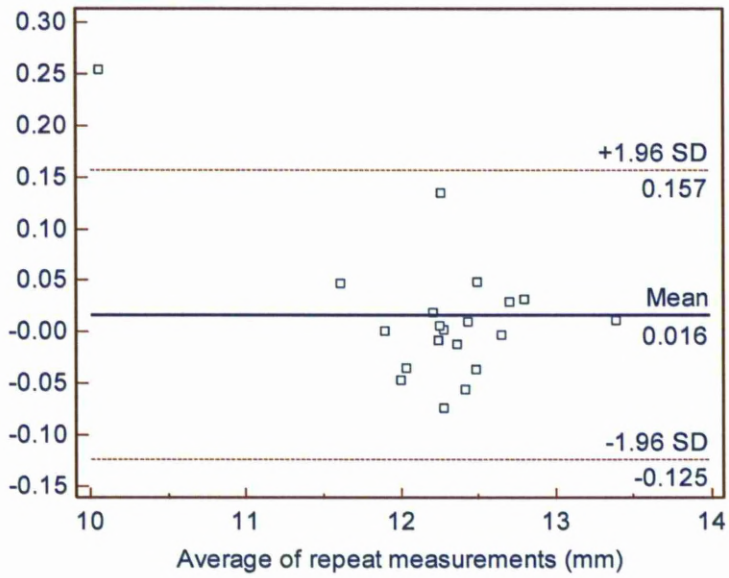

Intra-operator repeatability (ICC 0.810-0.997) was classified as excellent (Donner and Eliasziw, 1987); right lingual *ascending-height* (ICC $\geq$ 0.810) showed the lowest repeatability and right buccal *mandible-angle* (ICC $\leq$ 0.997) showed the highest repeatability (Appendix 1. Tables 3. and 4.).

5.1.2.3. Inter-Operator Reproducibility Operators I and II (TLC and JHH):

Table 4. Inter-operator Statistics - left mandible buccal view *overall-length*

Mean Difference (mm)	-0.069
Standard Deviation of Difference (mm)	0.113
Standard Error (mm)	0.025
Bias	0.049
Limits of Agreement ±	0.221
Intra Class Correlation Coefficient	0.980

Figure 59. Inter-operator Bland-Altman Plot - left mandible buccal view *overall-length*

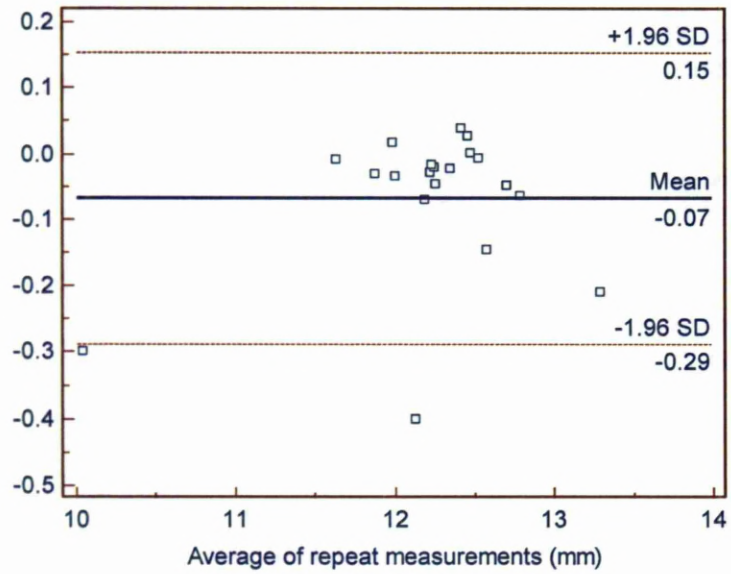

Inter-operator reproducibility (ICC 0.820-0.979) was classified as excellent (Donner and Eliasziw, 1987); left mandible lingual *diagonal-length* (ICC $\geq$ 0.820) showed the lowest reproducibility and left lingual *mandible-area* (ICC $\leq$ 0.993) showed the highest reproducibility (Appendix 1. Tables 5. and 6.).

5.1.3. Reliability - 2D Incisor Measurement

This section gives the statistics of one example variable from each of the intra-operator repeatability and the inter-operator reproducibility datasets for brevity. The full data is recorded in Appendix 1. Tables 7-9.

5.1.3.1. Intra-Operator Repeatability Operator I (TLC):

Table 5. Intra-operator I Statistics – left 2D incisor buccal view *overall-length*

Mean Difference (mm)	0.087
Standard Deviation of Difference (mm)	0.387
Standard Error (mm)	0.087
Bias	0.171
Coefficient of Repeatability ±	0.759
Intra Class Correlation Coefficient	0.908

Figure 60. Intra-operator I Bland-Altman Plot – left 2D incisor buccal view *overall-length*

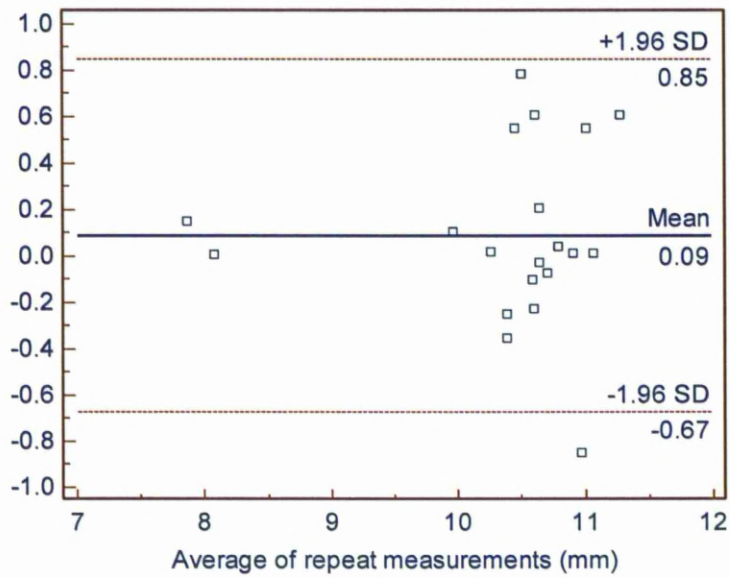

Intra-operator repeatability (ICC 0.826-1.000) was classified as excellent (Donner and Eliasziw, 1987); right buccal *angle-of-curvature* (ICC $\geq$ 0.826) showed the lowest repeatability and all *width-at-midpoint* (ICC 1.000) measurements showed equally high repeatability (Appendix 1. Table 7.).

5.1.3.2. Intra-Operator Repeatability Operator II (JHH):

Table 6. Intra-operator II Statistics - left 2D incisor buccal view *overall-length*

Mean Difference (mm)	-0.011
Standard Deviation of Difference (mm)	0.168
Standard Error (mm)	0.038
Coefficient of Repeatability ±	0.329
Bias	0.074
Intra-class Correlation Coefficient	0.987

Figure 61. Intra-operator II Bland-Altman Plot - left 2D incisor buccal view *overall-length*

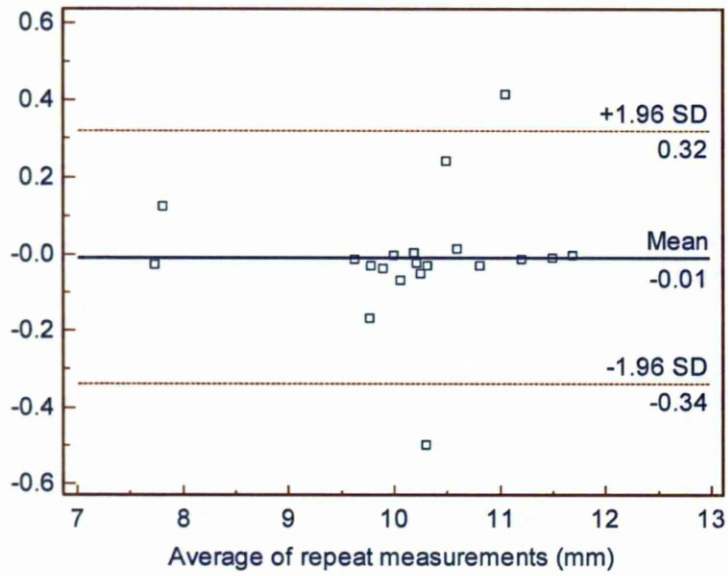

Intra-operator repeatability (ICC 0.925-1.000) was classified as excellent (Donner and Eliasziw, 1987); right lingual *overall-length* (ICC $\geq$ 0.955) showed the lowest repeatability and all *width-at-midpoint* (ICC 1.000) measurements showed equally high repeatability (Appendix 1. Table 8.).

5.1.3.3. Inter-Operator Reproducibility Operators I and II (TLC and JHH):

Table 7. Inter-operator Statistics - left 2D incisor buccal view *overall-length*

Mean Difference (mm)	0.270
Standard Deviation of Difference (mm)	0.467
Standard Error (mm)	0.104
Bias	0.203
Limits of Agreement ±	0.915
Intra Class Correlation Coefficient	0.852

Figure 62. Inter-operator Bland-Altman Plot – 2D left incisor buccal view *overall-length*

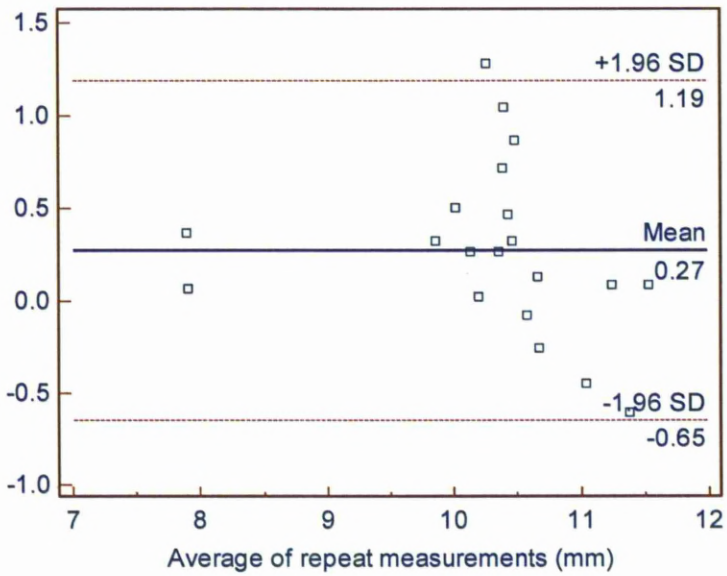

Inter-operator reproducibility (ICC 0.768-1.000) was classified as substantial to excellent (Donner and Eliasziw, 1987); right buccal *angle-of-curvature* (ICC ≥ 0.768) showed the lowest reproducibility and all *width-at-midpoint* (ICC 1.000) showed equally high reproducibility (Appendix 1. Table 9.).

5.1.4. Reliability - Colour and Whiteness Assessment

This section details one example variable from each of the intra-operator repeatability and inter-operator reproducibility datasets for brevity. The full data is recorded in Appendix 1 Tables 10-15.

5.1.4.1. Intra-Operator Repeatability Operator I (TLC):

Table 8. Intra-operator I Statistics - non-polarised *gingival* region *lightness*

Mean Difference	-0.081
Standard Deviation of Difference	2.083
Standard Error	0.466
Bias	0.953
Coefficient of Repeatability ±	4.083
Intra Class Correlation Coefficient	0.812

Figure 63. Intra-operator I Bland-Altman Plot - non-polarised *gingival* region *lightness*

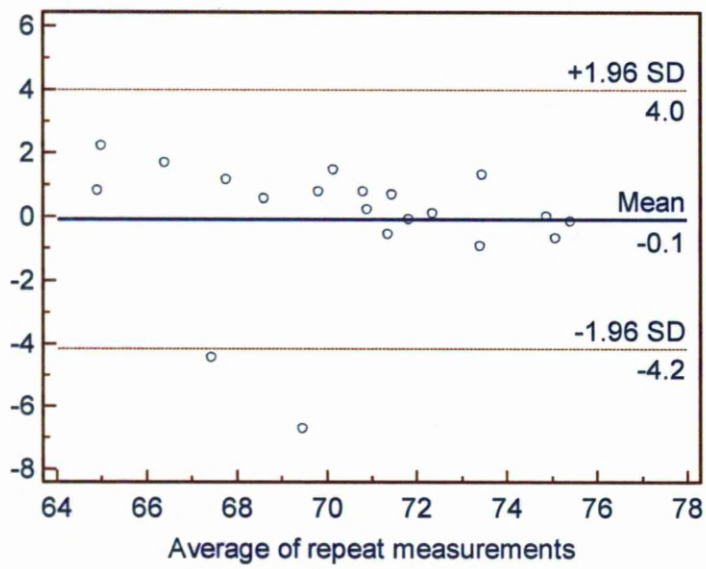

Intra-operator repeatability (ICC 0.731-0.999) was classified as substantial to excellent (Donner and Eliasziw, 1987); non-polarised *gingival* region *yellow/ blue* showed the lowest repeatability (ICC $\geq$ 0.731) and polarised *incisal* and *whole* region *red/ green* colour components showed the highest repeatability (ICC $\leq$ 0.999) (Appendix 1. Tables 10. and 11.).

5.1.4.2. Intra-Operator Repeatability Operator III (AS):

Table 9. Intra-operator III Statistics - non-polarised *gingival* region *lightness*

Mean Difference	1.417
Standard Deviation of Difference	4.756
Standard Error	1.063
Bias	2.083
Coefficient of Repeatability ±	9.322
Intra Class Correlation Coefficient	0.563

Figure 64. Intra-operator III Bland-Altman Plot - non-polarised *gingival* region *lightness*

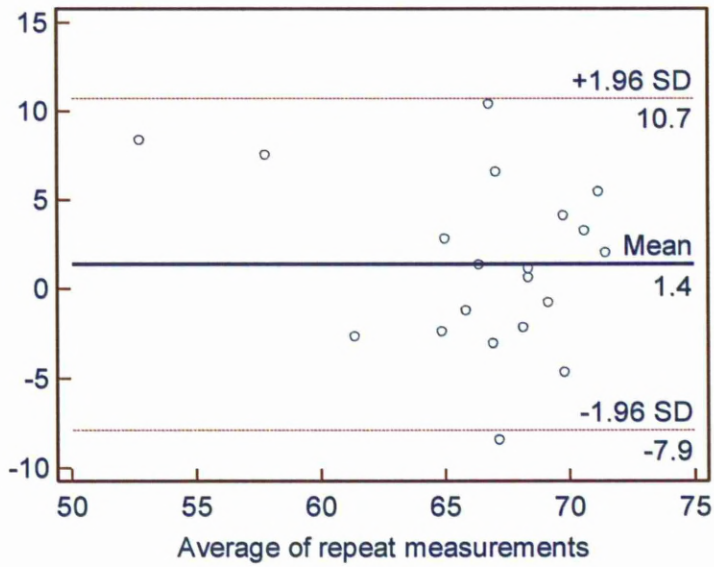

Intra-operator repeatability (ICC 0.400-0.973) was classified as fair to excellent (Donner and Eliasziw, 1987); non-polarised *gingival* region *yellow/ blue* showed the lowest repeatability (ICC $\geq$ 0.400) and polarised *whole* region *yellow/ blue* colour components showed the highest repeatability (ICC $\leq$ 0.973) (Appendix 1. Tables 12. and 13.).

5.1.4.3. Inter-Operator Reproducibility Operators I and III (TLC and AS):

Table 10. Inter-operator Statistics - non-polarised *gingival* region *lightness*

Mean Difference (mm)	3.331
Standard Deviation of Difference (mm)	4.676
Standard Error (mm)	1.046
Bias	2.050
Limits of Agreement ±	9.165
Intra Class Correlation Coefficient	0.219

Figure 65. Inter-operator Bland-Altman Plot - non-polarised *gingival* region *lightness*

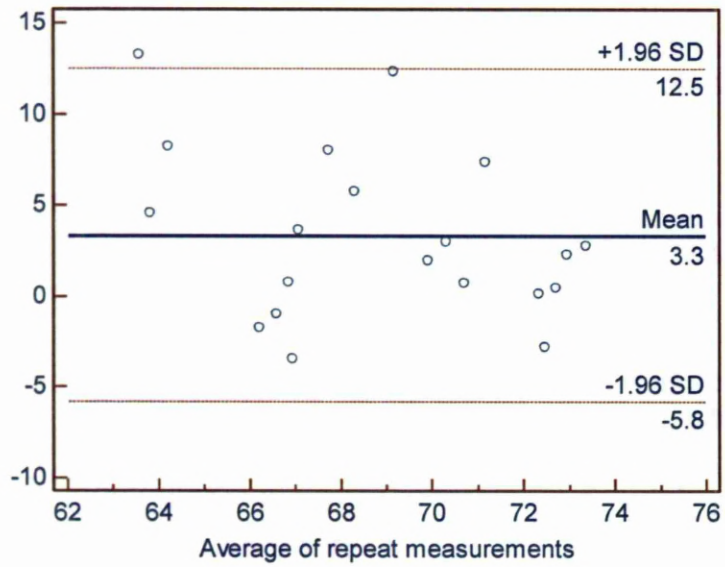

In the main, inter-operator reproducibility (ICC 0.126 - 0.939) was classified as slight to excellent (Donner and Eliasziw, 1987); non-polarised *gingival* region *yellow/ blue* showed the lowest reproducibility (ICC $\geq$ 0.126) and polarised *middle* region *red/ green* colour components showed the highest reproducibility (ICC $\leq$ 0.939) (Appendix 1. Tables 14. and 15.).

5.1.5. Reliability - 3D Incisor Measurement

This section details one example variable from each of the intra-operator repeatability and inter-operator reproducibility datasets for brevity. The full data is recorded in Appendix 1 Tables 16-20.

5.1.5.1. Intra-Operator Repeatability Operator I (TLC):

Table 11. Intra-operator I Statistics - left 3D incisor buccal view projected *overall-length*

Mean Difference (mm)	-0.028
Standard Deviation of Difference (mm)	0.282
Standard Error (mm)	0.063
Bias	0.124
Coefficient of Repeatability ±	0.553
Intra-class Correlation Coefficient	0.922

Figure 66. Intra-operator I Bland-Altman Plot - left 3D incisor buccal view projected *overall-length*

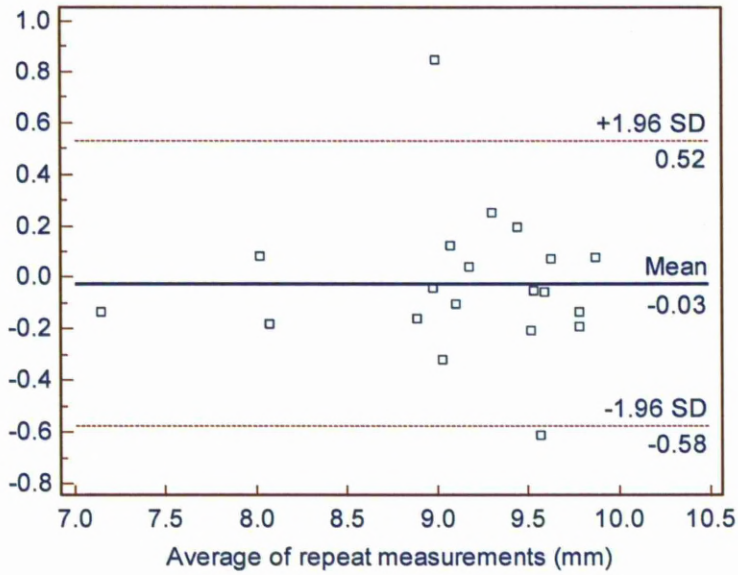

Intra-operator repeatability (ICC 0.750-1.000) was classified as substantial to excellent (Donner and Eliasziw, 1987); right lingual actual *width-at-midpoint* (ICC $\geq$ 0.750) showed the lowest repeatability and all projected *width-at-midpoint* measurements showed equally high repeatability (ICC $\leq$ 1.000) (Appendix 1. Tables 16. and 17.).

5.1.5.2. Inter-Operator Reproducibility Operators I and II (TLC and JHH):

Table 12. Inter-operator Statistics – left 3D incisor buccal view projected *overall-length*

Mean Difference (mm)	-0.068
Standard Deviation of Difference (mm)	0.104
Standard Error (mm)	0.023
Bias	0.045
Limits of Agreement ±	0.203
Intra Class Correlation Coefficient	0.986

Figure 67. Inter-operator Bland-Altman Plot – left 3D incisor buccal view projected *overall-length*

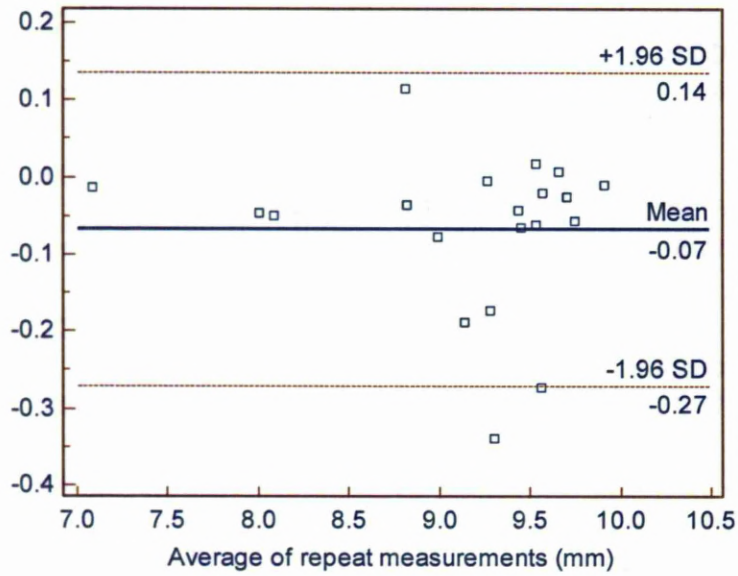

The inter-operator reproducibility (ICC 0.818-1.000) was classified as excellent (Donner and Eliasziw, 1987); right buccal actual *width-at-midpoint* (ICC $\geq$ 0.818) showed the lowest repeatability and left buccal and lingual projected *width-at-midpoint,* and *circumference* and right buccal projected *width-at-midpoint* and lingual projected and actual *width-at-midpoint* (ICC $\leq$ 1.000) showed equally high repeatability (Appendix 1. Tables 18. and 19.).

5.1.6. Validation - 2D and 3D Incisor Measurement

This section details of one example variable from the intra-operator repeatability and the inter-operator reproducibility datasets for brevity. The full data is recorded in Appendix 1 Tables 20.

5.1.6.1. 3D Method Validation Operator I (TLC):

Table 13. Validation Statistics - left incisor buccal view projected *overall-length*

Mean Difference (mm)	0.154
Standard Deviation of Difference (mm)	0.371
Standard Error (mm)	0.083
Bias	0.163
Limits of Agreement ±	0.727
***t*-test**	0.079*
Pearson's Correlation Coefficient	0.866**

*No significant difference at the 0.01 (1%) level (2-tailed). **Pearson's Correlation Coefficient was significant at the 0.01 (1%) level (2-tailed).

Figure 68. Validation Scatter Plot - left incisor buccal view projected *overall-length*

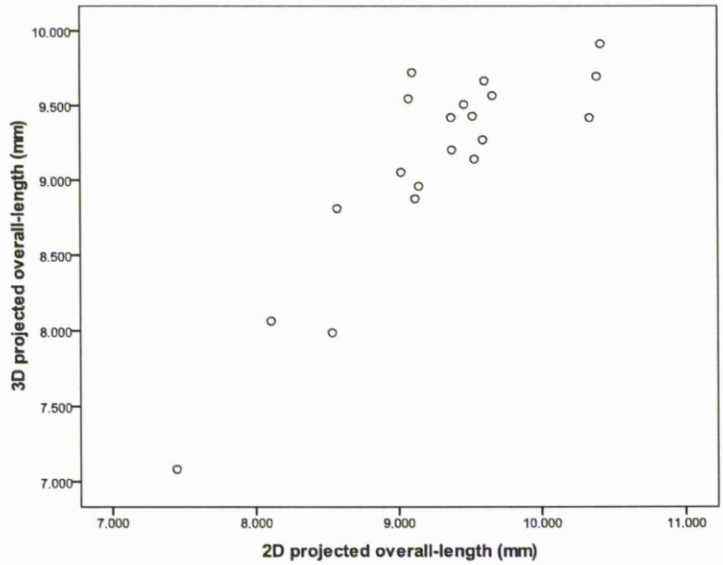

Figure 69. Validation Bland-Altman Plot - left incisor buccal view projected *overall-length*

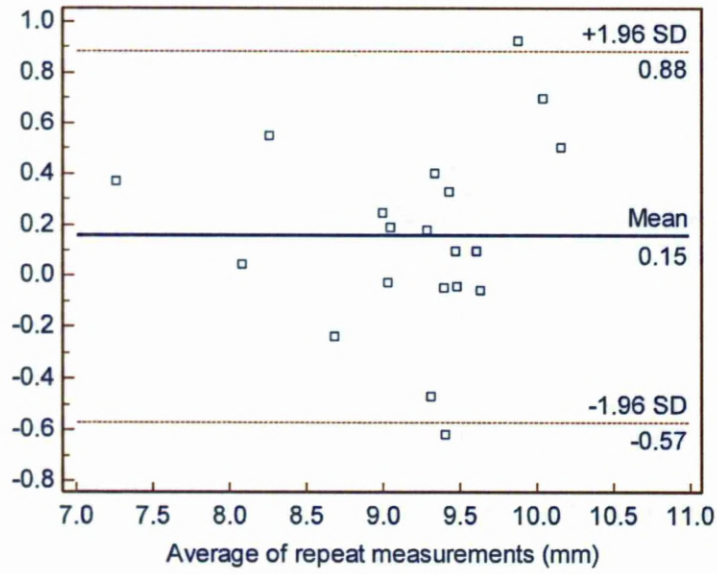

The 2D and 3D method agreement showed a significant ($p \leq 0.01$) large positive correlation (PCC 0.710 - 0.999) (Appendix 1. Table 20.). The repeated measures *t*-test showed there were no significant differences ($p \geq 0.01$) between the 2D IAS and 3D IAS measurements, except in the projected *width-at-midpoint* variable. The left lingual projected *width-at-midpoint* (PCC $\geq$ 0.710) showed the smallest positive correlation and the right labial projected *labial-length* (PCC $\geq$ 0.999) showed the largest positive correlation.

5.1.7. Summary

There was predominately substantial to excellent reliability for all three independent operators for all three measurement methods.

There were negligible differences in reliability between the left and right side mandibles and incisors, and between the buccal, lingual and labial views.

Bland-Altman plots indicated negligible systematic error, proportional error and bias.

The 2D IAS gold standard successfully validated the new 3D IAS and the two methods could be used interchangeably.

5.1.8. Impact on Null-Hypotheses

In relation to the hypotheses of this investigation, the null hypotheses were rejected in all cases in the reliability and validation studies indicating that all the methods were reliable, practical and objective and had good sensitivity for detecting differences between groups.

The methods identified macro-metric and micro-metric differences in a homogeneous congenic murine population. The methods were well suited to the small mammalian application.

5.2. PRINCIPAL COMPONENT ANALYSIS (PCA)

5.2.1. Introduction

Principal Components Analysis (PCA) established which variable relationships were responsible for describing shape. These formed the principal components derived from the factor analysis process. The values showed inter-relationships for each variable and were used to understand what each identified component signified. Following convention, components were only considered that scored over one Eigenvalue, as illustrated in the Scree plots.

5.2.2. PCA of 2D Mandible Measurement

This section gives the PCA statistics of the left side buccal view as an example for brevity as the data was similar for both the left and right sides, and for buccal and lingual views (Table 14. and Figure 70.). The full data is recorded in Appendix 2. Table 1.

Table 14. PCA Mandible Morphometry - left side buccal view

A

COMPONENT	Total Variance Explained Initial Eigenvalues Total	% of Variance	Cumulative %
1	4.368*	54.599	54.599
2	2.097*	26.216	80.815
3	0.990	12.375	93.190
4	0.337	4.216	97.406
5	0.126	1.577	98.983
6	0.048	0.605	99.588
7	0.026	0.323	99.911
8	0.007	0.089	100.000

B

MEASUREMENT VARIABLE	Component Matrix Component 1	2
mandible-area (mm^2)	0.902	-0.251
basal-length (mm)	0.882	0.372
mandible-perimeter (mm)	0.874	-0.349
ascending-height (mm)	0.850	0.219
overall-length (mm)	0.821	0.348
diagonal-length (mm)	0.766	-0.113
mandible-angle (°)	0.055	-0.963
coronoid-coronoid-length (mm)	-0.159	-0.815

(A) Total variance of shape explained; (B) Extracted components matrix. *Eigenvalue > 1.

Figure 70. PCA Scree Plot Mandible Morphometry - left side buccal view

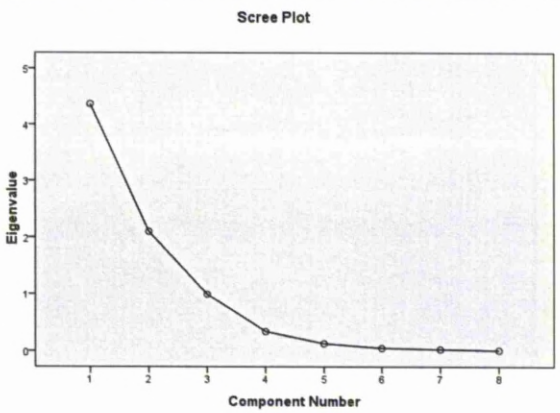

(C) Scree Plot.

Two components were identified; (i) component one (54.6%) and (ii) component two (26.2%) that accounted for 80.8% of the total variance in mandible shape (Appendix 2. Table 1). Component one highlighted a directly proportional size correlation between most variables. The *mandible-area*, *basal-length* and *mandible perimeter* showed the largest positive inter-relationships. The *coronoid-condyle-length* showed a negative relationship

which suggested a decrease in *coronoid-condyle-length* was related to an increase in mandible size. This later relationship was only small and may indicate that the size of this variable was static.

Component two highlighted an inversely proportional correlation between *coronoid-condyle-length* and *mandible-angle* and *diagonal-length*, which suggested a decrease in *coronoid-condyle-length* was related to an increase in *mandible-angle*. A larger *mandible-angle* gave a smaller mandible. This relationship was logical when studying the curved morphology of the incisor in the morphometric images (Figure 9.).

5.2.3. PCA of 2D Incisor Measurements

This section gives the PCA statistics of the left side buccal view as an example for brevity as the data was similar for both the left and right sides, and for buccal and lingual views (Table 15. and Figure 71.). The full data is recorded in Appendix 2. Table 2.

Table 15. PCA 2D Incisor Morphometry - left side buccal view

A

COMPONENT	Total Variance Explained Initial Eigenvalues		
	Total	% of Variance	Cumulative %
1	3.758*	75.165	75.165
2	1.067*	21.335	96.500
3	0.140	2.791	99.292
4	0.030	0.592	99.883
5	0.006	0.117	100.000

B

MEASUREMENT VARIABLE	Component Matrix Component	
	1	2
projected *perimeter* (mm)	0.989	-0.102
projected *overall-length* (mm)	0.979	-0.069
projected *surface-area* (mm^2)	0.970	0.192
angle-of-curvature (°)	-0.883	0.358
projected *width-at-midpoint* (mm)	0.316	0.941

(A) Total variance of shape explained; (B) Extracted components matrix. *Eigenvalue > 1.

Figure 71. PCA Scree Plot 2D Incisor Morphometry - left side buccal view

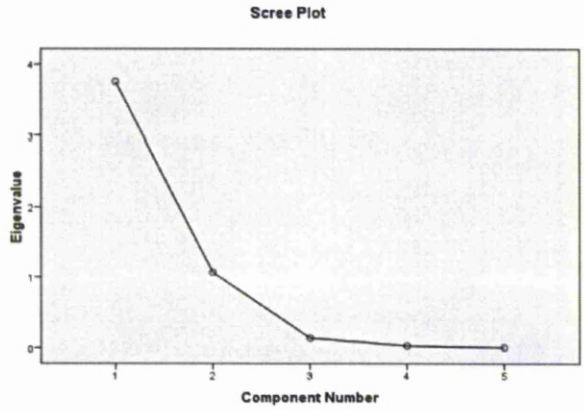

(C) Scree Plot.

Two components were identified; (i) component one (75.2%) and (ii) component two (21.3%) that accounted for 96.5% of the total variance in incisor shape (Appendix 2. Table 2). Component one highlighted a directly proportional size correlation between the majority of variables. The projected *perimeter*, projected *overall-length* and projected *surface-area* showed the largest positive inter-relationships. The *angle-of-curvature* showed a strong negative relationship which suggested a decrease in *angle-of-curvature* was related to an increase in incisor size. Component two highlighted a directly proportional relationship

between the *angle-of-curvature* and the projected *width-at-midpoint* variables. Therefore wider teeth were straighter. A large *angle-of-curvature* gave a small incisor because of the curved morphology of the incisor (Figure 18.).

5.2.4. PCA of Colour and Whiteness Assessment

PCA was not performed on the colour and whiteness assessment because of the different algorithmic relationships between the individual RGB values and the individual colour space outputs L A B and W. The PCA results would distort any relationship between the variables and elucidate no meaningful component correlations.

5.2.5. PCA of 3D Incisor Measurement

The PCA statistics of the left side buccal view was given as an example for brevity as the variance was similar for both the left and right sides, and for buccal and lingual views (Table 16. and Figure 72.). The 3D labial view was detailed separately (Table 17. and Figure 73.). The full data is recorded in Appendix 2. Tables 3. and 4.

5.2.5.1. Buccal and Lingual Views:

Table 16. PCA 3D Incisor Morphometry left side buccal view

A

COMPONENT	Total Variance Explained Initial Eigenvalues Total	% of Variance	Cumulative %
1	2.435*	48.693	48.693
2	2.159*	43.175	91.868
3	0.231	4.611	96.479
4	0.124	2.483	98.962
5	0.052	1.038	100.000

B

MEASUREMENT VARIABLE	Component Matrix Component 1	2
marked *surface-area* (mm^2)	0.909	0.266
projected *overall-length* (mm)	0.864	-0.352
actual *perimeter* (mm)	0.862	-0.430
projected *width-at-midpoint* (mm)	0.152	0.952
actual *width-at-midpoint* (mm)	0.309	0.934

(A) Total variance explained; (B) Extracted components matrix. *Eigenvalue > 1.

Figure 72. PCA Scree Plot 3D Incisor Morphometry left side buccal view

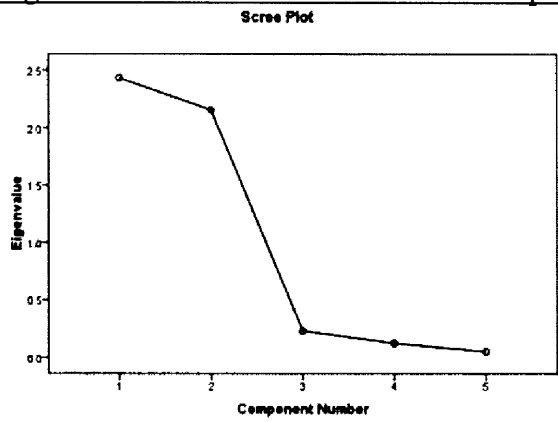

(C) Scree Plot.

Two components were identified; (i) component one (48.7%) and (ii) component two (43.2%) that accounted for 91.9% of the total variance in incisor shape (Appendix 2. Tables 3. and 4.). Component one highlighted a directly proportional size correlation between most variables. The marked *surface-area*, projected *overall-length* and actual *perimeter* showed

the largest positive inter-relationships. The projected and actual *width-at-midpoint* showed a lesser correlation, which may suggest they changed little compared to the other variables.

Component two highlighted a directly proportional link with projected *width-at-midpoint* and actual *width-at-midpoint.* Secondly, component two highlighted an inversely proportional correlation between *overall-length* and actual *perimeter* with projected and actual *width-at-midpoint*. The negative relationship suggested a reduced *width-at-midpoint* with increased incisor size in general.

5.2.5.2. Labial view:

Table 17. PCA 3D Incisor Morphometry left side labial view

A

COMPONENT	Total Variance Explained Initial Eigenvalues		
	Total	% of Variance	Cumulative %
1	2.946*	58.922	58.922
2	1.277*	25.538	84.460
3	0.474	9.475	93.935
4	0.187	3.733	97.668
5	0.117	2.332	100.000

B

MEASUREMENT VARIABLE	Component Matrix Component	
	1	2
total *surface-area* (mm^2)	0.926	-0.030
projected *labial-length* (mm)	0.918	-0.231
actual *labial-length* (mm)	0.904	-0.312
total *volume* (mm^3)	0.628	0.561
circumference (mm)	0.188	0.901

(A) Total variance explained; (B) Extracted components matrix. *Eigenvalue > 1

Figure 73. PCA Scree Plot 3D Incisor Morphometry left side labial view

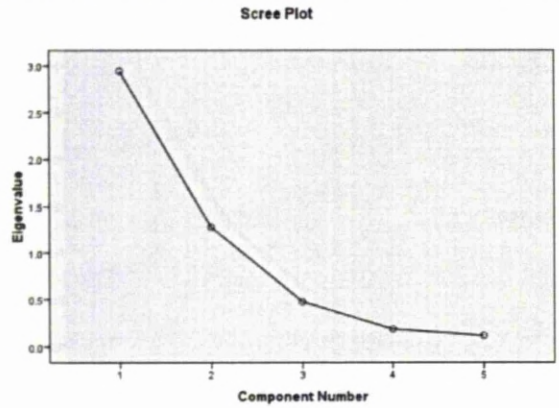

(C) Scree Plot.

Two components were identified; (i) component one (58.9%) and (ii) component two (25.5%) that accounted for 84.5% of the total variance in incisor shape (Appendix 2. Tables 3. and 4.). Component one highlighted a directly proportional size correlation between all variables. The total *surface-area*, projected *labial-length* and actual *labial-length* showed the strongest positive inter-relationships.

Firstly, component two highlighted a directly proportional relationship between total *volume* and *circumference*. Secondly, component two highlighted an inversely proportional relationship between total *surface-area*, projected *labial-length* and actual *labial-length* with *circumference* (and to a lesser extent with *total volume*). This relationship linked with the second component of the buccal view, showing that longer teeth are slimmer. Therefore, their *circumference* and *volume* remained largely unchanged or reduced.

5.2.6. Summary

The PCA predominantly revealed two main components for each method that described shape, e.g. 2D mandible measurement component one highlighted a directly proportional size correlation between variables.

The PCA identified a number of underlying morphological trends and associations that may not have otherwise been evident.

5.3. EXPERIMENTAL COMPARISON

5.3.1. Introduction

The following descriptive statistics summarised the experimental comparison data; Mean, Standard Deviation, Mean Difference, Standard Error and 95% Confidence Intervals.

A one-way ANOVA indicated the Bonferroni corrected significant differences ($p < 0.002$) in the experimental comparison. Post Hoc Multiple Comparison Tukey's HSD tests identified between which experimental groups the significant differences ($p < 0.05$) occurred.

The Bonferroni correction was considered to be a harsh adjustment and should ideally only be applied to independent variables. The variables within this study arguably had varying degrees of independence. For this reason any significant differences ($p < 0.05$) observed before the Bonferroni correction were also detailed.

Experimental measurements were carried out by operator I (TLC).

5.3.2. Amelx Experimental Comparison

This section details one example variable from each of the multiple *Amelx* experimental group comparisons for brevity. The full data is recorded in Appendix 3. Tables 1-22.

5.3.2.1. Amelx 2D Mandible Measurement:

Table 18. Statistics *Amelx* left mandible buccal view *overall-length*

HEMI-MANDIBLE			ANOVA									MULTIPLE COMPARISON					
VIEW/ ASPECT		MEASUREMENT VARIABLE	GROUP	Mean	SD	SE	95% CI of Mean lower bound	95% CI of Mean upper bound	min'	max'	F	Sig.	GROUPS	MD	SE	95% CI lower bound	95% CI upper bound	Sig.
LEFT	BUCCAL	*overall-length* (mm)	WT	11.782	0.132	0.059	11.618	11.947	11.611	11.922	2.495	0.097	WT-HET	0.126	0.284	-0.687	0.940	0.970
			HET	11.656	0.252	0.112	11.344	11.968	11.288	11.954			WT-HEMI	0.343		-0.470	1.157	0.631
			HEMI	11.439	0.649	0.290	10.633	12.245	10.338	11.924			WT-HOMO	0.725		-0.089	1.539	0.090
			HOMO	11.057	0.554	0.248	10.370	11.745	10.219	11.735			HET-HEMI	0.217		-0.596	1.031	0.869
													HET-HOMO	0.599		-0.215	1.412	0.193
													HEMI-HOMO	0.382		-0.432	1.195	0.551

Bonferroni corrected significant differences ($p \leq 0.002$) in the *mandible-angle* variable identified morphological variation between one and more of the four *Amelx* groups (Appendix 3. Tables 1-4.). The post hoc multiple comparisons indicated that the significant differences ($p \leq 0.05$) occurred between the *Amelx*^{WT} and *Amelx*$^{Y64H/Y64H}$ groups, between the *Amelx*$^{X/Y64H}$ and *Amelx*$^{Y64H/Y64H}$ groups, and between the *Amelx*$^{Y/Y64H}$ and *Amelx*$^{Y64H/Y64H}$ groups. For example, in accordance with the PCA, the *mandible-angle* showed the *Amelx*^{WT} mandibles (66.219°) were the smallest, followed in descending order of size by the *Amelx*$^{X/Y64H}$ (67.261°), *Amelx*$^{Y/Y64H}$ (67.838°) and *Amelx*$^{Y64H/Y64H}$ (71.885°) mandibles. The *mandible-angle* represented the overall bulk of the mandible as a combined measure of the *ascending-height* and *basal-length* variables.

Uncorrected significant differences ($p \leq 0.05$) occurred in eight of the thirty two (25%) mandible variables; between the *Amelx*^{WT} and *Amelx*$^{Y64H/Y64H}$ groups (x 7 variables), between the *Amelx*$^{X/Y64H}$ and *Amelx*$^{Y64H/Y64H}$ groups (x 5 variables) and between the *Amelx*$^{Y/Y64H}$ and *Amelx*$^{Y64H/Y64H}$ groups (x 2 variables).

5.3.2.2. Amelx 2D Incisor Measurement:

Table 19. Statistics *Amelx* left 2D incisor buccal view *overall-length*

MANDIBULAR INCISORS		ANOVA									MULTIPLE COMPARISON					
VIEW/ ASPECT	MEASUREMENT VARIABLE	GROUP	Mean	SD	SE	95% CI of Mean lower bound	95% CI of Mean upper bound	min'	max'	F	Sig.	GROUPS	MD	SE	95% CI lower bound	95% CI upper bound	Sig.
LEFT BUCCAL	*overall-length* (mm)	WT	10.560	0.758	0.339	9.619	11.501	9.808	11.699	9.165	0.001*	WT-HET	0.217	0.328	-0.721	1.154	0.910
		HET	10.343	0.474	0.212	9.755	10.931	9.521	10.701			WT-HEMI	0.369		-0.569	1.306	0.680
		HEMI	10.191	0.475	0.212	9.602	10.781	9.428	10.615			WT-HOMO	1.565		0.627	2.502	0.001**
		HOMO	8.995	0.223	0.100	8.719	9.271	8.738	9.247			HET-HEMI	0.152		-0.786	1.089	0.966
												HET-HOMO	1.348		0.411	2.285	0.004**
												HEMI-HOMO	1.196		0.259	2.134	0.010**

*Bonferroni corrected Significant Difference ($p \leq 0.002$).
**Significant Difference ($p \leq 0.05$).

Bonferroni corrected significant differences ($p \leq 0.002$) in all the incisor variables - except *overall-length* ($p \geq 0.008$), *width-at-midpoint* ($p \geq 0.051$) and *labial-length* ($p \geq 0.243$) that did indicate considerable differences - identified morphological variation between one and more of the four *Amelx* groups (Appendix 3. Tables 5-8.). The post hoc multiple comparisons indicated that the significant differences ($p \leq 0.05$) occurred between the *Amelx*^{WT} and *Amelx*$^{Y/Y64H}$ groups (x 3 variables), between the *Amelx*^{WT} and *Amelx*$^{Y64H/Y64H}$ groups (x 15 variables), between the *Amelx*$^{X/Y64H}$ and *Amelx*$^{Y64H/Y64H}$ groups (x 15 variables), and between the *Amelx*$^{Y/Y64H}$ and *Amelx*$^{Y64H/Y64H}$ groups (x 14 variables). For example, the *overall-length* showed the *Amelx*^{WT} incisors (10.566mm) were the largest, followed in descending order of size by the *Amelx*$^{X/Y64H}$ (10.343mm), *Amelx*$^{Y/Y64H}$ (10.191mm) and *Amelx*$^{Y64H/Y64H}$ (8.995mm) incisors. There were no significant differences between the *Amelx*^{WT} and *Amelx*$^{X/Y64H}$ groups or between the *Amelx*$^{X/Y64H}$ and *Amelx*$^{Y/Y64H}$ groups.

Uncorrected significant differences ($p \leq 0.05$) occurred in eighteen of the twenty two (82%) incisor variables between the *Amelx*^{WT} and *Amelx*$^{Y/Y64H}$ groups (x 3 variables), between the *Amelx*^{WT} and *Amelx*$^{Y64H/Y64H}$ groups (x 18 variables), between the *Amelx*$^{X/Y64H}$ and *Amelx*$^{Y64H/Y64H}$ groups (x 18 variables), and between the *Amelx*$^{Y/Y64H}$ and *Amelx*$^{Y64H/Y64H}$ groups (x 15 variables).

5.3.2.3. Amelx Colour and Whiteness Assessment:

Table 20. Statistics *Amelx* left *gingival* region *lightness*

MANDIBULAR INCISORS			ANOVA									MULTIPLE COMPARISON					
							95% CI of Mean								95% CI		
SIDE	REGION/ STAGE	COLOUR COMPONENT	GROUP	Mean	SD	SE	lower bound	upper bound	min'	max'	F	Sig.	GROUPS	MD	SE	lower bound	upper bound	Sig.
LEFT	GINGIVAL/ SECRETORY	*lightness*	WT	48.519	2.385	1.066	45.558	51.480	45.235	51.083	11.590	0.000*	WT-HET	10.855	2.046	5.001	16.709	0.000**
			HET	37.664	4.760	2.129	31.754	43.574	34.154	44.923			WT-HEMI	9.522		3.668	15.376	0.001**
			HEMI	38.998	2.996	1.340	35.278	42.718	35.079	43.418			WT-HOMO	8.690		2.836	14.545	0.003**
			HOMO	39.829	2.134	0.954	37.179	42.479	37.616	42.754			HET-HEMI	-1.333		-7.187	4.521	0.913
													HET-HOMO	-2.165		-8.019	3.690	0.719
													HEMI-HOMO	-0.831		-6.686	5.023	0.977

* Bonferroni corrected Significant Difference ($p \leq 0.002$).
** Significant Difference ($p \leq 0.05$).

Bonferroni corrected significant differences ($p \leq 0.002$) in nineteen of the thirty two (59%) variables identified colour and whiteness variation between one and more of the four *Amelx* groups (Appendix 3. Tables 9-16.). The post hoc multiple comparisons indicated that the significant differences ($p \leq 0.05$) occurred in the *lightness* colour component, in all four enamel surface regions, and in the *yellow/ blue* and *whiteness* colour components in the *middle*, *incisal* and *whole* regions; between the *Amelx*^{WT} and *Amelx*$^{X/Y64H}$ groups (x 10 components), between the *Amelx*^{WT} and *Amelx*$^{Y/Y64H}$ groups (x 15 components), between the *Amelx*^{WT} and *Amelx*$^{Y64H/Y64H}$ groups (x 12 components), between the *Amelx*$^{X/Y64H}$ and *Amelx*$^{Y/Y64H}$ groups (x 12 components), between the *Amelx*$^{X/Y64H}$ and *Amelx*$^{Y64H/Y64H}$ groups (x 16 components), and between the *Amelx*$^{Y/Y64H}$ and *Amelx*$^{Y64H/Y64H}$ groups (x 6 components).

Uncorrected significant differences ($p \leq 0.05$) occurred in twenty seven of the thirty two (84%) incisor variables between the *Amelx*^{WT} and *Amelx*$^{X/Y64H}$ groups (x 13 components), between the *Amelx*^{WT} and *Amelx*$^{Y/Y64H}$ groups (x 17 components), between the *Amelx*^{WT} and *Amelx*$^{Y64H/Y64H}$ groups (x 12 components), between the *Amelx*$^{X/Y64H}$ and *Amelx*$^{Y/Y64H}$ groups (x 15 components), between the *Amelx*$^{X/Y64H}$ and *Amelx*$^{Y64H/Y64H}$ groups (x 17 components), and between the *Amelx*$^{Y/Y64H}$ and *Amelx*$^{Y64H/Y64H}$ groups (x 6 components).

The enamel surface constituted: *gingival* region *lightness* (33.144 - 49.034), *green* (-5.114 - 1.086), *yellow* (1.970 - 8.998) and *whiteness* (39.292 - 88.966); *middle* region *lightness* (36.862 - 51.694), *green* (-4.036 - -0.782), *yellow* (0.074 - 6.482) *blue* (-0.514) and *whiteness*

(58.068 - 97.603); *incisal* region *lightness* (32.826 - 54.707), *green* (-7.198 - -0.316), *blue* (-1.552 - -0.660) *yellow* (8.386 - 12.344) and *whiteness* (18.800 - 107.451); *whole* region *lightness* (36.334 - 51.694), *green* (-5.322 - -1.084), *yellow* (0.354 - 7.632) and *whiteness* (49.926 - 97.930). *Lightness* and *whiteness* values were higher than *yellow/ blue* values in all regions. The *green* values were similar throughout.

The significant differences observed between the *Amelx*^{WT} group and the three mutant groups occurred specifically in the *lightness*, *yellow/ blue* and *whiteness* colour components in the *incisal* and *whole* enamel surface regions.

5.3.2.4. Amelx 3D Incisor Measurement:

Table 21. Statistics *Amelx* left 3D incisor buccal view projected *overall-length*

MANDIBULAR INCISORS			ANOVA									MULTIPLE COMPARISON					
VIEW/ ASPECT		MEASUREMENT VARIABLE	GROUP	Mean	SD	SE	95% CI of Mean lower bound	95% CI of Mean upper bound	min'	max'	F	Sig.	GROUPS	MD	SE	95% CI lower bound	95% CI upper bound	Sig.
LEFT	BUCCAL	projected *overall-length* (mm)	WT	10.041	0.684	0.306	9.191	10.891	9.294	10.804	4.879	0.014	WT-HET	0.819	0.378	-0.263	1.901	0.175
			HET	9.222	0.603	0.270	8.472	9.971	8.627	9.917			WT-HEMI	0.935		-0.147	2.017	0.103
			HEMI	9.106	0.402	0.180	8.607	9.604	8.552	9.482			WT-HOMO	1.423		0.341	2.505	0.008
			HOMO	8.618	0.661	0.295	7.798	9.438	7.447	9.042			HET-HEMI	0.116		-0.966	1.198	0.990
													HET-HOMO	0.604		-0.478	1.686	0.408
													HEMI-HOMO	0.488		-0.594	1.570	0.582

Bonferroni corrected significant differences ($p \leq 0.002$) in the *surface-area* and *volume* variables identified morphological variation between one and more of the four *Amelx* groups (Appendix 3. Tables 17-22.). The post hoc multiple comparisons indicated that the significant differences ($p \leq 0.05$) occurred between the $Amelx^{WT}$ and $Amelx^{X/Y64H}$ groups (x 4 variables), between the $Amelx^{WT}$ and $Amelx^{Y/Y64H}$ groups (x 4 variables), and between the $Amelx^{WT}$ and $Amelx^{Y64H/Y64H}$ groups (x 4 variables). For example, the $Amelx^{WT}$ incisors *surface-area* ($14.375mm^2$) and *volume* ($5.373mm^3$) were the largest, and the $Amelx^{Y64H/Y64H}$ incisors *surface-area* ($11.344mm^2$) and *volume* ($4.320mm^3$) were the smallest; the $Amelx^{X/Y64H}$ and $Amelx^{Y/Y64H}$ incisors were of intermediate size. There were no significant differences between the $Amelx^{X/Y64H}$ and $Amelx^{Y/Y64H}$ groups, between the $Amelx^{X/Y64H}$ and $Amelx^{Y64H/Y64H}$ groups, or between the $Amelx^{Y/Y64H}$ and $Amelx^{Y64H/Y64H}$ groups.

Uncorrected significant differences ($p \leq 0.05$) occurred in twenty two of the thirty (73%) incisor variables between the $Amelx^{WT}$ and $Amelx^{X/Y64H}$ groups (x 10 variables), between the $Amelx^{WT}$ and $Amelx^{Y/Y64H}$ groups (x 15 variables), and between the $Amelx^{WT}$ and $Amelx^{Y64H/Y64H}$ groups (x 21 variables).

5.3.3. Enam Experimental Comparison

This section details one example variable from each of the multiple *Enam* experimental group comparisons for brevity. The full data is recorded in Appendix 3. Tables 23-39.

5.3.3.1. Enam 2D Mandible Measurement:

Table 22. Statistics *Enam* left mandible buccal view *overall-length*

HEMI-MANDIBLES		ANOVA									MULTIPLE COMPARISON					
VIEW/ ASPECT	MEASUREMENT VARIABLE	GROUP	Mean	SD	SE	95% CI of Mean lower bound	95% CI of Mean upper bound	min'	max'	F	Sig.	GROUPS	MD	SE	95% CI lower bound	95% CI upper bound	Sig.
LEFT BUCCAL	*overall-length* (mm)	WT	12.138	0.465	0.208	11.561	12.714	11.716	12.85			WT-HOMO	0.089		-0.616	0.794	0.940
		HOMO	12.049	0.438	0.196	11.505	12.592	11.470	12.457	0.167	0.848	WT-HET	0.152	0.264	-0.553	0.857	0.836
		HET	11.986	0.341	0.153	11.562	12.409	11.687	12.560			HOMO-HET	0.063		-0.642	0.768	0.969

There were no statistically significant differences ($p < 0.002$) in mandible variables between any of the three *Enam* groups (Appendix 3. Tables 23-26.). No follow up post hoc multiple comparisons were implemented. However, the $Enam^{WT}$ group appeared to have the largest mandibles, followed in descending order of size by the $Enam^{Rgsc395}$ *heterozygous* and the $Enam^{Rgsc395}$ *homozygous* mandibles, e.g. *overall-length* $Enam^{WT}$ (12.138 mm), $Enam^{Rgsc395}$ *homozygous* (12.049 mm) and $Enam^{Rgsc395}$ *heterozygous* (11.986 mm).

5.3.3.2. Enam 2D Incisor Measurement:

Table 23. Statistics *Enam* left 2D incisor buccal view *overall-length*

MANDIBULAR INCISORS				ANOVA								MULTIPLE COMPARISON					
VIEW/ ASPECT		MEASUREMENT VARIABLE	GROUP	Mean	SD	SE	95% CI of Mean		min'	max'	F	Sig.	GROUPS	MD	SE	95% CI		Sig.
							lower bound	upper bound								lower bound	upper bound	
LEFT	BUCCAL	*overall-length* (mm)	WT	9.705	0.406	0.182	9.201	10.210	9.186	10.244			WT-HOMO	0.225		-0.391	0.841	0.607
			HOMO	9.481	0.315	0.141	9.089	9.872	9.136	9.926	0.516	0.609	WT-HET	0.054	0.231	-0.562	0.670	0.971
			HET	9.652	0.368	0.165	9.195	10.109	9.086	10.032			HOMO-HET	-0.171		-0.787	0.445	0.745

There were no significant differences ($p < 0.002$) in incisor variables between any of the three *Enam* groups (Appendix 3. Tables 27-28.). No follow up post hoc multiple comparisons were implemented. However, there were uncorrected significant differences ($p \leq 0.05$) identified in the *angle-of-curvature* variable between the $Enam^{WT}$ and $Enam^{Rgsc395}$ *heterozygous* groups (x 3 variables). In accordance with the PCA, the *angle-of-curvature* showed that the $Enam^{WT}$ (128.688°) incisors were the largest, followed in descending order of size by the $Enam^{Rgsc395}$ *homozygous* (128.715) and the $Enam^{Rgsc395}$ *heterozygous* (130.808°) incisors.

5.3.3.3. Enam Colour and Whiteness Assessment:

Table 24. Statistics *Enam* left *gingival* region *lightness*

MANDIBULAR INCISORS			ANOVA									MULTIPLE COMPARISON					
SIDE	REGION/ STAGE	COLOUR COMPONENT	GROUP	Mean	SD	SE	95% CI of Mean		min'	max'	F	Sig.	GROUPS	MD	SE	95% CI		Sig.
							lower bound	upper bound								lower bound	upper bound	
LEFT	GINGIVAL/ SECRETORY	*lightness*	WT	59.602	7.387	3.304	50.429	68.775	46.520	63.810	16.390	0.000*	WT-HOMO	26.596	4.919	13.473	39.719	0.000**
			HOMO	33.006	9.865	4.412	20.757	45.255	20.391	43.139			WT-HET	21.320		8.197	34.444	0.000**
			HET	38.281	5.439	2.432	31.528	45.035	34.818	47.834			HOMO-HET	-5.275		-18.399	7.848	0.548

* Bonferroni corrected Significant Difference ($p \leq 0.002$).
** Significant Difference ($p \leq 0.05$).

Bonferroni corrected significant differences ($p \leq 0.002$) in nine of the thirty two (28%) variables identified colour and whiteness variation between one and more of the three *Enam* groups (Appendix 3. Tables 29-36.). The post hoc multiple comparisons indicated that the significant differences ($p \leq 0.05$) occurred in the *lightness*, *yellow/ blue* and *whiteness* colour components, predominately in the *incisal* and *whole* regions; between the $Enam^{WT}$ and $Enam^{Rgsc395}$ *homozygous* (x 9 components) and the $Enam^{WT}$ and $Enam^{Rgsc395}$ *heterozygous* (x 9 components) groups. There were no significant differences identified between the $Enam^{Rgsc395}$ *homozygous* and $Enam^{Rgsc395}$ *heterozygous* groups.

Uncorrected significant differences ($p \leq 0.05$) occurred in thirteen of the thirty two (41%) colour and whiteness variables between the $Enam^{WT}$ and $Enam^{Rgsc395}$ *homozygous* (x 12 components) and between the $Enam^{WT}$ and $Enam^{Rgsc395}$ *heterozygous* groups (x 13 components), most notably in the additional *middle* enamel surface region.

The enamel surface constituted: *gingival* region *lightness* (33.006 - 59.602), *green* (-3.202 - -0.380), *yellow* (4.336 - 7.064) and *whiteness* (50.204-70.158); *middle* region *lightness* (42.079 - 47.467), *green* (-3.058 - -1.858), *yellow* (0.392 - 6.638) and *whiteness* (55.944 - 63.408); *incisal* region *lightness* (42.773 - 48.884), *green* (-4.326 - -2.114), *yellow /blue* (-3.020 - 14.120) and *whiteness* (8.948 - 114.262); *whole* region *lightness* (41.097 - 44.432), *green* (-3.176 - -1.580), *yellow* (1.594 - 8.150) and *whiteness* (46.550 - 88.236). *Lightness* and *whiteness* values were higher than *yellow/ blue* values in all regions.

The significant differences that were observed between the *Enam*^{WT} group and the two mutant groups occurred specifically in the *lightness*, *yellow/ blue* and *whiteness* colour components in the *middle*, *incisal* and *whole* enamel surface regions.

5.3.3.4. Enam 3D Incisor Measurement

Table 25. Statistics *Enam* left 3D incisor buccal view projected *overall-length*

MANDIBULAR INCISORS		ANOVA									MULTIPLE COMPARISON					
VIEW/ ASPECT	MEASUREMENT VARIABLE	GROUP	Mean	SD	SE	95% CI of Mean lower bound	95% CI of Mean upper bound	min'	max'	F	Sig.	GROUPS	MD	SE	95% CI lower bound	95% CI upper bound	Sig.
LEFT BUCCAL	projected *overall-length* (mm)	WT	9.777	0.675	0.302	8.940	10.615	9.118	10.847			WT-HET	0.703		-0.280	1.686	0.178
		HOMO	9.074	0.620	0.277	8.304	9.843	8.070	9.490	5.525	0.023	WT-HOMO	1.187	0.368	0.204	2.170	0.019
		HET	8.590	0.423	0.189	8.065	9.115	8.099	9.261			HET-HOMO	0.484		-0.499	1.467	0.415

Bonferroni corrected significant differences ($p \leq 0.002$) in the *overall-length* variable identified morphological variation between one and more of the three *Enam* groups (Appendix 3. Tables 37-39.). The post hoc multiple comparisons indicated that the significant differences ($p \leq 0.05$) occurred between the $Enam^{WT}$ and $Enam^{Rgsc395}$ *heterozygous* groups and between the $Enam^{Rgsc395}$ *homozygous* and $Enam^{Rgsc395}$ *heterozygous* groups. For example, the projected *overall-length* showed the $Enam^{WT}$ (9.777mm) incisors were largest, followed in descending order of size by the $Enam^{Rgsc395}$ *homozygous* (9.074mm), and the $Enam^{Rgsc395}$ *heterozygous* (8.590mm) incisors.

Uncorrected significant differences ($p \leq 0.05$) occurred in twelve of the fifteen (80%) incisor variables between the $Enam^{WT}$ and $Enam^{Rgsc395}$ *heterozygous* groups (x12 variables), between the $Enam^{WT}$ and $Enam^{Rgsc395}$ *homozygous* groups (x1 variable) and between the $Enam^{Rgsc395}$ *heterozygous* and $Enam^{Rgsc395}$ *homozygous* groups (x1 variable).

5.3.4. *Amelx* and *Enam* 3D Surface Analysis

The *surface-roughness* measured one individual incisor from each genotype group, so no group averages were obtained (Table 26. and Appendix 3. Table 40.).

Table 26. 3D Surface Analysis

MANDIBULAR INCISORS		GROUP (n = 1)						
MEASUREMENT VARIABLE	REGION/ STAGE	*Amelx*				*Enam*		
		WILD-TYPE	HETEROZYGOUS	HEMIZYGOUS	HOMOZYGOUS	WILD-TYPE	HETEROZYGOUS	HOMOZYGOUS
surface-roughness (µm)	*gingival/ pre-secretory*	2.000	1.900	1.500	2.000	2.800	2.400	1.900
	middle/ secretory	3.200	2.100	1.900	2.300	3.600	2.800	2.300
	incisal/ mature	5.400	2.300	2.100	3.400	5.100	3.500	4.200

Each value was a single measurement. No statistical analysis performed.

Amelx^{WT} and *Enam*^{WT} had similar and higher *surface-roughness* values compared to their respective mutant groups. In all groups the *surface-roughness* value increased from the *gingival*, *middle* through to the *incisal* enamel surface regions.

5.3.5. Summary

The 2D IAS mandible morphometry identified significant differences between the *Amelx*^{WT} and *Amelx*$^{Y64H/Y64H}$ groups, but not between any of the *Enam* groups; the *Amelx*^{WT} mandibles were the largest followed in descending order of size by the *Amelx*$^{X/Y64H}$, *Amelx*$^{Y/Y64H}$ and *Amelx*$^{Y64H/Y64H}$ mandibles.

The 2D IAS incisor morphometry identified significant differences between the *Amelx*^{WT} and *Amelx*$^{Y/Y64H}$ groups, between the *Amelx*^{WT} and *Amelx*$^{Y64H/Y64H}$ groups, between the *Amelx*$^{X/Y64H}$ and *Amelx*$^{Y64H/Y64H}$ groups, and between the *Amelx*$^{Y/Y64H}$ and *Amelx*$^{Y64H/Y64H}$ groups; the *Amelx*^{WT} incisors were the largest followed in descending order of size by the *Amelx*$^{X/Y64H}$, *Amelx*$^{Y/Y64H}$ and *Amelx*$^{Y64H/Y64H}$ incisors. The 2D IAS incisor morphometry identified significant differences between the *Enam*^{WT} and *Enam*^{Rgsc395} *heterozygous* groups; the *Enam*^{WT} incisors were the largest followed in descending order of size by the *Enam*^{Rgsc395} *homozygous* and the *Enam*^{Rgsc395} *heterozygous* incisors.

The colour and whiteness assessment indicated significant differences between the *Amelx*^{WT} group and all three of the *Amelx* mutant groups, and between the *Enam*^{WT} and *Enam*^{Rgsc395} *heterozygous* groups and between the *Enam*^{WT} and *Enam*^{Rgsc395} *homozygous* groups. The *Amelx*^{WT} and *Enam*^{WT} groups constituted low *lightness*, high *yellow/ blue* and low *whiteness* colour components, whereas the mutants groups constituted high *lightness*, low *yellow/ blue* and high *whiteness* colour components. The site of these significant differences varied between the *Amelx* groups and the *Enam* groups; in the *Amelx* incisors the differences were identified in the *incisal* and *whole* regions, while in the *Enam* incisors the differences were identified in the *middle*, *incisal* and *whole* regions.

The 3D IAS incisor morphometry identified significant differences between the *Amelx*^{WT} and *Amelx*$^{X/Y64H}$, between the *Amelx*^{WT} and *Amelx*$^{Y/Y64H}$ and between the *Amelx*^{WT} and *Amelx*$^{Y64H/Y64H}$ groups; the *Amelx*^{WT} incisors were the largest, the *Amelx*$^{Y64H/Y64H}$ incisors were the smallest and the *Amelx*$^{X/Y64H}$ incisors were of an intermediate size. Also, the 3D IAS incisor morphometry identified significant differences between the *Enam*^{WT} and *Enam*^{Rgsc395} *heterozygous* groups, between the *Enam*^{WT} and *Enam*^{Rgsc395} *homozygous* groups and between the *Enam*^{Rgsc395} *heterozygous* and *Enam*^{Rgsc395} *homozygous*; the *Enam*^{WT} incisors were the

largest and the *Enam*^{Rgsc395} *heterozygous* incisors were the smallest. The 3D IAS identified significant differences between the *Amelx*^{WT} controls and all three mutant groups only.

The incisor enamel *surface-roughness* values were higher in the *Amelx*^{WT} and in the *Enam*^{WT} controls compared to their respective mutant groups. The *surface-roughness* values increased through the *gingival*, *middle* and *incisal* enamel surface regions.

5.3.6. Impact on Null-Hypotheses

In the *Amelx* experimental group comparisons, the null hypotheses were rejected because all the methods identified significant differences between the control and the mutant groups.

In the *Enam* experimental group comparisons, the null hypotheses were rejected because all the methods identified significant differences between the control and the mutant groups, except in the 2D IAS mandible morphology.

6. DISCUSSION

6.1. METHOD DEVELOPMENT, RELIABILITY AND VALIDATION

6.1.1 Introduction

The development of the materials and methods involved considerable personal and departmental input, and hardware and software customisation to suit the experimental phenotype to genotype comparison. All methods provided practical, objective and quantitative analysis of mouse mandibles and incisors with low levels of experimental and systematic error (Donner and Eliasziw, 1987), high levels of operator consistency (Fleiss, 1986a, 1986b) and high levels of method agreement (Bland and Altman, 1986, 1999).

6.1.2. Morphological Measurement

The 2D morphometric methods were more reliable than the previous direct manual measurement methods (Moorees *et al.,* 1957; Hillson *et al.,* 2005) and equalled the substantial to excellent reliability of the gold standard in 2D clinical image analysis (Brook *et al.,* 2005; Brook *et al.,* 2007; Smith *et al.,* 2009b). The novel murine application benefitted from a macro-lens modification and highly standardised orientation, magnification and illumination conditions. Intra-operator repeatability was higher than inter-operator reproducibility, as would be expected (Harris and Smith, 2009).

The original concept of the 3D IAS was to exploit the recent advances in 3D technologies (Hajeer *et al.,* 2004) and to provide a small mammalian tooth imaging tool that could be applied to the molecular model of choice for human dental disease (Qui, 2006; Fleishmannova *et al.,* 2008). The NCSP device was modified with a novel rotary stage designed to be largely automated but versatile, e.g. the stage was removable so the system could be switched between human and murine tooth analysis. The equipment was successfully adapted to obtain multiple 3D images from multiple angles in 360° with less measurement error than other clinically acceptable 3D systems e.g. Santoro *et al.,* (2003), Quimby *et al.,* (2004) and Stevens *et al.,* (2006). The novel method of image indexing was introduced to reconstruct the 3D models and the powerful analytical software realised the full potential of the new system with actual on surface measurement variables that accounted for the 3D topographical contours of the tooth surface.

The resolution of the new 3D macro-metric structure and 3D micro-metric surface analysis system on the mineralised dental tissues compared well with the laser scanning method of Halazonetis *et al.,* (2001), and required less specimen preparation than confocal microscopy (Evans *et al.,* 2001). The high systematic resolution (1.0 μm) provided enhanced discriminatory powers over other techniques e.g. Apuzzo *et al.,* (2006) and gave excellent economy compared to X-ray μCT (Rowe *et al.,* 2001; Kim *et al.,* 2007).

The 2D IAS was proven to be a highly reliable method suitable for validating the 3D IAS (Rodgers and Nicewander, 1988). In the 2D and 3D IAS the multiple independent intra-operator repeatability tested total system error (including experimental error and systematic error), which was often overlooked in the literature (Harris and Smith, 2009). The 2D IAS and 3D IAS were complementary and showed significant method agreement and measurement correlations. The 3D IAS incisor morphometry was validated with excellent reliability and could be used interchangeably with the 2D IAS. However, the limitation of a small sample population (n = 1) for the *surface-roughness* assessment was recognised and will form part of the Future Work.

6.1.3. Principal Component Analysis

The Principal Component Analysis defined mandible and incisor morphology and revealed a number of interesting size relationships with biomechanical implications, e.g. the *mandible-angle* variable and the incisor *angle-of-curvature* variable were inversely proportional to mandible and incisor size respectively. The variables with the highest reliability scores (e.g. the incisor *width-at-midpoint*) also accounted for the majority of the morphological variation, which will strengthen the experimental interpretation.

6.1.4. Colour and Whiteness Assessment

The colour and whiteness assessment contained a highly novel software algorithm designed and developed in-house to calculate international standard CIE LAB and WI colour space values (Joiner, 2004; Wee *et al.,* 2006). The bespoke method was a great improvement compared to the conventional methods used in human studies, e.g. shade guides (Paul *et al.,* 2002), spectrophotometers (Guan *et al.,* 2005) and colourimeters (Khurana *et al.,* 2007). The predominantly excellent reliability exceeded that of any existing methods apparent in the

literature (Joiner *et al.,* 2008) and compared well with the translated human application that was validated during clinical trials (Smith *et al.,* 2008a). The method was especially sensitive and selective as it quantified tooth colour and whiteness in three separate surface regions that corresponded to three stages of enamel developmental, reaching beyond the limitations of the more subjective descriptions (Smith and Warshawsky, 1975, 1976; Robinson *et al.,* 1983).

6.1.5. Summary

All four measurement methods showed predominantly excellent reliability. The modified 2D IAS, the novel colour and whiteness assessment and the novel 3D IAS greatly extended the measurement capacity for the comparative experimental investigation. A combination of established parameters and new morphometric variables delivered a more comprehensive repertoire for objective and quantitative macro-metric and micro-metric dental phenotyping. These unique biometric methods enabled innovative novel ways of empirically exploring anatomical growth, biological development and organic mineralisation in the mouse model.

6.2. EXPERIMENTAL COMPARISONS

6.2.1 Introduction

The 2D IAS mandible and incisor morphology, incisor enamel colour and whiteness assessment and 3D IAS incisor morphometry and surface assessment will be discussed in terms of the separate *Amelx* and *Enam* experimental comparisons.

6.2.2. *Amelx* Experimental Comparison

The *Amelx*^{WT} group displayed normal mandible and incisor morphology (Gaunt, 1964; Atchley *et al.,* 1985; Bailey, 1985) with typical enamel deposition, thickness and colour distribution (Hay, 1961; Moinchen *et al.,* 1996). The *Amelx*$^{Y64H/Y64H}$ and *Amelx*$^{Y/Y64H}$ groups were most affected, displaying slightly dysmorphic mandibles and severely pathological incisor enamel (Gibson *et al.,* 2001, 2007, Wright *et al.,* 2009). The *Amelx*$^{X/Y64H}$ group incisors were mildly affected (Figure 74.).

Figure 74. *Amelx* Phenotype Comparison - 2D IAS Mandible Measurement, Incisor Measurement and Colour and Whiteness Assessment

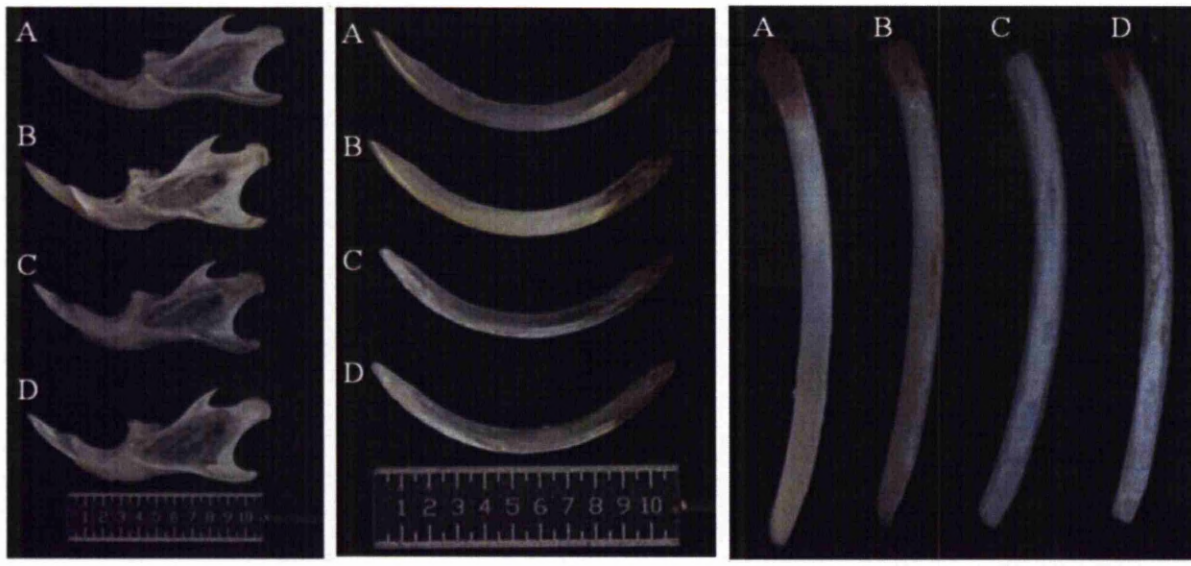

(A) *Amelx*^{WT}; (B) *Amelx*$^{X/Y64H}$; (C) *Amelx*$^{Y/Y64H}$; (D) *Amelx*$^{Y64H/Y64H}$. Scale = 10.0mm.

In humans, the P→T mutation in the conserved tri-tyrosyl motif of amelogenin N-terminus underlies a unique but consistent AI phenotype (Collier *et al.,* 1997; Hart *et al.,* 2000; Ravassipour *et al.,* 2000; Wright *et al.,* 2003). The murine *Amelx* Y64H mutation within the same tri-tyrosyl motif was recently shown to result in hypomineralised enamel in the *Amelx*$^{X/Y64H}$ group and result in severely hypoplastic enamel in the *Amelx*$^{Y/Y64H}$ and *Amelx*$^{Y64H/Y64H}$ groups (Barron *et al.,* 2010). The significant differences observed here between the *Amelx*^{WT} and *Amelx*$^{X/Y64H}$ groups, between the *Amelx*^{WT} and *Amelx*$^{Y/Y64H}$ groups and between the *Amelx*^{WT} and *Amelx*$^{Y64H/Y64H}$ groups, suggested that the amelogenin protein was involved in mandible and incisor morphological development, as well as enamel mineralisation.

Amelogenin has been shown to be expressed in various developing tissues (Hu *et al.,* 2006), including the dental supporting tissues (Deutsch *et al.,* 2006). The significant differences observed here (e.g. *mandible-angle*) between the *Amelx*^{WT} and *Amelx*$^{Y64H/Y64H}$ groups, and between the *Amelx*$^{X/Y64H}$ and *Amelx*$^{Y64H/Y64H}$ groups, suggested that the amelogenin protein was involved in mandible morphological development. These results were consistent with the involvement of the amelogenin protein in alveolar bone formation and remodelling (Haze *et al.,* 2007), and supported amelogenin's multifunctional role in the craniofacial-complex (Gruenbaum-Cohen *et al.,* 2008).

Amelogenin functions during enamel structural organisation (Robinson *et al.,* 1981a, 1983). Full length amelogenin localised to early prism cores was present in secretory stage enamel ECM deposits (Deutsch, 1989; Robinson *et al.,* 1989). The *Amelx*^{WT} mice expressed a functional *Amelx* gene (Hu *et al.,* 2001b), which led to the secretion of a full length amelogenin (Gibson *et al.,* 2005) and was essential for generating full thickness correctly mineralised enamel (Gibson *et al.,* 2001, 2007, 2009). The *Amelx*$^{Y/Y64H}$ and *Amelx*$^{Y64H/Y64H}$ groups expressed only the *Amelx* Y64H mutation containing allele (Masuya *et al,* 2005), which led to the absence of full length amelogenin in the secretory stage enamel ECM extracts and was shown to be the primary causality of aberrant enamel mineralisation (Barron *et al.,* 2010). The significant differences in incisor morphology observed here (e.g. *incisor-perimeter*) between the *Amelx*^{WT} and *Amelx*$^{X/Y64H}$ groups, between the *Amelx*^{WT} and *Amelx*$^{Y/Y64H}$ and between the *Amelx*^{WT} and *Amelx*$^{Y64H/Y64H}$ groups, supported the involvement of the amelogenin protein in incisor morphological development.

Biochemical and histological analysis showed the ameloblast cells of the affected *Amelx*$^{Y/Y64H}$ and *Amelx*$^{Y64H/Y64H}$ mice contain engorged cellular organelles with large accumulations of the truncated Y64H amelogenin (Barron *et al.,* 2010). This considerable intracellular protein retention suggested that the Y64H mutation caused the impaired secretion of a truncated Y64H amelogenin protein and that the subsequent loss of amelogenin function disrupted enamel mineralisation (Barron *et al.,* 2010). The failure to successfully traffic and secrete amelogenin down the usual pathways into the enamel ECM was proposed to be a key mechanistic factor underpinning the aberrant incisor morphology and enamel mineralisation of AIH1.

Amelogenin interacts directly with the ameloblastin protein through its tri-tyrosyl motif (Ravindranath *et al.,* 1999, 2003; Wright *et al.,* 2003). The two proteins are proposed to share a common secretory pathway (Zalzal *et al.,* 2008) and they potentially function by way of synergistic interactions (Hatakeyama *et al.,* 2009). The enamel hypoplasia of the affected *Amelx*$^{Y/Y64H}$ and *Amelx*$^{Y64H/Y64H}$ mutant mice had a similar pathology to the ameloblastin mutant mice that expressed a truncated ameloblastin variant (Fukumoto *et al.,* 2004; Smith *et al.,* 2009c; Wazen *et al.,* 2009). Therefore, enamel defects involving ameloblastin secretion and function may rely on similar protein-protein interactions that were compromised in the presence of the Y64H mutant amelogenin, e.g. Y64H amelogenin-ameloblastin interactions that regulate correct nanosphere self-assembly (Fincham *et al.,* 1995; Paine *et al.,* 2002) may have resulted in the structurally abnormal protein complexes that were not appropriately trafficked prior to secretion (Barron *et al.,* 2010).

Furthermore, abnormal amelogenin-ameloblastin interactions may be only a part of the pathology of impaired Y64H amelogenin secretion as it has also been proposed that cytokeratin protein-protein interactions at the dentino-enamel junction (Ravindranath *et al,* 1999; Wright, 2006) may also be important in amelogenin protein chaperoning, trafficking and secretory processes (Ravindranath *et al.,* 2003, 2004) that may have been affected in the presence of the Y64H amelogenin variant (Barron *et al.,* 2010). This has led to the suggestion that the actual mechanism responsible for AI may be related to amelogenin cell binding activity and cell signalling functions, but also the cell proliferation functions of ameloblastin (Gibson *et al.,* 2007, 2009).

The significant differences in incisor morphometry observed here (e.g. *overall-length*) between the *Amelx*$^{Y/Y64H}$ and *Amelx*$^{Y64H/Y64H}$ groups and between the *Amelx*$^{X/Y64H}$ and *Amelx*$^{Y64H/Y64H}$ groups was not readily explained by the expression of the single *Amelx* mutation containing allele in the *Amelx*$^{Y/Y64H}$ and *Amelx*$^{Y64H/Y64H}$ groups, which would have been expected to have produced more similar incisor morphology in the *Amelx*$^{Y/Y64H}$ and *Amelx*$^{Y64H/Y64H}$ groups than was observed in the *Amelx*^{WT} and *Amelx*$^{X/Y64H}$ that showed no significant differences. However, the similar incisor morphology in the *Amelx*^{WT} and *Amelx*$^{X/Y64H}$ groups and the significant differences between the *Amelx*$^{X/Y64H}$ and the *Amelx*$^{Y64H/Y64H}$ groups indicated that the *Amelx*$^{X/Y64H}$ incisors were of an intermediate size. The significant colour and whiteness differences observed between the *Amelx*$^{X/Y64H}$ and *Amelx*$^{Y/Y64H}$ groups and between the *Amelx*$^{X/Y64H}$ and *Amelx*$^{Y64H/Y64H}$ groups (e.g. *incisal* region *lightness* colour component) provided further evidence that the *Amelx*$^{X/Y64H}$ group had an intermediate enamel phenotype.

The *Amelx*$^{X/Y64H}$ females displayed mildly affected enamel hypomineralisation because of a mosaic pattern of expression of both the normal functional *Amelx* gene and the Y64H mutation containing *Amelx* allele reflecting the lyonisation hypotheses (Lyon, 1961) of X-chromosomal inactivation (Huynh and Lee, 2005). Clusters of ameloblasts alternately expressed either the normal gene or the mutant allele and secreted either the functional or defective amelogenin protein (Witkop, 1967; Gibson *et al.*, 2001). Therefore, it was proposed that both the full length amelogenin and the partial secretion of the truncated Y64H amelogenin may have contributed to the more normal and more affected intermediate morphology and enamel mineralisation observed in the *Amelx*$^{X/Y64H}$ incisors. The 2D and 3D incisor morphology and colour and whiteness assessment presented here strongly supported the *Amelx*$^{X/Y64H}$ group intermediate phenotype.

The significant colour and whiteness differences that were observed between the *Amelx*^{WT} and *Amelx*$^{X/Y64H}$ groups, between the *Amelx*^{WT} and *Amelx*$^{Y/Y64H}$ and between the *Amelx*^{WT} and *Amelx*$^{Y64H/Y64H}$ groups, occurred specifically in the *lightness*, *yellow/ blue* and *whiteness* colour components in the *incisal* and *whole* enamel surface regions. The *incisal* region represented the *secretory* stage and the *whole* region represented all three developmental stages of enamel formation (Smith and Warshawsky, 1975, 1976; Smith and Nanci, 1989). The *Amelx*^{WT} incisors were smooth with typically distributed enamel composed of low *lightness*, high *yellow/ blue* and low *whiteness* colour components that were consistent with

normal intact enamel containing iron pigment (Halse, 1972). In contrast, the *Amelx*$^{Y/Y64H}$ and *Amelx*$^{Y64H/Y64H}$ incisor enamel was rough where present and was composed of high *lightness,* low *yellow/ blue* and high *whiteness* colour components, which had the most severely affected and similar enamel phenotypes, e.g. the high *lightness* values in the *incisal* region.

This discolouration was consistent with the presence of aberrantly mineralised enamel and the absence of correctly mineralised enamel, comparable to that observed in humans with similar gene mutations (Witkop and Sauk, 1976; Collier *et al.,* 1997; Ravassipour *et al.,* 2000; Hart *et al.,* 2000; Wright *et al.,* 2003). The presence of normal intact enamel in the *Amelx*^{WT} incisors, of hypomineralised enamel in the *Amelx*$^{X/Y64H}$ incisors, and hypoplastic enamel in the *Amelx*$^{Y/Y64H}$ and *Amelx*$^{Y64H/Y64H}$ mutant incisors provided further evidence of the important role of amelogenin in enamel mineralisation.

The significant incisor morphological differences in the 3D *surface-area* and *volume* variables supported the 2D incisor morphometry that also showed the *Amelx*^{WT} group had the largest incisors and the *Amelx*$^{Y64H/Y64H}$ group had smallest incisors (Figure 75.).

Figure 75. *Amelx* Phenotype Comparison - 3D IAS Incisor Morphology and *surface-roughness* Analysis

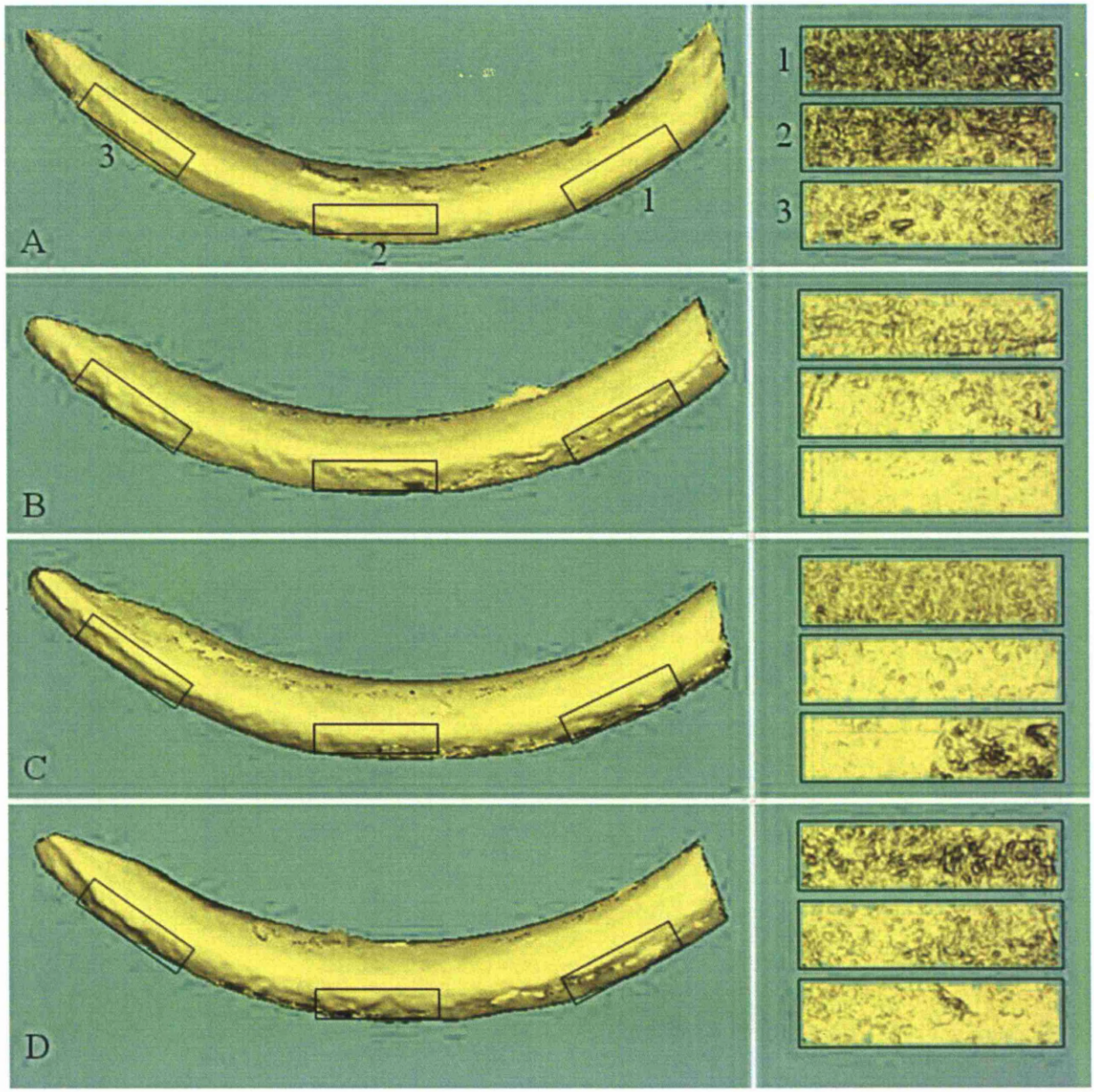

(A) *Amelx*^{WT}; (B) *Amelx*$^{X/Y64H}$; (C) *Amelx*$^{Y/Y64H}$; (D) *Amelx*$^{Y64H/Y64H}$; (1) *incisal*; (2) *middle*; (3) *gingival* enamel surface regions. Rectangles = 200x500µm. No scale.

The 3D IAS presents the first report of a 3D micro-metric surface analysis of murine enamel using NCSP technology and the ISO Ra standard measurement (Figure 75.). In the *Amelx*^{WT} group the incisor enamel *surface-roughness* increases through the *gingival*, *middle* and *incisal* surface regions that represent the progressive developmental stages of enamel mineralisation. This contrasts with the diminishing surface roughness that would be expected

from a loss of organic matrix and the increasingly smooth crystal surface morphology as revealed by Atomic Force Microscopy (Kirkham *et al.,* 1998). Nevertheless, the increasing *surface-roughness* observed in all the affected *Amelx*$^{X/Y64H}$, *Amelx*$^{Y/Y64H}$ and *Amelx*$^{Y64H/Y64H}$ incisors is consistent with the presence of pathological enamel. As mutations that lead to defective ECM processing are thought to impair enamel mineral initiation, fusion, and crystal growth leading to short mineral segments in hypoplastic AI or abnormally large crystals in hypomature AI (Robinson *et al.,* 2003).

The areas of missing enamel in the *Amelx*$^{Y/Y64H}$ and *Amelx*$^{Y64H/Y64H}$ groups make it difficult to carry out meaningful enamel thickness measurements on severely affected incisors. However, TMR images demonstrate significantly reduced enamel mineral content in the *Amelx*$^{X/Y64H}$ group incisors (Barron *et al.,* 2010) and are supported by the nano-CT images of unerupted incisors in the *Amelx*$^{Y/Y64H}$ and *Amelx*$^{Y64H/Y64H}$ groups (Myers *et al.,* 2009).

The 3D IAS incisor morphology presented here identifies significant differences between the *Amelx*^{WT} group and between each of the individual mutant groups. In contrast to the 2D IAS, the 3D IAS identifies significant differences between the *Amelx*^{WT} and *Amelx*$^{X/Y64H}$ groups, while showing no significant differences between the *Amelx*$^{Y/Y64H}$ and *Amelx*$^{Y64H/Y64H}$ groups. This suggests that the novel 3D IAS is particularly sensitive in detecting differences in incisor morphology and is more representative of the actual phenotype. The 3D IAS more accurately differentiated between the different phenotypes of the different genotype groups than the 2D IAS equivalent. The 3D IAS was well suited to the mouse incisor application.

The 2D IAS incisor morphology and colour and whiteness assessment findings and the 3D IAS incisor morphology and surface analysis findings were complementary and supported one another respectively. The new 3D IAS provided further morphological and topographical information that improved sensitivity in detecting the subtle morphological differences between the more affected and more unaffected *Amelx* mice incisors, e.g. the new actual *surface-area* and *volume* variables that measure the 360° of tooth bulk and enamel deposition.

The phenotype comparison presented here quantitatively supported the effect of amelogenin on enamel mineralisation in a mouse model of AIH1.

6.2.3. *Amelx* Summary

The significant differences observed between the wild-type and the mutant groups identified abnormal mandible morphology, incisor morphology and colour and whiteness in the mutant groups. This may be directly attributed to the loss of amelogenin protein function caused by the Y64H mutation.

The significant differences between the normal $Amelx^{WT}$ control mandibles and the abnormal $Amelx^{Y64H/Y64H}$ mutant mandibles supported a role for amelogenin in mandible development. The significant phenotype deviation in the mandible and incisor morphology and in the incisor colour and whiteness between the normal $Amelx^{WT}$ controls and the severely abnormal *Amelx* mutants was evidence both of the important role of amelogenin in development and of the pathological effects of mutations in the gene. Thus, the abnormal morphology exhibited in the *Amelx* mutant mandibles and incisors was directly attributed to the Y64H mutation. The aberrant mineralisation and apparent absence of enamel in the *Amelx* mutant incisors, particularly in the *incisal* region, was not the result of post-eruptive breakdown but was primarily a developmental defect related to the *Amelx* gene Y64H mutation that led to the disruption of the amelogenin protein function, leading to the enamel defects. The results demonstrate that amelogenin affects mandible and incisor morphology - reflecting enamel quantity, growth and development - and also that amelogenin affected enamel colour and whiteness - reflecting enamel quality and mineralisation.

The significant deviations between the enamel phenotypes of control and mutant animal groups presented here, along with recently published parallel findings (Barron *et al.,* 2010), infer that the failed secretion and the loss of function of the Y64H amelogenin protein may be the causative mechanism underpinning the dysplastic enamel mineralisation observed. These studies demonstrate that the mutation of the amelogenin gene was the outstanding factor in the pathogenesis of AIH1.

6.2.4. *Enam* Experimental Comparison

The *Enam*^{WT} group displayed normal mandible morphology (Gaunt, 1964; Atchley *et al.,* 1985; Bailey, 1985) and incisors with typical enamel deposition, thickness and colour distribution (Hay, 1961; Moinchen *et al.,* 1996). The *Enam*^{Rgsc395} *heterozygous* and *homozygous* groups both displayed severely affected pathological incisor enamel (Masuya *et al.,* 2005; Seedorf *et al.,* 2007; Hu *et al.,* 2008; Smith *et al.,* 2009c; Wright *et al.,* 2009) (Figure 76.).

Figure 76. *Enam* Phenotype Comparison - 2D IAS Mandible Measurement, Incisor Measurement and Colour and Whiteness Assessment

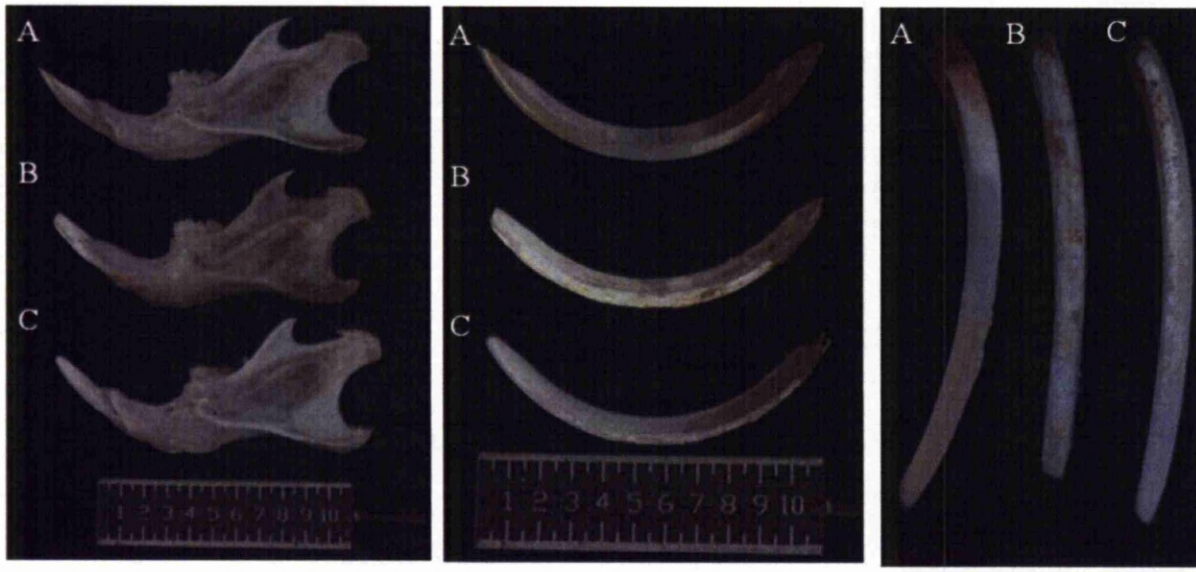

(A) *Enam*^{WT}; (B) *Enam*^{Rgsc395} *heterozygous*; (C) *Enam*^{Rgsc395} *homozygous*. Scale = 10.0mm.

In humans, *ENAM* mutations cause autosomal dominant AI (Rajpar *et al.,* 2001; Kida *et al.,* 2001; Mardh *et al.,* 2002; Hart *et al.,* 2003a, 2003b; Kim *et al.,* 2005b) and show haploinsufficiency (Hu and Yamakoshi, 2003; Ozdemir *et al.,* 2005). In mouse models of AI, the *Enam* gene mutations in similar sequences reflected this dose effect in the hypoplastic enamel of the *Enam*^{Rgsc395} *heterozygous* and *homozygous* mice (Matsuya *et al.,* 2005) and in the enamel agenesis of the *Enam*-null mice (Seedorf *et al.,* 2007; Hu *et al.,* 2008; Smith *et al.,* 2009c; Wright *et al.,* 2009). The significant differences in incisor morphology and colour and whiteness between the *Enam*^{WT} and *Enam*^{Rgsc395} *homozygous* and between the *Enam*^{WT} and

Enam^{Rgsc395} *heterozygous* suggested that the enamelin protein was involved in incisor morphological development, as well as enamel mineralisation.

There were no statistically significant differences between the three *Enam* group mandibles. This suggested that the enamelin protein had no effect on mandible morphology in contrast to *Amelx*. However, the significant differences in incisor morphology observed here suggested that the *Enam*^{WT} incisors were the largest, followed in descending order of size by the *Enam*^{Rgsc395} *homozygous* and *heterozygous* groups, e.g. in the *angle-of-curvature* variable.

The *Enam*^{WT} mice expressed the functional *Enam* gene (Hu *et al.,* 2001b). This led to the secretion of the full length enamelin protein essential for generating full thickness and correctly mineralised enamel (Hay, 1961; Moinchen *et al.,* 1996). The *Enam*^{Rgsc395} *homozygous* and *heterozygous* groups, that expressed the *Enam* S55I mutation containing allele, displayed thin aberrantly mineralised enamel that lacked the full length enamelin and its functionally important processing products (Masuya *et al.,* 2005). Failed secretion and loss of function of a similar truncated enamelin variant was unable to mediate proper enamel mineralisation (Seedorf *et al.,* 2007). The significant differences in incisor morphology observed here between the *Enam*^{WT} and *Enam*^{Rgsc395} *heterozygous* groups (e.g. *angle-of-curvature*) and between the *Enam*^{WT} and *Enam*^{Rgsc395} *homozygous* groups (e.g marked *surface-area*), are compatible with the enamelin protein involvement in incisor morphological development.

The significant colour and whiteness differences that were observed between *Enam*^{WT} and *Enam*^{Rgsc395} *homozygous* groups and between the *Enam*^{Rgsc395} *heterozygous* groups occurred specifically in the *lightness*, *yellow/ blue* and *whiteness* colour components in the *middle*, *incisal* and *whole* enamel surface regions. The *middle* and *incisal* regions represented the *secretory* and *mature* stages, and the *whole* region represented all three developmental stages of enamel formation (Smith and Warshawsky, 1975, 1976; Smith and Nanci, 1989). The *Enam*^{WT} incisor enamel was smooth, normally distributed and demonstrated low *lightness*, high *yellow* and low *whiteness* colour components, consistent with the normal enamel colour containing iron pigment (Halse, 1972). In marked contrast, the *Enam*^{Rgsc395} *homozygous* and *heterozygous* incisor enamel was rough and where present demonstrated high *lightness*, low *yellow* and high *whiteness* colour components. This discolouration was consistent with the presence of aberrantly mineralised enamel and/ or the absence of correctly mineralised

enamel (Masuya *et al.,* 2005). Similar enamel discolouration and severely pathological enamel mineralisation was the result of a similar loss of enamelin protein function in a number of other *Enam* mutant mouse models of AI (Seedorf *et al.,* 2007; Hu *et al.,* 2008; Smith *et al.,* 2009c; Wright *et al.,* 2009). This enamel defect was indicative of localised enamel hypoplasia similar to that observed in humans with similar mutations (Rajpar *et al.,* 2001; Kida *et al.,* 2002; Mardh *et al.,* 2002; Hart *et al.,* 2003a, 2003b; Kim *et al.,* 2005b).

The significant phenotype deviation in incisor morphology and enamel colour and whiteness, between the $Enam^{WT}$ control incisors and the enamel in the $Enam^{Rgsc395}$ *homozygous* and *heterozygous* mutant incisors, was suggested to be directly attributable to the *Enam* S55I mutation that disrupted the secretion of the truncated enamelin S55I protein and caused the subsequent loss of function. The absence of any significant colour and whiteness differences between the $Enam^{Rgsc395}$ *homozygous* and *heterozygous* groups suggested they had similar pathological enamel phenotypes (Figure 77.).

Figure 77. *Enam* Phenotype Comparison - 3D IAS Incisor Morphology and *surface-roughness* Analysis

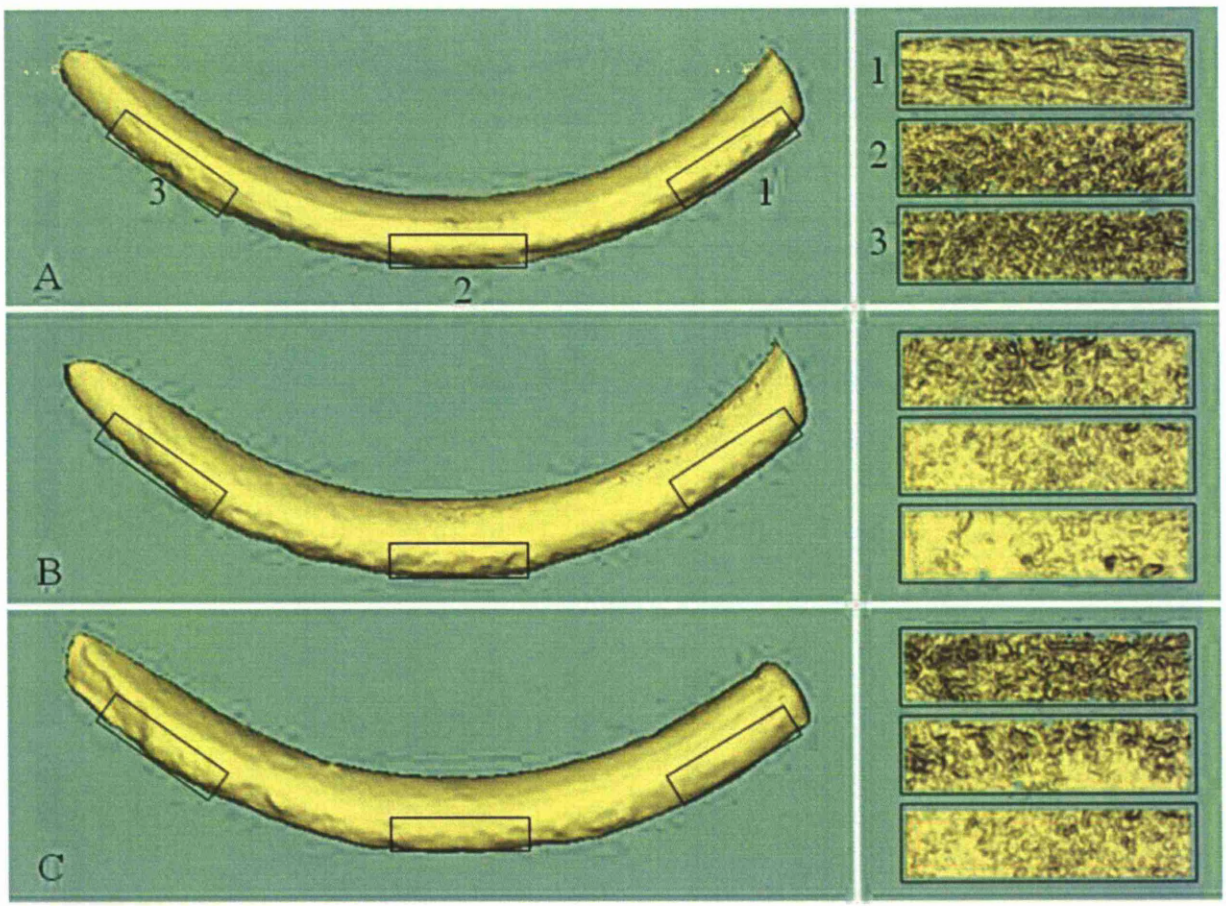

(A) *Enam*^{WT}; (B) *Enam*^{Rgsc395} *homozygous*; (C) *Enam*^{Rgsc395} *heterozygous*; (1) *incisal*; (2) *middle*; (3) *gingival* enamel surface regions. Rectangles = 200x500µm. No scale.

The 3D IAS provided the first report of a 3D micro-metric surface analysis of murine enamel using NCSP technology and the ISO Ra standard measurement (Figure 77.). In the *Enam*^{WT} group the incisor enamel *surface-roughness* increased through the *gingival*, *middle* and *incisal* surface regions that represented the progressive developmental stages of enamel mineralisation. This contrasted with the diminishing surface roughness that would be expected from a loss of organic matrix and the increasingly smooth crystal surface morphology as revealed by Atomic Force Microscopy (Kirkham *et al.,* 1998). Nevertheless, the increasing *surface-roughness* observed in the two affected *Enam*^{Rgsc395} *heterozygous* and *homozygous* incisors is consistent with the presence of pathological enamel, as mutations that lead to defective ECM processing are thought to impair enamel mineral initiation, fusion, and crystal growth leading to short mineral segments in hypoplastic AI (Robinson *et al.,* 2003).

The 2D IAS incisor morphology and colour and whiteness assessment findings and the 3D IAS incisor morphology and surface analysis findings were complementary and supported one another respectively. The new 3D IAS provided further morphological and topographical information that improved sensitivity in detecting the subtle morphological differences between the more affected and less affected *Enam* mice incisors, e.g. the new actual *surface-area* and *volume* variables that measure the 360° of tooth bulk and enamel deposition.

The phenotype comparison presented here quantitatively supported the effect of enamelin on enamel mineralisation in a mouse model of AIH2 that phenocopied AI patients presenting with similar mutations.

6.2.5. *Enam* Summary

The significant phenotype variation in incisor morphology and incisor colour and whiteness between the normal $Enam^{WT}$ control group and the severely abnormal *Enam* mutant groups was indicative of the pathological enamel defect. Enamelin variants and functionally important enamelin processing products were either absent or truncated significantly in *Enam* mutant mice suggesting that the non-functional enamelin S55I was unable to mediate proper enamel mineralisation because of impaired secretion. Failed enamelin secretion was also observed in a number of other *Enam* models that displayed similar severely aberrant enamel mineralisation.

The aberrant incisor morphology and enamel mineralisation, and apparent areas of absent enamel in the *Enam* mutant incisors, particularly in the *middle* and *incisal* regions, was not the result of post-eruptive breakdown but was primarily a developmental defect directly attributed to the *Enam* gene S55I mutation and subsequent disruption to the enamelin protein function. The results demonstrated that enamelin affected incisor morphology - reflecting enamel quantity, growth and development - and also that enamelin affected enamel colour and whiteness - reflecting enamel quality and mineralisation.

The phenotype comparison presented here quantitatively supports the affect of enamelin on enamel mineralisation in a mouse model of AIH2 that phenocopies AI patients presenting with similar mutations. The significant deviations between the enamel phenotypes of control and mutant animal groups suggests that the failed secretion and the loss of function of the enamelin S55I protein was the underpinning mechanism evident in the dysplastic enamel mineralisation observed. The $Enam^{WT}$ control group displayed normal intact enamel compared to the $Enam^{Rgsc395}$ *homozygous* and *heterozygous* mutant groups that displayed hypoplastic enamel or completely absent enamel indicative of AIH2. The supports the suggestion that enamelin mutations are the outstanding factor in the pathogenesis of AIH2.

6.2.6. *Amelx* and *Enam* Summary

The *Amelx*^{WT} and *Enam*^{WT} controls demonstrated normal enamel and the mutant groups were affected.

Significant differences in mandible morphology were observed between the *Amelx* groups but not between the *Enam* groups. This infers that amelogenin affected mandible development but that enamelin did not.

The significant differences in incisor morphology were observed between the *Amelx* groups and also between the *Enam* groups. This infers that both amelogenin and enamelin affected incisor enamel quantity, growth and development.

There were more significant differences between the *Amelx* groups than between the *Enam* groups. This suggested amelogenin had a greater affect on incisor development than enamelin.

The significant differences in enamel discolouration and the differences in enamel surface roughness observed between the *Amelx* groups and between the *Enam* mutant groups suggest that the amelogenin and enamelin proteins affect incisor enamel quality and mineralisation.

The 2D IAS and 3D IAS incisor morphology results were similar and supported one another. The colour and whiteness assessment and 3D IAS surface analysis results were similar and supported one another. There was no statistical support for the *surface-roughness* findings, which will be addressed in the Future Work.

The sites of the significant enamel discolouration were different between the *Amelx* groups and the *Enam* groups: in the *Amelx* incisors the differences were found only in *incisal* and *whole* regions, while in the *Enam* incisors the differences occurred in the *middle*, *incisal* and *whole* regions. The *middle* and *incisal* regions represented the *secretory* and *mature* stages of enamel formation, while the *whole* region represented all three developmental stages of enamel formation. Thus, the significant differences suggested that enamelin mutation affected the *secretory* stage of enamel formation and that amelogenin mutation did not. This implies that enamelin had an earlier, more localised effect on the secretory stage of amelogenesis

than amelogenin and supported the regulatory functions of the different ECM proteins during the different stages of enamel growth and formation.

The colour and whiteness assessment differentiated between hypomineralised *Amelx*$^{X/Y64H}$, hypoplastic *Amelx*$^{Y/Y64H}$ and *Amelx*$^{Y64H/Y64H}$ and local hypoplastic *Enam*^{Rgsc395} *homozygous* and *heterozygous* enamel phenotypes. According to the different gene mutation and subsequent protein disruption, the enamel defects were observed in a surface region specific manner that correlated to the distinct developmental stages of enamel formation.

Translating the phenotype observations made here in mice to the human counterpart must be undertaken with caution, with respect to the alternative splicing of amelogenin and the various cleavage products of enamelin that contribute to variable protein function, and also the considerable epigenetic effects within the broader genetic background of the human population.

7. CONCLUSIONS

7.1. METHOD RELIABILITY AND VALIDATION

Four novel measurement methods were successfully applied for murine dental phenotyping; 2D IAS (i) mandible morphology, (ii) incisor morphology (iii) enamel colour and whiteness assessment and (iv) 3D IAS incisor morphology and surface analysis.

The reliability of the 2D IAS mandible and incisor morphology was substantial to excellent. The reliability of the colour and whiteness assessment was predominately excellent. The reliability of the 3D IAS incisor morphology was substantial to excellent.

The 2D IAS and the 3D IAS incisor morphology gave significant method agreement and the 3D IAS was validated by large measurement correlations. Potential experimental and systematic error testing gave highly satisfactory results.

The 2D IAS and 3D IAS could be used with equal validity for incisor morphology.

7.1.1. Summary

In relation to the Aims of this investigation, the 2D IAS and 3D IAS were highly reliable measurement methods that were validated to provide additional morphological information.

These innovations were complementary and provided practical and objective approaches to the quantitative macro-metric and micro-metric characterisation of murine mandible morphology, incisor morphology and enamel mineralisation.

7.2. EXPERIMENTAL COMPARISON

7.2.1. Introduction

In relation to the aims and hypotheses of this investigation, there was significant phenotype variation between the wild-type control mice and the experimental mutant mice. The significant differences in the mandible and incisor morphology and in the colour and whiteness variables demonstrated the effect of the amelogenin protein and the enamelin protein on normal and abnormal enamel mineralisation. In complimentary studies (Barron *et al.,* 2010) the gene mutations were proposed to have truncated their respective protein products that led to the loss of function and the observed pathological enamel phenotypes.

The *Amelx*^{WT} and *Enam*^{WT} mice did not contain gene mutations and were unaffected so served as a baseline for the explicit phenotype to genotype correlation of the two models of AI: the *Amelx*$^{Y/Y64H}$ and *Amelx*$^{Y64H/Y64H}$ mutant mice displayed severely hypoplastic enamel characteristic of AIH1; the *Amelx*$^{X/Y64H}$ mutant mice displayed hypomineralised enamel characteristic of AIH1; the *Enam*^{Rgsc395} *homozygous* and *Enam*^{Rgsc395} *heterozygous* mutant mice displayed hypoplastic enamel characteristic of AIH2.

The enamel colour and whiteness phenotypes presented here were representative of enamel mineralisation and were differentiated by specific surface region and developmental stage comparisons.

7.2.2. *Amelx*

The significant morphological differences between the groups of *Amelx* mice suggested an active role for amelogenin in mandible bone formation and in generating the full thickness of enamel during mandibular incisor development; the unaffected $Amelx^{WT}$ mice had the largest mandibles and incisors while the affected $Amelx^{X/Y64H}$, $Amelx^{Y/Y64H}$ and $Amelx^{Y64H/Y64H}$ mutant mice displayed smaller mandibles and incisors. The observed phenotypes supported the multifunctional role of the amelogenin protein in the development of the craniofacial-complex.

The significant colour and whiteness differences between the groups of *Amelx* mice suggested an essential role for amelogenin in incisor enamel mineralisation; the unaffected $Amelx^{WT}$ mice incisors displayed normal smooth enamel in contrast with the affected $Amelx^{Y/Y64H}$ and $Amelx^{Y64H/Y64H}$ mutant mice incisors that displayed discoloured and rough pathological enamel. The more mildly affected $Amelx^{X/Y64H}$ mutant mice displayed intermediate incisor morphology and incisor enamel phenotype, which reinforced the phenotype to genotype correlation. The phenotype variation in the *incisal* surface region corresponded to a delayed function of amelogenin in the specific *mature* developmental stage of enamel formation. The 3D surface analysis corroborated the presence of abnormal enamel in the *Amelx* mutant mice.

Similar to the known mutational affects of *AMELX* in humans, the $Amelx^{Y64H/Y64H}$ and $Amelx^{Y/Y64H}$ mouse incisor enamel was hypoplastic and the $Amelx^{X/Y64H}$ mouse incisor enamel was hypomineralised and indicative of AIH1.

7.2.3. *Enam*

The absence of significant difference between the groups of *Enam* mice mandibles suggested the enamelin protein had no role in mandible development. The significant morphological differences between the groups of *Enam* mice incisors suggested a role for the enamelin protein in incisor development; the unaffected $Enam^{WT}$ mice had the largest incisors and the affected $Enam^{Rgsc395}$ *homozygous* and $Enam^{Rgsc395}$ *heterozygous* mutant mice incisors were smaller. The phenotype variation in 2D incisor morphology supported the essential function of the enamelin protein in generating full thickness enamel.

The significant colour and whiteness differences between the *Enam* mice incisors supported the role of enamelin in enamel mineralisation; the $Enam^{WT}$ mice incisors displayed normal smooth enamel in contrast with the affected $Enam^{Rgsc395}$ *homozygous* and $Enam^{Rgsc395}$ *heterozygous* mice incisors that displayed discoloured and rough pathological enamel. The similar aberrant enamel phenotypes in the $Enam^{Rgsc395}$ *homozygous* and $Enam^{Rgsc395}$ *heterozygous* mice incisors reinforced the phenotype to genotype correlation. The phenotype variation in the *middle* and *incisal* surface regions corresponded to the earlier more localised effect of enamelin in the *secretory* and subsequent *maturational* developmental stages of enamel formation. The 3D surface analysis corroborated the presence of pathological enamel in the *Enam* mutant mice.

Similar to the known mutational affects of *ENAM* in humans, the $Enam^{Rgsc395}$ *homozygous* and $Enam^{Rgsc395}$ *heterozygous* enamel was hypoplastic and indicative of AIH2.

7.2.4. *Amelx* and *Enam* Summary

The study showed that the *Amelx* and *Enam* gene mutations in mice, in similar domains to the *AMELX* and *ENAM* gene mutations in humans, produced comparable enamel defects that served as exploratory models for studying the aetiology of AI; the *Amelx* mutants displayed hypoplastic/ hypomineralised enamel indicative of X-linked AI (AIH1,OMIM301200) and *Enam* mutants displayed local hypoplastic enamel indicative of autosomal dominant AI (AIH2, OMIM104500).

The experimental comparison presented evidence of significant phenotype variation between the controls and the experimental mutants in two relevant mouse models that reflected human AI. The measurement methods correlated the phenotype to the genotype and supported the role of the amelogenin and enamelin proteins in incisor morphological development and enamel mineralisation.

The study successfully linked phenotype with underlying genetic lesion and supported protein-protein secretory interactions proposed to be a pathological mechanism underpinning abnormal enamel formation.

7.3. IMPACT ON AIMS

i. Four new measurement methods were successfully developed; (i) a 2D image analysis system (IAS) to measure murine mandible morphology, (ii) incisor morphology and (iii) incisor enamel colour and whiteness, and (iv) a 3D IAS to measure incisor morphology and enamel surface structure.

ii. The novel repertoires of variables were highly reliable and valid.

iii. The 2D IAS and 3D IAS approaches demonstrated complementary practical solutions that facilitated both the macro-metric and micro-metric investigation of the reliability population, with additive 3D IAS information.

iv. The mandible morphology and incisor morphology represented enamel quantity, growth and development. The colour and whiteness and 3D surface assessment represented enamel quality and mineralisation.

v. The new measurement methods were used to characterise the two populations of mice with specific gene mutations in the enamel ECM proteins amelogenin (*Amelx*, OMIM300391) and enamelin (*Enam*, OMIM606585). The *Amelx* and *Enam* populations were suitable mouse models of X-linked *Amelogenesis imperfecta* (AIH1, OMIM301200) and autosomal dominant local hypoplastic *Amelogenesis imperfecta* (AIH2, OMIM104500) respectively.

vi. The wild-type control groups were successfully compared with the experimental mutant groups.

vii. Significant phenotype differences were indentified in the mandible dimensions and incisor dimensions, and in the colour and whiteness assessment.

viii. This quantitatively supported the involvement of amelogenin and enamelin in mandible and incisor morphology and enamel mineralisation. The multifunctional role of amelogenin in the development of the craniofacial complex was supported.

ix. The enamel colour and whiteness assessment successfully differentiated between overlapping phenotypes according to the *Amelx* and *Enam* gene mutations in a surface region specific manner that correlated to the distinct developmental stages of enamel formation.

7.4. IMPACT ON NULL HYPOTHESES

xiv. The 2D IAS will not be reliable – reject

xv. The colour and whiteness assessment will not be reliable - reject

xvi. The 3D IAS will not be reliable – reject

xvii. The 3D IAS will not be valid – reject

xviii. The mandible and incisor morphometry, and colour and whiteness assessment will not quantify phenotype – reject

xix. The mandible and incisor morphology will not represent enamel quantity, growth and development – reject

xx. The colour and whiteness and 3D surface assessment will not represent enamel quality and mineralisation – reject

xxi. The control and mutant groups will not show evidence of statistically significant phenotypic variation – reject

xxii. There will be no significant differences in the mandible dimensions between wild-type and mutant populations – reject

xxiii. There will be no significant differences in the incisor dimensions between wild-type and mutant populations – reject

xxiv. There will be no significant differences in the enamel phenotype between wild-type and mutant populations – reject

xxv. The *Amelx* mutants will not display hypoplastic/ hypomineralised enamel indicative of X-linked AI (AIH1,OMIM301200) – reject

xxvi. The *Enam* mutants will not display local hypoplastic enamel indicative of autosomal dominant AI (AIH2, OMIM104500) – reject

8. FUTURE WORK

8.1. Reliability and Validation

Further 3D incisor morphometry intra-operator repeatability data would corroborate the exceptionally high reproducibility presented. Also, incisor intra-operator and inter-operator reliability data would validate the 3D IAS for *surface-roughness* measurement.

8.2. Method Development

The study demonstrates the successful modification of existing methods for new applications and presents original methods. This establishes a strong precedent for expanding the new methods to future applications, e.g. an alternative NCSP chromatic sensor may include 3D mandible morphology.

8.3. Experimental Comparison

The mandibular molars and maxillary incisors and molars of the experimental populations remain preserved for future use. The existing image archive and data records may be used in future studies.

Increasing the small sample population ($n = 1$) for the *surface-roughness* assessment would provide the necessary statistical support to strength the experimental comparison.

The current investigation provides collaborative potential for a broader series of similar investigations using other mouse models of AI, e.g. the recently described ECM protein amelobastin mice (Seedorf *et al.,* 2007) and enamelin-null mice (Hu *et al.,* 2008) and/ or the ECM proteases kallikrien *Klk-4* (Simmer *et al.,* 2009) and enamelysin *Mmp-20* (Wright *et al.,* 2009).

Indeed this was positively discussed with Dr. Jan Hu from The University of Michigan at Ann Arbor Dental School, USA at the American Association of Dental Research and Canadian Association of Dental Research conference in Washington DC USA in April 2010.

There is considerable potential for applying the novel measurement methods beyond the mouse model and to other small mammalian dental applications, e.g. rodents and bats (Evans *et al.*, 2001).

At the time of writing, example incisors from each experimental group are with Dr. Paul Anderson at Queen Mary, University of London awaiting X-ray Micro-Tomography (Anderson *et al.*, 1996). It is hoped this will provide valuable quantitative enamel mineral density data and additional 3D structural information.

9. REFERENCES

ABLAL, M.A., KAUR, J.S., COOPER, L., JARAD, F.D., MILOSEVIC, A., HIGHAM, S.M. & PRESTON, A.J. (2009) The erosive potential of some alcopops using bovine enamel: An *in vitro* study, *Journal of Dentistry*, vol. 37, no. 11, pp. 835-839.

ADDISON, W.H. & APPLETON, J.L. (1915) The structure and growth of the incisor teeth of the albino rat, *Journal of Morphology.*, vol. 26, pp. 43-96.

ALDRED, M.J., CRAWFORD, P.J., ROBERTS, E., GILLESPIE, C.M., THOMAS, N.S., FENTON, I., SANDKMJL, L.A. & HARPER, P.S. (1992a) Genetic heterogeneity in X-linked *Amelogenesis imperfecta*, *Genomics*, vol. 14, pp. 567-573.

ALDRED, M.J., CRAWFORD, P.J.M., ROBERTS, E. & THOMAS, N.S.T. (1992b) Identification of a nonsense mutation in the amelogenin gene (*AMELX*) in a family with X-linked *Amelogenesis imperfecta* (AIH1), *Human Genetics*, vol. 90, pp. 413-416.

ALDRED, M.J., SAVARIRAYAN, R. & CRAWFORD, P.J.M. (2003) *Amelogenesis imperfecta*: a classification and catalogue for the 21st century, *Oral Diseases*, vol. 9 no. 1, pp. 19-23.

AMAR, S., KARCHER-DJURICIC, V., MEYER, J.M. & RUCH, J.V. (1986) The lingual (root analogue) and the labial (crown analogue) mouse incisor promotes ameloblast differentiation, *Arch. Anat. Microsc. Morphol*, no. 75, pp. 229-239.

ANDERSON, P., BOLLET-QUIVOGNE, F.R., DOWKER, S.E.P. & ELLIOTT, J.C. (2004) Demineralization in enamel and Hydroxyapatite aggregates at increasing ionic strength, *Archives of Oral Biology*, vol. 49, pp. 199-207.

ANDERSON, P., ELLIOTT, J.C., BOSE, U. & JONES, S.J. (1996) A comparison of the mineral content of enamel and dentine in human premolars and enamel pearls measured by X-ray microtomography, *Archives of Oral Biology*, vol. 41, no. 3, pp. 281-290.

ANDERSON, P., LEVINKIND, M. & ELLIOTT. J.C. (1998) Scanning microradiographic studies of rates of *in vitro* demineralisation in human and bovine dental enamel, *Archives of Oral Biology*, vol. 43, pp. 649-656.

ANSORGE, H. (2001) Assessing non-metric skeleton characters as a morphological tool, *Zoology*, vol. 104, no. 3-4, pp. 268-277.

APUZZO, N.D. (2006) Overview of 3D surface digitization technologies in Europe, in B. Corner, D., P. Li & M. Tocheri (eds), *Three-Dimensional Image Capture and Applications VI, Proc. of SPIE-IS&T Electronic Imaging*, vol. 6056, SPIE, San Jose, pp. 1-13.

ARENDS, J. & TEN BOSCH, J.J. (1992) Demineralization and remineralisation evaluation techniques, *Journal of Dental Research*, vol. 71, no. suppl 1, pp. 924-928.

ASQUITH, J., GILLGRASS, T. & MOSSEY, P. (2007) Three-dimensional imaging of orthodontic models: a pilot study *European Journal of Orthodontics*, vol. 29, pp. 517-522.

ATCHLEY, W.R. & HALL, B.K. (1991) A model for development and evolution of complex morphological structures, *Biological Reviews*, vol. 66, no. 2, pp. 101-157.

ATCHLEY, W.R., PLUMMER, A.A. & RISKA, B. (1985) Genetics of mandible form in the mouse, *Genetics*, vol. 111, no. 3, pp. 555-577.

AYOUB, A.F., WRAY, D., MOOS, K.F., JIN, J., NIBLETT, T.B., & URQUHART, C. (1997) A three-dimensional imaging system for archiving dental study casts: a preliminary report, *International Journal of Adult Orthodontics and Orthognathic surgery*, vol. 12, pp. 79-84.

BABA, O., TAKAHASHI, N., TERASHIMA, T., LI, W., DENBESTEN, P.K. & TAKANO, Y. (2002) Expression of alternatively spliced RNA transcripts of amelogenin gene exons 8 and 9 and its end products in the rat incisor, *Journal of Histochemistry and Cytochemistry*, vol. 50, pp. 1229-1236.

BACKMAN, B. (1988) *Amelogenesis imperfecta*--clinical manifestations in 51 families in a northern Swedish county, *Scandinavian Journal of Dental Research*, vol. 96, pp. 505-516.

BACKMAN, B. & HOLM, A.K. (1986) *Amelogenesis imperfecta*: prevalence and incidence in a northern Swedish county, *Community Dentistry & Oral Epidemiology*, vol. 14, pp. 43-47.

BADER, R.S. (1965) Heritability of Dental Characters in the House Mouse, *Evolution*, vol. 19, no. 3, pp. 378-384.

BAILEY, D.W. (1985) Genes that affect the shape of the murine mandible: Congenic strain analysis, *Journal of Heredity*, vol. 76, no. 2, pp. 107-114.

BAILEY, D.W. (1986) Genes that affect morphogenesis of the murine mandible: Recombinant-inbred strain analysis, *Journal of Heredity*, vol. 77, no. 1, pp. 17-25.

BARRETT, M.J., BROWN, T. & LUKE, J.I. (1963) Dental observations on Australian aborigines: mesiodistal crown diameters of deciduous teeth, *Australian Dental Journal*, vol. 8, pp. 299-302.

BARRON, M.J., BROOKES, S.J., KIRKHAM, J., SHORE, R.C., HUNT, C., MIRONOV, A., KINGSWELL, N.J., MAYCOCK, J., SHUTTLEWORTH, C.A. & DIXON, M.J. (2010) A mutation in the mouse *Amelx* tri-tyrosyl domain results in impaired secretion of amelogenin and phenocopies human X-linked *Amelogenesis imperfecta*, *Human Molecular Genetics*, p. ddq001.

BARTLETT, J.D., BENIASH, E., LEE, D.H. & SMITH, C.E. (2004) Decreased Mineral Content in MMP-20 Null Mouse Enamel is Prominent During the Maturation Stage, *Journal of Dental Research*, vol. 83, no. 12, pp. 909-913.

BARTLETT, J.D., SIMMER, J.P., XUE, J., MARGOLIS, H.C. & MORENO, E.C. (1996) Molecular cloning and mRNA tissue distribution of a novel matrix metalloproteinase isolated from porcine enamel organ, *Gene*, vol. 183, no. 123-128.

BARTLETT, J.D., SKOBE, Z., LEE, D.H., WRIGHT, J.T., LI, Y., KULKARNI, A.B. & GIBSON , C.W. (2006) A developmental comparison of matrix metalloproteinase-20 and amelogenin null mouse enamel, *European Journal of Oral Science*, vol. 114, no. Suppl. 1, pp. 18-23.

BEAMER, W.G., DONAHUE, L.R., ROSEN, C.J. & BAYLINK, D.J. (1996) Genetic variability in adult bone density among inbred strains of mice, *Bone*, vol. 18, pp. 397-403.

BELL, A., AYOUB, A.F. & SIEBERT, P. (2003) Assessment of the accuracy of a three-dimensional imaging system for archiving dental study models, *Journal of Orthodontics*, vol. 30, pp. 219-223.

BENATAR, M., WYNCHANK, S. & ADAMS, L.P. (1989) Measurements of reflection hologram images, *Physics in Medicine and Biology*, vol. 34, pp. 1259-1268.

BERKOWITZ, S. & PRUZANSKY, S. (1968) Stereophotogrammetry of serial casts of cleft palate, *Angle Orthodontist*, vol. 38, no. 136-149.

BHATIA, S.N. & HARRISON, V.E. (1987) Operational performance of the travelling microscope in the measurement of dental casts, *British Journal of Orthodontics*, vol. 14, pp. 147-153.

BIGGERSTAFF, R.H. (1969) Electronic methods for the analysis of the human post-canine dentition, *American Journal of Physical Anthropology*, vol. 31, pp. 235-242.

BLAND, J.M. & ALTMAN, D.G. (1986) 'Statistical methods for assessing agreement between two methods of clinical measurement', *The Lancet*, vol. i, pp. 307-310.

BLAND, J.M. & ALTMAN, D.G. (1999) 'Measuring agreement in method comparison studies', *Statistical Methods in Medical Research*, vol. 8, no. 2, pp. 135-160.

BOLTON, W.A. (1962) The clinical application of a tooth-size analysis, *American Journal of Orthodontics*, vol. 48, pp. 504-529.

BOOKSTEIN, F.L. (1984) A statistical method for biological shape comparisons, *Journal of Theoretical Biology*, vol. 107, pp. 475-520.

BOOKSTEIN, F.L. (1997) Landmark methods for forms without landmarks: morphometrics of group differences in outline shape, *Medical Image Analysis*, vol. 1, no. 3, pp. 225-243.

BOOKSTEIN, F.L. (1998) A hundred years of morphometrics, in C.P. Kingenburg & F.L. Bookstein (eds) vol. 44(1-2), *ACTA Zool. Sci. Hung.*, pp. 7-59.

BOURSOT, P., DIN, W., ANAND, R., DARVICHE, D., DOD, B., VON DEIMLING, F., TALWAR, G.P. & BONHOMME, F. (1996) Origin and radiation of the house mouse: mitochondrial DNA phylogeny, *Journal of Evolutionary Biology*, vol. 9, no. 4, pp. 391-415.

BOYDE, A. (1967) The Development of Enamel Structure, *Proceedings of the Royal Society of Medicine*, vol. 60, pp. 13-18.

BROOK, A.H. (2009) Multilevel complex interactions between genetic, epigenetic and environmental factors in the aetiology of anomalies of dental development, *Archives of Oral Biology*, vol. 54, pp. S3-S17.

BROOK, A.H., ELCOCK, C., AL-SHAROOD, M.H., MCKEOWN, H.F., KHALAF, K. & SMITH, R.N.P. (2002) Further studies of a model for the aetiology of anomalies of tooth number and size in humans, *Connective Tissue Research*, vol. 43 no. 2-3, pp. 289-295.

BROOK, A.H., ELCOCK, C., HALLONSTEN, A.L., ET AL. & ROBINSON, D.L. (2001) The development of a new index to measure enamel defects. , in A.H. Brook (ed.), *Dental Morphology*, Sheffield University Academic Press UK Sheffield, pp. 59-66.

BROOK, A.H. & JOHNS, C.C. (1995) Dental anomalies of number and size in a Romano-British population, *International Symposium on Dental Morphology*, ed. R. Radlanski, Brunne, GBR, Berlin, pp. 177-180.

BROOK, A.H., LATH, D.L., BROOK, B.J. & SMITH, R.N. (2005b) Further consideration of the aetiology of development anomalies of the dentition, in E. Zadzinska (ed.), *Current Trends in Dental Morphology Research,13th International Symposium on Dental Morphology* University of Lodz Press, Poland, pp. 467-474.

BROOK, A.H., PITTS, N.B. & RENSON, C.E. (1983) Determination of tooth dimensions from study casts using an image analysis system, *Journal of International Association of Dentistry for Children*, vol. 14, pp. 55-60.

BROOK, A.H., PITTS, N.B., YAU, F. & SANDAR, P.K. (1986) An image analysis system for the determination of tooth dimensions from study casts: comparison with manual measurements of mesio-distal diameter, *Journal of Dental Research*, vol. 65, no. 3, pp. 428-431.

BROOK, A.H., SMITH, R.N., ELCOCK, C., AL-SHAROOD, M.H., SHAH, A.A., KARMO, M., KHALAF K. & ROBINSON, D.L. (1999) Accurate tooth morphology measurement using a new image analysis system, *Journal of Dental Research*, vol. 78, no. 5, pp. 386.

BROOK, A.H., SMITH, R.N., ELCOCK, C., AL-SHAROOD, M.H., SHAH, A.A., KHALAF, K., ROBINSON, D.L., LATH, D.L. & KARMO, M. (2005a) The measurement of tooth morphology: Validation of an image analysis system, in E. Zadzinska (ed.), *Current Trends In Dental Morphology Research*, University of Lodz Press, Poland. pp. 475-482.

BROOK, A.H., SMITH, R.N. & LATH, D.J. (2007) The clinical Measurement of tooth Colour and Stain, *International Dental Journal*, vol. 57, no. 5, pp. 234-330.

BROOK, A.H., UNDERHILL, C., FOO, L.K. & HECTOR, M. (2006) Approximal attrition and permanent tooth crown size in a Romano-British population, *Dental Anthropology*, vol. 19, pp. 23-28.

BROOKES, S.J., KIRKHAM, J., SHORE, R.C., WOOD, S.R., SLABY, I. & ROBINSON, C. (2001) Amelin extracellular processing and aggregation during rat incisor amelogenesis., *Archives of Oral Biology*, vol. 46, pp. 201-208.

BROOKES, S.J., ROBINSON, C., KIRKHAM, J. & BONASS, W.A. (1995) Biochemistry and molecular biology of amelogenin proteins of developing dental enamel, *Archives of Oral Biology*, vol. 40, pp. 1-14.

BROWN, S., LAD, H., GREEN, E., GKOUTOS, G., GATES, H. & ANGELIS, M.H.D. (2008) Eumorphia and the European Mouse Phenotyping Resource for Standardized Screens (EMPReSS), in Standards of Mouse Model Phenotyping. Prof. Dr. Martin Hrabé de Angelis (ed.), *Standards of Mouse Model Phenotyping*, pp. 311-320. (www.eumorphia.org)

BUCHAILLARD, S.I., ONG, S.H., PAYAN, Y. & FOONG, K. (2007) 3D statistical models for tooth surface reconstruction, *Computers in Biology and Medicine*, vol. 37, no. 10, pp. 1461-1471.

BUTCHER, G.W. & STEPHENS, C.I. (1981) The reflex optical plotter; a preliminary report, *British Dental Journal*, vol. 151, pp. 304-305.

BUTLER, P.M. (1939) Studies of the mammalian dentition. Differentiation of the postcanine dentition, *Proceedings of the Zoological Society of London,* vol. 109 no. B, pp. 329-356.

BUTLER, P.M. (1956) The ontogeny of molar pattern, *Biological Review*, vol. 31, pp. 30-70.

BUTLER, P.M. (1995a) Ontogenetic aspects of dental evolution, *International Journal of Developmental Biology*, vol. 39, pp. 25-34.

BUTLER, W.T. (1995b) Dentin matrix proteins and dentinogenesis, *Connective Tissue Research*, vol. 33, pp. 59- 65.

BUTLER, W.T., BRUNN, J.C., QIN, C. & MCKEE, M.D. (2002) Extracellular Matrix Proteins and the Dynamics of Dentin Formation, *Connective Tissue Research*, vol. 43, no. 2-3, pp. 301-307.

CARLSSON, K. & ALUND, N. (1987) Confocal imaging for 3-D digital microscopy, *Applied Optics*, vol. 26, no. 16, pp. 3232-3238.

CHAMPAGNE, M. (1992) Reliability of measurements from photocopies of study models, *Journal of Clinical Orthodontics*, vol. 26, pp. 648-650.

CHEN, E., YUAN, Z.A., WRIGHT, J.T., HONG, S.P., LI, Y., COLLIER, P.M., HALL, B., D'ANGELO, M., DECKER, S., PIDDINGTON, R., ABRAMS, W.R., KULKARNI, A.B. & GIBSON, C.W. (2003) The Small Bovine Amelogenin LRAP Fails to Rescue the Amelogenin Null Phenotype, *Calcified Tissue International*, vol. 73, no. 5, pp. 487-495.

CHEN, F., BROWN, G.M. & SONG, M. (2000) Overview of three-dimensional shape measurement using optical methods, *Optical Engineering*, vol. 39, no. 1, pp. 10-22.

CHEVERUD, J.M., HARTMAN, S.E., RICHTSMEIER, J.T. & ATCHLEY, W.R. (1990) Quantitative genetic analysis of localized morphology in inbred mouse mandibles using finite element scaling analysis, *Journal of Craniofacial Genetics and Developmental Biology*, vol. 11, no. 3, pp. 122-137.

CHEVERUD, J.M., LEWIS, J.L., BACHRACH, W.M. & LEW, W.D. (1983) The measurement of form and variation in form: an application of three-dimensional quantitative morphology by finite element methods, *American Journal of Physical Anthropology*, vol. 62, pp. 151-165.

CHEVERUD, J.M., ROUTMAN, E.J., DUARTE, F.A.M., VAN-SWINDEREN, B., COTHRAN, K. & PEREL, C. (1996) Quantitative Trait Loci for Murine Growth, *Genetics*, vol. 142, no. 4, pp. 1305-1319.

CHOSACK, A., EIDELMAN, E., WISOTSKI, I. & COHEN, T. (1979) *Amelogenesis imperfecta* among Israeli Jews and the description of a new type of local hypoplastic autosomal recessive *Amelogenesis imperfecta*, *Oral Surgery, Oral Medicine, Oral Pathology, Oral Radiology, and Endodontology*, vol. 47, pp. 148-156.

CHRZANOWSKI, W., ARMITAGE, D.A., KNOWLES, J.C., SZADE, J., KORLACKI, W. & MARCINIAK, J. (2008) Chemical, Corrosion and Topographical Analysis of Stainless Steel Implants after Different Implantation Periods, *Journal of Biomaterials Applications*, vol. 23, no. 1, pp. 51-71.

CHUAH, J.H., ONG, S.H., KONDO, T., FOONG, K.W.C. & YONG, T.F. (2001) 3D space analysis of dental models, *564 Proceedings of SPIE*, vol. 4319 ed. K.M. Seong, pp. 564-573.

CIAMBOTTI, C., NGAN, P., DURKEE, M., KOHLI, K. & KIM, H. (2001) Comparison of dental and dentoalveolar changes between rapid palatal expansion and nickel-titanium palatal expansion appliances, *American Journal of Orthodontics and Dentofacial Orthopedics*, vol. 119, no. 1, pp. 11-20.

COLLIER, P.M., SAUKK J.J., ROSENBLOOM, S.J., YUAN, Z.A. & GIBSON, C.W. (1997) An amelogenin gene defect associated with human X-linked *Amelogenesis imperfecta*, *Arch Oral Biol*, vol. 42, pp. 235-242.

COMMISSION INTERNATIONALE DE L' E'CLAIRAGE, C.I.E. (1986) *Commission Internationale de l' E'clairage colorimetry*, 2nd edition, Central bureau of the CIE, Paris.

COOPER, W.J. & ALBERTSON, R.C. (2008) Quantification and variation in experimental studies of morphogenesis, *Developmental Biology*, vol. 321, no. 2, pp. 295-302.

CRAWFORD, P., ALDRED, M. & BLOCH-ZUPAN, A. (2007) *Amelogenesis imperfecta*, *Orphanet Journal of Rare Diseases*, vol. 2, no. 1, p. 17.

CROMPTON, A.W. (1963) The Evolution of the Mammalian Jaw, *Evolution*, vol. 17, no. 4, pp. 431-439.

CURLESS, B. & LEVOY, M. (1996) A Volumetric Method for Building Complex Models from Range Images, *Computer Graphics, SIGGRAPH*; 303-312.

DACULSI, G. & KEREBEL, B. (1978) High-resolution electron microscope study of human enamel crystallites: size, shape, and growth, *Journal of Ultrastructural Research*, vol. 65, pp. 163-172.

DAHLBERG, A.A. (1945) The changing dentition of man, *Journal of the American Dental Association*, vol. 32, pp. 676-690.

DAVIS, G.R. & WONG, F.S.L. (1996) X-ray microtomography of bones and teeth, *Physiological Measurements*, vol. 17, no. 3, pp. 121-146.

DEUTSCH, D. (1989) Structure and function of enamel gene products, *The Anatomical Record*, vol. 224, no. 2, pp. 189-210.

DEUTSCH, D., CATALANO-SHERMAN, J., DAFNI, L., DAVID, S. & PALMON, A. (1995) Enamel Matrix Proteins and Ameloblast Biology, *Connective Tissue Research*, vol. 32, no. 1-4, pp. 97-107.

DEUTSCH, D., HAZE-FILDERMAN, A., BLUMENFELD, A., DAFNI, L., LEISER, Y., SHAY, B., GRUENBAUM-COHEN, Y., ROSENFELD, E., FERMON, E., ZIMMERMANN, B., HAEGEWALD, S., BERNIMOULIN, J.P. & TAYLOR, A.L. (2006) Amelogenin, a major structural protein in mineralizing enamel, is also expressed in soft tissues: brain and cells of the hematopoietic system, *European Journal of Oral Sciences*, vol. 114, no. Suppl 1, pp. 183-189.

DIBIASE, A.T., ELCOCK, C., SMITH, R.N. & BROOK, A.H. (2006) A new technique for symmetry determination in tooth morphology using image analysis: Application in the diagnosis of solitary maxillary median central incisor, *Archives of Oral Biology*, vol. 51, no. 10, pp. 870-875.

DONG, J., GU, T.T., SIMMONS, D. & MACDOUGALL, M. (2000) Enamelin maps to human chromosome 4q21 within the autosomal dominant *Amelogenesis imperfecta* locus, *European Journal of Oral Sciences*, vol. 108, no. 5, pp. 353-358.

DONNER, A. & ELIASZIW, M. (1987) 'Sample size requirements for reliability studies', *Statistics in Medicine*, vol. 6, pp. 441-448.

DOUGLAS, R.D. (1997) Precision of *in vivo* colorimetric assessments of teeth, *The Journal of Prosthetic Dentistry*, vol. 77, no. 5, pp. 464-470.

DOWKER, S.E.P., ELLIOTT, J.C., DAVIS, G.R. & WASSIF, H.S. (2003) Longitudinal Study of the Three-Dimensional Development of Subsurface Enamel Lesions during *in vitro* Demineralisation, *Caries Research*, vol. 37, no. 4, pp. 237-245.

DU, C., FALINI, G., FERMANI, S., ABBOTT, C. & MORADIAN-OLDAK, J. (2005) Supramolecular Assembly of Amelogenin Nanospheres into Birefringent Microribbons, *Science*, vol. 307, no. 5714, pp. 1450-1454.

DURET, F., BLOUIN, J.L. & DURET, B. (1988) CAD CAM in dentistry, *Journal of the American Dental Association*, vol. 117, pp. 715-720.

ELCOCK, C., LATH, D.L., LUTY, J.D., GALLAGHER, M.G., ABDELLATIF, A., BÄCKMAN, B. & BROOK, A.H. (2006) The new Enamel Defects Index: testing and expansion, *European Journal of Oral Sciences*, vol. 114, no. s1, pp. 35-38.

ELLIOTT, J.C., ANDERSON, P., GAO, X.J., WONG, F.S.L., DAVIS, G.R. & DOWKER, S.E.P. (1994) Application of scanning microradiography and X-ray microtomography to studies of bones and teeth, *Journal of X-Ray Science and Technology*, vol. 4, no. 2, pp. 102-117.

ELTON, V., COOPER, L., HIGHAM, S.M. & PENDER, N. (2009) Validation of enamel erosion *in vitro*, *Journal of Dentistry*, vol. 37, no. 5, pp. 336-341.

ENCISO, R., LEWIS, J.P., NEUMANN, U. & MAH, J. (2003) 3D tooth shape from radiographs using thin-plate splines, *MMVR11-NextMed: Health Horizon, The 11th Annual Medicine Meets Virtual Reality Conference*, pp. 62-64.

EVANS, A.R., HARPER, I.S. & SANSON, G.D. (2001) Confocal imaging, visualization and 3-D surface measurement of small mammalian teeth, *Journal of Microscopy*, vol. 204, no. 2, pp. 108-119.

FEARNE, J.M., ANDERSON, P. & DAVIS, G.R. (2004) 3D X-ray microscopic study of the extent of variations in enamel density in first permanent molars with idiopathic enamel hypomineralisation, *British Dental Journal*, vol. 94, pp. 634-638.

FEARNHEAD, R.W. (1960) Mineralization of Rat Enamel, *Nature*, vol. 188, no. 4749, pp. 509-510.

FEDERATION DENTAIRE INTERNATIONAL, (FDI) (1992) A review of the developmental defects of dental enamel index (DDE index), *International Dentistry Journal,* 42, 411-426.

FESTING, M. (1972) Mouse strain identification, *Nature*, vol. 238, pp. 351-352.

FINCHAM, A.G., BELCOURT, A.B., TERMINE, J.D., BUTLER, W.T. & COTHRAN, W.C. (1983) Amelogenins. Sequence homologies in enamel-matrix proteins from three mammalian species, *Biochemistry Journal*, vol. 211, pp. 149-154.

FINCHAM, A.G., MORADIAN-OLDAK, J., DIEKWISCH, T.G.H., LYARUU, D.M., WRIGHT, J.T., BRINGAS, P. & SLAVKIN, H.C. (1995) Evidence for Amelogenin Nanospheres as Functional Components of Secretory-Stage Enamel Matrix, *Journal of Structural Biology*, vol. 115, no. 1, pp. 50-59.

FINCHAM, A.G., MORADIAN-OLDAK. J. & SIMMER, J.P. (1999) The structural biology of the developing dental enamel matrix, *The Journal of Structural Biology*, vol. 126, no. 3, pp. 270-299.

FLEISCHMANNOVA, J., MATALOVA, E., TUCKER, A.S. & SHARPE, P.T. (2008) Mouse models of tooth abnormalities, *European Journal of Oral Sciences*, vol. 116, no. 1, pp. 1-10.

FLEISS, J.L. (1986a) The design and analysis of clinical experiments, in, *Reliability of measurement* , Wiley and Sons Inc, New York, pp. 1-32.

FLEISS, J.L. (1986b) 'Confidence intervals vs significance tests: quantitative interpretation ', *American Journal of Public Health*, vol. 76, no. 5, pp. 587-588.

FLEISS, J.L. & SHROUT, P.E. (1977) 'The effects of measurements on some multivariate procedures', *American Journal of Public Health*, vol. 67, pp. 1188-1191.

FONG, C.D., CEMY, R., HAMMARSTROM, L. & SLABY, I. (1998) Sequential expression of an amelin gene in mesenchymal and epithelial cells during odontogenesis in rats, *European Journal of Oral Sciences*, vol. 106, pp. 324-330.

FONG, C.D. & HAMMARSTROM, L. (2000) Expression of amelin and amelogenin in epithelial root sheath remnants of fully formed rat molars, *Oral Surgery, Oral Medicine, Oral Pathology, Oral Radiology, and Endodontology*, vol. 90, pp. 218-223.

FROMMER, J. (1964) Prenatal development of the mandibular joint in mice, *The Anatomical Record*, vol. 150, pp. 449-461.

FRYE, M.S. & HEDGES, S.B. (1995) Monophyly of the order Rodentia inferred from mitochondrial DNA sequences of the genes for 12S rRNA, 16S rRNA, and tRNA-valine, *Molecular Biology and Evolution*, vol. 12, no. 1, pp. 168-176.

FUCHS, T.O.J., KACHELRIESS, M. & KALENDER, W.A. (2000) System performance of multislice spiral computed tomography, *IEEE Engineering in Medicine and Biology*, vol. 19, no. 5, pp. 63-70.

FUKUMOTO, S., KIBA, T., HALL, B., LEHARA, N., NAKAMURA, T., LONGENECKER, G., KREBSBACH, P.H., NANCI, A., KULKARNI, A.B. & YAMADA, Y. (2004) Ameloblastin is a cell adhesion molecule required for maintaining the differentiation state of ameloblasts, *Journal of Cell Biology*, vol. 167, pp. 973-983.

FUKUMOTO, S. & YAMADA, Y. (2005) Review: Extracellular Matrix Regulates Tooth Morphogenesis, *Connective Tissue Research*, vol. 46, no. 4, pp. 220 - 226.

GANT, D.G., KAPPELMAN, J. & KETCHAM, R.A. (2001) Hominid enamel and dentin volumes by means of HRXCT 3D reconstuction, in E. Zadzinska (ed.), *Current Trends in Dental Morphology Research*, University of Lodz Press, Poland, pp. 483-499.

GARCÍA-GODOY, F., VILLALTA, P., BARTIZEK, R.D., BARKER, M.L. & BIESBROCK, A.R. (2004) Tooth whitening effects of an experimental whitening toothbrush relative to an 8.7% hydrogen peroxide paint-on gel control., *American Journal of Dentistry*, vol. 17 no. Spec pp. 25A-30A.

GAUNT, W.A. (1955) The development of the molar pattern of the mouse, *Mus musculus*, *ACTA Anatomica*, no. 24, pp. 249-268.

GAUNT, W.A. (1956) The development of enamel and dentine on the molars of the mouse, with an account of the enamel-free areas, *ACTA Anatomica (Basel)*, vol. 28, no. (1-2), pp. 111-134.

GAUNT, W.A. (1964) The development of the teeth and jaws of the albino mouse, *ACTA Anatomica*, vol. 57, pp. 115-151.
GIBSON, C.W., KULKARNI, A.B. & WRIGHT, J.T. (2005) The Use of Animal Models to Explore Amelogenin Variants in *Amelogenesis imperfecta*, *Cells Tissues Organs*, vol. 181, pp. 196-201.

GIBSON, C.W., LI, Y., DALY, B., SUGGS, C., YUAN, Z., FONG, H., SIMMONS, D., ARAGON, M., KULKARNI, A.B. & WRIGHT, J.T. (2009) The Leucine-Rich Amelogenin Peptide Alters the Amelogenin Null Enamel Phenotype, *Cells Tissues Organs*, vol. 189, no. 1-4, pp. 169-174.

GIBSON, C.W., YUAN, Z.A., HALL, B., LONGENECKER, G., CHEN, E., THYAGARAJAN, T.T., SREENATH, T., WRIGHT, J.T., DECKER, S., PIDDINGTON, R., HARRISON, G. & KULKARNI, A.B. (2001) Amelogenin-deficient mice display an *Amelogenesis imperfecta* phenotype, *Journal of Biological Chemistry*, vol. 276, no. 34, pp. 31871-31875.

GIBSON, C.W., YUAN, Z.A., LI, Y., DALY B, SUGGS, C., ARAGON, M.A., ALAWI, F., KULKARNI, A.B. & WRIGHT, J.T. (2007) Transgenic mice that express normal and mutated amelogenins, *Journal of Dental Research*, vol. 86, no. 4, pp. 331-335.

GOODKIND, R.J. & SCHWABACHER, W.B. (1987) Use of a fiber-optic colorimeter for *in vivo* color measurements of 2830 anterior teeth, *The Journal of Prosthetic Dentistry*, vol. 58, no. 5, pp. 535-542.

GOSHTASBY, A.A., NAMBALA, S., DERIJK, S.G. & CAMPBELL, S.D. (1997) A system for digital reconstruction of gypsum dental casts, *IEEE Transactions on Medical Imaging*, vol. 16, no. 5, pp. 664-674.

GREEN, E.C.J., GKOUTOS, G.V., LAD, H.V., BLAKE, A., WEEKES, J. & HANCOCK, J.M. (2005) EMPReSS: European Mouse Phenotyping Resource for Standardized Screens, *Bioinformatics*, vol. 21, no. 12, pp. 2930-2931. (http://www.empress.har.mrc.ac.uk/)

GREENE, S.R., YUAN, Z.A., WRIGHT, J.T., AMJAD, H., ABRAMS, W.R., BUCHANAN, J.A., TRACHTENBERG, D.I. & GIBSON, C.W. (2002) A new frameshift mutation encoding a truncated amelogenin leads to X-linked *Amelogenesis imperfecta*, *Archives of Oral Biology*, vol. 47, no. 3, pp. 211-217.

GRUENBAUM-COHEN, Y., TUCKER, A.S., HAZE, A., SHILO, D., TAYLOR, A.L., SHAY, B., SHARPE, P.T., MITSIADIS, T.A., ORNOY, A., BLUMENFELD, A. & DEUTSCH, D. (2008) Amelogenin in cranio-facial development: the tooth as a model to study the role of amelogenin during embryogenesis, *Journal of Experimental Zoology Part B: Molecular and Developmental Evolution*, vol. 310B, pp. 1-13.

GRÜNBERG, H. (1951) The genetics of a tooth defect in the mouse, *Proceedings of the Royal Society of London*, vol. 138, no. 892 pp. 437-451.

GRÜNBERG, H. (1963) *The Pathology of Development: A Study of Inherited Skeletal Disorders in Animals*, Blackwell Scientific, Oxford.

GRÜNBERG, H. (1965) Genes and genotypes affecting the teeth of the mouse, *Journal of Embryology & Experimental Morphology*, vol. 14, pp. 137-159.

GUAN, Y.H., LATH, D.L., LILLEY, T.H., WILLMOT, D.R., MARLOW, I. & BROOK, A.H. (2005) The measurement of tooth whiteness by image analysis and spectrophotometry: a comparison, *Journal of Oral Rehabilitation*, vol. 32, no. 1, pp. 7-15.

GUÉNET, J.-L. & BONHOMME, F. (2004) Origin of the Laboratory Mouse and Related Subspecies, in J.H. Professor Hans & B. Professor Gillian (eds), *The Laboratory Mouse*, Academic Press, London, pp. 1-11.

GUILD, J. (1931) The colorimetric properties of the spectrum, *Philosophical Transactions of the Royal Society of London*, vol. 230, pp. 149-187.

GUTIERREZ, S.J., CHAVES, M., TORRES, D.M. & BRICEÑO, I. (2007) Identification of a novel mutation in the enamelin gene in a family with autosomal-dominant *Amelogenesis imperfecta*, *Archives of Oral Biology*, vol. 52, no. 5, pp. 503-506.

HAJEER, M.Y., MILLETT, D.T., AYOUB, A.F. & SIEBERT, J.P. (2004) Current Products and Practices: Applications of 3D imaging in orthodontics, *Journal of Orthodontics*, vol. 31, pp. 154-162

HALAZONETIS, D.J. (2001) Acquisition of 3-dimensional shapes from images, *American Journal of Orthodontics and Dentofacial Orthopedics*, vol. 119, pp. 556-560.

HALL, B.K. (1991) Cellular interactions during cartilage and bone development, *Journal of Craniofacial Genetics and Developmental Biology*, no. 11, pp. 238-250.

HALSE, A. (1972) Location and first appearance of rat incisor pigmentation, *Scandinavian Journal of Dental Research*, vol. 80, pp. 428-433.

HAMMAD, I.A. (2003) Intra-rater repeatability of shade selections with two shade guides, *The Journal of Prosthetic Dentistry*, vol. 89, no. 1, pp. 50-53.

HAMMARSTROM, L., HEIJL, L. & GESTRELIUS, S. (1997) Periodontal regeneration in a buccal dehiscence model in monkeys after application of enamel matrix proteins, *Journal of Clinical Periodontology*, vol. 24, pp. 669-677.

HARADA, H., KETTUNEN, P., JUNG, H.S., MUSTONEN, T., WANG, Y.A. & THESLEFF, I. (1999) Localization of putative stem cells in dental epithelium and their association with Notch and FGF signalling, *Journal of Cell Biol.*, vol. 147, pp. 105-120.

HARRIS, E.F. & BAILIT, H.L. (1988) A principal components analysis of human odontometrics, *American Journal of Physical Anthropology*, vol. 75, no. 1, pp. 87 - 99.

HART, P.S., ALDRED, M.J., CRAWFORD, P.J.M., WRIGHT, N.J., HART T.C. & WRIGHT, J.T. (2002b) *Amelogenesis imperfecta* phenotype-genotype correlations with two amelogenin gene mutations, *Archives of Oral Biology*, vol. 47, no. 4, pp. 261-265.

HART, P.S., HART, T.C., MICHALEC, M.D., RYU, O.H., SIMMONS, D., HONG, S. & WRIGHT, J.T. (2004) Mutation in kallikrein 4 causes autosomal recessive hypomaturation *Amelogenesis imperfecta*, *Journal of Medical Genetics*, vol. 41, no. 7, pp. 545-549.

HART, P.S., HART, T.C., SIMMER, J.P. & WRIGHT, J.T. (2002a) A nomenclature for X-linked *Amelogenesis imperfecta*, *Archives of Oral Biology*, vol. 47, no. 4, pp. 255-260.

HART, P.S., MICHALEC, M.D., SEOW, W.K., HART, T.C. & WRIGHT, J.T. (2003a) Identification of the enamelin (g.8344delG) mutation in a new kindred and presentation of a standardized ENAM nomenclature, *Archives of Oral Biology*, vol. 48, pp. 589-596.

HART, P.S., HART, T., GIBSON, C.W. & WRIGHT, J.T. (2000) Mutational analysis of X-linked *Amelogenesis imperfecta* in multiple families, *Archives of Oral Biology*, vol. 45, pp. 79-86.

HART, T.C., HART, P.S., GORRY, M.C., MICHALEC, M.D., RYU, O.H., UYGUR, C., OZDEMIR, D., FIRATLI, S., AREN, G. & FIRATLI, E. (2003b) Novel ENAM mutation responsible for autosomal recessive *Amelogenesis imperfecta* and localised enamel defects, *Journal of Medical Genetics*, vol. 40, no. 12, pp. 900-906.

HATAKEYAMA, J., FUKUMOTO, S., NAKAMURA, T., HARUYAMA, N., SUZUKI, S., HATAKEYAMA, Y., SHUM, L., GIBSON, C.W., YAMADA, Y. & KULKARNI, A.B. (2009) Synergistic Roles of Amelogenin and Ameloblastin, *Journal of Dental Research*, vol. 88, no. 4, pp. 318-322.

HAY, M.F. (1961) The development *in vivo* and *in vitro* of the lower incisor and molars of the mouse, *Archives of Oral Biology*, vol. 3, p. 86-109.

HAYASHI, K., UECHI, J. & MIZOGUCHI, I. (2003) Three-Dimensional Analysis of Dental Casts Based on a Newly Defined Palatal Reference Plane, *The Angle Orthodontist*, vol. 73, no. 5, pp. 539-544.

HAZE, A., TAYLOR, A.L., BLUMENFELD, A., ROSENFELD, E., LEISER, Y., DAFNI, L., SHAY, B., GRUENBAUM-COHEN, Y., FERMON, E., HAEGEWALD, S., BERNIMOULIN, J.-P. & DEUTSCH, D. (2007) Amelogenin expression in long bone and cartilage cells and in bone marrow progenitor cells, *The Anatomical Record*, vol. 290, pp. 455-460.

HEARD, E. & DISTECHE, C.M. (2006) Dosage compensation in mammals: fine-tuning the expression of the X chromosome, *Genes and Development*, vol. 20, no. 14, pp. 1848-1867.

HIGHAM, S.M., PENDER, N., DE JONG, E.D.J. & SMITH, P.W. (2009) Application of biophysical technologies in dental research, *Journal of Applied Physics*, vol. 105, no. 10, pp. 102048-102048.

HILLER, C.R., ROBINSON, C. & WEATHERELL, J.A. (1975) Variations in the composition of developing rat incisor enamel, *Calcified Tissue Research*, vol. 18, no. 1, pp. 1-12.

HILLSON, S., FITZGERALD, C. & FLINN, H. (2005) Alternative dental measurements: Proposals and relationships with other measurements, *American Journal of Physical Anthropology*, vol. 126, no. 4, pp. 413-426.

HIROGAKI, Y., SOHUMURA, T., SATOH, H., TAKAHASHI, J. & TAKADA, K. (2001) Complete 3-D reconstruction of dental cast shape using perceptual grouping, *IEEE Transactions on Medical Imaging*, vol. 20, pp. 1093-1101.

HIXON, E.H. & OLDFATHER, R.E. (1958) Estimation of the sizes of unerupted cuspid and bicuspid teeth, *The Angle Orthodontist*, vol. 28, no. 4, pp. 236-240.

HO, C.T. & FREER, T., J. (1999) A computerized tooth-width analysis, *Journal of Clinical Orthodontics*, no. 33, pp. 498-503.

HOLLAND, N.D. & CHEN, J. (2001) Origin and early evolution of the vertebrates: New insights from advances in molecular biology, anatomy, and palaeontology, *BioEssays*, vol. 23, no. 2, pp. 142-151.

HORROCKS, L.R., BROOK, A.H., ALVESALO, L. & SMITH, R.N. (2009) A Three-Dimensional Comparison of the Modifying Effects of Familial Genetic Contribution in Turner Syndrome, in T. Koppe, G. Meyer & K.W. Alt (eds), *Comparative Dental Morphology. Frontiers of Oral Biology*, vol. 13, Karger, Basel, pp. 148-152.

HOUSTON, W.J.B. (1983) The analysis of errors in orthodontic measurements, *American Journal of Orthodontics*, vol. 83, pp. 382-390.

HU, B., NADIRI, A., KUCHLER-BOPP, S., PERRIN-SCHMITT, F., PETERS, H. & LESOT, H. (2006) Tissue Engineering of Tooth Crown, Root, and Periodontium, *Tissue Engineering*, vol. 12, no. 8, pp. 2069-2075.

HU, J.C.C., HART, T.C., DUPONT, B.R., CHEN, J.J., SUN, X., QIAN, Q., ZHANG, C.H., JIANG, H., MATTERN, V.L. & WRIGHT, J.T. (2000) Cloning human enamelin cDNA, chromosomal localization, and analysis of expression during tooth development, *Journal of Dental Research*, vol. 79, no. 912-919.

HU, J.C.C., SIMMER, J.P., BARTLETT, J.D., NANCI, A., QIAN, Q., ZHANG, C., RYU, O.H., XUE, J., FUKAE, M., UCHIDA, T. & MACDOUGAL, M. (1998) Cloning and characterization of mouse enamelin, *Connective Tissue Research*, vol. 39, pp. 47-61.

HU, C.C., RYU, O.H., QIAN, Q., ZHANG, C.H. & SIMMER, J.P. (1997) Cloning, Characterization, and Heterologous Expression of Exon-4-containing Amelogenin mRNAs, *Journal of Dental Research*, vol. 76, no. 2, pp. 641-647.

HU, J.C.C. & YAMAKOSHI, F. (2003) Enamelin and autosomal-dominant *Amelogenesis imperfecta*, *Critical Reviews in Oral Biology & Medicine.*, vol. 14, pp. 387-398.

HU, J.C.C. & SIMMER, J.P. (2007) Developmental biology and genetics of dental malformations, *Orthodontics and Craniofacial Research*, vol. 10, no. 2, pp. 45-52.

HU, J.C.C., CHUN, Y.-H.P., HAZZAZZI, T.A. & SIMMER, J.P. (2007) Enamel Formation and *Amelogenesis imperfecta*, *Cells Tissues Organs*, vol. 186, pp. 78-85.

HU, J.C.C., HU, Y., SMITH, C.E., MCKEE, M.D., WRIGHT, J.T., YAMAKOSHI, Y., PAPAGERAKIS, P., HUNTER, G.K., FENG, J.Q., YAMAKOSHI, F. & SIMMER, J.P. (2008) Enamel Defects and Ameloblast-specific Expression in Enam Knock-out/lacZ Knock-in Mice, *Journal of Biological Chemistry*, vol. 283, no. 16, pp. 10858-10871.

HU, J.C.C., SUN, X., ZHANG, C. & SIMMER, J.P. (2001b) A comparison of enamelin and amelogenin expression in developing mouse molars, *European Journal of Oral Sciences*, vol. 109, no. 2, pp. 125-132.

HU, J.C.C., SUN, X., ZHANG, C., LIU, S., BARTLETT, J.D. & SIMMER, J.P. (2002) Enamelysin and kallikrein-4 mRNA expression in developing mouse molars, *European Journal of Oral Sciences*, vol. 110, no. 4, pp. 307-315.

HU, J.C.C., ZHANG, C.H., YANG, Y., KARRMAN-MARDH, C., FORSMAN-SEMB, K. & SIMMER, J.P. (2001a) Cloning and Characterization of the Mouse and Human Enamelin Genes, *Journal of Dental Research*, vol. 80, no. 3, pp. 898-902.

HUNTER, W.S. & PRIEST, W.R. (1960) Errors and discrepancies in measurement of tooth size, *Journal of Dental Research*, vol. 39, pp. 405-414.

HUYNH, K.D. & LEE, J.T. (2005) X-chromosome inactivation: a hypothesis linking ontogeny and phylogeny, *Nature Reviews Genetics*, vol. 6, no. 5, pp. 410-418.

INTERNATIONAL STANDARD ORGANISATION, (ISO) *Rules and Procedures for Assessment of Surface Texture*, no. 4288-1996.

IWASAKI, K., BAJENOVA, E., SOMOGYI-GANSS, E., MILLER, M., NGUYEN, V., NOURKEYHANI, H., GAO, Y., WENDEL, M. & GANSS, B. (2005) Amelotin-a novel secreted, ameloblast-specific protein, *Journal of Dental Research*, vol. 84, pp. 1127-1132.

IWATA, T., YAMAKOSHI, Y., HU, J.C.C., ISHIKAWA, I., BARTLETT, J.D., KREBSBACH, P.H. & SIMMER, J.P. (2007) Processing of Ameloblastin by MMP-20, *Journal of Dental Research*, vol. 86, no. 2, pp. 153-157.

JARAD, F.D., RUSSELL, M.D. & MOSS, B.W. (2005) The use of digital imaging for colour matching and communication in restorative dentistry, *British Dental Journal*, vol. 199, pp. 43-49.

JERNVALL, J., KERÄNEN, S.V.E. & THESLEFF, I. (2000) Evolutionary modification of development in mammalian teeth: Quantifying gene expression patterns and topography, *Proceedings of the National Academy of Sciences*, vol. 97, no. 26, pp. 14444-14448.

JERNVALL, J., KETTUNEN, P., KARAVANOVA, I., MARTIN, L.B. & THESLEFF, I. (1994) Evidence for the role of the enamel knot as a control centre in mammalian tooth cusp formation: non-dividing cells express growth stimulating Fgf-4 gene, *International Journal of Developmental Biology*, vol. 38, pp. 463- 469.

JERNVALL, J. & SELAENNE, L. (1999) Laser confocal microscopy and geographic information systems in the study of dental morphology, *Palaeontologia Electronica*, vol. 2, p. 18.

JERNVALL, J. & THESLEFF, I. (2000a) Reiterative signaling and patterning during mammalian tooth morphogenesis, *Mechanisms of Development*, vol. 92, no. 1, pp. 19-29.

JERNVALL, J. & THESLEFF, I. (2000b) Return of lost structure in the developmental control of tooth shape, in M.F. Teaford, M.M. Smith & M.W.J. Ferguson (eds), *Development, Function and Evolution of Teeth* Cambridge University Press, Cambridge, pp. 13-21.

JOFFE, L. (2004) Current Products and Practices OrthoCAD™: digital models for a digital era, *Journal of Orthodontics*, vol. 31, no. 4, pp. 344-347.

JOINER, A. (2004) Tooth colour: a review of the literature, *Journal of Dentistry*, vol. 32, no. Supplement 1, pp. 3-12.

JOINER, A., HOPKINSON, I., DENG, Y. & WESTLAND, S. (2008) A review of tooth colour and whiteness, *Journal of Dentistry*, vol. 36, no. Supplement 1, pp. 2-7.

KANAZAWA, E., SEKIKAWA, M. & OZAKI, T. (1984) Three-dimensional measurements of the occlusal surfaces of the upper molars in a Dutch population, *Journal of Dental Research*, vol. 63, pp. 1298-1301.

KARRMAN, C., BACKMAN, B., DIXON, M., HOLMGREN, G. & FORSMAN, K. (1997) Mapping of the locus for autosomal dominant *Amelogenesis imperfecta* (AIH2) to a 4-Mb YAC contig on chromosome 4qll-q21, *Genomics*, vol. 39, pp. 164-170.

KARRMAN, C., BACKMAN, B., HOLMGREN, G. & FORSMAN, K. (1996) Genetic heterogeneity of autosomal dominant *Amelogenesis imperfecta* demonstrated by its exclusion from the AIH2 region on human chromosome 4Q, *Archives of Oral Biology*, vol. 41, pp. 893-900.

KAWASAKI, K. & WEISS, K.M. (2003) Mineralized tissue and vertebrate evolution: the secretory calcium-binding phosphoprotein gene cluster, *Proceedings of the National Academy of Sciences*, vol. 100, no. 7, pp. 4060-4065.

KEISER, G.A. (1990) *Human adult odontometrics*, Cambridge University Press.

KELLER, U. & HIBST, R. (1993) Lasers in dentistry: clinical application today and tomorrow, *Dental Applications of Lasers*, vol. 2080, SPIE, Budapest, Hungary, pp. 2-9.

KHALAF, K., ELCOCK, C., SMITH, R.N. & BROOK, A.H. (2005b) Fluctuating dental asymmetry of multiple crown variables measured by image analysis system, *Archives of Oral Biology*, vol. 50, pp. 249-253.

KHALAF, K., ROBINSON, D.L., ELCOCK, C., SMITH, R.N. & BROOK, A.H. (2001) Determination and comparison of size variables of upper central incisors in patients with supernumerary teeth, in A.H. Brook (ed.), *Dental Morphology*, Sheffield University Academic Press UK pp. 343-350.

KHALAF, K., ROBINSON, D.L., ELCOCK, C., SMITH, R.N. & BROOK, A.H. (2005a) Tooth size in patients with supernumerary teeth and a control group measured by image analysis system, *Archives of Oral Biology*, vol. 50, no. 2, pp. 243-248.

KHALAF, K., SMITH, R.N., ELCOCK, C. & BROOK, A.H. (2009) Multiple crown size variables of the upper incisors in patients with supernumerary teeth compared with controls, *Archives of Oral Biology*, vol. 54, pp. S71-S78.

KHAMBAY, B.S., NEBEL, J.C., BOWMAN, J., AYOUB, A.F., WALKER, F. & HADLEY, D. (2002) A pilot study: 3D stereo photogrammetric image superimposition on to 3D CT scan images — the future of orthognathic surgery, *International Journal of Adult Orthodontics and Orthognathic Surgery*, vol. 17, pp. 244-252.

KHURANA, R., TREDWIN, C.J., WEISBLOOM, M. & MOLES, D.R. (2007) A clinical evaluation of the individual repeatability of three commercially available colour measuring devices, *British Dental Journal*, vol. 203, no. 12, pp. 675 -680

KIDA, M., ARIGA, T., SHIRAKAWA, T., OGUCHI, H. & SAKIYAMA, Y. (2002) Autosomal-dominant hypoplastic form of *Amelogenesis imperfecta* caused by an enamelin gene mutation at the exon-intron boundary, *Journal of Dental Research*, vol. 81, pp. 738-742.

KIDA, M., SAKIYAMA, Y., MATSUDA, A., TAKABAYASHI, S., OCHI, H., SEKIGUCHI, H., MINAMITAKE, S. & ARIGA, T. (2007) A Novel Missense Mutation (p.P52R) in Amelogenin Gene Causing X-linked *Amelogenesis imperfecta*, *Journal of Dental Research*, vol. 86, pp. 69-72.

KIM, I., PAIK, K.-S. & LEE, S.-P. (2007) Quantitative evaluation of the accuracy of micro-computed tomography in tooth measurement, *Clinical Anatomy*, vol. 20, no. 1, pp. 27-34.

KIM, J.W., SEYMEN, F., LIN, B.P., KIZILTAN, B., GENCAY, K., SIMMER, J.P. & HU, J.C. (2005b) ENAM mutations in autosomal-dominant *Amelogenesis imperfecta*, *Journal of Dental Research*, vol. 84, pp. 278-282.

KIM, J.W., SIMMER, J.P., HU, Y.Y., LIN, B.P.L., BOYD, C., WRIGHT, J.T., YAMADA, C.J.M., RAYES, S.K., FEIGAL, R.J. & HU, J.C.C. (2004) Amelogenin p.M1T and p.W4S Mutations Underlying Hypoplastic X-linked *Amelogenesis imperfecta*, *Journal of Dental Research*, vol. 83, no. 5, pp. 378-383.

KIM, J.W., SIMMER, J.P., LIN, B.P., SEYMEN, F., BARTLETT, J.D. & HU, J.C. (2006b) Mutational analysis of candidate genes in 24 *Amelogenesis imperfecta* families, *European Journal of Oral Science*, vol. 114 no. Suppl 1, pp. 3-12.

KIM, J.-W., LEE, S.-K., LEE, Z.H., PARK, J.-C., LEE, K.-E., LEE, M.-H., PARK, J.-T., SEO, B.-M., HU, J.C.C. & SIMMER, J.P. (2008) FAM83H Mutations in Families with Autosomal-Dominant Hypocalcified *Amelogenesis imperfecta*, *The American Journal of Human Genetics*, vol. 82, no. 2, pp. 489-494.

KIM, J.-W., SIMMER, J.P., HART, T.C., HART, P.S., RAMASWAMI, M.D., BARTLETT, J.D. & HU, J.C.-C. (2005a) MMP-20 mutation in autosomal recessive pigmented hypomaturation *Amelogenesis imperfecta*, *Journal of Medical Genetics*, vol. 42, no. 3, pp. 271-275.

KIM, J.Y., CHA, Y.G., CHO, S.W., KIM, E.J., LEE, M.J., LEE, J.M., CAI, J., OHSHIMA, H. & JUNG, H.S. (2006a) Inhibition of Apoptosis in Early Tooth Development Alters Tooth Shape and Size, *Journal of Dental Research*, vol. 85, pp. 530-535

KIRKHAM, J., BROOKES, S.J., SHORE, R.C., BONASS, W.A., SMITH, D.A., WALLWORK, M.L. & ROBINSON, C. (1998) Atomic force microscopy studies of crystal surface topology during enamel development., *Connect Tissue Research*, vol. 38(1-4), no. 91-100, pp. 139-145.

KIRKHAM, J., BROOKES, S.J., SHORE, R.C., WOOD, S.R., SMITH, D.A., ZHANG, J., CHEN, H. & ROBINSON, C. (2002) Physico-chemical properties of crystal surfaces in matrix-mineral interactions during mammalian biomineralisation, *Current Opinion in Colloid & Interface Science*, vol. 7, no. 1-2, pp. 124-132.

KIRKHAM, J., ZHANG, J., BROOKES, S.J., SHORE, R.C., WOOD, S.R., SMITH, D.A., WALLWORK, M.L., RYU, O.H. & ROBINSON, C. (2000) Evidence for charge domains on developing enamel crystal surfaces, *Journal of Dental Research*, vol. 79, no. 12, pp. 1943-1947.

KLINGENBERG, C.P. (2002) Morphometrics and the role of the phenotype in studies of the evolution of developmental mechanisms, *Gene*, vol. 287, no. 1-2, pp. 3-10.

KLINGENBERG, C.P., LEAMY, L.J. & CHEVERUD, J.M. (2004) Integration and Modularity of Quantitative Trait Locus Effects on Geometric Shape in the Mouse Mandible, *Genetics*, vol. 166, no. 4, pp. 1909-1921.

KLINGENBERG, C.P., LEAMY, L.J., ROUTMAN, E.J. & CHEVERUD, J.M. (2001) Genetic Architecture of Mandible Shape in Mice: Effects of Quantitative Trait Loci Analyzed by Geometric Morphometrics, *Genetics*, vol. 157, no. 2, pp. 785-802.

KONDO, T., ONG, S.H. & FOONG, K.W.C. (2004) Tooth segmentation of dental study models using range images, *IEEE Transactions on Medical Imaging*, vol. 23, no. 3, pp. 350-362.

KORKHAUS, G. (1930) A new orthodontic Symmetrograph, *International Journal of Orthodontics*, vol. 16, pp. 665-668.

KRINKE, G.J. (2004) Normative Histology of Organs, in H.J. Hedrich & G. Bullock (eds), *The Laboratory Mouse*, Academic Press, London, pp. 133-166.

KURODA, T., MOTOHASHI, N., TOMINAGA, R. & IWATA, K. (1996) Three-dimensional cast analysing system using laser scanning, *American Journal of Orthodontics and Dentofacial Orthoptics*, vol. 110, pp. 365-369.

LAGERSTRÖM-FERMÉR, M., DAHL, N., NAKAHORI, Y., NAKAGOME, Y., BÄCKMAN, B., LANDEGREN, U. & PETTERSSON, U. (1991) A deletion in the amelogenin gene (AMG) causes X-linked *Amelogenesis imperfecta* (AIH1), *Genomics*, vol. 10, no. 4, pp. 971-975.

LAGERSTRÖM-FERMÉR, M. & LANDEGREN, U. (1995) Understanding Enamel Formation from Mutations Causing X-Linked *Amelogenesis imperfecta*, *Connective Tissue Research*, vol. 32, no. 1-4, pp. 241-246.

LAGERSTRÖM-FERMÉR, M., NILSSON, M., BÄCKMAN, B., SALIDO, E., SHAPIRO, L., PETTERSSON, U. & LANDEGREN, U. (1995) Amelogenin signal peptide mutation: correlation between mutations in the amelogenin gene (AMGX) and manifestations of X-linked *Amelogenesis imperfecta*, *Genomics*, vol. 26, no. 1, pp. 159-162.

LATH, D.L., JOHNSON, C., SMITH, R.N. & BROOK, A.H. (2006) Measurement of stain removal *in vitro*: a comparison of two instrumental methods, *International Journal of Dental Hygiene*, vol. 4, no. 3, pp. 129-132.

LATH, D.L., SMITH, R.N., GUAN, Y.H., KARMO, M. & BROOK, A.H. (2007b) Measurement of stain on extracted teeth using spectrophotometry and digital image analysis, *International Journal of Dental Hygiene*, vol. 5, no. 3, pp. 174-179.

LATH, D.L., WILDGOOSE, D.G., GUAN, Y.H., LILLEY, T.H., SMITH, R.N. & BROOK, A.H. (2007a) A digital image analysis system for the assessment of tooth whiteness compared to visual shade matching, *Journal of Clinical Dentistry*, vol. 18 no. 1, pp. 17-20.

LAU, E.C., MOHANDAS, T.K., SHAPIRO, L.J., SLAVKIN, H.C. & SNEAD, M.L. (1989) Human and mouse amelogenin gene loci are on the sex chromosomes, *Genomics*, vol. 4, no. 2, pp. 162-168.

LAVELLE, C.L.B. (1972) Maxillary and mandibular tooth size in different racial groups and different occlusal categories, *American Journal of Orthodontics*, vol. 61, pp. 29-37.

LAVELLE, C.L.B. (1983) Study of mandibular shape in the mouse, *ACTA Anatomica*, vol. 314-320, no. 117 p. 4.

LAZZARI, V., TAFFOREAU, P., AGUILAR, J.-P. & MICHAUX, J. (2009) Topographic maps applied to comparative molar morphology: the case of murine and cricetine dental plans (Rodentia, Muroidea), *Paleobiology*, vol. 34, no. 1, pp. 46-64.

LEBLOND, C.P. & WARSHAWSKY, H. (1979) Dynamics of enamel formation in the rat incisor tooth, *Journal of Dental Research,* vol. 58(B), pp. 950-975.

LEE, S.J. & CHANG, D.Y. (2005) Laser scanning probe with multiple detectors used for sculptured surface digitization in reverse engineering, *Journal of Physics*, vol. 13, pp. 155-158.

LELE, S. & RICHTSMEIER, J.T. (1991) Euclidean distance matrix analysis: a coordinate-free approach for comparing biological shapes using landmark data, *American Journal of Physical Anthropology*, vol. 86, no. 3, pp. 415-427.

LENCH, N.J., BROOK, A.H. & WINTER, G.B. (1994) SSCP detection of a nonsense mutation in exon 5 of the amelogenin gene (AMGX) causing X-linked *Amelogenesis imperfecta* (AIH1), *Human Molecular Genetics*, vol. 3, pp. 827-828.

LENCH, N.J. & WINTER, G.B. (1995) Characterisation of molecular defects in X-linked *Amelogenesis imperfecta* (AIH1), *Human Mutation*, vol. 5, pp. 251-259.

LESOT, H. & BROOK, A.H. (2009) Epithelial histogenesis during tooth development, *Archives of Oral Biology*, vol. 54, pp. S25-S33.

LESOT, H., PETERKOVA R, VONESCH J-L, VIRIOT L, TURECKOVA J, PETERKA M & RUCH, J.V. (1998) Early stages of tooth morphogenesis in mouse analyzed by 3D reconstructions, *European Journal of Oral Sciences*, no. 106, pp. 64-70.

LESOT, H., VONESCH, J.L., PETERKA, M., TURECKOVA, J., PETERKAKOVA, R. & RUCH, J.V. (1996) Mouse molar morphogenes revisited by three dimensional reconstruction: (II). Spatial distribution 01 mitoses and apoptosis in cap to bell staged first and second upper molar teeth. , *International Journal of Developmental Biology*, vol. 40, pp. 1017-1031.

LEZOT, F., DESCROIX, V., MESBAH, M., HOTTON, D., BLIN, C., PAPAGERAKIS, P., MAURO, N., KATO, S., MACDOUGALL, M., SHARPE, P. & BERDAL, A. (2002) Cross-Talk Between Msx/Dlx Homeobox Genes and Vitamin D During Tooth Mineralization, *Connective Tissue Research*, vol. 43, no. 2, pp. 509 - 514.

LEZOT, F., THOMAS, B., HOTTON, D., FOREST, N., ORESTES-CARDOSO, S., ROBERT, B., SHARPE, P. & BERDAL, A. (2000) Biomineralization, Life-Time of Odontogenic Cells and Differential Expression of the Two Homeobox Genes MSX-1 and DLX-2 in Transgenic Mice, *Journal of Bone and Mineral Research*, vol. 15, no. 3, pp. 430-441.

LEZOT, L., THOMAS, B., GREENE, S.R., HOTTON, D., YUAN, Z.-A., CASTANEDA, B., BOLAÑOS, A., DEPEW, M., SHARPE, P. & GIBSON, C., W., BERDAL, A. (2008) Physiological implications of DLX homeoproteins in enamel formation, *Journal of Cellular Physiology*, vol. 216, no. 3, pp. 688-697.

LI, W., GIBSON, C.W., ABRAMS, W.R., ANDREWS, D.W. & DENBESTEN, P.K. (2001) Reduced hydrolysis of amelogenin may result in X-linked *Amelogenesis imperfecta*, *Matrix Biology*, vol. 19, no. 8, pp. 755-760.

LI, W., MATHEWS, C., GAO, C. & DENBESTEN, P.K. (1998) Identification of two additional exons at the 3' end of the amelogenin gene, *Archives of Oral Biology*, vol. 43, no. 6, pp. 497-504.

LI, Y., YUAN, Z.-A., ARAGON, M.A., KULKARNI, A.B. & GIBSON, C.W. (2006) Comparison of body weight and gene expression in amelogenin null and wild-type mice, *European Journal of Oral Sciences*, vol. 114, no. s1, pp. 190-193.

LIAO, B.-Y. & ZHANG, J. (2008) Null mutations in human and mouse orthologs frequently result in different phenotypes, *Proceedings of the National Academy of Sciences`*, vol. 105, pp. 6987-6992.

LINDE, A. & GOLDBERG, M. (1993) Dentinogenesis, *Critical Reviews in Oral Biology & Medicine*, vol. 4, no. 5, pp. 679-728.

LINE, S.R.P. (2001) Molecular morphogenetic fields in the development of human dentition, *Journal of Theoretical Biology*, vol. 211, no. 1, pp. 67-75.

LINE, S.R.P. (2003) Variation of tooth number in mammalian dentition: connecting genetics, development, and evolution, *Evolution and Development*, vol. 5, no. 3, pp. 295-304.

LOEW, F.M. & COHEN, B.J. (2002) Laboratory Animal Medicine Historical Perspectives, in J.G. Fox, L.C. Anderson, F.M. Loew & F.W. Quimby (eds), *Laboratory Animal Medicine (Electronic Book)*, Academic Press, Amsterdam; Oxford.

LU, Y., PAPAGERAKIS, P., YAMAKOSHI, Y., HU, J.C.C., BARTLETT, J.D. & SIMMER, J.P. (2008) Functions of KLK4 and MMP-20 in dental enamel formation, *Biological Chemistry*, vol. 389, no. 6, pp. 695-700.

LUCKETT, W.P. & HARTENBERGER, J.L. (eds) (1985) *Evolutionary Relationships among Rodents. A Multidisciplinary Analysis*, Plenum, New York.

LUMSDEN, A.G.S. (1988) Spatial organisation of the epithelium and the role of neural crest cells in the initiation of the mammalian tooth germ, *Development*, vol. 103, pp. 155-169.
LUTHER, P. G. (1949) Enzymatic maceration of skeletons, *Proceedings of the Linnean Society*, 161, 146-147.

LYNGSTADAAS, S.P., MOINICHEN, C.B. & RISNES, S. (1998) Crown morphology, enamel distribution and enamel structure in mouse molars, *The Anatomical Record*, vol. 250, pp. 268-280.

LYON, M. (1961) Gene action in the X chromosome of the mouse (*Mus musculus* L.), *Nature*, vol. 190, pp. 372-373.
MAAS, R., & BEI, M. (1997) The genetic control of early tooth development, *Critical Reviews in Oral Biology & Medicine,* vol. 8, no. 4-39.

MACDOUGALL, M. (2003) Dental structural diseases mapping to human chromosome 4q21, *Connective Tissue Research*, vol. 44, pp. 285-291.

MACDOUGALL, M., DUPONT, B.R., SIMMONS, D., REUS, B., KREBSBACH, P., KÄRRMAN, C., HOLMGREN, G., LEACH, R.J. & FORSMAN, K. (1997) Ameloblastin Gene (AMBN) Maps within the Critical Region for Autosomal Dominant *Amelogenesis imperfecta* at Chromosome 4q21, *Genomics*, vol. 41, no. 1, pp. 115-118.

MACDOUGALL, M., NYDEGGER, J., GU, T.T., SIMMONS, D., LUAN, X., CAVENDER, A. & D'SOUZA, R.N. (1998) Developmental Regulation of Dentin Sialophosphoprotein during Ameloblast Differentiation: A Potential Enamel Matrix Nucleator, *Connective Tissue Research*, vol. 39, no. 1, pp. 25 - 37.

MACDOUGALL, M., SIMMONS, D., GU, T.T. & DONG, J. (2002) MEPE/OF45, a new dentin/bone matrix protein and candidate gene for dentin diseases mapping to chromosome 4q21, *Connective Tissue Research*, vol. 43, no. 320- 330.

MACENTEE, M. & LAKOWSKI, R. (1981) Instrumental colour measurement of vital and extracted human teeth, *Journal of Oral Rehabilitation*, vol. 8, no. 3, pp. 203-208.

MAO, J.J. & NAH, H.-D. (2004) Growth and development: hereditary and mechanical modulations, *American Journal of Orthodontics and Dentofacial Orthopedics*, vol. 125, no. 6, pp. 676-689.

MARDH, K.C., BACKMAN, B., HOLMGREN, G., HU, J.C., SIMMER, J.P. & FORSMAN-SEMB, K. (2002) A nonsense mutation in the enamelin gene causes local hypoplastic autosomal dominant *Amelogenesis imperfecta* (AIH2), *Human Molecular Genetics*, vol. 11, pp. 1069-1074.

MARGOLIS, H.C., BENIASH, E. & FOWLER, C.E. (2006) Role of macromolecular assembly of enamel matrix proteins in enamel formation, *Journal of Dental Research*, vol. 85, no. 9, pp. 775-793.

MASUYA, H., SHIMIZU, K., SEZUTSU, H., SAKURABA, Y., NAGANO, J., SHIMIZU, A., FUJIMOTO, N., KAWAI, A., MIURA, I., KANEDA, H., KOBAYASHI, K., ISHIJIMA, J., MAEDA, T., GONDO, Y., NODA, T., WAKANA, S. & SHIROISHI, T. (2005) Enamelin (Enam) is essential for amelogenesis: ENU-induced mouse mutants as models for different clinical subtypes of human *Amelogenesis imperfecta* (AI), *Human Molecular Genetics*, vol. 14, no. 5, pp. 575-583.

MASUYAMA, T., MIYAJIMA, K., OHSHIMA, H., OSAWA, M., YOKOI, NORIHIDE.,, OIKAWA, T. & TANIGUCHI, K. (2005) A novel autosomal-recessive mutation, whitish chalk-like teeth, resembling *Amelogenesis imperfecta*, maps to rat chromosome 14 corresponding to human 4q21, *European Journal of Oral Sciences*, vol. 113, no. 6, pp. 451-456.

MAYERS, M., FIRESTONE, A.R., RASHID, R. & VIG, K.W.L. (2005) Comparison of peer assessment rating (PAR) index scores of plaster and computer-based digital models, *American Journal of Orthodontics and Dentofacial Orthopedics*, vol. 128, no. 4, pp. 431-434.

MAYHALL, J.T. & ALVESALO, L. (1992) Sexual dimorphism in the three-dimensional determinations of the maxillary first molar; cusp height, area, volume and position, in Smith.P. & Freund (eds), *Structure, Function and Evolution of Teeth*, Tel Aviv.

MAYHALL, J.T. & KAGEYAMA, I. (1997) A new, three-dimensional method for determining tooth wear, *American Journal of Physical Anthropology*, vol. 103, pp. 463-469.

MCCOLLUM, M.A. & SHARPE, P.T. (2001a) Evolution and development of teeth, *Journal of Anatomy*, vol. 199, no. 1-2, pp. 153-159.

MCCOLLUM, M.A. & SHARPE, P.T. (2001b) Developmental genetics and early hominid craniodental evolution, *Bio Essays*, vol. 23, no. 6, pp. 481-493.

MCKEOWN, H.F., ROBINSON, D.L., ELCOCK, C., AL-SHAROOD, M. & BROOK, A.H. (2002) Tooth dimensions in hypodontia patients, their unaffected relatives and a control group measured by a new image analysis system, *European journal of Orthodontics*, vol. 24, no. 2, pp. 131-141.

MECKEL, A.H., GRIEBSTEIN, W.J. & NEAL, R.J. (1965) Structure of mature human dental enamel as observed by electron microscopy, *Archives of Oral Biology*, vol. 10, no. 5, pp. 775-783.

MIK, K.H.Y. & COOKE, M.S. (1998) Space analysis a comparison between sonic digitization (DigiGraphTM Workstation) and the digital calliper, *European Journal of Orthodontics*, vol. 20, no. 653-661.

MILETICH, I. & SHARPE, P.T. (2003) Normal and abnormal dental development, *Human Molecular Genetics*, vol. 12, no. Review Issue 1, pp. R69-R73.

MINDERMANN, A., NIEMZ, M.H., EISENMANN, L., LOESEL, F.H. & BILLE, J.F. (1993) Comparison of three different laser systems for application in dentistry, *Dental Applications of Lasers*, vol. 2080, SPIE, Budapest, Hungary, pp. 68-76.

MITSIADIS, T.A. & SMITH, M.M. (2006) How do genes make teeth to order through development? *Journal of Experimental Zoology Part B: Molecular and Developmental Evolution*, vol. 306B, no. 3, pp. 177-182.

MOINICHEN, C.B., LYNGSTADAAS, S.P. & RISNES, S. (1996) Morphological Characteristics of Mouse Incisor Enamel, *Journal of Anatomy*, vol. 189, no. 2, pp. 325-333.

MOORE, W.J. (1973) An experimental study of the functional components of growth in the rat mandible, *ACTA Anatomica (Basel)*, vol. 85, pp. 378-385.

MOORREES, C.F.A. & REED, R.B. (1964) Correlations among crown diameters of human teeth, *Archives of Oral Biology*, vol. 9, pp. 685-697.

MOORREES, C.F.A., THOMSEN, S.O., JENSEN, E. & YEN, P.K. (1957) Mesiodistal crown diameters of the deciduous and permanent teeth in individuals, *Journal of Dental Research*, vol. 36, no. 39-47.

MORADIAN-OLDAK, J., PAINE, M.L., LEI, Y.P., FINCHAM. A.G. & SNEAD, M.L. (2000) Self-assembly properties of recombinant engineered amelogenin proteins analyzed by dynamic light scattering and atomic force microscopy, *Journal of Structural Biology*, vol. 131, pp. 27-37.

MOSS, M.L. (1988) Finite element method comparison of murine mandibular form difference, *Journal Craniofacial Genetics and Developmental Biology*, vol. 8, pp. 3-20.

MOTOHASHI, N. & KURODA, T. (1999) A 3D computer-aided design system applied to diagnosis and treatment planning in orthodontics and orthognathic surgery, *European journal of Orthodontics*, vol. 21, pp. 263-274.

MOYERS, R.E. (1988) *A handbook of orthodonics*, Fourth Edition, Year Book Medical Publishers

MYERS, S.L., SHORE, R.C., BROOKES, S.J., BARRON, M.J., DIXON, M.J. & KIRKHAM, J. (2009) Non-destructive Quantitative Phenotyping of Murine Enamel (227), *British Society for Dental Research*, Glasgow, September 1-4.

NAGANO, T., KAKEGAWA, A., YAMAKOSHI, Y., TSUCHIYA, S., HU, J.C.-C., GOMI, K., ARAI, T., BARTLETT, J.D. & SIMMER, J.P. (2009) Mmp-20 and Klk4 Cleavage Site Preferences for Amelogenin Sequences, *Journal of Dental Research*, vol. 88, no. 9, pp. 823-828.

NAKAHORI, Y., TAKENAKA, O. & NAKAGOME, Y. (1991) A human X-Y homologous region encodes 'amelogenin, *Genomics*, vol. 9, pp. 264-269.

NAKASIMA, A., TERAJIMA, M., MORI, N., HOSHINO, Y., TOKUMORI, K., AOKI, Y. & HASHIMOTO, S. (2005) Three-dimensional computer-generated head model reconstructed from cephalograms, facial photographs, and dental cast models, *American Journal of Orthodontics and Dentofacial Orthopedics*, vol. 127, no. 3, pp. 282-292.

NANCI, A.R. (2003) *Ten Cate's Oral Histology; Development, Structure, and Function*, Seventh Edition, Mosby, St Louis.

NEBGEN, D.R., INOUE, H., SABSAY, B., WEI, K., HO, C.S. & VEIS, A. (1999) Identification of the chondrogenic-inducing activity from bovine dentin (bcia) as a low-molecular-mass amelogenin polypeptide, *Journal of Dental Research*, vol. 78, pp. 1484-1494.

NISHII, Y., NOJIMA, K. & TAKANE, Y., ET AL. (1998) Integration of the maxillofacial three-dimensional CT image and the three dimensional dental surface image, *Journal of the Japanese Orthodontic Society*, vol. 57, no. 189-194.

OHSHIMA, H., NAKASONE, N., HASHIMOTO, E., SAKAI, H., NAKAKURA-OHSHIMA, K. & HARADA, H. (2005) The eternal tooth germ is formed at the apical end of continuously growing teeth, *Archives of Oral Biology*, vol. 50, no. 2, pp. 153-157.

OKUBO, S.R., KANAWATI, A., RICHARDS, M.W. & CHILDRESS, S. (1998) Evaluation of visual and instrumental shade matching, *Journal of Prosthetic Dentistry*, vol. 80, pp. 642-648.

OLT, S. & JAKOB, P.M. (2004) Contrast-enhanced dental MRI for visualization of the teeth and jaw, *Magnetic Resonance in Medicine*, vol. 52, no. 1, pp. 174-176.

ONLINE MENDELIAN INHERITANCE IN MAN, (OMIM) *National Centre for Biotechnology Information, USA.* National Library of Medicine, USA, National Institute of Medicine, USA. http://www.ncbi.nlm.nih.gov/omim

OSBORN, J.W. (1971) The ontogeny of tooth succession in *Lacerta vivipara*, *Proceedings of the Royal Society of London,* vol. 179, pp. 261-289.

OSBORN, J.W. (1978) Morphogenetic gradients: fields versus clones, in P.M. Butler & K.M. Joysey (eds), *Development, Function and Evolution of Teeth*, Academic Press, London, pp. 171-201.

OTHMAN, S.A. & HARRADINE, N.W.T. (2006) Tooth-size Discrepancy and Bolton's Ratios: a literature review, *Journal of Orthodontics*, no. 33, pp. 45-51.

OZDEMIR, D., HART, P.S., FIRATLI, E., AREN, G., RYU, O.H. & HART, T.C. (2005) Phenotype of ENAM Mutations is Dosage-dependent, *Journal of Dental Research*, vol. 84, no. 11, pp. 1036-1041.

PAINE, M.L., LEI, Y.-P., DICKERSON, K. & SNEAD, M.L. (2002) Altered Amelogenin Self-assembly Based on Mutations Observed in Human X-linked *Amelogenesis imperfecta* (AIH1), *Journal of Biological Chemistry*, vol. 277, no. 19, pp. 17112-17116.

PAINE, M.L. & SNEAD, M.L. (2005) Tooth developmental biology: disruptions to enamel-matrix assembly and its impact on biomineralization, *Orthodontics and Craniofacial Research*, vol. 8, no. 4, pp. 239-251.

PAINE, M.L., ZHU, D.-H., LUO, W., BRINGAS, P., GOLDBERG, M., WHITE, S.N., LEI, Y.-P., SARIKAYA, M., FONG, H.K. & SNEAD, M.L. (2000) Enamel Biomineralization Defects Result from Alterations to Amelogenin Self-Assembly, *Journal of Structural Biology*, vol. 132, no. 3, pp. 191-200.

PAINE, M.L., ZHU, D.-H., LUO, W. & SNEAD, M.L. (2004) Overexpression of TRAP in the Enamel Matrix Does Not Alter the Enamel Structural Hierarchy, *Cells Tissues Organs*, vol. 176, pp. 7-16.

PAPAGERAKIS, P., IBARRA, J.M., INOZENTSEVA, N., DENBESTEN, P. & MACDOUGALL, M. (2005) Mouse Amelogenin Exons 8 and 9: Sequence Analysis and Protein Distribution, *Journal of Dental Research*, vol. 84, no. 7, pp. 613-617.

PAPAGERAKIS, P., LIN, H.K., LEE, K.Y., HU, Y., SIMMER, J.P., BARTLETT, J.D. & HU, J.C.C. (2008) Premature Stop Codon in MMP20 Causing *Amelogenesis imperfecta*, *Journal of Dental Research*, vol. 87, no. 1, pp. 56-59.

PAPAGERAKIS, P., MACDOUGALL, M., HOTTON, D., BAILLEUL-FORESTIER, I., OBOEUF, M. & BERDAL, A. (2003) Expression of amelogenin in odontoblasts, *Bone*, vol. 32, pp. 228-240.

PARKINSON, C.R. & SASOV, A. (2008) High-resolution non-destructive 3D interrogation of dentin using X-ray nanotomography, *Dental Materials*, vol. 24, no. 6, pp. 773-777.

PARSONS, T.E., KRISTENSEN, E., HORNUNG, L., DIEWERT, V.M., BOYD, S.K., GERMAN, R.Z. & HALLGRÍMSSON, B. (2008) Phenotypic variability and craniofacial dysmorphology: Increased shape variance in a mouse model for cleft lip, *Journal of Anatomy*, vol. 212, no. 2, pp. 135-143.

PAUL, S., PETER, A., PIETROBON, N. & HAMMERLE, C.H.F. (2002) Visual and Spectrophotometric Shade Analysis of Human Teeth, *Journal of Dental Research*, vol. 81, no. 8, pp. 578-582.

PIRTTINIEMI, P., ALVESALO, L., PIRILÄ-PARKKINEN, K., SILVÉN, O., HEIKKILÄ, J., JULKU, J. & KARJALAHTI, P. (1999) A new method for measuring three-dimensional dental morphology, *Proceedings of the 11th International Symposium on Dental Morphology*, University of Oulu.

PISPA, J. & THESLEFF, I. (2003) Mechanisms of ectodermal organogenesis, *Developmental Biology*, vol. 262, pp. 195-205.

PLATT, J.P. (1893) Ectodermic origin of the cartilages of the head, *Anat Ans*, vol. 8, pp. 506-509.

PLYUSNIN, I., EVANS, A.R., KARME, A., GIONIS, A. & JERNVALL, J. (2008) Automated 3D Phenotype Analysis Using Data Mining, *Public Library of Science ONE*, vol. 3, no. 3, p. e1742.

QUI (2006) Mighty Mouse, *Nature*, vol. 444, pp. 814-816.

QUIMBY, M.L., VIG, K.W.L., ROBERT, G.R. & FIRESTONE, A.R. (2004) The Accuracy and Reliability of Measurements Made on Computer-Based Digital Models, *Angle Orthodontist*, vol. 74, no. 3, pp. 298-303.

RAJPAR, M.H., HARLEY, K., LAING, C., DAVIES, R.M. & DIXON, M.J. (2001) Mutation of the gene encoding the enamel-specific protein, enamelin, causes autosomal-dominant *Amelogenesis imperfecta*, *Human Molecular Genetics*, vol. 10, pp. 1673-1677.

RAMAESH, T., AND BARD, J.B.L. (2003) The growth and morphogenesis of the early mouse mandible: a quantitative analysis, *Journal of Anatomy*, vol. 203, no. 2, pp. 213-222.

RAVASSIPOUR, D.B., HART, S., HART, T.C., RITTER, A.V., YAMAUCHI, R.M., GIBSON, C. & WRIGHT, J.T. (2000) Unique enamel phenotype associated with amelogenin gene (*AMELX*) codon 41 point mutation, *Journal of Dental Research*, vol. 79, pp. 1476-1481.

RAVINDRANATH, H.H., CHEN, L.S., ZEICHNER-DAVID, M., ISHIMA, R. & RAVINDRANATH, R.M. (2004) Interaction between the enamel matrix proteins amelogenin and ameloblastin, *Biochemical and Biophysical Research Communications*, vol. 323, pp. 1075-1083.

RAVINDRANATH, R.M.H., BASILROSE, R.M., RAVINDRANATH, N.H. & VAITHEESVARAN, B. (2003) Amelogenin interacts with cytokeratin-5 in ameloblasts during enamel growth, *Journal of Biological Chemistry*, vol. 278, pp. 20293-20302.

RAVINDRANATH, R.M.H., MORADIAN-OLDAK, J. & FINCHAM, A.G. (1999) Tyrosyl motif in amelogenins binds N-acetyl-D-glucosamine, *Journal of Biological Chemistry*, vol. 274, pp. 2464-2471.

REICH, C. (1998) Photogrammetric matching of point clouds for 3D measurement of complex objects, *Proceedings of SPIE*, vol. 3520, pp. 100-110.

REIF, W.E. (1982) Evolution of dermal skeleton and dentition in vertebrates: the odontode-regulation theory, *Evolutionary Biology*, vol. 15, pp. 287-368.

REKOW, E.D. (2006) Dental CAD/CAM systems: A 20-year success story, *Journal of the American Dental Association*, vol. 137, no. suppl1, pp. 5S-6.

RICHMOND, S. (1987) Recording the dental cast in three dimensions, *American Journal of Orthodontics and Dentofacial Orthopedics*, vol. 92, pp. 199-206.

RINSES, S. (1979b) Amethod of calculating the speed of movement of ameloblasts during rat incisor amelogenesis, *Archives of Oral Biology*, vol. 24, pp. 299-306.

RISNES, S. (1979a) A scanning electron microscope study of aberrations in the prism pattern of rat incisor inner enamel, *American Journal of Anatomy*, vol. 154, pp. 419-436.

RISNES, S. (1987) Multiplane sectioning and scanning electron microscopy as a method for studying the three-dimensional structure of mature dental enamel, *Scanning Microscopy*, vol. 1, pp. 1893-1902.

RISNES, S. (1998) Mature enamel morphology and forming enamel dynamics: Crystal orientation, crystal continuity, prism diameter, Retzius lines, and prism cross-striations, *Proceedings of the 11th International Symposium on Dental Morphology Research*, eds J.T. Mayhall & T. Heikkinen, Oulu University Press, Finland, pp. 312-322.

RISNES, S., SEPTIER, D., DE PERIERE, D.D. & GOLDBERG, M. (2002) TEM Observations on the Ameloblast/Enamel Interface in the Rat Incisor, *Connective Tissue Research*, vol. 43, no. 2-3, pp. 496-504.

ROBINSON, C., BRIGGS, H.D. & ATKINSON, P.J. (1981a) Histology of enamel organ and chemical composition of adjacent enamel in rat incisors, *Calcified Tissue International*, vol. 33, no. 5, pp. 513-520.

ROBINSON, C., FUCHS, P. & WEATHERELL, J.A. (1981b) The appearance of developing rat incisor enamel using a freeze fracturing technique, *Journal of Crystal Growth*, vol. 53, pp. 160-165.

ROBINSON, C., BRIGGS, H.D., KIRKHAM, J. & ATKINSON, P.J. (1983) Changes in the protein components of rat incisor enamel during tooth development, *Archives of Oral Biology*, vol. 28, pp. 993-1000.

ROBINSON, C., KIRKHAM, J., STONEHOUSE, N.J. & SHORE, R.C. (1989) Control of crystal growth during enamel maturation, *Connective Tissue Research*, vol. 22, pp. 139-145.

ROBINSON, C., BROOKES, S.J., SHORE, R.C. & KIRKHAM, J. (1998) The developing enamel matrix: nature and function, *European Journal of Oral Sciences*, vol. 106, pp. 282-291.

ROBINSON, D.L., BLACKWELL, P.G., STILLMAN, E.C. & BROOK, A.H. (2001) Planar Procrustes analysis of tooth shape, *Archives of Oral Biology*, vol. 46, no. 3, pp. 191-199.

ROBINSON, D.L., BLACKWELL, P.G., STILLMAN, E.C. & BROOK, A.H. (2002) Impact of landmark reliability on the planar Procrustes analysis of tooth shape, *Archives of Oral Biology*, vol. 47, no. 7, pp. 545-554.

ROBINSON, C., SHORE, R.C., WOOD, S.R., BROOKES, S.J., SMITH, D.A.M., WRIGHT, J.T., CONNELL, S. & KIRKHAM, J. (2003) Subunit Structures in Hydroxyapatite Crystal Development in Enamel: Implications for *Amelogenesis imperfecta*, *Connective Tissue Research*, vol. 44, pp. 65-71.

RODGERS, J.L. & NICEWANDER, W.A. (1988) Thirteen Ways to Look at the Correlation Coefficient, *The American Statistician*, vol. 42, no. 1, pp. 59-66.

ROSSOUW, P.E., PRESTON, C.B., LOMBARD, C.J. & TRUTER, J.W. (1993) A longitudinal evaluation of the anterior border of the dentition, *American Journal of Orthodontics and Dentofacial Orthopedics*, vol. 104, no. 146-152.

ROTH, V.L. (1988) The biological basis of homology, in C.J. Humphries (ed.), *Ontogeny and Systematics*, Columbia University Press, New
York.

ROWE, S.H. & WELFORD, W.T. (1967) Surface Topography of Non-Optical Surfaces by Projected Interference Fringes, *Nature*, vol. 216, no. 5117, pp. 786-787.

ROWE, T., COLBERT, M.W., KETCHAM, R.A., MAISANO, J.A. & OWEN, P.R. (2001) High-resolution X-ray computed tomography in vertebrate morphology, *Journal of Morphology*, vol. 248, no. 3, p. 277.

RUCH, J.V. & LESOT, H. (2000) Molecules implicated in odontoblast terminal differentiation and dentinogenesis, in M.F. Teaford, M.M. Smith & M.W.J. Ferguson (eds), *Development, Function and Evolution of Teeth* Cambridge University Press, Cambridge, pp. 22-36.

SAKAKURA, Y., FUJIWARA, N. & NAWA, T. (1989) Epithelial cytodifferentiation and extracellular matrix formation in enamel-free areas of the occlusal cusp during development of mouse molars: light and electron microscopic studies, *American Journal of Anatomy*, vol. 184, pp. 287-297.

SALAZAR-CIUDAD, I. & JERNVALL, J. (2002) A gene network model accounting for development and evolution of mammalian teeth, *Proceedings of the National Academy of Sciences*, vol. 99, no. 12, pp. 8116-8120.

SALAZAR-CIUDAD, I., JERNVALL, J. & NEWMAN, S.A. (2003) Mechanisms of pattern formation in development and evolution, *Development*, vol. 130, no. 10, pp. 2027-2037.

SALIDO, E.C., YEN, P.H., KOPRIVNIKAR, K., YU, L.C. & SHAPIRO, L.J. (1992) The human enamel protein gene amelogenin is expressed from both the X and the Y chromosomes, *American Journal of Human Genetics*, vol. 50, no. 2, pp. 303-316.

SALMIVIRTA, K., SOROKIN, L.M. & EKBLOM, P. (1997) Differential expression of laminin alpha chains during murine tooth development, *Developmental Dynamics*, vol. 210, pp. 206-215.

SANTORO, M., GALKIN, S., TEREDESAI, M., NICOLAY, O.F. & CANGIALOSI, T.J. (2003) Comparison of measurements made on digital and plaster models, *American Journal of Orthodontics and Dentofacial Orthopedics*, vol. 124, no. 1, pp. 101-105.

SATO, K., HATTORI, M. & AOBA, T. (1996) Disturbed enamel mineralization in a rat incisor model, *Advances in Dental Research*, vol. 10, no. 2, pp. 216-224.

SAUK, J.J., LYON, H.W. & WITKOP, C.J. (1972) Electron optic microanalysis of two gene products in enamel of females heterozygous for X-linked hypomaturation *Amelogenesis imperfecta*, *American Journal of Human Genetics*, vol. 24, no. 3, pp. 267-276.

SAVARA, B.S. (1965) Applications of photogrammetry for quantitative study of tooth and face morphology, *American Journal of Physical Anthropology*, vol. 23, pp. 427-434.

SAVARA, B.S. & SANIN, C. (1969) Data acquisition method for measuring dentitions and tests for accuracy, *American Journal of Physical Anthropology*, vol. 30, pp. 315-318.

SCOTT, P.J. (1981) The Reflex Plotters: Measurement without Photographs, *The Photogrammetric Record*, vol. 10, pp. 435-446.

SEEDORF, H., KLAFTEN, M., EKE, F., FUCHS, H., SEEDORF, U. & HRABE DE ANGELIS, M. (2007) A Mutation in the Enamelin Gene in a Mouse Model, *Journal of Dental Research*, vol. 86, no. 8, pp. 764-768.

SEEDORF, H., SPRINGER, I.N., GRUNDNER-CULEMANN, E., ALBERS, H.K., REIS, A., FUCHS, H., HRABE DE ANGELIS, M. & AÇIL, Y. (2004) *Amelogenesis imperfecta* in a New Animal Model-a Mutation in Chromosome 5 (human 4q21), *Journal of Dental Research*, vol. 83, no. 8, pp. 608-612.

SEKIGUCHI, H., ALALUUSUA, S., MINAGUCHI, K. & YAKUSHUI, M. (2001) A new mutation in the amelogenin gene causes X-linked *Amelogenesis imperfecta*, *Journal of Dental Research*, vol. 80, p. 617.

SHARPE, P.T. (1995) Homeobox genes and orofacial development, *Connective Tissue Research*, vol. 32, no. 1-4, pp. 17-25.

SHARPE, P.T. (2000) Homeobox genes in initiation and shape of teeth during develpment in mammaian embryos, in M.F. Teaford, M.M. Smith & M.W.J. Ferguson (eds), *Development, Function and Evolution of Teeth,* Cambridge University Press, Cambridge, pp. 3-12.

SHELLHART, W.C., LANGE, D.W., KLEUMPER, G.T., HICKS, E.P. & KAPLAN, A.L. (1995) Reliability of the Bolton tooth-size analysis when applied to crowded dentitions, *Angle Orthodontist*, vol. 65, pp. 327-334.

SHELLIS, P. & BERKOVITZ, B.K.B. (1981) Comparative anatomy of dentition. The dentition of laboratory rodents and lagomorphs., in J.W. Osborn (ed.), *Dental Anatomy and Embryology.*, vol. 1, Blackwell Scientific Publications, Oxford, pp. 432-439.

SIMMER, J.P. (1995) Alternative splicing of amelogenins, *Connective Tissue Research*, vol. 32, pp. 131-136.

SIMMER, J.P. & FINCHAM, A.G. (1995) Molecular mechanisms of dental enamel formation, *Critical Reviews in Oral Biology & Medicine*, vol. 6, pp. 84-108.

SIMMER, J.P., FUKAE, M., TANABE, T., YAMAKOSHI, Y., UCHIDA, T., XUE, J., MARGOLIS, H.C., SHIMIZU, M., DEHART, B.C. & HU, C.C. (1998) Purification, characterization, and cloning of enamel matrix serine proteinase 1, *Journal of Dental Research*, vol. 77, pp. 377-386.

SIMMER, J.P., HU, C.C., LAU, E.C., SARTE, P., SLAVKIN, H.C. & FINCHAM, A.G. (1994) Alternative splicing of the mouse amelogenin primary RNA transcript, *Calcified Tissue International*, vol. 55, pp. 302-310.

SIMMER, J.P., HU, Y., LERTLAM, R., YAMAKOSHI, Y. & HU, J.C.-C. (2009) Hypomaturation enamel defects in Klk4 knock-out/ lacZ knock-in mice, *Journal of Biological Chemistry*, vol. 284, pp. 19110-19121.

SINGH, I.J. & SAVARA, B.S. (1964) Methods for making tooth and dental arch measurements, *Journal of the American Dental Association*, vol. 69, pp. 719-721.

SMITH, C.E. (1998) Cellular and Chemical Events During Enamel Maturation, *Critical Reviews in Oral Biology & Medicine*, vol. 9, no. 2, pp. 128-161.

SMITH, C.E. & NANCI, A. (1989) A method for sampling the stages of amelogenesis on mandibular rat incisors using the molars as a reference for dissection, *The Anatomical Record*, vol. 225, no. 3, pp. 257-266.

SMITH, C.E. & WARSHAWSKY, H. (1975) Cellular renewal in the enamel organ and the odontoblast layer of the rat incisor as followed by radio autography using 3H-thymidine, *The Anatomical Record*, vol. 183, no. 4, pp. 523-561.

SMITH, C.E. & WARSHAWSKY, H. (1976) Movement of entire cell populations during renewal of the rat incisor as shown by radio autography after labelling with 3Hthymidine. The concept of a continuously differentiating cross-sectional segment, *American Journal of Anatomy*, vol. 145, pp. 225-259.

SMITH, C.E., WAZEN, R., HU, Y., ZALZAL, S.F., NANCI, A., SIMMER, J.P. & HU, J.C.C. (2009c) Consequences for enamel development and mineralization resulting from loss of function of ameloblastin or enamelin, *European Journal of Oral Sciences*, vol. 117, no. 5, pp. 485-497.

SMITH, M.M. (2003) Vertebrate dentitions at the origin of jaws: when and how pattern evolved, *Evolution and Development*, vol. 5, pp. 394-413

SMITH, M.M. & COATES, M.I. (2000) Evolutionary origins of teeth and jaws: developmental models and phylogenetic patterns, in M.F. Teaford, M.M. Smith & M.W.J. Ferguson (eds), *Development, Function and Evolution of Teeth,* Cambridge University Press, Cambridge, pp. 133-152.

SMITH, M.M. & JOHANSON, Z. (2003) Separate evolutionary origins of teeth from evidence in fossil jawed vertebrates, *Science*, vol. 299, pp. 1235-1236.

SMITH, R.N, LATH, D., RAWLINSON, A., KARMO, M. & BROOK, A. (2008b) Gingival inflammation assessment by image analysis: measurement and validation, *International Journal of Dental Hygiene*, vol. 6, no. 2, pp. 137-142.

SMITH, R.N., COLLINS, L.Z., NAEENI, M., JOINER, A., PHILPOTTS, C.J., HOPKINSON, I., JONES, C., LATH, D.L., COXON, T.L., HIBBARD, J.H. & BROOK, A.H. (2008a) The *in vitro* and *in vivo* validation of a mobile non-contact camera-based digital imaging system for tooth colour measurement, *Journal of Dentistry*, vol. 36, no. Supplement 1, pp. 15-20.

SMITH, R.N., ELCOCK, C., ABDELLATIF, A., BÄCKMAN, B., RUSSELL, J.M. & BROOK, A.H. (2009a) Enamel defects in extracted and exfoliated teeth from patients with *Amelogenesis imperfecta*, measured using the extended enamel defects index and image analysis, *Archives of Oral Biology*, vol. 54, pp. S86-S92.

SMITH, R.N., KARMO, M., RUSSELL, J. & BROOK, A.H. (2007) The variability of the curvature of the labial surface of the upper anterior teeth along the facial axis of the clinical crown, *Archives of Oral Biology*, vol. 52, no. 11, pp. 1037-1042.

SMITH, R.N., RAWLINSON, A., LATH, D.L. & BROOK, A.H. (2006) A digital SLR or intra-oral camera: preference for acquisition within an image analysis system for measurement of disclosed dental plaque area within clinical trials, *Journal of Periodontal Research*, vol. 41, no. 1, pp. 55-61.

SMITH, R.N., RAWLINSON, A., LATH, D.L., ELCOCK, C., WALSH, T.F. & BROOK, A.H. (2004) Quantification of dental plaque on lingual tooth surfaces using image analysis: reliability and validation, *Journal of Clinical Periodontology*, vol. 31 no. 7, pp. 569-573.

SMITH, R.N., ZAITOUN, H., COXON, T.L., KARMO, M., KAUR, G., TOWNSEND, G., HARRIS, E.F. & BROOK, A.H. (2009b) Defining new dental phenotypes using 3-D image analysis to enhance discrimination and insights into biological processes, *Archives of Oral Biology*, vol. 54, pp. S118-S125.

SNEAD, M.L., LAU, E.C., FINCHAM, A.G., ZEICHNER-DAVID, M., DAVIS, C. & SLAVKIN, H.C. (1989) Of mice and men: Anatomy of the amelogenin gene, *Connective Tissue Research,* vol. 22, pp. 101-109.

SOFAER, J.A. (1975) Genetic variation and tooth development, *British Medical Bulletin*, vol. 31, pp. 107-110.

SOHMURA, T., NAGAO, M., SAKAI, M., WAKABAYASHI, K., KOJIMA, T., KINUTA, S., NAKAMURA, T. & TAKAHASHI, J. (2004a) High-resolution 3-D shape integration of dentition and face measured by new laser scanner, *IEEE Transactions on Medical Imaging*, vol. 23, no. 5, pp. 633-638.

SOHMURA, T., TOJIMA, T., WAKABAYASHI, K. & TAKAHASHI, J. (2000) Use of an ultrahigh-speed laser scanner for constructing three-dimensional shapes of dentition and occlusion, *The Journal of Prosthetic Dentistry*, vol. 84, no. 3, pp. 345-352.

SOHMURA, T., WAKABAAYSHI, K., LOMUNKONG, R., HOJO, H., KUSUMOTO, N., OKUDA, H., KOJIMA, T., NAKAMURA, T., YATANI, H. & TAKAHASHI, J. (2004b) 3D shape measurement of dental casts using medical x-ray CT, *Dental Materials Journal*, vol. 23, pp. 121-128.

STANTON, F.L., FISH, G.D. & ASHLEY-MONTAGUE, M.F. (1931) Description of three instruments for use in orthodontic and cephalometric investigations, with some remarks on map construction *Journal of Dental Research*, vol. 11, pp. 885-902.

STEPHANOPOULOS, G., GAREFALAKI, M.E. & LYROUDIA, K. (2005) Genes and Related Proteins Involved in *Amelogenesis imperfecta*, *Journal of Dental Research*, vol. 84, no. 1117-1126.

STEVENS, D.R., FLORES-MIR, C., NEBBE, B., RABOUD, D.W., HEO, G. & MAJOR, P.W. (2006) Validity, reliability, and reproducibility of plaster vs digital study models, *American Journal of Orthodontics and Dentofacial Orthopedics*, vol. 129, no. 6, pp. 794 - 803.

STRAUSS, R.E. & F.L., B. (1982) The truss: body form reconstructions in morphometrics, *Syst. Zool*, vol. 31, pp. 113-135.

TACHIBANA, H. & MATSUMOTO, K. (1990) Applicability of X-ray computerized tomography in endodontics, *Endodontics & Dental Traumatology*, vol. 6, no. 1, pp. 16-20.

TAKADA, K., LOWE, A.A. & DECOU, R. (1983) Operational performance of the reflex metrograph and its applicability to the three-dimensional analysis of dental casts, *American Journal of Orthodontics*, no. 83, pp. 195-199.

TEN BOSCH, J.J. & COOPS, J.C. (1995) Tooth color and reflectance as related to light scattering and enamel hardness, *Journal of Dental Research*, vol. 74, no. 1, pp. 374-380.

TERAI, H., SHIMAHARA, M., SAKINAKA, Y. & S., T. (1999) Accuracy of integration of dental casts in three-dimensional models., *Journal of Oral and Maxillofacial Surgery*, vol. 57, no. 662-665.

TERMINE, J.D., BELCOURT, A.B., CHRISTNER, P.J., CONN, K.M. & NYLEN, M.U. (1980) Properties of dissociatively extracted fetal tooth matrix proteins. Principal molecular species in developing bovine enamel, *Journal of Biological Chemistry*, vol. 120, pp. 9760-9768.

THAM, P. (1957) Photogrammetric application in dentistry, *Photogrammetric Engineering*, vol. 23, pp. 668-670.

THESLEFF, I. (2006) The genetic basis of tooth development and dental defects, *American Journal of Medical Genetics*, vol. 140A, no. 23, pp. 2530-2535.

THIELKE, S., SERANO, J.G. & LEPE, X. (1998) A method for true coordinate three-dimensional measurement of casts using the measuring microscope, *The Journal of Prosthetic Dentistry*, vol. 80, pp. 506-510.

THOMAS, T.R. (1982) Profile description, in T.R. Thomas (ed.), *Rough Surfaces*, Longmans, London, pp. 72-90.

THOMAS, B.L. & SHARPE, P.T. (1998) Patterning of the murine dentition by homeobox genes, *European Journal of Oral Sciences*, vol. 106, no. Suppl 1, pp. 48-54.

TIZIANI, H.J. & UHDE, H. (1994) Three-dimensional image sensing by chromatic confocal microscopy, *Applied Optics*, vol. 33, pp. 1838-1843.

TOMASSETTI, J.J., TALOUMIS, L.J., DENNY, J.M. & FISCHER, J.R. (2001) A comparison of 3 computerized Bolton tooth size analyses with a commonly used method, *Angle Orthodontist*, vol. 71, no. 351-357.

TOMES, J. (1850) On the structure of the dental tissues of the order Rodentia, *Philosophical Transactions of the Royal Society of London*, vol. 140, pp. 529-567.

TOWNSEND, G., HARRIS, E.F., LESOT, H., CLAUSS, F. & BROOK, A. (2009) Morphogenetic fields within the human dentition: A new, clinically relevant synthesis of an old concept, *Archives of Oral Biology*, vol. 54, pp. S34-S44.

TOYOSAWA, S., FUJIWARA, T., OOSHIMA, T., SHINTANI, S., SATO, A., OGAWA, Y., SOBUE, S. & LJUHIN, N. (2000) Cloning and characterization of the human ameloblastin gene, *Gene*, vol. 256, pp. 1-11.

TSUTSUI, T.W., RIMINUCCI, M., HOLMBECK, K., BIANCO, P. & ROBEY, P.G. (2008) Development of craniofacial structures in transgenic mice with constitutively active PTH/PTHrP receptor, *Bone*, vol. 42, no. 2, pp. 321-331.

TUCKER, A. & SHARPE, P. (2004) The cutting-edge of mammalian development; how the embryo makes teeth, *Nature Reviews Genetics*, vol. 5, no. 7, pp. 499-508.

TUCKER, A.S. (2006) *Encyclopedia of Life Sciences*, TUCKER, A.S., John Wiley & Sons, www.mrw.interscience.wiley.com/emrw/978047005902/els/article/a0005989/current/html

TUCKER, A.S., MATTHEWS, K.L. & SHARPE, P.T. (1998) Transformation of tooth type induced by inhibition of BMP signalling, *Science*, vol. 82, pp. 1136–1138.

TUCKER, A.S. & SHARPE, P.T. (1999) Molecular genetics of tooth morphogenesis and patterning: the right shape in the right place, *Journal of Dental Research*, vol. 78, pp. 826-834.

VAAHTOKARI, A., ABERG, T., JERNVALL, J., KERÄNEN, S.V.E. & THESLEFF, I. (1996) The enamel knot as a signalling center in the developing mouse tooth, *Mechanisms of Development*, vol. 54, pp. 39-43.

VAN DER BURGT, T.P., TEN BOSCH, J.J., BORSBOOM, P.C.F. & KORTSMIT, W.J.P.M. (1990) A comparison of new and conventional methods for quantification of tooth color, *Journal of Prosthetic Dentistry*, vol. 63, pp. 155-162.

VAN DER LINDEN, F.P.G.M., BOERSMA, H., ZELDERS, T., PETERS, K.A. & RAABEN, J.H. (1972) Three-dimensional analysis of dental casts by means of the Optocom, *Journal of Dental Research*, vol. 51.

VAN VALEN, L.M. (1982) Homology and causes, *Journal of Morphology*, vol. 173, no. 3, pp. 305-312.

VEIS, A. (2003a) Amelogenin gene splice products: potential signalling molecules, *Cellular and Molecular Life Sciences*, vol. 60, pp. 38-55.

VEIS, A. (2003b) Mineralization in Organic Matrix Frameworks, *Reviews in Mineralogy and Geochemistry*, vol. 54, no. 1, pp. 249-289.

VEIS, A. (2005) A window on biomineralization, *Science*, vol. 307, pp. 1419-1420.

WANG, X.-P., SUOMALAINEN, M., FELSZEGHY, S., ZELARAYAN, L.C., ALONSO, M.T., PLIKUS, M.V., MAAS, R.L., CHUONG, C.-M., SCHIMMANG, T. & THESLEFF, I. (2007) An Integrated Gene Regulatory Network Controls Stem Cell Proliferation in Teeth, *Public Library of Science ONE Biology*, vol. 5, no. 6, p. e159.

WANG, X.-P., SUOMALAINEN, M., JORGEZ, C.J., MATZUK, M.M., WERNER, S. & THESLEFF, I. (2004) Follistatin Regulates Enamel Patterning in Mouse Incisors by Asymmetrically Inhibiting BMP Signalling and Ameloblast Differentiation, *Developmental Cell*, vol. 7, no. 5, pp. 719-730.

WARSHAWSKY, H., BAI, P. & NANCI, A. (1987) Analysis of crystallite shape in rat incisor enamel, *Anatomical Record*, vol. 218, no. 380-390.

WARSHAWSKY, H., JOSEPHSEN, K., THYLSTRUP A. & FEJERSKOV, O. (1981) The development of enamel structure in rat incisors as compared to the teeth of monkey and man, *Anatomical Record*, vol. 200, pp. 371-399.

WATERSTON, R.H., LINDBLAD-TOH K, BIRNEY E, and LANDER ES. (2002) Initial sequencing and comparative analysis of the mouse genome, *Nature*, vol. 420, no. 6915, pp. 520-562.

WATTS, A. & ADDY, M. (2001) Tooth discolouration and staining: Tooth discolouration and staining: a review of the literature, *British Dental Journal*, vol. 190, no. 6, pp. 309-316.

WAZEN, R.M., MOFFATT, P., ZALZAL, S.F., YAMADA, Y. & NANCI, A. (2009) A mouse model expressing a truncated form of ameloblastin exhibits dental and junctional epithelium defects, *Matrix Biology*, vol. 28, no. 5, pp. 292-303.

WEE, A.G., LINDSEY, D.T., KUO, S. & JOHNSTON, W.M. (2006) Color accuracy of commercial digital cameras for use in dentistry, *Dental Materials*, vol. 22, no. 6, pp. 553-559.

WEISS, K.M., STOCK, D.W. & ZHAO, Z. (1998) Dynamic interactions and the evolutionary genetics of dental patterning, *Critical Reviews in Oral Biology & Medicine*, vol. 9, pp. 369-398.

WENTWORTH-THOMPSON, D.A. (1942) *On Growth and Form*, Cambridge University Press, Cambridge

WHITEHOUSE, D.J. (1994) *Handbook of Surface Metrology*, Institute of Physics Publishing, Bristol.

WINTER, G.B. & BROOK, A.H. (1975) Enamel hypoplasia and anomalies of the enamel, *Dental clinics of North America*, vol. 19, pp. 3-24.

WITKOP, C.J. (1957) Hereditary defects in enamel and dentin, *ACTA Genetica et Statistica Medica,* vol. 7, pp. 236-239.

WITKOP, C.J. (1967) Partial expression of sex-linked recessive *Amelogenesis imperfecta* in females compatible with the Lyon hypothesis, *Oral Surgery, Oral Medicine, Oral Pathology, Oral Radiology, and Endodontology*, vol. 23, pp. 174-182.

WITKOP, C.J. (1975) Hereditary defects of dentin, *Dental clinics of North America*, vol. 19, pp. 25-45.

WITKOP, C.J. (1989) *Amelogenesis imperfecta*, Dentinogenesis Imperfecta and Dentin Dysplasia revisited - problems in classification., *Journal of Oral Pathology and Medicine*, vol. 17, pp. 547-553.

WITKOP, C.J. & SAUK, J.J. (1976) *Heritable defects of enamel*, in R.E. Stewart & G.H. Prescott (eds), Oral Facial Genetics, Mosby, St. Louis. pp. 151-226.

WOLPERT, L. (1969) Positional information and the spatial pattern of cellular differentiation, *Journal of Theoretical Biology*, vol. 25, pp. 1-47.

WONG, F.S., ELLIOTT, J.C., ANDERSON, P. & DAVIS, G.R. (1995) Three dimensional mineral distribution in the enamel of a rat incisor measured by X-ray microtomography, *Bone*, vol. 16, no. 6, pp. 690-690.

WONG, F.S., ELLIOTT, J.C., DAVIS, G.R. & ANDERSON, P. (2000) X-ray microtomographic study of mineral distribution in enamel of mandibular rat incisors, *Journal of Anatomy*, vol. 196, no. 03, pp. 405-413.

WRIGHT, J.T. (2006) The Molecular Etiologies and Associated Phenotypes of *Amelogenesis imperfecta*, *American Journal of Medical Genetics*, vol. 140, no. 23, pp. 2547-2555.

WRIGHT, J.T., HART, P.S., ALDRED, M.J., SEOW, K., CRAWFORD, P.J., HONG, S.P., GIBSON, C.W. & HART, T.C. (2003) Relationship of phenotype and genotype in X-linked *Amelogenesis imperfecta*, *Connective Tissue Research*, vol. 44(Suppl 1), pp. 72-78.

WRIGHT, J.T., HART, T.C., HART, P.S., SIMMONS, D., SUGGS, C., DALEY, B., SIMMER, J.P., HU, J.C.C., BARTLETT, J.D., LI, Y., YUAN, Z.-A., SEOW, W.K. & GIBSON, C.W. (2009) Human and Mouse Enamel Phenotypes Resulting from Mutation or Altered Expression of *AMEL, ENAM , MMP20* and *KLK4*, *Cells Tissues Organs*, vol. 189, no. 1-4, pp. 224-229.

WRIGHT, W.D. (1928) A re-determination of the trichromatic coefficients of the spectral colours, *Transactions of the Optical Society*, vol. 30, pp. 141-164.

XIAO, S., YU, C., CHOU, X., YUAN, W., WANG, Y., BU, L., FU, G., QIAN, M., YANG, J., SHI, Y., HU, L., HAN, B., WANG, Z., HUANG, W., LIU, J., CHEN, Z., ZHAO, G. & KONG, X. (2001) Dentinogenesis imperfecta 1 with or without progressive hearing loss is associated with distinct mutations in DSPP, *Nature Genetics*, vol. 27, pp. 201-204.

ZALZAL, S.F., SMITH, C.E. & NANCI, A. (2008) Ameloblastin and amelogenin share a common secretory pathway and are co-secreted during enamel formation, *Matrix Biology*, vol. 27, no. 4, pp. 352-359.

ZELDITCH, M.L., DEBRY, R.W. & STRANEY, D.O. (1989) Triangulation-Measurement Schemes in the Multivariate Analysis of Size and Shape, *Journal of Mammalogy*, vol. 70, no. 3, pp. 571-579.

ZHANG, X., ZHAO, J., LI, C., GAO, S., QIU, C., LIU, P., WU, G., QIANG, B., LO, W.H. & SHEN, Y. (2001) DSPP mutation in dentinogenesis imperfecta Shields type II, *Nature Genetics*, vol. 27, pp. 151-152.

ZHANG, X.Z., ANDERSON, P., DOWKER, S.E.P. & ELLIOTT, J.C. (2000) Optical Profilometric Study of Changes in Surface Roughness of Enamel during *in vitro* Demineralization, *Caries Research*, vol. 34, no. 2, pp. 164-174.

ZHU, D., PAINE, M.L., LUO, W., BRINGAS, P., JR. & SNEAD, M.L. (2006) Altering Biomineralization by Protein Design, *Journal of Biological Chemistry*, vol. 281, no. 30, pp. 21173-21182.

ZHU, Q., SUN, Y., LU, Y., WANG, X., PRASAD, M., FENG, J. & QIN, C. (2010) Cleavage-Site Residue Substitution Blocks Processing of Dentin Sialophosphoprotein *in vivo*, *American Association of Dental Research*, Abstract 1249, Washington DC, USA

ZILBERMAN, O., HUGGARE, J.A.V. & PARIKAKIS, K.A. (2003) Evaluation of the Validity of Tooth Size and Arch Width Measurements Using Conventional and Three-Dimensional Virtual Orthodontic Models, *The Angle Orthodontist*, vol. 73, no. 3, pp. 301-306.

Websites:

Digital Morphology Resource, National Science Foundation Digital Library at The University of Austin, Texas, USA. (http://digimorph.org/index.phtml)

European Mouse Phenotyping Resource of Standardised Screens (www.empress.har.mrc.ac.uk)

Gene Expression, Tooth and Craniofacial Development Group of the Developmental Biology Programme, Institute of Biotechnology, University of Helsinki (http://bite-it.helsinki.fi)

Mouse Dental Anomalies Record Form (www.eumorphia.org)

Mouse Genome Informatics (http://www.informatics.jax.org/)

National Centre for Biotechnology Information, National Library of Medicine, USA, National Institute of Medicine, USA. (www.ncbi.nlm.nih.gov/genome/guide/mouse/)

Parliament of the United Kingdom, Animal (*Scientific Procedures*) Act 1986 (Chapter 14) (www.archive.official-documents.co.uk/document/hoc/321/321-xa.htm)

RIKEN BioResources Center, Japan. ENU mutagenesis screening (www.brc.riken.jp/lab/gsc/mouse/)

Scantron Industrial Products Ltd., Taunton, UK (www.scantron-net.co.uk/proscan2000)

10. APPENDIX

10.1. APPENDIX 1. RELIABILITY AND VALIDATION

Table 1. 2D *left* Mandible Morphometry Intra-Operator Repeatability (TLC)

HEMI-MANDIBLES			CD-1 RELIABILITY																											
			INTRA-OPERATOR (TLC) $n = 20$																						Statistics						
VIEW/ ASPECT	MEASUREMENT VARIABLE	REPEAT	1	2	3	4	5	6	7	8	9	10	11	12	13	14	15	16	17	18	19	20	Mean	SD	Mean Dif.	SD. Dif.	SE	CR	Bias	ICC
BUCCAL	*overall-length* (mm)	1	12.508	12.519	9.893	13.186	12.233	12.476	11.997	12.212	11.867	12.339	11.986	12.153	12.434	12.678	11.628	11.929	12.241	12.224	12.473	12.755	12.187	0.643	0.025	0.243	0.054	0.476	0.106	0.919
		2	12.546	12.470	10.692	13.271	12.126	12.358	11.959	12.159	11.834	12.328	12.006	12.120	12.301	12.709	11.623	11.828	12.133	11.581	12.464	12.728	12.162	0.530						
	ascending-height (mm)	1	6.381	6.569	4.873	6.601	6.134	6.146	6.097	6.478	4.359	6.424	6.144	6.342	6.463	6.812	6.204	5.971	6.203	6.317	6.778	6.876	6.208	0.605	0.033	0.106	0.024	0.208	0.047	0.983
		2	6.218	6.581	4.897	6.590	6.103	6.150	6.016	6.486	4.383	6.503	6.153	6.244	6.249	6.683	6.183	6.249	6.133	6.140	6.726	6.826	6.176	0.582						
	basal-length (mm)	1	7.441	7.557	6.060	7.557	7.562	7.336	7.133	7.363	6.914	7.471	7.063	7.168	7.754	7.746	6.967	6.946	6.988	7.464	7.701	8.054	7.312	0.431	0.114	0.213	0.048	0.418	0.094	0.839
		2	7.493	7.445	5.955	7.510	7.238	7.239	7.065	7.297	7.050	7.185	7.062	7.148	7.092	7.761	6.970	7.203	6.926	6.914	7.518	7.891	7.198	0.396						
	mandible-angle (°)	1	52.050	65.210	86.730	68.100	49.050	51.170	63.660	51.540	49.410	62.650	64.330	62.280	53.610	62.620	48.110	51.230	67.910	61.626	56.460	64.640	59.619	9.344	0.053	1.805	0.404	3.538	0.792	0.942
		2	52.340	65.070	84.260	67.230	54.770	53.900	63.440	50.660	49.070	61.590	64.200	61.980	52.253	62.550	48.010	51.250	68.300	58.440	57.150	64.860	59.566	8.641						
	coronoid-coronoid-length (mm)	1	4.343	2.943	3.306	2.807	4.098	4.052	2.880	4.220	3.097	3.080	3.204	3.248	3.854	3.162	4.192	3.923	3.004	3.528	3.869	3.215	3.501	0.511	-0.025	0.262	0.059	0.514	0.116	0.877
		2	4.390	2.986	3.382	3.035	3.684	3.832	3.027	4.550	3.194	3.305	3.341	3.145	3.283	3.077	4.224	4.327	2.932	4.036	3.690	3.082	3.526	0.527						
	diagonal-length (mm)	1	9.060	8.867	8.881	9.041	8.968	8.804	8.442	8.965	8.233	8.722	8.745	8.509	8.976	8.989	8.208	8.365	8.564	8.879	8.986	9.537	8.787	0.323	0.087	0.149	0.033	0.292	0.065	0.853
		2	9.058	8.765	8.657	9.015	8.843	8.668	8.367	8.951	8.391	8.478	8.706	8.435	8.439	8.978	8.169	8.525	8.519	8.848	8.852	9.333	8.700	0.288						
	mandible-perimeter (mm)	1	34.993	36.998	32.290	38.921	33.924	33.650	34.684	34.209	33.017	35.569	35.219	35.060	35.197	36.795	32.050	32.996	36.389	36.782	35.101	37.120	35.048	1.781	0.367	1.236	0.276	2.423	0.541	0.807
		2	35.126	36.933	32.099	40.508	33.459	33.486	34.719	34.133	30.863	35.222	34.923	34.824	35.977	36.569	32.068	32.613	35.870	31.997	35.024	37.202	34.681	2.242						
	mandible-area (mm^2)	1	38.790	39.041	36.311	42.136	37.261	37.697	35.716	37.993	30.958	38.593	37.426	34.905	37.568	40.078	34.153	32.613	38.278	38.698	38.748	42.800	37.488	2.853	0.196	0.302	0.068	0.592	0.133	0.807
		2	39.035	38.982	36.081	42.657	36.770	37.510	35.610	37.865	30.083	38.081	37.190	34.491	37.341	39.916	34.109	32.526	38.254	38.058	38.708	42.569	37.292	3.001						
LEFT																														
LINGUAL	*overall-length* (mm)	1	12.608	12.570	10.778	13.591	12.369	12.633	11.973	12.319	12.290	12.528	12.057	12.349	12.405	12.776	11.684	12.263	12.322	12.280	12.572	13.030	12.370	0.544	0.008	0.092	0.021	0.181	0.041	0.987
		2	12.711	12.573	10.740	13.612	12.381	12.627	11.997	12.310	11.969	12.512	12.064	12.359	12.584	12.783	11.697	12.296	12.216	12.249	12.564	12.999	12.362	0.561						
	ascending-height (mm)	1	6.496	6.609	4.729	6.556	6.044	6.322	5.985	6.486	4.383	6.531	6.090	6.215	6.504	6.510	6.092	5.830	6.053	6.690	6.494	6.821	6.172	0.615	0.030	0.116	0.026	0.227	0.051	0.981
		2	6.233	6.578	4.743	6.504	5.868	6.251	5.985	6.219	4.407	6.501	6.143	6.207	6.465	6.764	6.003	5.855	5.993	6.676	6.600	6.851	6.142	0.614						
	basal-length (mm)	1	7.307	7.496	6.053	7.583	7.587	7.445	7.093	7.447	6.387	7.476	7.161	7.155	7.645	7.828	7.022	7.035	6.998	7.407	7.676	7.872	7.284	0.451	-0.026	0.150	0.034	0.294	0.067	0.943
		2	7.546	7.533	6.000	7.533	7.433	7.340	7.042	7.372	6.928	7.537	7.144	7.154	7.651	7.824	6.919	7.036	7.077	7.375	7.793	7.949	7.309	0.430						
	mandible-angle (°)	1	52.699	64.529	84.736	67.080	50.043	50.054	63.624	51.818	49.858	61.100	63.908	62.161	53.630	63.423	47.367	51.059	68.011	59.830	56.811	63.997	59.287	8.915	-0.038	1.110	0.248	2.176	0.486	0.992
		2	51.732	65.458	84.710	66.790	54.065	50.123	63.364	51.306	48.973	60.787	63.925	62.163	53.470	61.651	48.050	51.420	67.964	60.020	57.072	63.463	59.325	8.746						
	coronoid-coronoid-length (mm)	1	4.408	2.940	3.236	2.913	3.940	4.119	2.828	4.206	3.265	3.322	3.157	3.200	3.770	2.943	4.101	3.814	2.977	3.532	3.738	3.621	3.501	0.490	0.012	0.151	0.034	0.296	0.067	0.948
		2	4.409	2.933	3.273	2.948	3.815	4.039	3.036	3.936	3.327	3.361	3.177	3.167	3.853	3.304	3.913	3.843	2.908	3.580	3.658	3.303	3.489	0.425						
	diagonal-length (mm)	1	9.157	8.834	8.744	9.154	8.975	8.943	8.427	9.006	8.986	8.837	8.860	8.449	8.881	9.070	8.241	8.387	8.587	8.902	9.004	9.487	8.846	0.303	0.039	0.151	0.034	0.296	0.874	0.874
		2	9.125	8.879	8.745	9.051	8.961	8.851	8.443	8.975	8.344	8.827	8.837	8.495	8.855	9.051	8.184	8.431	8.643	8.849	9.121	9.487	8.808	0.312						
	mandible-perimeter (mm)	1	35.635	38.731	33.962	40.856	35.537	33.000	35.620	34.306	33.469	37.788	35.877	36.252	36.940	38.930	33.405	35.199	37.302	34.720	36.915	39.659	36.205	2.186	-0.146	0.401	0.090	0.786	0.176	0.980
		2	36.626	38.917	34.467	40.589	35.789	33.885	36.235	34.282	34.126	37.728	35.892	36.558	36.692	38.700	33.512	35.242	37.224	34.549	36.455	39.550	36.351	1.989						
	mandible-area (mm^2)	1	38.227	38.973	35.786	42.935	37.386	38.754	35.322	38.586	30.928	38.537	36.590	35.283	37.726	40.962	33.289	32.831	37.694	39.217	38.651	43.692	37.568	3.136	0.078	0.290	0.065	0.568	0.127	0.996
		2	38.333	39.092	35.908	43.106	37.423	38.653	35.394	38.349	30.890	38.169	36.775	34.615	37.338	41.120	33.172	32.786	36.919	39.118	39.042	43.613	37.491	3.191						

Table 2. 2D *right* Mandible Morphometry Intra-Operator Repeatability (TLC)

HEMI-MANDIBLES			CD-1 RELIABILITY																												
				INTRA-OPERATOR (TLC)																							Statistics					
VIEW/ ASPECT		MEASUREMENT VARIABLE	REPEAT	n = 20																					Mean	SD	Mean Dif.	SD. Dif.	SE	CR	Bias	ICC
				1	2	3	4	5	6	7	8	9	10	11	12	13	14	15	16	17	18	19	20								
RIGHT	BUCCAL	*overall-length* (mm)	1	12.148	12.447	12.490	13.052	12.532	12.717	12.040	12.340	12.335	12.717	12.270	12.004	12.258	12.794	12.385	12.016	12.378	12.393	12.763	12.718	12.440	0.286	0.010	0.054	0.012	0.105	0.031	0.988
			2	12.164	12.556	12.565	13.031	12.530	12.652	12.017	12.350	12.205	12.687	12.190	12.033	12.278	12.764	12.318	12.001	12.371	12.390	12.738	12.764	12.430	0.288						
		ascending-height (mm)	1	6.064	6.733	6.225	6.410	6.089	6.339	6.394	6.668	6.656	6.209	5.941	6.194	6.355	6.804	6.044	5.965	6.425	6.611	6.381	6.980	6.374	0.293	0.058	0.180	0.040	0.353	0.054	0.819
			2	6.003	6.848	6.272	6.468	5.747	6.443	6.405	6.690	5.996	6.186	6.079	6.033	6.285	6.743	5.959	5.995	6.378	6.460	6.447	6.897	6.317	0.320						
		basal-length (mm)	1	7.183	7.618	7.467	7.650	7.362	7.302	7.263	7.574	7.600	7.697	7.306	7.226	7.376	8.084	7.250	7.031	7.338	7.417	8.242	7.309	7.465	0.295	0.033	0.124	0.028	0.244	0.061	0.921
			2	7.225	7.680	7.244	7.595	7.409	7.402	7.192	7.656	7.494	7.814	7.069	6.970	7.296	7.998	7.108	6.920	7.306	7.506	8.261	7.486	7.431	0.339						
		mandible-angle (°)	1	55.916	40.705	66.656	68.684	47.242	59.636	48.229	44.986	44.918	67.625	63.748	64.802	58.640	63.063	64.330	63.185	51.171	64.157	63.394	65.984	58.354	8.846	-0.353	1.871	0.418	3.667	0.496	0.976
			2	56.932	40.207	66.369	65.635	53.381	57.740	48.137	44.911	47.902	67.884	64.468	65.434	59.454	63.243	65.975	63.193	51.105	64.571	63.508	64.090	58.707	8.275						
		coronoid-coronoid-length (mm)	1	3.757	4.868	2.807	2.601	4.027	3.343	4.439	4.749	2.971	2.471	3.070	3.150	3.625	3.141	2.776	3.088	4.467	3.156	2.835	3.292	3.432	0.722	0.007	0.223	0.050	0.437	0.067	0.955
			2	3.767	5.017	3.033	2.786	3.414	3.562	4.422	5.062	2.684	2.526	3.204	3.008	3.494	3.157	2.567	3.155	4.339	3.146	3.087	3.075	3.425	0.744						
		diagonal-length (mm)	1	8.794	8.839	8.982	9.114	8.737	8.748	8.683	8.964	9.218	8.845	8.790	8.657	8.939	9.542	8.502	8.530	8.845	8.977	9.176	8.739	8.881	0.247	0.061	0.161	0.036	0.316	0.029	0.791
			2	8.873	8.965	8.817	9.122	8.783	8.799	8.613	9.083	8.751	8.496	8.784	8.465	8.853	9.425	8.410	8.328	8.787	9.038	9.089	8.914	8.820	0.269						
		mandible-perimeter (mm)	1	33.990	33.600	35.270	37.748	34.302	35.301	34.523	36.427	33.597	36.979	34.899	35.035	35.221	36.160	36.107	35.035	35.223	35.967	36.789	37.001	35.459	1.169	-0.153	0.578	0.129	1.133	0.202	0.887
			2	33.937	34.384	36.637	38.139	34.471	36.731	34.137	35.931	33.566	36.785	34.843	34.889	34.818	36.054	35.685	35.434	35.162	35.991	36.591	38.046	35.611	1.284						
		mandible-area (mm^2)	1	36.882	36.938	38.924	42.154	36.529	39.857	35.788	37.841	37.454	39.928	37.701	34.767	37.828	40.792	35.347	34.955	37.974	39.581	39.623	41.766	38.131	2.160	0.156	0.969	0.217	1.899	0.139	0.907
			2	36.918	36.917	40.145	42.763	36.506	38.570	35.640	37.740	33.980	39.651	37.398	35.144	37.745	40.383	36.538	35.265	37.924	38.799	39.477	42.009	37.976	2.288						
	LINGUAL	*overall-length* (mm)	1	12.158	12.507	12.518	12.949	12.549	12.549	11.982	12.272	12.313	12.507	12.210	12.094	12.461	12.295	12.511	11.894	12.385	12.410	12.780	12.718	12.403	0.261	-0.020	0.158	0.035	0.310	0.980	0.836
			2	12.186	12.556	12.554	12.981	12.548	12.705	12.023	12.236	12.167	12.422	12.148	12.432	12.309	12.777	12.325	11.921	12.314	12.331	12.756	12.764	12.423	0.279						
		ascending-height (mm)	1	6.140	6.817	6.374	6.466	6.032	6.378	6.452	6.648	6.647	6.206	5.949	6.161	6.512	6.927	6.137	5.971	6.533	6.473	6.402	6.980	6.410	0.300	0.051	0.159	0.036	0.312	0.059	0.856
			2	6.147	6.845	6.504	6.431	5.993	6.497	6.431	6.637	6.014	6.107	6.039	6.189	6.339	6.865	5.999	5.969	6.547	6.338	6.392	6.897	6.359	0.301						
		basal-length (mm)	1	7.186	7.601	7.679	7.572	7.543	7.344	7.012	7.526	7.573	7.737	7.102	7.128	7.660	7.316	7.260	7.038	7.324	7.363	8.189	7.309	7.423	0.285	0.067	0.182	0.041	0.357	0.024	0.802
			2	7.199	7.364	7.440	7.555	7.273	7.436	7.012	7.549	7.396	7.675	7.009	7.221	7.290	7.681	7.068	6.694	7.212	7.333	8.224	7.486	7.356	0.317						
		mandible-angle (°)	1	55.820	40.300	64.390	67.720	47.320	58.420	47.540	44.570	44.790	66.780	63.900	64.380	52.970	63.140	65.327	61.550	50.930	63.480	62.560	65.084	57.549	8.734	-0.201	1.681	0.376	3.290	0.396	0.981
			2	56.060	39.250	62.620	66.490	53.220	58.919	47.410	44.887	47.790	66.730	63.980	64.830	52.990	61.930	64.220	61.680	51.010	64.240	62.650	64.090	57.750	8.135						
		coronoid-coronoid-length (mm)	1	3.909	4.731	3.086	2.630	4.037	3.341	4.358	4.807	3.147	2.538	3.035	2.941	3.846	3.653	2.731	3.224	4.537	3.147	3.102	3.292	3.505	0.694	-0.011	0.229	0.051	0.449	0.051	0.953
			2	3.895	5.089	3.395	2.825	3.597	3.499	4.633	5.129	2.889	2.444	3.092	3.117	3.596	3.332	2.780	3.151	4.591	3.152	3.039	3.075	3.516	0.770						
		diagonal-length (mm)	1	8.846	8.788	9.183	9.167	8.924	8.767	8.457	9.002	9.298	8.944	8.633	8.628	8.798	8.942	8.549	8.518	8.936	8.866	9.152	8.739	8.857	0.233	-0.010	0.139	0.031	0.272	0.041	0.862
			2	8.911	8.923	9.039	9.118	8.800	8.805	8.462	9.231	9.336	8.907	8.636	8.801	8.800	9.198	8.230	8.441	8.825	8.871	9.098	8.914	8.867	0.275						
		mandible-perimeter (mm)	1	35.482	36.005	37.812	38.808	36.358	36.492	35.619	35.453	35.483	37.877	35.547	35.664	36.519	36.702	34.746	35.869	36.723	36.775	38.021	37.001	36.448	1.049	0.031	0.477	0.107	0.935	0.150	0.901
			2	35.603	35.619	37.502	38.021	36.100	35.550	35.480	35.362	35.176	37.872	35.721	35.590	36.529	37.452	35.493	35.721	36.444	36.842	38.210	38.046	36.417	1.056						
		mandible-area (mm^2)	1	37.449	36.772	39.598	40.862	36.303	38.561	35.062	37.372	37.544	38.714	36.834	34.591	37.416	40.305	36.074	34.183	38.106	38.645	39.082	41.766	37.762	2.014	0.258	1.143	0.256	2.240	0.104	0.872
			2	37.459	36.620	39.618	40.630	36.572	39.933	35.101	36.994	32.906	38.561	36.571	34.598	37.281	41.087	34.856	33.835	37.946	38.637	38.865	42.009	37.504	2.475						

Table 3. 2D *left* Mandible Morphometry Intra-Operator Repeatability (JHH)

HEMI-MANDIBLES		CD-1 RELIABILITY																												
		INTRA-OPERATOR (JHH)																						Statistics						
VIEW/ ASPECT	MEASUREMENT VARIABLE	REPEAT	n = 20																				Mean	SD	Mean Dif.	SD. Dif.	SE	Bias	CR	ICC
			1	2	3	4	5	6	7	8	9	10	11	12	13	14	15	16	17	18	19	20								
LEFT BUCCAL	*overall-length* (mm)	1	12.654	12.526	10.192	13.396	12.280	12.475	11.980	12.241	11.897	12.362	12.020	12.223	12.396	12.726	11.636	12.329	12.262	12.241	12.446	12.820	12.255	0.611	0.016	0.072	0.016	0.031	0.141	0.993
		2	12.658	12.478	9.938	13.385	12.278	12.512	12.027	12.250	11.896	12.374	12.055	12.205	12.452	12.697	11.589	12.195	12.256	12.315	12.436	12.789	12.239	0.655						
	ascending-height (mm)	1	6.217	6.578	5.314	6.568	6.039	6.151	6.010	6.153	4.380	6.473	6.187	6.362	6.313	6.753	5.772	6.008	6.252	6.646	6.563	6.852	6.180	0.554	0.054	0.224	0.050	0.098	0.439	0.916
		2	5.635	6.508	5.891	6.608	5.865	5.989	6.027	6.201	4.412	6.510	6.207	6.359	6.331	6.801	5.800	5.656	6.118	6.362	6.358	6.874	6.126	0.534						
	basal-length (mm)	1	7.524	7.689	5.537	7.514	7.560	7.294	7.114	7.448	6.883	7.755	7.075	7.191	7.640	8.160	7.004	7.342	7.127	7.501	7.866	7.925	7.357	0.542	0.045	0.137	0.031	0.061	0.269	0.971
		2	7.540	7.629	4.991	7.540	7.494	7.277	7.078	7.419	7.046	7.659	7.075	7.215	7.684	8.202	7.047	7.183	7.058	7.452	7.743	7.922	7.313	0.633						
	mandible-angle (°)	1	52.701	65.416	87.055	67.096	53.719	51.730	63.957	54.410	44.736	62.334	64.233	62.821	57.253	63.088	51.414	51.628	66.501	60.201	57.556	65.156	60.150	8.942	-0.464	1.131	0.253	0.496	2.217	0.991
		2	54.133	66.001	87.090	66.958	58.064	52.025	63.368	53.875	45.031	62.192	64.395	62.599	56.754	63.115	50.995	53.014	67.656	61.055	58.965	65.002	60.614	8.743						
	coronoid-coronoid-length (mm)	1	4.380	3.199	3.657	3.061	3.828	4.035	3.170	4.290	3.511	3.295	3.212	3.326	3.449	3.247	3.793	3.896	3.141	3.584	3.636	3.488	3.560	0.381	0.075	0.151	0.034	0.067	0.296	0.891
		2	3.936	3.057	3.539	3.123	3.498	3.787	3.109	4.232	3.518	3.325	3.321	3.351	3.536	3.329	3.687	3.652	3.004	3.573	3.579	3.544	3.485	0.302						
	diagonal-length (mm)	1	9.059	8.875	8.869	9.030	9.100	8.834	8.492	9.021	8.230	8.986	8.813	8.489	8.839	9.310	8.212	8.760	8.720	8.960	9.033	9.515	8.857	0.321	0.016	0.068	0.015	0.029	0.133	0.980
		2	9.066	8.917	8.801	9.033	8.994	8.713	8.413	9.023	8.375	8.907	8.854	8.502	8.857	9.379	8.268	8.698	8.649	8.879	9.013	9.484	8.841	0.308						
	mandible-perimeter (mm)	1	35.355	37.091	31.727	38.786	34.811	34.007	34.900	34.254	33.377	35.597	35.600	35.484	34.893	36.541	32.051	33.976	35.717	36.369	35.470	37.363	35.168	1.693	-0.008	0.459	0.103	0.202	0.900	0.967
		2	35.114	37.271	32.825	39.037	34.120	33.862	34.659	34.125	33.196	35.398	35.410	35.239	34.958	36.452	31.953	33.412	36.325	37.335	35.108	37.724	35.176	1.788						
	mandible-area (mm^2)	1	39.036	38.936	35.614	42.248	37.410	38.181	35.729	38.110	30.760	38.474	37.502	35.103	37.447	38.831	34.326	33.035	38.430	38.816	39.011	43.091	37.505	2.852	0.060	0.319	0.071	0.139	0.625	0.994
		2	38.602	38.854	36.464	42.322	37.134	37.958	35.700	37.915	31.002	37.998	37.884	34.926	37.455	39.054	34.247	32.746	38.465	38.275	38.919	42.965	37.444	2.803						
LEFT LINGUAL	*overall-length* (mm)	1	12.800	12.811	10.756	13.643	12.347	12.647	12.057	12.356	12.011	12.627	12.082	12.320	12.557	12.744	11.714	12.264	12.274	12.217	12.642	13.110	12.399	0.576	0.034	0.254	0.500	0.980	0.498	0.909
		2	12.798	12.638	10.796	13.985	12.430	12.709	12.057	12.336	11.994	12.596	12.102	12.352	12.570	12.767	11.747	12.209	12.356	12.204	12.568	12.077	12.365	0.589						
	ascending-height (mm)	1	6.240	6.543	4.773	6.565	5.646	6.047	5.970	6.497	4.346	6.580	6.035	6.278	6.557	6.779	5.581	5.877	5.973	6.710	6.405	6.842	6.112	0.646	0.029	0.133	0.030	0.059	0.261	0.979
		2	5.730	6.605	4.724	6.655	5.572	6.173	5.989	6.352	4.407	6.549	6.089	6.274	6.486	6.802	5.613	5.756	5.945	6.654	6.380	6.903	6.083	0.653						
	basal-length (mm)	1	7.399	7.555	6.237	7.591	7.400	7.340	6.961	7.340	6.899	7.606	7.067	7.113	7.572	8.083	7.071	7.128	7.078	7.484	7.808	8.045	7.339	0.423	-0.016	0.053	0.012	0.024	0.104	0.994
		2	7.510	7.593	6.156	7.660	7.399	7.387	6.998	7.398	6.934	7.590	7.094	7.104	7.604	8.031	7.083	7.133	7.141	7.548	7.696	8.041	7.355	0.424						
	mandible-angle (°)	1	51.880	63.544	83.934	67.223	57.455	53.503	63.811	51.712	49.290	61.266	63.902	62.045	52.247	61.884	51.212	51.436	68.536	60.268	56.953	63.683	59.789	8.209	-0.154	0.903	0.202	0.396	1.770	0.994
		2	53.052	64.958	84.041	66.746	59.217	51.301	63.647	51.843	49.470	60.959	62.951	62.118	52.948	61.673	50.724	52.560	68.524	60.768	57.934	63.433	59.943	8.145						
	coronoid-coronoid-length (mm)	1	4.206	2.721	3.305	2.963	3.290	3.816	3.104	4.307	3.207	3.407	3.209	3.175	3.974	3.319	3.598	3.816	2.893	3.670	3.596	3.623	3.460	0.425	0.019	0.115	0.026	0.051	0.225	0.962
		2	3.908	2.865	3.282	3.142	3.124	3.919	3.144	4.257	3.280	3.396	3.295	3.191	3.889	3.289	3.527	3.768	2.906	3.565	3.635	3.440	3.441	0.365						
	diagonal-length (mm)	1	8.910	8.652	8.835	9.132	8.917	8.781	8.374	8.905	8.315	8.900	8.738	8.407	8.893	9.260	8.296	8.612	8.678	9.018	9.060	9.638	8.816	0.332	-0.039	0.095	0.021	0.041	0.186	0.957
		2	8.990	8.877	8.857	9.461	8.913	8.844	8.390	8.992	8.325	8.820	8.768	8.479	8.902	9.301	8.275	8.580	8.734	8.972	9.052	9.576	8.855	0.345						
	mandible-perimeter (mm)	1	35.921	38.432	33.446	40.911	36.560	35.953	36.394	36.199	34.109	36.877	36.297	36.806	37.184	38.125	33.581	35.236	37.591	34.871	36.891	39.663	36.552	1.870	0.009	0.339	0.076	0.150	0.664	0.984
		2	35.780	38.669	33.982	41.369	36.180	36.073	36.302	36.514	34.131	36.072	36.352	36.777	36.958	38.316	33.416	35.368	36.922	34.986	37.180	39.529	36.544	1.890						
	mandible-area (mm^2)	1	38.750	38.698	35.805	42.270	37.262	38.743	35.992	38.250	31.120	38.183	36.058	34.938	37.629	40.716	32.815	33.045	37.038	39.040	38.919	43.663	37.447	3.057	0.053	0.360	0.080	0.104	0.706	0.993
		2	38.519	38.722	35.486	43.290	37.045	38.251	35.905	37.998	30.989	38.749	36.152	35.069	37.485	40.533	33.135	32.738	36.888	39.018	38.369	43.531	37.394	3.128						

Table 4. 2D *right* Mandible Morphometry Intra-Operator Repeatability (JHH)

HEMI-MANDIBLES			CD-1 RELIABILITY																											
			INTRA-OPERATOR (JHH)																						Statistics						
VIEW/ ASPECT	MEASUREMENT VARIABLE	REPEAT	$n = 20$																				Mean	SD	Mean Dif.	SD. Dif.	SE	Bias	CR	ICC
			1	2	3	4	5	6	7	8	9	10	11	12	13	14	15	16	17	18	19	20								
RIGHT BUCCAL	*overall-length* (mm)	1	12.025	12.504	12.984	13.141	12.536	12.756	12.008	12.424	12.143	12.791	12.381	12.060	12.401	12.833	12.602	12.108	12.414	12.430	12.796	12.801	12.507	0.331	-0.032	0.178	0.040	0.078	0.349	0.840
		2	12.184	12.494	13.273	12.825	12.541	12.794	12.067	12.428	12.233	12.577	12.376	12.649	12.352	12.806	12.612	12.059	12.453	12.437	12.820	12.788	12.538	0.298						
	ascending-height (mm)	1	6.002	6.488	6.363	6.428	5.864	6.202	6.101	6.652	6.301	6.477	5.990	6.108	6.529	6.787	6.063	6.083	6.308	6.402	6.406	6.900	6.323	0.275	0.065	0.158	0.035	0.069	0.310	0.818
		2	5.951	6.456	6.289	6.220	5.920	6.271	6.007	6.102	6.354	6.412	6.006	6.123	6.436	6.810	6.067	5.952	5.955	6.404	6.564	6.846	6.257	0.278						
	basal-length (mm)	1	7.245	7.700	7.455	7.657	7.427	7.362	7.194	7.511	7.533	7.671	7.142	6.978	7.223	7.987	7.075	7.013	7.363	7.444	8.297	7.399	7.434	0.324	-0.032	0.195	0.044	0.086	0.382	0.848
		2	7.188	7.677	7.434	7.587	7.359	7.425	7.052	7.487	7.499	7.649	7.125	6.943	7.279	8.024	7.102	7.105	7.383	7.412	8.371	8.223	7.466	0.381						
	mandible-angle (°)	1	58.111	41.828	66.112	68.384	48.351	60.224	49.780	49.786	45.635	64.048	64.362	62.811	58.390	63.356	65.491	61.600	52.927	64.688	62.789	65.974	58.732	7.832	0.008	0.616	0.138	0.270	1.207	0.997
		2	57.419	42.289	66.098	69.088	47.234	59.555	50.002	48.894	44.565	64.892	64.082	62.762	58.747	62.978	65.427	62.102	53.275	65.182	63.397	66.499	58.724	8.113						
	coronoid-coronoid-length (mm)	1	3.311	4.863	2.766	2.601	3.899	3.196	4.063	3.800	3.863	2.909	3.112	3.005	3.554	3.139	2.571	3.203	3.897	3.056	2.862	3.105	3.339	0.574	-0.036	0.113	0.025	0.049	0.221	0.977
		2	3.513	4.682	2.801	2.703	3.854	3.359	3.922	3.889	3.955	2.841	3.193	3.103	3.525	3.111	2.586	3.158	3.910	3.324	3.008	3.067	3.375	0.529						
	diagonal-length (mm)	1	8.865	8.989	8.981	9.152	8.796	8.762	8.617	8.960	8.804	8.771	8.766	8.391	8.858	9.373	8.320	8.454	8.814	8.845	9.111	8.664	8.815	0.254	-0.016	0.070	0.016	0.031	0.137	0.970
		2	8.781	8.911	9.001	9.171	8.682	8.766	8.598	9.127	8.801	8.801	8.672	8.390	8.902	9.393	8.402	8.503	8.903	8.920	9.188	8.691	8.830	0.263						
	mandible-perimeter (mm)	1	33.700	33.711	37.255	37.783	34.520	34.920	33.542	34.290	33.183	37.121	35.683	35.597	35.156	36.590	36.007	34.896	35.389	36.361	36.736	37.265	35.485	1.390	-0.044	0.357	0.080	0.157	0.700	0.967
		2	33.701	34.403	37.329	37.522	34.976	35.195	33.695	34.446	33.265	37.936	35.683	35.605	34.778	36.356	36.161	35.005	35.322	36.203	35.974	37.029	35.529	1.310						
	mandible-area (mm^2)	1	36.763	36.839	41.266	42.151	37.163	40.380	35.491	37.828	34.324	40.143	37.935	35.128	37.607	40.647	36.836	35.134	38.163	39.204	39.579	42.162	38.237	2.370	0.229	0.304	0.068	0.133	0.596	0.987
		2	36.794	37.065	41.094	41.767	36.891	40.552	35.816	37.601	33.978	39.789	37.827	34.895	37.536	40.423	36.465	35.177	37.742	38.430	38.758	41.563	38.008	2.268						
LINGUAL	*overall-length* (mm)	1	12.251	12.529	12.572	13.023	12.557	12.697	12.040	12.340	12.186	12.466	12.200	12.129	12.289	12.745	12.487	11.954	12.385	12.395	12.832	12.773	12.443	0.280	-0.023	0.095	0.021	0.041	0.186	0.933
		2	12.238	12.568	12.492	13.067	12.568	12.774	12.093	12.282	12.222	12.685	12.317	12.174	12.324	12.769	12.524	12.003	12.443	12.456	12.543	12.777	12.466	0.267						
	ascending-height (mm)	1	6.164	6.684	6.362	6.470	5.931	6.231	6.140	6.652	6.592	6.196	5.956	6.046	6.308	6.893	6.109	6.021	5.902	6.504	6.506	6.825	6.325	0.303	0.075	0.166	0.037	0.073	0.325	0.810
		2	6.046	6.289	6.283	6.561	5.940	6.290	6.027	6.549	5.969	6.183	5.974	6.025	6.265	6.798	6.085	5.985	6.022	6.492	6.425	6.791	6.250	0.273						
	basal-length (mm)	1	7.258	7.640	7.640	7.567	7.474	7.418	7.183	7.474	7.504	7.644	7.075	7.226	7.253	7.590	7.170	6.983	7.345	7.433	8.068	7.361	7.415	0.247	-0.009	0.098	0.022	0.043	0.192	0.924
		2	7.294	7.630	7.496	7.703	7.435	7.438	7.127	7.509	7.401	7.712	7.104	7.199	7.244	7.858	7.204	6.903	7.474	7.514	7.973	7.265	7.424	0.267						
	mandible-angle (°)	1	56.690	39.989	62.575	67.482	47.582	59.001	50.131	51.719	47.766	67.100	64.250	64.904	52.495	61.927	64.367	61.546	52.696	63.802	61.030	65.315	58.118	7.764	-0.517	1.535	0.343	0.672	3.009	0.979
		2	57.130	41.920	65.290	66.042	48.025	57.870	48.810	52.045	48.540	67.834	64.201	64.766	57.988	62.036	64.563	61.639	52.396	63.905	62.421	65.289	58.636	7.506						
	coronoid-coronoid-length (mm)	1	3.887	5.258	3.553	2.674	4.083	3.401	4.012	3.950	3.773	2.526	3.153	3.160	3.675	3.292	2.717	3.212	4.156	3.245	3.251	3.257	3.512	0.623	0.045	0.164	0.037	0.073	0.321	0.958
		2	4.010	4.747	3.281	2.940	3.883	3.558	4.045	3.911	3.566	2.499	3.205	3.156	3.631	3.265	2.735	3.136	4.104	3.266	3.195	3.195	3.466	0.532						
	diagonal-length (mm)	1	8.923	8.774	9.016	9.124	8.836	8.832	8.608	9.247	9.308	8.835	8.690	8.737	8.737	9.370	8.364	8.467	8.883	8.930	9.038	8.763	8.874	0.260	0.005	0.161	0.036	0.071	0.316	0.821
		2	8.965	9.014	9.093	9.162	8.757	8.810	8.601	9.304	8.700	8.868	8.721	8.747	8.733	9.338	8.421	8.404	8.913	9.081	9.098	8.658	8.869	0.262						
	mandible-perimeter (mm)	1	35.879	35.532	38.171	39.130	35.288	35.865	35.635	35.655	34.296	37.673	35.219	35.657	35.928	37.543	34.501	35.422	36.520	37.052	38.384	39.279	36.431	1.469	-0.184	0.514	0.115	0.225	1.007	0.925
		2	35.543	35.594	38.352	38.841	36.012	36.843	35.601	35.730	34.866	37.356	35.425	35.498	35.957	37.556	36.278	35.481	36.808	37.245	37.940	39.383	36.615	1.282						
	mandible-area (mm^2)	1	37.348	36.982	40.158	40.442	36.710	38.443	35.507	37.947	32.587	38.562	36.212	34.690	37.112	40.966	35.486	33.810	38.336	38.589	39.008	41.390	37.514	2.358	-0.113	0.502	0.112	0.220	0.984	0.976
		2	37.394	36.743	39.214	41.127	36.638	39.253	35.498	37.304	33.852	39.012	36.445	34.865	37.201	41.025	35.369	34.216	38.073	38.873	38.633	41.816	37.628	2.269						

Table 5. 2D *left* Mandible Morphometry Inter-Operator Reproducibility (TLC & JHH)

HEMI-MANDIBLES		CD-1 RELIABILITY																					Statistics							
			INTER-OPERATOR																											
			$n = 20$																											
VIEW/ ASPECT	MEASUREMENT VARIABLE	OPERATOR	1	2	3	4	5	6	7	8	9	10	11	12	13	14	15	16	17	18	19	20	Mean	SD	Mean Dif.	SD. Dif.	SE	Bias	LOA	ICC
LEFT BUCCAL	*overall-length* (mm)	TLC	12.508	12.519	9.893	13.186	12.233	12.476	11.997	12.212	11.867	12.339	11.986	12.153	12.434	12.678	11.628	11.929	12.241	12.224	12.473	12.755	12.187	0.643	-0.069	0.113	0.025	0.049	0.221	0.980
		JHH	12.654	12.526	10.192	13.396	12.280	12.475	11.980	12.241	11.897	12.362	12.020	12.223	12.396	12.726	11.636	12.329	12.262	12.241	12.446	12.820	12.255	0.611						
	ascending-height (mm)	TLC	6.381	6.569	4.873	6.601	6.134	6.146	6.097	6.478	4.359	6.424	6.144	6.342	6.463	6.812	6.204	5.971	6.203	6.317	6.778	6.876	6.208	0.605	0.029	0.193	0.043	0.084	0.378	0.946
		JHH	6.217	6.578	5.314	6.568	6.039	6.151	6.010	6.153	4.380	6.473	6.187	6.362	6.313	6.753	5.772	6.008	6.252	6.646	6.563	6.852	6.180	0.554						
	basal-length (mm)	TLC	7.441	7.557	6.060	7.557	7.562	7.336	7.133	7.363	6.914	7.471	7.063	7.168	7.754	7.746	6.967	6.946	6.988	7.464	7.701	8.054	7.312	0.431	-0.045	0.200	0.045	0.088	0.392	0.917
		JHH	7.524	7.689	5.537	7.514	7.560	7.294	7.114	7.448	6.883	7.755	7.075	7.191	7.640	8.160	7.004	7.342	7.127	7.501	7.866	7.925	7.357	0.542						
	mandible-angle (°)	TLC	52.050	65.210	86.730	68.100	49.050	51.170	63.660	51.540	49.410	62.650	64.330	62.280	53.610	62.620	48.110	51.230	67.910	61.626	56.460	64.640	59.619	9.344	-0.531	2.035	0.455	0.892	3.989	0.975
		JHH	52.701	65.416	87.055	67.096	53.719	51.730	63.957	54.410	44.736	62.334	64.233	62.821	57.253	63.088	51.414	51.628	66.501	60.201	57.556	65.156	60.150	8.942						
	coronoid-coronoid-length (mm)	TLC	4.343	2.943	3.306	2.807	4.098	4.052	2.880	4.220	3.097	3.080	3.204	3.248	3.854	3.162	4.192	3.923	3.004	3.528	3.869	3.215	3.501	0.511	-0.059	0.236	0.053	0.104	0.463	0.862
		JHH	4.380	3.199	3.657	3.061	3.828	4.035	3.170	4.290	3.511	3.295	3.212	3.326	3.449	3.247	3.793	3.896	3.141	3.584	3.636	3.488	3.560	0.381						
	diagonal-length (mm)	TLC	9.060	8.867	8.881	9.041	8.968	8.804	8.442	8.965	8.233	8.722	8.745	8.509	8.976	8.989	8.208	8.365	8.564	8.879	8.986	9.537	8.787	0.323	-0.070	0.128	0.029	0.057	0.251	0.906
		JHH	9.059	8.875	8.869	9.030	9.100	8.834	8.492	9.021	8.230	8.986	8.813	8.489	8.839	9.310	8.212	8.760	8.720	8.960	9.033	9.515	8.857	0.321						
	mandible-perimeter (mm)	TLC	34.993	36.998	32.290	38.921	33.924	33.650	34.684	34.209	33.017	35.569	35.219	35.060	35.197	36.795	32.050	32.996	36.389	36.782	35.101	37.120	35.048	1.781	-0.120	0.432	0.097	0.190	0.847	0.968
		JHH	35.355	37.091	31.727	38.786	34.811	34.007	34.900	34.254	33.377	35.597	35.600	35.484	34.893	36.541	32.051	33.976	35.717	36.369	35.470	37.363	35.168	1.693						
	mandible-area (mm^2)	TLC	38.790	39.041	36.311	42.136	37.261	37.697	35.716	37.993	30.958	38.593	37.426	34.905	37.568	40.078	34.153	32.613	38.278	38.698	38.748	42.800	37.488	2.853	-0.016	0.391	0.087	0.171	0.766	0.991
		JHH	39.036	38.936	35.614	42.248	37.410	38.181	35.729	38.110	30.760	38.474	37.502	35.103	37.447	38.831	34.326	33.035	38.430	38.816	39.011	43.091	37.505	2.852						
LINGUAL	*overall-length* (mm)	TLC	12.608	12.570	10.778	13.591	12.369	12.633	11.973	12.319	12.290	12.528	12.057	12.349	12.405	12.776	11.684	12.263	12.322	12.280	12.572	13.030	12.370	0.544	-0.029	0.108	0.024	0.047	0.217	0.981
		JHH	12.800	12.811	10.756	13.643	12.347	12.647	12.057	12.356	12.011	12.627	12.082	12.320	12.557	12.744	11.714	12.264	12.274	12.217	12.642	13.110	12.399	0.576						
	ascending-height (mm)	TLC	6.496	6.609	4.729	6.556	6.044	6.322	5.985	6.486	4.383	6.531	6.090	6.215	6.504	6.510	6.092	5.830	6.053	6.690	6.494	6.821	6.172	0.615	0.060	0.178	0.040	0.078	0.349	0.957
		JHH	6.240	6.543	4.773	6.565	5.646	6.047	5.970	6.497	4.346	6.580	6.035	6.278	6.557	6.779	5.581	5.877	5.973	6.710	6.405	6.842	6.112	0.646						
	basal-length (mm)	TLC	7.307	7.496	6.053	7.583	7.587	7.445	7.093	7.447	6.387	7.476	7.161	7.155	7.645	7.828	7.022	7.035	6.998	7.407	7.676	7.872	7.284	0.451	-0.055	0.161	0.036	0.071	0.316	0.927
		JHH	7.399	7.555	6.237	7.591	7.400	7.340	6.961	7.340	6.899	7.606	7.067	7.113	7.572	8.083	7.071	7.128	7.078	7.484	7.808	8.045	7.339	0.423						
	mandible-angle (°)	TLC	52.699	64.529	84.736	67.080	50.043	50.054	63.624	51.818	49.858	61.100	63.908	62.161	53.630	63.423	47.367	51.059	68.011	59.830	56.811	63.997	59.287	8.915	-0.502	2.106	0.471	0.923	4.128	0.970
		JHH	51.880	63.544	83.934	67.223	57.455	53.503	63.811	51.712	49.290	61.266	63.902	62.045	52.247	61.884	51.212	51.436	68.536	60.268	56.953	63.683	59.789	8.209						
	coronoid-coronoid-length (mm)	TLC	4.408	2.940	3.236	2.913	3.940	4.119	2.828	4.206	3.265	3.322	3.157	3.200	3.770	2.943	4.101	3.814	2.977	3.532	3.738	3.621	3.501	0.490	0.041	0.247	0.055	0.108	0.484	0.829
		JHH	4.206	2.721	3.305	2.963	3.290	3.816	3.104	4.307	3.207	3.407	3.209	3.175	3.974	3.319	3.598	3.816	2.893	3.670	3.596	3.623	3.460	0.425						
	diagonal-length (mm)	TLC	9.157	8.834	8.744	9.154	8.975	8.943	8.427	9.006	8.986	8.837	8.860	8.449	8.881	9.070	8.241	8.387	8.587	8.902	9.004	9.487	8.846	0.303	0.030	0.197	0.044	0.086	0.386	0.820
		JHH	8.910	8.652	8.835	9.132	8.917	8.781	8.374	8.905	8.315	8.900	8.738	8.407	8.893	9.260	8.296	8.612	8.678	9.018	9.060	9.638	8.816	0.332						
	mandible-perimeter (mm)	TLC	35.635	38.731	33.962	40.856	35.537	33.000	35.620	34.306	33.469	37.788	35.877	36.252	36.940	38.930	33.405	35.199	37.302	34.720	36.915	39.659	36.205	2.186	-0.347	0.875	0.196	0.384	1.715	0.899
		JHH	35.921	38.432	33.446	40.911	36.560	35.953	36.394	36.199	34.109	36.877	36.297	36.806	37.184	38.125	33.581	35.236	37.591	34.871	36.891	39.663	36.552	1.870						
	mandible-area (mm^2)	TLC	38.227	38.973	35.786	42.935	37.386	38.754	35.322	38.586	30.928	38.537	36.590	35.283	37.726	40.962	33.289	32.831	37.694	39.217	38.651	43.692	37.568	3.136	0.122	0.364	0.081	0.159	0.713	0.993
		JHH	38.750	38.698	35.805	42.270	37.262	38.743	35.992	38.250	31.120	38.183	36.058	34.938	37.629	40.716	32.815	33.045	37.038	39.040	38.919	43.663	37.447	3.057						

Table 6. 2D *right* Mandible Morphometry Inter-Operator Reproducibility (TLC & JHH)

HEMI-MANDIBLES			CD-1 RELIABILITY																												
			INTER-OPERATOR $n = 20$																							Statistics						
VIEW/ ASPECT	MEASUREMENT VARIABLE	OPERATOR	1	2	3	4	5	6	7	8	9	10	11	12	13	14	15	16	17	18	19	20	Mean	SD	Mean Dif.	SD. Dif.	SE	Bias	LOA	ICC
RIGHT BUCCAL	*overall-length* (mm)	TLC	12.148	12.447	12.490	13.052	12.532	12.717	12.040	12.340	12.335	12.717	12.270	12.004	12.258	12.794	12.385	12.016	12.378	12.393	12.763	12.718	12.440	0.286	-0.067	0.133	0.030	0.059	0.226	0.888
		JHH	12.025	12.504	12.984	13.141	12.536	12.756	12.008	12.424	12.143	12.791	12.381	12.060	12.401	12.833	12.602	12.108	12.414	12.430	12.796	12.801	12.507	0.331						
	ascending-height (mm)	TLC	6.064	6.733	6.225	6.410	6.089	6.339	6.394	6.668	6.656	6.209	5.941	6.194	6.355	6.804	6.044	5.965	6.425	6.611	6.381	6.980	6.374	0.293	0.051	0.163	0.036	0.071	0.319	0.829
		JHH	6.002	6.488	6.363	6.428	5.864	6.202	6.101	6.652	6.301	6.477	5.990	6.108	6.529	6.787	6.063	6.083	6.308	6.402	6.406	6.900	6.323	0.275						
	basal-length (mm)	TLC	7.183	7.618	7.467	7.650	7.362	7.302	7.263	7.574	7.600	7.697	7.306	7.226	7.376	8.084	7.250	7.031	7.338	7.417	8.242	7.309	7.465	0.295	0.031	0.097	0.022	0.043	0.190	0.948
		JHH	7.245	7.700	7.455	7.657	7.427	7.362	7.194	7.511	7.533	7.671	7.142	6.978	7.223	7.987	7.075	7.013	7.363	7.444	8.297	7.399	7.434	0.324						
	mandible-angle (°)	TLC	55.916	40.705	66.656	68.684	47.242	59.636	48.229	44.986	44.918	67.625	63.748	64.802	58.640	63.063	64.330	63.185	51.171	64.157	63.394	65.984	58.354	8.846	-0.379	1.717	0.384	0.753	3.365	0.979
		JHH	58.111	41.828	66.112	68.384	48.351	60.224	49.780	49.786	45.635	64.048	64.362	62.811	58.390	63.356	65.491	61.600	52.927	64.688	62.789	65.974	58.732	7.832						
	coronoid-coronoid-length (mm)	TLC	3.757	4.868	2.807	2.601	4.027	3.343	4.439	4.749	2.971	2.471	3.070	3.150	3.625	3.141	2.776	3.088	4.467	3.156	2.835	3.292	3.432	0.722	0.093	0.366	0.082	0.161	0.717	0.840
		JHH	3.311	4.863	2.766	2.601	3.899	3.196	4.063	3.800	3.863	2.909	3.112	3.005	3.554	3.139	2.571	3.203	3.897	3.056	2.862	3.105	3.339	0.574						
	diagonal-length (mm)	TLC	8.794	8.839	8.982	9.114	8.737	8.748	8.683	8.964	9.218	8.845	8.790	8.657	8.939	9.542	8.502	8.530	8.845	8.977	9.176	8.739	8.881	0.247	0.066	0.126	0.028	0.055	0.247	0.846
		JHH	8.865	8.989	8.981	9.152	8.796	8.762	8.617	8.960	8.804	8.771	8.766	8.391	8.858	9.373	8.320	8.454	8.814	8.845	9.111	8.664	8.815	0.254						
	mandible-perimeter (mm)	TLC	33.990	33.600	35.270	37.748	34.302	35.301	34.523	36.427	33.597	36.979	34.899	35.035	35.221	36.160	36.107	35.035	35.223	35.967	36.789	37.001	35.459	1.169	-0.027	0.773	0.173	0.339	1.515	0.827
		JHH	33.700	33.711	37.255	37.783	34.520	34.920	33.542	34.290	33.183	37.121	35.683	35.597	35.156	36.590	36.007	34.896	35.389	36.361	36.736	37.265	35.485	1.390						
	mandible-area (mm^2)	TLC	36.882	36.938	38.924	42.154	36.529	39.857	35.788	37.841	37.454	39.928	37.701	34.767	37.828	40.792	35.347	34.955	37.974	39.581	39.623	41.766	38.131	2.160	-0.106	0.993	0.222	0.435	1.946	0.907
		JHH	36.763	36.839	41.266	42.151	37.163	40.380	35.491	37.828	34.324	40.143	37.935	35.128	37.607	40.647	36.836	35.134	38.163	39.204	39.579	42.162	38.237	2.370						
RIGHT LINGUAL	*overall-length* (mm)	TLC	12.158	12.507	12.518	12.949	12.549	12.549	11.982	12.272	12.313	12.507	12.210	12.094	12.461	12.295	12.511	11.894	12.385	12.410	12.780	12.718	12.403	0.261	-0.039	0.121	0.027	0.053	0.237	0.904
		JHH	12.251	12.529	12.572	13.023	12.557	12.697	12.040	12.340	12.186	12.466	12.200	12.129	12.289	12.745	12.487	11.954	12.385	12.395	12.832	12.773	12.443	0.280						
	ascending-height (mm)	TLC	6.140	6.817	6.374	6.466	6.032	6.378	6.452	6.648	6.647	6.206	5.949	6.161	6.512	6.927	6.137	5.971	6.533	6.473	6.402	6.980	6.410	0.300	0.086	0.162	0.036	0.071	0.318	0.830
		JHH	6.164	6.684	6.362	6.470	5.931	6.231	6.140	6.652	6.592	6.196	5.956	6.046	6.308	6.893	6.109	6.021	5.902	6.504	6.506	6.825	6.325	0.303						
	basal-length (mm)	TLC	7.186	7.601	7.679	7.572	7.543	7.344	7.012	7.526	7.573	7.737	7.102	7.128	7.660	7.316	7.260	7.038	7.324	7.363	8.189	7.309	7.423	0.285	0.008	0.135	0.302	0.592	0.265	0.870
		JHH	7.258	7.640	7.640	7.567	7.474	7.418	7.183	7.474	7.504	7.644	7.075	7.226	7.253	7.590	7.170	6.983	7.345	7.433	8.068	7.361	7.415	0.247						
	mandible-angle (°)	TLC	55.820	40.300	64.390	67.720	47.320	58.420	47.540	44.570	44.790	66.780	63.900	64.380	52.970	63.140	65.327	61.550	50.930	63.480	62.560	65.084	57.549	8.734	-0.570	1.967	0.440	0.862	3.855	0.972
		JHH	56.690	39.989	62.575	67.482	47.582	59.001	50.131	51.719	47.766	67.100	64.250	64.904	52.495	61.927	64.367	61.546	52.696	63.802	61.030	65.315	58.118	7.764						
	coronoid-coronoid-length (mm)	TLC	3.909	4.731	3.086	2.630	4.037	3.341	4.358	4.807	3.147	2.538	3.035	2.941	3.846	3.653	2.731	3.224	4.537	3.147	3.102	3.292	3.505	0.694	-0.007	0.336	0.075	0.147	0.659	0.875
		JHH	3.887	5.258	3.553	2.674	4.083	3.401	4.012	3.950	3.773	2.526	3.153	3.160	3.675	3.292	2.717	3.212	4.156	3.245	3.251	3.257	3.512	0.623						
	diagonal-length (mm)	TLC	8.846	8.788	9.183	9.167	8.924	8.767	8.457	9.002	9.298	8.944	8.633	8.628	8.798	8.942	8.549	8.518	8.936	8.866	9.152	8.739	8.857	0.233	-0.017	0.144	0.032	0.063	0.282	0.836
		JHH	8.923	8.774	9.016	9.124	8.836	8.832	8.608	9.247	9.308	8.835	8.690	8.737	8.737	9.370	8.364	8.467	8.883	8.930	9.038	8.763	8.874	0.260						
	mandible-perimeter (mm)	TLC	35.482	36.005	37.812	38.808	36.358	36.492	35.619	35.453	35.483	37.877	35.547	35.664	36.519	36.702	34.746	35.869	36.723	36.775	38.021	37.001	36.448	1.049	0.016	0.743	0.166	0.325	1.456	0.838
		JHH	35.879	35.532	38.171	39.130	35.288	35.865	35.635	35.655	34.296	37.673	35.219	35.657	35.928	37.543	34.501	35.422	36.520	37.052	38.384	39.279	36.431	1.469						
	mandible-area (mm^2)	TLC	37.449	36.772	39.598	40.862	36.303	38.561	35.062	37.372	37.544	38.714	36.834	34.591	37.416	40.305	36.074	34.183	38.106	38.645	39.082	41.766	37.762	2.014	0.248	1.175	0.263	0.263	2.303	0.857
		JHH	37.348	36.982	40.158	40.442	36.710	38.443	35.507	37.947	32.587	38.562	36.212	34.690	37.112	40.966	35.486	33.810	38.336	38.589	39.008	41.390	37.514	2.358						

Table 7. 2D Incisor Morphometry Intra-Operator Repeatability (TLC)

MANDIBULAR INCISORS			CD-I RELIABILITY																											
			INTRA-OPERATOR (TLC)																					Statistics						
VIEW/ ASPECT	MEASUREMENT VARIABLE	REPEAT	$n = 20$																					Mean	SD	Mean Dif.	SD. Dif.	SE	Bias	CR	ICC
			1	2	3	4	5	6	7	8	9	10	11	12	13	14	15	16	17	18	19	20								
LEFT	BUCCAL *overall-length* (mm)	1	10.544	10.818	11.077	7.942	10.628	11.581	10.920	10.919	10.902	10.214	10.488	10.730	10.263	10.546	10.017	10.266	10.668	11.293	10.746	8.079	10.432	0.907	0.087	0.387	0.087	0.171	0.759	0.908
		2	10.646	10.777	11.064	7.793	10.659	10.975	10.315	10.908	10.121	10.570	10.719	10.184	10.512	11.395	9.915	10.249	10.743	10.742	10.539	8.073	10.345	0.895						
		1	112.040	113.920	116.220	127.230	116.000	115.750	114.520	115.390	115.710	114.810	112.790	115.410	115.810	116.870	115.120	115.040	113.290	114.210	113.130	135.160	116.421	5.360	0.166	1.496	0.335	0.657	2.932	0.963
	angle-of-curvature (°)	2	112.600	113.800	115.490	126.570	117.180	115.830	114.190	115.640	114.210	113.200	115.890	115.530	116.220	112.080	116.330	115.020	113.280	114.430	112.120	135.490	116.255	5.450						
		1	1.070	1.028	1.054	1.052	1.040	1.127	1.082	1.066	1.066	1.054	1.079	1.037	1.021	1.018	1.036	0.993	1.042	1.153	1.093	1.081	1.060	0.037	0.014	0.035	0.008	0.016	0.069	1.000
	BUCCAL *width-at-midpoint* (mm)	2	1.089	1.040	1.024	1.055	1.022	1.042	1.005	1.071	1.022	1.072	1.027	1.016	1.055	1.025	1.056	0.989	1.056	1.089	1.077	1.087	1.046	0.029						
		1	25.472	26.754	27.098	19.316	25.118	28.206	26.762	26.811	26.848	25.287	26.003	26.464	25.026	25.653	24.225	25.224	25.888	28.120	26.165	17.753	25.410	2.570	0.116	1.058	0.237	0.116	2.074	0.918
	incisor-perimeter (mm)	2	25.510	26.729	27.216	19.259	25.040	26.815	25.651	26.956	24.800	26.011	26.484	25.308	25.731	28.656	24.245	25.121	26.016	26.547	26.089	17.692	25.294	2.542						
		1	11.466	12.077	12.007	8.825	10.820	13.748	12.695	12.340	12.386	11.236	11.981	11.917	11.083	11.548	10.761	10.938	11.840	13.843	12.646	8.301	11.623	1.348	0.166	0.741	0.166	0.325	1.452	0.829
	incisor-area (mm^2)	2	11.510	12.111	11.975	8.886	10.792	12.388	11.487	12.366	11.107	12.029	11.965	11.073	11.565	13.136	10.622	10.882	11.899	12.463	12.581	8.308	11.457	1.182						
	LINGUAL *overall-length* (mm)	1	10.541	10.844	11.070	7.881	10.596	11.041	10.918	10.920	10.901	10.282	10.611	10.750	10.330	11.418	10.082	10.358	10.611	10.743	10.866	8.082	10.442	0.897	0.063	0.275	0.061	0.120	0.539	0.948
		2	10.615	10.841	11.014	7.941	10.649	11.011	10.427	10.913	10.140	10.560	10.725	10.162	10.495	11.340	9.967	10.280	10.580	10.756	10.689	8.476	10.379	0.816						
		1	112.430	113.910	115.800	127.210	116.640	116.500	114.450	115.440	115.480	115.570	113.140	115.900	116.200	111.740	115.540	114.820	112.900	114.290	114.470	136.410	116.442	5.630	0.071	0.981	0.219	0.429	1.923	0.958
	angle-of-curvature (°)	2	112.790	113.960	115.190	127.620	117.070	116.120	114.830	115.580	114.210	113.560	115.650	115.650	116.770	111.610	116.000	115.450	112.530	114.700	112.800	135.330	116.371	5.512						
		1	1.090	1.038	1.037	1.051	1.020	1.039	1.075	1.069	1.055	1.053	1.097	1.008	1.022	1.040	1.071	1.030	1.063	1.087	1.073	1.073	1.055	0.025	0.000	0.024	0.005	0.010	0.047	1.000
	LINGUAL *width-at-midpoint* (mm)	2	1.095	1.038	1.064	1.056	1.026	1.043	1.039	1.088	1.071	1.087	1.038	1.023	1.022	1.056	1.038	1.005	1.071	1.090	1.090	1.044	1.054	0.027						
		1	25.315	26.648	27.240	19.320	25.012	26.826	26.779	26.786	26.842	25.371	25.951	26.415	25.204	28.599	24.250	25.299	25.958	26.713	26.143	17.693	25.418	2.564	0.179	0.667	0.149	0.292	1.307	0.965
	incisor-perimeter (mm)	2	25.449	26.719	27.155	19.286	24.975	26.778	25.377	26.782	24.611	26.014	26.484	25.405	25.742	28.355	24.218	25.113	26.001	26.606	26.078	17.634	25.239	2.521						
		1	11.426	12.201	11.923	8.903	10.786	12.430	12.757	12.351	12.487	11.308	12.035	12.011	11.104	13.220	10.848	10.980	11.860	12.493	12.775	8.362	11.613	1.231	0.103	0.490	0.110	0.216	0.960	0.920
	incisor-area (mm^2)	2	11.544	12.143	12.061	8.874	10.919	12.414	11.526	12.455	11.255	12.107	12.062	11.148	11.577	13.209	10.858	10.849	11.908	12.465	12.631	8.204	11.510	1.205						
		1	11.547	10.379	10.607	10.503	10.532	11.284	11.553	10.444	10.547	9.357	10.065	12.057	10.795	11.268	10.107	11.785	10.960	10.076	9.559	8.440	10.593	0.877	-0.048	0.249	0.056	0.109	0.488	0.961
	labial-length (mm)	2	11.490	10.406	10.506	10.491	10.493	11.243	11.613	11.183	11.230	9.392	10.102	12.042	10.380	11.222	10.164	11.864	10.956	10.075	9.525	8.439	10.641	0.896						
RIGHT	BUCCAL *overall-length* (mm)	1	10.825	9.695	10.371	10.883	8.791	10.320	9.951	10.426	9.573	10.467	9.645	9.475	10.234	10.298	8.030	10.470	9.752	10.223	9.775	9.263	9.923	0.691	0.043	0.334	0.075	0.147	0.655	0.890
		2	10.344	9.294	10.536	10.906	8.846	9.542	10.003	9.764	9.578	10.538	9.662	9.496	10.180	10.370	8.068	10.463	9.703	11.010	9.979	9.326	9.880	0.709						
		1	116.200	119.280	119.140	120.590	123.550	124.840	114.950	121.220	121.340	116.050	124.800	121.280	123.950	122.190	129.490	119.180	122.990	123.020	119.150	123.880	121.355	3.475	0.200	2.388	0.534	1.047	4.681	0.826
	angle-of-curvature (°)	2	116.540	118.955	122.000	120.630	124.510	129.980	114.380	121.340	121.980	116.360	124.420	122.200	124.830	119.610	129.070	118.890	121.580	117.990	113.150	124.670	121.154	4.401						
		1	1.116	1.045	1.030	0.982	1.027	1.115	1.032	1.169	1.044	1.047	1.008	1.030	1.030	1.025	0.996	0.998	1.014	1.046	1.024	1.094	1.043	0.046	0.003	0.038	0.009	0.018	0.074	1.000
	BUCCAL *width-at-midpoint* (mm)	2	1.056	1.026	1.039	0.982	1.047	1.054	1.036	1.087	1.053	1.054	1.006	1.004	0.994	1.040	1.008	0.992	1.073	1.129	1.015	1.108	1.040	0.039						
		1	26.554	23.014	24.943	25.409	19.663	23.221	23.846	24.101	22.609	25.128	24.565	21.796	23.268	24.462	19.105	24.552	24.826	25.429	23.429	21.855	23.589	1.885	0.250	0.690	0.154	0.301	1.352	0.928
	incisor-perimeter (mm)	2	25.195	22.078	24.806	25.343	19.830	22.057	23.920	22.858	22.609	25.279	24.614	21.739	23.372	24.371	19.159	24.524	23.123	26.718	23.430	21.749	23.339	1.894						
		1	12.844	10.120	11.129	11.279	7.884	11.013	10.526	11.694	10.046	11.616	10.570	9.632	10.319	10.957	8.016	10.877	10.697	11.454	10.700	10.235	10.580	1.144	0.119	0.559	0.125	0.245	1.096	0.879
	incisor-area (mm^2)	2	11.695	9.615	11.052	11.413	8.098	9.987	10.626	10.561	10.092	11.743	10.536	9.531	10.318	10.891	8.065	10.910	10.187	12.842	10.711	10.349	10.461	1.123						
		1	10.338	9.427	10.658	10.819	8.823	9.804	10.594	9.748	10.086	10.643	9.683	9.435	10.109	10.324	8.030	10.461	9.732	10.285	9.673	9.170	9.892	0.694	0.013	0.254	0.057	0.112	0.498	0.935
	overall-length (mm)	2	10.330	9.310	10.477	10.856	8.861	9.550	9.958	9.724	9.615	11.217	9.703	9.444	10.217	10.373	8.310	10.434	9.689	10.484	9.717	9.314	9.879	0.687						
		1	117.800	119.330	119.100	120.290	123.670	124.740	114.640	125.320	121.280	118.070	124.180	120.670	121.460	122.620	128.640	118.760	122.760	122.450	124.870	127.110	121.888	3.435	-0.109	2.241	0.501	0.982	4.392	0.834
	angle-of-curvature (°)	2	116.860	119.047	122.470	121.150	124.180	130.140	114.070	127.360	122.470	118.180	124.240	121.160	123.050	118.960	129.250	118.410	123.020	117.570	123.350	125.010	121.997	4.146						
		1	1.065	1.016	1.051	1.005	1.045	1.038	1.150	1.104	1.093	1.068	1.018	1.028	1.011	1.053	1.012	1.023	1.072	1.065	1.049	1.104	1.053	0.038	0.008	0.037	0.008	0.016	0.073	1.000
	LINGUAL *width-at-midpoint* (mm)	2	1.074	1.007	1.047	0.952	1.008	1.056	1.240	1.089	1.039	1.131	1.038	1.020	1.005	1.041	1.026	0.974	1.027	1.046	1.004	1.089	1.046	0.061						
		1	25.458	22.006	25.077	25.397	19.575	22.158	25.494	22.853	23.820	25.184	24.493	21.790	23.286	24.413	19.174	24.499	23.551	25.386	23.386	21.671	23.434	1.892	0.072	0.507	0.113	0.221	0.994	0.965
	incisor-perimeter (mm)	2	25.244	21.973	25.016	25.401	19.799	22.083	24.074	22.848	22.666	26.410	24.456	21.758	23.355	24.366	19.106	24.587	23.486	25.475	23.413	21.713	23.361	1.903						
		1	11.513	9.666	10.992	11.367	7.912	9.962	11.933	10.492	11.163	11.581	10.483	9.522	10.248	10.830	8.013	10.936	10.359	11.487	10.700	10.277	10.472	1.074	0.046	0.481	0.108	0.212	0.943	0.909
	incisor-area (mm^2)	2	11.666	9.609	10.966	11.324	8.021	9.919	10.731	10.505	10.058	12.885	10.494	9.487	10.230	10.892	7.953	10.900	10.302	11.583	10.709	10.281	10.426	1.137						
		1	12.189	11.144	10.901	12.055	9.015	10.375	10.969	11.217	9.353	12.072	11.672	9.966	9.836	12.326	8.844	10.931	11.114	10.549	9.568	10.484	10.729	1.055	-0.009	0.189	0.042	0.083	0.370	0.985
	labial-length (mm)	2	12.193	10.877	11.090	12.054	9.000	10.420	11.059	11.266	8.875	12.054	11.662	9.776	10.198	12.427	9.186	10.763	11.139	10.570	9.590	10.567	10.738	1.065						

Table 8. 2D Incisor Morphometry Intra-Operator Repeatability (JHH)

MANDIBULAR INCISORS			CD-1 RELIABILITY																											
			INTRA-OPERATOR (JHH)																						Statistics						
			n = 20																											
VIEW/ ASPECT	MEASUREMENT VARIABLE	REPEAT	1	2	3	4	5	6	7	8	9	10	11	12	13	14	15	16	17	18	19	20	Mean	SD	Mean Dif.	SD. Dif.	SE	Bias	CR	ICC
LEFT BUCCAL	*overall-length* (mm)	1	10.621	11.268	11.687	7.878	10.307	11.494	9.879	10.057	9.620	10.193	10.227	10.603	9.999	10.800	9.693	9.766	10.202	11.207	10.032	7.718	10.163	1.007	-0.011	0.168	0.038	0.074	0.329	0.987
		2	10.380	10.854	11.689	7.754	10.338	11.505	9.915	10.556	9.634	10.189	10.280	10.590	10.002	10.832	9.860	9.796	10.226	11.221	10.101	7.746	10.173	0.996						
	angle-of-curvature (°)	1	112.095	112.678	116.753	127.071	113.831	113.988	112.152	113.852	112.706	111.405	113.963	112.530	114.159	110.296	112.525	113.400	110.659	111.432	109.719	136.882	114.605	6.351	-0.340	0.694	0.155	0.304	1.360	0.993
		2	111.409	112.356	116.917	129.689	114.130	113.698	112.235	114.106	112.562	112.017	114.125	114.078	114.654	110.864	112.789	113.560	111.001	111.647	110.039	137.026	114.945	6.601						
	width-at-midpoint (mm)	1	1.073	1.022	1.059	1.071	1.053	1.054	0.987	1.057	1.040	1.068	1.014	1.004	1.065	1.019	1.067	1.002	1.050	1.070	1.097	1.098	1.049	0.031	-0.013	0.020	0.004	0.008	0.039	1.000
		2	1.082	1.017	1.065	1.073	1.058	1.039	1.036	1.073	1.075	1.108	1.046	1.041	1.031	1.043	1.060	1.014	1.057	1.082	1.103	1.120	1.061	0.029						
	incisor-perimeter (mm)	1	25.686	26.996	27.381	19.079	25.099	26.590	25.503	26.836	24.211	26.025	26.550	25.325	25.563	28.316	23.980	25.145	26.026	26.277	25.882	17.566	25.202	2.573	0.046	0.155	0.035	0.069	0.304	0.988
		2	25.324	26.867	27.175	18.798	25.021	26.486	25.603	26.616	24.277	26.081	26.623	25.232	25.514	28.513	24.094	24.956	25.947	26.284	26.050	17.655	25.156	2.584						
	incisor-area (mm^2)	1	11.594	12.209	12.064	8.917	10.866	12.249	11.532	12.413	10.977	12.001	11.950	11.094	11.458	12.971	10.724	10.795	11.823	12.277	12.379	8.157	11.423	1.170	-0.036	0.117	0.026	0.051	0.229	0.995
		2	11.387	12.187	12.029	8.855	10.811	12.168	11.660	12.395	11.115	12.114	12.139	11.205	11.573	13.073	10.560	10.723	11.937	12.389	12.552	8.291	11.458	1.189						
LINGUAL	*overall-length* (mm)	1	10.578	11.335	11.706	6.861	10.356	10.520	9.892	10.623	9.630	10.213	10.218	9.653	10.321	10.824	9.749	9.795	10.264	10.147	10.169	7.659	10.026	1.088	0.030	0.112	0.025	0.049	0.220	0.995
		2	10.461	10.925	11.541	6.826	10.339	10.557	9.924	10.588	9.631	10.237	10.210	9.562	10.245	10.922	9.841	9.826	10.293	10.208	10.127	7.643	9.995	1.061						
	angle-of-curvature (°)	1	111.417	114.659	116.668	126.612	114.023	113.596	112.246	114.055	112.725	112.021	114.143	114.048	114.365	110.608	113.079	113.026	111.023	111.078	110.015	135.989	114.770	6.072	-0.134	1.809	0.405	0.794	3.546	0.955
		2	111.304	111.795	116.639	126.573	114.000	113.716	111.205	114.213	112.354	111.753	113.887	113.896	114.441	110.863	112.875	113.125	117.797	112.899	110.557	134.182	114.904	5.728						
	width-at-midpoint (mm)	1	1.072	1.040	1.066	1.071	1.036	1.055	1.021	1.053	1.050	1.068	1.034	1.002	1.073	1.024	1.059	0.972	1.051	1.097	1.067	1.072	1.049	0.029	-0.012	0.017	0.004	0.008	0.033	1.000
		2	1.088	1.047	1.049	1.068	1.026	1.058	1.040	1.075	1.065	1.120	1.048	1.024	1.054	1.046	1.073	0.993	1.069	1.095	1.097	1.086	1.061	0.029						
	incisor-perimeter (mm)	1	25.566	26.968	27.359	19.172	25.104	26.751	25.547	26.803	24.181	25.973	26.428	25.098	25.925	28.323	24.183	25.162	26.020	26.238	26.485	17.721	25.250	2.546	0.066	0.171	0.038	0.074	0.335	0.991
		2	25.452	26.800	26.989	19.167	25.047	26.589	25.545	26.907	24.350	26.169	26.457	25.137	25.711	28.243	23.935	25.191	25.746	26.359	26.104	17.792	25.185	2.502						
	incisor-area (mm^2)	1	11.537	12.241	12.055	8.907	10.919	12.302	11.534	12.425	10.966	12.076	11.980	11.038	12.054	13.062	10.757	10.830	11.808	12.248	12.421	8.154	11.466	1.190	-0.059	0.134	0.030	0.059	0.263	0.993
		2	11.478	12.168	11.993	8.908	10.873	12.245	11.756	12.500	11.071	12.291	12.139	11.138	11.871	13.203	10.564	10.926	12.012	12.441	12.544	8.382	11.525	1.191						
RIGHT BUCCAL	*overall-length* (mm)	1	10.990	9.326	10.561	10.440	8.649	10.449	9.655	10.681	9.357	9.996	9.978	8.995	9.738	9.954	8.105	9.949	9.507	10.285	9.631	8.952	9.760	0.727	-0.037	0.050	0.110	0.216	0.098	0.996
		2	11.004	9.393	10.613	10.457	8.657	10.501	9.716	10.696	9.283	10.021	10.013	9.021	9.743	10.033	8.276	9.919	9.581	10.274	9.705	9.022	9.796	0.710						
	angle-of-curvature (°)	1	111.185	118.372	117.825	120.443	121.970	122.339	111.762	117.711	116.493	112.856	115.012	118.570	118.866	114.663	118.713	115.158	114.740	111.605	114.239	127.259	116.989	4.075	-0.051	0.360	0.080	0.157	0.706	0.996
		2	110.586	119.066	117.989	120.351	121.789	122.210	111.595	118.001	116.048	112.665	115.364	118.639	119.165	114.856	119.079	114.898	114.189	112.024	114.625	127.655	117.040	4.185						
	width-at-midpoint (mm)	1	1.052	1.018	1.018	1.001	1.021	1.041	1.035	1.089	1.025	1.021	1.015	0.997	1.016	1.035	0.998	0.982	1.039	1.073	1.039	1.071	1.029	0.027	-0.009	0.015	0.003	0.006	0.029	1.000
		2	1.056	1.011	1.025	0.985	1.030	1.054	1.043	1.091	0.998	1.052	1.020	1.022	1.041	1.038	1.022	1.007	1.055	1.069	1.050	1.089	1.038	0.028						
	incisor-perimeter (mm)	1	25.113	22.169	24.627	25.140	19.717	21.880	23.772	22.813	22.548	24.935	24.235	21.540	23.159	24.137	18.875	24.281	23.068	25.165	23.211	21.832	23.111	1.754	-0.144	0.161	0.036	0.071	0.316	0.992
		2	24.968	22.101	24.712	25.295	19.801	22.061	24.052	22.956	23.108	24.999	24.527	21.790	23.312	24.295	19.095	24.569	22.937	25.221	23.412	21.876	23.254	1.739						
	incisor-area (mm^2)	1	11.512	9.415	10.763	11.081	7.940	9.771	10.430	10.397	9.899	11.506	10.235	9.319	10.112	10.720	7.820	10.684	10.116	11.179	10.510	9.823	10.162	0.993	-0.174	0.074	0.017	0.033	0.145	0.982
		2	11.583	9.545	10.845	11.211	8.085	10.121	10.685	10.543	10.154	11.607	10.480	9.584	10.241	10.946	7.993	10.919	10.234	11.301	10.670	9.963	10.336	0.977						
LINGUAL	*overall-length* (mm)	1	10.083	9.336	10.611	10.687	8.652	9.576	9.668	9.657	9.253	9.913	9.960	9.124	9.621	9.981	8.150	9.887	9.476	10.331	9.609	8.980	9.628	0.617	0.017	0.248	0.055	0.108	0.486	0.925
		2	9.940	9.562	10.556	10.466	8.701	9.625	9.714	9.740	9.283	9.984	10.047	9.168	9.704	10.061	8.239	9.922	8.480	10.333	9.652	9.035	9.611	0.630						
	angle-of-curvature (°)	1	112.499	119.006	118.907	120.656	121.947	122.687	112.012	118.100	115.336	112.566	115.625	118.489	118.752	115.002	119.056	115.277	114.501	111.613	115.101	117.596	116.736	3.267	-0.040	0.360	0.080	0.157	0.706	0.994
		2	111.987	119.465	118.667	120.685	122.054	122.724	111.934	118.124	114.658	112.441	116.063	118.698	119.654	115.212	119.057	114.878	114.612	111.765	114.889	117.963	116.777	3.397						
	width-at-midpoint (mm)	1	1.050	1.018	1.069	1.011	1.030	1.037	1.041	1.086	1.031	1.039	0.999	1.013	1.011	1.023	1.033	0.989	1.031	1.047	0.998	1.076	1.032	0.026	-0.012	0.013	0.003	0.006	0.025	1.000
		2	1.059	1.045	1.060	0.992	1.038	1.059	1.049	1.102	1.032	1.071	1.025	1.026	1.008	1.038	1.040	1.008	1.055	1.056	1.023	1.095	1.044	0.027						
	incisor-perimeter (mm)	1	25.386	22.071	24.635	25.985	19.656	21.923	23.773	22.745	22.538	24.972	24.320	21.544	23.090	24.170	19.001	24.348	23.102	25.382	23.213	21.737	23.180	1.849	-0.036	0.184	0.041	0.080	0.361	0.995
		2	25.260	22.147	24.699	25.556	19.672	21.930	23.978	22.724	22.812	25.240	24.318	21.746	23.066	24.336	19.097	24.644	23.103	25.163	23.298	21.515	23.215	1.816						
	incisor-area (mm^2)	1	11.438	9.412	10.837	11.761	7.889	9.737	10.506	10.357	9.964	11.420	10.355	9.287	10.107	10.653	7.875	10.706	10.170	11.243	10.514	10.066	10.215	1.030	-0.162	0.093	0.021	0.041	0.182	0.984
		2	11.539	9.656	11.057	11.665	8.068	9.878	10.725	10.575	10.161	11.655	10.412	9.517	10.199	10.982	7.983	10.953	10.315	11.388	10.678	10.125	10.377	1.021						

Table 9. 2D Incisor Morphometry Inter-Operator Reproducibility (TLC & JHH)

MANDIBULAR INCISORS			CD-1 RELIABILITY																				Statistics							
			INTER-OPERATOR $n = 20$																											
VIEW/ ASPECT	MEASUREMENT VARIABLE	OPERATOR	1	2	3	4	5	6	7	8	9	10	11	12	13	14	15	16	17	18	19	20	Mean	SD	Mean Dif.	SD. Dif.	SE	Bias	LOA	ICC
LEFT BUCCAL	*overall-length* (mm)	TLC	10.544	10.818	11.077	7.942	10.628	11.581	10.920	10.919	10.902	10.214	10.488	10.730	10.263	10.546	10.017	10.266	10.668	11.293	10.746	8.079	10.432	0.907	0.270	0.467	0.104	0.203	0.915	0.852
		JHH	10.621	11.268	11.687	7.878	10.307	11.494	9.879	10.057	9.620	10.193	10.227	10.603	9.999	10.800	9.693	9.766	10.202	11.207	10.032	7.718	10.163	1.007						
	angle-of-curvature (°)	TLC	112.040	113.920	116.220	127.230	116.000	115.750	114.520	115.390	115.710	114.810	112.790	115.410	115.810	116.870	115.120	115.040	113.290	114.210	113.130	135.160	116.421	5.360	1.816	1.872	0.419	0.821	3.669	0.908
		JHH	112.095	112.678	116.753	127.071	113.831	113.988	112.152	113.852	112.706	111.405	113.963	112.530	114.159	110.296	112.525	113.400	110.659	111.432	109.719	136.882	114.605	6.351						
	width-at-midpoint (mm)	TLC	1.070	1.028	1.054	1.052	1.040	1.127	1.082	1.066	1.066	1.054	1.079	1.037	1.021	1.018	1.036	0.993	1.042	1.153	1.093	1.081	1.060	0.037	0.011	0.039	0.009	0.018	0.076	1.000
		JHH	1.073	1.022	1.059	1.071	1.053	1.054	0.987	1.057	1.040	1.068	1.014	1.004	1.065	1.019	1.067	1.002	1.050	1.070	1.097	1.098	1.049	0.031						
	incisor-perimeter (mm)	TLC	25.472	26.754	27.098	19.316	25.118	28.206	26.762	26.811	26.848	25.287	26.003	26.464	25.026	25.653	24.225	25.224	25.888	28.120	26.165	17.753	25.410	2.570	0.208	1.135	0.254	0.408	2.225	0.907
		JHH	25.686	26.996	27.381	19.079	25.099	26.590	25.503	26.836	24.211	26.025	26.550	25.325	25.563	28.316	23.980	25.145	26.026	26.277	25.882	17.566	25.202	2.573						
	incisor-area (mm^2)	TLC	11.466	12.077	12.007	8.825	10.820	13.748	12.695	12.340	12.386	11.236	11.981	11.917	11.083	11.548	10.761	10.938	11.840	13.843	12.646	8.301	11.623	1.348	0.200	0.755	0.169	0.331	1.480	0.818
		JHH	11.594	12.209	12.064	8.917	10.866	12.249	11.532	12.413	10.977	12.001	11.950	11.094	11.458	12.971	10.724	10.795	11.823	12.277	12.379	8.157	11.423	1.170						
LINGUAL	*overall-length* (mm)	TLC	10.541	10.844	11.070	7.881	10.596	11.041	10.918	10.920	10.901	10.282	10.611	10.750	10.330	11.418	10.082	10.358	10.611	10.743	10.866	8.082	10.442	0.897	0.417	0.491	0.110	0.216	0.962	0.812
		JHH	10.578	11.335	11.706	6.861	10.356	10.520	9.892	10.623	9.630	10.213	10.218	9.653	10.321	10.824	9.749	9.795	10.264	10.147	10.169	7.659	10.026	1.088						
	angle-of-curvature (°)	TLC	112.430	113.910	115.800	127.210	116.640	116.500	114.450	115.440	115.480	115.570	113.140	115.900	116.200	111.740	115.540	114.820	112.900	114.290	114.470	136.410	116.442	5.630	1.672	1.473	0.329	0.645	2.887	0.932
		JHH	111.417	114.659	116.668	126.612	114.023	113.596	112.246	114.055	112.725	112.021	114.143	114.048	114.365	110.608	113.079	113.026	111.023	111.078	110.015	135.989	114.770	6.072						
	width-at-midpoint (mm)	TLC	1.090	1.038	1.037	1.051	1.020	1.039	1.075	1.069	1.055	1.053	1.097	1.008	1.022	1.040	1.071	1.030	1.063	1.087	1.073	1.073	1.055	0.025	0.005	0.029	0.006	0.012	0.057	1.000
		JHH	1.072	1.040	1.066	1.071	1.036	1.055	1.021	1.053	1.050	1.068	1.034	1.002	1.073	1.024	1.059	0.972	1.051	1.097	1.067	1.072	1.049	0.029						
	incisor-perimeter (mm)	TLC	25.315	26.648	27.240	19.320	25.012	26.826	26.779	26.786	26.842	25.371	25.951	26.415	25.204	28.599	24.250	25.299	25.958	26.713	26.143	17.693	25.418	2.564	0.168	0.779	0.174	0.341	1.527	0.954
		JHH	25.566	26.968	27.359	19.172	25.104	26.751	25.547	26.803	24.181	25.973	26.428	25.098	25.925	28.323	24.183	25.162	26.020	26.238	26.485	17.721	25.250	2.546						
	incisor-area (mm^2)	TLC	11.426	12.201	11.923	8.903	10.786	12.430	12.757	12.351	12.487	11.308	12.035	12.011	11.104	13.220	10.848	10.980	11.860	12.493	12.775	8.362	11.613	1.231	0.147	0.570	0.033	0.065	0.288	0.887
		JHH	11.537	12.241	12.055	8.907	10.919	12.302	11.534	12.425	10.966	12.076	11.980	11.038	12.054	13.062	10.757	10.830	11.808	12.248	12.421	8.154	11.466	1.190						
RIGHT BUCCAL	*overall-length* (mm)	TLC	10.825	9.695	10.371	10.883	8.791	10.320	9.951	10.426	9.573	10.467	9.645	9.475	10.234	10.298	8.030	10.470	9.752	10.223	9.775	9.263	9.923	0.691	0.163	0.279	0.062	0.122	0.547	0.903
		JHH	10.990	9.326	10.561	10.440	8.649	10.449	9.655	10.681	9.357	9.996	9.978	8.995	9.738	9.954	8.105	9.949	9.507	10.285	9.631	8.952	9.760	0.727						
	angle-of-curvature (°)	TLC	116.200	119.280	119.140	120.590	123.550	124.840	114.950	121.220	121.340	116.050	124.800	121.280	123.950	122.190	129.490	119.180	122.990	123.020	119.150	123.880	121.355	3.475	1.865	2.511	0.561	1.100	4.922	0.768
		JHH	111.185	118.372	117.825	120.443	121.970	122.339	111.762	117.711	116.493	112.856	125.012	118.570	118.866	124.663	128.713	115.158	124.740	121.605	114.239	127.259	119.489	5.059						
	width-at-midpoint (mm)	TLC	1.116	1.045	1.030	0.982	1.027	1.115	1.032	1.169	1.044	1.047	1.008	1.030	1.030	1.025	0.996	0.998	1.014	1.046	1.024	1.094	1.043	0.046	0.014	0.031	0.007	0.014	0.061	1.000
		JHH	1.052	1.018	1.018	1.001	1.021	1.041	1.035	1.089	1.025	1.021	1.015	0.997	1.016	1.035	0.998	0.982	1.039	1.073	1.039	1.071	1.029	0.027						
	incisor-perimeter (mm)	TLC	26.554	23.014	24.943	25.409	19.663	23.221	23.846	24.101	22.609	25.128	24.565	21.796	23.268	24.462	19.105	24.552	24.826	25.429	23.429	21.855	23.589	1.885	0.478	0.539	0.027	0.053	1.056	0.926
		JHH	25.113	22.169	24.627	25.140	19.717	21.880	23.772	22.813	22.548	24.935	24.235	21.540	23.159	24.137	18.875	24.281	23.068	25.165	23.211	21.832	23.111	1.754						
	incisor-area (mm^2)	TLC	12.844	10.120	11.129	11.279	7.884	11.013	10.526	11.694	10.046	11.616	10.570	9.632	10.319	10.957	8.016	10.877	10.697	11.454	10.700	10.235	10.580	1.144	0.419	0.411	0.092	0.180	0.806	0.864
		JHH	11.512	9.415	10.763	11.081	7.940	9.771	10.430	10.397	9.899	11.506	10.235	9.319	10.112	10.720	7.820	10.684	10.116	11.179	10.510	9.823	10.162	0.993						
LINGUAL	*overall-length* (mm)	TLC	10.338	9.427	10.658	10.819	8.823	9.804	10.594	9.748	10.086	10.643	9.683	9.435	10.109	10.324	8.030	10.461	9.732	10.285	9.673	9.170	9.892	0.694	0.264	0.312	0.070	0.137	0.612	0.824
		JHH	10.083	9.336	10.611	10.687	8.652	9.576	9.668	9.657	9.253	9.913	9.960	9.124	9.621	9.981	8.150	9.887	9.476	10.331	9.609	8.980	9.628	0.617						
	angle-of-curvature (°)	TLC	117.800	119.330	119.100	120.290	123.670	124.740	114.640	125.320	121.280	118.070	124.180	120.670	121.460	122.620	128.640	118.760	122.760	122.450	124.870	127.110	121.888	3.435	1.152	2.570	0.575	0.575	5.037	0.815
		JHH	112.499	119.006	118.907	120.656	121.947	122.687	112.012	128.100	115.336	112.566	125.625	118.489	118.752	125.002	129.056	115.277	124.501	121.613	125.101	127.596	120.736	5.316						
	width-at-midpoint (mm)	TLC	1.065	1.016	1.051	1.005	1.045	1.038	1.150	1.104	1.093	1.068	1.018	1.028	1.011	1.053	1.012	1.023	1.072	1.065	1.049	1.104	1.053	0.038	0.022	0.030	0.007	0.014	0.059	1.000
		JHH	1.050	1.018	1.069	1.011	1.030	1.037	1.041	1.086	1.031	1.039	0.999	1.013	1.011	1.023	1.033	0.989	1.031	1.047	0.998	1.076	1.032	0.026						
	incisor-perimeter (mm)	TLC	25.458	22.006	25.077	25.397	19.575	22.158	25.494	22.853	23.820	25.184	24.493	21.790	23.286	24.413	19.174	24.499	23.551	25.386	23.386	21.671	23.434	1.892	0.254	0.485	0.108	0.212	0.951	0.959
		JHH	25.386	22.071	24.635	25.985	19.656	21.923	23.773	22.745	22.538	24.972	24.320	21.544	23.090	24.170	19.001	24.348	23.102	25.382	23.213	21.737	23.180	1.849						
	incisor-area (mm^2)	TLC	11.513	9.666	10.992	11.367	7.912	9.962	11.933	10.492	11.163	11.581	10.483	9.522	10.248	10.830	8.013	10.936	10.359	11.487	10.700	10.277	10.472	1.074	0.257	0.389	0.087	0.171	0.762	0.908
		JHH	11.438	9.412	10.837	11.761	7.889	9.737	10.506	10.357	9.964	11.420	10.355	9.287	10.107	10.653	7.875	10.706	10.170	11.243	10.514	10.066	10.215	1.030						

Table 10. Reliability Colour and Whiteness Assessment Intra-Operator Repeatability (TLC) *non-polarised*

COLOUR AND WHITENESS (non-polarised)			CD-1 RELIABILITY																											
			INTRA-OPERATOR (TLC)																				Statistics							
REGION/ STAGE	COLOUR COMPONENT	REPEAT	*n* = 20																				Mean	SD	Mean Dif.	SD. Dif.	SE	Bias	CR	ICC
			1	2	3	4	5	6	7	8	9	10	11	12	13	14	15	16	17	18	19	20								
GINGIVAL / PRE-SECRETORY	*lightness*	1	72.411	71.188	74.747	75.335	70.211	72.938	71.082	71.773	65.202	70.880	66.098	71.020	74.100	71.796	74.866	66.101	65.317	68.336	67.239	68.890	70.477	3.238	-0.081	2.083	0.466	0.953	4.083	0.812
		2	72.296	70.409	75.408	75.487	69.411	73.862	71.623	71.859	69.662	69.406	72.819	70.777	72.772	71.083	74.864	63.879	64.503	67.172	65.546	68.314	70.558	3.401						
	red/ green	1	69.516	68.787	66.843	65.003	58.640	54.606	63.352	63.452	66.760	66.108	63.374	63.440	70.956	63.559	69.004	69.510	64.368	67.290	66.146	64.963	65.284	3.842	-0.219	1.453	0.33	0.637	2.848	0.925
		2	69.773	68.320	66.811	65.534	58.168	56.886	64.032	64.145	64.316	65.273	68.473	63.417	70.528	64.094	69.588	69.119	64.011	67.199	65.571	64.792	65.503	3.533						
	yellow/ blue	1	67.272	68.162	66.972	67.942	66.060	59.249	65.540	64.620	65.943	67.346	62.748	62.770	65.374	66.494	67.513	68.238	63.830	66.074	66.554	61.817	65.526	2.378	-0.296	1.592	0.356	0.698	3.120	0.731
		2	67.270	67.682	66.692	68.110	65.465	60.245	65.886	64.964	65.292	66.437	65.871	62.783	65.348	66.054	67.735	67.505	63.577	65.922	65.816	67.780	65.822	1.907						
	whiteness	1	69.747	69.442	69.941	69.765	64.949	62.368	66.875	66.903	65.663	67.914	64.187	66.046	70.410	67.468	70.882	67.474	64.470	67.310	66.293	65.412	67.176	2.328	-0.124	1.299	0.290	0.568	2.546	0.838
		2	69.855	68.920	69.330	70.111	64.452	63.929	67.331	67.336	66.564	67.405	69.109	65.917	69.748	67.576	70.992	66.367	63.969	66.828	65.502	64.763	67.300	2.151						
MIDDLE/ SECRETORY	*lightness*	1	2.710	3.440	1.770	0.700	2.440	1.750	2.170	1.300	3.580	5.670	-0.140	1.640	2.460	0.730	1.480	6.210	5.580	7.060	5.740	4.240	3.027	2.077	-0.057	0.246	0.055	0.108	0.482	0.993
		2	2.830	3.530	1.650	0.460	2.310	1.580	2.280	1.490	4.310	5.660	-0.340	1.490	2.410	0.800	1.570	6.830	5.660	7.030	5.730	4.390	3.084	2.183						
	red/ green	1	-1.660	-0.310	-1.190	0.100	0.990	2.690	-0.730	-1.000	1.510	0.420	-2.330	-2.120	-2.910	-1.560	-1.550	0.670	0.680	-0.310	-0.040	2.320	-0.317	1.523	0.044	0.291	0.065	0.127	0.570	0.982
		2	-1.800	-0.280	-1.480	-0.450	0.700	2.440	-0.610	-0.840	1.040	0.110	-2.560	-2.270	-2.440	-1.210	-1.790	0.580	0.940	-0.100	0.210	2.600	-0.361	1.488						
	yellow/ blue	1	-5.170	-4.820	-4.180	-4.250	-3.760	-2.530	-4.870	-4.860	-3.730	-4.900	-4.880	-3.890	-5.130	-4.670	-4.110	-3.430	-3.990	-4.460	-3.960	-3.750	-4.267	0.666	0.012	0.319	0.071	0.139	0.624	0.880
		2	-4.620	-4.890	-4.260	-4.320	-3.960	-2.930	-4.810	-4.710	-4.310	-4.770	-4.470	-4.430	-5.250	-4.630	-3.640	-3.320	-4.160	-4.720	-4.090	-3.290	-4.279	0.598						
	whiteness	1	-1.110	-0.280	-0.980	-0.900	0.170	0.830	-0.910	-1.240	0.770	0.760	-2.280	-1.350	-1.620	-1.580	-1.120	1.610	1.330	1.440	0.980	1.160	-0.216	1.226	0.006	0.171	0.038	0.074	0.335	0.991
		2	-0.940	-0.250	-1.100	-1.180	-0.030	0.550	-0.820	-1.110	0.640	0.650	-2.290	-1.610	-1.540	-1.440	-1.020	1.860	1.230	1.460	1.040	1.450	-0.223	1.240						
INCISAL/ MATURE	*lightness*	1	3.910	2.620	3.930	3.290	2.200	3.680	2.540	4.240	4.980	5.290	3.800	2.520	3.720	5.560	2.210	8.760	5.340	7.230	6.520	8.140	4.524	1.939	0.253	0.498	0.111	0.218	0.976	0.960
		2	3.430	2.220	3.590	3.190	1.970	3.560	2.470	3.650	3.760	4.940	5.300	2.450	3.290	5.320	1.820	8.570	5.410	6.810	6.230	7.440	4.271	1.909						
	red/ green	1	10.140	9.530	8.170	8.790	12.330	5.290	9.920	13.640	2.610	3.090	9.650	15.150	11.750	11.100	5.970	9.080	4.560	5.650	6.510	4.410	8.367	3.516	0.120	0.535	0.120	0.235	1.049	0.988
		2	9.780	9.080	8.110	8.710	12.320	5.280	9.270	13.350	3.980	2.910	10.960	15.140	11.320	10.820	5.740	8.910	3.950	5.190	6.170	3.960	8.248	3.484						
	yellow/ blue	1	14.300	12.450	13.300	10.010	13.290	10.700	13.940	13.440	15.260	10.250	13.610	18.260	13.210	11.160	11.370	10.000	14.780	7.720	15.510	20.770	13.167	2.995	0.127	0.487	0.109	0.214	0.955	0.987
		2	13.020	12.130	13.060	9.960	13.090	11.130	13.810	13.000	15.160	10.020	14.750	18.690	13.480	11.160	10.640	9.930	14.700	7.490	15.420	20.160	13.040	3.010						
	whiteness	1	9.060	7.840	8.080	6.920	8.730	6.320	8.360	9.990	7.050	5.970	8.610	11.340	9.250	8.970	6.020	9.180	7.800	6.790	9.090	10.580	8.298	1.482	0.184	0.405	0.091	0.178	0.794	0.958
		2	8.350	7.440	7.820	6.840	8.520	6.380	8.110	9.550	7.100	5.740	9.900	11.410	9.050	8.810	5.600	9.030	7.520	6.390	8.810	9.910	8.114	1.517						
WHOLE/ ALL	*lightness*	1	76.450	81.560	75.940	78.170	83.450	77.210	81.920	75.380	73.670	71.480	78.330	82.050	76.820	70.370	82.160	58.350	72.170	64.340	67.190	60.710	74.386	7.211	-0.524	2.118	0.474	0.929	4.151	0.956
		2	77.950	82.960	76.770	78.240	84.260	77.160	81.750	77.240	77.180	72.650	70.840	82.040	78.390	70.980	83.340	58.490	71.460	65.560	68.000	62.950	74.911	7.143						
	red/ green	1	52.720	55.160	60.520	58.040	42.030	74.490	53.200	37.400	82.880	81.200	54.290	30.850	46.570	48.180	69.170	56.970	75.620	70.650	67.340	76.070	59.668	14.701	0.089	2.063	0.461	0.904	4.043	0.991
		2	53.570	56.330	60.170	57.700	41.000	73.310	55.270	38.020	77.510	81.710	48.700	29.980	47.570	48.690	69.540	57.060	77.720	72.020	68.230	77.470	59.579	14.727						
	yellow/ blue	1	35.410	43.180	39.490	53.040	39.350	49.230	36.410	38.230	31.120	51.970	36.940	16.950	39.400	48.170	47.480	53.110	32.370	62.330	30.300	5.480	39.498	12.974	0.277	1.281	0.286	0.561	2.511	0.995
		2	35.910	43.630	39.630	52.610	39.220	46.580	36.240	39.390	30.390	52.150	36.300	14.000	37.400	47.390	49.800	52.700	31.730	62.680	29.550	7.120	39.221	13.092						
	whiteness	1	57.010	61.820	60.840	65.380	58.270	68.550	59.760	53.160	65.190	69.280	58.690	47.530	56.270	57.280	68.760	56.530	62.170	66.090	56.870	50.730	60.009	5.994	-0.140	1.627	0.364	0.713	3.189	0.966
		2	59.250	62.870	61.330	65.150	58.500	67.530	60.190	54.340	64.330	69.760	53.010	46.480	56.450	57.360	69.910	56.490	62.720	67.220	57.330	52.750	60.149	6.167						

Table 11. Reliability Colour and Whiteness Assessment Intra-Operator Repeatability (TLC) *polarised*

COLOUR AND WHITENESS (polarised)			CD-1 RELIABILITY																										
			INTRA-OPERATOR (TLC) $n = 20$																					Statistics						
REGION/ STAGE	COLOUR COMPONENT	REPEAT	1	2	3	4	5	6	7	8	9	10	11	12	13	14	15	16	17	18	19	20	Mean	SD	Mean Dif.	SD. Dif.	SE	Bias	CR	ICC
GINGIVAL / PRE-SECRETORY	*lightness*	1	71.797	69.668	74.854	74.014	66.928	74.467	70.915	69.222	70.173	68.264	72.832	68.194	73.376	71.692	73.792	66.141	64.169	65.839	64.663	66.450	69.873	3.432	0.383	0.953	0.213	0.417	1.868	0.956
		2	71.688	69.267	73.357	73.358	67.768	73.860	70.768	69.286	70.156	67.071	72.181	69.087	73.267	71.445	74.117	62.869	63.235	66.746	64.808	65.451	69.489	3.557						
	red/ green	1	69.302	67.948	62.831	63.039	56.297	59.432	63.800	60.510	66.167	62.208	69.496	59.319	72.019	64.964	65.495	69.423	62.659	68.393	64.366	65.975	64.682	4.047	-0.402	0.571	0.128	0.251	1.119	0.985
		2	69.379	67.581	63.582	62.859	57.001	59.851	63.898	61.113	66.135	62.290	69.054	60.561	72.091	64.978	67.022	69.561	63.266	69.922	65.202	66.344	65.085	3.894						
	yellow/ blue	1	64.236	64.139	60.956	63.642	60.928	57.422	62.182	59.330	63.349	61.815	64.726	56.935	63.914	63.966	61.303	65.731	60.288	63.637	62.359	59.125	61.999	2.444	-0.253	0.641	0.143	0.280	1.256	0.960
		2	64.571	63.673	60.965	63.389	61.519	57.401	62.148	59.421	63.338	61.032	64.042	58.393	64.311	63.761	62.444	66.053	60.900	65.279	62.940	59.467	62.252	2.333						
	whiteness	1	68.645	67.464	66.625	67.644	61.571	64.160	65.957	63.329	66.942	64.363	69.308	61.843	70.063	66.918	67.398	66.129	62.442	65.991	64.158	64.065	65.751	2.428	-0.086	0.582	0.130	0.255	1.141	0.971
		2	68.766	67.207	66.423	67.086	62.273	64.050	65.963	63.708	66.790	63.586	68.846	63.065	70.177	66.789	68.293	65.498	62.459	67.370	64.354	64.039	65.837	2.301						
MIDDLE/ SECRETORY	*lightness*	1	3.300	3.500	1.600	0.290	2.450	1.630	2.790	1.340	5.050	5.840	-0.320	1.360	2.620	0.750	0.720	6.990	6.140	7.960	6.020	5.180	3.261	2.448	-0.049	0.306	0.068	0.133	0.600	0.993
		2	3.140	2.980	1.570	0.340	2.340	2.010	2.950	1.290	4.990	5.860	-0.470	1.390	2.440	0.890	0.580	7.970	6.590	8.220	6.060	5.050	3.310	2.589						
	red/ green	1	-2.140	0.080	-0.610	0.340	1.780	2.550	0.170	-0.530	1.610	1.010	-1.850	-1.390	-2.030	-0.930	-1.090	1.700	1.740	-0.100	0.430	2.990	0.187	1.531	0.035	0.161	0.036	0.071	0.316	0.994
		2	-2.150	-0.310	-0.640	0.220	1.550	2.570	0.090	-0.600	1.540	0.790	-2.010	-1.140	-1.910	-0.900	-1.190	1.970	1.780	-0.010	0.550	2.840	0.152	1.517						
	yellow/ blue	1	-5.280	-4.210	-3.830	-3.540	-3.580	-1.700	-3.830	-4.440	-3.090	-4.630	-3.760	-3.360	-4.700	-4.540	-2.890	-2.590	-3.460	-3.200	-3.510	-2.240	-3.619	0.879	0.080	0.213	0.048	0.094	0.417	0.970
		2	-5.430	-5.010	-3.910	-3.630	-3.550	-1.500	-3.890	-4.570	-3.010	-4.450	-3.800	-3.470	-4.690	-4.640	-3.100	-2.500	-3.440	-3.540	-3.470	-2.380	-3.699	0.948						
	whiteness	1	-1.110	0.070	-0.740	-0.790	0.480	0.940	-0.080	-0.950	1.390	1.140	-1.850	-1.030	-1.190	-1.300	-0.910	2.790	1.970	2.220	1.300	2.130	0.224	1.412	0.026	0.171	0.038	0.075	0.335	0.993
		2	-1.210	-0.500	-0.800	-0.810	0.380	1.140	-0.050	-1.050	1.530	1.160	-1.990	-0.970	-1.210	-1.280	-1.040	3.030	2.090	2.150	1.410	1.990	0.199	1.481						
INCISAL/ MATURE	*lightness*	1	4.010	3.240	3.950	3.500	2.550	4.250	2.890	4.470	4.910	5.380	6.290	2.920	3.960	6.440	2.070	8.790	5.430	8.340	6.790	8.640	4.941	2.035	-0.025	0.275	0.061	0.120	0.539	0.992
		2	4.090	3.610	4.070	3.280	2.610	3.920	2.790	4.440	4.550	5.240	6.320	2.610	3.920	6.300	2.360	9.520	5.890	8.450	6.800	8.550	4.966	2.117						
	red/ green	1	12.740	11.040	9.370	10.330	14.060	7.510	10.800	14.530	5.290	4.120	12.210	15.350	13.120	13.270	5.940	10.150	5.140	6.560	7.470	5.440	9.722	3.563	0.016	0.172	0.038	0.074	0.234	0.999
		2	12.600	11.310	9.210	10.270	14.130	7.340	10.900	14.860	5.560	3.890	12.310	15.410	12.960	13.260	6.010	10.140	4.870	6.460	7.300	5.330	9.706	3.634						
	yellow/ blue	1	17.430	15.180	15.480	10.900	15.450	13.890	15.870	14.920	17.990	11.230	16.650	18.760	16.320	13.640	12.170	11.530	16.280	7.650	17.800	24.010	15.158	3.502	-0.212	0.301	0.067	0.131	0.590	0.995
		2	17.500	16.100	15.800	10.950	15.590	13.770	15.990	15.170	18.060	11.110	16.670	19.540	16.390	13.710	12.880	11.340	16.490	8.120	17.870	24.330	15.369	3.546						
	whiteness	1	10.880	9.350	9.090	7.750	10.000	8.180	9.340	10.820	8.800	6.630	11.250	11.650	10.740	10.690	6.180	10.310	8.480	7.500	10.120	12.000	9.488	1.649	-0.034	0.164	0.036	0.071	0.321	0.995
		2	10.860	9.870	9.160	7.620	10.070	8.010	9.340	10.950	8.730	6.440	11.310	11.770	10.690	10.650	6.500	10.200	8.530	7.580	10.110	12.050	9.522	1.661						
WHOLE/ ALL	*lightness*	1	76.230	79.620	75.870	77.730	83.140	74.840	80.690	75.010	73.050	71.520	67.480	81.340	76.100	67.000	83.080	58.110	71.950	59.930	66.310	58.670	72.884	7.770	0.225	1.110	0.248	0.486	2.176	0.990
		2	75.830	78.170	75.590	78.600	82.530	76.070	80.970	74.980	74.310	72.130	67.300	82.200	76.180	67.420	81.810	54.850	70.010	59.330	66.070	58.830	72.659	8.113						
	red/ green	1	42.150	48.880	55.350	51.260	33.080	63.600	49.340	32.240	72.280	78.010	44.350	27.950	41.270	39.040	69.700	52.670	73.500	66.850	63.450	71.670	53.832	15.328	0.115	0.706	0.158	0.310	1.377	0.999
		2	42.560	47.530	55.850	51.300	32.720	64.090	48.720	30.730	70.990	78.780	43.670	28.020	41.730	38.900	69.050	52.560	74.370	66.940	63.930	71.910	53.718	15.558						
	yellow/ blue	1	20.630	30.360	27.800	48.710	27.950	33.890	26.610	29.540	18.050	46.920	24.380	10.510	25.300	36.910	42.740	46.390	23.920	62.660	18.290	-11.540	29.501	15.855	1.081	1.262	0.282	0.553	2.474	0.995
		2	20.230	25.870	26.120	48.240	27.320	34.170	25.810	28.170	17.520	47.090	23.740	7.630	24.960	36.290	39.680	47.050	23.020	60.400	18.040	-12.950	28.420	15.982						
	whiteness	1	49.550	55.680	56.660	62.140	52.580	60.480	55.650	49.130	57.930	66.990	48.120	45.290	50.260	50.090	68.480	51.770	59.230	63.240	52.310	44.450	55.002	6.851	0.327	0.688	0.154	0.301	1.348	0.994
		2	49.460	53.330	56.170	62.510	52.090	61.020	55.440	48.410	58.040	67.660	47.610	44.780	50.300	50.080	66.930	51.970	58.830	62.680	52.190	44.000	54.675	6.907						

Table 12. Reliability Colour and Whiteness Assessment Intra-Operator Repeatability (AS) *non-polarised*

COLOUR AND WHITENESS (non-polarised)			CD-1 RELIABILITY																											
			INTRA-OPERATOR (AS)																						Statistics						
REGION/ STAGE	COLOUR COMPONENT	REPEAT	$n = 20$																				Mean	SD	Mean Dif.	SD. Dif.	SE	Bias	CR	ICC
			1	2	3	4	5	6	7	8	9	10	11	12	13	14	15	16	17	18	19	20								
GINGIVAL / PRE-SECRETORY	*lightness*	1	72.256	65.392	71.953	62.982	56.923	72.460	70.329	63.693	68.679	68.909	61.530	73.884	71.798	68.780	67.467	67.076	67.076	60.067	66.428	65.235	67.146	4.505	1.417	4.756	1.063	2.083	9.322	0.563
		2	68.980	68.453	61.567	71.405	48.579	70.457	63.815	66.052	68.020	67.792	54.027	68.435	67.706	69.511	72.114	69.209	65.692	62.707	63.611	66.451	65.729	5.744						
	red/ green	1	67.954	64.800	60.516	63.789	54.485	65.521	64.227	63.252	71.014	66.433	62.854	64.932	68.494	65.516	64.449	68.719	68.719	68.728	65.520	66.190	65.306	3.568	2.766	2.705	0.605	1.186	5.390	0.568
		2	60.048	63.101	58.274	62.344	51.036	60.850	60.788	61.999	65.913	65.289	60.414	58.116	68.943	65.048	65.527	68.169	60.044	66.963	62.005	65.925	62.540	4.179						
	yellow/ blue	1	67.001	64.964	61.667	64.552	61.212	65.495	63.490	64.537	64.854	64.665	62.308	62.178	66.577	66.273	64.544	67.622	67.622	63.494	63.584	63.966	64.530	1.874	1.415	1.797	0.402	3.522	3.522	0.400
		2	63.200	64.955	62.023	64.225	58.779	60.903	62.076	63.791	63.237	63.807	61.929	60.872	64.623	65.715	65.209	67.373	60.984	62.418	62.134	64.052	63.115	2.005						
	whiteness	1	68.876	64.328	64.401	63.640	57.294	67.787	66.022	62.154	67.837	66.535	61.488	67.047	68.850	66.458	65.023	66.998	66.953	63.930	65.431	65.208	65.313	2.763	1.527	2.585	0.578	1.133	5.067	0.604
		2	64.116	65.487	60.736	66.173	52.260	64.041	62.379	63.946	65.801	65.648	58.845	62.682	67.587	66.815	67.814	68.130	62.361	63.310	62.167	65.421	63.786	3.644						
MIDDLE/ SECRETORY	*lightness*	1	-0.010	1.770	0.650	-0.340	1.670	0.640	0.580	0.110	3.090	3.440	-0.780	0.650	-1.450	-1.820	-0.520	4.650	3.720	7.690	4.630	2.730	1.555	2.411	0.685	1.184	0.265	0.519	2.321	0.836
		2	-1.310	0.310	0.480	-2.360	1.560	0.290	1.160	-1.480	2.020	2.310	-1.300	-0.580	0.040	-1.780	0.120	1.280	2.060	6.470	3.930	4.190	0.871	2.223						
	red/ green	1	-1.500	-0.540	-0.990	-0.550	1.200	0.880	-1.090	-1.210	0.010	-0.140	-2.060	-2.030	-1.940	-2.340	-1.610	0.490	0.460	0.870	0.410	2.140	-0.477	1.263	0.312	0.569	0.127	0.249	1.115	0.871
		2	-1.320	0.050	-1.480	-1.670	0.530	0.790	-0.550	-1.150	0.440	-0.440	-3.080	-1.810	-2.120	-2.590	-1.780	-1.030	-0.210	-0.030	-0.150	1.820	-0.789	1.230						
	yellow/ blue	1	-3.330	-3.250	-3.820	-3.260	-2.970	-3.150	-4.030	-4.360	-3.780	-4.370	-4.820	-4.480	-3.140	-4.640	-3.050	-3.480	-3.990	-3.090	-4.460	-2.400	-3.694	0.674	0.473	0.622	0.139	0.272	1.219	0.420
		2	-4.370	-3.520	-5.460	-4.380	-3.320	-3.960	-4.310	-4.260	-3.880	-4.440	-5.140	-3.750	-3.650	-5.720	-4.410	-3.250	-3.780	-4.120	-4.340	-3.270	-4.167	0.681						
	whiteness	1	-1.570	-0.490	-1.230	-1.320	0.090	-0.450	-1.460	-1.490	-0.180	-0.310	-2.340	-1.840	-2.140	-2.800	-1.610	0.870	0.190	2.090	0.290	0.860	-0.742	1.246	0.472	0.499	0.112	0.220	0.978	0.858
		2	-2.270	-0.890	-2.040	-2.710	-0.230	-0.800	-1.180	-2.180	-0.270	-0.780	-3.080	-2.080	-1.880	-3.240	-1.810	-0.800	-0.460	1.220	0.140	1.060	-1.214	1.259						
INCISAL/ MATURE	*lightness*	1	1.940	5.060	3.770	5.180	2.390	2.310	3.210	5.700	5.570	6.280	3.800	2.410	5.580	8.620	1.340	7.940	4.790	11.240	5.790	10.610	5.177	2.760	0.161	1.020	0.228	0.447	2.000	0.917
		2	2.560	5.770	2.800	6.080	3.700	2.350	4.180	6.390	5.440	5.700	4.260	2.090	5.410	8.250	1.450	5.990	4.900	9.310	5.530	8.150	5.016	2.136						
	red/ green	1	13.090	11.250	7.110	10.470	12.130	9.720	11.900	13.920	5.360	3.310	9.250	18.120	11.730	12.030	7.990	7.150	6.640	3.030	4.380	8.430	9.351	3.844	0.470	1.250	0.280	0.549	2.450	0.939
		2	9.760	9.440	7.400	10.430	11.750	9.260	10.790	13.210	4.250	3.330	9.590	17.700	11.490	12.130	4.660	8.810	6.430	3.990	5.310	7.880	8.881	3.597						
	yellow/ blue	1	10.260	11.020	12.690	8.420	11.440	12.590	12.890	12.140	16.150	9.540	13.420	18.850	12.370	11.280	9.520	9.760	13.790	7.650	14.220	16.760	12.238	2.823	0.058	0.811	0.181	0.355	1.590	0.957
		2	10.020	10.650	12.240	9.140	11.110	12.760	12.580	12.500	15.390	9.430	13.730	17.020	11.910	12.410	10.930	9.470	12.620	8.000	13.580	18.100	12.180	2.569						
	whiteness	1	8.330	9.040	7.650	7.980	8.380	7.910	10.410	8.640	8.640	6.260	8.640	12.610	9.820	10.580	6.100	8.350	8.180	7.260	7.830	11.800	8.721	1.641	0.251	0.673	0.150	0.294	1.319	0.910
		2	7.290	8.470	7.230	8.350	8.600	7.830	9.100	10.470	7.940	6.030	8.910	11.790	9.440	10.840	5.240	8.010	7.710	7.130	7.880	11.140	8.470	1.659						
WHOLE/ ALL	*lightness*	1	83.960	73.490	77.210	73.490	87.300	82.520	79.680	71.160	70.900	68.140	79.670	81.780	70.460	58.960	87.840	61.780	73.960	47.940	70.370	50.980	72.580	10.997	-0.583	4.114	0.920	1.803	8.063	0.918
		2	82.250	69.600	83.330	68.090	83.440	82.630	76.870	67.360	70.990	69.980	78.960	84.240	71.160	59.700	85.570	68.670	73.510	55.420	71.220	60.250	73.162	8.835						
	red/ green	1	41.170	48.130	65.580	51.250	42.430	54.520	45.290	36.590	71.400	80.330	56.270	19.580	46.640	44.930	61.590	64.740	66.870	80.780	76.210	59.810	55.706	15.729	-0.873	5.027	0.453	0.888	9.852	0.950
		2	52.910	54.640	63.520	50.220	41.930	55.280	48.460	38.060	76.130	80.080	53.650	16.160	46.740	43.340	74.560	57.450	67.770	76.980	72.410	61.280	56.579	15.758						
	yellow/ blue	1	52.290	48.960	41.230	59.730	46.640	42.530	40.750	44.150	27.500	55.030	38.100	14.580	43.650	47.990	55.160	54.350	37.550	63.010	35.120	24.740	43.653	12.054	1.136	3.224	0.721	1.413	6.319	0.959
		2	51.950	49.500	41.980	55.810	46.510	39.470	40.570	41.370	28.780	54.540	35.380	20.530	44.130	42.120	48.330	54.670	40.140	60.700	36.220	17.640	42.517	11.220						
	whiteness	1	60.110	57.230	62.990	61.660	60.110	61.790	56.290	51.290	58.920	68.490	58.860	42.870	54.230	50.940	69.320	60.080	60.780	64.700	62.260	46.020	58.447	6.718	-0.251	1.712	0.383	0.751	3.356	0.970
		2	63.690	58.780	64.130	59.230	57.870	61.460	55.990	50.210	60.980	68.880	56.580	44.330	54.830	48.970	71.820	60.680	62.020	64.480	61.280	47.760	58.699	6.954						

Table 13. Reliability Colour and Whiteness Assessment Intra-Operator Repeatability (AS) *polarised*

COLOUR AND WHITENESS (polarised)			CD-1 RELIABILITY																										
			INTRA-OPERATOR (AS)																				Statistics						
REGION/ STAGE	COLOUR COMPONENT	REPEAT	$n = 20$																				Mean	SD	Mean Dif.	SD. Dif.	SE	Bias	CR	ICC
			1	2	3	4	5	6	7	8	9	10	11	12	13	14	15	16	17	18	19	20								
GINGIVAL / PRE-SECRETORY	*lightness*	1	71.508	63.647	73.698	60.871	56.723	72.124	69.283	60.262	68.770	66.701	57.552	72.972	71.350	67.705	67.092	64.424	65.252	57.921	63.109	64.781	65.787	5.266	-0.071	4.703	1.052	2.062	9.218	0.648
		2	70.305	66.485	61.552	70.503	52.406	72.022	70.034	59.416	69.499	67.291	52.423	67.631	68.658	68.392	73.202	69.925	66.864	63.010	62.123	65.433	65.859	5.827						
	red/ green	1	67.378	62.640	62.604	60.295	54.609	65.044	65.318	62.096	71.834	64.756	64.809	62.390	69.477	65.800	66.154	67.611	65.003	71.721	61.055	67.172	64.888	3.995	1.672	2.629	0.588	5.153	5.153	0.723
		2	62.356	61.777	60.384	60.319	55.776	59.356	63.877	56.461	68.835	62.171	65.007	57.098	70.219	64.478	67.341	67.500	65.043	66.212	64.150	65.960	63.216	4.075						
	yellow/ blue	1	65.172	61.679	61.500	61.285	59.578	62.088	61.859	60.737	63.924	61.427	61.426	56.667	64.013	64.240	63.002	64.710	61.990	63.626	58.442	62.672	62.002	2.107	0.816	1.769	0.396	3.467	3.467	0.557
		2	61.302	60.216	61.132	61.494	61.273	57.208	61.189	57.930	62.709	60.172	61.355	57.341	62.919	63.729	63.201	64.836	62.499	60.857	60.896	61.467	61.186	1.980						
	whiteness	1	67.687	62.660	65.805	61.347	56.909	66.658	65.626	60.323	68.334	64.387	61.409	64.669	68.527	65.878	66.222	65.980	64.178	64.477	60.936	64.941	64.348	2.958	0.888	2.007	0.449	2.007	3.934	0.758
		2	64.850	62.967	61.640	64.190	56.071	63.219	65.072	57.995	67.201	62.715	59.317	60.706	66.402	65.511	68.209	67.693	65.047	63.556	62.574	64.255	63.460	3.160						
MIDDLE/ SECRETORY	*lightness*	1	0.590	2.380	1.450	0.320	2.210	1.350	1.990	0.560	4.080	4.900	-0.370	1.520	0.440	-1.060	0.490	5.290	3.890	10.310	5.300	4.520	2.508	2.675	0.752	1.019	0.228	0.447	1.997	0.885
		2	-0.130	1.000	1.180	-1.780	1.940	0.970	1.640	-0.570	3.350	3.650	-0.320	-0.110	1.030	-0.840	0.660	1.710	2.950	8.470	5.290	5.030	1.756	2.462						
	red/ green	1	-0.880	0.650	-0.610	0.940	2.420	1.890	-0.200	-0.710	1.190	0.590	-2.190	-0.970	-1.520	-1.320	-0.510	0.390	0.940	1.180	0.210	2.900	0.220	1.341	0.285	0.508	0.114	0.223	0.996	0.902
		2	-0.580	0.320	-0.610	-0.710	1.540	1.630	-0.270	-0.070	1.120	0.350	-2.370	-1.120	-1.370	-1.800	-1.260	-0.120	0.530	0.360	0.610	2.510	-0.066	1.222						
	yellow/ blue	1	-2.750	-2.940	-3.380	-2.390	-2.430	-2.460	-3.170	-3.370	-2.810	-3.160	-3.540	-2.930	-2.410	-4.070	-2.310	-3.080	-3.230	-2.450	-3.600	-1.060	-2.877	0.644	0.326	0.447	0.100	0.196	0.876	0.654
		2	-3.000	-2.770	-4.370	-3.310	-2.970	-2.800	-3.290	-3.410	-3.190	-3.590	-4.020	-3.080	-2.510	-4.280	-3.760	-2.580	-3.230	-2.530	-3.550	-1.830	-3.204	0.628						
	whiteness	1	-0.970	0.150	-0.730	-0.320	0.810	0.330	-0.420	-1.010	0.960	0.830	-2.050	-0.880	-1.190	-2.040	-0.790	0.950	0.650	3.270	0.790	2.170	0.026	1.332	0.433	0.453	0.101	0.198	0.888	0.890
		2	-1.250	-0.370	-1.390	-1.880	0.330	0.050	-0.590	-1.280	0.610	0.320	-2.190	-1.520	-0.670	-2.230	-1.290	-0.270	0.250	2.290	0.930	2.000	-0.408	1.274						
INCISAL/ MATURE	*lightness*	1	2.350	6.080	4.220	6.590	3.880	2.510	3.720	7.000	6.230	6.620	5.920	2.920	4.950	9.730	1.880	9.050	5.230	12.870	7.740	10.340	5.992	2.907	0.203	1.043	0.233	0.457	2.044	0.926
		2	2.650	7.460	3.900	6.320	5.870	2.580	4.120	6.290	6.170	6.200	5.990	2.300	5.820	9.420	1.670	6.330	5.470	10.780	6.780	9.650	5.789	2.446						
	red/ green	1	16.260	11.910	8.810	11.940	14.380	11.290	13.860	15.800	6.780	4.980	12.150	19.610	13.590	13.470	9.380	9.610	7.930	4.230	6.580	10.400	11.148	3.964	0.079	1.271	0.284	0.557	2.491	0.946
		2	13.470	12.220	9.760	12.040	14.410	11.490	13.010	13.720	6.280	5.450	13.100	19.570	13.760	13.850	6.400	10.510	8.870	6.240	7.300	9.920	11.069	3.580						
	yellow/ blue	1	13.420	12.660	14.950	9.420	14.500	15.530	15.580	14.880	18.820	10.300	15.890	19.880	14.180	12.750	12.110	11.150	15.830	9.180	16.380	20.070	14.374	3.116	0.030	0.784	0.175	0.343	1.537	0.971
		2	12.390	13.120	14.650	9.710	14.460	14.340	15.130	14.040	18.190	10.210	16.890	19.640	14.340	12.730	14.130	10.510	16.230	8.310	17.150	20.720	14.345	3.243						
	whiteness	1	10.490	10.150	9.110	9.290	10.550	9.380	10.860	12.380	10.160	7.180	11.050	13.570	10.780	11.910	7.330	9.800	9.400	8.610	9.910	13.400	10.266	1.691	0.135	0.553	0.124	0.243	1.084	0.947
		2	9.330	10.790	9.050	9.230	11.290	9.080	10.620	11.070	9.700	7.260	11.670	13.250	11.150	11.950	6.800	9.050	9.800	8.330	10.040	13.150	10.131	1.720						
WHOLE/ ALL	*lightness*	1	83.960	73.490	77.210	73.490	87.300	82.520	79.680	71.160	70.900	68.140	79.670	81.780	70.460	58.960	87.840	61.780	73.960	47.940	70.370	50.980	72.580	10.997	1.633	4.761	1.065	2.087	9.332	0.884
		2	82.240	64.310	79.810	68.310	73.370	81.960	76.700	70.100	68.990	69.170	72.850	84.420	70.490	56.490	84.950	68.330	72.120	51.100	67.550	55.660	70.946	9.355						
	red/ green	1	30.260	46.750	59.550	46.310	34.200	49.610	39.250	30.280	66.800	74.860	45.900	14.440	41.090	40.840	57.200	56.350	63.060	76.160	69.030	53.310	49.763	16.097	0.701	4.781	1.069	2.095	9.371	0.956
		2	39.230	44.490	54.870	44.910	33.260	47.310	41.520	36.520	68.680	73.150	41.260	9.910	39.870	38.070	68.410	52.190	58.690	69.210	65.160	54.520	49.062	15.511						
	yellow/ blue	1	40.790	43.240	33.390	56.990	34.800	31.220	30.860	33.450	18.270	53.210	29.320	9.260	37.440	43.250	45.780	49.920	29.850	57.980	25.940	12.680	35.882	13.494	1.055	3.148	0.704	1.380	6.170	0.973
		2	43.450	40.050	33.460	55.020	34.440	33.640	31.480	35.190	19.040	52.760	23.830	9.380	35.520	42.370	36.390	51.870	27.270	61.120	22.540	7.720	34.827	14.231						
	whiteness	1	52.870	54.030	58.260	57.570	52.000	57.230	51.280	44.290	54.220	66.110	50.070	40.210	51.790	47.050	65.320	55.580	57.130	60.360	55.000	41.160	53.577	6.871	0.251	2.318	0.518	1.015	4.543	0.948
		2	56.780	50.670	57.940	57.160	47.660	57.850	51.520	48.830	55.390	65.480	46.290	39.700	49.520	46.090	66.760	57.960	54.890	60.980	53.810	41.220	53.325	7.236						

Table 14. Reliability Colour and Whiteness Assessment Inter-Operator Reproducibility (TLC & AS) *non-polarised*

COLOUR AND WHITENESS (non-polarised)			CD-1 RELIABILITY																											
			INTER-OPERATOR																						Statistics						
			$n = 20$																											
REGION/ STAGE	COLOUR COMPONENT	OPERATOR	1	2	3	4	5	6	7	8	9	10	11	12	13	14	15	16	17	18	19	20	Mean	SD	Mean Dif.	SD. Dif.	SE	Bias	LOA	ICC
GINGIVAL / PRE-SECRETORY	*lightness*	TLC	72.411	71.188	74.747	75.335	70.211	72.938	71.082	71.773	65.202	70.880	66.098	71.020	74.100	71.796	74.866	66.101	65.317	68.336	67.239	68.890	70.477	3.238	3.331	4.676	1.046	2.050	9.165	0.219
		AS	72.256	65.392	71.953	62.982	56.923	72.460	70.329	63.693	68.679	68.909	61.530	73.884	71.798	68.780	67.467	67.076	67.076	60.067	66.428	65.235	67.146	4.505						
	red/ green	TLC	69.516	68.787	66.843	65.003	58.640	54.606	63.352	63.452	66.760	66.108	63.374	63.440	70.956	63.559	69.004	69.510	64.368	67.290	66.146	64.963	65.284	3.842	0.022	3.783	0.846	1.659	7.415	0.492
		AS	67.954	64.800	60.516	63.789	54.485	65.521	64.227	63.252	71.014	66.433	62.854	64.932	68.494	65.516	64.449	68.719	68.719	68.728	65.520	66.190	65.306	3.568						
	yellow/ blue	TLC	67.272	68.162	66.972	67.942	66.060	59.249	65.540	64.620	65.943	67.346	62.748	62.770	65.374	66.494	67.513	68.238	63.830	66.074	66.554	61.817	65.526	2.378	-0.996	2.818	0.630	1.235	5.523	0.126
		AS	67.001	64.964	61.667	64.552	61.212	65.495	63.490	64.537	64.854	64.665	62.308	62.178	66.577	66.273	64.544	67.622	67.622	63.494	63.584	63.966	64.530	1.874						
	whiteness	TLC	69.747	69.442	69.941	69.765	64.949	62.368	66.875	66.903	65.663	67.914	64.187	66.046	70.410	67.468	70.882	67.474	64.470	67.310	66.293	65.412	67.176	2.328	-1.863	3.311	0.740	1.440	6.490	0.131
		AS	68.876	64.328	64.401	63.640	57.294	67.787	66.022	62.154	67.837	66.535	61.488	67.047	68.850	66.458	65.023	66.998	66.953	63.930	65.431	65.208	65.313	2.763						
MIDDLE/ SECRETORY	*lightness*	TLC	2.710	3.440	1.770	0.700	2.440	1.750	2.170	1.300	3.580	5.670	-0.140	1.640	2.460	0.730	1.480	6.210	5.580	7.060	5.740	4.240	3.027	2.077	-1.472	0.951	0.213	0.417	1.864	0.753
		AS	-0.010	1.770	0.650	-0.340	1.670	0.640	0.580	0.110	3.090	3.440	-0.780	0.650	-1.450	-1.820	-0.520	4.650	3.720	7.690	4.630	2.730	1.555	2.411						
	red/ green	TLC	-1.660	-0.310	-1.190	0.100	0.990	2.690	-0.730	-1.000	1.510	0.420	-2.330	-2.120	-2.910	-1.560	-1.550	0.670	0.680	-0.310	-0.040	2.320	-0.317	1.523	-0.161	0.704	0.157	1.380	1.380	0.873
		AS	-1.500	-0.540	-0.990	-0.550	1.200	0.880	-1.090	-1.210	0.010	-0.140	-2.060	-2.030	-1.940	-2.340	-1.610	0.490	0.460	0.870	0.410	2.140	-0.477	1.263						
	yellow/ blue	TLC	-5.170	-4.820	-4.180	-4.250	-3.760	-2.530	-4.870	-4.860	-3.730	-4.900	-4.880	-3.890	-5.130	-4.670	-4.110	-3.430	-3.990	-4.460	-3.960	-3.750	-4.267	0.666	0.574	0.795	0.178	0.349	1.558	0.222
		AS	-3.330	-3.250	-3.820	-3.260	-2.970	-3.150	-4.030	-4.360	-3.780	-4.370	-4.820	-4.480	-3.140	-4.640	-3.050	-3.480	-3.990	-3.090	-4.460	-2.400	-3.694	0.674						
	whiteness	TLC	-1.110	-0.280	-0.980	-0.900	0.170	0.830	-0.910	-1.240	0.770	0.760	-2.280	-1.350	-1.620	-1.580	-1.120	1.610	1.330	1.440	0.980	1.160	-0.216	1.226	-0.526	0.464	0.104	0.204	0.910	0.855
		AS	-1.570	-0.490	-1.230	-1.320	0.090	-0.450	-1.460	-1.490	-0.180	-0.310	-2.340	-1.840	-2.140	-2.800	-1.610	0.870	0.190	2.090	0.290	0.860	-0.742	1.246						
INCISAL/ MATURE	*lightness*	TLC	3.910	2.620	3.930	3.290	2.200	3.680	2.540	4.240	4.980	5.290	3.800	2.520	3.720	5.560	2.210	8.760	5.340	7.230	6.520	8.140	4.524	1.939	-0.653	1.590	0.356	0.698	3.116	0.758
		AS	1.940	5.060	3.770	5.180	2.390	2.310	3.210	5.700	5.570	6.280	3.800	2.410	5.580	8.620	1.340	7.940	4.790	11.240	5.790	10.610	5.177	2.760						
	red/ green	TLC	10.140	9.530	8.170	8.790	12.330	5.290	9.920	13.640	2.610	3.090	9.650	15.150	11.750	11.100	5.970	9.080	4.560	5.650	6.510	4.410	8.367	3.516	0.984	2.014	0.450	0.882	3.947	0.827
		AS	13.090	11.250	7.110	10.470	12.130	9.720	11.900	13.920	5.360	3.310	9.250	18.120	11.730	12.030	7.990	7.150	6.640	3.030	4.380	8.430	9.351	3.844						
	yellow/ blue	TLC	14.300	12.450	13.300	10.010	13.290	10.700	13.940	13.440	15.260	10.250	13.610	18.260	13.210	11.160	11.370	10.000	14.780	7.720	15.510	20.770	13.167	2.995	-0.929	1.422	0.318	0.623	2.787	0.843
		AS	10.260	11.020	12.690	8.420	11.440	12.590	12.890	12.140	16.150	9.540	13.420	18.850	12.370	11.280	9.520	9.760	13.790	7.650	14.220	16.760	12.238	2.823						
	whiteness	TLC	9.060	7.840	8.080	6.920	8.730	6.320	8.360	9.990	7.050	5.970	8.610	11.340	9.250	8.970	6.020	9.180	7.800	6.790	9.090	10.580	8.298	1.482	0.423	1.017	0.227	0.445	1.993	0.768
		AS	8.330	9.040	7.650	7.980	8.380	7.910	10.410	8.640	8.640	6.260	8.640	12.610	9.820	10.580	6.100	8.350	8.180	7.260	7.830	11.800	8.721	1.641						
WHOLE/ ALL	*lightness*	TLC	76.450	81.560	75.940	78.170	83.450	77.210	81.920	75.380	73.670	71.480	78.330	82.050	76.820	70.370	82.160	58.350	72.170	64.340	67.190	60.710	74.386	7.211	-1.807	6.316	1.412	2.768	12.380	0.764
		AS	83.960	73.490	77.210	73.490	87.300	82.520	79.680	71.160	70.900	68.140	79.670	81.780	70.460	58.960	87.840	61.780	73.960	47.940	70.370	50.980	72.580	10.997						
	red/ green	TLC	52.720	55.160	60.520	58.040	42.030	74.490	53.200	37.400	82.880	81.200	54.290	30.850	46.570	48.180	69.170	56.970	75.620	70.650	67.340	76.070	59.668	14.701	-3.962	8.325	1.862	3.650	16.317	0.829
		AS	41.170	48.130	65.580	51.250	42.430	54.520	45.290	36.590	71.400	80.330	56.270	19.580	46.640	44.930	61.590	64.740	66.870	80.780	76.210	59.810	55.706	15.729						
	yellow/ blue	TLC	35.410	43.180	39.490	53.040	39.350	49.230	36.410	38.230	31.120	51.970	36.940	16.950	39.400	48.170	47.480	53.110	32.370	62.330	30.300	5.480	39.498	12.974	4.155	6.080	1.359	2.664	11.917	0.841
		AS	52.290	48.960	41.230	59.730	46.640	42.530	40.750	44.150	27.500	55.030	38.100	14.580	43.650	47.990	55.160	54.350	37.550	63.010	35.120	24.740	43.653	12.054						
	whiteness	TLC	57.010	61.820	60.840	65.380	58.270	68.550	59.760	53.160	65.190	69.280	58.690	47.530	56.270	57.280	68.760	56.530	62.170	66.090	56.870	50.730	60.009	5.994	-1.562	3.546	0.793	1.554	6.950	0.826
		AS	60.110	57.230	62.990	61.660	60.110	61.790	56.290	51.290	58.920	68.490	58.860	42.870	54.230	50.940	69.320	60.080	60.780	64.700	62.260	46.020	58.447	6.718						

Table 15. Reliability Colour and Whiteness Assessment Inter-Operator Reproducibility (TLC & AS) *polarised*

COLOUR AND WHITENESS (polarised)		CD-1 RELIABILITY																											
			INTER-OPERATOR																					Statistics						
REGION/ STAGE	COLOUR COMPONENT	OPERATOR	$n = 20$																					Mean	SD	Mean Dif.	SD. Dif.	SE	Bias	LOA	ICC
			1	2	3	4	5	6	7	8	9	10	11	12	13	14	15	16	17	18	19	20								
GINGIVAL/ PRE-SECRETORY	*lightness*	TLC	71.797	69.668	74.854	74.014	66.928	74.467	70.915	69.222	70.173	68.264	72.832	68.194	73.376	71.692	73.792	66.141	64.169	65.839	64.663	66.450	69.873	3.432	4.085	4.957	1.108	2.172	9.716	0.272
		AS	71.508	63.647	73.698	60.871	56.723	72.124	69.283	60.262	68.770	66.701	57.552	72.972	71.350	67.705	67.092	64.424	65.252	57.921	63.109	64.781	65.787	5.266						
	red/ green	TLC	69.302	67.948	62.831	63.039	56.297	59.432	63.800	60.510	66.167	62.208	69.496	59.319	72.019	64.964	65.495	69.423	62.659	68.393	64.366	65.975	64.682	4.047	-0.206	3.142	0.703	1.378	6.158	0.705
		AS	67.378	62.640	62.604	60.295	54.609	65.044	65.318	62.096	71.834	64.756	64.809	62.390	69.477	65.800	66.154	67.611	65.003	71.721	61.055	67.172	64.888	3.995						
	yellow/ blue	TLC	64.236	64.139	60.956	63.642	60.928	57.422	62.182	59.330	63.349	61.815	64.726	56.935	63.914	63.966	61.303	65.731	60.288	63.637	62.359	59.125	61.999	2.444	-0.003	2.112	0.472	1.411	4.140	0.584
		AS	65.172	61.679	61.500	61.285	59.578	62.088	61.859	60.737	63.924	61.427	61.426	56.667	64.013	64.240	63.002	64.710	61.990	63.626	58.442	62.672	62.002	2.107						
	whiteness	TLC	68.645	67.464	66.625	67.644	61.571	64.160	65.957	63.329	66.942	64.363	69.308	61.843	70.063	66.918	67.398	66.129	62.442	65.991	64.158	64.065	65.751	2.428	1.403	2.863	0.640	1.254	5.612	0.398
		AS	67.687	62.660	65.805	61.347	56.909	66.658	65.626	60.323	68.334	64.387	61.409	64.669	68.527	65.878	66.222	65.980	64.178	64.477	60.936	64.941	64.348	2.958						
MIDDLE/ SECRETORY	*lightness*	TLC	3.300	3.500	1.600	0.290	2.450	1.630	2.790	1.340	5.050	5.840	-0.320	1.360	2.620	0.750	0.720	6.990	6.140	7.960	6.020	5.180	3.261	2.448	0.753	1.013	0.233	0.457	1.985	0.874
		AS	0.590	2.380	1.450	0.320	2.210	1.350	1.990	0.560	4.080	4.900	-0.370	1.520	0.440	-1.060	0.490	5.290	3.890	10.310	5.300	4.520	2.508	2.675						
	red/ green	TLC	-2.140	0.080	-0.610	0.340	1.780	2.550	0.170	-0.530	1.610	1.010	-1.850	-1.390	-2.030	-0.930	-1.090	1.700	1.740	-0.100	0.430	2.990	0.187	1.531	-0.033	0.677	0.151	0.286	1.327	0.939
		AS	-0.880	0.650	-0.610	0.940	2.420	1.890	-0.200	-0.710	1.190	0.590	-2.190	-0.970	-1.520	-1.320	-0.510	0.390	0.940	1.180	0.210	2.900	0.220	1.341						
	yellow/ blue	TLC	-5.280	-4.210	-3.830	-3.540	-3.580	-1.700	-3.830	-4.440	-3.090	-4.630	-3.760	-3.360	-4.700	-4.540	-2.890	-2.590	-3.460	-3.200	-3.510	-2.240	-3.619	0.879	-0.742	0.812	0.182	0.357	1.590	0.309
		AS	-2.750	-2.940	-3.380	-2.390	-2.430	-2.460	-3.170	-3.370	-2.810	-3.160	-3.540	-2.930	-2.410	-4.070	-2.310	-3.080	-3.230	-2.450	-3.600	-1.060	-2.877	0.644						
	whiteness	TLC	-1.110	0.070	-0.740	-0.790	0.480	0.940	-0.080	-0.950	1.390	1.140	-1.850	-1.030	-1.190	-1.300	-0.910	2.790	1.970	2.220	1.300	2.130	0.224	1.412	0.199	0.627	0.140	0.274	1.229	0.891
		AS	-0.970	0.150	-0.730	-0.320	0.810	0.330	-0.420	-1.010	0.960	0.830	-2.050	-0.880	-1.190	-2.040	-0.790	0.950	0.650	3.270	0.790	2.170	0.026	1.332						
INCISAL/ MATURE	*lightness*	TLC	4.010	3.240	3.950	3.500	2.550	4.250	2.890	4.470	4.910	5.380	6.290	2.920	3.960	6.440	2.070	8.790	5.430	8.340	6.790	8.640	4.941	2.035	-1.051	0.621	0.130	0.255	1.217	0.735
		AS	2.350	6.080	4.220	6.590	3.880	2.510	3.720	7.000	6.230	6.620	5.920	2.920	4.950	9.730	1.880	9.050	5.230	12.870	7.740	10.340	5.992	2.907						
	red/ green	TLC	12.740	11.040	9.370	10.330	14.060	7.510	10.800	14.530	5.290	4.120	12.210	15.350	13.120	13.270	5.940	10.150	5.140	6.560	7.470	5.440	9.722	3.563	-1.426	1.958	0.438	0.858	3.838	0.812
		AS	16.260	11.910	8.810	11.940	14.380	11.290	13.860	15.800	6.780	4.980	12.150	19.610	13.590	13.470	9.380	9.610	7.930	4.230	6.580	10.400	11.148	3.964						
	yellow/ blue	TLC	17.430	15.180	15.480	10.900	15.450	13.890	15.870	14.920	17.990	11.230	16.650	18.760	16.320	13.640	12.170	11.530	16.280	7.650	17.800	24.010	15.158	3.502	0.783	1.544	0.345	0.676	3.026	0.872
		AS	13.420	12.660	14.950	9.420	14.500	15.530	15.580	14.880	18.820	10.300	15.890	19.880	14.180	12.750	12.110	11.150	15.830	9.180	16.380	20.070	14.374	3.116						
	whiteness	TLC	10.880	9.350	9.090	7.750	10.000	8.180	9.340	10.820	8.800	6.630	11.250	11.650	10.740	10.690	6.180	10.310	8.480	7.500	10.120	12.000	9.488	1.649	-0.778	0.747	0.167	0.327	1.464	0.816
		AS	10.490	10.150	9.110	9.290	10.550	9.380	10.860	12.380	10.160	7.180	11.050	13.570	10.780	11.910	7.330	9.800	9.400	8.610	9.910	13.400	10.266	1.691						
WHOLE/ ALL	*lightness*	TLC	76.230	79.620	75.870	77.730	83.140	74.840	80.690	75.010	73.050	71.520	67.480	81.340	76.100	67.000	83.080	58.110	71.950	59.930	66.310	58.670	72.884	7.770	0.304	6.191	1.384	2.731	12.134	0.797
		AS	83.960	73.490	77.210	73.490	87.300	82.520	79.680	71.160	70.900	68.140	79.670	81.780	70.460	58.960	87.840	61.780	73.960	47.940	70.370	50.980	72.580	10.997						
	red/ green	TLC	42.150	48.880	55.350	51.260	33.080	63.600	49.340	32.240	72.280	78.010	44.350	27.950	41.270	39.040	69.700	52.670	73.500	66.850	63.450	71.670	53.832	15.328	4.070	7.682	1.718	3.367	15.057	0.857
		AS	30.260	46.750	59.550	46.310	34.200	49.610	39.250	30.280	66.800	74.860	45.900	14.440	41.090	40.840	57.200	56.350	63.060	76.160	69.030	53.310	49.763	16.097						
	yellow/ blue	TLC	20.630	30.360	27.800	48.710	27.950	33.890	26.610	29.540	18.050	46.920	24.380	10.510	25.300	36.910	42.740	46.390	23.920	62.660	18.290	-11.540	29.501	15.855	-6.381	6.967	1.558	3.054	13.655	0.816
		AS	40.790	43.240	33.390	56.990	34.800	31.220	30.860	33.450	18.270	53.210	29.320	9.260	37.440	43.250	45.780	49.920	29.850	57.980	25.940	12.680	35.882	13.494						
	whiteness	TLC	49.550	55.680	56.660	62.140	52.580	60.480	55.650	49.130	57.930	66.990	48.120	45.290	50.260	50.090	68.480	51.770	59.230	63.240	52.310	44.450	55.002	6.851	1.425	2.911	0.651	1.276	5.706	0.895
		AS	52.870	54.030	58.260	57.570	52.000	57.230	51.280	44.290	54.220	66.110	50.070	40.210	51.790	47.050	65.320	55.580	57.130	60.360	55.000	41.160	53.577	6.871						

Table 16. Reliability 3D *left* Incisor Morphometry Intra-Operator Repeatability (TLC)

MANDIBULAR INCISORS			CD-1 RELIABILITY																											
			INTRA-OPERATOR (TLC)																						Statistics						
			n = 20																											
VIEW/ ASPECT		MEASUREMENT VARIABLE	REPEAT	1	2	3	4	5	6	7	8	9	10	11	12	13	14	15	16	17	18	19	20	Mean	SD	Mean Dif.	SD Dif.	SE	Bias	CR	ICC
LEFT	BUCCAL	projected *overall-length* (mm)	1	9.268	8.957	9.419	9.912	9.720	9.138	9.428	9.200	9.417	8.063	8.809	9.694	9.545	9.507	7.986	9.566	9.050	8.874	9.664	7.081	9.115	0.695	-0.028	0.282	0.063	0.124	0.553	0.922
			2	9.883	9.002	8.573	9.838	9.859	9.017	9.181	9.164	9.626	7.986	8.973	9.886	9.351	9.561	8.168	9.626	9.156	9.196	9.595	7.217	9.143	0.702						
		projected *width-at-midpoint* (mm)	1	1.234	1.070	1.023	1.056	1.057	1.145	1.106	1.146	1.188	1.132	1.090	1.152	1.293	1.108	1.120	1.092	1.092	1.148	1.195	1.217	1.474	0.109	0.012	0.032	0.007	0.022	0.063	1.000
			2	1.243	1.074	1.022	1.053	1.030	1.137	1.090	1.097	1.141	1.177	1.120	1.098	1.253	1.150	1.130	1.091	1.134	1.164	1.190	1.188	1.461	0.106						
		actual *width-at-midpoint* (mm)	1	1.577	1.336	1.253	1.404	1.336	1.532	1.443	1.537	1.559	1.472	1.453	1.566	1.744	1.479	1.429	1.425	1.419	1.427	1.492	1.597	3.066	0.199	-0.002	0.051	0.011	0.014	0.101	0.909
			2	1.574	1.343	1.312	1.399	1.253	1.490	1.388	1.451	1.483	1.489	1.401	1.505	1.738	1.553	1.398	1.420	1.508	1.448	1.526	1.552	3.067	0.182						
		actual *perimeter* (mm)	1	22.097	21.961	22.956	24.016	24.409	23.038	24.258	23.391	23.431	20.114	21.429	23.801	23.807	23.456	19.047	23.439	22.685	21.915	23.977	16.786	22.501	1.931	0.105	1.085	0.243	0.475	2.126	0.843
			2	22.385	21.798	23.099	24.087	24.326	22.563	24.063	25.902	21.444	19.285	21.807	22.840	22.774	23.451	20.584	21.049	22.647	22.604	23.724	17.479	22.395	1.865						
		marked *surface-area* (mm^2)	1	14.908	13.247	13.446	16.226	13.946	16.814	15.936	16.460	15.563	13.502	13.893	16.771	17.821	15.919	12.175	15.616	15.413	15.031	16.636	13.263	15.129	1.522	0.171	0.563	0.126	0.247	1.103	0.923
			2	15.044	13.436	13.265	16.276	14.593	16.745	15.588	16.307	15.150	13.850	13.963	16.251	17.048	16.353	11.809	13.608	15.355	14.881	16.076	13.567	14.958	1.410						
	LINGUAL	projected *overall-length* (mm)	1	9.225	8.986	9.426	9.905	9.648	9.164	9.661	9.277	9.446	8.088	8.965	9.658	9.521	9.436	7.930	9.546	9.158	8.941	9.655	7.024	9.133	0.703	-0.016	0.159	0.035	0.070	0.311	0.974
			2	9.242	9.010	9.596	9.808	9.862	9.062	9.484	9.090	9.621	7.987	9.004	9.372	9.581	9.324	8.161	9.625	9.186	9.206	9.540	7.216	9.149	0.659						
		projected *width-at-midpoint* (mm)	1	1.165	1.074	0.956	1.052	1.055	1.138	1.090	1.166	1.145	1.117	1.106	1.125	1.266	1.098	1.096	1.114	1.116	1.160	1.201	1.208	1.122	0.066	-0.001	0.028	0.006	0.012	0.056	1.000
			2	1.176	1.065	1.009	1.082	1.058	1.135	1.098	1.156	1.110	1.137	1.116	1.117	1.241	1.110	1.020	1.139	1.101	1.199	1.181	1.218	1.123	0.061						
		actual *width-at-midpoint* (mm)	1	1.322	1.272	1.153	1.268	1.128	1.285	1.253	1.334	1.298	1.207	1.182	1.260	1.511	1.280	1.208	1.292	1.464	1.273	1.368	1.397	1.288	0.095	0.027	0.048	0.011	0.021	0.093	0.857
			2	1.281	1.137	1.148	1.267	1.127	1.292	1.243	1.295	1.283	1.221	1.214	1.259	1.417	1.247	1.180	1.331	1.328	1.232	1.330	1.392	1.261	0.078						
		actual *perimeter* (mm)	1	21.835	21.812	22.300	24.353	24.531	23.798	24.365	23.629	22.991	20.098	21.631	24.535	23.382	23.138	19.276	23.437	22.331	21.800	23.776	17.563	22.529	1.847	0.178	1.005	0.225	0.440	1.969	0.870
			2	20.257	22.336	20.614	24.557	24.195	23.269	23.086	25.297	21.554	19.437	21.354	23.471	22.421	24.351	19.581	23.941	22.700	23.451	23.786	17.369	22.351	2.046						
		marked *surface-area* (mm^2)	1	13.875	11.643	11.254	14.632	12.723	14.218	14.736	14.590	14.176	11.570	12.163	14.428	16.006	13.839	11.135	14.234	15.405	12.922	15.193	10.239	13.449	1.631	0.190	0.883	0.198	0.387	1.731	0.878
			2	14.395	11.684	10.607	14.487	11.775	14.715	15.264	14.898	14.403	11.136	12.231	13.609	15.790	14.535	10.636	14.286	15.314	14.170	12.300	8.941	13.259	1.932						
	LABIAL	projected *labial-length* (mm)	1	9.216	8.910	9.359	9.824	9.688	9.223	9.637	9.185	9.359	8.034	8.882	9.667	9.495	9.502	7.939	9.539	9.209	8.928	9.654	7.053	9.115	0.698	-0.030	0.297	0.066	0.130	0.582	0.914
			2	9.873	8.956	8.574	9.817	9.852	9.092	9.159	9.161	9.686	8.002	8.944	9.883	9.351	9.579	8.153	9.626	9.173	9.236	9.566	7.222	9.145	0.702						
		actual *labial-length* (mm)	1	10.165	9.784	10.496	10.883	11.601	10.229	11.119	10.306	10.855	9.135	9.987	11.284	10.805	10.622	8.825	10.964	10.607	9.896	11.174	7.523	10.313	0.959	0.036	0.492	0.110	0.216	0.964	0.888
			2	9.520	9.877	9.409	11.033	11.896	10.151	11.998	10.631	9.915	8.676	10.010	11.070	10.635	10.936	9.068	10.624	10.418	10.546	11.496	7.643	10.277	1.072						
		circumference (mm)	1	3.226	3.001	2.529	2.965	2.687	3.156	3.061	3.198	3.123	3.131	3.078	3.199	3.465	3.091	2.969	2.991	2.982	3.023	3.237	3.200	3.066	0.199	-0.002	0.106	0.024	0.046	0.207	0.857
			2	3.222	2.969	2.606	2.958	2.667	3.154	2.984	3.187	3.135	3.175	3.073	3.185	3.271	3.181	2.924	3.265	2.975	3.229	3.119	3.070	3.067	0.182						
		total *surface-area* (mm^2)	1	35.551	32.106	30.785	34.528	35.971	39.000	36.225	35.605	34.613	28.079	33.736	36.076	38.413	34.015	28.734	36.216	35.140	32.644	35.464	24.525	33.871	3.552	0.332	1.425	0.319	0.625	2.793	0.917
			2	34.786	32.106	32.651	34.479	34.284	38.051	36.759	36.725	33.371	26.020	33.736	34.775	35.599	34.880	30.562	34.812	35.850	34.504	33.165	23.665	33.539	3.443						
		total *volume* (mm^3)	1	5.644	5.240	6.205	6.501	4.838	7.693	7.041	9.703	7.211	7.432	6.752	8.420	7.646	8.159	4.943	6.804	7.701	7.130	7.715	4.753	6.877	1.306	0.130	0.352	0.079	0.154	0.691	0.960
			2	5.279	5.240	6.558	6.473	4.846	7.526	6.622	9.580	7.666	7.120	6.752	7.995	6.468	7.886	4.956	7.166	7.741	6.802	7.681	4.577	6.747	1.271						

Table 17. Reliability 3D *right* Incisor Morphometry Intra-Operator Repeatability (TLC)

MANDIBULAR INCISORS			CD-1 RELIABILITY																											
			INTRA-OPERATOR (TLC)																				Statistics							
VIEW/ ASPECT	MEASUREMENT VARIABLE	REPEAT	$n = 20$																				Mean	SD	Mean Dif.	SD. Dif.	SE	Bias	CR	ICC
			1	2	3	4	5	6	7	8	9	10	11	12	13	14	15	16	17	18	19	20								
RIGHT BUCCAL	projected *overall-length* (mm)	1	9.756	8.911	9.192	9.933	7.186	8.764	9.611	9.341	8.332	9.819	9.300	7.999	8.919	9.741	7.567	9.426	9.123	8.727	8.962	8.827	8.972	0.741	0.082	0.117	0.026	0.051	0.228	0.982
		2	9.648	8.628	9.021	9.972	6.973	8.698	9.547	9.091	8.456	9.753	9.111	8.129	8.769	9.689	7.582	9.405	9.154	8.684	8.867	8.618	8.890	0.739						
	projected *width-at-midpoint* (mm)	1	1.138	1.148	1.123	1.056	1.109	1.132	1.063	1.185	1.181	1.096	1.131	1.108	1.137	1.118	1.092	1.073	1.114	1.132	1.189	1.209	1.437	0.092	0.002	0.027	0.006	0.012	0.053	1.000
		2	1.152	1.137	1.092	1.084	1.078	1.154	1.109	1.182	1.167	1.084	1.140	1.082	1.096	1.071	1.097	1.108	1.153	1.141	1.169	1.192	1.452	0.083						
	actual *width-at-midpoint* (mm)	1	1.456	1.479	1.412	1.401	1.433	1.450	1.262	1.525	1.688	1.275	1.440	1.409	1.468	1.501	1.383	1.341	1.376	1.445	1.482	1.512	3.049	0.093	-0.015	0.045	0.010	0.020	0.089	0.875
		2	1.481	1.460	1.392	1.427	1.438	1.433	1.299	1.556	1.641	1.260	1.499	1.429	1.455	1.492	1.384	1.471	1.480	1.483	1.431	1.533	3.038	0.083						
	actual *perimeter* (mm)	1	24.282	21.763	22.209	25.686	16.817	21.276	24.389	23.350	19.831	25.287	22.458	19.382	21.378	23.325	18.334	22.863	22.430	20.969	21.803	21.281	21.956	2.230	0.273	0.701	0.157	0.307	1.374	0.942
		2	23.250	20.533	22.490	25.616	16.710	20.798	22.916	21.830	20.710	24.433	22.421	19.481	21.890	23.928	18.161	23.376	21.750	20.991	21.830	20.539	21.683	2.090						
	marked *surface-area* (mm^2)	1	15.757	15.635	14.316	16.144	10.214	13.255	14.957	17.435	16.136	15.323	14.361	11.578	16.100	15.745	11.219	14.607	14.135	13.717	14.101	14.565	14.465	1.807	0.221	0.845	0.189	0.370	1.656	0.898
		2	15.115	14.913	13.108	14.837	9.814	13.950	14.677	15.820	16.978	16.248	14.308	11.592	16.836	16.240	10.323	13.683	13.927	13.702	15.405	13.403	14.244	1.955						
LINGUAL	projected *overall-length* (mm)	1	9.738	8.896	9.168	9.978	7.106	8.806	9.221	9.301	8.261	9.857	9.316	7.992	8.854	9.697	7.548	9.495	9.115	8.715	8.925	8.798	8.939	0.748	0.100	0.146	0.033	0.064	0.286	0.972
		2	9.363	8.616	9.048	9.999	6.956	8.649	9.227	9.073	8.465	9.744	9.162	8.204	8.795	9.678	7.426	9.326	8.888	8.714	8.871	8.578	8.839	0.725						
	projected *width-at-midpoint* (mm)	1	1.123	1.155	1.118	1.088	1.098	1.112	1.084	1.172	1.142	1.116	1.100	1.126	1.048	1.113	1.102	1.074	1.113	1.145	1.173	1.194	1.120	0.036	-0.001	0.030	0.007	0.013	0.059	1.000
		2	1.121	1.137	1.093	1.040	1.079	1.133	1.058	1.189	1.110	1.158	1.131	1.076	1.168	1.082	1.121	1.095	1.154	1.125	1.194	1.155	1.121	0.042						
	actual *width-at-midpoint* (mm)	1	1.293	1.348	1.310	1.475	1.265	1.329	1.239	1.317	1.356	1.218	1.201	1.325	1.320	1.282	1.276	1.208	1.248	1.278	1.285	1.344	1.296	0.063	0.005	0.033	0.007	0.014	0.065	0.750
		2	1.254	1.352	1.301	1.440	1.270	1.369	1.213	1.321	1.319	1.261	1.256	1.261	1.321	1.249	1.254	1.230	1.282	1.256	1.298	1.300	1.290	0.053						
	actual *perimeter* (mm)	1	24.115	21.956	22.007	24.188	18.431	20.841	22.995	23.047	19.986	24.823	22.738	19.675	21.125	24.937	19.031	23.117	22.802	20.958	21.312	20.833	21.946	1.869	0.505	0.871	0.195	0.382	1.706	0.871
		2	22.953	21.061	21.774	24.675	16.159	21.673	22.693	21.876	19.932	23.855	22.054	19.775	21.466	23.368	17.687	22.665	21.322	20.439	22.435	20.954	21.441	1.994						
	marked *surface-area* (mm^2)	1	14.608	12.807	12.418	14.921	12.316	12.726	13.226	14.023	12.873	14.285	13.175	10.477	12.606	14.166	10.033	13.096	12.820	12.234	14.074	12.219	12.955	1.236	0.039	0.400	0.089	0.175	0.784	0.979
		2	14.358	11.960	12.090	14.247	12.152	13.052	13.028	14.669	12.835	14.759	12.950	10.851	12.103	14.600	9.715	13.138	12.775	12.367	14.470	12.204	12.916	1.335						
LABIAL	projected *labial-length* (mm)	1	9.726	8.835	9.112	9.958	7.162	8.769	9.609	9.343	8.296	9.772	9.313	8.016	8.894	9.722	7.582	9.450	9.122	8.699	8.973	8.828	8.959	0.740	0.082	0.139	0.031	0.061	0.272	0.976
		2	9.316	8.663	8.988	10.038	6.946	8.622	9.613	9.153	8.491	9.708	9.124	8.135	8.751	9.756	7.529	9.371	8.935	8.714	8.836	8.853	8.877	0.738						
	actual *labial-length* (mm)	1	10.978	9.673	10.053	11.170	7.703	9.639	11.233	10.454	9.395	11.098	10.432	8.719	9.722	10.886	8.296	10.635	10.283	9.668	9.962	9.836	9.992	0.956	0.128	0.281	0.063	0.123	0.551	0.952
		2	10.070	9.601	9.917	11.300	7.366	9.590	11.582	10.177	9.591	11.002	10.051	8.871	9.636	11.019	8.234	10.564	9.802	9.632	9.812	9.459	9.864	0.992						
	circumference (mm)	1	3.122	3.110	3.134	2.999	2.953	3.131	2.985	3.288	3.030	3.031	3.011	2.972	3.002	3.076	2.922	2.916	2.990	3.068	3.058	3.191	3.049	0.093	0.011	0.047	0.011	0.021	0.093	0.875
		2	3.081	3.114	3.093	2.991	2.898	3.119	3.035	3.225	2.960	3.125	3.019	2.921	2.946	3.044	2.957	2.975	3.029	3.075	3.028	3.126	3.038	0.083						
	total *surface-area* (mm^2)	1	34.066	35.142	30.823	34.965	22.332	37.215	34.100	33.102	30.468	34.627	34.086	25.749	30.192	33.858	26.158	31.855	32.245	32.069	35.175	31.737	31.998	3.659	-0.217	1.143	0.256	0.501	2.240	0.957
		2	35.906	34.910	30.588	36.174	21.224	36.297	34.214	33.880	32.122	34.947	35.246	26.341	32.065	34.602	24.970	31.917	32.200	32.069	35.690	28.937	32.215	4.077						
	total *volume* (mm^3)	1	7.200	5.800	6.173	6.917	4.204	5.796	6.724	6.910	7.368	6.310	7.798	4.838	7.081	6.976	4.950	5.766	5.666	7.493	5.557	5.908	6.272	0.970	-0.233	0.467	0.104	0.205	0.916	0.878
		2	7.328	6.638	6.008	7.586	3.956	6.296	7.005	6.003	7.846	7.022	8.041	5.558	7.590	7.559	5.026	5.777	5.657	7.493	6.344	5.368	6.505	1.088						

Table 18. Reliability 3D *left* Incisor Morphometry Inter-Operator Reproducibility (TLC & JHH)

MANDIBULAR INCISORS			CD-1 RELIABILITY																					Statistics						
				INTER-OPERATOR $n = 20$																										
VIEW/ ASPECT		MEASUREMENT VARIABLE	OPERATOR	1	2	3	4	5	6	7	8	9	10	11	12	13	14	15	16	17	18	19	20	Mean	SD	Mean Dif.	SD. Dif.	SE	Bias	CR	ICC
LEFT	BUCCAL	projected *overall-length* (mm)	TLC	9.268	8.957	9.419	9.912	9.720	9.138	9.428	9.200	9.417	8.063	8.809	9.694	9.545	9.507	7.986	9.566	9.050	8.874	9.664	7.081	9.115	0.695	-0.068	0.104	0.023	0.045	0.203	0.986
			JHH	9.274	9.035	9.484	9.922	9.777	9.478	9.701	9.374	9.460	8.113	8.846	9.720	9.529	9.569	8.033	9.587	9.239	8.760	9.658	7.096	9.183	0.709						
		projected *width-at-midpoint* (mm)	TLC	1.234	1.070	0.982	1.056	1.057	1.145	1.106	1.146	1.188	1.132	1.090	1.152	1.293	1.108	1.120	1.092	1.092	1.148	1.195	1.217	1.131	0.071	-0.007	-0.008	-0.002	-0.004	-0.016	1.000
			JHH	1.237	1.089	0.961	1.062	1.015	1.165	1.120	1.186	1.168	1.146	1.106	1.120	1.287	1.115	1.148	1.129	1.107	1.161	1.227	1.225	1.139	0.076						
		actual *width-at-midpoint* (mm)	TLC	1.577	1.336	1.253	1.404	1.336	1.532	1.443	1.537	1.559	1.472	1.453	1.566	1.744	1.479	1.429	1.425	1.419	1.427	1.492	1.597	1.474	0.109	-0.031	0.054	0.012	0.024	0.106	0.917
			JHH	1.592	1.412	1.245	1.357	1.266	1.583	1.471	1.611	1.532	1.501	1.524	1.521	1.715	1.507	1.470	1.520	1.470	1.539	1.604	1.667	1.505	0.119						
		actual *perimeter* (mm)	TLC	22.097	21.961	22.956	24.016	24.409	23.038	24.258	23.391	23.431	20.114	21.429	23.801	23.807	23.456	19.047	23.439	22.685	21.915	23.977	16.786	22.501	1.931	-0.236	0.335	0.075	0.147	0.656	0.979
			JHH	21.950	22.455	23.212	24.704	24.596	23.635	24.378	23.723	23.490	20.005	22.091	24.575	23.283	23.780	19.661	23.497	22.543	22.144	24.056	16.945	22.736	1.942						
		marked *surface-area* (mm^2)	TLC	14.908	13.247	13.446	16.226	13.946	16.814	15.936	16.460	15.563	13.502	13.893	16.771	17.821	15.919	12.175	15.616	15.413	15.031	16.636	13.263	15.129	1.522	0.106	0.210	0.047	0.092	0.411	0.988
			JHH	14.867	13.345	13.418	15.703	13.976	16.231	15.940	16.656	15.680	13.251	13.788	16.435	17.865	15.665	12.241	15.651	15.233	14.798	16.646	13.079	15.023	1.490						
	LINGUAL	projected *overall-length* (mm)	TLC	9.225	8.986	9.426	9.905	9.648	9.164	9.661	9.277	9.446	8.088	8.965	9.658	9.521	9.436	7.930	9.546	9.158	8.941	9.655	7.024	9.133	0.703	-0.055	0.078	0.017	0.034	0.152	0.992
			JHH	9.262	8.941	9.511	9.854	9.784	9.442	9.753	9.362	9.427	8.099	8.981	9.669	9.550	9.555	8.018	9.538	9.184	8.985	9.673	7.180	9.188	0.687						
		projected *width-at-midpoint* (mm)	TLC	1.165	1.074	0.956	1.052	1.055	1.138	1.090	1.166	1.145	1.117	1.106	1.125	1.266	1.098	1.096	1.114	1.116	1.160	1.201	1.208	1.122	0.066	-0.010	0.014	0.003	0.006	0.027	1.000
			JHH	1.171	1.074	0.965	1.046	1.045	1.162	1.118	1.190	1.164	1.127	1.125	1.122	1.256	1.131	1.109	1.104	1.130	1.177	1.224	1.199	1.132	0.067						
		actual *width-at-midpoint* (mm)	TLC	1.322	1.272	1.153	1.268	1.128	1.285	1.253	1.334	1.298	1.207	1.182	1.260	1.511	1.280	1.208	1.292	1.464	1.273	1.368	1.397	1.288	0.095	-0.016	0.054	0.012	0.024	0.106	0.889
			JHH	1.368	1.235	1.090	1.358	1.181	1.239	1.249	1.382	1.337	1.250	1.209	1.304	1.494	1.369	1.229	1.272	1.368	1.346	1.448	1.352	1.304	0.096						
		actual *perimeter* (mm)	TLC	21.835	21.812	22.300	24.353	24.531	23.798	24.365	23.629	22.991	20.098	21.631	24.535	23.382	23.138	19.276	23.437	22.331	21.800	23.776	17.563	22.529	1.847	-0.401	0.398	0.089	0.175	0.780	0.957
			JHH	22.508	21.989	22.898	25.312	25.185	23.866	25.356	23.466	23.379	21.045	21.892	24.934	23.928	23.415	19.805	23.651	21.762	22.629	23.996	17.596	22.930	1.923						
		marked *surface-area* (mm^2)	TLC	13.875	11.643	11.254	14.632	12.723	14.218	14.736	14.590	14.176	11.570	12.163	14.428	16.006	13.839	11.135	14.234	15.405	12.922	15.193	10.239	13.449	1.631	-0.035	0.234	0.052	0.102	0.458	0.990
			JHH	13.598	11.575	11.345	15.156	12.968	14.113	14.445	14.540	14.301	11.747	12.200	14.514	15.568	14.130	11.102	14.196	15.198	13.232	15.275	10.485	13.484	1.560						
	LABIAL	projected *labial-length* (mm)	TLC	9.216	8.910	9.359	9.824	9.688	9.223	9.637	9.185	9.359	8.034	8.882	9.667	9.495	9.502	7.939	9.539	9.209	8.928	9.654	7.053	9.115	0.698	-0.052	0.076	0.017	0.033	0.149	0.992
			JHH	9.213	8.932	9.203	9.906	9.867	9.457	9.707	9.215	9.433	8.106	8.941	9.678	9.525	9.510	7.988	9.589	9.272	8.956	9.672	7.171	9.167	0.692						
		actual *labial-length* (mm)	TLC	10.165	9.784	10.496	10.883	11.601	10.229	11.119	10.306	10.855	9.135	9.987	11.284	10.805	10.622	8.825	10.964	10.607	9.896	11.174	7.523	10.313	0.959	-0.087	0.135	0.030	-0.002	0.265	0.987
			JHH	10.206	9.768	10.412	11.102	11.941	10.574	11.280	10.504	11.048	9.198	9.982	11.174	10.746	10.645	8.839	10.942	10.602	9.964	11.302	7.772	10.400	0.963						
		circumference (mm)	TLC	3.226	3.001	2.529	2.965	2.687	3.156	3.061	3.198	3.123	3.131	3.078	3.199	3.465	3.091	2.969	2.991	2.982	3.023	3.237	3.200	3.066	0.199	-0.002	0.028	0.006	0.012	0.055	1.000
			JHH	3.197	3.021	2.555	2.976	2.674	3.174	3.058	3.171	3.178	3.150	3.097	3.124	3.466	3.108	2.963	2.990	2.989	3.047	3.203	3.208	3.067	0.194						

Table 19. Reliability 3D *right* Incisor Morphometry Inter-Operator Reproducibility (TLC & JHH)

MANDIBULAR INCISORS			CD-1 RELIABILITY																											
			INTER-OPERATOR																				Statistics							
			$n = 20$																											
VIEW/ ASPECT	MEASUREMENT VARIABLE	OPERATOR	1	2	3	4	5	6	7	8	9	10	11	12	13	14	15	16	17	18	19	20	Mean	SD	Mean Dif.	SD. Dif.	SE	Bias	CR	ICC
RIGHT BUCCAL	projected *overall-length* (mm)	TLC	9.756	8.911	9.192	9.933	7.186	8.764	9.611	9.341	8.332	9.819	9.300	7.999	8.919	9.741	7.567	9.426	9.123	8.727	8.962	8.827	8.972	0.741	-0.027	0.047	0.010	0.020	0.091	0.998
		JHH	9.707	8.925	9.214	10.036	7.219	8.822	9.575	9.348	8.331	9.834	9.312	8.040	8.892	9.783	7.581	9.592	9.162	8.756	8.997	8.857	8.999	0.745						
	projected *width-at-midpoint* (mm)	TLC	1.138	1.148	1.123	1.056	1.109	1.132	1.063	1.185	1.181	1.096	1.131	1.108	1.137	1.118	1.092	1.073	1.114	1.132	1.189	1.209	1.127	0.041	-0.022	0.015	0.003	0.007	0.029	1.000
		JHH	1.159	1.167	1.123	1.097	1.125	1.134	1.126	1.201	1.201	1.121	1.143	1.127	1.159	1.130	1.112	1.103	1.152	1.175	1.208	1.216	1.149	0.036						
	actual *width-at-midpoint* (mm)	TLC	1.456	1.479	1.412	1.401	1.433	1.450	1.262	1.525	1.688	1.275	1.440	1.409	1.468	1.501	1.383	1.341	1.376	1.445	1.482	1.512	1.437	0.092	-0.036	0.038	0.008	0.017	0.074	0.818
		JHH	1.534	1.572	1.484	1.452	1.511	1.487	1.288	1.548	1.750	1.238	1.475	1.484	1.487	1.483	1.449	1.350	1.363	1.512	1.466	1.527	1.473	0.108						
	actual *perimeter* (mm)	TLC	24.282	21.763	22.209	25.686	16.817	21.276	24.389	23.350	19.831	25.287	22.458	19.382	21.378	23.325	18.334	22.863	22.430	20.969	21.803	21.281	21.956	2.230	-0.133	0.519	0.116	0.227	1.017	0.970
		JHH	24.723	21.629	22.576	24.354	17.453	21.499	23.386	23.333	20.045	25.467	23.231	19.509	22.151	23.565	18.329	23.125	22.385	21.275	22.422	21.314	22.089	2.052						
	marked *surface-area* (mm^2)	TLC	15.757	15.635	14.316	16.144	10.214	13.255	14.957	17.435	16.136	15.323	14.361	11.578	16.100	15.745	11.219	14.607	14.135	13.717	14.101	14.565	14.465	1.807	0.068	0.330	0.074	0.144	0.646	0.983
		JHH	15.340	14.961	14.102	15.904	10.228	13.597	14.156	17.715	15.959	15.970	14.345	11.756	16.265	15.740	11.004	14.624	13.976	13.704	14.018	14.574	14.397	1.810						
RIGHT LINGUAL	projected *overall-length* (mm)	TLC	9.738	8.896	9.168	9.978	7.106	8.806	9.221	9.301	8.261	9.857	9.316	7.992	8.854	9.697	7.548	9.495	9.115	8.715	8.925	8.798	8.939	0.748	-0.034	0.036	0.008	0.016	0.071	0.996
		JHH	9.746	8.930	9.216	10.035	7.165	8.840	9.256	9.381	8.346	9.857	9.359	8.049	8.784	9.684	7.594	9.561	9.170	8.710	8.949	8.831	8.973	0.740						
	projected *width-at-midpoint* (mm)	TLC	1.123	1.155	1.118	1.088	1.098	1.112	1.084	1.172	1.142	1.116	1.100	1.126	1.148	1.113	1.102	1.074	1.113	1.145	1.173	1.194	1.125	0.032	-0.010	0.031	0.007	0.014	0.062	1.000
		JHH	1.163	1.155	1.137	1.094	1.085	1.139	1.090	1.193	1.138	1.131	1.029	1.121	1.176	1.078	1.185	1.096	1.121	1.126	1.204	1.229	1.134	0.049						
	actual *width-at-midpoint* (mm)	TLC	1.293	1.348	1.310	1.475	1.265	1.329	1.239	1.317	1.356	1.218	1.201	1.325	1.320	1.282	1.276	1.208	1.248	1.278	1.285	1.344	1.296	0.063	-0.007	0.027	0.006	0.012	0.053	1.000
		JHH	1.323	1.329	1.338	1.461	1.274	1.301	1.203	1.291	1.377	1.229	1.191	1.316	1.348	1.324	1.302	1.271	1.261	1.258	1.274	1.380	1.303	0.063						
	actual *perimeter* (mm)	TLC	24.115	21.956	22.007	24.188	18.431	20.841	22.995	23.047	19.986	24.823	22.738	19.675	21.125	24.937	19.031	23.117	22.802	20.958	21.312	20.833	21.946	1.869	-0.195	0.304	0.068	0.133	0.596	0.981
		JHH	23.679	22.334	22.191	24.027	18.609	21.294	23.342	22.917	19.682	25.015	23.110	19.649	21.589	24.869	19.698	23.596	23.015	21.036	21.929	21.225	22.140	1.797						
	marked *surface-area* (mm^2)	TLC	14.608	12.807	12.418	14.921	12.316	12.726	13.226	14.023	12.873	14.285	13.175	10.477	12.606	14.166	10.033	13.096	12.820	12.234	14.074	12.219	12.955	1.236	0.015	0.413	0.092	0.181	0.810	0.940
		JHH	14.207	12.645	12.621	14.586	12.645	12.025	12.501	14.010	12.987	14.435	13.085	10.871	12.606	13.998	10.111	13.131	13.235	12.967	13.353	12.787	12.940	1.097						
	projected *labial-length* (mm)	TLC	9.726	8.835	9.112	9.958	7.162	8.769	9.609	9.343	8.296	9.772	9.313	8.016	8.894	9.722	7.582	9.450	9.122	8.699	8.973	8.828	8.959	0.740	-0.055	0.066	0.015	0.029	0.129	0.995
		JHH	9.762	8.977	9.269	9.982	7.208	8.839	9.628	9.401	8.338	9.848	9.331	8.018	8.894	9.735	7.588	9.482	9.133	8.965	8.980	8.899	9.014	0.742						
	actual *labial-length* (mm)	TLC	10.978	9.673	10.053	11.170	7.703	9.639	11.233	10.454	9.395	11.098	10.432	8.719	9.722	10.886	8.296	10.635	10.283	9.668	9.962	9.836	9.992	0.956	-0.074	0.162	0.036	0.071	0.318	0.980
		JHH	11.113	9.708	10.036	11.144	7.843	9.697	11.362	10.475	9.562	11.124	10.454	8.796	9.768	10.984	8.332	10.796	10.369	9.759	9.994	9.998	10.066	0.949						
	circumference (mm)	TLC	3.122	3.110	3.134	2.999	2.953	3.131	2.985	3.288	3.030	3.031	3.011	2.972	3.002	3.076	2.922	2.916	2.990	3.068	3.058	3.191	3.049	0.093	-0.020	0.047	0.011	0.021	0.092	0.857
		JHH	3.107	3.121	3.047	2.981	2.966	3.139	3.046	3.285	3.044	3.054	3.006	3.033	3.098	3.116	3.029	2.930	3.057	3.111	3.095	3.131	3.070	0.077						

Table 20. 2D And 3D Incisor Morphometry Validation

MANDIBULAR INCISORS				CD-I VALIDATION																											
				METHOD VALIDATION																						Statistics							
VIEW/ ASPECT		MEASUREMENT VARIABLE	METHOD	n = 20																				Mean	SD	Mean Dif.	SD. Dif.	SE	Bias	LOA	t-test	PCC
				1	2	3	4	5	6	7	8	9	10	11	12	13	14	15	16	17	18	19	20									
LEFT	BUCCAL	projected *overall-length* (mm)	2D	9.594	9.144	9.372	10.415	9.100	9.534	9.522	9.377	10.338	8.106	8.569	10.389	9.075	9.463	8.533	9.661	9.020	9.118	9.606	7.447	9.269	0.731	0.154	0.371	0.083	0.163	0.727	0.079*	0.866**
			3D	9.268	8.957	9.419	9.912	9.720	9.138	9.428	9.200	9.417	8.063	8.809	9.694	9.545	9.507	7.986	9.566	9.050	8.874	9.664	7.081	9.115	0.695							
		projected *width-at-midpoint* (mm)	2D	1.081	1.016	1.023	0.972	1.001	1.041	1.002	1.043	1.043	1.030	1.067	1.024	1.210	1.012	1.010	0.974	1.050	1.071	1.070	1.079	1.041	0.051	-0.090	0.035	0.008	0.015	0.069	0.000	0.885**
			3D	1.234	1.070	0.982	1.056	1.057	1.145	1.106	1.146	1.188	1.132	1.090	1.152	1.293	1.108	1.120	1.092	1.092	1.148	1.195	1.217	1.131	0.071							
	LINGUAL	projected *overall-length* (mm)	2D	9.572	9.169	9.777	10.475	9.075	9.563	9.578	9.376	10.376	8.085	8.606	10.480	9.097	9.851	8.567	9.608	9.097	9.089	9.495	7.466	9.320	0.756	0.187	0.403	0.090	0.177	0.790	0.052*	0.850**
			3D	9.225	8.986	9.426	9.905	9.648	9.164	9.661	9.277	9.446	8.088	8.965	9.658	9.521	9.436	7.930	9.546	9.158	8.941	9.655	7.024	9.133	0.703							
		projected *width-at-midpoint* (mm)	2D	1.079	1.036	1.056	0.975	1.001	1.049	1.012	1.136	1.048	1.020	1.044	1.012	1.213	1.005	1.007	1.084	1.045	1.097	1.106	1.083	1.055	0.055	-0.067	0.027	0.006	0.012	0.052	0.000	0.710**
			3D	1.165	1.074	0.956	1.052	1.055	1.138	1.090	1.166	1.145	1.117	1.106	1.125	1.266	1.098	1.096	1.114	1.116	1.160	1.201	1.208	1.122	0.066							
	LABIAL	projected *labial-length* (mm)	2D	9.268	8.957	9.419	9.912	9.720	9.138	9.428	9.200	9.417	8.063	8.809	9.694	9.545	9.507	7.986	9.566	9.050	8.874	9.664	7.081	9.115	0.695	0.000	0.077	0.017	0.034	0.151	0.989*	0.994**
			3D	9.216	8.910	9.359	9.824	9.688	9.223	9.637	9.185	9.359	8.034	8.882	9.667	9.495	9.502	7.939	9.539	9.209	8.928	9.654	7.053	9.115	0.698							
		projected *labial-length* (mm)	2D	10.547	10.379	10.607	10.503	10.532	11.284	11.553	10.444	10.547	9.357	10.065	12.057	10.795	11.268	9.107	11.785	10.960	10.076	9.559	8.440	10.493	0.902	0.257	0.498	0.111	0.218	0.976	0.032*	0.856**
			3D	10.165	9.784	10.496	10.883	11.601	10.229	11.119	10.306	10.855	9.135	9.987	11.284	10.805	10.622	8.825	10.964	10.607	9.896	9.630	7.523	10.236	0.948							
RIGHT	BUCCAL	projected *overall-length* (mm)	2D	9.604	9.022	9.178	10.045	7.131	8.937	9.210	9.505	8.270	9.771	9.706	8.361	8.782	9.641	7.882	9.216	9.292	8.960	9.095	8.898	9.025	0.695	0.054	0.204	0.046	0.089	0.400	0.256*	0.962**
			3D	9.756	8.911	9.192	9.933	7.186	8.764	9.611	9.341	8.332	9.819	9.300	7.999	8.919	9.741	7.567	9.426	9.123	8.727	8.962	8.827	8.972	0.741							
		projected *width-at-midpoint* (mm)	2D	1.127	1.100	1.062	0.957	1.097	1.043	0.993	1.164	1.099	1.037	1.076	0.995	1.010	0.994	0.989	0.965	1.027	1.091	1.077	1.145	1.052	0.060	-0.074	0.036	0.008	0.071	0.071	0.000	0.814**
			3D	1.138	1.148	1.123	1.056	1.109	1.132	1.063	1.185	1.181	1.096	1.131	1.108	1.137	1.118	1.092	1.073	1.114	1.132	1.189	1.209	1.127	0.041							
	LINGUAL	projected *overall-length* (mm)	2D	9.890	9.027	9.489	10.294	7.025	8.873	9.212	9.594	8.106	9.816	9.197	8.164	9.231	9.893	7.868	9.358	9.093	9.007	8.653	8.868	9.033	0.782	0.094	0.192	0.043	0.084	0.377	0.042*	0.969**
			3D	9.738	8.896	9.168	9.978	7.106	8.806	9.221	9.301	8.261	9.857	9.316	7.992	8.854	9.697	7.548	9.495	9.115	8.715	8.925	8.798	8.939	0.748							
		projected *width-at-midpoint* (mm)	2D	1.059	1.082	1.035	0.996	0.998	1.004	1.026	1.069	1.071	1.039	0.998	1.037	1.066	1.055	1.011	0.984	1.038	1.082	1.085	1.090	1.041	0.034	-0.079	0.016	0.004	0.007	0.032	0.000	0.777**
			3D	1.123	1.155	1.118	1.088	1.098	1.112	1.084	1.172	1.142	1.116	1.100	1.126	1.048	1.113	1.102	1.074	1.113	1.145	1.173	1.194	1.120	0.036							
	LABIAL	projected *labial-length* (mm)	2D	9.756	8.911	9.192	9.933	7.186	8.764	9.611	9.341	8.332	9.819	9.300	7.999	8.919	9.741	7.567	9.426	9.123	8.727	8.962	8.827	8.972	0.741	0.013	0.031	0.007	0.013	0.060	0.077*	0.999**
			3D	9.726	8.835	9.112	9.958	7.162	8.769	9.609	9.343	8.296	9.772	9.313	8.016	8.894	9.722	7.582	9.450	9.122	8.699	8.973	8.828	8.959	0.740							
		projected *labial-length* (mm)	2D	11.189	10.144	10.901	12.055	8.015	10.375	10.969	11.217	9.353	12.072	10.672	8.966	9.836	10.326	8.844	10.931	11.114	9.549	9.568	10.484	10.329	1.057	0.337	0.450	0.101	0.197	0.882	0.030*	0.905**
			3D	10.978	9.673	10.053	11.170	7.703	9.639	11.233	10.454	9.395	11.098	10.432	8.719	9.722	10.886	8.296	10.635	10.283	9.668	9.962	9.836	9.992	0.956							

*No Significant Difference at the 0.01 (1%) level (2-tailed). ** Significant Pearson's Correlation at the 0.01 (1%) level (2-tailed).

10.2. APPENDIX 2. PRINCIPAL COMPONENT ANALYSIS

Table 1. 2D PCA Mandible Morphometry

PCA 2D Mandible Morphometry - left buccal

A

Total Variance Explained

COMPONENT	Initial Eigenvalues Total	% of Variance	Cumulative %
1	4.368*	54.599	54.599
2	2.097*	26.216	80.815
3	0.990	12.375	93.190
4	0.337	4.216	97.406
5	0.126	1.577	98.983
6	0.048	0.605	99.588
7	0.026	0.323	99.911
8	0.007	0.089	100.000

B

C

Component Matrix

MEASUREMENT VARIABLE	Component 1	2
mandible-area (mm^2)	0.902	-0.251
basal-length (mm)	0.882	0.372
mandible-perimeter (mm)	0.874	-0.349
ascending-height (mm)	0.850	0.219
overall-length (mm)	0.821	0.348
diagonal-length (mm)	0.766	-0.113
mandible-angle (°)	0.055	-0.963
coronoid-coronoid-length (mm)	-0.159	0.815

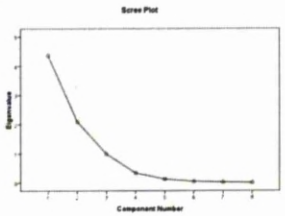

PCA 2D Mandible Morphometry - left lingual

A

Total Variance Explained

COMPONENT	Initial Eigenvalues Total	% of Variance	Cumulative %
1	4.174*	52.179	52.179
2	2.085*	26.059	78.237
3	0.834	10.424	88.662
4	0.609	7.616	96.277
5	0.140	1.752	98.029
6	0.110	1.379	99.408
7	0.035	0.435	99.842
8	0.013	0.158	100.000

B

C

Component Matrix

MEASUREMENT VARIABLE	Component 1	2
mandible-area (mm^2)	0.913	-0.175
basal-length (mm)	0.901	0.299
overall-length (mm)	0.858	0.137
ascending-height (mm)	0.831	0.236
mandible-perimeter (mm)	0.801	-0.479
diagonal-length (mm)	0.678	0.032
mandible-angle (°)	0.017	-0.925
coronoid-coronoid-length (mm)	-0.051	0.897

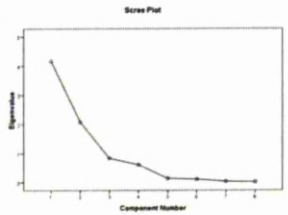

PCA 2D Mandible Morphometry - right buccal

A

Total Variance Explained

COMPONENT	Initial Eigenvalues Total	% of Variance	Cumulative %
1	4.023*	50.286	50.286
2	2.164*	27.056	77.342
3	0.783	9.792	87.135
4	0.407	5.088	92.222
5	0.335	4.192	96.414
6	0.171	2.142	98.556
7	0.080	0.999	99.555
8	0.036	0.445	100.000

B

C

Component Matrix

MEASUREMENT VARIABLE	Component 1	2
mandible-area (mm^2)	0.912	0.064
overall-length (mm)	0.888	0.045
mandible-perimeter (mm)	0.763	-0.356
basal-length (mm)	0.761	0.375
diagonal-length (mm)	0.715	0.462
mandible-angle (°)	0.493	-0.822
coronoid-coronoid-length (mm)	-0.504	0.729
ascending-height (mm)	0.482	0.686

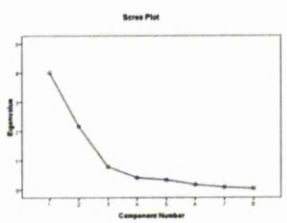

PCA 2D MandibleMorphometry - right lingual

A

Total Variance Explained

COMPONENT	Initial Eigenvalues Total	% of Variance	Cumulative %
1	3.878*	48.480	48.480
2	2.099*	26.239	74.719
3	0.930	11.620	86.339
4	0.407	5.087	91.426
5	0.326	4.074	95.500
6	0.215	2.694	98.193
7	0.109	1.358	99.551
8	0.036	0.449	100.000

B

C

Component Matrix

MEASUREMENT VARIABLE	Component 1	2
mandible-area (mm^2)	0.873	0.058
overall-length (mm)	0.872	0.020
mandible-perimeter (mm)	0.868	-0.159
basal-length (mm)	0.770	0.253
diagonal-length (mm)	0.765	0.302
mandible-angle (°)	0.354	-0.876
coronoid-coronoid-length (mm)	-0.360	0.859
ascending-height (mm)	0.410	0.640

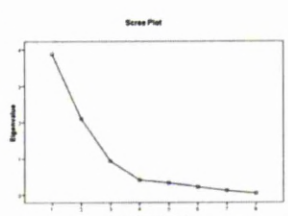

*Eigenvalue > 1.

Table 2. 2D PCA Incisor Morphometry

*Eigenvalue > 1.

PCA 2D Incisor Morphometry - left buccal

A

Total Variance Explained

COMPONENT	Initial Eigenvalues Total	% of Variance	Cumulative %
1	3.758*	75.165	75.165
2	1.067*	21.335	96.500
3	0.140	2.791	99.292
4	0.030	0.592	99.883
5	0.006	0.117	100.000

B

MEASUREMENT VARIABLE	Component Matrix Component 1	2
projected *perimeter* (mm)	0.989	-0.102
projected *overall-length* (mm)	0.979	-0.069
projected *surface-area* (mm^2)	0.970	0.192
angle-of-curvature (°)	-0.883	0.358
projected *width-at-midpoint* (mm)	0.316	0.941

C

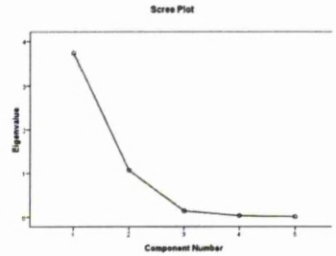

PCA 2D Incisor Morphometry - left lingual

A

Total Variance Explained

COMPONENT	Initial Eigenvalues Total	% of Variance	Cumulative %
1	3.766*	75.326	75.326
2	1.017*	20.339	95.665
3	0.166	3.322	98.987
4	0.043	0.853	99.840
5	0.008	0.160	100.000

B

MEASUREMENT VARIABLE	Component Matrix Component 1	2
projected *perimeter* (mm)	0.995	-0.055
projected *overall-length* (mm)	0.983	-0.045
projected *surface-area* (mm^2)	0.961	0.121
angle-of-curvature (°)	-0.938	-0.061
projected *width-at-midpoint* (mm)	-0.075	0.997

C

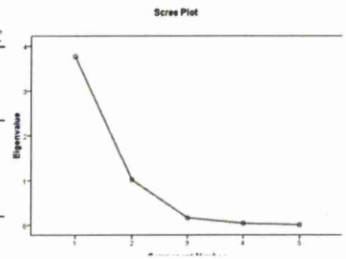

PCA 2D Incisor Morphometry - right buccal

A

Total Variance Explained

COMPONENT	Initial Eigenvalues Total	% of Variance	Cumulative %
1	3.376*	67.522	67.522
2	0.964	19.271	86.793
3	0.533	10.656	97.448
4	0.111	2.222	99.670
5	0.016	0.330	100.000

B

MEASUREMENT VARIABLE	Component 1
projected *surface-area* (mm^2)	0.970
projected *overall-length* (mm)	0.947
projected *perimeter* (mm)	0.937
angle-of-curvature (°)	-0.725
projected *width-at-midpoint* (mm)	0.368

C

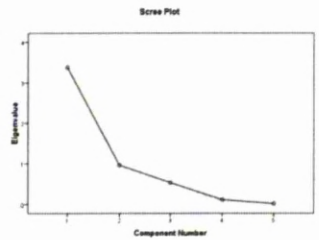

PCA 2D Incisor Morphometry - right lingual

A

Total Variance Explained

COMPONENT	Initial Eigenvalues Total	% of Variance	Cumulative %
1	3.527*	70.551	70.551
2	0.929	18.588	89.139
3	0.453	9.056	98.196
4	0.066	1.323	99.518
5	0.024	0.482	100.000

B

MEASUREMENT VARIABLE	Component 1
projected *perimeter* (mm)	0.959
projected *surface-area* (mm^2)	0.958
projected *overall-length* (mm)	0.956
angle-of-curvature (°)	-0.790
projected *width-at-midpoint* (mm)	0.391

C

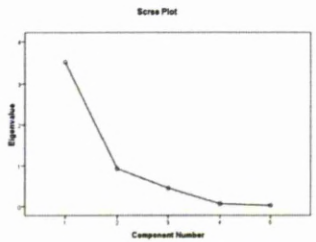

Table 3. PCA 3D Incisor Morphometry - *left*

*Eigenvalue > 1.

PCA 3D Incisor Morphometry - left buccal

A

COMPONENT	Total Variance Explained: Initial Eigenvalues Total	% of Variance	Cumulative %
1	2.435*	48.693	48.693
2	2.159*	43.175	91.868
3	0.231	4.611	96.479
4	0.124	2.483	98.962
5	0.052	1.038	100.000

B

C

MEASUREMENT VARIABLE	Component Matrix Component 1	2
marked *surface-area* (mm^2)	0.909	0.266
projected *overall-length* (mm)	0.864	-0.352
actual *perimeter* (mm)	0.862	-0.430
projected *width-at-midpoint* (mm)	0.152	0.952
actual *width-at-midpoint* (mm)	0.309	0.934

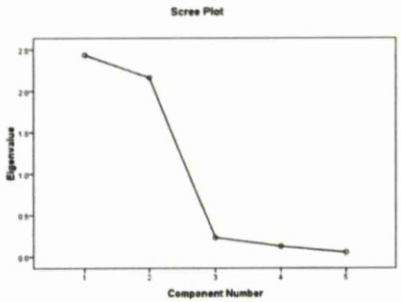

PCA 3D Incisor Morphometry - left lingual

A

COMPONENT	Total Variance Explained: Initial Eigenvalues Total	% of Variance	Cumulative %
1	2.525*	50.499	50.499
2	1.933*	38.663	89.162
3	0.253	5.065	94.228
4	0.152	3.037	97.265
5	0.137	2.735	100.000

B

C

MEASUREMENT VARIABLE	Component Matrix Component 1	2
marked *surface-area* (mm^2)	0.923	0.213
actual *perimeter* (mm)	0.895	-0.314
projected *overall-length* (mm)	0.865	-0.404
projected *width-at-midpoint* (mm)	0.175	0.914
actual *width-at-midpoint* (mm)	0.307	0.889

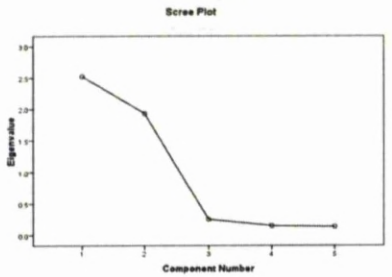

PCA 3D Incisor Morphometry - left labial

A

COMPONENT	Total Variance Explained: Initial Eigenvalues Total	% of Variance	Cumulative %
1	2.946*	58.922	58.922
2	1.277*	25.538	84.460
3	0.474	9.475	93.935
4	0.187	3.733	97.668
5	0.117	2.332	100.000

B

C

MEASUREMENT VARIABLE	Component Matrix Component 1	2
total *surface-area* (mm^2)	0.926	-0.030
projected *labial-length* (mm)	0.918	-0.231
actual *labial-length* (mm)	0.904	-0.312
total *volume* (mm^3)	0.628	0.561
circumference (mm)	0.188	0.901

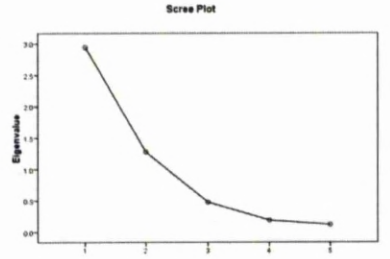

*Eigenvalue > 1.

Table 4. PCA 3D Incisor Morphometry - *right*

PCA 3D Incisor Morphometry - right buccal

A

COMPONENT	Total Variance Explained Initial Eigenvalues Total	% of Variance	Cumulative %
1	2.645*	52.893	52.893
2	1.817*	36.339	89.232
3	0.343	6.866	96.098
4	0.179	3.573	99.672
5	0.016	0.328	100.000

B

C

MEASUREMENT VARIABLE	Component Matrix Component 1	2
actual *perimeter* (mm)	0.981	-0.094
projected *overall-length* (mm)	0.980	-0.007
marked *surface-area* (mm^2)	0.819	0.454
projected *width-at-midpoint* (mm)	-0.102	0.895
actual *width-at-midpoint* (mm)	-0.203	0.895

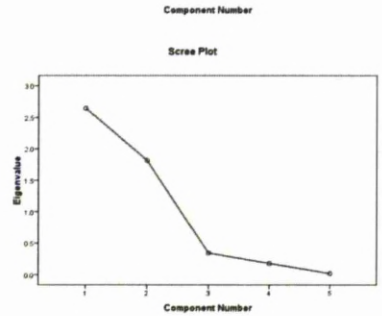

PCA 3D Incisor Morphometry - right lingual

A

COMPONENT	Total Variance Explained Initial Eigenvalues Total	% of Variance	Cumulative %
1	2.676*	53.528	53.528
2	1.179*	23.587	77.116
3	0.833	16.665	93.781
4	0.278	5.550	99.331
5	0.033	0.669	100.000

B

C

MEASUREMENT VARIABLE	Component Matrix Component 1	2
projected *overall-length* (mm)	0.968	-0.078
actual *perimeter* (mm)	0.966	-0.106
marked *surface-area* (mm^2)	0.889	0.102
projected *width-at-midpoint* (mm)	-0.006	0.786
actual *width-at-midpoint* (mm)	0.127	0.731

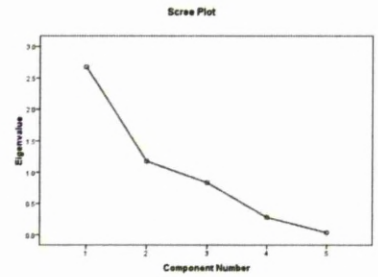

PCA 3D Incisor Morphometry - right labial

A

COMPONENT	Total Variance Explained Initial Eigenvalues Total	% of Variance	Cumulative %
1	3.465*	69.300	69.300
2	0.849*	16.989	86.289
3	0.463	9.256	95.545
4	0.205	4.107	99.652
5	0.017	0.348	100.000

B

C

MEASUREMENT VARIABLE	Component 1
projected *labial-length* (mm)	0.946
actual *labial-length* (mm)	0.934
total *surface-area* (mm^2)	0.917
total *volume* (mm^3)	0.775
circumference (mm)	0.508

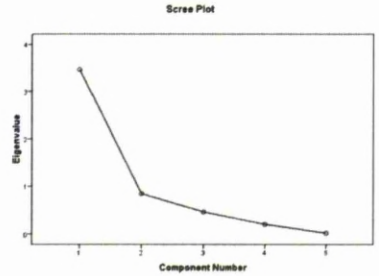

*Eigenvalue > 1.

10.3. EXPERIMENTAL COMPARISON

Table 1. *Amelx* 2D Mandible Morphometry – left buccal

HEMI-MANDIBLE		ANOVA									MULTIPLE COMPARISON					
VIEW/ ASPECT	MEASUREMENT VARIABLE	GROUP	Mean	SD	SE	95% CI of Mean lower bound	95% CI of Mean upper bound	min	max	F	Sig	GROUPS	MD	SE	95% CI lower bound	95% CI upper bound	Sig
LEFT BUCCAL	*overall-length* (mm)	WT	11.782	0.132	0.059	11.618	11.947	11.611	11.922	2.495	0.097	WT-HET	0.126	0.284	-0.687	0.940	0.970
		HET	11.656	0.252	0.112	11.344	11.968	11.288	11.954			WT-HEMI	0.343		-0.470	1.157	0.631
		HEMI	11.439	0.649	0.290	10.633	12.245	10.338	11.924			WT-HOMO	0.725		-0.089	1.539	0.090
		HOMO	11.057	0.554	0.248	10.370	11.745	10.219	11.735			HET-HEMI	0.217		-0.596	1.031	0.869
												HET-HOMO	0.599		-0.215	1.412	0.193
												HEMI-HOMO	0.382		-0.432	1.195	0.551
	ascending-height (mm)	WT	6.005	0.139	0.062	5.832	6.178	5.782	6.163	5.110	0.007**	WT-HET	0.112	0.119	-0.227	0.451	0.781
		HET	5.892	0.188	0.084	5.659	6.126	5.618	6.113			WT-HEMI	0.246		-0.093	0.585	0.203
		HEMI	5.759	0.270	0.121	5.424	6.094	5.336	6.039			WT-HOMO	0.466		0.127	0.805	0.006**
		HOMO	5.539	0.114	0.051	5.398	5.680	5.444	5.697			HET-HEMI	0.134		-0.205	0.473	0.679
												HET-HOMO	0.354		0.015	0.693	0.039**
												HEMI-HOMO	0.220		-0.119	0.559	0.285
	basal-length (mm)	WT	7.070	0.159	0.071	6.872	7.267	6.843	7.271	0.732	0.548	WT-HET	0.161	0.196	-0.399	0.721	0.843
		HET	6.909	0.092	0.041	6.795	7.023	6.772	7.013			WT-HEMI	0.208		-0.352	0.769	0.715
		HEMI	6.861	0.460	0.206	6.290	7.432	6.110	7.359			WT-HOMO	0.279		-0.281	0.839	0.503
		HOMO	6.791	0.372	0.166	6.329	7.252	6.407	7.351			HET-HEMI	0.047		-0.513	0.608	0.995
												HET-HOMO	0.118		-0.442	0.678	0.930
												HEMI-HOMO	0.071		-0.490	0.631	0.983
	mandible-angle (°)	WT	66.219	1.273	0.569	64.638	67.799	64.349	67.620	7.500	0.002*	WT-HET	-1.042	1.282	-4.709	2.625	0.847
		HET	67.261	3.033	1.357	63.494	71.027	63.937	72.041			WT-HEMI	-1.620		-5.286	2.047	0.597
		HEMI	67.838	2.037	0.911	65.309	70.368	65.700	70.078			WT-HOMO	-5.666		-9.333	-2.000	0.002**
		HOMO	71.885	1.205	0.539	70.388	73.382	70.357	73.060			HET-HEMI	-0.578		-4.244	3.089	0.969
												HET-HOMO	-4.624		-8.291	-0.958	0.011**
												HEMI-HOMO	-4.046		-7.713	-0.380	0.028**
	coronoid-coronoid-length (mm)	WT	2.739	0.111	0.050	2.601	2.877	2.590	2.864	0.707	0.562	WT-HET	-0.155	0.121	-0.502	0.191	0.586
		HET	2.895	0.308	0.138	2.512	3.277	2.588	3.383			WT-HEMI	-0.021		-0.368	0.326	0.998
		HEMI	2.760	0.118	0.053	2.614	2.906	2.638	2.911			WT-HOMO	-0.016		-0.363	0.330	0.999
		HOMO	2.756	0.160	0.072	2.557	2.955	2.501	2.932			HET-HEMI	0.134		-0.212	0.481	0.689
												HET-HOMO	0.139		-0.208	0.486	0.667
												HEMI-HOMO	0.005		-0.342	0.351	1.000
	diagonal-length (mm)	WT	8.504	0.134	0.060	8.337	8.671	8.279	8.592	1.421	0.273	WT-HET	0.039	0.209	-0.557	0.636	0.998
		HET	8.465	0.193	0.086	8.225	8.704	8.156	8.625			WT-HEMI	0.032		-0.565	0.628	0.999
		HEMI	8.472	0.537	0.240	7.806	9.139	7.746	8.980			WT-HOMO	-0.326		-0.923	0.270	0.425
		HOMO	8.830	0.303	0.136	8.454	9.206	8.558	9.335			HET-HEMI	-0.008		-0.604	0.589	1.000
												HET-HOMO	-0.366		-0.962	0.231	0.330
												HEMI-HOMO	-0.358		-0.954	0.239	0.348
	mandible-perimeter (mm)	WT	34.001	0.645	0.288	33.200	34.801	33.367	34.921	0.861	0.481	WT-HET	0.313	0.653	-1.554	2.180	0.963
		HET	33.688	0.348	0.156	33.256	34.120	33.223	34.128			WT-HEMI	0.633		-1.234	2.500	0.768
		HEMI	33.368	1.777	0.795	31.162	35.574	30.468	35.085			WT-HOMO	0.998		-0.869	2.865	0.444
		HOMO	33.003	0.752	0.336	32.069	33.936	32.022	34.005			HET-HEMI	0.320		-1.547	2.187	0.960
												HET-HOMO	0.685		-1.182	2.552	0.723
												HEMI-HOMO	0.365		-1.502	2.232	0.943
	mandible-area (mm^2)	WT	34.072	0.626	0.280	33.295	34.850	33.207	34.881	0.088	0.965	WT-HET	-0.406	1.228	-3.918	3.106	0.987
		HET	34.478	1.448	0.647	32.680	36.276	32.094	35.591			WT-HEMI	0.155		-3.358	3.667	0.999
		HEMI	33.918	3.456	1.546	29.626	38.209	28.598	36.581			WT-HOMO	0.123		-3.389	3.635	1.000
		HOMO	33.949	0.798	0.357	32.958	34.940	32.957	35.097			HET-HEMI	0.560		-2.952	4.073	0.967
												HET-HOMO	0.529		-2.983	4.041	0.972
												HEMI-HOMO	-0.031		-3.544	3.481	1.000

* Bonferroni Corrected Significant Difference ($p \leq 0.002$)
** Significant Difference ($p \leq 0.05$)

Table 2. *Amelx* 2D Mandible Morphometry – left lingual

HEMI-MANDIBLE		ANOVA									MULTIPLE COMPARISON					
VIEW/ ASPECT	MEASUREMENT VARIABLE	GROUP	Mean	SD	SE	95% CI of Mean lower bound	95% CI of Mean upper bound	min'	max'	F	Sig.	GROUPS	MD	SE	95% CI lower bound	95% CI upper bound	Sig.
LEFT LINGUAL	*overall-length* (mm)	WT	11.798	0.109	0.049	11.662	11.933	11.691	11.916	1.873	0.175	WT-HET	-0.048	0.266	-0.810	0.714	0.998
		HET	11.846	0.341	0.152	11.423	12.269	11.279	12.159			WT-HEMI	0.263		-0.499	1.025	0.758
		HEMI	11.534	0.674	0.301	10.698	12.371	10.395	11.995			WT-HOMO	0.508		-0.254	1.270	0.264
		HOMO	11.289	0.357	0.160	10.846	11.733	11.029	11.868			HET-HEMI	0.312		-0.450	1.074	0.653
												HET-HOMO	0.557		-0.205	1.319	0.198
												HEMI-HOMO	0.245		-0.517	1.007	0.795
	ascending-height (mm)	WT	6.047	0.196	0.088	5.803	6.290	5.795	6.298	5.607	0.008**	WT-HET	0.028	0.153	-0.410	0.467	0.998
		HET	6.018	0.240	0.107	5.721	6.316	5.611	6.205			WT-HEMI	0.333		-0.106	0.771	0.174
		HEMI	5.714	0.350	0.157	5.279	6.148	5.129	6.009			WT-HOMO	0.536		0.097	0.975	0.014**
		HOMO	5.511	0.129	0.058	5.350	5.671	5.347	5.694			HET-HEMI	0.304		-0.134	0.743	0.234
												HET-HOMO	0.508		0.069	0.946	0.021**
												HEMI-HOMO	0.203		-0.235	0.642	0.561
	basal-length (mm)	WT	7.098	0.149	0.066	6.914	7.283	6.893	7.312	1.118	0.371	WT-HET	0.104	0.199	-0.467	0.674	0.953
		HET	6.995	0.169	0.076	6.785	7.204	6.722	7.154			WT-HEMI	0.180		-0.390	0.750	0.804
		HEMI	6.918	0.447	0.200	6.364	7.473	6.251	7.480			WT-HOMO	0.354		-0.217	0.924	0.321
		HOMO	6.745	0.384	0.172	6.268	7.221	6.435	7.347			HET-HEMI	0.076		-0.494	0.647	0.980
												HET-HOMO	0.250		-0.321	0.820	0.604
												HEMI-HOMO	0.174		-0.397	0.744	0.820
	mandible-angle (°)	WT	65.167	1.311	0.586	63.539	66.795	63.600	66.770	7.299	0.003**	WT-HET	-1.056	1.336	-4.879	2.767	0.858
		HET	66.223	3.303	1.477	62.123	70.324	63.055	71.389			WT-HEMI	-1.109		-4.931	2.714	0.840
		HEMI	66.276	1.899	0.849	63.917	68.634	64.234	68.720			WT-HOMO	-5.723		-9.546	-1.901	0.003**
		HOMO	70.891	1.273	0.569	69.310	72.471	68.982	72.236			HET-HEMI	-0.053		-3.875	3.770	1.000
												HET-HOMO	-4.667		-8.490	-0.845	0.014**
												HEMI-HOMO	-4.615		-8.438	-0.792	0.016**
	coronoid-coronoid-length (mm)	WT	2.844	0.127	0.057	2.686	3.002	2.663	2.987	0.731	0.548	WT-HET	-0.113	0.130	-0.485	0.258	0.819
		HET	2.958	0.349	0.156	2.524	3.391	2.743	3.571			WT-HEMI	0.077		-0.295	0.449	0.933
		HEMI	2.767	0.146	0.065	2.586	2.949	2.572	2.958			WT-HOMO	-0.027		-0.398	0.345	0.997
		HOMO	2.871	0.097	0.043	2.750	2.992	2.766	3.018			HET-HEMI	0.190		-0.181	0.562	0.480
												HET-HOMO	0.087		-0.285	0.458	0.908
												HEMI-HOMO	-0.104		-0.475	0.268	0.854
	diagonal-length (mm)	WT	8.564	0.113	0.051	8.423	8.704	8.385	8.671	0.785	0.520	WT-HET	-0.063	0.216	-0.680	0.555	0.991
		HET	8.626	0.304	0.136	8.249	9.004	8.205	8.999			WT-HEMI	0.067		-0.550	0.685	0.989
		HEMI	8.496	0.484	0.217	7.895	9.098	7.852	8.911			WT-HOMO	-0.247		-0.864	0.370	0.668
		HOMO	8.811	0.354	0.158	8.371	9.251	8.513	9.405			HET-HEMI	0.130		-0.487	0.747	0.930
												HET-HOMO	-0.184		-0.802	0.433	0.828
												HEMI-HOMO	-0.314		-0.932	0.303	0.484
	mandible-perimeter (mm)	WT	35.657	0.951	0.425	34.476	36.838	34.272	36.813	0.620	0.612	WT-HET	-0.107	0.932	-2.774	2.560	0.999
		HET	35.764	1.050	0.470	34.460	37.068	34.459	36.867			WT-HEMI	0.613		-2.054	3.279	0.911
		HEMI	35.044	2.465	1.102	31.984	38.105	30.894	37.217			WT-HOMO	0.990		-1.677	3.657	0.717
		HOMO	34.667	0.778	0.348	33.701	35.633	33.697	35.665			HET-HEMI	0.719		-1.947	3.386	0.866
												HET-HOMO	1.097		-1.570	3.764	0.649
												HEMI-HOMO	0.377		-2.289	3.044	0.977
	mandible-area (mm^2)	WT	34.687	0.819	0.366	33.670	35.704	33.634	35.900	0.656	0.591		-1.017	1.440	-5.138	3.104	0.893
		HET	35.704	2.310	1.033	32.836	38.572	31.986	38.278			WT-HEMI	0.530		-3.591	4.650	0.982
		HEMI	34.157	3.690	1.650	29.575	38.739	28.583	36.805			WT-HOMO	0.875		-3.246	4.995	0.928
		HOMO	33.812	1.058	0.473	32.498	35.126	32.750	35.204			HET-HEMI	1.547		-2.574	5.668	0.710
												HET-HOMO	1.892		-2.229	6.013	0.568
												HEMI-HOMO	0.345		-3.776	4.466	0.995

* Bonferroni Corrected Significant Difference ($p \leq 0.002$)
** Significant Difference ($p \leq 0.05$)

Table 3. *Amelx* 2D Mandible Morphometry – right buccal

HEMI-MANDIBLE VIEW/ ASPECT	MEASUREMENT VARIABLE	ANOVA GROUP	Mean	SD	SE	95% CI of Mean lower bound	95% CI of Mean upper bound	min	max	F	Sig.	MULTIPLE COMPARISON GROUPS	MD	SE	95% CI lower bound	95% CI upper bound	Sig.
RIGHT BUCCAL	*overall-length* (mm)	WT	11.879	0.239	0.107	11.583	12.176	11.487	12.110	1.132	0.366	WT-HET	0.239	0.336	-0.724	1.202	0.892
		HET	11.640	0.137	0.061	11.470	11.811	11.408	11.767			WT-HEMI	0.375		-0.588	1.338	0.686
		HEMI	11.504	0.987	0.441	10.279	12.729	9.886	12.235			WT-HOMO	0.605		-0.358	1.567	0.310
		HOMO	11.275	0.287	0.128	10.918	11.631	10.966	11.704			HET-HEMI	0.136		-0.827	1.099	0.977
												HET-HOMO	0.366		-0.597	1.328	0.702
												HEMI-HOMO	0.230		-0.733	1.192	0.902
	ascending-height (mm)	WT	6.012	0.138	0.061	5.841	6.182	5.863	6.234	3.908	0.029**	WT-HET	0.066	0.120	-0.276	0.408	0.945
		HET	5.946	0.222	0.099	5.670	6.222	5.620	6.148			WT-HEMI	0.225		-0.117	0.567	0.275
		HEMI	5.787	0.251	0.112	5.476	6.098	5.473	6.078			WT-HOMO	0.373		0.031	0.715	0.030**
		HOMO	5.639	0.109	0.049	5.504	5.774	5.518	5.734			HET-HEMI	0.159		-0.183	0.501	0.558
												HET-HOMO	0.307		-0.035	0.649	0.087
												HEMI-HOMO	0.148		-0.194	0.490	0.613
	basal-length (mm)	WT	6.913	0.123	0.055	6.760	7.066	6.741	7.033	0.498	0.708	WT-HET	-0.142	0.265	-0.901	0.618	0.950
		HET	7.055	0.234	0.105	6.764	7.346	6.693	7.350			WT-HEMI	-0.113		-0.873	0.646	0.973
		HEMI	7.026	0.762	0.341	6.081	7.972	5.753	7.695			WT-HOMO	0.141		-0.618	0.900	0.950
		HOMO	6.772	0.232	0.104	6.484	7.060	6.413	7.040			HET-HEMI	0.028		-0.731	0.787	1.000
												HET-HOMO	0.283		-0.477	1.042	0.715
												HEMI-HOMO	0.254		-0.505	1.014	0.774
	mandible-angle (°)	WT	62.554	1.917	0.857	60.174	64.934	59.878	64.604	7.282	0.003**	WT-HET	-3.650	1.612	-8.262	0.962	0.148
		HET	66.205	1.373	0.614	64.500	67.909	64.380	67.922			WT-HEMI	-4.168		-8.780	0.444	0.084
		HEMI	66.722	3.534	1.581	62.334	71.111	63.164	72.663			WT-HOMO	-7.514		-12.126	-2.902	0.001**
		HOMO	70.068	2.817	1.260	66.570	73.566	67.518	74.810			HET-HEMI	-0.518		-5.130	4.094	0.988
												HET-HOMO	-3.863		-8.475	0.749	0.118
												HEMI-HOMO	-3.346		-7.958	1.266	0.203
	coronoid-coronoid-length (mm)	WT	2.926	0.273	0.122	2.587	3.265	2.537	3.284	0.066	0.977	WT-HET	0.061	0.147	-0.359	0.482	0.975
		HET	2.865	0.138	0.062	2.693	3.037	2.624	2.972			WT-HEMI	0.049		-0.371	0.470	0.986
		HEMI	2.877	0.064	0.029	2.797	2.957	2.789	2.971			WT-HOMO	0.034		-0.386	0.454	0.996
		HOMO	2.893	0.343	0.154	2.466	3.319	2.406	3.341			HET-HEMI	-0.012		-0.432	0.408	1.000
												HET-HOMO	-0.028		-0.448	0.393	0.998
												HEMI-HOMO	-0.016		-0.436	0.405	1.000
	diagonal-length (mm)	WT	8.347	0.074	0.033	8.256	8.438	8.246	8.450	2.622	0.086	WT-HET	-0.219	0.156	-0.666	0.227	0.514
		HET	8.566	0.271	0.121	8.230	8.903	8.140	8.877			WT-HEMI	-0.389		-0.836	0.057	0.099
		HEMI	8.736	0.366	0.164	8.282	9.191	8.247	9.148			WT-HOMO	-0.364		-0.811	0.082	0.131
		HOMO	8.711	0.176	0.079	8.493	8.930	8.461	8.897			HET-HEMI	-0.170		-0.616	0.276	0.701
												HET-HOMO	-0.145		-0.591	0.301	0.790
												HEMI-HOMO	0.025		-0.421	0.471	0.998
	mandible-perimeter (mm)	WT	34.721	2.195	0.982	31.995	37.447	33.340	38.569	0.895	0.465	WT-HET	0.458	1.069	-2.601	3.517	0.973
		HET	34.263	0.988	0.442	33.036	35.490	33.147	35.680			WT-HEMI	1.256		-1.802	4.315	0.650
		HEMI	33.464	2.189	0.979	30.747	36.182	30.046	35.237			WT-HOMO	1.556		-1.503	4.615	0.485
		HOMO	33.165	0.919	0.411	32.024	34.306	32.180	34.169			HET-HEMI	0.798		-2.260	3.857	0.877
												HET-HOMO	1.098		-1.961	4.157	0.737
												HEMI-HOMO	0.299		-2.759	3.358	0.992
	mandible-area (mm^2)	WT	34.615	1.768	0.791	32.420	36.811	33.035	37.637	0.020	0.996	WT-HET	0.096	1.388	-3.875	4.066	1.000
		HET	34.520	1.218	0.545	33.008	36.032	32.400	35.320			WT-HEMI	0.227		-3.743	4.198	0.998
		HEMI	34.388	3.399	1.520	30.167	38.609	29.227	37.316			WT-HOMO	-0.097		-4.067	3.873	1.000
		HOMO	34.713	1.758	0.786	32.530	36.896	32.299	36.305			HET-HEMI	0.132		-3.838	4.102	1.000
												HET-HOMO	-0.193		-4.163	3.777	0.999
												HEMI-HOMO	-0.325		-4.295	3.646	0.995

* Bonferroni Corrected Significant Difference ($p \leq 0.002$)
** Significant Difference ($p \leq 0.05$)

Table 4. *Amelx* 2D Mandible Morphometry – right lingual

HEMI-MANDIBLE		ANOVA									MULTIPLE COMPARISON					
VIEW/ ASPECT	MEASUREMENT VARIABLE	GROUP	Mean	SD	SE	95% CI of Mean lower bound	95% CI of Mean upper bound	min	max	F	Sig.	GROUPS	MD	SE	95% CI lower bound	95% CI upper bound	Sig.
RIGHT LINGUAL	*overall-length* (mm)	WT	11.936	0.221	0.099	11.662	12.211	11.591	12.175	0.867	0.478	WT-HET	0.048	0.335	-0.911	1.007	0.999
		HET	11.888	0.125	0.056	11.733	12.043	11.742	12.020			WT-HEMI	0.336		-0.623	1.294	0.751
		HEMI	11.601	0.985	0.440	10.378	12.823	9.990	12.285			WT-HOMO	0.455		-0.504	1.413	0.542
		HOMO	11.482	0.298	0.133	11.112	11.851	11.003	11.748			HET-HEMI	0.288		-0.671	1.246	0.826
												HET-HOMO	0.407		-0.552	1.365	0.627
												HEMI-HOMO	0.119		-0.839	1.078	0.984
	ascending-height (mm)	WT	6.060	0.151	0.067	5.873	6.247	5.861	6.273	5.719	0.007**	WT-HET	0.023	0.121	-0.324	0.370	0.997
		HET	6.037	0.117	0.052	5.892	6.182	5.890	6.146			WT-HEMI	0.299		-0.048	0.646	0.105
		HEMI	5.761	0.321	0.144	5.363	6.160	5.332	6.089			WT-HOMO	0.415		0.068	0.762	0.017**
		HOMO	5.645	0.087	0.039	5.537	5.754	5.565	5.781			HET-HEMI	0.276		-0.071	0.623	0.146
												HET-HOMO	0.392		0.045	0.739	0.024**
												HEMI-HOMO	0.116		-0.231	0.463	0.775
	basal-length (mm)	WT	7.006	0.108	0.049	6.871	7.141	6.901	7.184	0.686	0.574	WT-HET	-0.168	0.244	-0.866	0.531	0.901
		HET	7.174	0.180	0.081	6.950	7.397	7.021	7.463			WT-HEMI	-0.064		-0.762	0.635	0.993
		HEMI	7.070	0.709	0.317	6.189	7.950	5.877	7.557			WT-HOMO	0.173		-0.525	0.872	0.892
		HOMO	6.833	0.221	0.099	6.558	7.107	6.469	7.070			HET-HEMI	0.104		-0.595	0.802	0.973
												HET-HOMO	0.341		-0.358	1.039	0.520
												HEMI-HOMO	0.237		-0.462	0.936	0.768
	mandible-angle (°)	WT	61.434	2.125	0.950	58.796	64.072	58.480	63.566	6.785	0.004**	WT-HET	-3.447	1.690	-8.283	1.390	0.215
		HET	64.880	1.403	0.627	63.138	66.622	63.090	66.680			WT-HEMI	-3.880		-8.717	0.956	0.141
		HEMI	65.314	3.891	1.740	60.482	70.146	61.973	72.050			WT-HOMO	-7.612		-12.448	-2.775	0.002**
		HOMO	69.046	2.636	1.179	65.772	72.319	66.605	73.521			HET-HEMI	-0.434		-5.270	4.403	0.994
												HET-HOMO	-4.165		-9.002	0.671	0.105
												HEMI-HOMO	-3.731		-8.568	1.105	0.163
	coronoid-coronoid-length (mm)	WT	3.100	0.185	0.083	2.871	3.330	2.818	3.267	0.789	0.518	WT-HET	0.060	0.113	-0.262	0.382	0.951
		HET	3.041	0.084	0.038	2.937	3.145	2.923	3.115			WT-HEMI	0.083		-0.239	0.405	0.882
		HEMI	3.018	0.135	0.061	2.850	3.186	2.822	3.197			WT-HOMO	0.170		-0.152	0.492	0.452
		HOMO	2.930	0.259	0.116	2.608	3.252	2.603	3.267			HET-HEMI	0.023		-0.299	0.345	0.997
												HET-HOMO	0.111		-0.211	0.433	0.760
												HEMI-HOMO	0.088		-0.234	0.410	0.862
	diagonal-length (mm)	WT	8.458	0.107	0.048	8.326	8.591	8.352	8.616	0.952	0.439	WT-HET	0.941	0.885	-1.592	3.474	0.716
		HET	7.517	2.769	1.238	4.079	10.955	2.569	8.884			WT-HEMI	-0.358		-2.891	2.174	0.977
		HEMI	8.817	0.335	0.150	8.400	9.233	8.395	9.135			WT-HOMO	-0.345		-2.877	2.188	0.979
		HOMO	8.803	0.212	0.095	8.539	9.067	8.510	9.026			HET-HEMI	-1.299		-3.832	1.233	0.478
												HET-HOMO	-1.286		-3.818	1.247	0.487
												HEMI-HOMO	0.014		-2.519	2.546	1.000
	mandible-perimeter (mm)	WT	34.150	2.028	0.907	31.631	36.668	31.017	36.220	0.963	0.434	WT-HET	-1.644	1.041	-4.623	1.334	0.417
		HET	35.794	0.815	0.365	34.782	36.806	34.887	36.740			WT-HEMI	-0.934		-3.913	2.044	0.806
		HEMI	35.084	2.231	0.998	32.313	37.855	31.553	37.018			WT-HOMO	-0.336		-3.315	2.642	0.988
		HOMO	34.486	1.039	0.465	33.196	35.777	33.093	35.856			HET-HEMI	0.710		-2.268	3.688	0.902
												HET-HOMO	1.308		-1.670	4.286	0.602
												HEMI-HOMO	0.598		-2.380	3.576	0.958
	mandible-area (mm^2)	WT	34.822	1.283	0.574	33.229	36.415	33.602	36.917	0.376	0.772	WT-HET	-0.705	1.229	-4.221	2.810	0.938
		HET	35.528	0.342	0.153	35.102	35.953	35.096	35.925			WT-HEMI	0.047		-3.468	3.563	1.000
		HEMI	34.775	3.396	1.519	30.558	38.992	29.519	37.597			WT-HOMO	0.594		-2.922	4.110	0.962
		HOMO	34.228	1.342	0.600	32.561	35.895	32.030	35.489			HET-HEMI	0.753		-2.763	4.268	0.927
												HET-HOMO	1.299		-2.216	4.815	0.719
												HEMI-HOMO	0.547		-2.969	4.062	0.970

* Bonferroni Corrected Significant Difference ($p \leq 0.002$)
** Significant Difference ($p \leq 0.05$)

Table 5. *Amelx* 2D Incisor Morphometry – left buccal

MANDIBULAR INCISORS			ANOVA									MULTIPLE COMPARISON					
VIEW/ ASPECT		MEASUREMENT VARIABLE	GROUP	Mean	SD	SE	95% CI of Mean lower bound	95% CI of Mean upper bound	min'	max'	F	Sig.	GROUPS	MD	SE	95% CI lower bound	95% CI upper bound	Sig.
LEFT	BUCCAL	*overall-length* (mm)	WT	10.560	0.758	0.339	9.619	11.501	9.808	11.699	9.165	0.001*	WT-HET	0.217	0.328	-0.721	1.154	0.910
			HET	10.343	0.474	0.212	9.755	10.931	9.521	10.701			WT-HEMI	0.369		-0.569	1.306	0.680
			HEMI	10.191	0.475	0.212	9.602	10.781	9.428	10.615			WT-HOMO	1.565		0.627	2.502	0.001**
			HOMO	8.995	0.223	0.100	8.719	9.271	8.738	9.247			HET-HEMI	0.152		-0.786	1.089	0.966
													HET-HOMO	1.348		0.411	2.285	0.004**
													HEMI-HOMO	1.196		0.259	2.134	0.010**
		angle-of-curvature (°)	WT	117.476	2.535	1.134	114.328	120.624	113.427	120.321	73.047	0.000*	WT-HET	1.003	1.379	-2.942	4.947	0.885
			HET	116.473	2.477	1.108	113.398	119.549	113.953	120.000			WT-HEMI	-1.751		-5.696	2.193	0.594
			HEMI	119.228	1.704	0.762	117.112	121.343	118.266	122.234			WT-HOMO	-16.758		-20.703	-12.813	0.000**
			HOMO	134.234	1.882	0.842	131.897	136.572	132.324	136.997			HET-HEMI	-2.754		-6.699	1.190	0.230
													HET-HOMO	-17.761		-21.705	-13.816	0.000**
													HEMI-HOMO	-15.007		-18.951	-11.062	0.000**
		width-at-midpoint (mm)	WT	0.987	0.032	0.014	0.947	1.027	0.952	1.033	5.407	0.009**	WT-HET	0.009	0.022	-0.055	0.073	0.979
			HET	0.978	0.038	0.017	0.931	1.025	0.926	1.028			WT-HEMI	0.049		-0.015	0.113	0.165
			HEMI	0.938	0.029	0.013	0.901	0.974	0.910	0.980			WT-HOMO	0.079		0.015	0.143	0.013**
			HOMO	0.908	0.040	0.018	0.858	0.958	0.848	0.956			HET-HEMI	0.040		-0.024	0.104	0.305
													HET-HOMO	0.070		0.006	0.134	0.029**
													HEMI-HOMO	0.030		-0.034	0.094	0.556
		incisor-perimeter (mm)	WT	25.014	1.940	0.868	22.605	27.423	22.821	27.560	18.866	0.000*	WT-HET	-0.163	0.791	-2.426	2.100	0.997
			HET	25.177	1.348	0.603	23.503	26.851	22.800	26.137			WT-HEMI	0.725		-1.538	2.988	0.796
			HEMI	24.289	0.556	0.249	23.598	24.980	23.687	25.042			WT-HOMO	4.985		2.722	7.248	0.000**
			HOMO	20.029	0.605	0.271	19.278	20.781	19.302	20.699			HET-HEMI	0.888		-1.375	3.151	0.681
													HET-HOMO	5.147		2.885	7.411	0.000**
													HEMI-HOMO	4.256		1.997	6.523	0.000**
		incisor-area (mm^2)	WT	10.956	1.132	0.506	9.551	12.362	9.696	12.554	15.231	0.000*	WT-HET	0.122	0.455	-1.180	1.425	0.993
			HET	10.834	0.804	0.360	9.835	11.833	9.455	11.528			WT-HEMI	0.850		-0.453	2.153	0.280
			HEMI	10.106	0.336	0.150	9.689	10.523	9.701	10.615			WT-HOMO	2.723		1.420	4.025	0.000**
			HOMO	8.234	0.182	0.081	8.008	8.459	7.968	8.383			HET-HEMI	0.728		-0.575	2.031	0.407
													HET-HOMO	2.600		1.297	3.903	0.000**
													HEMI-HOMO	1.872		0.570	3.175	0.004**

* Bonferroni Corrected Significant Difference ($p \leq 0.002$)

** Significant Difference ($p \leq 0.05$)

Table 6. *Amelx* 2D Incisor Morphometry – left lingual

MANDIBULAR INCISORS			ANOVA									MULTIPLE COMPARISON					
VIEW/ ASPECT	MEASUREMENT VARIABLE	GROUP	Mean	SD	SE	95% CI of Mean lower bound	95% CI of Mean upper bound	min'	max'	F	Sig.	GROUPS	MD	SE	95% CI lower bound	95% CI upper bound	Sig.
LEFT LINGUAL	*overall-length* (mm)	WT	10.463	0.563	0.252	9.764	11.161	9.834	11.118	5.681	0.008**	WT-HET	-0.056	0.330	-0.999	0.887	0.998
		HET	10.518	0.741	0.331	9.598	11.438	9.578	11.280			WT-HEMI	0.195		-0.748	1.138	0.933
		HEMI	10.268	0.433	0.194	9.730	10.805	9.606	10.617			WT-HOMO	1.137		0.194	2.080	0.016**
		HOMO	9.326	0.182	0.082	9.099	9.553	9.044	9.545			HET-HEMI	0.251		-0.692	1.194	0.871
												HET-HOMO	1.192		0.249	2.135	0.011**
												HEMI-HOMO	0.942		-0.001	1.885	0.050**
	angle-of-curvature (°)	WT	117.317	2.848	1.274	113.780	120.853	112.824	120.689	46.247	0.000*	WT-HET	0.865	1.517	-3.477	5.206	0.940
		HET	116.452	2.770	1.239	113.012	119.892	113.580	120.731			WT-HEMI	-2.183		-6.524	2.159	0.495
		HEMI	119.499	1.606	0.718	117.505	121.494	117.944	122.171			WT-HOMO	-14.806		-19.147	-10.465	0.000**
		HOMO	132.123	2.158	0.965	129.443	134.802	129.980	135.133			HET-HEMI	-3.047		-7.389	1.294	0.226
												HET-HOMO	-15.671		-20.012	-11.329	0.000**
												HEMI-HOMO	-12.623		-16.965	-8.282	0.000**
	width-at-midpoint (mm)	WT	0.991	0.024	0.011	0.961	1.021	0.964	1.017	7.616	0.002*	WT-HET	0.012	0.017	-0.036	0.061	0.884
		HET	0.978	0.026	0.012	0.946	1.011	0.959	1.015			WT-HEMI	0.0544		0.006	0.103	0.026**
		HEMI	0.936	0.021	0.009	0.910	0.963	0.911	0.960			WT-HOMO	0.0696		0.021	0.118	0.004**
		HOMO	0.921	0.034	0.015	0.879	0.964	0.870	0.955			HET-HEMI	0.042		-0.007	0.091	0.104
												HET-HOMO	0.0572		0.009	0.106	0.019**
												HEMI-HOMO	0.015		-0.033	0.064	0.808
	incisor-perimeter (mm)	WT	24.882	1.487	0.665	23.036	26.729	22.956	26.463	16.117	0.000*	WT-HET	-0.212	0.717	-2.265	1.841	0.991
		HET	25.094	1.389	0.621	23.369	26.820	23.059	26.358			WT-HEMI	0.631		-1.422	2.684	0.815
		HEMI	24.251	0.610	0.273	23.493	25.009	23.611	25.066			WT-HOMO	4.150		2.097	6.203	0.000**
		HOMO	20.732	0.796	0.356	19.745	21.720	19.537	21.771			HET-HEMI	0.843		-1.210	2.896	0.650
												HET-HOMO	4.362		2.309	6.415	0.000**
												HEMI-HOMO	3.519		1.466	5.572	0.001**
	incisor-area (mm^2)	WT	11.015	0.867	0.388	9.939	12.091	10.008	11.967	13.333	0.000*	WT-HET	0.179	0.435	-1.066	1.424	0.976
		HET	10.836	0.951	0.425	9.654	12.017	9.640	11.666			WT-HEMI	0.850		-0.395	2.095	0.246
		HEMI	10.165	0.355	0.159	9.723	10.606	9.729	10.705			WT-HOMO	2.467		1.223	3.712	0.000**
		HOMO	8.547	0.332	0.149	8.135	8.960	8.087	8.942			HET-HEMI	0.671		-0.574	1.916	0.437
												HET-HOMO	2.288		1.043	3.533	0.000**
												HEMI-HOMO	1.617		0.373	2.862	0.009**
	labial-length (mm)	WT	10.924	0.520	0.232	10.279	11.569	10.167	11.516	1.541	0.243	WT-HET	0.469	0.337	-0.496	1.435	0.522
		HET	10.455	0.581	0.260	9.733	11.176	9.718	11.248			WT-HEMI	0.703		-0.262	1.668	0.200
		HEMI	10.221	0.654	0.292	9.410	11.033	9.536	11.193			WT-HOMO	0.296		-0.669	1.261	0.816
		HOMO	10.628	0.321	0.144	10.229	11.027	10.285	10.975			HET-HEMI	0.233		-0.732	1.199	0.899
												HET-HOMO	-0.173		-1.139	0.792	0.955
												HEMI-HOMO	-0.407		-1.372	0.558	0.632

* Bonferroni Corrected Significant Difference ($p \leq 0.002$)
** Significant Difference ($p \leq 0.05$)

Table 7. *Amelx* 2D Incisor Morphometry – right buccal

MANDIBULAR INCISORS			ANOVA									MULTIPLE COMPARISON					
VIEW/ ASPECT		MEASUREMENT VARIABLE	GROUP	Mean	SD	SE	95% CI of Mean lower bound	95% CI of Mean upper bound	min'	max'	F	Sig.	GROUPS	MD	SE	95% CI lower bound	95% CI upper bound	Sig.
RIGHT	BUCCAL	*overall-length* (mm)	WT	10.626	0.421	0.188	10.102	11.149	9.919	10.982	9.157	0.001*	WT-HET	-0.051	0.307	-0.930	0.829	0.998
			HET	10.676	0.649	0.290	9.871	11.482	9.801	11.374			WT-HEMI	0.488		-0.391	1.367	0.412
			HEMI	10.137	0.534	0.239	9.474	10.801	9.281	10.643			WT-HOMO	1.368		0.489	2.247	0.002**
			HOMO	9.258	0.246	0.110	8.952	9.563	8.846	9.494			HET-HEMI	0.539		-0.340	1.418	0.330
													HET-HOMO	1.419		0.539	2.298	0.001**
													HEMI-HOMO	0.880		0.001	1.759	0.050**
		angle-of-curvature (°)	WT	116.801	2.834	1.268	113.282	120.321	112.810	119.088	61.606	0.000*	WT-HET	-1.011	1.355	-4.887	2.866	0.877
			HET	117.812	1.329	0.594	116.162	119.463	116.471	119.577			WT-HEMI	-4.635		-8.512	-0.759	0.017**
			HEMI	121.437	2.030	0.908	118.916	123.958	118.306	123.937			WT-HOMO	-16.385		-20.262	-12.509	0.000**
			HOMO	133.187	2.106	0.942	130.572	135.802	130.267	135.558			HET-HEMI	-3.625		-7.501	0.252	0.071
													HET-HOMO	-15.374		-19.251	-11.498	0.000**
													HEMI-HOMO	-11.750		-15.626	-7.873	0.000**
		width-at-midpoint (mm)	WT	0.979	0.039	0.017	0.931	1.028	0.912	1.008	3.212	0.051	WT-HET	0.009	0.029	-0.074	0.092	0.989
			HET	0.970	0.067	0.030	0.887	1.054	0.859	1.041			WT-HEMI	0.060		-0.023	0.143	0.203
			HEMI	0.919	0.029	0.013	0.884	0.955	0.878	0.947			WT-HOMO	0.074		-0.009	0.157	0.089
			HOMO	0.905	0.039	0.017	0.857	0.954	0.868	0.967			HET-HEMI	0.051		-0.032	0.134	0.325
													HET-HOMO	0.065		-0.018	0.148	0.154
													HEMI-HOMO	0.014		-0.069	0.097	0.963
		incisor-perimeter (mm)	WT	25.308	1.140	0.510	23.893	26.724	23.740	26.608	21.020	0.000*	WT-HET	-0.091	0.696	-2.082	1.900	0.999
			HET	25.399	1.608	0.719	23.403	27.395	23.083	27.174			WT-HEMI	1.209		-0.782	3.199	0.338
			HEMI	24.100	0.851	0.381	23.043	25.156	23.077	24.916			WT-HOMO	4.726		2.735	6.717	0.000**
			HOMO	20.582	0.482	0.216	19.983	21.181	19.792	21.049			HET-HEMI	1.299		-0.691	3.290	0.280
													HET-HOMO	4.817		2.826	6.808	0.000**
													HEMI-HOMO	3.517		1.527	5.508	0.0001**
		incisor-area (mm^2)	WT	10.916	0.682	0.305	10.069	11.763	9.914	11.546	9.324	0.001*	WT-HET	-0.212	0.521	-1.702	1.278	0.977
			HET	11.128	1.389	0.621	9.403	12.853	9.003	12.449			WT-HEMI	0.682		-0.808	2.172	0.571
			HEMI	10.234	0.462	0.207	9.661	10.808	9.643	10.815			WT-HOMO	2.272		0.782	3.762	0.002**
			HOMO	8.644	0.321	0.144	8.245	9.043	8.097	8.941			HET-HEMI	0.893		-0.597	2.383	0.348
													HET-HOMO	2.484		0.994	3.974	0.001**
													HEMI-HOMO	1.591		0.101	3.081	0.034**

* Bonferroni Corrected Significant Difference ($p \leq 0.002$)
** Significant Difference ($p \leq 0.05$)

Table 8. *Amelx* 2D Incisor Morphometry – right lingual

MANDIBULAR INCISORS			ANOVA									MULTIPLE COMPARISON					
VIEW/ ASPECT	MEASUREMENT VARIABLE	GROUP	Mean	SD	SE	95% CI of Mean lower bound	95% CI of Mean upper bound	min[1]	max[2]	F	Sig.	GROUPS	MD	SE	95% CI lower bound	95% CI upper bound	Sig.
RIGHT LINGUAL	*overall-length* (mm)	WT	10.635	0.379	0.169	10.164	11.105	10.030	10.981	7.022	0.003**	WT-HET	0.187	0.332	-0.764	1.137	0.942
		HET	10.448	0.884	0.395	9.351	11.546	9.089	11.272			WT-HEMI	0.497		-0.453	1.447	0.462
		HEMI	10.138	0.336	0.150	9.720	10.555	9.801	10.593			WT-HOMO	1.403		0.453	2.354	0.003**
		HOMO	9.231	0.256	0.114	8.914	9.549	8.930	9.553			HET-HEMI	0.310		-0.640	1.261	0.787
												HET-HOMO	1.217		0.266	2.167	0.010**
												HEMI-HOMO	0.906		-0.044	1.857	0.064
	angle-of-curvature (°)	WT	116.540	2.648	1.184	113.252	119.827	112.785	118.580	103.342	0.000*	WT-HET	-2.445	1.107	-5.611	0.722	0.163
		HET	118.984	1.301	0.582	117.369	120.600	117.156	120.362			WT-HEMI	-5.175		-8.341	-2.009	0.001**
		HEMI	121.715	1.516	0.678	119.832	123.597	119.324	123.434			WT-HOMO	-17.878		-21.044	-14.711	0.000**
		HOMO	134.417	1.115	0.499	133.032	135.802	132.821	135.800			HET-HEMI	-2.730		-5.897	0.436	0.104
												HET-HOMO	-15.433		-18.599	-12.267	0.000**
												HEMI-HOMO	-12.703		-15.869	-9.536	0.000**
	width-at-midpoint (mm)	WT	0.974	0.027	0.012	0.939	1.008	0.930	0.995	7.022	0.003**	WT-HET	0.012	0.026	-0.062	0.086	0.969
		HET	0.962	0.062	0.028	0.885	1.039	0.862	1.026			WT-HEMI	0.053		-0.021	0.127	0.216
		HEMI	0.921	0.027	0.012	0.887	0.955	0.890	0.963			WT-HOMO	0.064		-0.010	0.138	0.104
		HOMO	0.910	0.036	0.016	0.865	0.955	0.864	0.964			HET-HEMI	0.041		-0.033	0.115	0.413
												HET-HOMO	0.052		-0.022	0.126	0.222
												HEMI-HOMO	0.011		-0.063	0.085	0.972
	incisor-perimeter (mm)	WT	25.305	1.354	0.605	23.625	26.986	23.573	26.995	19.245	0.000*	WT-HET	0.130	0.741	-1.991	2.251	0.998
		HET	25.175	1.751	0.783	22.001	27.349	22.653	27.156			WT-HEMI	1.419		-0.702	3.540	0.261
		HEMI	23.886	0.558	0.250	23.193	24.579	23.281	24.461			WT-HOMO	4.933		2.813	7.054	0.000**
		HOMO	20.372	0.534	0.239	19.708	21.035	19.804	21.086			HET-HEMI	1.289		-0.832	3.410	0.337
												HET-HOMO	4.803		2.682	6.924	0.000**
												HEMI-HOMO	3.514		1.394	5.635	0.001**
	incisor-area (mm^2)	WT	10.827	0.760	0.340	9.884	11.771	9.886	11.634	9.603	0.001*	WT-HET	-0.085	0.505	-1.531	1.361	0.998
		HET	10.913	1.337	0.598	9.253	12.572	8.849	12.229			WT-HEMI	0.701		-0.745	2.147	0.525
		HEMI	10.126	0.266	0.119	9.796	10.456	9.747	10.427			WT-HOMO	2.305		0.859	3.751	0.002**
		HOMO	8.522	0.347	0.155	8.091	8.953	8.184	8.901			HET-HEMI	0.786		-0.660	2.232	0.430
												HET-HOMO	2.390		0.945	3.837	0.001**
												HEMI-HOMO	1.604		0.158	3.050	0.027**
	labial-length (mm)	WT	10.865	0.783	0.350	9.893	11.837	9.664	11.833	2.232	0.124	WT-HET	0.188	0.377	-0.891	1.268	0.958
		HET	10.677	0.622	0.278	9.904	11.449	9.758	11.426			WT-HEMI	0.731		-0.349	1.810	0.252
		HEMI	10.134	0.564	0.252	9.434	10.834	9.481	10.848			WT-HOMO	-0.195		-1.275	0.884	0.954
		HOMO	11.060	0.326	0.146	10.655	11.465	10.503	11.366			HET-HEMI	0.543		-0.537	1.622	0.495
												HET-HOMO	-0.383		-1.463	0.696	0.743
												HEMI-HOMO	-0.926		-2.006	0.154	0.106

* Bonferroni Corrected Significant Difference ($p \leq 0.002$)
** Significant Difference ($p \leq 0.05$)

Table 9. *Amelx* 2D Colour and Whiteness – left gingival/ pre-secretory

MANDIBULAR INCISORS			ANOVA									MULTIPLE COMPARISON					
							95% CI of Mean								95% CI		
SIDE	REGION/ STAGE	COLOUR COMPONENT	GROUP	Mean	SD	SE	lower bound	upper bound	min'	max'	F	Sig.	GROUPS	MD	SE	lower bound	upper bound	Sig.
LEFT	GINGIVAL/ PRE-SECRETORY	*lightness*	WT	48.519	2.385	1.066	45.558	51.480	45.235	51.083	11.590	0.000*	WT-HET	10.855	2.046	5.001	16.709	0.000**
			HET	37.664	4.760	2.129	31.754	43.574	34.154	44.923			WT-HEMI	9.522		3.668	15.376	0.001**
			HEMI	38.998	2.996	1.340	35.278	42.718	35.079	43.418			WT-HOMO	8.690		2.836	14.545	0.003**
			HOMO	39.829	2.134	0.954	37.179	42.479	37.616	42.754			HET-HEMI	-1.333		-7.187	4.521	0.913
													HET-HOMO	-2.165		-8.019	3.690	0.719
													HEMI-HOMO	-0.831		-6.686	5.023	0.977
		red/ green	WT	-4.316	0.688	0.308	-5.171	-3.461	-5.240	-3.420	2.358	0.110	WT-HET	-2.618	1.012	-5.513	0.277	0.084
			HET	-1.698	3.042	1.361	-5.476	2.080	-5.260	1.790			WT-HEMI	-1.650		-4.545	1.245	0.390
			HEMI	-2.666	0.576	0.258	-3.381	-1.951	-3.470	-1.990			WT-HOMO	-1.028		-3.923	1.867	0.743
			HOMO	-3.288	0.419	0.187	-3.808	-2.768	-3.850	-2.850			HET-HEMI	0.968		-1.927	3.863	0.775
													HET-HOMO	1.590		-1.305	4.485	0.421
													HEMI-HOMO	0.622		-2.273	3.517	0.926
		yellow/ blue	WT	3.092	2.988	1.336	-0.618	6.802	-1.960	5.700	1.534	0.244	WT-HET	-2.906	1.955	-8.500	2.688	0.468
			HET	5.998	4.417	1.975	0.514	11.482	0.940	10.620			WT-HEMI	1.122		-4.472	6.716	0.938
			HEMI	1.970	2.037	0.911	-0.559	4.499	0.000	5.040			WT-HOMO	-0.138		-5.732	5.456	1.000
			HOMO	3.230	2.378	1.064	0.277	6.183	0.140	5.610			HET-HEMI	4.028		-1.566	9.622	0.208
													HET-HOMO	2.768		-2.826	8.362	0.508
													HEMI-HOMO	-1.260		-6.854	4.334	0.916
		whiteness	WT	76.681	17.914	8.012	54.438	98.925	61.390	107.107	1.791	0.189	WT-HET	15.337	11.943	-18.832	49.507	0.585
			HET	61.344	27.061	12.102	27.744	94.944	28.950	92.170			WT-HEMI	-12.284		-46.454	21.885	0.736
			HEMI	88.966	11.001	4.920	75.306	102.625	72.130	101.108			WT-HOMO	0.571		-33.598	34.741	1.000
			HOMO	76.110	15.880	7.102	56.393	95.827	60.340	96.680			HET-HEMI	-27.622		-61.791	6.548	0.137
													HET-HOMO	-14.766		-48.936	19.404	0.614
													HEMI-HOMO	12.856		-21.314	47.025	0.708

* Bonferroni Corrected Significant Difference ($p \leq 0.002$)
** Significant Difference ($p \leq 0.05$)

Table 10. *Amelx* 2D Colour and Whiteness – left middle/ secretory

MANDIBULAR INCISORS			ANOVA									MULTIPLE COMPARISON					
							95% CI of Mean								95% CI		
SIDE	REGION/ STAGE	COLOUR COMPONENT	GROUP	Mean	SD	SE	lower bound	upper bound	min'	max'	F	Sig.	GROUPS	MD	SE	lower bound	upper bound	Sig.
LEFT	MIDDLE/ SECRETORY	*lightness*											WT-HET	8.097	2.988	-0.450	16.645	0.067
			WT	44.960	5.280	2.361	38.403	51.516	37.934	52.044	8.321	0.001*	WT-HEMI	-0.766		-9.314	7.781	0.994
			HET	36.862	7.096	3.174	28.051	45.674	31.156	48.536			WT-HOMO	-6.734		-15.282	1.814	0.151
			HEMI	45.726	2.629	1.176	42.461	48.991	42.757	48.632			HET-HEMI	-8.864		-17.411	-0.316	0.041**
			HOMO	51.694	2.026	0.906	49.178	54.209	49.431	53.724			HET-HOMO	-14.831		-23.379	-6.284	0.001**
													HEMI-HOMO	-5.968		-14.515	2.580	0.230
		red/ green											WT-HET	-3.240	0.823	-5.595	-0.885	0.006**
			WT	-4.036	0.552	0.247	-4.721	-3.351	-4.700	-3.240	6.011	0.006**	WT-HEMI	-2.358		-4.713	-0.003	0.050**
			HET	-0.796	2.258	1.010	-3.600	2.008	-2.630	2.950			WT-HOMO	-1.052		-3.407	1.303	0.589
			HEMI	-1.678	0.731	0.327	-2.585	-0.771	-2.830	-1.010			HET-HEMI	0.882		-1.473	3.237	0.711
			HOMO	-2.984	0.915	0.409	-4.120	-1.848	-4.290	-1.910			HET-HOMO	2.188		-0.167	4.543	0.073**
													HEMI-HOMO	1.306		-1.049	3.661	0.413
		yellow/ blue											WT-HET	-1.986	2.569	-9.336	5.364	0.865
			WT	4.496	0.460	0.206	3.925	5.067	4.040	5.140	3.509	0.040**	WT-HEMI	4.422		-2.928	11.772	0.345
			HET	6.482	7.580	3.390	-2.930	15.894	-1.600	18.390			WT-HOMO	5.010		-2.340	12.360	0.247
			HEMI	0.074	1.443	0.645	-1.717	1.865	-1.990	1.110			HET-HEMI	6.408		-0.942	13.758	0.099
			HOMO	-0.514	2.500	1.118	-3.618	2.590	-3.490	2.280			HET-HOMO	6.996		-0.354	14.346	0.065
													HEMI-HOMO	0.588		-6.762	7.938	0.996
		whiteness											WT-HET	9.806	16.635	-37.787	57.399	0.934
			WT	67.874	3.088	1.381	64.040	71.708	63.790	71.000	2.901	0.067	WT-HEMI	-29.729		-77.322	17.864	0.315
			HET	58.068	49.997	22.359	-4.011	120.147	-22.140	111.152			WT-HOMO	-28.447		-76.040	19.146	0.351
			HEMI	97.603	7.298	3.264	88.541	106.665	89.610	108.841			HET-HEMI	-39.535		-87.128	8.058	0.122
			HOMO	96.321	14.310	6.400	78.552	114.089	80.640	113.428			HET-HOMO	-38.252		-85.845	9.341	0.140
													HEMI-HOMO	1.282		-46.311	48.875	1.000

* Bonferroni Corrected Significant Difference ($p \leq 0.002$)
** Significant Difference ($p \leq 0.05$)

Table 11. *Amelx* 2D Colour and Whiteness – left incisal/ mature

MANDIBULAR INCISORS			ANOVA									MULTIPLE COMPARISON					
							95% CI of Mean								95% CI		
SIDE	REGION/ STAGE	COLOUR COMPONENT	GROUP	Mean	SD	SE	lower bound	upper bound	min'	max'	F	Sig.	GROUPS	MD	SE	lower bound	upper bound	Sig.
LEFT	INCISAL/ MATURE	*lightness*	WT	44.263	2.361	1.056	41.331	47.195	40.787	46.437	26.326	0.000*	WT-HET	11.437	2.497	4.294	18.580	0.002**
			HET	32.826	5.970	2.670	25.414	40.238	27.509	42.817			WT-HEMI	3.300		-3.843	10.444	0.563
			HEMI	40.962	2.375	1.062	38.014	43.911	37.253	43.320			WT-HOMO	-10.444		-17.587	-3.301	0.004**
			HOMO	54.707	3.935	1.760	49.821	59.593	51.078	61.229			HET-HEMI	-8.136		-15.280	-0.993	0.023**
													HET-HOMO	-21.881		-29.024	-14.738	0.000**
													HEMI-HOMO	-13.745		-20.888	-6.601	0.000**
		red/ green	WT	-4.806	0.479	0.214	-5.401	-4.211	-5.230	-4.080	57.609	0.000*	WT-HET	-4.490	0.478	-5.858	-3.122	0.000**
			HET	-0.316	1.019	0.456	-1.582	0.950	-1.630	0.820			WT-HEMI	-4.388		-5.756	-3.020	0.000**
			HEMI	-0.418	0.492	0.220	-1.029	0.193	-0.990	0.090			WT-HOMO	0.012		-1.356	1.380	1.000
			HOMO	-4.818	0.881	0.394	-5.912	-3.724	-5.870	-3.500			HET-HEMI	0.102		-1.266	1.470	0.996
													HET-HOMO	4.502		3.134	5.870	0.000**
													HEMI-HOMO	4.400		3.032	5.768	0.000**
		yellow/ blue	WT	11.256	1.529	0.684	9.358	13.154	9.390	13.590	39.406	0.000*	WT-HET	2.870	1.477	-1.357	7.097	0.250
			HET	8.386	3.523	1.576	4.011	12.761	2.210	10.930			WT-HEMI	12.406		8.179	16.633	0.000**
			HEMI	-1.150	2.418	1.081	-4.153	1.853	-3.350	2.290			WT-HOMO	12.808		8.581	17.035	0.000**
			HOMO	-1.552	1.109	0.496	-2.929	-0.175	-2.590	0.290			HET-HEMI	9.536		5.309	13.763	0.000**
													HET-HOMO	9.938		5.711	14.165	0.000**
													HEMI-HOMO	0.402		-3.825	4.629	0.993
		whiteness	WT	26.062	8.874	3.969	15.043	37.081	13.640	38.620	37.335	0.000*	WT-HET	-16.120	9.507	-43.319	11.079	0.358
			HET	42.182	25.249	11.292	10.831	73.533	24.950	84.880			WT-HEMI	-81.389		-108.588	-54.190	0.000**
			HEMI	107.451	11.930	5.335	92.637	122.264	90.070	118.589			WT-HOMO	-74.879		-102.078	-47.680	0.000**
			HOMO	100.941	6.722	3.006	92.594	109.288	89.550	106.198			HET-HEMI	-65.269		-92.468	-38.070	0.000**
													HET-HOMO	-58.759		-85.958	-31.560	0.000**
													HEMI-HOMO	6.510		-20.689	33.709	0.901

* Bonferroni Corrected Significant Difference ($p \leq 0.002$)
** Significant Difference ($p \leq 0.05$)

Table 12. *Amelx* 2D Colour and Whiteness – left whole/ all

MANDIBULAR INCISORS			ANOVA									MULTIPLE COMPARISON					
							95% CI of Mean								95% CI		
SIDE	REGION/ STAGE	COLOUR COMPONENT	GROUP	Mean	SD	SE	lower bound	upper bound	min'	max'	F	Sig.	GROUPS	MD	SE	lower bound	upper bound	Sig.
LEFT	WHOLE/ ALL	*lightness*	WT	45.885	3.314	1.482	41.769	50.000	41.242	49.478	17.331	0.000*	WT-HET	9.913	1.854	4.609	15.216	0.000**
			HET	35.972	3.545	1.585	31.570	40.374	33.069	41.909			WT-HEMI	4.253		-1.051	9.556	0.141
			HEMI	41.632	2.435	1.089	38.609	44.655	38.911	44.737			WT-HOMO	-2.568		-7.872	2.735	0.526
			HOMO	48.453	2.209	0.988	45.710	51.196	45.820	51.665			HET-HEMI	-5.660		-10.963	-0.357	0.034**
													HET-HOMO	-12.481		-17.785	-7.178	0.000**
													HEMI-HOMO	-6.821		-12.125	-1.518	0.010**
		red/ green	WT	-4.406	0.278	0.124	-4.751	-4.061	-4.800	-4.120	13.547	0.000*	WT-HET	-3.324	0.619	-5.096	-1.552	0.000**
			HET	-1.082	1.718	0.769	-3.216	1.052	-3.320	1.090			WT-HEMI	-2.852		-4.624	-1.080	0.002**
			HEMI	-1.554	0.615	0.275	-2.317	-0.791	-2.230	-0.840			WT-HOMO	-0.728		-2.500	1.044	0.650
			HOMO	-3.678	0.655	0.293	-4.491	-2.865	-4.420	-2.810			HET-HEMI	0.472		-1.300	2.244	0.870
													HET-HOMO	2.596		0.824	4.368	0.003**
													HEMI-HOMO	2.124		0.352	3.896	0.016**
		yellow/ blue	WT	6.054	1.119	0.501	4.664	7.444	4.110	6.850	11.114	0.000*	WT-HET	-0.742	1.485	-4.990	3.506	0.958
			HET	6.796	3.886	1.738	1.972	11.620	2.900	12.700			WT-HEMI	5.700		1.452	9.948	0.007**
			HEMI	0.354	1.695	0.758	-1.751	2.459	-1.310	2.200			WT-HOMO	5.636		1.388	9.884	0.008**
			HOMO	0.418	1.679	0.751	-1.667	2.503	-1.460	1.930			HET-HEMI	6.442		2.194	10.690	0.003**
													HET-HOMO	6.378		2.130	10.626	0.003
													HEMI-HOMO	-0.064		-4.312	4.184	1.000
		whiteness	WT	58.834	6.694	2.994	50.523	67.145	53.290	70.240	12.203	0.000*	WT-HET	2.342	8.785	-22.792	27.476	0.993
			HET	56.492	23.651	10.577	27.125	85.859	19.170	79.960			WT-HEMI	-39.096		-64.229	-13.962	0.002**
			HEMI	97.930	8.012	3.583	87.982	107.878	89.060	107.608			WT-HOMO	-33.192		-58.326	-8.058	0.008**
			HOMO	92.026	10.167	4.547	79.402	104.650	82.700	103.041			HET-HEMI	-41.439		-66.571	-16.304	0.001**
													HET-HOMO	-35.534		-60.668	-10.400	0.005**
													HEMI-HOMO	5.904		-19.230	31.037	0.906

* Bonferroni Corrected Significant Difference ($p \leq 0.002$)
** Significant Difference ($p \leq 0.05$)

Table 13. *Amelx* 2D Colour and Whiteness – right gingival/ pre-secretory

MANDIBULAR INCISORS			ANOVA									MULTIPLE COMPARISON					
							95% CI of Mean								95% CI		
SIDE	REGION/ STAGE	COLOUR COMPONENT	GROUP	Mean	SD	SE	lower bound	upper bound	min'	max'	F	Sig.	GROUPS	MD	SE	lower bound	upper bound	Sig.
RIGHT	GINGIVAL/ PRE-SECRETORY	*lightness*	WT	49.034	0.647	0.289	48.231	49.837	48.384	49.849	21.888	0.000*	WT-HET	14.187	2.164	7.996	20.379	0.000**
			HET	34.847	5.785	2.587	27.664	42.029	27.181	41.990			WT-HEMI	11.460		5.269	17.652	0.000**
			HEMI	37.574	2.179	0.975	34.868	40.280	35.531	40.790			WT-HOMO	15.890		9.698	22.081	0.000**
			HOMO	33.144	2.864	1.281	29.588	36.701	29.497	36.190			HET-HEMI	-2.727		-8.919	3.465	0.600
													HET-HOMO	1.703		-4.489	7.894	0.859
													HEMI-HOMO	4.430		-1.762	10.621	0.213
		red/ green	WT	-5.114	0.875	0.391	-6.200	-4.028	-6.390	-4.110	4.504	0.018**	WT-HET	-4.028	1.140	-7.291	-0.765	0.013**
			HET	-1.086	3.001	1.342	-4.812	2.640	-5.100	2.190			WT-HEMI	-2.868		-6.131	0.395	0.095
			HEMI	-2.246	1.579	0.706	-4.206	-0.286	-3.760	0.150			WT-HOMO	-2.800		-6.063	0.463	0.106
			HOMO	-2.314	0.860	0.385	-3.382	-1.246	-3.040	-0.850			HET-HEMI	1.160		-2.103	4.423	0.742
													HET-HOMO	1.228		-2.035	4.491	0.708
													HEMI-HOMO	0.068		-3.195	3.331	1.000
		yellow/ blue	WT	3.452	2.605	1.165	0.218	6.686	-0.520	6.570	3.501	0.040**	WT-HET	-5.546	2.054	-11.423	0.331	0.068
			HET	8.998	4.669	2.088	3.200	14.796	4.350	15.530			WT-HEMI	0.398		-5.479	6.275	0.997
			HEMI	3.054	2.896	1.295	-0.542	6.650	-2.050	4.990			WT-HOMO	-2.028		-7.905	3.849	0.759
			HOMO	5.480	2.284	1.021	2.644	8.316	2.010	7.580			HET-HEMI	5.944		0.067	11.821	0.047**
													HET-HOMO	3.518		-2.359	9.395	0.350
													HEMI-HOMO	-2.426		-8.303	3.451	0.647
		whiteness	WT	74.224	14.984	6.701	55.619	92.829	56.090	96.940	3.946	0.028**	WT-HET	34.932	13.427	-3.482	73.346	0.081
			HET	39.292	32.139	14.373	-0.613	79.197	-8.540	69.960			WT-HEMI	-8.144		-46.558	30.269	0.928
			HEMI	82.368	16.412	7.340	61.990	102.746	71.540	110.952			WT-HOMO	14.046		-24.368	52.460	0.726
			HOMO	60.178	16.612	7.429	39.551	80.805	44.720	85.340			HET-HEMI	-43.076		-81.490	-4.663	0.025**
													HET-HOMO	-20.886		-59.300	17.528	0.430
													HEMI-HOMO	22.190		-16.223	60.604	0.379

* Bonferroni Corrected Significant Difference ($p \leq 0.002$)
** Significant Difference ($p \leq 0.05$)

Table 14. *Amelx* 2D Colour and Whiteness – right middle/ secretory

MANDIBULAR INCISORS			ANOVA									MULTIPLE COMPARISON					
							95% CI of Mean								95% CI		
SIDE	REGION/ STAGE	COLOUR COMPONENT	GROUP	Mean	SD	SE	lower bound	upper bound	min'	max'	F	Sig.	GROUPS	MD	SE	lower bound	upper bound	Sig.
RIGHT	MIDDLE/ SECRETORY	*lightness*	WT	44.157	1.920	0.858	41.773	46.540	40.963	45.821	4.097	0.025**	WT-HET	6.322	2.685	-1.360	14.003	0.127
			HET	37.835	7.573	3.387	28.432	47.238	28.357	48.929			WT-HEMI	0.645		-7.037	8.326	0.995
			HEMI	43.512	1.842	0.824	41.225	45.799	41.109	46.142			WT-HOMO	-2.855		-10.537	4.826	0.716
			HOMO	47.012	2.768	1.238	43.575	50.449	43.001	50.730			HET-HEMI	-5.677		-13.358	2.005	0.191
													HET-HOMO	-9.177		-16.858	-1.495	0.017**
													HEMI-HOMO	-3.500		-11.182	4.182	0.574
		red/ green	WT	-3.770	0.424	0.190	-4.296	-3.244	-4.260	-3.220	6.366	0.005**	WT-HET	-2.988	0.730	-5.077	-0.899	0.004
			HET	-0.782	1.683	0.753	-2.872	1.308	-2.700	1.000			WT-HEMI	-2.302		-4.391	-0.213	0.028**
			HEMI	-1.468	1.207	0.540	-2.966	0.030	-2.890	0.200			WT-HOMO	-1.260		-3.349	0.829	0.343
			HOMO	-2.510	0.927	0.415	-3.661	-1.359	-3.950	-1.650			HET-HEMI	0.686		-1.403	2.775	0.784
													HET-HOMO	1.728		-0.361	3.817	0.124
													HEMI-HOMO	1.042		-1.047	3.131	0.501
		yellow/ blue	WT	3.984	1.654	0.740	1.930	6.038	2.540	6.520	2.689	0.081	WT-HET	-1.694	1.931	-7.219	3.831	0.817
			HET	5.678	5.185	2.319	-0.760	12.116	-1.910	11.080			WT-HEMI	2.960		-2.565	8.485	0.442
			HEMI	1.024	1.255	0.561	-0.534	2.582	-0.540	2.920			WT-HOMO	2.716		-2.809	8.241	0.513
			HOMO	1.268	2.469	1.104	-1.798	4.334	-1.230	3.940			HET-HEMI	4.654		-0.871	10.179	0.115
													HET-HOMO	4.410		-1.115	9.935	0.144
													HEMI-HOMO	-0.244		-5.769	5.281	0.999
		whiteness	WT	71.100	10.173	4.549	58.469	83.731	55.470	79.900	3.236	0.050**	WT-HET	8.046	11.058	-23.592	39.684	0.885
			HET	63.054	29.377	13.138	26.578	99.531	33.170	105.471			WT-HEMI	-22.268		-53.906	9.370	0.224
			HEMI	93.368	6.979	3.121	84.702	102.033	84.130	101.099			WT-HOMO	-16.316		-47.954	15.322	0.474
			HOMO	87.416	14.411	6.445	69.523	105.309	71.980	102.006			HET-HEMI	-30.314		-61.952	1.325	0.063
													HET-HOMO	-24.362		-56.000	7.276	0.165
													HEMI-HOMO	5.952		-25.687	37.590	0.948

* Bonferroni Corrected Significant Difference ($p \leq 0.002$)
** Significant Difference ($p \leq 0.05$)

Table 15. *Amelx* 2D Colour and Whiteness – right incisal/ mature

MANDIBULAR INCISORS			ANOVA									MULTIPLE COMPARISON					
							95% CI of Mean								95% CI		
SIDE	REGION/ STAGE	COLOUR COMPONENT	GROUP	Mean	SD	SE	lower bound	upper bound	min'	max'	F	Sig.	GROUPS	MD	SE	lower bound	upper bound	Sig.
RIGHT	INCISAL/ MATURE	*lightness*											WT-HET	8.418	1.764	3.370	13.466	0.001**
			WT	44.442	2.786	1.246	40.983	47.901	39.845	46.541	24.110	0.000*	WT-HEMI	2.600		-2.448	7.648	0.475
			HET	36.024	4.335	1.939	30.641	41.407	29.875	41.315			WT-HOMO	-6.355		-11.403	-1.308	0.012**
			HEMI	41.842	0.988	0.442	40.615	43.069	41.078	43.468			HET-HEMI	-5.818		-10.866	-0.770	0.021**
			HOMO	50.797	1.897	0.848	48.443	53.152	48.925	53.715			HET-HOMO	-14.774		-19.821	-9.726	0.000**
													HEMI-HOMO	-8.955		-14.003	-3.908	0.001**
		red/ green											WT-HET	-5.624	0.616	-7.387	-3.861	0.000**
			WT	-7.198	1.232	0.551	-8.728	-5.668	-8.250	-5.250	34.432	0.000*	WT-HEMI	-5.074		-6.837	-3.311	0.000**
			HET	-1.574	1.117	0.500	-2.961	-0.187	-2.530	0.090			WT-HOMO	-2.850		-4.613	-1.087	0.001**
			HEMI	-2.124	0.970	0.434	-3.328	-0.920	-3.420	-0.850			HET-HEMI	0.550		-1.213	2.313	0.809
			HOMO	-4.348	0.301	0.134	-4.721	-3.975	-4.640	-3.840			HET-HOMO	2.774		1.011	4.537	0.002**
													HEMI-HOMO	2.224		0.461	3.987	0.011**
		yellow/ blue											WT-HET	3.886	1.801	-1.265	9.037	0.177
			WT	12.344	1.101	0.492	10.977	13.711	10.730	13.560	26.222	0.000*	WT-HEMI	12.786		7.635	17.937	0.000**
			HET	8.458	5.258	2.352	1.929	14.987	1.660	14.390			WT-HOMO	13.004		7.853	18.155	0.000**
			HEMI	-0.442	1.682	0.752	-2.530	1.646	-2.530	1.560			HET-HEMI	8.900		3.749	14.051	0.001**
			HOMO	-0.660	0.853	0.382	-1.719	0.399	-1.940	0.160			HET-HOMO	9.118		3.967	14.269	0.001**
													HEMI-HOMO	0.218		-4.933	5.369	0.999
		whiteness											WT-HET	-25.088	12.028	-59.500	9.324	0.200
			WT	18.800	7.229	3.233	9.824	27.776	10.750	30.190	23.390	0.000*	WT-HEMI	-84.145		-118.558	-49.733	0.000**
			HET	43.888	36.139	16.162	-0.985	88.761	4.560	87.160			WT-HOMO	-78.731		-113.143	-44.319	0.000**
			HEMI	102.945	8.086	3.616	92.906	112.985	93.110	112.164			HET-HEMI	-59.057		-93.470	-24.645	0.000**
			HOMO	97.531	4.798	2.146	91.573	103.488	92.160	104.234			HET-HOMO	-53.643		-88.055	-19.231	0.002**
													HEMI-HOMO	5.415		-28.998	39.827	0.969

* Bonferroni Corrected Significant Difference ($p \leq 0.002$)
** Significant Difference ($p \leq 0.05$)

Table 16. *Amelx* 2D Colour and Whiteness – right whole/ all

MANDIBULAR INCISORS			ANOVA									MULTIPLE COMPARISON					
							95% CI of Mean								95% CI		
SIDE	REGION/ STAGE	COLOUR COMPONENT	GROUP	Mean	SD	SE	lower bound	upper bound	min'	max'	F	Sig.	GROUPS	MD	SE	lower bound	upper bound	Sig.
RIGHT	WHOLE/ ALL	*lightness*	WT	45.804	1.281	0.573	44.213	47.394	43.832	47.177	11.128	0.000*	WT-HET	9.470	1.758	4.440	14.500	0.000**
			HET	36.334	5.120	2.290	29.976	42.692	28.596	42.787			WT-HEMI	5.425		0.395	10.455	0.032**
			HEMI	40.379	1.073	0.480	39.047	41.711	38.590	41.336			WT-HOMO	2.034		-2.996	7.064	0.661
			HOMO	43.769	1.378	0.616	42.058	45.481	42.462	45.801			HET-HEMI	-4.045		-9.075	0.985	0.139
													HET-HOMO	-7.435		-12.465	-2.405	0.003**
													HEMI-HOMO	-3.390		-8.420	1.640	0.256
		red/ green	WT	-5.322	0.123	0.055	-5.474	-5.170	-5.500	-5.190	11.879	0.000*	WT-HET	-4.106	0.741	-6.225	-1.987	0.000**
			HET	-1.216	1.869	0.836	-3.537	1.105	-3.260	1.000			WT-HEMI	-3.440		-5.559	-1.321	0.001**
			HEMI	-1.882	1.294	0.579	-3.489	-0.275	-3.370	-0.010			WT-HOMO	-2.218		-4.337	-0.099	0.039**
			HOMO	-3.104	0.552	0.247	-3.790	-2.418	-3.920	-2.470			HET-HEMI	0.666		-1.453	2.785	0.805
													HET-HOMO	1.888		-0.231	4.007	0.090
													HEMI-HOMO	1.222		-0.897	3.341	0.381
		yellow/ blue	WT	6.248	1.544	0.691	4.331	8.165	4.400	8.650	8.205	0.002*	WT-HET	-1.384	1.532	-5.766	2.998	0.803
			HET	7.632	4.027	1.801	2.632	12.632	1.480	11.580			WT-HEMI	4.890		0.508	9.272	0.026**
			HEMI	1.358	1.588	0.710	-0.614	3.330	-1.240	2.700			WT-HOMO	4.254		-0.128	8.636	0.059
			HOMO	1.994	1.527	0.683	0.098	3.890	0.240	3.540			HET-HEMI	6.274		1.892	10.656	0.004**
													HET-HOMO	5.638		1.256	10.020	0.010**
													HEMI-HOMO	-0.636		-5.018	3.746	0.975
		whiteness	WT	57.442	9.437	4.220	45.725	69.159	42.600	68.470	9.624	0.001*	WT-HET	7.516	9.344	-19.218	34.250	0.851
			HET	49.926	25.208	11.273	18.626	81.226	23.230	87.890			WT-HEMI	-35.174		-61.908	-8.440	0.008**
			HEMI	92.616	7.821	3.498	82.905	102.327	86.320	105.740			WT-HOMO	-26.414		-53.148	0.320	0.053
			HOMO	83.856	9.351	4.182	72.245	95.467	74.430	94.420			HET-HEMI	-42.690		-69.424	-15.956	0.000**
													HET-HOMO	-33.930		-60.664	-7.196	0.011**
													HEMI-HOMO	8.760		-17.974	35.494	0.785

* Bonferroni Corrected Significant Difference ($p \leq 0.002$)
** Significant Difference ($p \leq 0.05$)

Table 17. *Amelx* 3D Incisor Morphometry – left buccal

MANDIBULAR INCISORS				ANOVA								MULTIPLE COMPARISON					
VIEW/ ASPECT		MEASUREMENT VARIABLE	GROUP	Mean	SD	SE	95% CI of Mean lower bound	95% CI of Mean upper bound	min'	max'	F	Sig.	GROUPS	MD	SE	95% CI lower bound	95% CI upper bound	Sig.
LEFT	BUCCAL	projected *overall-length* (mm)	WT	10.041	0.684	0.306	9.191	10.891	9.294	10.804	4.879	0.014**	WT-HET	0.819	0.378	-0.263	1.901	0.175
			HET	9.222	0.603	0.270	8.472	9.971	8.627	9.917			WT-HEMI	0.935		-0.147	2.017	0.103
			HEMI	9.106	0.402	0.180	8.607	9.604	8.552	9.482			WT-HOMO	1.423		0.341	2.505	0.008**
			HOMO	8.618	0.661	0.295	7.798	9.438	7.447	9.042			HET-HEMI	0.116		-0.966	1.198	0.990
													HET-HOMO	0.604		-0.478	1.686	0.408
													HEMI-HOMO	0.488		-0.594	1.570	0.582
		projected *width-at-midpoint* (mm)	WT	1.068	0.068	0.030	0.984	1.152	0.964	1.144	2.289	0.117	WT-HET	0.056	0.040	-0.059	0.170	0.526
			HET	1.012	0.074	0.033	0.920	1.104	0.932	1.110			WT-HEMI	0.050		-0.065	0.165	0.611
			HEMI	1.018	0.036	0.016	0.973	1.063	0.980	1.073			WT-HOMO	0.105		-0.010	0.220	0.079
			HOMO	0.963	0.069	0.031	0.877	1.048	0.870	1.058			HET-HEMI	-0.006		-0.121	0.109	0.999
													HET-HOMO	0.049		-0.065	0.164	0.617
													HEMI-HOMO	0.055		-0.060	0.170	0.531
		actual *width-at-midpoint* (mm)	WT	1.418	0.042	0.019	1.366	1.470	1.366	1.463	3.562	0.038**	WT-HET	0.127	0.055	-0.029	0.284	0.133
			HET	1.291	0.088	0.040	1.181	1.401	1.162	1.376			WT-HEMI	0.070		-0.086	0.227	0.585
			HEMI	1.348	0.090	0.040	1.236	1.460	1.255	1.457			WT-HOMO	0.168		0.012	0.325	0.033**
			HOMO	1.250	0.111	0.049	1.113	1.387	1.088	1.348			HET-HEMI	-0.057		-0.214	0.100	0.729
													HET-HOMO	0.041		-0.116	0.198	0.876
													HEMI-HOMO	0.098		-0.059	0.255	0.314
		actual *perimeter* (mm)	WT	23.466	1.606	0.718	21.471	25.460	21.347	24.685	5.806	0.007**	WT-HET	2.393	0.723	0.325	4.461	0.021**
			HET	21.073	1.037	0.464	19.786	22.360	19.549	22.231			WT-HEMI	2.388		0.320	4.456	0.021**
			HEMI	21.078	0.554	0.248	20.390	21.766	20.293	21.714			WT-HOMO	2.588		0.520	4.656	0.012**
			HOMO	20.878	1.123	0.502	19.483	22.273	18.965	21.952			HET-HEMI	-0.005		-2.073	2.063	1.000
													HET-HOMO	0.195		-1.873	2.263	0.993
													HEMI-HOMO	0.200		-1.868	2.268	0.992
		marked *surface-area* (mm^2)	WT	14.375	1.158	0.518	12.937	15.812	12.899	15.407	8.407	0.001*	WT-HET	2.477	0.658	0.594	4.360	0.008**
			HET	11.898	1.508	0.674	10.026	13.770	10.241	13.805			WT-HEMI	2.421		0.538	4.304	0.010**
			HEMI	11.954	0.418	0.187	11.434	12.473	11.570	12.650			WT-HOMO	3.030		1.147	4.914	0.002**
			HOMO	11.344	0.739	0.330	10.427	12.261	10.125	11.964			HET-HEMI	-0.056		-1.939	1.827	1.000
													HET-HOMO	0.553		-1.330	2.437	0.834
													HEMI-HOMO	0.609		-1.274	2.493	0.792

* Bonferroni Corrected Significant Difference ($p \leq 0.002$)
** Significant Difference ($p \leq 0.05$)

Table 18. *Amelx* 3D Incisor Morphometry – left lingual

MANDIBULAR INCISORS			ANOVA									MULTIPLE COMPARISON					
VIEW/ ASPECT		MEASUREMENT VARIABLE	GROUP	Mean	SD	SE	95% CI of Mean lower bound	95% CI of Mean upper bound	min'	max'	F	Sig.	GROUPS	MD	SE	95% CI lower bound	95% CI upper bound	Sig.
LEFT	LINGUAL	projected *overall-length* (mm)	WT	10.032	0.700	0.313	9.163	10.900	9.285	10.823	4.445	0.019**	WT-HET	0.788	0.389	-0.324	1.900	0.219
			HET	9.244	0.674	0.301	8.407	10.081	8.593	10.097			WT-HEMI	0.942		-0.170	2.054	0.113
			HEMI	9.090	0.372	0.166	8.628	9.552	8.571	9.399			WT-HOMO	1.391		0.278	2.503	0.012**
			HOMO	8.641	0.655	0.293	7.828	9.454	7.483	9.074			HET-HEMI	0.154		-0.958	1.266	0.978
													HET-HOMO	0.603		-0.510	1.715	0.433
													HEMI-HOMO	0.449		-0.663	1.561	0.663
		projected *width-at-midpoint* (mm)	WT	1.095	0.133	0.060	0.929	1.261	0.944	1.311	2.218	0.126	WT-HET	0.081	0.053	-0.071	0.232	0.448
			HET	1.015	0.070	0.031	0.928	1.101	0.938	1.100			WT-HEMI	0.067		-0.084	0.219	0.594
			HEMI	1.028	0.041	0.018	0.977	1.079	0.988	1.084			WT-HOMO	0.136		-0.016	0.287	0.088
			HOMO	0.960	0.061	0.027	0.884	1.035	0.881	1.048			HET-HEMI	-0.013		-0.165	0.138	0.994
													HET-HOMO	0.055		-0.096	0.206	0.730
													HEMI-HOMO	0.068		-0.083	0.220	0.581
		actual *width-at-midpoint* (mm)	WT	1.184	0.098	0.044	1.062	1.306	1.044	1.279	0.576	0.639	WT-HET	-0.019	0.058	-0.184	0.147	0.988
			HET	1.203	0.078	0.035	1.106	1.299	1.135	1.327			WT-HEMI	-0.032		-0.198	0.133	0.942
			HEMI	1.216	0.063	0.028	1.138	1.294	1.150	1.293			WT-HOMO	0.039		-0.126	0.204	0.905
			HOMO	1.145	0.117	0.052	0.999	1.291	1.036	1.279			HET-HEMI	-0.014		-0.179	0.152	0.995
													HET-HOMO	0.058		-0.108	0.223	0.751
													HEMI-HOMO	0.071		-0.094	0.237	0.614
		actual *perimeter* (mm)	WT	23.622	1.452	0.649	21.819	25.424	21.140	24.869	4.997	0.012**	WT-HET	3.086	0.884	0.558	5.614	0.014**
			HET	20.535	0.686	0.307	19.683	21.387	19.830	21.455			WT-HEMI	2.379		-0.149	4.907	0.069
			HEMI	21.243	0.756	0.338	20.304	22.182	20.041	21.921			WT-HOMO	2.734		0.206	5.262	0.032**
			HOMO	20.888	2.158	0.965	18.208	23.568	17.118	22.343			HET-HEMI	-0.708		-3.236	1.820	0.853
													HET-HOMO	-0.353		-2.881	2.175	0.978
													HEMI-HOMO	0.355		-2.173	2.883	0.977
		marked *surface-area* (mm^2)	WT	13.851	1.151	0.515	12.422	15.279	12.406	15.270	10.078	0.001*	WT-HET	3.577	0.694	1.593	5.562	0.000**
			HET	10.273	1.122	0.502	8.880	11.666	9.042	11.572			WT-HEMI	2.433		0.449	4.417	0.014**
			HEMI	11.418	0.504	0.226	10.791	12.044	10.696	11.947			WT-HOMO	2.894		0.910	4.878	0.004**
			HOMO	10.956	1.405	0.628	9.212	12.700	8.571	11.994			HET-HEMI	-1.144		-3.129	0.840	0.380
													HET-HOMO	-0.683		-2.667	1.301	0.760
													HEMI-HOMO	0.461		-1.523	2.445	0.909

* Bonferroni Corrected Significant Difference ($p \leq 0.002$)
** Significant Difference ($p \leq 0.05$)

Table 19. *Amelx* 3D Incisor Morphometry – left labial

MANDIBULAR INCISORS			ANOVA									MULTIPLE COMPARISON					
VIEW/ ASPECT		MEASUREMENT VARIABLE	GROUP	Mean	SD	SE	95% CI of Mean lower bound	95% CI of Mean upper bound	min'	max'	F	Sig.	GROUPS	MD	SE	95% CI lower bound	95% CI upper bound	Sig.
LEFT	LABIAL	projected *labial-length* (mm)											WT-HET	0.615	0.396	-0.519	1.749	0.432
			WT	9.831	0.803	0.359	8.834	10.829	9.040	10.799			WT-HEMI	0.729		-0.405	1.864	0.292
			HET	9.216	0.609	0.272	8.460	9.973	8.605	9.907	3.365	0.045**	WT-HOMO	1.253		0.118	2.387	0.023**
			HEMI	9.102	0.380	0.170	8.630	9.574	8.577	9.432			HET-HEMI	0.114		-1.020	1.249	0.991
			HOMO	8.579	0.641	0.287	7.782	9.375	7.462	9.096			HET-HOMO	0.638		-0.497	1.772	0.402
													HEMI-HOMO	0.523		-0.611	1.658	0.564
		actual *labial-length* (mm)											WT-HET	0.884	0.511	-0.578	2.346	0.341
			WT	10.911	1.059	0.473	9.596	12.226	9.186	11.998			WT-HEMI	0.877		-0.585	2.339	0.348
			HET	10.027	0.890	0.398	8.922	11.131	9.278	11.074	3.241	0.050**	WT-HOMO	1.588		0.127	3.050	0.031**
			HEMI	10.034	0.403	0.180	9.533	10.535	9.485	10.390			HET-HEMI	-0.007		-1.469	1.455	1.000
			HOMO	9.323	0.732	0.327	8.414	10.231	8.086	9.914			HET-HOMO	0.704		-0.758	2.166	0.530
													HEMI-HOMO	0.711		-0.750	2.173	0.522
		circumference (mm)											WT-HET	0.264	0.106	-0.040	0.568	0.100
			WT	2.962	0.144	0.065	2.783	3.142	2.804	3.189			WT-HEMI	0.155		-0.148	0.459	0.480
			HET	2.698	0.128	0.057	2.540	2.857	2.616	2.923	5.062	0.012**	WT-HOMO	0.399		0.095	0.702	0.008**
			HEMI	2.807	0.243	0.109	2.505	3.109	2.424	3.040			HET-HEMI	-0.109		-0.412	0.195	0.738
			HOMO	2.564	0.127	0.057	2.406	2.721	2.388	2.685			HET-HOMO	0.135		-0.169	0.438	0.595
													HEMI-HOMO	0.243		-0.060	0.547	0.141
		total *surface-area* (mm^2)											WT-HET	4.030	1.239	0.487	7.574	0.023
			WT	27.954	1.310	0.586	26.328	29.580	26.206	29.487			WT-HEMI	5.154		1.611	8.698	0.004**
			HET	23.924	1.737	0.777	21.767	26.081	22.411	26.664	6.765	0.004**	WT-HOMO	4.142		0.599	7.686	0.019**
			HEMI	22.799	0.955	0.427	21.613	23.986	21.817	24.059			HET-HEMI	1.124		-2.419	4.668	0.801
			HOMO	23.811	3.114	1.392	19.945	27.677	20.962	28.775			HET-HOMO	0.112		-3.431	3.656	1.000
													HEMI-HOMO	-1.012		-4.556	2.532	0.846
		volume (mm^3)											WT-HET	0.664	0.217	0.044	1.284	0.034**
			WT	5.373	0.496	0.222	4.756	5.989	4.687	6.027			WT-HEMI	1.024		0.404	1.643	0.001**
			HET	4.709	0.203	0.091	4.457	4.961	4.497	4.979	10.228	0.001*	WT-HOMO	1.053		0.433	1.672	0.001**
			HEMI	4.349	0.275	0.123	4.008	4.690	4.071	4.754			HET-HEMI	0.360		-0.260	0.979	0.375
			HOMO	4.320	0.325	0.145	3.916	4.724	4.087	4.871			HET-HOMO	0.389		-0.231	1.008	0.312
													HEMI-HOMO	0.029		-0.591	0.649	0.999

* Bonferroni Corrected Significant Difference ($p \leq 0.002$)
** Significant Difference ($p \leq 0.05$)

Table 20. *Amelx* 3D Incisor Morphometry – right buccal

MANDIBULAR INCISORS			ANOVA									MULTIPLE COMPARISON					
VIEW/ ASPECT		MEASUREMENT VARIABLE	GROUP	Mean	SD	SE	95% CI of Mean lower bound	95% CI of Mean upper bound	min'	max'	F	Sig.	GROUPS	MD	SE	95% CI lower bound	95% CI upper bound	Sig.
RIGHT	BUCCAL	projected *overall-length* (mm)	WT	10.082	0.450	0.201	9.524	10.641	9.461	10.669	5.783	0.007**	WT-HET	0.865	0.260	0.121	1.609	0.020**
			HET	9.218	0.388	0.174	8.736	9.700	8.726	9.765			WT-HEMI	0.887		0.143	1.631	0.017**
			HEMI	9.195	0.321	0.143	8.797	9.593	8.652	9.431			WT-HOMO	0.900		0.156	1.644	0.015**
			HOMO	9.182	0.469	0.210	8.599	9.765	8.643	9.694			HET-HEMI	0.022		-0.722	0.767	1.000
													HET-HOMO	0.035		-0.709	0.780	0.999
													HEMI-HOMO	0.013		-0.731	0.757	1.000
		projected *width-at-midpoint* (mm)	WT	1.080	0.029	0.013	1.044	1.115	1.047	1.121	1.292	0.311	WT-HET	0.047	0.048	-0.091	0.185	0.767
			HET	1.033	0.069	0.031	0.947	1.118	0.913	1.083			WT-HEMI	0.056		-0.082	0.195	0.656
			HEMI	1.023	0.118	0.053	0.877	1.169	0.897	1.173			WT-HOMO	0.095		-0.044	0.233	0.246
			HOMO	0.985	0.063	0.028	0.906	1.064	0.900	1.077			HET-HEMI	0.009		-0.129	0.148	0.997
													HET-HOMO	0.048		-0.091	0.186	0.761
													HEMI-HOMO	0.038		-0.100	0.177	0.858
		actual *width-at-midpoint* (mm)	WT	1.370	0.056	0.025	1.301	1.439	1.324	1.433	0.626	0.609	WT-HET	0.053	0.063	-0.128	0.234	0.835
			HET	1.317	0.077	0.035	1.221	1.413	1.196	1.411			WT-HEMI	0.065		-0.116	0.245	0.737
			HEMI	1.305	0.139	0.062	1.132	1.478	1.173	1.485			WT-HOMO	0.082		-0.099	0.262	0.578
			HOMO	1.288	0.107	0.048	1.156	1.421	1.189	1.470			HET-HEMI	0.012		-0.169	0.192	0.998
													HET-HOMO	0.029		-0.152	0.209	0.967
													HEMI-HOMO	0.017		-0.164	0.198	0.993
		actual *perimeter* (mm)	WT	23.568	0.622	0.278	22.795	24.341	22.670	24.348	5.198	0.011**	WT-HET	0.964	0.718	-1.091	3.020	0.551
			HET	22.604	1.502	0.672	20.739	24.469	20.527	24.669			WT-HEMI	2.708		0.652	4.763	0.008**
			HEMI	20.860	0.877	0.392	19.771	21.949	19.794	21.557			WT-HOMO	1.809		-0.246	3.865	0.095
			HOMO	21.759	1.322	0.591	20.117	23.401	20.216	23.658			HET-HEMI	1.743		-0.312	3.799	0.112
													HET-HOMO	0.845		-1.210	2.900	0.650
													HEMI-HOMO	-0.898		-2.954	1.157	0.605
		marked *surface-area* (mm^2)	WT	13.984	1.541	0.689	12.071	15.898	11.786	15.621	7.029	0.003**	WT-HET	1.414	0.647	-0.438	3.266	0.170
			HET	12.570	0.850	0.380	11.515	13.626	11.098	13.225			WT-HEMI	2.295		0.443	4.146	0.013**
			HEMI	11.690	0.939	0.420	10.524	12.855	10.291	12.707			WT-HOMO	2.758		0.906	4.610	0.003**
			HOMO	11.226	0.460	0.206	10.655	11.797	10.640	11.636			HET-HEMI	0.881		-0.971	2.732	0.540
													HET-HOMO	1.344		-0.508	3.196	0.203
													HEMI-HOMO	0.464		-1.388	2.315	0.889

* Bonferroni Corrected Significant Difference ($p \leq 0.002$)
** Significant Difference ($p \leq 0.05$)

Table 21. *Amelx* 3D Incisor Morphometry – right lingual

MANDIBULAR INCISORS				ANOVA								MULTIPLE COMPARISON					
VIEW/ ASPECT		MEASUREMENT VARIABLE	GROUP	Mean	SD	SE	95% CI of Mean lower bound	95% CI of Mean upper bound	min'	max'	F	Sig.	GROUPS	MD	SE	95% CI lower bound	95% CI upper bound	Sig.
RIGHT	LINGUAL	projected *overall-length* (mm)	WT	9.949	0.458	0.205	9.381	10.518	9.515	10.638	4.608	0.017**	WT-HET	0.788	0.250	0.072	1.503	0.029**
			HET	9.161	0.373	0.167	8.698	9.625	8.767	9.712			WT-HEMI	0.717		0.002	1.433	0.049**
			HEMI	9.232	0.239	0.107	8.935	9.529	8.852	9.432			WT-HOMO	0.766		0.051	1.482	0.034**
			HOMO	9.183	0.469	0.210	8.601	9.765	8.621	9.682			HET-HEMI	-0.071		-0.786	0.645	0.992
													HET-HOMO	-0.022		-0.737	0.694	1.000
													HEMI-HOMO	0.049		-0.667	0.765	0.997
		projected *width-at-midpoint* (mm)	WT	1.070	0.030	0.013	1.032	1.107	1.023	1.107	1.916	0.168	WT-HET	0.001	0.039	-0.110	0.113	1.000
			HET	1.068	0.033	0.015	1.027	1.110	1.021	1.106			WT-HEMI	0.037		-0.074	0.149	0.775
			HEMI	1.032	0.102	0.046	0.905	1.159	0.899	1.162			WT-HOMO	0.081		-0.031	0.193	0.203
			HOMO	0.988	0.053	0.024	0.922	1.055	0.925	1.070			HET-HEMI	0.036		-0.076	0.148	0.794
													HET-HOMO	0.080		-0.032	0.192	0.215
													HEMI-HOMO	0.044		-0.068	0.156	0.683
		actual *width-at-midpoint* (mm)	WT	1.249	0.068	0.031	1.164	1.334	1.158	1.351	0.311	0.817	WT-HET	0.047	0.074	-0.166	0.259	0.922
			HET	1.203	0.131	0.059	1.040	1.365	1.021	1.350			WT-HEMI	0.021		-0.192	0.234	0.992
			HEMI	1.228	0.167	0.075	1.021	1.436	1.031	1.409			WT-HOMO	0.067		-0.146	0.280	0.804
			HOMO	1.182	0.074	0.033	1.091	1.274	1.104	1.273			HET-HEMI	-0.026		-0.238	0.187	0.985
													HET-HOMO	0.020		-0.192	0.233	0.992
													HEMI-HOMO	0.046		-0.167	0.259	0.924
		actual *perimeter* (mm)	WT	23.460	0.677	0.303	22.620	24.300	22.484	24.354	4.391	0.020**	WT-HET	0.978	0.731	-1.114	3.070	0.554
			HET	22.482	1.722	0.770	20.343	24.620	20.686	24.997			WT-HEMI	2.579		0.487	4.671	0.013**
			HEMI	20.881	0.691	0.309	20.023	21.739	20.149	21.650			WT-HOMO	1.605		-0.487	3.697	0.167
			HOMO	21.855	1.203	0.538	20.361	23.348	20.111	23.192			HET-HEMI	1.601		-0.491	3.693	0.169
													HET-HOMO	0.627		-1.465	2.719	0.826
													HEMI-HOMO	-0.974		-3.066	1.118	0.557
		marked *surface-area* (mm^2)	WT	14.041	1.384	0.619	12.322	15.760	11.825	15.257	7.623	0.002*	WT-HET	2.191	0.661	0.301	4.081	0.020**
			HET	11.850	0.664	0.297	11.025	12.675	11.055	12.786			WT-HEMI	2.184		0.294	4.073	0.021**
			HEMI	11.857	1.313	0.587	10.227	13.487	9.998	13.431			WT-HOMO	3.007		1.117	4.897	0.002**
			HOMO	11.034	0.531	0.238	10.374	11.693	10.223	11.637			HET-HEMI	-0.007		-1.897	1.882	1.000
													HET-HOMO	0.816		-1.074	2.706	0.614
													HEMI-HOMO	0.824		-1.066	2.713	0.608

* Bonferroni Corrected Significant Difference ($p \leq 0.002$)
** Significant Difference ($p \leq 0.05$)

Table 22. *Amelx* 3D Incisor Morphometry – right labial

MANDIBULAR INCISORS				ANOVA								MULTIPLE COMPARISON					
VIEW/ ASPECT		MEASUREMENT VARIABLE	GROUP	Mean	SD	SE	95% CI of Mean lower bound	95% CI of Mean upper bound	min'	max'	F	Sig.	GROUPS	MD	SE	95% CI lower bound	95% CI upper bound	Sig.
RIGHT	LABIAL	projected *labial-length* (mm)	WT	10.086	0.417	0.186	9.568	10.603	9.533	10.653	6.668	0.004**	WT-HET	0.887	0.245	0.187	1.587	0.011**
			HET	9.198	0.392	0.175	8.712	9.685	8.700	9.737			WT-HEMI	0.875		0.175	1.575	0.012**
			HEMI	9.211	0.262	0.117	8.886	9.536	8.779	9.429			WT-HOMO	0.916		0.216	1.616	0.009**
			HOMO	9.170	0.450	0.201	8.611	9.729	8.636	9.669			HET-HEMI	-0.012		-0.712	0.687	1.000
													HET-HOMO	0.029		-0.671	0.728	0.999
													HEMI-HOMO	0.041		-0.659	0.741	0.998
		actual *labial-length* (mm)	WT	10.864	0.582	0.260	10.141	11.587	10.023	11.542	2.899	0.067	WT-HET	0.678	0.410	-0.495	1.851	0.379
			HET	10.186	0.485	0.217	9.584	10.788	9.623	10.695			WT-HEMI	0.838		-0.335	2.011	0.213
			HEMI	10.026	0.390	0.174	9.542	10.510	9.584	10.390			WT-HOMO	1.174		0.001	2.346	0.050
			HOMO	9.690	0.977	0.437	8.478	10.903	8.132	10.803			HET-HEMI	0.160		-1.013	1.333	0.979
													HET-HOMO	0.496		-0.677	1.668	0.630
													HEMI-HOMO	0.336		-0.837	1.508	0.845
		circumference (mm)	WT	2.993	0.135	0.060	2.825	3.160	2.891	3.216	6.579	0.004**	WT-HET	0.172	0.090	-0.087	0.431	0.267
			HET	2.821	0.075	0.033	2.728	2.914	2.751	2.905			WT-HEMI	0.285		0.026	0.544	0.028**
			HEMI	2.708	0.203	0.091	2.455	2.960	2.492	2.937			WT-HOMO	0.382		0.123	0.641	0.003**
			HOMO	2.611	0.129	0.058	2.451	2.771	2.420	2.747			HET-HEMI	0.113		-0.146	0.372	0.605
													HET-HOMO	0.210		-0.049	0.469	0.134
													HEMI-HOMO	0.097		-0.162	0.356	0.711
		total *surface-area* (mm^2)	WT	29.038	1.362	0.609	27.347	30.729	26.773	30.239	4.972	0.013**	WT-HET	2.995	1.259	-0.608	6.597	0.122
			HET	26.044	1.694	0.757	23.941	28.146	23.551	27.568			WT-HEMI	3.729		0.126	7.332	0.041**
			HEMI	25.309	2.538	1.135	22.158	28.460	22.039	28.431			WT-HOMO	4.557		0.954	8.159	0.011**
			HOMO	24.481	2.166	0.969	21.791	27.171	21.531	26.709			HET-HEMI	0.734		-2.868	4.337	0.936
													HET-HOMO	1.562		-2.040	5.165	0.611
													HEMI-HOMO	0.828		-2.775	4.430	0.911
		volume (mm^3)	WT	5.772	0.959	0.429	4.581	6.962	4.769	6.904	6.625	0.004**	WT-HET	0.961	0.361	-0.073	1.995	0.073
			HET	4.811	0.338	0.151	4.391	5.231	4.419	5.334			WT-HEMI	1.288		0.254	2.322	0.012**
			HEMI	4.484	0.362	0.162	4.034	4.934	3.945	4.923			WT-HOMO	1.482		0.448	2.516	0.004**
			HOMO	4.290	0.377	0.168	3.822	4.758	3.807	4.704			HET-HEMI	0.327		-0.707	1.361	0.803
													HET-HOMO	0.521		-0.513	1.555	0.494
													HEMI-HOMO	0.194		-0.840	1.228	0.949

* Bonferroni Corrected Significant Difference ($p \leq 0.002$)
** Significant Difference ($p \leq 0.05$)

Table 23. *Enam* 2D Mandible Morphometry – left buccal

HEMI-MANDIBLES				ANOVA								MULTIPLE COMPARISON					
VIEW/ ASPECT		MEASUREMENT VARIABLE	GROUP	Mean	SD	SE	95% CI of Mean lower bound	95% CI of Mean upper bound	min'	max'	F	Sig.	GROUPS	MD	SE	95% CI lower bound	95% CI upper bound	Sig.
LEFT	BUCCAL	*overall-length* (mm)	WT	12.138	0.465	0.208	11.561	12.714	11.716	12.85	0.167	0.848	WT-HOMO	0.089	0.264	-0.616	0.794	0.940
			HOMO	12.049	0.438	0.196	11.505	12.592	11.470	12.457			WT-HET	0.152		-0.553	0.857	0.836
			HET	11.986	0.341	0.153	11.562	12.409	11.687	12.560			HOMO-HET	0.063		-0.642	0.768	0.969
		ascending-height (mm)	WT	6.351	0.224	0.100	6.073	6.629	6.115	6.683	0.792	0.475	WT-HOMO	0.049	0.155	-0.366	0.463	0.948
			HOMO	6.302	0.232	0.104	6.014	6.590	6.037	6.582			WT-HET	0.188		-0.226	0.603	0.469
			HET	6.162	0.278	0.124	5.818	6.507	5.894	6.621			HOMO-HET	0.140		-0.275	0.555	0.651
		basal-length (mm)	WT	7.241	0.403	0.180	6.740	7.741	6.770	7.673	2.761	0.103	WT-HOMO	0.387	0.188	-0.114	0.888	0.140
			HOMO	6.853	0.268	0.120	6.521	7.186	6.494	7.106			WT-HET	0.376		-0.124	0.877	0.153
			HET	6.864	0.173	0.077	6.649	7.079	6.689	7.095			HOMO-HET	-0.011		-0.512	0.490	0.998
		mandible-angle (°)	WT	66.056	1.682	0.752	63.967	68.145	63.662	68.331	0.679	0.526	WT-HOMO	0.249	1.482	-3.705	4.204	0.985
			HOMO	65.807	2.822	1.262	62.303	69.311	62.792	69.852			WT-HET	-1.355		-5.310	2.599	0.642
			HET	67.412	2.384	1.066	64.451	70.372	64.659	70.530			HOMO-HET	-1.605		-5.559	2.350	0.542
		coronoid-coronoid-length (mm)	WT	3.153	0.318	0.142	2.759	3.548	2.799	3.650	0.291	0.753	WT-HOMO	-0.080	0.128	-0.422	0.262	0.810
			HOMO	3.233	0.124	0.055	3.080	3.387	3.126	3.410			WT-HET	-0.089		-0.431	0.254	0.773
			HET	3.242	0.084	0.037	3.138	3.346	3.156	3.353			HOMO-HET	-0.009		-0.351	0.334	0.997
		diagonal-length (mm)	WT	8.910	0.365	0.163	8.456	9.363	8.564	9.44	1.119	0.358	WT-HOMO	0.282	0.194	-0.237	0.801	0.348
			HOMO	8.628	0.301	0.135	8.254	9.002	8.252	9.039			WT-HET	0.203		-0.316	0.722	0.565
			HET	8.707	0.244	0.109	8.404	9.010	8.449	9.042			HOMO-HET	-0.079		-0.598	0.440	0.914
		mandible-perimeter (mm)	WT	35.089	1.255	0.561	33.530	36.647	34.083	37.198	0.088	0.916	WT-HOMO	0.237	0.837	-1.996	2.470	0.957
			HOMO	34.852	1.597	0.714	32.869	36.834	32.414	36.336			WT-HET	0.343		-1.890	2.576	0.912
			HET	34.746	1.063	0.475	33.426	36.066	33.435	36.115			HOMO-HET	0.106		-2.127	2.339	0.991
		mandible-area (mm^2)	WT	38.281	1.800	0.805	36.046	40.516	36.653	41.044	0.118	0.890	WT-HOMO	-0.003	1.203	-3.213	3.207	1.000
			HOMO	38.284	2.086	0.933	35.694	40.875	35.204	40.605			WT-HET	-0.508		-3.718	2.702	0.907
			HET	38.788	1.807	0.808	36.544	41.033	36.339	41.167			HOMO-HET	-0.504		-3.714	2.706	0.908

* Bonferroni Corrected Significant Difference ($p \leq 0.002$)
** Significant Difference ($p \leq 0.05$)

Table 24. *Enam* 2D Mandible Morphometry – left lingual

HEMI-MANDIBLES				ANOVA								MULTIPLE COMPARISON					
VIEW/ ASPECT		MEASUREMENT VARIABLE	GROUP	Mean	SD	SE	95% CI of Mean lower bound	95% CI of Mean upper bound	min'	max'	F	Sig.	GROUPS	MD	SE	95% CI lower bound	95% CI upper bound	Sig.
LEFT	LINGUAL	*overall-length* (mm)	WT	12.190	0.488	0.218	11.583	12.795	11.721	12.911	0.311	0.738	WT-HOMO	0.145	0.269	-0.573	0.863	0.855
			HOMO	12.045	0.395	0.177	11.554	12.535	11.445	12.459			WT-HET	0.207		-0.511	0.925	0.728
			HET	11.982	0.386	0.173	11.503	12.462	11.698	12.643			HOMO-HET	0.062		-0.656	0.780	0.971
		ascending-height (mm)	WT	6.373	0.241	0.108	6.074	6.672	6.111	6.702	1.025	0.388	WT-HOMO	0.139	0.167	-0.308	0.586	0.692
			HOMO	6.234	0.240	0.107	5.937	6.532	6.019	6.557			WT-HET	0.239		-0.208	0.685	0.360
			HET	6.135	0.308	0.138	5.752	6.517	5.819	6.636			HOMO-HET	0.100		-0.347	0.546	0.825
		basal-length (mm)	WT	7.147	0.344	0.154	6.719	7.574	6.901	7.640	1.530	0.256	WT-HOMO	0.282	0.169	-0.170	0.734	0.258
			HOMO	6.865	0.260	0.116	6.542	7.188	6.481	7.182			WT-HET	0.220		-0.232	0.672	0.423
			HET	6.927	0.170	0.076	6.716	7.138	6.696	7.061			HOMO-HET	-0.062		-0.514	0.390	0.929
		mandible-angle (°)	WT	65.117	1.848	0.826	62.823	67.411	63.216	67.820	0.813	0.467	WT-HOMO	0.171	1.611	-4.127	4.468	0.994
			HOMO	64.946	2.903	1.298	61.342	68.551	62.275	68.851			WT-HET	-1.687		-5.985	2.610	0.563
			HET	66.804	2.761	1.235	63.376	70.233	64.031	70.097			HOMO-HET	-1.858		-6.156	2.440	0.502
		coronoid-coronoid-length (mm)	WT	3.271	0.268	0.120	2.938	3.603	3.006	3.712	0.670	0.530	WT-HOMO	-0.083	0.122	-0.408	0.242	0.779
			HOMO	3.354	0.094	0.042	3.237	3.471	3.262	3.464			WT-HET	0.057		-0.268	0.383	0.886
			HET	3.213	0.176	0.079	2.995	3.432	3.005	3.470			HOMO-HET	0.140		-0.185	0.466	0.503
		diagonal-length (mm)	WT	8.926	0.357	0.160	8.483	9.370	8.585	9.494	1.039	0.384	WT-HOMO	0.246	0.173	-0.215	0.707	0.360
			HOMO	8.680	0.210	0.094	8.419	8.942	8.324	8.862			WT-HET	0.156		-0.305	0.616	0.650
			HET	8.771	0.228	0.102	8.488	9.054	8.518	9.131			HOMO-HET	-0.091		-0.551	0.370	0.861
		mandible-perimeter (mm)	WT	37.157	1.613	0.721	35.154	39.160	35.619	38.935	1.603	0.242	WT-HOMO	0.783	0.891	-1.595	3.161	0.663
			HOMO	36.374	1.201	0.537	34.884	37.865	34.965	37.957			WT-HET	1.596		-0.782	3.974	0.214
			HET	35.562	1.383	0.619	33.844	37.279	34.086	37.648			HOMO-HET	0.813		-1.565	3.191	0.643
		mandible-area (mm^2)	WT	38.012	1.860	0.832	35.703	40.321	36.682	40.898	0.388	0.686	WT-HOMO	0.009	1.286	-3.421	3.439	1.000
			HOMO	38.003	2.092	0.936	35.405	40.601	34.656	39.922			WT-HET	-0.977		-4.406	2.453	0.734
			HET	38.989	2.135	0.955	36.337	41.640	36.820	41.934			HOMO-HET	-0.986		-4.415	2.444	0.730

* Bonferroni Corrected Significant Difference ($p \leq 0.002$)
** Significant Difference ($p \leq 0.05$)

Table 25. *Enam* 2D Mandible Morphometry – right buccal

HEMI-MANDIBLES				ANOVA								MULTIPLE COMPARISON					
VIEW/ ASPECT		MEASUREMENT VARIABLE	GROUP	Mean	SD	SE	95% CI of Mean lower bound	95% CI of Mean upper bound	min'	max'	F	Sig.	GROUPS	MD	SE	95% CI lower bound	95% CI upper bound	Sig.
RIGHT	BUCCAL	*overall-length* (mm)	WT	11.916	0.341	0.153	11.492	12.340	11.567	12.282	0.125	0.884	WT-HOMO	-0.032	0.231	-0.649	0.585	0.989
			HOMO	11.948	0.351	0.157	11.512	12.384	11.458	12.369			WT-HET	-0.112		-0.729	0.505	0.880
			HET	12.028	0.401	0.180	11.529	12.526	11.653	12.710			HOMO-HET	-0.080		-0.697	0.537	0.936
		ascending-height (mm)	WT	6.291	0.284	0.127	5.938	6.643	5.856	6.622	0.251	0.782	WT-HOMO	0.146	0.207	-0.406	0.698	0.765
			HOMO	6.145	0.352	0.158	5.707	6.582	5.648	6.562			WT-HET	0.084		-0.468	0.636	0.914
			HET	6.207	0.341	0.152	5.784	6.630	5.889	6.785			HOMO-HET	-0.062		-0.614	0.490	0.952
		basal-length (mm)	WT	6.942	0.183	0.082	6.714	7.169	6.712	7.223	1.099	0.364	WT-HOMO	-0.159	0.115	-0.467	0.148	0.381
			HOMO	7.101	0.210	0.094	6.840	7.362	6.867	7.382			WT-HET	-0.026		-0.334	0.282	0.973
			HET	6.967	0.149	0.066	6.783	7.152	6.788	7.166			HOMO-HET	0.134		-0.174	0.441	0.499
		mandible-angle (°)	WT	65.704	1.453	0.650	63.901	67.508	63.552	67.356	0.560	0.585	WT-HOMO	-0.842	1.101	-3.778	2.095	0.731
			HOMO	66.546	1.997	0.893	64.066	69.026	63.819	68.531			WT-HET	-1.118		-4.055	1.818	0.581
			HET	66.823	1.728	0.773	64.677	68.968	64.742	68.949			HOMO-HET	-0.277		-3.213	2.659	0.966
		coronoid-coronoid-length (mm)	WT	3.215	0.180	0.081	2.992	3.439	3.057	3.517	1.036	0.385	WT-HOMO	-0.214	0.149	-0.612	0.184	0.356
			HOMO	3.429	0.225	0.101	3.149	3.709	3.164	3.650			WT-HET	-0.089		-0.487	0.309	0.824
			HET	3.304	0.289	0.129	2.945	3.664	2.848	3.647			HOMO-HET	0.125		-0.273	0.523	0.689
		diagonal-length (mm)	WT	8.704	0.161	0.072	8.504	8.904	8.538	8.962	0.664	0.533	WT-HOMO	-0.153	0.148	-0.547	0.242	0.572
			HOMO	8.857	0.261	0.117	8.532	9.181	8.414	9.060			WT-HET	-0.142		-0.537	0.253	0.615
			HET	8.846	0.264	0.118	8.518	9.174	8.649	9.195			HOMO-HET	0.011		-0.384	0.405	0.997
		mandible-perimeter (mm)	WT	34.780	0.636	0.284	33.990	35.570	34.018	35.527	0.065	0.937	WT-HOMO	0.017	0.466	-1.225	1.260	0.999
			HOMO	34.763	0.478	0.214	34.169	35.357	34.340	35.398			WT-HET	-0.136		-1.378	1.106	0.954
			HET	34.916	0.997	0.446	33.679	36.154	34.195	36.668			HOMO-HET	-0.153		-1.396	1.089	0.942
		mandible-area (mm^2)	WT	37.621	1.789	0.800	35.400	39.841	35.219	39.893	1.378	0.289	WT-HOMO	-0.291	1.100	-3.225	2.642	0.962
			HOMO	37.912	1.939	0.867	35.505	40.319	34.709	39.474			WT-HET	-1.706		-4.640	1.227	0.303
			HET	39.327	1.453	0.650	37.523	41.131	37.818	41.692			HOMO-HET	-1.415		-4.349	1.519	0.429

* Bonferroni Corrected Significant Difference ($p \leq 0.002$)
** Significant Difference ($p \leq 0.05$)

Table 26. *Enam* 2D Mandible Morphometry – right lingual

HEMI-MANDIBLES				ANOVA								MULTIPLE COMPARISON					
VIEW/ ASPECT		MEASUREMENT VARIABLE	GROUP	Mean	SD	SE	95% CI of Mean lower bound	95% CI of Mean upper bound	min'	max'	F	Sig.	GROUPS	MD	SE	95% CI lower bound	95% CI upper bound	Sig.
RIGHT	LINGUAL	*overall-length* (mm)	WT	11.953	0.470	0.210	11.369	12.537	11.382	12.475	0.182	0.836	WT-HOMO	-0.103	0.266	-0.813	0.607	0.921
			HOMO	12.056	0.395	0.177	11.565	12.547	11.521	12.489			WT-HET	-0.158		-0.868	0.552	0.826
			HET	12.111	0.392	0.175	11.625	12.597	11.647	12.731			HOMO-HET	-0.055		-0.765	0.655	0.977
		ascending-height (mm)	WT	6.264	0.258	0.115	5.944	6.585	5.885	6.588	0.303	0.744	WT-HOMO	0.165	0.218	-0.416	0.747	0.734
			HOMO	6.099	0.395	0.177	5.608	6.590	5.594	6.534			WT-HET	0.116		-0.466	0.698	0.858
			HET	6.148	0.366	0.164	5.694	6.603	5.772	6.737			HOMO-HET	-0.050		-0.631	0.532	0.972
		basal-length (mm)	WT	6.941	0.206	0.092	6.685	7.197	6.734	7.274	1.301	0.308	WT-HOMO	-0.201	0.130	-0.549	0.147	0.308
			HOMO	7.142	0.245	0.110	6.837	7.446	6.872	7.496			WT-HET	-0.046		-0.394	0.301	0.933
			HET	6.987	0.157	0.070	6.792	7.183	6.828	7.175			HOMO-HET	0.154		-0.193	0.502	0.484
		mandible-angle (°)	WT	64.939	1.458	0.652	63.130	66.749	62.723	66.359	0.816	0.465	WT-HOMO	-1.279	1.117	-4.258	1.700	0.506
			HOMO	66.218	2.028	0.907	63.700	68.736	64.167	68.887			WT-HET	-1.187		-4.166	1.792	0.554
			HET	66.127	1.765	0.789	63.935	68.318	63.743	68.360			HOMO-HET	0.092		-2.888	3.071	0.996
		coronoid-coronoid-length (mm)	WT	3.201	0.186	0.083	2.970	3.432	2.979	3.489	1.647	0.233	WT-HOMO	-0.224	0.124	-0.554	0.106	0.208
			HOMO	3.425	0.179	0.080	3.203	3.647	3.181	3.606			WT-HET	-0.097		-0.427	0.233	0.721
			HET	3.298	0.220	0.098	3.025	3.571	2.987	3.574			HOMO-HET	0.127		-0.203	0.457	0.575
		diagonal-length (mm)	WT	8.762	0.19	0.09	8.5241	8.9991	8.557	9.032	0.689	0.521	WT-HOMO	-0.166	0.159	-0.589	0.257	0.564
			HOMO	8.927	0.278	0.124	8.582	9.272	8.453	9.147			WT-HET	-0.156		-0.579	0.267	0.600
			HET	8.918	0.274	0.122	8.578	9.258	8.649	9.266			HOMO-HET	0.010		-0.414	0.433	0.998
		mandible-perimeter (mm)	WT	35.870	1.082	0.484	34.526	37.214	35.020	37.377	0.000	1.000	WT-HOMO	0.011	0.950	-2.522	2.545	1.000
			HOMO	35.858	1.956	0.875	33.429	38.288	32.903	37.690			WT-HET	0.025		-2.508	2.559	1.000
			HET	35.844	1.328	0.594	34.195	37.494	34.467	37.805			HOMO-HET	0.014		-2.519	2.547	1.000
		mandible-area (mm^2)	WT	37.411	2.068	0.925	34.843	39.980	35.137	40.145	0.884	0.438	WT-HOMO	-0.228	1.248	-3.558	3.101	0.982
			HOMO	37.639	2.334	1.044	34.742	40.537	33.852	39.813			WT-HET	-1.537		-4.867	1.792	0.458
			HET	38.949	1.398	0.625	37.213	40.684	37.813	41.234			HOMO-HET	-1.309		-4.639	2.020	0.562

* Bonferroni Corrected Significant Difference ($p \leq 0.002$)
** Significant Difference ($p \leq 0.05$)

Table 27. *Enam* 2D Incisor Morphometry – left

MANDIBULAR INCISORS				ANOVA									MULTIPLE COMPARISON					
VIEW/ ASPECT		MEASUREMENT VARIABLE	GROUP	Mean	SD	SE	95% CI of Mean lower bound	95% CI of Mean upper bound	min'	max'	F	Sig.	GROUPS	MD	SE	95% CI lower bound	95% CI upper bound	Sig.
LEFT	BUCCAL	*overall-length* (mm)	WT	9.705	0.406	0.182	9.201	10.210	9.186	10.244	0.516	0.609	WT-HOMO	0.225	0.231	-0.391	0.841	0.607
			HOMO	9.481	0.315	0.141	9.089	9.872	9.136	9.926			WT-HET	0.054		-0.562	0.670	0.971
			HET	9.652	0.368	0.165	9.195	10.109	9.086	10.032			HOMO-HET	-0.171		-0.787	0.445	0.745
		angle-of-curvature (°)	WT	128.498	1.713	0.766	126.371	130.625	126.500	131.050	1.056	0.378	WT-HOMO	-0.387	1.100	-3.320	2.547	0.934
			HOMO	128.885	1.617	0.723	126.877	130.893	126.570	130.721			WT-HET	-1.536		-4.469	1.398	0.373
			HET	130.034	1.876	0.839	127.705	132.363	127.087	132.323			HOMO-HET	-1.149		-4.083	1.784	0.564
		width-at-midpoint (mm)	WT	0.994	0.044	0.019	0.940	1.048	0.947	1.043	0.559	0.586	WT-HOMO	0.023	0.025	-0.044	0.089	0.649
			HOMO	0.972	0.029	0.013	0.936	1.007	0.924	0.999			WT-HET	-0.001		-0.067	0.066	1.000
			HET	0.995	0.045	0.020	0.940	1.050	0.942	1.061			HOMO-HET	-0.023		-0.090	0.044	0.634
		incisor-perimeter (mm)	WT	21.763	1.099	0.491	20.399	23.127	20.135	23.020	0.167	0.848	WT-HOMO	-0.381	0.688	-2.218	1.455	0.847
			HOMO	22.144	1.135	0.507	20.735	23.553	20.914	23.719			WT-HET	-0.092		-1.928	1.745	0.990
			HET	21.855	1.029	0.460	20.576	23.133	20.607	22.829			HOMO-HET	0.289		-1.547	2.126	0.908
		incisor-area (mm^2)	WT	9.573	0.652	0.292	8.763	10.382	8.650	10.300	1.483	0.266	WT-HOMO	0.614	0.466	-0.629	1.857	0.413
			HOMO	8.959	0.807	0.361	7.957	9.961	8.114	10.075			WT-HET	-0.141		-1.384	1.102	0.951
			HET	9.713	0.743	0.332	8.791	10.636	8.979	10.760			HOMO-HET	-0.755		-1.998	0.488	0.275
	LINGUAL	*overall-length* (mm)	WT	9.670	0.171	0.076	9.458	9.882	9.545	9.971	0.366	0.701	WT-HOMO	0.005	0.184	-0.487	0.496	1.000
			HOMO	9.665	0.297	0.133	9.296	10.034	9.348	10.143			WT-HET	0.139		-0.353	0.630	0.737
			HET	9.531	0.370	0.165	9.072	9.991	9.062	9.937			HOMO-HET	0.134		-0.357	0.625	0.752
		angle-of-curvature (°)	WT	128.688	0.669	0.299	127.857	129.518	127.833	129.454	4.676	0.032**	WT-HOMO	-0.028	0.795	-2.150	2.095	0.999
			HOMO	128.715	1.325	0.592	127.070	130.360	126.897	130.454			WT-HET	-2.120		-4.243	0.002	0.050**
			HET	130.808	1.595	0.713	128.828	132.788	128.881	133.285			HOMO-HET	-2.093		-4.215	0.029	0.053
		width-at-midpoint (mm)	WT	0.983	0.056	0.025	0.914	1.052	0.931	1.047	1.395	0.285	WT-HOMO	0.041	0.032	-0.043	0.126	0.420
			HOMO	0.941	0.031	0.014	0.902	0.980	0.901	0.984			WT-HET	-0.008		-0.093	0.077	0.966
			HET	0.991	0.059	0.026	0.917	1.064	0.941	1.092			HOMO-HET	-0.049		-0.134	0.035	0.301
		incisor-perimeter (mm)	WT	21.670	0.414	0.185	21.156	22.184	21.290	22.302	1.930	0.188	WT-HOMO	-0.241	0.406	-1.325	0.843	0.827
			HOMO	21.911	0.891	0.398	20.804	23.017	20.915	22.831			WT-HET	0.539		-0.545	1.623	0.408
			HET	21.131	0.523	0.234	20.482	21.781	20.511	21.933			HOMO-HET	0.780		-0.305	1.864	0.176
		incisor-area (mm^2)	WT	9.563	0.409	0.183	9.055	10.071	9.094	10.212	3.049	0.085	WT-HOMO	0.715	0.301	-0.089	1.519	0.083
			HOMO	8.848	0.650	0.290	8.042	9.655	8.299	9.713			WT-HET	0.179		-0.625	0.983	0.826
			HET	9.384	0.303	0.136	9.008	9.760	9.082	9.755			HOMO-HET	-0.536		-1.340	0.268	0.218
		labial-length (mm)	WT	11.630	0.762	0.341	10.683	12.576	10.451	12.501	0.111	0.896	WT-HOMO	0.203	0.444	-0.981	1.388	0.892
			HOMO	11.426	0.794	0.355	10.441	12.411	10.727	12.758			WT-HET	0.143		-1.042	1.328	0.945
			HET	11.487	0.518	0.232	10.843	12.130	10.846	12.249			HOMO-HET	-0.060		-1.245	1.124	0.990

* Bonferroni Corrected Significant Difference ($p \leq 0.002$)
** Significant Difference ($p \leq 0.05$)

Table 28. *Enam* 2D Incisor Morphometry – right

MANDIBULAR INCISORS				ANOVA								MULTIPLE COMPARISON					
VIEW/ ASPECT		MEASUREMENT VARIABLE	GROUP	Mean	SD	SE	95% CI of Mean		min'	max'	F	Sig.	GROUPS	MD	SE	95% CI		Sig.
							lower	upper								lower	upper	
RIGHT	BUCCAL	*overall-length* (mm)	WT	9.679	0.199	0.089	9.431	9.926	9.486	10.011	1.066	0.375	WT-HOMO	0.167	0.249	-0.497	0.830	0.785
			HOMO	9.512	0.612	0.274	8.752	10.272	8.971	10.489			WT-HET	0.363		-0.301	1.026	0.344
			HET	9.316	0.222	0.099	9.040	9.592	8.965	9.552			HOMO-HET	0.196		-0.467	0.860	0.717
		angle-of-curvature (°)	WT	127.491	0.951	0.425	126.310	128.671	125.982	128.417	7.333	0.008**	WT-HOMO	-1.470	0.970	-4.057	1.118	0.319
			HOMO	128.960	0.933	0.417	127.802	130.119	127.615	130.146			WT-HET	-3.689		-6.276	-1.101	0.007**
			HET	131.179	2.298	1.028	128.326	134.032	129.294	134.755			HOMO-HET	-2.219		-4.806	0.368	0.096
		width-at-midpoint (mm)	WT	0.980	0.033	0.015	0.940	1.021	0.953	1.036	0.304	0.743	WT-HOMO	0.011	0.025	-0.057	0.079	0.906
			HOMO	0.969	0.050	0.023	0.907	1.032	0.915	1.044			WT-HET	-0.009		-0.077	0.059	0.934
			HET	0.989	0.035	0.016	0.945	1.033	0.957	1.030			HOMO-HET	-0.020		-0.088	0.048	0.723
		incisor-perimeter (mm)	WT	21.490	0.833	0.373	20.455	22.524	20.547	22.312	3.138	0.080	WT-HOMO	-0.459	0.461	-1.690	0.772	0.594
			HOMO	21.949	0.622	0.278	21.177	22.721	21.372	22.672			WT-HET	0.689		-0.542	1.920	0.328
			HET	20.800	0.718	0.321	19.909	21.692	19.691	21.521			HOMO-HET	1.148		-0.083	2.380	0.068
		incisor-area (mm^2)	WT	9.422	0.553	0.247	8.736	10.109	8.903	10.184	0.944	0.416	WT-HOMO	0.479	0.369	-0.504	1.463	0.422
			HOMO	8.943	0.503	0.225	8.319	9.567	8.353	9.453			WT-HET	0.097		-0.886	1.081	0.962
			HET	9.325	0.679	0.304	8.482	10.168	8.589	10.230			HOMO-HET	-0.382		-1.365	0.602	0.570
	LINGUAL	*overall-length* (mm)	WT	9.698	0.235	0.105	9.406	9.990	9.423	10.052	2.356	0.137	WT-HOMO	0.384	0.178	-0.092	0.859	0.121
			HOMO	9.314	0.200	0.089	9.066	9.562	9.045	9.525			WT-HET	0.235		-0.241	0.710	0.414
			HET	9.463	0.378	0.169	8.993	9.933	8.832	9.751			HOMO-HET	-0.149		-0.625	0.326	0.688
		angle-of-curvature (°)	WT	127.409	1.076	0.481	126.072	128.746	126.167	129.011	8.633	0.005**	WT-HOMO	-2.428	0.916	-4.872	0.016	0.052
			HOMO	129.837	1.026	0.459	128.564	131.110	128.611	130.935			WT-HET	-3.752		-6.196	-1.309	0.004**
			HET	131.161	2.020	0.903	128.653	133.670	128.265	133.563			HOMO-HET	-1.324		-3.768	1.119	0.350
		width-at-midpoint (mm)	WT	0.981	0.052	0.023	0.917	1.046	0.939	1.051	1.213	0.331	WT-HOMO	0.210	0.160	-0.217	0.637	0.416
			HOMO	0.771	0.433	0.194	0.234	1.309	0.000	1.002			WT-HET	-0.011		-0.438	0.416	0.997
			HET	0.993	0.045	0.020	0.937	1.049	0.958	1.054			HOMO-HET	-0.221		-0.648	0.206	0.380
		incisor-perimeter (mm)	WT	21.686	0.378	0.169	21.217	22.155	21.368	22.280	1.647	0.233	WT-HOMO	-0.051	0.390	-1.091	0.990	0.991
			HOMO	21.736	0.609	0.272	20.980	22.493	20.806	22.394			WT-HET	0.586		-0.454	1.627	0.324
			HET	21.100	0.792	0.354	20.116	22.083	19.938	22.017			HOMO-HET	0.637		-0.404	1.677	0.270
		incisor-area (mm^2)	WT	9.471	0.401	0.179	8.974	9.969	9.166	10.123	2.548	0.120	WT-HOMO	0.626	0.327	-0.246	1.498	0.177
			HOMO	8.845	0.540	0.242	8.174	9.516	8.062	9.307			WT-HET	-0.025		-0.897	0.847	0.997
			HET	9.496	0.591	0.264	8.762	10.230	8.854	10.233			HOMO-HET	-0.651		-1.523	0.221	0.157
		labial-length (mm)	WT	11.421	1.173	0.525	9.964	12.878	9.393	12.447	0.270	0.768	WT-HOMO	0.133	0.529	-1.278	1.544	0.966
			HOMO	11.288	0.833	0.372	10.254	12.322	10.049	12.343			WT-HET	0.383		-1.028	1.794	0.754
			HET	11.038	0.170	0.076	10.827	11.249	10.777	11.206			HOMO-HET	0.250		-1.161	1.661	0.885

* Bonferroni Corrected Significant Difference ($p \leq 0.002$)
** Significant Difference ($p \leq 0.05$)

Table 29. *Enam* 2D Colour and Whiteness – left gingival/ pre-secretory

MANDIBULAR INCISORS				ANOVA								MULTIPLE COMPARISON					
SIDE	REGION/ STAGE	COLOUR COMPONENT	GROUP	Mean	SD	SE	95% CI of Mean lower bound	95% CI of Mean upper bound	min'	max'	F	Sig.	GROUPS	MD	SE	95% CI lower bound	95% CI upper bound	Sig.
LEFT	GINGIVAL/ PRE-SECRETORY	*lightness*	WT	59.602	7.387	3.304	50.429	68.775	46.520	63.810	16.390	0.000*	WT-HOMO	26.596	4.919	13.473	39.719	0.000**
			HOMO	33.006	9.865	4.412	20.757	45.255	20.391	43.139			WT-HET	21.320		8.197	34.444	0.000**
			HET	38.281	5.439	2.432	31.528	45.035	34.818	47.834			HOMO-HET	-5.275		-18.399	7.848	0.548
		red/ green	WT	-3.202	1.937	0.866	-5.608	-0.796	-5.530	-0.220	1.840	0.201	WT-HOMO	-2.822	1.508	-6.844	1.200	0.189
			HOMO	-0.380	2.934	1.312	-4.023	3.263	-4.350	2.950			WT-HET	-1.960		-5.982	2.062	0.422
			HET	-1.242	2.165	0.968	-3.930	1.446	-4.320	0.800			HOMO-HET	0.862		-3.160	4.884	0.837
		yellow/ blue	WT	5.172	1.317	0.589	3.537	6.807	3.290	7.000	1.424	0.279	WT-HOMO	-1.892	1.322	-5.419	1.635	0.357
			HOMO	7.064	2.854	1.276	3.520	10.608	3.990	11.230			WT-HET	0.078		-3.449	3.605	0.998
			HET	5.094	1.796	0.803	2.863	7.325	2.500	6.980			HOMO-HET	1.970		-1.557	5.497	0.330
		whiteness	WT	65.028	9.370	4.190	53.394	76.662	52.560	78.580	1.582	0.246	WT-HOMO	14.824	9.818	-11.370	41.018	0.321
			HOMO	50.204	23.009	10.290	21.634	78.774	18.640	74.200			WT-HET	-0.582		-26.776	25.612	0.998
			HET	65.610	10.284	4.599	52.840	78.380	56.140	81.330			HOMO-HET	-15.406		-41.600	10.788	0.296

* Bonferroni Corrected Significant Difference ($p \leq 0.002$)
** Significant Difference ($p \leq 0.05$)

Table 30. *Enam* 2D Colour and Whiteness – left middle/ secretory

MANDIBULAR INCISORS				ANOVA								MULTIPLE COMPARISON					
							95% CI of Mean								95% CI		
SIDE	REGION/ STAGE	COLOUR COMPONENT	GROUP	Mean	SD	SE	lower bound	upper bound	min'	max'	F	Sig.	GROUPS	MD	SE	lower bound	upper bound	Sig.
LEFT	MIDDLE/ SECRETORY	*lightness*	WT	42.079	4.696	2.100	36.248	47.910	35.647	46.413	0.630	0.549	WT-HOMO	-2.386	2.989	-10.360	5.587	0.711
			HOMO	44.466	6.272	2.805	36.678	52.253	35.036	50.256			WT-HET	-3.234		-11.208	4.739	0.542
			HET	45.314	2.367	1.059	42.374	48.253	43.186	48.255			HOMO-HET	-0.848		-8.821	7.126	0.957
		red/ green	WT	-2.692	0.661	0.295	-3.512	-1.872	-3.260	-1.570	1.060	0.377	WT-HOMO	-0.834	0.704	-2.713	1.045	0.484
			HOMO	-1.858	1.203	0.538	-3.352	-0.364	-3.650	-0.720			WT-HET	0.100		-1.779	1.979	0.989
			HET	-2.792	1.356	0.606	-4.476	-1.108	-4.410	-0.810			HOMO-HET	0.934		-0.945	2.813	0.408
		yellow/ blue	WT	6.638	2.812	1.258	3.146	10.130	3.430	10.500	5.413	0.021**	WT-HOMO	4.076	1.545	-0.046	8.198	0.053
			HOMO	2.562	2.354	1.053	-0.361	5.485	-1.180	5.250			WT-HET	4.6700		0.548	8.792	0.027**
			HET	1.968	2.111	0.944	-0.653	4.589	0.470	5.360			HOMO-HET	0.594		-3.528	4.716	0.922
		whiteness	WT	55.944	17.606	7.874	34.084	77.804	32.120	74.560	6.254	0.014**	WT-HOMO	-25.959	8.968	-49.885	-2.034	0.033**
			HOMO	81.903	13.886	6.210	64.661	99.145	64.310	102.967			WT-HET	-28.762		-52.687	-4.837	0.019**
			HET	84.706	10.020	4.481	72.265	97.147	69.780	93.190			HOMO-HET	-2.803		-26.728	21.123	0.948

* Bonferroni Corrected Significant Difference ($p \leq 0.002$)
** Significant Difference ($p \leq 0.05$)

Table 31. *Enam* 2D Colour and Whiteness – left incisal/ mature

MANDIBULAR INCISORS				ANOVA								MULTIPLE COMPARISON					
							95% CI of Mean								95% CI		
SIDE	REGION/ STAGE	COLOUR COMPONENT	GROUP	Mean	SD	SE	lower bound	upper bound	min'	max'	F	Sig.	GROUPS	MD	SE	lower bound	upper bound	Sig.
LEFT	INCISAL/ MATURE	*lightness*	WT	42.773	6.969	3.117	34.120	51.426	33.297	49.404	0.777	0.482	WT-HOMO	-3.093	3.734	-13.053	6.868	0.693
			HOMO	45.865	6.853	3.065	37.356	54.375	40.085	57.566			WT-HET	-4.558		-14.519	5.403	0.464
			HET	47.331	3.003	1.343	43.602	51.060	42.308	50.378			HOMO-HET	-1.465		-11.426	8.495	0.919
		red/ green	WT	-3.406	2.069	0.925	-5.975	-0.837	-5.480	-0.880	0.516	0.610	WT-HOMO	-1.292	1.326	-4.829	2.245	0.606
			HOMO	-2.114	2.026	0.906	-4.630	0.402	-5.510	-0.310			WT-HET	-0.318		-3.855	3.219	0.969
			HET	-3.088	2.189	0.979	-5.807	-0.369	-5.440	-0.140			HOMO-HET	0.974		-2.563	4.511	0.748
		yellow/ blue	WT	13.330	3.443	1.540	9.055	17.605	7.440	16.380	14.393	0.001*	WT-HOMO	16.350	3.084	8.122	24.578	0.000**
			HOMO	-3.020	0.513	0.229	-3.657	-2.383	-3.850	-2.450			WT-HET	10.376		2.148	18.604	0.014**
			HET	2.954	7.695	3.441	-6.601	12.509	-2.820	16.150			HOMO-HET	-5.974		-14.202	2.254	0.171
		whiteness	WT	13.328	21.913	9.800	-13.880	40.536	-1.490	51.360	15.575	0.000*	WT-HOMO	-100.934	18.335	-149.850	-52.018	0.000**
			HOMO	114.262	2.935	1.313	110.617	117.906	111.179	117.978			WT-HET	-65.083		-113.999	-16.167	0.010**
			HET	78.411	45.084	20.162	22.431	134.391	0.260	111.092			HOMO-HET	35.851		-13.065	84.767	0.166

* Bonferroni Corrected Significant Difference ($p \leq 0.002$)
** Significant Difference ($p \leq 0.05$)

Table 32. *Enam* 2D Colour and Whiteness – left whole/ all

MANDIBULAR INCISORS				ANOVA								MULTIPLE COMPARISON					
							95% CI of Mean								95% CI		
SIDE	REGION/ STAGE	COLOUR COMPONENT	GROUP	Mean	SD	SE	lower bound	upper bound	min'	max'	F	Sig.	GROUPS	MD	SE	lower bound	upper bound	Sig.
LEFT	WHOLE/ ALL	*lightness*	WT	42.669	4.621	2.067	36.931	48.407	36.974	48.305	0.330	0.725	WT-HOMO	1.572	3.042	-6.544	9.687	0.865
			HOMO	41.097	6.513	2.913	33.010	49.184	32.162	47.285			WT-HET	-0.867		-8.983	7.249	0.956
			HET	43.536	2.372	1.061	40.591	46.481	40.683	46.946			HOMO-HET	-2.439		-10.554	5.677	0.709
		red/ green	WT	-3.166	1.435	0.642	-4.948	-1.384	-4.460	-0.950	1.247	0.322	WT-HOMO	-1.586	1.005	-4.266	1.094	0.292
			HOMO	-1.580	1.541	0.689	-3.494	0.334	-3.250	0.100			WT-HET	-0.752		-3.432	1.928	0.740
			HET	-2.414	1.771	0.792	-4.612	-0.216	-4.320	-0.060			HOMO-HET	0.834		-1.846	3.514	0.692
		yellow/ blue	WT	8.150	1.388	0.621	6.426	9.874	7.020	10.560	11.650	0.002*	WT-HOMO	6.042	1.326	2.504	9.580	0.002**
			HOMO	2.108	1.398	0.625	0.372	3.844	0.060	3.800			WT-HET	4.852		1.314	8.390	0.009**
			HET	3.298	3.051	1.364	-0.490	7.086	0.470	7.950			HOMO-HET	-1.190		-4.728	2.348	0.652
		whiteness	WT	46.550	8.777	3.925	35.652	57.448	31.080	52.280	13.114	0.001*	WT-HOMO	-38.944	8.013	-60.322	-17.566	0.001**
			HOMO	85.494	9.037	4.041	74.274	96.714	72.390	97.180			WT-HET	-30.680		-52.058	-9.302	0.006**
			HET	77.230	17.969	8.036	54.919	99.541	47.690	93.460			HOMO-HET	8.264		-13.114	29.642	0.572

* Bonferroni Corrected Significant Difference ($p \leq 0.002$)
** Significant Difference ($p \leq 0.05$)

Table 33. *Enam* 2D Colour and Whiteness – right gingival/ pre-secretory

MANDIBULAR INCISORS				ANOVA								MULTIPLE COMPARISON					
SIDE	REGION/ STAGE	COLOUR COMPONENT	GROUP	Mean	SD	SE	95% CI of Mean lower bound	95% CI of Mean upper bound	min'	max'	F	Sig.	GROUPS	MD	SE	95% CI lower bound	95% CI upper bound	Sig.
RIGHT	GINGIVAL/ PRE-SECRETORY	*lightness*	WT	42.672	7.082	3.167	33.879	51.466	37.851	55.118	2.346	0.138	WT-HOMO	7.683	3.566	-1.830	17.196	0.120
			HOMO	34.989	4.501	2.013	29.401	40.578	29.372	39.738			WT-HET	4.523		-4.990	14.036	0.438
			HET	38.149	4.993	2.233	31.949	44.350	33.076	44.265			HOMO-HET	-3.160		-12.673	6.353	0.659
		red/ green	WT	-2.628	0.647	0.289	-3.432	-1.824	-3.710	-2.020	0.736	0.499	WT-HOMO	-1.082	0.912	-3.514	1.350	0.483
			HOMO	-1.546	1.469	0.657	-3.370	0.278	-3.350	0.500			WT-HET	-0.740		-3.172	1.692	0.703
			HET	-1.888	1.912	0.855	-4.262	0.486	-4.730	-0.330			HOMO-HET	0.342		-2.090	2.774	0.926
		yellow/ blue	WT	5.444	1.347	0.602	3.771	7.117	3.140	6.530	2.399	0.133	WT-HOMO	-0.806	0.877	-3.147	1.535	0.639
			HOMO	6.250	1.222	0.546	4.733	7.767	4.910	7.630			WT-HET	1.108		-1.233	3.449	0.441
			HET	4.336	1.571	0.702	2.386	6.286	2.290	6.100			HOMO-HET	1.914		-0.427	4.255	0.115
		whiteness	WT	62.672	8.561	3.829	52.042	73.302	53.520	75.900	2.222	0.151	WT-HOMO	4.538	5.761	-10.832	19.908	0.717
			HOMO	58.134	9.381	4.195	46.486	69.782	46.920	68.410			WT-HET	-7.486		-22.856	7.884	0.422
			HET	70.158	9.362	4.187	58.534	81.782	56.170	81.930			HOMO-HET	-12.024		-27.394	3.346	0.134

* Bonferroni Corrected Significant Difference ($p \leq 0.002$)
** Significant Difference ($p \leq 0.05$)

Table 34. *Enam* 2D Colour and Whiteness – right middle/ secretory

MANDIBULAR INCISORS				ANOVA								MULTIPLE COMPARISON					
							95% CI of Mean								95% CI		
SIDE	REGION/ STAGE	COLOUR COMPONENT	GROUP	Mean	SD	SE	lower bound	upper bound	min'	max'	F	Sig.	GROUPS	MD	SE	lower bound	upper bound	Sig.
RIGHT	MIDDLE/ SECRETORY	*lightness*	WT	43.063	6.495	2.904	34.999	51.127	37.749	54.200	1.013	0.392	WT-HOMO	-3.462	3.258	-12.154	5.229	0.554
			HOMO	46.526	3.162	1.414	42.599	50.452	42.505	49.154			WT-HET	-4.403		-13.095	4.288	0.395
			HET	47.467	5.237	2.342	40.964	53.970	40.108	53.827			HOMO-HET	-0.941		-9.633	7.751	0.955
		red/ green	WT	-2.544	0.597	0.267	-3.285	-1.803	-3.210	-1.900	1.274	0.315	WT-HOMO	-0.676	0.748	-2.671	1.319	0.648
			HOMO	-1.868	0.493	0.220	-2.480	-1.256	-2.510	-1.360			WT-HET	0.514		-1.481	2.509	0.775
			HET	-3.058	1.896	0.848	-5.412	-0.704	-5.210	0.010			HOMO-HET	1.190		-0.805	3.185	0.287
		yellow/ blue	WT	5.298	2.609	1.167	2.059	8.537	1.040	7.880	6.483	0.012**	WT-HOMO	4.906	1.432	1.086	8.726	0.013**
			HOMO	0.392	1.159	0.519	-1.048	1.832	-0.960	2.130			WT-HET	3.826		0.006	7.646	0.050**
			HET	1.472	2.688	1.202	-1.866	4.810	-0.610	6.160			HOMO-HET	-1.080		-4.900	2.740	0.737
		whiteness	WT	63.408	15.478	6.922	44.190	82.626	46.620	87.090	8.443	0.005**	WT-HOMO	-30.784	7.839	-51.698	-9.871	0.005**
			HOMO	94.192	7.245	3.240	85.197	103.188	83.950	101.241			WT-HET	-23.610		-44.523	-2.697	0.027**
			HET	87.018	12.993	5.811	70.885	103.151	65.060	99.150			HOMO-HET	7.174		-13.739	28.088	0.641

* Bonferroni Corrected Significant Difference ($p \leq 0.002$)
** Significant Difference ($p \leq 0.05$)

Table 35. *Enam* 2D Colour and Whiteness – right incisal/ mature

MANDIBULAR INCISORS				ANOVA								MULTIPLE COMPARISON					
SIDE	REGION/ STAGE	COLOUR COMPONENT	GROUP	Mean	SD	SE	95% CI of Mean lower bound	95% CI of Mean upper bound	min'	max'	F	Sig.	GROUPS	MD	SE	95% CI lower bound	95% CI upper bound	Sig.
RIGHT	INCISAL/ MATURE	*lightness*	WT	43.651	8.121	3.632	33.567	53.735	34.284	54.262	1.101	0.364	WT-HOMO	-5.233	3.630	-14.918	4.452	0.352
			HOMO	48.884	4.569	2.044	43.210	54.558	45.443	56.702			WT-HET	-3.727		-13.412	5.958	0.575
			HET	47.378	3.465	1.549	43.076	51.680	41.345	50.066			HOMO-HET	1.506		-8.179	11.191	0.910
		red/ green	WT	-4.278	1.547	0.692	-6.199	-2.357	-6.390	-2.460	0.082	0.922	WT-HOMO	-0.350	1.076	-3.220	2.520	0.944
			HOMO	-3.928	1.103	0.493	-5.298	-2.558	-5.790	-2.970			WT-HET	0.048		-2.822	2.918	0.999
			HET	-4.326	2.252	1.007	-7.122	-1.530	-6.220	-0.740			HOMO-HET	0.398		-2.472	3.268	0.928
		yellow/ blue	WT	14.120	3.834	1.714	9.360	18.880	7.500	17.050	18.996	0.000*	WT-HOMO	16.458	2.686	9.291	23.625	0.000**
			HOMO	-2.338	1.254	0.561	-3.895	-0.781	-3.720	-0.630			WT-HET	9.800		2.633	16.967	0.008**
			HET	4.320	6.152	2.751	-3.319	11.959	-1.140	14.930			HOMO-HET	-6.658		-13.825	0.509	0.070
		whiteness	WT	8.948	24.121	10.787	-21.002	38.898	-7.580	50.850	19.434	0.000*	WT-HOMO	-99.547	16.121	-142.555	-56.539	0.000**
			HOMO	108.495	5.777	2.584	101.322	115.668	99.480	114.369			WT-HET	-61.749		-104.757	-18.742	0.006**
			HET	70.697	36.522	16.333	25.349	116.045	7.470	100.747			HOMO-HET	37.798		-5.210	80.805	0.087

* Bonferroni Corrected Significant Difference ($p \leq 0.002$)
** Significant Difference ($p \leq 0.05$)

Table 36. *Enam* 2D Colour and Whiteness – right whole/ all

MANDIBULAR INCISORS			ANOVA									MULTIPLE COMPARISON					
							95% CI of Mean								95% CI		
SIDE	REGION/ STAGE	COLOUR COMPONENT	GROUP	Mean	SD	SE	lower bound	upper bound	min'	max'	F	Sig.	GROUPS	MD	SE	lower bound	upper bound	Sig.
RIGHT	WHOLE/ ALL	*lightness*	WT	43.093	6.355	2.842	35.203	50.984	38.288	53.921	0.148	0.864	WT-HOMO	0.086	2.943	-7.765	7.938	1.000
			HOMO	43.007	3.608	1.613	38.527	47.487	38.861	46.416			WT-HET	-1.339		-9.191	6.512	0.893
			HET	44.432	3.399	1.520	40.212	48.653	38.866	47.080			HOMO-HET	-1.425		-9.277	6.426	0.880
		red/ green	WT	-3.176	0.681	0.305	-4.022	-2.330	-3.930	-2.490	0.621	0.554	WT-HOMO	-0.698	0.712	-2.598	1.202	0.603
			HOMO	-2.478	0.759	0.339	-3.420	-1.536	-3.140	-1.290			WT-HET	-0.022		-1.922	1.878	0.999
			HET	-3.154	1.663	0.744	-5.219	-1.089	-4.760	-0.340			HOMO-HET	0.676		-1.224	2.576	0.621
		yellow/ blue	WT	7.994	0.969	0.433	6.791	9.197	6.670	8.850	22.933	0.000*	WT-HOMO	6.400	0.982	3.780	9.020	0.000**
			HOMO	1.594	1.045	0.467	0.297	2.891	0.380	3.270			WT-HET	4.764		2.144	7.384	0.001**
			HET	3.230	2.280	1.020	0.398	6.062	0.360	5.970			HOMO-HET	-1.636		-4.256	0.984	0.257
		whiteness	WT	47.144	6.647	2.973	38.891	55.397	40.320	56.950	26.729	0.000*	WT-HOMO	-41.092	5.824	-56.631	-25.553	0.000**
			HOMO	88.236	6.477	2.896	80.194	96.278	78.170	95.010			WT-HET	-30.226		-45.765	-14.687	0.001**
			HET	77.370	12.973	5.802	61.262	93.478	59.360	93.720			HOMO-HET	10.866		-4.673	26.405	0.191

* Bonferroni Corrected Significant Difference ($p \leq 0.002$)
** Significant Difference ($p \leq 0.05$)

Table 37. *Enam* 3D Incisor Morphometry left buccal

MANDIBULAR INCISORS				ANOVA								MULTIPLE COMPARISON					
VIEW/ ASPECT		MEASUREMENT VARIABLE	GROUP	Mean	SD	SE	95% CI of Mean lower bound	95% CI of Mean upper bound	min'	max'	F	Sig.	GROUPS	MD	SE	95% CI lower bound	95% CI upper bound	Sig.
LEFT	BUCCAL	projected *overall-length* (mm)	WT	9.777	0.675	0.302	8.940	10.615	9.118	10.847	5.525	0.023**	WT-HOMO	0.703	0.368	-0.280	1.686	0.178
			HOMO	9.074	0.620	0.277	8.304	9.843	8.070	9.490			WT-HET	1.187		0.204	2.170	0.019**
			HET	8.590	0.423	0.189	8.065	9.115	8.099	9.261			HOMO-HET	0.484		-0.499	1.467	0.415
		projected *width-at-midpoint* (mm)	WT	1.095	0.146	0.065	0.914	1.276	0.909	1.309	3.109	0.082	WT-HOMO	0.089	0.067	-0.089	0.267	0.406
			HOMO	1.006	0.080	0.036	0.906	1.106	0.912	1.083			WT-HET	0.166		-0.012	0.344	0.068
			HET	0.929	0.076	0.034	0.835	1.022	0.817	1.019			HOMO-HET	0.077		-0.101	0.255	0.498
		actual *width-at-midpoint* (mm)	WT	1.388	0.132	0.059	1.224	1.552	1.192	1.492	4.392	0.037**	WT-HOMO	0.066	0.075	-0.133	0.266	0.658
			HOMO	1.321	0.125	0.056	1.166	1.476	1.134	1.446			WT-HET	0.216		0.017	0.416	0.034**
			HET	1.171	0.095	0.042	1.054	1.289	1.051	1.308			HOMO-HET	0.150		-0.050	0.350	0.153
		actual *perimeter* (mm)	WT	24.157	1.547	0.692	22.237	26.078	23.012	26.304	0.867	0.005**	WT-HOMO	1.642	0.741	-0.335	3.619	0.109
			HOMO	22.515	0.856	0.383	21.452	23.579	21.199	23.270			WT-HET	3.083		1.106	5.060	0.003**
			HET	21.074	0.997	0.446	19.836	22.312	20.083	22.668			HOMO-HET	1.441		-0.536	3.418	0.169
		marked *surface-area* (mm^2)	WT	13.605	1.154	0.516	12.173	15.037	12.257	14.936	3.977	0.047**	WT-HOMO	0.729	0.634	-0.963	2.421	0.504
			HOMO	12.876	0.731	0.327	11.968	13.784	11.845	13.804			WT-HET	1.779		0.087	3.471	0.039**
			HET	11.826	1.073	0.480	10.494	13.158	10.149	12.769			HOMO-HET	1.050		-0.642	2.742	0.261

* Bonferroni Corrected Significant Difference ($p \leq 0.002$)
** Significant Difference ($p \leq 0.05$)

Table 38. *Enam* 3D Incisor Morphometry left lingual

MANDIBULAR INCISORS				ANOVA								MULTIPLE COMPARISON					
VIEW/ ASPECT		MEASUREMENT VARIABLE	GROUP	Mean	SD	SE	95% CI of Mean lower bound	95% CI of Mean upper bound	min'	max'	F	Sig.	GROUPS	MD	SE	95% CI lower bound	95% CI upper bound	Sig.
LEFT	LINGUAL	projected *overall-length* (mm)	WT	9.615	0.402	0.180	9.116	10.114	9.019	10.033	11.409	0.002*	WT-HOMO	0.371	0.220	-0.215	0.956	0.249
			HOMO	9.244	0.270	0.121	8.909	9.579	8.864	9.485			WT-HET	1.035		0.449	1.620	0.001**
			HET	8.580	0.357	0.159	8.137	9.023	8.159	9.092			HOMO-HET	0.664		0.078	1.250	0.027**
		projected *width-at-midpoint* (mm)	WT	1.050	0.048	0.022	0.990	1.109	0.989	1.120	6.135	0.015**	WT-HOMO	0.055	0.040	-0.052	0.162	0.389
			HOMO	0.995	0.072	0.032	0.906	1.084	0.905	1.053			WT-HET	0.140		0.032	0.247	0.012**
			HET	0.910	0.068	0.030	0.825	0.995	0.826	1.011			HOMO-HET	0.085		-0.022	0.192	0.129
		actual *width-at-midpoint* (mm)	WT	1.205	0.088	0.039	1.095	1.314	1.061	1.290	1.314	0.305	WT-HOMO	0.039	0.069	-0.144	0.222	0.836
			HOMO	1.165	0.139	0.062	0.993	1.338	1.032	1.385			WT-HET	0.110		-0.073	0.293	0.283
			HET	1.095	0.091	0.041	0.982	1.208	0.969	1.189			HOMO-HET	0.070		-0.113	0.253	0.575
		actual *perimeter* (mm)	WT	24.192	1.523	0.681	22.301	26.083	22.258	26.268	9.067	0.004**	WT-HOMO	2.088	0.747	0.094	4.082	0.040**
			HOMO	22.104	1.045	0.467	20.807	23.401	20.868	23.321			WT-HET	3.124		1.130	5.118	0.003**
			HET	21.068	0.883	0.395	19.971	22.164	20.553	22.623			HOMO-HET	1.036		-0.958	3.030	0.378
		marked *surface-area* (mm^2)	WT	12.663	1.138	0.509	11.250	14.076	11.565	13.854	3.676	0.057	WT-HOMO	0.459	0.532	-0.959	1.878	0.672
			HOMO	12.204	0.626	0.280	11.426	12.982	11.377	12.997			WT-HET	1.413		-0.005	2.831	0.051
			HET	11.250	0.657	0.294	10.434	12.066	10.427	12.028			HOMO-HET	0.954		-0.465	2.372	0.213

* Bonferroni Corrected Significant Difference ($p \leq 0.002$)
** Significant Difference ($p \leq 0.05$)

Table 39. *Enam* 3D Incisor Morphometry left labial

MANDIBULAR INCISORS				ANOVA								MULTIPLE COMPARISON					
VIEW/ ASPECT		MEASUREMENT VARIABLE	GROUP	Mean	SD	SE	95% CI of Mean lower bound	95% CI of Mean upper bound	min'	max'	F	Sig.	GROUPS	MD	SE	95% CI lower bound	95% CI upper bound	Sig.
LEFT	LABIAL	projected *labial-length* (mm)	WT	9.820	0.674	0.301	8.983	10.657	9.116	10.872	5.870	0.017**	WT-HOMO	0.763	0.363	-0.206	1.731	0.132
			HOMO	9.057	0.593	0.265	8.321	9.793	8.104	9.504			WT-HET	1.233		0.264	2.201	0.014**
			HET	8.587	0.428	0.191	8.056	9.119	8.135	9.280			HOMO-HET	0.470		-0.499	1.439	0.425
		actual *labial-length* (mm)	WT	10.687	0.920	0.411	9.545	11.829	9.433	11.827	4.775	0.030**	WT-HOMO	0.516	0.467	-0.729	1.761	0.529
			HOMO	10.171	0.818	0.366	9.156	11.186	8.775	10.794			WT-HET	1.424		0.179	2.670	0.025**
			HET	9.263	0.346	0.155	8.833	9.692	8.762	9.725			HOMO-HET	0.908		-0.337	2.154	0.168
		circumference (mm)	WT	2.899	0.197	0.088	2.655	3.144	2.552	3.035	5.070	0.025**	WT-HOMO	0.138	0.118	-0.178	0.453	0.496
			HOMO	2.762	0.232	0.104	2.473	3.050	2.515	3.067			WT-HET	0.372		0.057	0.688	0.021**
			HET	2.527	0.110	0.049	2.390	2.664	2.374	2.666			HOMO-HET	0.235		0.158	-0.081	0.158
		total *surface-area* (mm^2)	WT	26.873	1.437	0.643	25.088	28.657	25.212	29.067	5.980	0.016**	WT-HOMO	1.214	1.295	-2.240	4.668	0.628
			HOMO	25.659	2.954	1.321	21.991	29.326	21.527	29.167			WT-HET	4.339		0.885	7.793	0.015**
			HET	22.533	1.334	0.597	20.877	24.190	21.134	24.042			HOMO-HET	3.125		-0.329	6.579	0.078
		volume (mm^3)	WT	6.232	1.234	0.552	4.700	7.764	5.213	8.276	6.112	0.015**	WT-HOMO	1.207	0.555	-0.272	2.687	0.116
			HOMO	5.024	0.686	0.307	4.173	5.876	4.337	6.023			WT-HET	1.918		0.438	3.398	0.012**
			HET	4.314	0.561	0.251	3.617	5.010	3.855	5.253			HOMO-HET	0.711		-0.769	2.190	0.432

* Bonferroni Corrected Significant Difference ($p \leq 0.002$)
** Significant Difference ($p \leq 0.05$)

Table 40. 3D Surface Analysis

MANDIBULAR INCISORS		GROUP (n = 1)						
MEASUREMENT VARIABLE	REGION/ STAGE	*Amelx*				*Enam*		
		WILD-TYPE	HETEROZYGOUS	HEMIZYGOUS	HOMOZYGOUS	WILD-TYPE	HETEROZYGOUS	HOMOZYGOUS
surface-roughness (µm)	*gingival/ pre-secretory*	2.000	1.900	1.500	2.000	2.800	2.400	1.900
	middle/ secretory	3.200	2.100	1.900	2.300	3.600	2.800	2.300
	incisal/ mature	5.400	2.300	2.100	3.400	5.100	3.500	4.200

Table shows raw data. Values are single measurements. No statistical analysis performed.

* Bonferroni Corrected Significant Difference ($p \leq 0.002$)
** Significant Difference ($p \leq 0.05$)

10.4. APPENDIX 4. LIST OF ORIGINAL PUBLICATIONS

As a direct result of this project I was a contributing author on two peer reviewed journal articles; (i) the first paper was a multiple operator clinical trial that employed and validated the novel colour and whiteness assessment translated for the human application (in industrial partnership with Unilever PLC, Port Sunlight, UK.); (ii) the second paper employed the customised 3D analytical software translated for the human dental study model application (in collaboration with colleagues at the University College London).

i. SMITH, R.N., COLLINS, L.Z., NAEENI, M., JOINER, A., PHILPOTTS, C.J., HOPKINSON, I., JONES, C., LATH, D.L., COXON, T.L., HIBBARD, J. & BROOK, A.H. (2008) 'The in vitro and in vivo validation of a mobile non-contact camera-based digital imaging system for tooth colour measurement', *Journal of Dentistry*, vol. 36, no. Supplement 1, pp. 15-20.

ii. SMITH, R.N., ZAITOUN, H., COXON, T.L., KARMO, M., KAUR, G., TOWNSEND, G., HARRIS, E.F. & BROOK, A.H. (2009) 'Defining new dental phenotypes using 3-D image analysis to enhance discrimination and insights into biological processes', *Archives of Oral Biology*, vol. 54, pp. S118-S125.

CONFERENCE ABSTRACTS

1. 14.07.10-17.07.10
   COXON, T.L., BROOK, A.H., ANDERSON, P., & SMITH. R.N.
   3D morphometric and surface phenotyping mouse models of AI (138531)
   International Association of Dental Research (IADR) & Pan European Federation (PEF) Joint Scientific meeting in Barcelona, Spain.
   http://iadr.confex.com/iadr/2010barce/webprogram/Paper138531.html

2. 03.03.10-06.03.10
   COXON, T.L., BROOK, A.H., & SMITH. R.N.
   Quantifying phenotyping variation in mice with *Amelx* and *Enam* mutations (1405)
   Joint American & Canadian Association of Dental Research in Washington DC, USA.
   http://iadr.confex.com/iadr/2010dc/webprogram/Paper129170.html

3. 30.10.09
   COXON, T.L., BROOK, A.H., & SMITH. R.N.
   Phenotype-Genotype correlations in two mouse models of *Amelogenesis imperfecta*
   Postgraduate Researchers in Science & Medicine (PRISM) Conference 2009
   The University of Manchester, Manchester, UK.

4. 01.09.09-04.09.09
   COXON, T.L., BROOK, A.H., & SMITH. R.N.
   Phenotyping mouse models of *Amelogenesis imperfecta.*
   GSK - Mineralised Tissue Group Travel Award #124716
   British Society for Dental Research (BSDR), Glasgow, UK.

5. 01.04.09-04.04.09
   COXON, T.L., BROOK, A.H., ANDERSON, P., ADAMS, P., & SMITH. R.N.
   Measuring genotype-phenotype relationships in the murine dentition (0731)
   International Association of Dental Research (IADR) in Miami, USA.

6. 19.09.08
   COXON, T.L., HIBBARD, J.H., BROOK, A.H., & SMITH. R.N.
   Phenotyping mouse models of *Amelogenesis imperfecta.*
   Postgraduate Researchers in Science & Medicine Conference (PRISM) 2008
   The University of Liverpool, Liverpool, UK.

7. 10.09.08-12.09.08
   COXON, T.L., HIBBARD, J.H., BROOK, A.H., & SMITH. R.N.
   Murine oro-facial morphology: a model for human dental anomalies. (0212)
   Pan European Federation (PEF) British Society for Dental Research (BSDR), London, UK.

8. 02.07.08-05.07.08
   COXON, T.L., HIBBARD, J.H., KARMO, M., SMITH, R.N., & BROOK, A.H.
   Morphometric macro-measurement of murine mandibles and incisors. (2071)
   International Association of Dental Research (IADR) in Toronto, Canada.

9. 02.07.08-05.07.08
   SMITH, R.N., STRETTON, A., COXON, T.L., & BROOK, A.H.
   Automated calibrated measurement of murine tooth colour and whiteness
   International Association of Dental Research (IADR) in Toronto, Canada.

10. 12.10.07
    SMITH, R.N., KARMO, M., COXON, T.L., PETERS, H., & BROOK, A.H.
    Phenotyping of a murine model for dental anomalies.
    5th Annual Research & Development Open Day, Royal Liverpool University Hospital Research & Development Directorate and Clinical Trials Unit. Education Centre, Royal Liverpool University Hospital.

11. 04.04.07
    SMITH, R.N., KARMO, M., COXON, T., PETERS, H., & BROOK A.
    A new methodology for 2D imaging of murine dentition. (0190)
    British Society for Dental Research (BSDR) & Nordisk Odontogisk Förening Joint Scientific Meeting - University of Durham.

12. 03.04.07-05.05.07
    ZAITOUN, H., COXON, T.L., KARMO, M., BROOK, A.H., & SMITH R.N.
    Validation and applications of a 3D Laser Scanner for odontometry. (0174)
    British Society for Dental Research (BSDR) & Nordisk Odontogisk Förening Joint Scientific Meeting - University of Durham.